Selected Technical Papers

STP 1544

Performance of Protective Clothing and Equipment:

9th Volume, Emerging Issues and Technologies

Editor:
Angie M. Shepherd

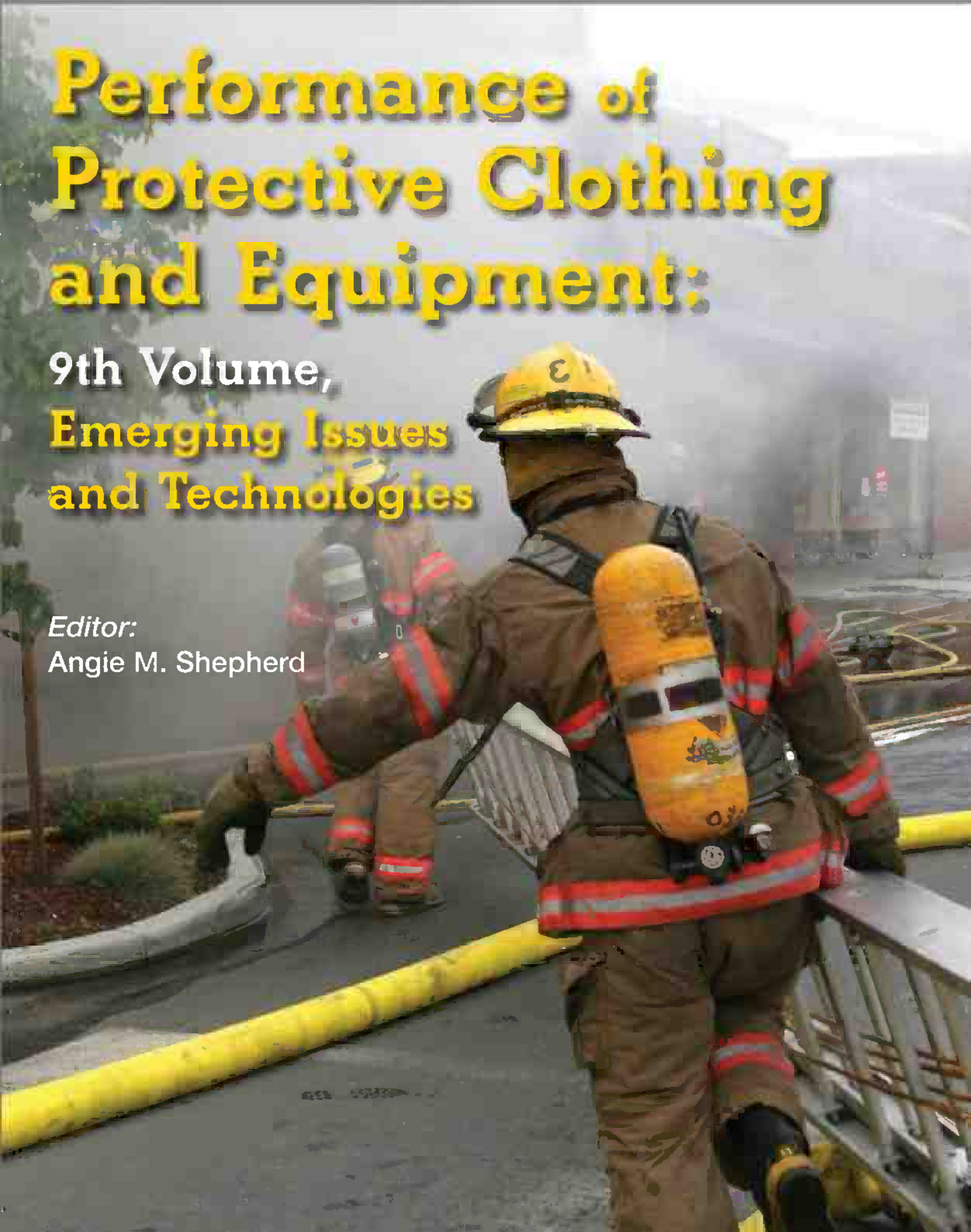

Selected Technical Papers STP1544

Performance of Protective Clothing and Equipment: Emerging Issues and Technologies

Editor:

Angie M. Shepherd

ASTM International
100 Barr Harbor Drive
PO Box C700
West Conshohocken, PA 19428-2959

Printed in the U.S.A.

ASTM Stock #: STP1544

Library of Congress Cataloging-in-Publication Data

ISBN: 978-0-8031-7530-3

This publication has been registered with the Library of Congress.
Library of Congress control number 2012036736

Peer Review Policy

Each paper published in this volume was evaluated by two peer reviewers and at least one editor. The authors addressed all of the reviewers' comments to the satisfaction of both the technical editor(s) and the ASTM International Committee on Publications.

The quality of the papers in this publication reflects not only the obvious efforts of the authors and the technical editor(s), but also the work of the peer reviewers. In keeping with long-standing publication practices, ASTM International maintains the anonymity of the peer reviewers. The ASTM International Committee on Publications acknowledges with appreciation their dedication and contribution of time and effort on behalf of ASTM International.

Citation of Papers

When citing papers from this publication, the appropriate citation includes the paper authors, "paper title", J. ASTM Intl., volume and number, Paper doi, ASTM International, West Conshohocken, PA, Paper, year listed in the footnote of the paper. A citation is provided as a footnote on page one of each paper.

Printed in Bay Shore, NY
October, 2012

Foreword

THIS COMPILATION OF *Selected Technical Papers*, STP1544, on *Performance of Protective Clothing and Equipment: Emerging Issues and Technologies, 9th Volume*, contains 22 papers presented at the symposium with the same name held in Anaheim, CA, June 16–17, 2011. The symposium was sponsored by the ASTM International Committee F23 on Personal Protective Clothing and Equipment.

The Symposium Chairman and STP Editor is Angie M. Shepherd, NIOSH/NPPTL, Pittsburgh, PA, USA.

Contents

Field Analysis of Arc-Flash Incidents and the Related PPE Protective Performance
D. R. Doan, E. "Hugh" Hoagland IV, and T. E. Neal 1

Evaluation of Fire-resistant Clothing Using an Instrumented Mannequin: A Comparison of Exposure Test Conditions Set With a Cylinder Form or Mannequin Form
M. Y. Ackerman, E. M. Crown, J. D. Dale, and S. Paskaluk. 13

Translation between Heat Loss Measured Using Guarded Sweating Hot Plate, Sweating Manikin, and Physiologically Assessed Heat Stress of Firefighter Turnout Ensembles
K. Ross, R. Barker, and A. S. Deaton 27

Analysis of Physical and Thermal Comfort Properties of Chemical Protective Clothing
S. Wen, G. Song, and S. Duncan 48

Chemical Protection Garment Redesign for Military Use by the Laboratory for Engineered Human Protecton Years 2005–2011
K. L. Hultzapple, S. S. Hirsch, J. Venafro, S. Frumkin, J. Brady, C. Winterhalter, and S. Proodian 74

Evaluation of Thermal Comfort of Fabrics Using a Controlled-Environment Chamber
J. D. Pierce, Jr., S. S. Hirsch, S. B. Kane, J. A. Venafro, and C. A. Winterhalter 108

Effects of Overgarment Moisture Vapor Transmission Rate on Human Thermal Comfort
C. Winterhalter, Q. Truong, T. Endrusick, A. Cardello, and L. Lesher 129

Assessing User Needs and Perceptions of Firefighter PPE
J. Barker, L. M. Boorady, S.-H. Lin, Y.-A. Lee, B. Esponnette, and S. P. Ashdown 158

Developing a Thermal Sensor for Use in the Fingers of the PyroHands Fire Test System
A. Hummel, R. Barker, K. Lyons, A. S. Deaton, and J. Morton-Aslanis. 176

Interlaboratory Study of ASTM F2731, Standard Test Method for Measuring the Transmitted and Stored Energy of Firefighter Protective Clothing Systems
L. Deuser, R. Barker, A. S. Deaton, and A. Shepherd 188

Non-destructive Test Methods to Assess the Level of Damage to Firefighters' Protective Clothing
M. Rezazadeh, D. A. Torvi 202

Dual-mode Analytical Permeation System for Precise Evaluation of Porous and Nonporous Chemical Protective Materials
D. L. MacTaggart, S. O. Farwell, Z. Cai, and P. Smith. 227

Factors Influencing the Uptake Rate of Passive Adsorbent Dosimeters Used in the Man-in-Simulant-Test
R. B. Ormond, R. Barker, K. Beck, D. Thompson, and S. Deaton 247

Destructive Adsorption for Enhanced Chemical Protection
S. K. Obendorf and E. F. Spero 266

Protective Clothing for Pesticide Operators: The Past, Present, and Proposed Plans
A. Shaw. 280

Garment Specifications and Mock-ups for Protection from Steam and Hot Water
S. Yu, M. Strickfaden, E. Crown, and S. Olsen 290

Development of a Test Apparatus/Method and Material Specifications for Protection from Steam under Pressure
M. Y. Ackerman, E. M. Crown, J. D. Dale, G. Murtaza, J. Batcheller, and J. A. Gonzalez . . 308

Apparatus for Use in Evaluating Protection from Low Pressure Hot Water Jets
S. H. Jalbani, M. Y. Ackerman, E. M. Crown, M. van Keulen, and G. Song 329

Analysis of Test Parameters and Criteria for Characterizing and Comparing Puncture Resistance of Protective Gloves to Needles
C. Gauvin, O. Darveau, C. Robin, and J. Lara 340

Characterization of the Resistance of Protective Gloves to Pointed Blades
P. I. Dolez, M. Azaiez, and T. Vu-Khanh 354

Methods for Measuring the Grip Performance of Structural Firefighting Gloves
K. Ross, R. Barker, J. Watkins, and A. S. Deaton 371

A New Test Method to Characterize the Grip Adhesion of Protective Glove Materials
C. Gauvin, A. Airoldi, S. Proulx-Croteau, P. I. Dolez, and J. Lara 392

Author Index 407

Subject Index 409

Performance of Protective Clothing and Equipment: Emerging Issues and Technologies
STP 1544, 2012
Available online at www.astm.org
DOI:10.1520/STP104080

Daniel R. Doan,[1] *Elihu "Hugh" Hoagland IV,*[2]
and Thomas E. Neal[3]

Field Analysis of Arc-Flash Incidents and the Related PPE Protective Performance

REFERENCE: Doan, Daniel R., Hoagland IV, Elihu "Hugh", and Neal, Thomas E., "Field Analysis of Arc-Flash Incidents and the Related PPE Protective Performance," *Performance of Protective Clothing and Equipment: Emerging Issues and Technologies* on April 16, 2011 in Anaheim, CA; STP 1544, Angie M. Shepherd, Editor, pp. 1–12, doi:10.1520/STP104080, ASTM International, West Conshohocken, PA 2012.

ABSTRACT: This paper will provide a field analysis of the effectiveness of personal protective clothing and equipment and the related worker burn injuries in real-world electric arc-flash incidents, and a review of the ASTM test methods used for determining the arc rating of personal protective clothing and equipment used to protect workers from electric arc-flash hazards. New learning and conclusions relating to the causes of arc-flash burn injuries and personal protective clothing and equipment strategies that can be effective in reducing burn injuries will be discussed.

KEYWORDS: arc flash, arc rated, flame resistant, burn injury, total body surface area (TBSA), flash fire, personal protective equipment, arc-flash hazard analysis

Introduction

Over the past 15 years, the ASTM Committee F18 on Electrical Protective Equipment for Workers and Subcommittee F18.65 on Wearing Apparel

Manuscript received June 1, 2011; accepted for publication February 27, 2012; published online September 2012.

[1]Principal Consultant, DuPont Engineering, P.O. Box 80723, Wilmington, DE 19880, e-mail: doan@ieee.org

[2]ArcWear/ArcStore/e-Hazard.com, 13113 Eastpoint Park Blvd., Suite E, Louisville, KY 40223, e-mail: hugh@e-hazard.com

[3]Ph.D., Neal Associates Ltd., 24671 Canary Island Ct., Unit 202, Bonita Springs, FL 34134, e-mail: nealassoc@earthlink.net

have developed a series of standards aimed at better protection for electricians and electrical workers exposed to arc-flash hazards [1–9]. During the same period, researchers have written a series of papers with the objective of improving the understanding of the arc-flash phenomenon and quantifying the level of personnel exposure involved in an arc-flash event [10–19]. This arc-flash research contributed to the development of the IEEE 1584 "Guide for Performing Arc-Flash Hazard Calculations" [20] for determining the arc-flash heat exposure based on electrical parameters, equipment design, and the proximity of the electrician or electrical worker to the arc-flash event. The arc ratings and other content of the ASTM standards and IEEE 1584 were incorporated into the 2000, 2004, and 2009 editions of the NFPA 70E "Standard for Electrical Safety in the Workplace" [21]. This brought together the arc rating of protective clothing and equipment and the level of exposure to which an electrician or electrical worker would be exposed in the event that an arc-flash incident occurred while a specific electrical task was being performed on a specific piece of electrical equipment. One of the basic protection principles established by the NFPA 70E standard was the need to match the arc-flash incident energy potential of the task being performed with the arc rating of the protective clothing and equipment worn by the worker performing the task. As long as this match was provided, if an arc-flash incident occurred, the expected burn injury to the worker would either be eliminated or significantly reduced. As the use of arc-rated protective clothing and equipment grew in the late 1990s and early 2000s, and as industry adoptions of the NFPA 70E standard increased, electrical injury studies indicated a decreasing trend of burn injuries to electricians and electrical workers during the decade from 1992 and 2002 [22].

Over the past decade, many workers who were wearing arc-rated clothing and equipment have been involved in arc-flash incidents. Although there has been anecdotal evidence that arc-rated protective clothing and equipment protected workers in several arc-flash incidents, recent field studies [23–25] have confirmed the protective performance and overall effectiveness of arc-rated protective clothing and equipment in real-world arc-flash incidents; however, many of the workers involved in these arc-flash incidents continued to receive more serious burn injuries than expected, in spite of wearing arc-rated clothing and equipment.

What Is an Arc Flash and How Does It Compare to a Flash Fire?

An arc flash is basically a very large short circuit that occurs across an air gap from a conductor to ground or between two or more conductor phases. The electric current involved is typically thousands or tens of thousands of amps and is transmitted through a stream of plasma and ionized gases. The temperature within the arc reaches 15,000°C, but the duration on an arc flash is typically a fraction of a second, because the electrical equipment utilizes fuse or relay devices that will sense and terminate the electrical fault. As an arc flash is initiated, a blinding flash occurs followed by an explosion as the superheated gases in the vicinity of the arc rapidly expand in a fraction of a second. This explosion creates a shock wave and hazardous noise levels exceeding 150 dB. Because of the high temperatures involved, all metallic materials in the vicinity of the arc flash, including copper and steel, vaporize or melt and the molten-metal droplets are projected away from the source of the arc by the shock wave. In some cases, larger pieces of metal or other debris are also projected from the arc source by the shock wave as shrapnel. During the event, an opaque smoke consisting of oxidized copper vapor and other decomposition products reduces visibility to near zero. An arc flash, when slowed down using high speed video, appears as a type of fire, but the arc flash does not require fuel or air in the same way a fire does because electrical energy continues to flow until protective circuitry stops or "clears" the flow of current.

As shown in Table 1, a flash fire is a different phenomenon from an arc flash in several ways. First, the temperature of a flash fire is in the range of 800°C to 1000°C, but the exposure duration can be several seconds. A worker wearing flame-resistant clothing has a few seconds to escape from a flash-fire incident, but because the arc flash typically has a duration of only a fraction of a second, a worker normally has no time to escape from an arc-flash exposure. The temperature of a flash fire is lower than the melting temperature of steel, so the molten-metal hazard that is part of an arc-flash event is not usually present in a flash fire.

The protection approach provided in NFPA 2112 "Standard on Flame-Resistant Garments for Protection of Industrial Personnel against Flash Fire" [26] is to provide flame-resistant clothing that will result in a total body surface area (TBSA) burn injury of 50 % or less as determined by ASTM F1930 [27] using an instrumented manikin and a laboratory-simulated flash fire of controlled intensity for 3 s. As noted above, NFPA 70E provides protective clothing and equipment selected to eliminate most if not all burn injury for a worker. Table 1 compares the different arc-flash and flash-fire protection approaches.

ASTM Arc-Flash Testing Standards

ASTM F1506 "Standard Specification for Flame-Resistant and Arc-Rated Textile Materials for Wearing Apparel for Use by Electrical Workers Exposed to Momentary Electric Arc and Related Thermal Hazards" [1] was

TABLE 1—*Comparison of arc-flash and flash fire phenomena.*

	Arc Flash	Flash Fire
Protection approach	Quantify the arc-flash hazard and minimize burn injury by using PPE with arc rating equal to the exposure level	Select PPE to limit burn injury equal to or less than 50 % TBSA to increase the probability of survival
Ignition time of flammable clothing (s)	0.1 to 0.2	3 to 5
Protective clothing break open	Frequently observed in outer layers	Seldom observed
Heat flux (cal/cm^{2}s)	1 to 200	1 to 3
Typical exposure time (s)	0.1 to 1	1 to 5
Typical total exposure (cal/cm^2)	1 to 100	1 to 15
Maximum temperature (°C)	15,000	800 to 1000
Ignition	Requires reduced insulation	Requires ignition source
Re-ignition	Frequent based on equipment settings	Can occur
Fuel and Air	Not required, but can increase hazard	Requires specific fuel/air mixture
Momentary blinding flash	Yes	Infrequent
Molten metal hazard	Yes	No
Explosion	Yes	In some cases
Shock wave	Yes	When explosion occurs
Hazardous noise levels	Yes	When explosion occurs
Smoke	Yes	Yes

issued in 1994 as the first ASTM Committee F18 standard relating to the arc-flash hazard. This initial version of F1506 provided basic guidance on protective clothing and introduced the use of flame-resistant clothing to prevent clothing ignition in an arc-flash exposure. Preliminary test methods for ignition of flammable clothing and the determination of arc rating for flame-resistant clothing followed in the late 1990s and were formalized as F1958 [2] and F1959 [3] in 1999. Subsequent standards, including F1891 [4] for rating arc- and flame-resistant rainwear, F2178 [5] for rating face-protective equipment, F887 [6] for fall protection and positioning devices, F2621 [6] for finished products like arc-flash suits, F2522 [7] for rating arc-protective shields, and F2676 [8] for rating arc-protective blankets were developed over the next decade. Additional standards development is underway for arc-rated gloves and arc-in-a-box arc-flash hazards. Figures 1–4 show

FIG. 1—*8000-Amp arc-flash generated in arc testing.*

laboratory generated arc-flash exposures and test equipment for two of the arc test methods.

Figure 1 is created by initiating an arc flash with 8000 A of current flowing between two vertical stainless steel electrodes with a gap between the two electrodes of 305 mm (12 in.). The incident energy level of the arc flash is increased by increasing the duration of the arc flash within the range of 0.1 s to 2 s. This arc-flash geometry is used for the ASTM F1959 test method for determining the arc rating of fabrics or multilayer fabric systems and also the ASTM F2178 test method for face-protective equipment. The arc-flash incident

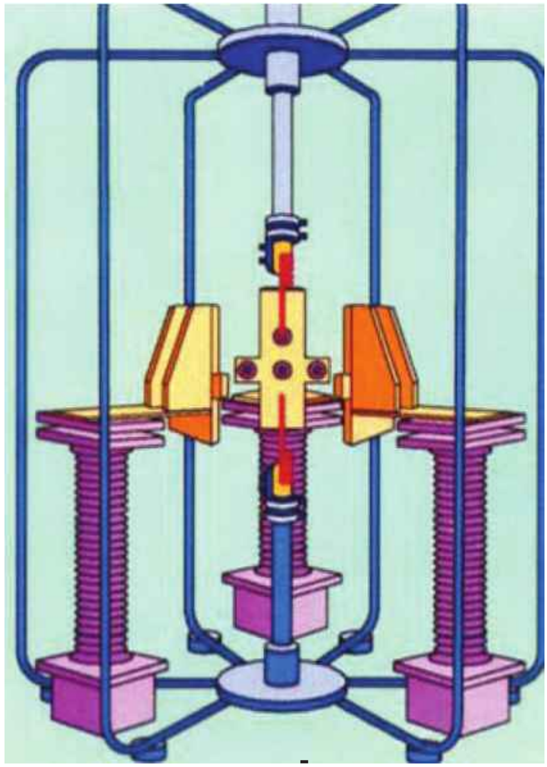

FIG. 2—*ASTM F1959 test method for fabric and system arc rating.*

energy from this arc geometry is a combination of radiant heat and convective heat.

Figure 2 shows the test setup for the F1959 test method. There are three test panels positioned around the two vertical electrodes 305 mm (12 in.) from the centerline of the vertical electrodes where the arc flash will be initiated. There are two heat sensors on each test panel and two monitor heat sensors, one positioned on each side of each test panel. The monitor sensors are also positioned 305 mm (12 in.) from the centerline of the vertical electrodes. A fabric test specimen is positioned on each of the three test panels covering the two heat sensors on each panel. The two monitor sensors are not covered by test specimens. An arc flash is initiated, and the heat at the panel sensors under the fabric test specimens is measured to determine how much heat is transmitted through the test specimen. The heat is also measured at the monitor sensors to determine the total incident energy of the arc flash on each test specimen. The incident energy is increased until the heat sensors under the fabric test specimens indicate sufficient heat transfer through the fabric to cause a second-degree-burn injury. A minimum of 20 test specimens are tested to determine

FIG. 3—*ASTM F2178 face-protection test setup.*

FIG. 4—*ASTM F2676 test method with plasma arc exposure for arc-protective blankets.*

the arc rating of the fabric or fabric system. The heat-sensor data is analyzed using logistic regression, and the arc rating is equal to the incident energy that has a 50 % probability of causing a second-degree-burn injury under the test specimen.

Figure 3 shows the test setup for the F2178 test method for face-protective products, such as arc-rated faceshields and hoods. There are two instrumented heads positioned around the two vertical electrodes 305 mm (12 in.) from the centerline of the vertical electrodes where the arc flash will be initiated. There are four heat sensors on each instrumented head, which are located in each eye area, the mouth area, and under the chin. There are also two monitor heat sensors for each head, one positioned on each side of each instrumented head. The monitor sensors are also positioned 305 mm (12 in.) from the centerline of the vertical electrodes. A face-protective test specimen is positioned on each of the two instrumented heads covering or shielding the four heat sensors on each instrumented head. The two monitor sensors for each head are not covered or shielded by test specimens. An arc flash is initiated and the heat at the head sensors shielded by the face-protective test specimens is measured to determine how much heat is transmitted through the test specimen. The heat is also determined at the monitor sensors to determine the total incident energy of the arc flash on each test specimen. The incident energy is increased until the heat sensors under or behind the face-protective test specimens indicate sufficient heat transfer through the test specimen to cause a second-degree-burn injury. A minimum of 20 test specimens are tested to determine the arc rating of the face-protective product. The heat sensor data is analyzed using logistic regression, and the arc rating is equal to the incident energy that has a 50 % probability of causing a second-degree-burn injury under or behind the face-protective test specimen.

Figure 4 shows a plasma stream arc exposure, which is used for testing arc-protective blankets. The plasma arc exposure is continued until it causes break open in all layers of the arc-protective blanket specimen. The arc-protective blanket is assigned a rating value based on the product of the plasma arc current and the time required for break open of all layers.

The type of arc exposure can significantly impact the arc rating of protective clothing and equipment. When fabrics or fabric systems used in protective clothing are tested using a plasma arc exposure or an arc flash created in and projected out of an enclosure, the arc rating is observed to decrease to approximately half the value determined by the F1959 test method because of the higher ratio of convective energy in these types of arc-flash exposures. On the other hand, face-protective products have increased arc ratings when tested using plasma arcs or arc flashes in enclosures. Real arc-flash incidents frequently involve enclosures and can involve plasma arcs, and consequently the level of protection provided by arc-rated clothing may be only half of the level that is expected based on the F1959 arc test method [19]. This dependence of arc rating results on the type and geometry of arc-flash exposure raises the question of how arc-rated protective clothing and equipment perform in real arc-flash incidents.

Protective Performance of Arc-Rated PPE

Recent studies have assessed the performance of arc-flash protective clothing and equipment worn by workers in real arc-flash incidents [22–24]. Figure 5 summarizes the findings from these studies relating to 40 arc-flash incidents involving 54 workers. In spite of the use of arc-rated protective clothing and equipment, 57 % of the workers received burn injuries. However, when selection and use of arc-rated protective clothing and equipment was based on an arc-flash hazard analysis, the arc-rated protective clothing and equipment provided the expected level of protection. Burn injuries resulted when an arc-flash hazard analysis was not performed leading to insufficient protection, when all elements of protective clothing and equipment were not worn, or when flammable clothing layers worn under arc-rated clothing ignited and/or melted. The authors' [24] conclusions based on their analyses of these arc-flash incidents included the following:

- Arc-rated protective clothing and equipment performs as expected in protecting workers from arc-flash exposures, as long as it is matched to the exposure level and worn in accordance with the NFPA 70E standard.
- Failing to use an arc-flash hazard analysis to assist in the selection of protective clothing and equipment increases the probability that workers will sustain a burn injury if involved in an arc-flash event. Two thirds of the workers involved in an arc-flash incident were burned when an arc-flash hazard analysis was not used to select protective clothing and equipment.
- Conducting an arc-flash hazard analysis to assist in the selection of protective clothing and equipment does not mean that workers will actually

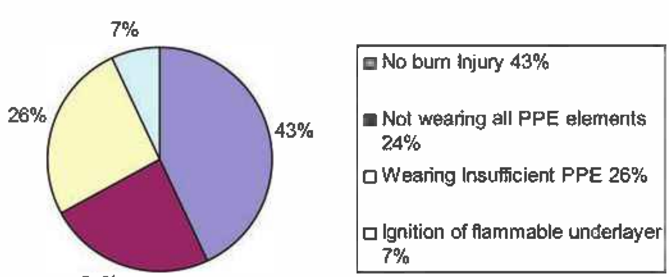

FIG. 5—*Arc-flash incident burn injury analysis and causes of burn injury.*

use all of the required protective clothing and equipment. Approximately half of the injured workers using a hazard-analysis approach to select protective clothing and equipment received a burn injury as a result of not wearing gloves or not wearing an arc-rated faceshield with a hard hat.

- Analysis of real arc-flash incidents reinforces the need to use all required protective clothing and equipment and to follow safe work practices outlined in the NFPA 70E standard:
  (1) Hard-hat protection from arc-flash shrapnel.
  (2) Fully buttoning or closing protective clothing.
  (3) Testing for the absence of voltage and applying safety grounds before beginning electrical work.

References

[1] ASTM F1506-10a, 2010, "Standard Specification for Flame-Resistant and Arc-Rated Textile Materials for Wearing Apparel for Use by Electrical Workers Exposed to Momentary Electric Arc and Related Thermal Hazards," *Annual Book of ASTM Standards*, Vol. 10.03, ASTM International, West Conshohocken, PA.

[2] ASTM F1958/F1958M-99, 2010, "Standard Arc Test Method for Determining the Ignitability of Non-Flame-Resistant Materials for Clothing by Electric Arc Exposure Method Using Mannequins," *Annual Book of ASTM Standards*, Vol. 10.03, ASTM International, West Conshohocken, PA.

[3] ASTM F1959/F1959M-06ae1, 2006, "Standard Arc Test Method for Determining the Arc Thermal Performance Value of Materials for Clothing," *Annual Book of ASTM Standards*, ASTM International, West Conshohocken, PA.

[4] ASTM F1891-06, 2006, "Standard Specification for Arc and Flame-Resistant Rainwear," *Annual Book of ASTM Standards*, Vol. 10.03, ASTM International, West Conshohocken, PA.

[5] ASTM F2178-08, 2008, "Standard Test Method for Determining the Arc Rating and Standard Specification for Face Protective Products," *Annual Book of ASTM Standards*, Vol. 10.03, ASTM International, West Conshohocken, PA.

[6] ASTM F887-11, 2011, "Standard Specification for Personal Climbing Equipment," *Annual Book of ASTM Standards*, Vol. 10.03, ASTM International, West Conshohocken, PA.

[7] ASTM F2621-06, 2006, "Standard Practice for Determining the Response Characteristics and Design Integrity of Arc-Rated Finished Products in an Electric Arc Exposure," *Annual Book of ASTM Standards*, Vol. 10.03, ASTM International, West Conshohocken, PA.

[8] ASTM F2522-05, 2005, "Standard Test Method for Determining the Protective Performance of a Shield Attached on Live Line Tools or on Racking Rods for Electric Arc Hazards," *Annual Book of ASTM Standards*, Vol. 10.03, ASTM International, West Conshohocken, PA.

[9] ASTM F2676-09, 2009, "Standard Test Method for Determining the Protective Performance of an Arc Protective Blanket for Electric Arc Hazards," *Annual Book of ASTM Standards*, Vol. 10.03, ASTM International, West Conshohocken, PA.

[10] Neal, T. E., Bingham, A. H., and Doughty, R. L., "Protective Clothing Guidelines for Electric Arc Exposure," *IEEE Trans. Ind. Appl.*, Vol. 33, No 4, 1997, pp. 1041–1054.

[11] Doughty, R. L., Neal, T. E., Dear, T. A., and Bingham, A. H., "Testing Update on Protective Clothing and Equipment for Electric Arc Exposure," *IEEE Ind. Appl. Mag.*, Vol. 5, No. 1, 1999, pp. 37–49.

[12] Doughty, R. L., Neal, T. E., and Floyd, H. L., II, "Predicting Incident Energy to Better Manage the Electric Arc Hazard on 600-V Power Distribution Systems," *IEEE Trans. Ind. Appl.*, Vol. 36, No. 1, 2000, pp. 257–269.

[13] Doughty, R. L., Neal, T. E., Macalady, T., Saporita, V., and Borgwald, K., "The Use of Low Voltage Current Limiting Fuses to Reduce Arc-Flash Energy," *IEEE PCIC-99-36 Conference Record 99-12*, Sept 1999, San Diego, CA.

[14] Landis Floyd, H. Andrews, J. J., Capelli-Schellpfeffer, M., Neal, T. E., and Saunders, L. F., "Electrical Safety: State of the Art in Technology, Work Practices and Management Systems," *American Society of Safety Engineers 2001 Professional Development Conference, Proceedings Safety*, June 13, 2001, Anaheim, CA.

[15] Doan, D. R. and Sweigart, R. A., "A Summary of Arc-Flash Hazard Calculations," *IEEE Trans. Ind. Appl.*, Vol. 39, No. 4, 2003, pp. 1200–1204.

[16] Doan, D. R., Floyd, H. L., II, and Neal, T. E., "Comparison of Methods for Selecting Personal Protective Equipment for Arc-Flash Hazards," *IEEE Trans. Ind. Appl.*, Vol. 40, No. 4, 2004, pp. 963–969.

[17] Neal T. E. and Parry, R. A., "Shrapnel, Pressure, and Noise," *IEEE Ind. Appl. Mag.*, Vol. 11, No. 3, 2005, pp. 49–53.

[18] Doan, D. R., Gregory, G. D., Kemp, H. O., McClung, B., Saporita, V., and Wellman, C. M., "Development of the Guide for Performing Arc-Flash Hazard Calculations," *IEEE Ind. Appl. Mag.*, Vol. 11, No. 3, 2005, pp. 30–39.

[19] Lang, M., Jones, K., and Neal, T. E., "Impact of Arc-flash Events with Outward Convective Flows on Worker Protection Strategies," *IEEE Electrical Safety Workshop, ESW2010-15*, Feb 2010, Memphis, TN.

[20] IEEE 1584, 2002, "IEEE Guide for Performing Arc-Flash Hazard Calculations," IEEE, NY.

[21] NFPA 70E, 2009, "Standard for Electrical Safety in the Workplace," National Fire Protection Association, Boston, MA.

[22] Cawley, J. C. and Homce, G. T., "Trends in Electrical Injury in the U. S., 1992–2002," *IEEE Trans. Ind. Appl.*, Vol. 44, No. 4, 2008, pp. 962–972.

[23] Doan D. R. and Neal, T. E., "Field Analysis of Arc-Flash Incidents and the Related PPE Protective Performance," *IEEE IAS PCIC Electrical Safety Workshop*, Feb 2009, St. Louis, MO.

[24] Doan D. R. and Neal, T. E., "Putting PPE Performance to the Test," *Electrical Construction & Maintenance (EC&M) Magazine*, May 2009, C24–C26.

[25] Doan, D. R., Elihu, P. E., Hoagland, H., IV, and Neal, T. E., "Update on Field Analysis of Arc-Flash Incidents, PPE Protective Performance Related Worker Injuries," *IEEE IAS PCIC Electrical Safety Workshop, ESW2010-15*, Feb 2010, Memphis, TN.

[26] NFPA 2112, "Standard on Flame-Resistant Garments for Protection of Industrial Personnel against Flash Fire," National Fire Protection Association, Boston, MA.

[27] ASTM F1930-08, 2008, "Standard Test Method for Evaluation of Flame-Resistant Clothing for Protection against Flash Fire Simulations Using an Instrumented Manikin, *Annual Book of ASTM Standards*, Vol. 11.03, ASTM International, West Conshohocken, PA.

Performance of Protective Clothing and Equipment: Emerging Issues and Technologies
STP 1544, 2012
Available online at www.astm.org
DOI:10.1520/STP104103

M. Y. Ackerman,[1] *E. M. Crown,*[1] *J. D. Dale,*[1]
and S. Paskaluk[1]

Evaluation of Fire-resistant Clothing Using an Instrumented Mannequin: A Comparison of Exposure Test Conditions Set With a Cylinder Form or Mannequin Form

REFERENCE: Ackerman, M. Y., Crown, E. M., Dale, J. D., and Paskaluk, S., "Evaluation of Fire-resistant Clothing Using an Instrumented Mannequin: A Comparison of Exposure Test Conditions Set With a Cylinder Form or Mannequin Form," *Performance of Protective Clothing and Equipment: Emerging Issues and Technologies* on April 16, 2011 in Anaheim, CA; STP 1544, Angie M. Shepherd, Editor, pp. 13–26, doi:10.1520/STP104103, ASTM International, West Conshohocken, PA 2012.

ABSTRACT: Setting up a manikin/burner system to evaluate FR clothing requires that the energy transfer to the surface of an instrumented manikin be measured and adjusted to meet the requirements of the test method being used (ASTM F1930 or ISO 11056). ISO 11056 makes provision for the use of an instrumented cylinder to initially set the physical position of burners before using the manikin. The idea behind the provision is that because of the symmetry of the cylinder the heat flux should be uniform over the surface enabling rapid initial setting of burner positions, fuel pressures, flow controls etc. This work experimentally evaluated the differences in heat flux that would be obtained if conditions were set with a cylinder and the cylinder then replaced with the manikin for. The work was undertaken as background to find out whether this procedure would be a useful addition to ASTM F1930. The study concluded that the additional cost/time associated with using a cylinder did not result in better exposure conditions on a manikin form primarily due to the non-uniform shape of the manikin.

Manuscript received June 2, 2011; accepted for publication March 15, 2012; published online September 2012.
[1]Univ. of Alberta, Edmonton, AB T6G 2G8, Canada.

Introduction

The evaluation of protective clothing using an instrumented mannequin system faces challenges in the measurement of energy transfer rates, spatial and time variations in rates, the fit of the garment on the mannequin, and the position and orientation of the burners used to generate the exposure. It is important to ensure that the exposure conditions meet specified tolerances if the results are to be compared to those obtained at other laboratories.

Setting up a mannequin flash fire exposure system involves calibrating the sensors used for the measurement of the heat flux, setting the position of the burners relative to the mannequin, adjusting fuel pressures and gas flow, and eventually achieving an exposure that meets the requirements of the standard being tested (either ASTM F1930 [1] or ISO 13506 [2]). This process can involve significant trial and error, as the movement of the burners relative to the mannequin form can result in changes in energy transfer on the surface of the mannequin that are not what was expected. The energy transfer from the hot combustion products primarily takes the form of convection and radiation, and because the mannequin surfaces do not all have the same orientation, the convection portion of the heat flux varies over the surface of the mannequin. The radiation portion of the total will vary as well but seems to be less sensitive as long as the flames are large enough to engulf the mannequin fully. This has not been verified experimentally, as the sensors used in mannequins around the world respond to the total energy transfer rather than individual components.

ISO 13506 contains a normative appendix that outlines the methods to be used in order to attain the required exposure conditions for an instrumented mannequin form. The appendix is normative, yet there is a provision, Section D.2, in which it appears that the use of an instrumented cylinder is optional. The quotation below, taken from Section D.2.1, outlines the procedure to be used in the event a cylinder is used to initially set up the system.

"D.2.1 The initial setup and positioning of the burners can be aided by using an instrumented vertical cylinder or multi-sided box. If a cylinder is used, it should be 2 000 mm tall and 300 mm in diameter and be fitted with at least 30 heat flux gauges. The gauges shall be spaced around the circumference in five equally spaced vertical columns. Thin-walled steel heating and air conditioning ductwork and paper concrete piling tubes have been used successfully. Software capable of converting the measured data into time-varying heat fluxes at each heat flux sensor is required. If a multi-sided box is used, six heat flux sensors should be equally spaced in each vertical face.

"Place the cylinder on the floor where the manikin is to be located. Space the burners equally around the cylinder, with about 800 mm distance between the burner head and the cylinder. Measure the intensity and uniformity of the flash fire with a 4 s exposure. Gather data for 60 s. Adjust the positions of the

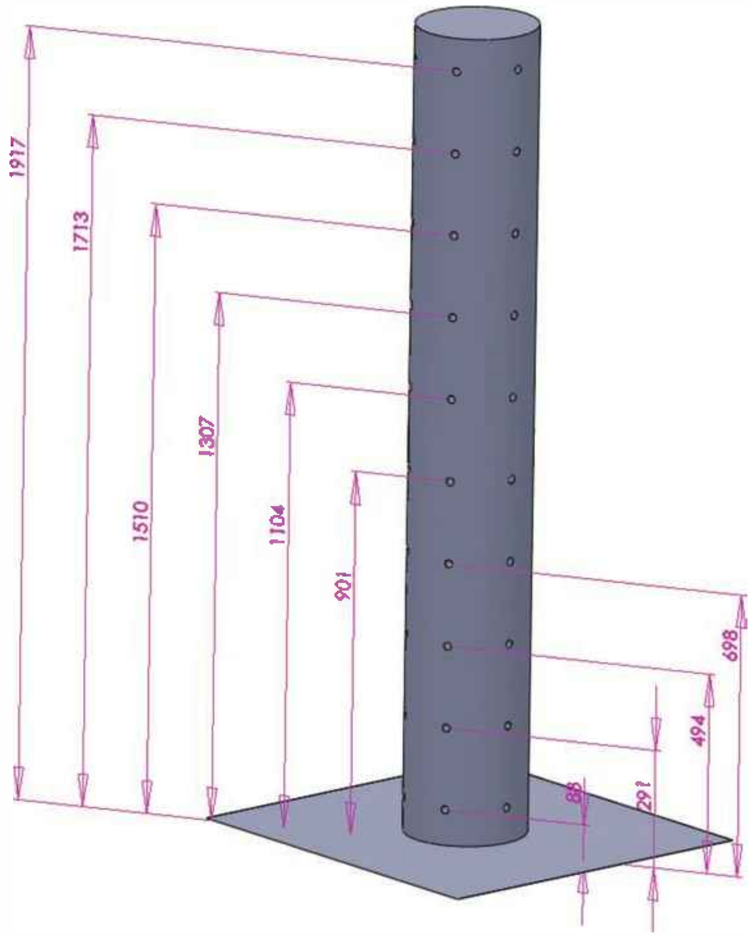

FIG. 1—*Fiberglass cylinder fitted with 60 heat flux sensors installed in burn chamber.*

burners to obtain a heat flux that is as uniform as possible over the surface of the cylinder. Modify the fuel orifice size in the burner heads and/or the fuel line pressure to obtain an average heat flux density of 84 kW/m^2 $\pm$ 2,5 %. Replace the cylinder or multi-sided box with the instrumented manikin" [2].

In order to evaluate the utility of using a cylinder to set the initial conditions for exposure, a fiberglass cylinder 300 mm (12 in.) in diameter and 2000 mm (78 in.) in length was constructed (Fig. 1). The cylinder was fitted with 60 heat flux sensors (base material with surface mounted thermocouple) arranged in 10 rows vertically and six columns equally spaced around the circumference. The vertical spacing of the rows of sensors was set at 200 mm, with the first row positioned 90 mm above the floor or bottom of the cylinder.

A USB data acquisition system was placed inside the cylinder and set up to measure the temperature of the thermocouples ten times per second. The exposure duration for the series of tests was set at 4 s.

Four sets of conditions were run so as to evaluate the differences between using the cylinder to set the exposure conditions and using the mannequin to set the exposure conditions. The four cases were as follows:

Case 1: burner heads normal position for testing—cylinder in place
Case 2: burner heads normal position for testing—mannequin in place
Case 3: burners positioned equidistant to cylinder—mannequin in place
Case 4: burners positioned equidistant to cylinder—cylinder in place

In each case, "normal" refers to the burner position that is usually used for mannequin testing, and these positions have been found experimentally to produce the best heat flux uniformity on the mannequin. "Equidistant" refers to the positioning of the burners so that each burner head is the same distance from the 300 mm diameter cylinder. In all cases, the exposure duration was set at 4 s as per ISO 13506.

The burn chamber used for testing consists of a masonry block room with inside dimensions of approximately 5.7 m × 5.7 m × 3.7 m (18.7 ft × 18.7 ft × 12 ft). The room was constructed with a suspended flooring system so there was an additional 1 m high crawl space beneath the floor. Fuel is delivered to the burners from an outside storage via a 50 mm (2 in.) diameter pipe system, and individual burners are fed from a 2.4 m × 2.4 m × 100 mm (8 ft × 8 ft × 4 in.) steel pipe ring located in the crawl space beneath the floor. The supply pressure is maintained via the use of four additional propane storage tanks charged to approximately 500 kPa (75 psig), which can be connected to the system as needed. The fuel pressure is typically 250 kPa (36 psig). Connecting any of the four higher pressure storage tanks results in the rapid transfer of fuel to the main fuel supply, quickly replenishing fuel that is burned during a test. The system was designed to maintain an absolute fuel pressure within ±10 % during exposures of up to 20 s in length. Figure 2 is a photograph of the burn chamber and burner systems with the mannequin in place. The 12 burners are positioned in groups of two at 60° angles from the center of the position normally occupied by the mannequin. Each of the six burner supports has two burner heads that can be independently adjusted for height, azimuth, and angle. When the burn room was commissioned, the burner positions were adjusted so as to maintain an average heat flux according to the requirements of ASTM F1930 while minimizing variations over the mannequin surface.

A summary of the test results for all cases is shown in Table 1. Note that in all cases, the torch positions relative to the cylinder or mannequin would have produced results that met the requirements of the ASTM F1930 test method. The primary difference lies in the variability of the heat flux readings, as indicated by the standard deviation, for either the 110 sensors that are in the mannequin or the 60 sensors in the cylinder.

FIG. 2—*Burn chamber showing placement of mannequin and burners.*

Section 10.2.2.2 of ASTM F1930 gives some guidance on the initial placement of burners and the requirements that must be met, as indicated in the following quote:

"Position the exposure burners and adjust the flames so that the standard deviation of the average exposure heat flux level of all of the manikin sensors does not exceed 21 kW/m^2 (0.5 cal/s · cm^2) for a nude manikin exposure" [1].

A similar statement appears in Section D.2.3 of ISO 13506 [2]:

"Position the exposure burners and adjust the flames so that the average exposure heat flux density is within ±5 % of the specified level. Confirm the standard deviation of the average heat flux density calculated for all the sensors to be equal to or less than 20 kW/m^2 for each nude manikin exposure and, if

TABLE 1—*Comparison of average heat flux changes with burner position.*

Case		Average Heat Flux,[a] kW/m^2 (cal/cm^2 s)	Standard Deviation of Heat Flux,[a] kW/m^2 (cal/cm^2 s)
1	Burners normal, cylinder in place	81.9 (1.95)	13.0 (0.31)
2	Burners normal, mannequin in place	81.5 (1.94)	14.3 (0.34)
3	Burners equidistant, mannequin in place	85.9 (2.05)	19.5 (0.46)
4	Burners equidistant, cylinder in place	81.0 (1.93)	21.8 (0.52)

[a]Determined using readings between 1.2 and 4 s.

necessary, adjust the burners to obtain the exposure uniformity. See also 5.6.4.4. Record the final position of each burner."

Note that with the exception of case 4 (burners equidistant, cylinder in place), all of the tests would meet the requirements of ASTM F1930 in that the heat flux average is 84 ± 5 % and the standard deviation of the average is less than 21 kW/m^2. Part of the challenge in running these comparisons is deciding which sensors on the cylinder should be included in the evaluation. Because we were interested in spatial and time variations in heat flux, the cylinder was constructed with ten rows of sensors vertically. The lowest row of sensors (closest to the burn chamber floor) is within 100 mm (4 in.) of the bottom of the cylinder. Because the hot gases produced are very buoyant, the combustion products rarely get to this level, and as a result the dominant mode of energy transfer to this lower row is radiation. Figure 3 shows the flux traces for each vertical row of sensors with the burners equidistant from the cylinder. Sensor flux readings at each level were averaged and plotted as a function of time in order to examine vertical differences. When our burn chamber was initially commissioned, it was found that the most uniform distribution of heat flux was obtained with the burners in a position that would not place them equidistant from a cylinder in the room center. This has to do largely with the fact that

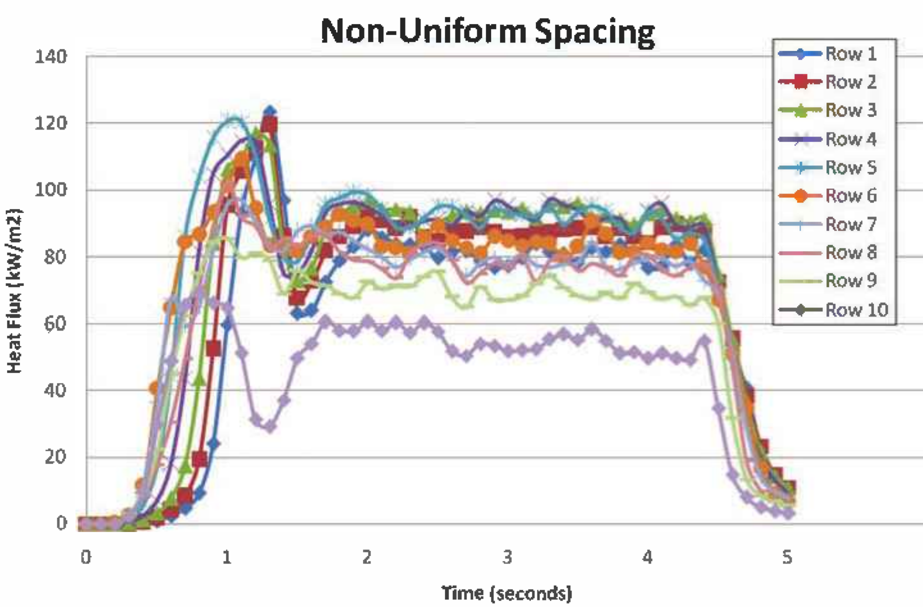

FIG. 3—*Heat flux on a cylindrical form. Burners are positioned so as to meet the requirements of ASTM F1930, Sections 10.1.3 and 10.1.4. Average heat flux = 84 ± 5 % kW/m^2; standard deviation lower than 21 kW/m^2; average heat flux measured for arms, thighs, shanks, and trunk is 84 ± 15 % kW/m^2 of the mannequin average.*

the human form, although often approximated as a cylinder, is quite different. Figure 4 shows the flux traces obtained from the cylinder placed in the center of the room and the burners left in the positions typically used for clothing evaluation.

Note that whereas the average heat flux in each case (determined according to ASTM F1930) is very similar (81.0 kW/m^2 versus 81.9 kW/m^2), the standard deviation of the system with uniform burner placement is much larger than that obtained when the burners are placed so as to meet ASTM F1930 specified flux requirements on the mannequin form. This would indicate that either method would be fine for the initial placement of burners relative to the mannequin position, but uniform spacing might not produce an ideal distribution, even on a simple geometric form such as a cylinder.

Figure 5 shows a comparison of the vertical distributions of heat flux for the two burner positions. In each case, the six sensors at each elevation were averaged over 0.7 s to 4 s (the start and end periods are arbitrary but in line with the requirements of ASTM F1930 for determining average heat flux). Uniform spacing of burners around the cylinder produced an average of 81 kW/m^2 with a standard deviation of 11.8 kW/m^2. Non-uniform spacing (set up to produce the most uniform flux on the mannequin) resulted in the same mean value of 81 kW/m^2 but a standard deviation almost twice as large (19.6 kW/m^2). Recognizing that most mannequin systems in existence do not have sensors in the feet, it would perhaps make more sense to exclude the row of sensors that were within 100 mm of the floor of the chamber. Excluding this row of sensors from the analysis increases the average heat flux on the cylinder to 83.9 kW/m^2 and 86.6 kW/m^2, respectively, and provides a substantial reduction in the standard deviation in both cases. As the location of sensors is not precisely specified in either test method, this could be problematic in that one could spend a lot of time attempting to achieve a uniform flux on the cylinder without knowing the impact on the measured flux on the mannequin form. It is our understanding that the use of a cylinder as an initial setup tool was intended to allow the rapid setting of initial burner positions. The idea was to produce as uniform a heat flux as possible on the cylinder and then put the mannequin in place, and it should meet the requirements of 84 ± 5 % kW/m^2; a standard deviation of 21 kW/m^2; and an average heat flux for arms, trunk, thighs, and shanks of 84 ± 15 % kW/m^2, thus eliminating a lot of the time spent positioning the burners with the mannequin in place.

Radial Variations in Heat Flux

In order to evaluate the radial variations in energy transfer to the cylinder, the heat flux data were grouped in vertical columns at 60° intervals. Thus there were ten sensors in each grouping for these tests. Two tests were run, one with burners at an equal offset from the cylinder and one with burners positioned so

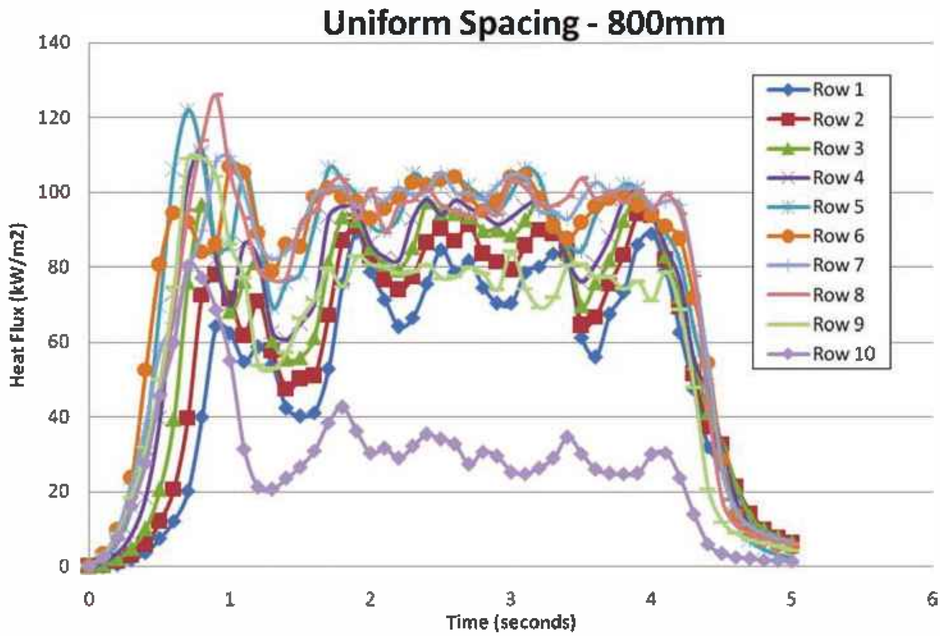

FIG. 4—*Heat flux on a cylindrical form; uniform spacing around cylinder.*

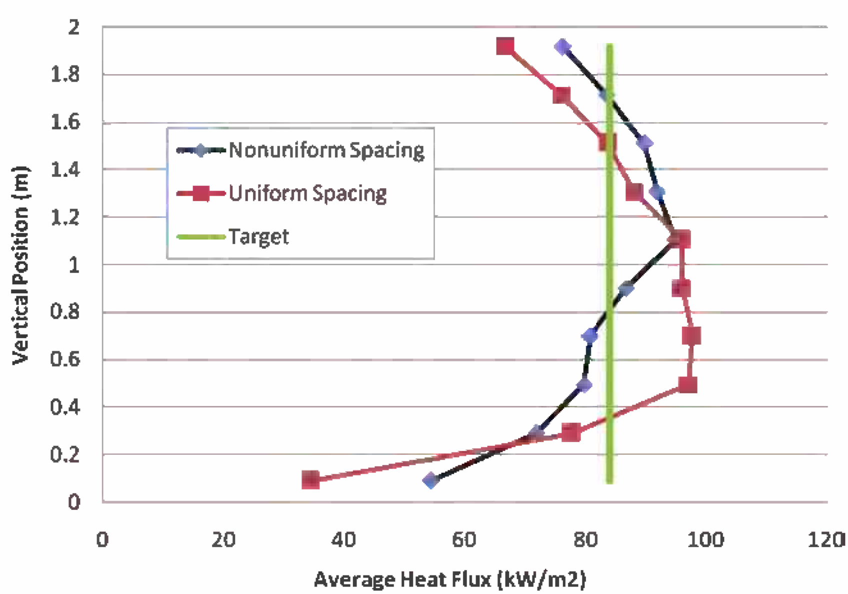

FIG. 5—*Vertical variation in heat flux on a 300 mm diameter, 2000 mm tall cylinder; exposure averaged 0.7 to 4 s.*

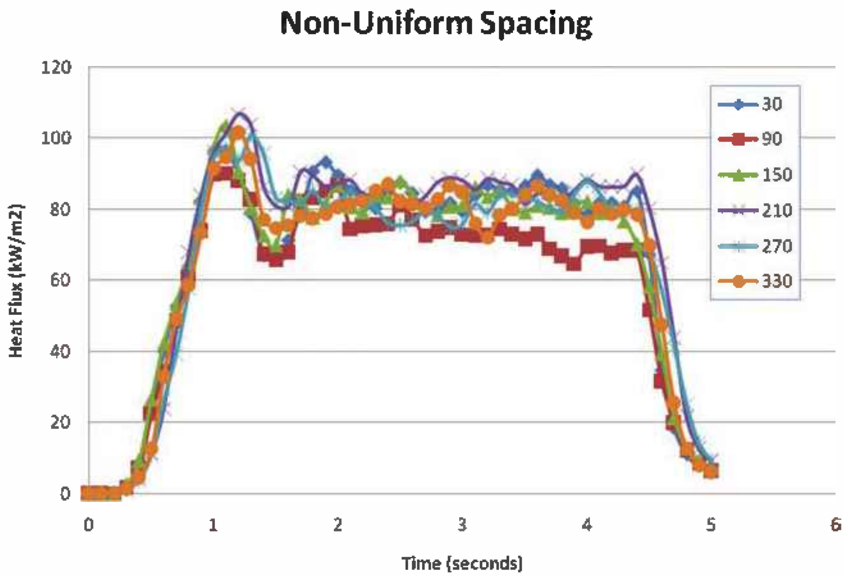

FIG. 6—*Radial distribution of heat flux on cylinder; burners placed so as to meet the requirements of ASTM F1930, Test 2557.*

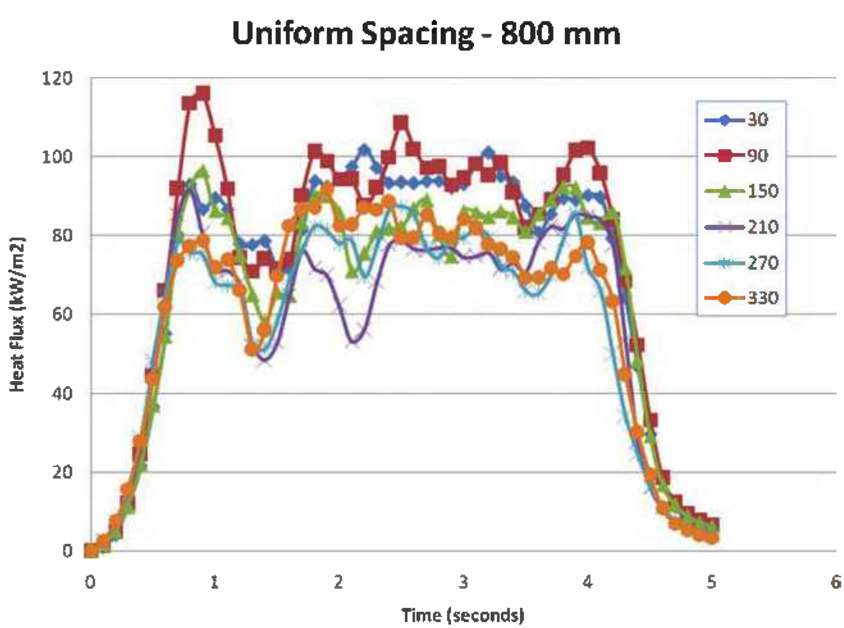

FIG. 7—*Radial distribution of heat flux on cylinder; burners positioned equidistant from cylinder, Test 2563.*

as to give a uniform flux on the mannequin form. Figures 6 and 7 show the experimental results for each case.

What is quite interesting in these results is that the uniform positioning of burners relative to the cylinder does not produce more uniform heat flux on the cylindrical form azimuthally. Part of this apparent contradiction comes from the interaction of the hot gas "plumes" that evolve from each burner. The torches in the burn chamber are not perfectly aligned, as they have been positioned by trial and error to result in a uniform heat flux distribution on a mannequin form that is obviously not a cylinder. As a result, even though the burner heads were all positioned equidistant from the cylinder, there are small alignment variations, and not all burner axes coincide with the center line of the cylinder. Small changes in burner position can have unexpected effects on the overall mannequin heat flux as the buoyant combustion gases from one burner interact strongly with those from the surrounding burners. Other factors that can affect these results are the dynamics of the fuel control valves and the gas flow. Ideally, the flow through each burner will be identical, as will the timing of the start-stop cycle. This has not been investigated in this study.

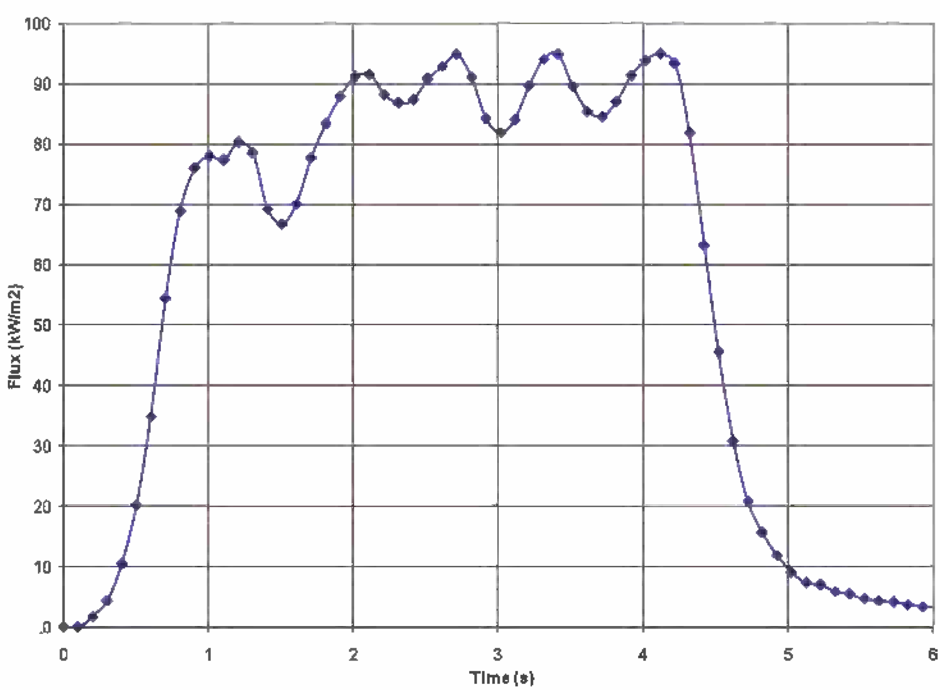

FIG. 8—*Average heat flux on mannequin form with burners positioned for uniform spacing on cylinder form.*

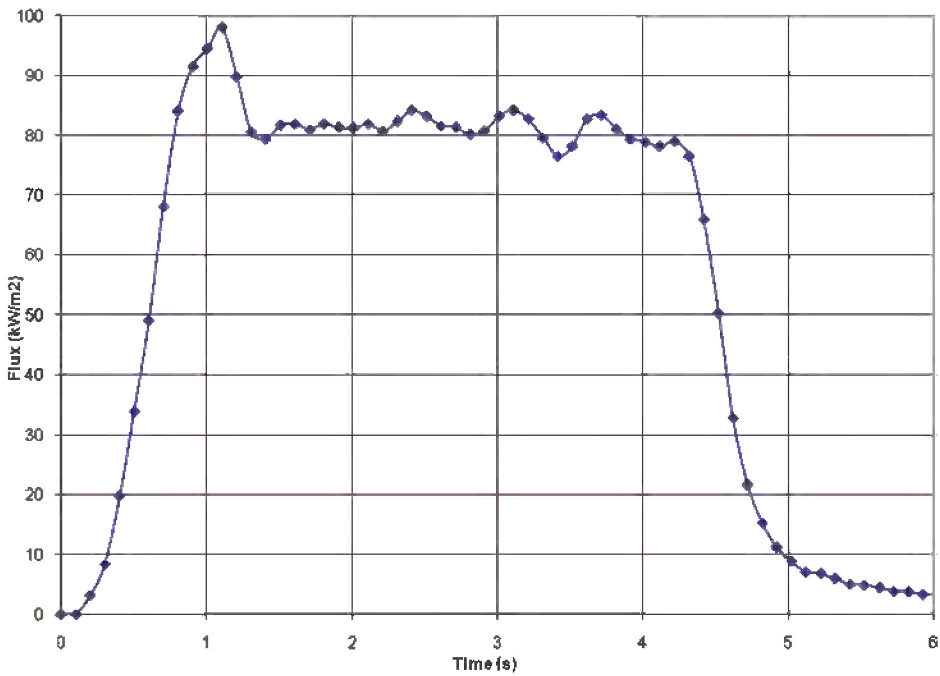

FIG. 9—*Average heat flux on mannequin form with burner positions set so as to produce uniform flux on mannequin form.*

Heat Flux on Mannequin Form

Two sets of tests were carried out using the mannequin form in order to examine the variations in heat flux that would occur with changes in burner position. In the first case, the burners were positioned equidistant from the cylinder (not equidistant from the mannequin form), and in the second they were positioned using successive tests on a nude mannequin so as to produce a flux that would meet the requirements of ASTM F1930. Four-second exposures were run for both configurations as indicated in Figs. 8 and 9. Sensor readings were grouped and area weighted (not all sensors are associated with an equal surface area on

TABLE 2—*Vertical distribution of heat flux on an instrumented cylinder.*

Configuration	Sensors Averaged	Average Heat Flux, kW/m^2 (cal/cm^2 s)	Standard Deviation, kW/m^2 (cal/cm^2 s)
Uniform burner placement	Rows 1–10	81.0 (1.93)	11.8 (0.28)
Non-uniform burner placement	Rows 1–10	81.3 (1.94)	19.6 (0.46)
Uniform burner placement	Rows 1–9	83.9 (2.0)	7.6 (0.18)
Non-uniform burner placement	Rows 1–9	86.6 (2.06)	11.2 (0.27)

TABLE 3—*Average heat flux on cylinder: Variation with radial position.*

	Angular Position					
Test 2563: Uniform Spacing	30°	90°	150°	210°	270°	330°
Average 1 to 4 s, kW/m^2	89.5	92.0	81.3	71.0	73.8	77.3
Standard deviation, kW/m^2	7.98	10.2	8.7	9.7	9.2	9.1
	Angular Position					
Test 2557: Non-Uniform Spacing	30°	90°	150°	210°	270°	330°
Average 1 to 4 s, kW/m^2	83.8	75.8	82.8	87.8	83.5	82.5
Standard deviation, kW/m^2	7.1	7.2	6.2	6.3	6.6	6.3

the mannequin) so as to produce an average flux for representative areas of the body. These results are presented in Tables 4 and 5. Note that the equidistant positioning of the burners (relative to where the cylinder would be positioned) resulted in an average heat flux and standard deviation that would meet the requirements of ASTM F1930, Section 10.1.3, but which would not meet the requirements of Section 10.1.4. That section states, "Distribution—The burners shall be positioned so that the average heat flux measured for the trunk, arms, thighs and shanks (lower legs) is each within ±15 % of the average heat flux required in 4.1." As indicated in Table 4, the back of the mannequin would be underexposed and the right leg would be overexposed. Repositioning the burners relative to the mannequin results in the distribution shown in Table 5, in which all segments of the mannequin meet the requirements.

As was seen with the cylinder tests, deliberate uniform spacing *does not* produce the best result on the mannequin in terms of uniform exposure heat flux due to the interaction of hot gas plumes from each burner. Positioning

TABLE 4—*Heat flux by mannequin area: Burner positions uniform for cylinder.*

	Flux Breakdown, kW/m^2	
1.2 to 4.0 s	Mean	Standard Deviation
Chest and abdomen	91.2	20.3
Back	71.3	11.6
Left arm	75.7	17.5
Right arm	83.3	18.5
Left leg (upper)	81.7	19.3
Left leg (lower)	90.0	14.7
Right leg (upper)	95.6	8.2
Right leg (lower)	106.2	11.1
Head	86.8	18.8
Overall average	85.9	19.5

TABLE 5—*Heat flux by mannequin area: Burner positions for uniform flux on mannequin form.*

	Flux Breakdown, kW/m^2	
1.2 to 4.0 s	Mean	Standard Deviation
Chest and abdomen	86.6	13.2
Back	79.7	9.8
Left arm	84.2	19.7
Right arm	83.0	17.7
Left leg (upper)	76.0	13.0
Left leg (lower)	74.2	6.8
Right leg (upper)	77.0	7.6
Right leg (lower)	76.8	5.2
Head	92.0	13.0
Overall	81.5	14.3

of the burner heads then becomes a trial and error process with the aim of producing an average heat flux over the entire surface of ~84 kW/m^2 (2 cal/cm^2 s) and at the same time minimizing the variations via minimization of the standard deviation of the heat flux measurements. Some of this is quite arbitrary (such as the start time and end time for determining the average heat flux). ASTM F1930 gives some guidance on this in Section 6.5.3, in which it states, "The average heat flux value reported is the average of the averages for each of the sensors for the steady region of the exposure duration." This statement is interpreted with the help of Fig. 2 in the standard, reproduced below as Fig. 10.

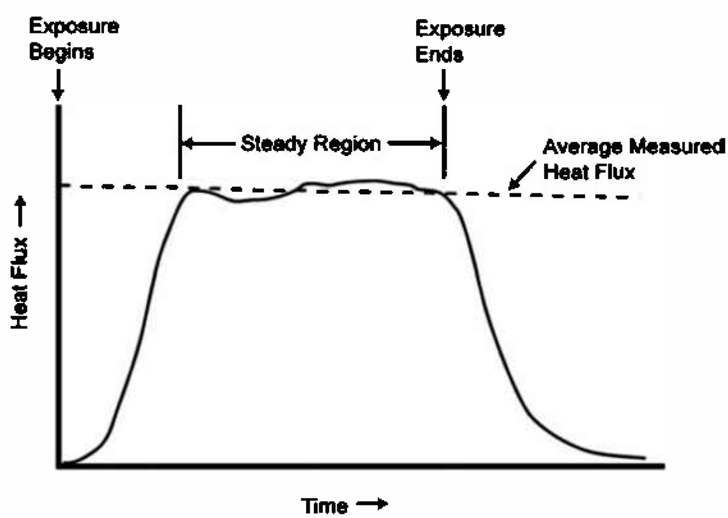

FIG. 10—*Determination of average heat flux from mannequin sensor readings (source: ASTM F1930, Fig. 2).*

Conclusions

Only the ISO 13506 test method recommends that an instrumented cylinder or multi-sided box be used to aid in the initial setup of a mannequin burner system in order to achieve the desired test conditions of heat flux and its distribution over the mannequin surface. The results from this investigation would suggest that the historical method of working only with the mannequin and using a trial and error process for setting the burner positions can just as easily meet both test method requirements for the average heat flux, its distribution on the mannequin, and its standard deviation as the use of an instrumented cylinder or multi-sided calibration box. The results also suggest that for a given burner configuration, some differences will be apparent, in both the average heat flux and the uniformity of exposure, between the cylinder and the mannequin form.

References

[1] ASTM F1930, 2012 "Standard Test Method for Evaluation of Flame Resistant Clothing for Protection against Flash Fire Simulations Using an Instrumented Manikin," *Annual Book of ASTM Standards*, Vol. 11.03, ASTM International, West Conshohocken, PA.

[2] ISO 13506, 2008, "Protective Clothing against Heat and Flame—Test Method for Complete Garments—Prediction of Burn Injury Using an Instrumented Manikin," International Organization for Standardization, Geneva, Switzerland.

Performance of Protective Clothing and Equipment: Emerging Issues and Technologies
STP 1544, 2012
Available online at www.astm.org
DOI:10.1520/STP104510

Kevin Ross,[1] *Roger Barker,*[2] *and A. Shawn Deaton*[3]

Translation between Heat Loss Measured Using Guarded Sweating Hot Plate, Sweating Manikin, and Physiologically Assessed Heat Stress of Firefighter Turnout Ensembles

REFERENCE: Ross, Kevin, Barker, Roger, and Shawn Deaton, A., "Translation between Heat Loss Measured Using Guarded Sweating Hot Plate, Sweating Manikin, and Physiologically Assessed Heat Stress of Firefighter Turnout Ensembles," *Performance of Protective Clothing and Equipment: Emerging Issues and Technologies* on April 16, 2011 in Anaheim, CA; STP 1544, Angie M. Shepherd, Editor, pp. 27–47, doi:10.1520/STP104510, ASTM International, West Conshohocken, PA 2012.

ABSTRACT: Sweating skin models and instrumented thermal manikins are commonly used to assess the heat stress potential of materials used in protective clothing. This research describes the relationship observed between heat loss through firefighter turnout ensembles measured using a sweating thermal manikin and that measured with a guarded sweating hot plate. Materials and garment level instrument measures are compared on the basis of their ability to predict human physiological responses related to heat stress in firefighter turnout systems. Sweating hot plate and manikin test results for selected firefighter turnout ensembles are compared to human wear studies in which firefighter turnout ensembles were worn in different environmental conditions. Sweating manikin tests are used to explain differences in the human physiological response and how these measures are related to turnout heat transfer properties measured using a sweating hot plate. This study confirms the utility of sweating manikins in characterizing the effects of clothing design, fit, and layers on heat and moisture transfer. Thermal manikins

Manuscript received November 1, 2011; accepted for publication March 16, 2012; published online September 2012.

[1]Research Associate, Center for Research on Textile Protection and Comfort, College of Textiles, North Carolina State Univ., Raleigh, NC 27695-8301.

[2]Professor, Dept. of Textiles Engineering, Chemistry and Science, North Carolina State Univ., Raleigh, NC 27695-8301.

[3]Special Projects Director, Center for Research on Textile Protection and Comfort, College of Textiles, North Carolina State Univ., Raleigh, NC 27695-8301.

are shown to be valuable tools for evaluating the distribution of heat loss through different areas of protective gear.

KEYWORDS: sweating manikin, heat stress, sweating hot plate, thermal manikin, total heat loss, thermal resistance, evaporative resistance, THL, physiological response

Introduction

Stress and overexertion are responsible for nearly half of all on-duty firefighter fatalities [1]. The sweating hot plate, the fabric level test for total heat loss (THL) required by NFPA 1971 [2], aims to combat this problem by limiting the thermal burden imposed by the materials used in the construction of turnout clothing. Studies have investigated how instrument level measures of heat stress relate to human physiological responses [3–8]. There is a continuing need, however, for a better understanding of the assessment potential of sweating manikins that provide instrumented heat loss measurements at the garment level. The research described here employed a sweating manikin as a heat loss evaluation means intermediate between a sweating hot plate and human subject physiological evaluations of heat stress. It used fabric- and systems-level test methods to characterize a selected group of structural firefighter turnout suits having known differences in the breathability of the moisture barrier component of the turnout composite system.

Methods and Materials

This research evaluated the heat loss and associated heat stress of a selected group of firefighter turnout systems measured on a flat sweating plate, a full-form sweating manikin, and humans.

Test Materials

Six firefighter turnout systems consisting of an outer shell fabric layered with an inner moisture barrier and thermal liner components were studied (Table 1). The layered fabric systems were deliberately assembled so as to achieve a range of THL values. This was accomplished by combining the same heat resistant outer shell fabric with different moisture barrier and thermal liner components.

Three different moisture barriers and three different thermal liners were layered so as to produce THL values ranging from 97 W/m^2 to 247 W/m^2. Moisture barriers A and B represent "breathable" moisture barrier technologies, and moisture barrier C represents a "non-breathable" moisture barrier system. The moisture vapor permeability of the moisture barriers was ranked as follows: $A > B > C$. The thermal liners varied in thermal resistance such that their thermal insulation values compared as $A \sim C < B$ [6].

TABLE 1—*Firefighter turnout ensembles.*

Garment ID	Outer Shell	Moisture Barrier	Thermal Liner	Composite Weight, oz/yd^2 [3]	Composite Thickness, mm [3]	Composite R_{cf},[a] °C · m^2/W	Composite AR_{ef},[a] kPa · m^2/W	Composite THL,[a] W/m^2
1	A	A	A	19.95	4.98	0.119	0.016	250
2	A	A	B	19.59	5.28	0.153	0.017	222
3	A	B	B	19.82	5.08	0.161	0.034	146
4	A	C	B	27.25	4.17	0.134	0.087	97
5	A	A	C	19.51	4.90	0.115	0.016	247
6	A	B	A	20.19	4.88	0.118	0.034	158

[a]Measured on the sweating guarded hot plate [3].

Total Heat Loss Test Method

The THL method provides a fabric-level measurement of the predicted heat burden imposed by clothing materials. The THL test method was first added as an appendix to NFPA 1971 in its 1991 revision. This addition came about as a result of recommendations of the NFPA Technical Committee on Protective Clothing and Equipment after a series of meetings regarding the issue of heat stress [9]. The THL method utilized existing hot plate methodology but was in large part a new method developed specifically for this application [9]. ASTM F1868, originally adopted in 1998, describes the THL test method (Part C) that is currently required by NFPA 1971 [2,10].

Prior to the addition of the guarded sweating hot plate THL method, there were no requirements in NFPA 1971 specifically aimed at dealing with the issue of heat stress in firefighting. Amid debate regarding the practicality of the test and its meaningfulness, it did not become a part of the standard until roughly a decade after its initial inclusion in the appendix. After much debate, the THL was added to the standard [5,9]. The 2000 edition of NFPA 1971 was the first edition to include the THL test method as part of the standard, with a performance requirement set at 130 W/m^2 [11]. In the 2007 edition, this requirement was raised to 205 W/m^2 [2]. The foundations for setting the original THL requirement and subsequent justifications for raising THL values were laid in two foundational physiological wear trials of structural firefighter turnout ensembles [12,13]. In one study, the measured THL values of the turnout composite materials were shown to correlate with physiological temperature responses, whereas in the other significant differences could be established only between breathable and non-breathable systems [3,4,7]. The turnout garments tested for the research discussed in this paper are the same garments that were used in the human subject wear trials previously reported based on protocols conducted at North Carolina State University [3,4]. The results of these foundational studies are further examined here in light of manikin test results and testing conditions.

Sweating Manikin Test Method

The sweating manikin was one of the National Fire Protection Agency's (NFPA) original considerations for evaluating heat stress but was rejected based on limited availability and cost [9]. Today, over 20 years later, the availability and cost are much less prohibitive. The sweating manikin measures thermal resistance, evaporative resistance, and heat loss using primarily the same principles and techniques as the sweating hot plate. The most prominent difference between the hot plate and the manikin is the human form of the manikin. The manikin's form allows garments to be dressed on the manikin to fit as they would on a human. This allows air layers to develop within fabric layers and between fabric layers and the body. It also allows assessments of fit, additional options and gear, garment construction, and overall design features.

Physiological Evaluations

Systematically designed human subject wear trials have been performed in order to evaluate the heat stress and comfort of the same firefighter turnout systems tested on the sweating manikin [3,4]. This study (the International Firefighter Protective Clothing Breathability Research Project), conducted in 1998 at North Carolina State University, consisted of two parts: a Mild Environment Protocol and a Warm Environment Protocol. For both protocols, the same six turnout ensembles were evaluated with a range of THL values from 97 to 251 W/m^2 [3,4]. The details of the ensemble materials can be found in Table 1. It is this set of turnout ensembles that was evaluated with the sweating manikin system.

The Mild Environment Protocol featured "light to moderate" work in mild climatic conditions (21°C, 65 % relative humidity [RH]) [3]. For this protocol, seven professional firefighters wore turnout test clothing over a station uniform and underwear. The firefighters did not wear gloves, hood, or helmet or don a self-contained breathing apparatus (SCBA) [3]. Table 2 describes the Mild Environment Protocol.

The Warm Environment Protocol determined the heat stress experienced by the same group of professional firefighters when performing "moderate work" activities in a warm environment (39°C, 35 % RH) [4]. For this warm environment study, test participants wore the complete firefighter protective ensemble: turnout suits equipped with accessories including a two-ply balaclava hood, gloves, sneaker-type jogging shoes (in lieu of firefighter boots), a mask, and a helmet. In both studies, trouser cuffs were sealed at shoe level with tape [4]. Table 3 describes the Warm Environment Protocol.

Table 4 compares the conditions of the two wear trial protocols (mild and warm climate), as well as the environmental conditions called for by the standard sweating hot plate test method used to determine the THL of turnout composite materials.

The findings of the firefighter wear studies, as documented in Refs 3 and 4, can be summarized as follows.

For low work loads, in a mild environment, physiological heat stress limits are not approached, regardless of the "breathability" of the turnout composite. No significant differences are seen in measured core temperature or heart rates that can be correlated with differences in turnout breathability.

For mild wear conditions, differences in turnout breathability are apparent at the comfort level: sweating plate heat loss values correlate with measured indexes that are associated with turnout comfort performance (higher sweating plate THL values correlate with lower skin temperatures and less indicated buildup of moisture vapor in the turnout microclimate). However, firefighters

TABLE 2—*Mild climate protocol (21°C, 65% RH) [3].*

Test Period	Time, min	Cumulative Time, min	Activity	Physiological Measurements[a]	Subjective Ratings
Pretest Baseline			Prior to donning turnout	Initial T_s, T_{re}, HR	
1	15	1–15	Rest	T_s, T_{re}, % RH, HR at 5 and 15 min	End of period
2	20	15–35	Walk 2 % grade treadmill at 2.5 mph	T_s, T_{re}, % RH, HR at 5 min intervals	End of period
3	30	35–65	Rest	T_s, T_{re}, % RH, HR at 5 and 25 min	End of period
4	20	65–85	Walk 2 % grade treadmill at 2.5 mph	T_s, T_{re}, % RH, HR at 5 min intervals	End of period
5	30	85–115	Rest and cool down	T_s, T_{re}, % RH, HR at 5 min intervals	End of period

[a]T_s = skin temperature of chest, back, arm, and thigh; T_{re} = rectal temperature; % RH = percent relative humidity in the clothing microclimate; HR = heart rate.

can decisively perceive and differentiate among composites on the basis of comfort sensations only in the case of the composite having the lowest THL ($Q_t = 97$ watts/m^2). Statistically significant differences in comfort performance can be related to feelings of warmth and skin wetness that occur in the non-breathable garment (#4) [3].

The Warm Environment Protocol similarly showed that sweating plate test scores differentiate at the lowest level of heat loss measured among turnout systems (97 W/m^2). Therefore, differences in the physiological heat stress performance of the 97 W/m^2 system are not indicated by core temperature, but they are indicated by higher skin temperatures and reduced tolerance time when working in heat. Subjective ratings show that the 97 W/m^2 system (garment #4) is perceived to be hotter, with greater sensations of skin wetness than experienced with the other test turnouts.

All of the "warm" experiments, regardless of the garment worn, proceeded to a point at which every firefighter complained that he could go no further.

No decisively significant differences in physiological heat stress response can be found in systems having total sweating hot plate heat loss values within the range of 146 to 251 W/m^2 [4].

Test conditions for the Warm Environment Protocol were hot (39°C) and dry (35 % RH). In these conditions, the ambient environment was slightly hotter than skin temperatures at the beginning of each session, with final skin temperatures within 0.3°C to 1.3°C of the ambient environment. In these conditions, the body cannot lose heat to the environment through conduction, convection, or radiation. Instead, the body gains heat from the environment.

TABLE 3—*Warm climate protocol (39°C, 35 % RH) [6].*

Test Period	Time, min	Cumulative Time, min	Activity	Physiological Measurements[a]	Subjective Ratings
Pretest Baseline 1			Prior to donning turnout	Initial T_s, T_{re}, HR	
Pretest Baseline 2			Prior to donning SCBA	T_s, T_{re}, HR	
1	15	1–15	Walk 2 % grade treadmill at 2.5 mph	T_s, T_{re}, HR at 5 min intervals, % RH every minute	
2	2	15–17	Rest	T_s, T_{re}, HR at end of period, % RH every minute	While resting
3	15	17–32	Walk 2 % grade treadmill at 2.5 mph	T_s, T_{re}, HR at 5 min intervals, % RH every minute	
4	2	32–34	Rest	T_s, T_{re}, HR at end of period, % RH every minute	While resting
$4+n$[b]	15	$17+17^*n$ to $19+17^*n$	Walk 2 % grade treadmill at 2.5 mph	T_s, T_{re}, HR at 5 min intervals, % RH every minute	At end of final work cycle
$5+n$	2	$19+17^*n$ to $21+17^*n$	Rest	T_s, T_{re}, HR at end of period, % RH every minute	While resting

[a]T_s = skin temperature of chest, back, arm, and thigh; T_{re} = rectal temperature; % RH = percent relative humidity in the clothing microclimate; HR = heart rate.

[b]Work/rest cycles continued until either subject's T_{re} reached 39°C or he was unwilling or unable to continue for any reason.

Therefore, in principle, the more thermally insulating the turnout ensemble, the more the body is shielded from the hot environment, provided only dry heat transfer is considered. Consequently, because of the small differences between skin and ambient temperatures, the majority of the heat must be transferred via sweat evaporation. Although the RH was very low in the Warm Environment Protocol, the approximate vapor pressure differential was slightly less than in the Mild Environment Protocol because of the higher temperature (and thus higher saturation vapor pressure), as shown in Table 2. Nevertheless, evaporative cooling played a much greater role in total heat transfer than the combined effects of conduction, convection, and radiation in the warm protocol conditions.

Sweating Manikin Evaluation

The six fabric ensembles identified in Table 1 were made into firefighter turnout suits of identical design and sized to fit the instrumented manikin. The

TABLE 4—*Physiological wear trials and standard sweating hot plate conditions [3,4,6,10].*

	Temperature, °C	Humidity, %	Skin Temperature Differential, °C, Instruments[a]	Vapor Pressure Differential, kPa, Instruments[b]	Skin Temperature Differential, °C, Humans[c]	Vapor Pressure Differential, kPa, Humans[d]	Activity Level[e]	Dress
Mild	21	65	14	4.01	11.7 to 14.8	3.32 to 4.27	Light to moderate (~238 W/m^2)	No SCBA, gloves, or head gear; sneakers instead of boots
Warm	39	35	−4	3.18	−3.78 to − 1.02	3.25 to 4.17	Moderate (~225 W/m^2)	Fully dressed, breathing ambient air; sneakers instead of boots
Standard THL Conditions	25	65	10	3.57	N/A	N/A	N/A	N/A

[a]Based on instrument skin temperature of 35°C ($T_{sk} - T_a$).

[b]Based on fully sweating skin at 35°C.

[c]Based on overall average initial and maximum skin temperatures for all test subjects and all garments ($T_{sk} - T_a$).

[d]Based on fully sweating skin and overall average initial and maximum skin temperatures for all test subjects and all garments.

[e]Activity levels as described by reference studies; 238 W/m^2 is converted from a reported 450 kal/h work rate and average surface area of 2.19 m^2.

a) b)

FIG 1—*Sweating manikin dressed in firefighter ensemble: (a) front view; (b) side view.*

turnout ensembles used were the same ones that had been used in the physiological assessments previously conducted at North Carolina State University [3,4]. The gear tested on the sweating manikin was selected to match gear used in the International Firefighter Protective Clothing Breathability Research Project Warm Environment Protocol [4]. This approach was employed because the garments and all raw data were readily available for testing and for examination. The manikin was dressed the same as the human subjects were in the Warm Environment Protocol of this study. Figure 1 shows the sweating manikin dressed in a firefighter test ensemble.

The sweating manikin was dressed as follows: a station uniform was worn consisting of a button-up woven short-sleeve station shirt and zipper-fly woven station pants, both constructed of 55 % fibrous flame retardant fiber and 45 % cotton. A fiberglass-reinforced Kevlar helmet was worn over a two-ply balaclava hood. Cotton briefs and crew-style socks were worn. Leather firefighting gloves were carefully deconstructed, and the outer shell was reconstructed in a mitt pattern so that it would fit onto the manikin (the inner components of the glove were not altered). The manikin was dressed in sneakers rather than boots, with the trouser legs taped at the ankle. The manikin wore the full facepiece assembly and harness components of an SCBA. The SCBA cylinder was removed for testing. As in the physiological trial, the SCBA regulator was not attached to the respirator face piece.

Sweating Manikin Heat Transfer Calculations

This research used a Coppelius-type sweating thermal manikin [14]. The Coppelius manikin has 18 individually controlled body zones, each capable of measuring thermal resistance, evaporative resistance, and heat loss. Sweat control is achieved by use of a pump that delivers water to 187 individual "sweat glands" located throughout the manikin body. The continuous supply of water kept the manikin "skin" saturated throughout testing. Calculations of thermal resistance, evaporative resistance, and heat loss were made using measurements of skin temperature, power consumption, ambient temperature, and ambient RH, assuming a 100 % wetted skin condition during the sweating portion of the test.

Thermal resistance was measured following procedures described in ASTM F1291 [15]. Evaporative resistance was measured according to procedures in ASTM F2370 [16]. If thermal and evaporative resistance are measured in identical, non-isothermal conditions, the measurements of total thermal and evaporative resistance with boundary air layers included can be used to calculate the heat loss for the manikin (similar to the THL measurement on the hot plate) according to Eq 1

$$Q_t = (T_s - T_a)/R_t + (P_s - P_a)/AR_{et} \tag{1}$$

where:

Q_t = THL from dry and evaporative components, W/m^2,
T_s = temperature at the manikin surface, °C,
T_a = temperature in the air surrounding the manikin, °C,
R_t = total thermal resistance of the test ensemble and surface air layer, $°C \cdot m^2/W$,
P_s = water vapor pressure at the manikin surface, kPa,
P_a = water vapor pressure in the air surrounding the manikin, kPa, and
AR_{et} = total evaporative resistance of the test ensemble and surface air layer, $kPa \cdot m^2/W$ [10].

This equation can be written as

$$Q_t = (T_s - T_a)/R_t + (P_s - P_a)/AR_{et} = C + E \tag{2}$$

where:

$C = (T_s - T_a)/R_t$ = dry component of heat loss, W/m^2, and
$E = (P_s - P_a)/AR_{et}$ = evaporative component of heat loss, W/m^2.

However, manikin testing per ASTM F1291 and ASTM F2370 requires testing in dissimilar environments. Manikin measurements of thermal and evaporative resistance were calculated in a 23°C environment for thermal resistance and at 35°C for evaporative resistance, consistent with the specifications of ASTM F1291 and ASTM F2370. It is important to point out that because the manikin THL is calculated based on measurements made in two different environments, these heat loss estimates are predictive calculations rather than actual measurements. They assume that condensation and absorption have a negligible effect on heat transfer through the test fabric system. They further assume that the thermal and evaporative resistance of the tested fabric is independent of the ambient temperature and humidity. With these assumptions, the manikin heat loss for different environmental temperatures and humidities can be estimated from the thermal and evaporative resistance properties (R_t and R_{et}) of the test ensemble measured in standard environmental conditions using Eq 3

$$Q_{t(\text{predicted},T,RH)} = (T_s - T_a)/R_t + (P_s - P_a)/R_{et} \tag{3}$$

where:

$Q_{t(\text{predicted},T,RH)}$ = predicted manikin THL for specified environmental conditions, W/m^2,

T = specified temperature condition, °C,

RH = specified relative humidity, %,

T_s = specified temperature at the manikin surface, °C,

T_a = specified temperature of the local environment, °C,

P_s = calculated water vapor pressure at the surface of the manikin, kPa,

P_a = calculated water vapor pressure in the specified local environment, kPa, and

R_{et} = total evaporative resistance of the test ensemble and surface air layer, kPa · m^2/W.

Vapor pressures were calculated from temperature and RH specifications based on Wexler's formulation according to Eq 4

$$\begin{aligned} e_s = a_1 + a_2(T - T_0) + a_3(T - T_0)^2 + a_4(T - T_0)^3 + a_5(T - T_0)^4 \\ + a_6(T - T_0)^5 + a_7(T - T_0)^6 \end{aligned} \tag{4}$$

where:

e_s = saturation vapor pressure, mb,

a_1–a_7 = coefficients of the sixth order polynomial fits to saturation vapor pressure (see Ref 17),

T = temperature, K, and

T_0 = 273.15 [17].

The ambient vapor pressure was calculated from the saturation vapor pressure as

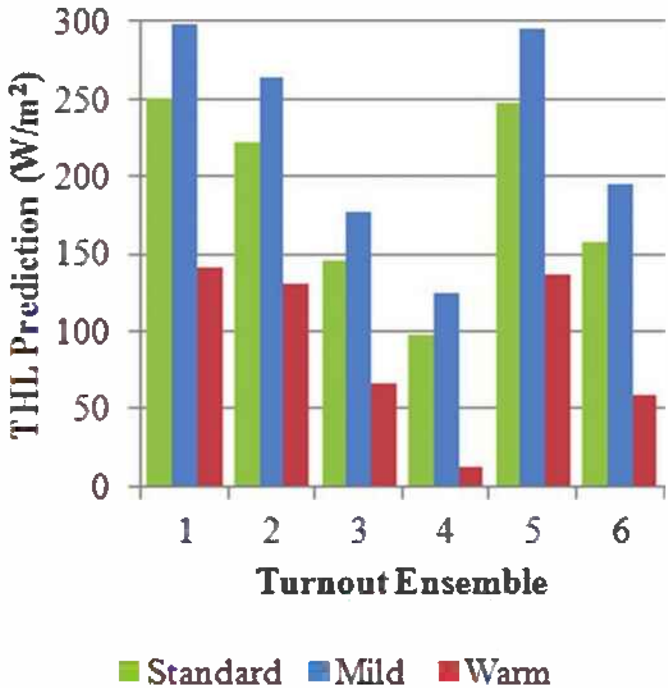

FIG. 2—*Hot plate THL predictions for test environments.*

$$P = [(\mathrm{RH} * e_s)/100]/10 \tag{5}$$

where:

P = water vapor pressure, kPa, and

RH = relative humidity, %.

A moisture vapor saturated, or 100 % humidity, condition is assumed to exist at the surface of the manikin skin.

Sweating Hot Plate Heat Transfer Predictions

Using the same assumptions and vapor pressure calculations given for the manikin heat loss predictions, the sweating hot plate THL was predicted for environmental conditions other than the standard condition (25°C, 65 % RH) of the test environment as

$$Q_{t(\text{predicted,T,RH})} = [(T_s - T_a)/(R_{cf} + C_1)] + [(P_s - P_a)/(AR_{ef} + C_2)] \tag{6}$$

where:

$Q_{t(\text{predicted,T,RH})}$ = predicted hot plate THL for specified environmental conditions, W/m^2,

R_{cf} = intrinsic thermal resistance of the fabric specimen, $°C \cdot m^2/W$,

TABLE 5—*Firefighter turnout ensemble heat loss predictions using sweating hot plate and sweating manikin instruments.*

		Sweating Hot Plate			Sweating Manikin		
Condition	Garment ID	C, W/m^2	E, W/m^2	THL, W/m^2	C, W/m^2	E, W/m^2	THL, W/m^2
ASTM F1868 standard THL conditions (25°C, 65 % RH)	1	64	187	250	30	38	67
	2	52	170	222	30	38	68
	3	50	96	146	31	34	65
	4	58	40	97	29	9	37
	5	65	182	247	30	39	69
	6	63	95	158	28	36	64
Mild Environment Protocol conditions (21°C, 65 % RH)	1	89	210	299	42	42	84
	2	73	191	264	42	43	85
	3	70	108	178	44	38	82
	4	81	45	125	40	10	50
	5	90	205	295	42	44	86
	6	89	107	195	39	40	80
Warm Environment Protocol conditions (39°C, 35 % RH)	1	−25	166	141	−12	33	22
	2	−21	152	131	−12	34	22
	3	−20	86	66	−12	30	18
	4	−23	35	12	−11	8	−4
	5	−26	162	137	−12	35	23
	6	−25	84	59	−11	32	21

C_1 = plate constant for standard air layer thermal resistance = 0.04,
AR_{ef} = intrinsic evaporative resistance of the fabric specimen, kPa · m^2/W, and
C_2 = plate constant for standard air layer evaporative resistance = 0.0035.

Results and Discussion

Sweating Hot Plate Predictions

Figure 2 compares the THL values measured for standard environmental conditions (25°C, 65 % RH) with predicted THL values for the Mild (21°C, 65 % RH) and Warm (39°C, 35 % RH) Environment Protocol conditions estimated using the heat transfer model described in Eq 6. Values are also provided in Table 5.

These measured and extrapolated THL estimates indicate similar levels of heat loss for each turnout composite in either standard hot plate or mild environment conditions. This result is not surprising because the environmental temperature and RH at which the Mild Environment Protocol was conducted

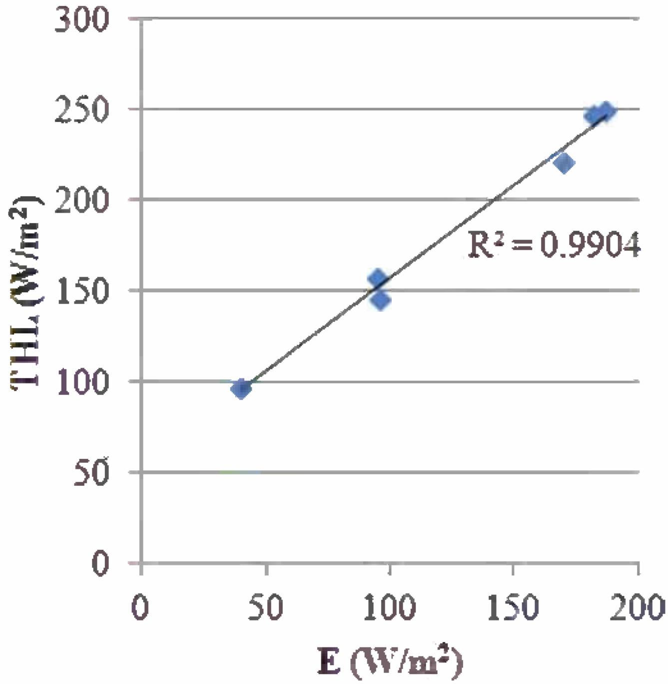

FIG. 3—*Relationship between THL and evaporative cooling (E) at 25°C and 65 % RH.*

did not substantially differ from standard sweating hot plate testing conditions. Figure 2 also predicts the dramatic effect that environmental conditions have on minimizing the opportunity for heat loss through turnout systems. For the warm protocol conditions (39°C, 35 % RH), THL values fall within the range of 59 to 141 W/m^2 for composites that use a breathable moisture barrier. It drops to a nearly negligible level for the non-breathable composite (system 4). These model predictions of THL clearly explain the results of the Warm Environment Wear Trial Protocol, which show the overwhelming effect of environmental factors on the heat stress relief that can be expected based on THL.

The model-calculated THL values, shown in Fig. 2, demonstrate that the comparative differences among tested turnout systems are similar, at or around the 130–170 W/m^2 level, regardless of the assumed environmental conditions. They also show that some level of heat loss can be expected through all the composites, even when the ambient temperature exceeds sweating plate, or nominal skin, temperature, as is the case for the warm protocol conditions (39°C, 35 % RH). This finding demonstrates the important role played by the evaporative component of THL and the obvious influence of the moisture vapor permeability, or breathability,

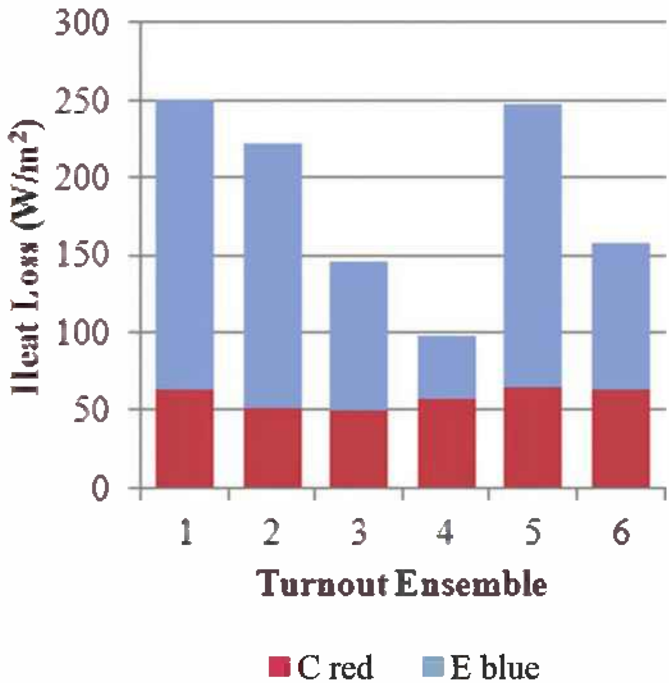

FIG. 4—*Contribution of dry (C) and evaporative (E) heat transfer to hot plate-measured THL (25°C, 65 % RH).*

of the moisture barrier composite layer. The influence of the breathability of the moisture barrier component on the THL is apparent and recognizable as three distinct levels of heat loss associated with the three different moisture barriers incorporated into the test composites. We can observe these three levels of THL in Fig. 2: the highest level is associated with turnout systems 1, 2, and 5, which incorporated moisture barrier component A. Systems 2 and 6, which use moisture barrier component B, show THL values intermediate between those of these systems and the results from system 4, which incorporates a moisture vapor impermeable barrier material (C).

Figures 3 and 4 show the dependence of the THL on the evaporative component of the heat loss (*E*) for standard hot plate test conditions.

Figure 3 demonstrates that even at standard hot plate conditions, the THL differences of the tested turnout composite are highly dependent on the level of evaporative cooling possible. Figure 4 provides a breakdown of the lump dry and evaporative heat loss components of THL for the six turnout composites studied.

These calculations show that evaporative heat transfer is the primary heat loss mechanism with breathable turnout composites (systems 1–3, 5, and 6).

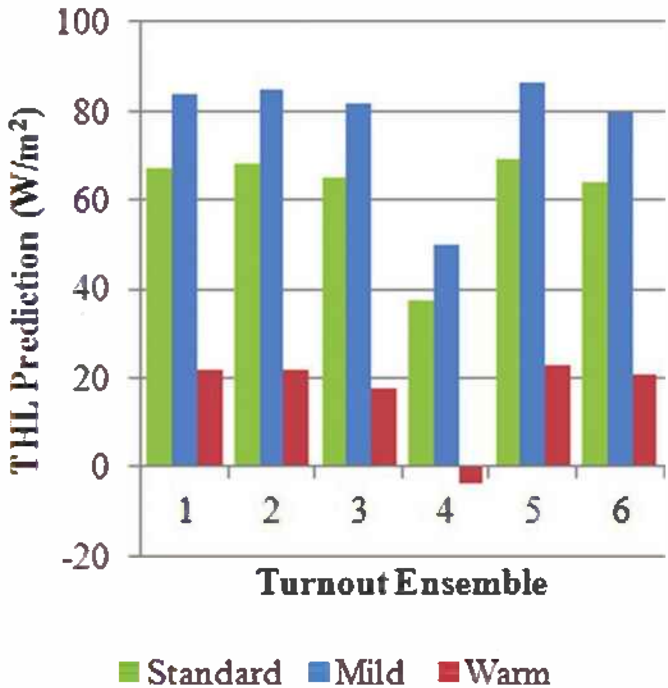

FIG. 5—*Manikin THL predictions for test environments.*

Dry heat transfer (conduction, convection, and heat radiation) dominates only in the moisture-vapor-impermeable composite (system 4). The fraction of evaporative heat transfer observed in the moisture-vapor-impermeable system can be attributed to thermal energy absorbed through the moisture condensation in the turnout composite.

Sweating Manikin Predictions

Differences in THL based on sweating plate estimates provide the basis for an expectation of three levels of differentiated heat stress performance in turnouts made of the tested composites. However, these distinct performance levels were not observed in the controlled physiologically based wear studies. In the wear tests, only the non-breathable turnout suit (system 4) showed a disadvantage based on human subject assessments of heat stress reduction and thermal comfort performance.

A primary objective of this research was to use sweating manikin measurements to shed light on the translation from plate THL measurement and garment level heat stress. To achieve this objective, an analysis of sweating manikin heat transfer was conducted similar to the above-discussed analysis of sweating plate heat loss assessments. Figure 5 compares the manikin THL

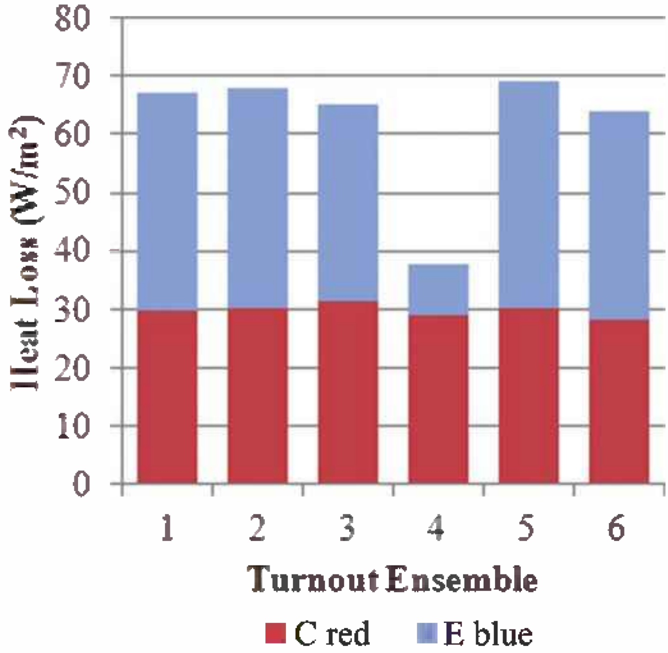

FIG. 6—*Contribution of dry (C) and evaporative (E) heat transfer to manikin-measured THL (25°C, 65 % RH).*

values, measured at the standard (ASTM F1868, Part C) environmental conditions (25°C, 65 % RH), with manikin THL values for the Mild and Warm Environment Protocol conditions (21°C, 65 % RH and 39°C, 35 % RH). Manikin THL values were estimated using the heat transfer model described in Eq 3.

Test results from sweating manikin testing are more consistent with the findings of the physiological testing. Figure 5 shows the manikin THL values predicted for each test environment.

The most obvious difference between sweating plate and sweating manikin results is the greatly reduced scale of heat losses in sweating manikin tests. Whereas flat plate THL predictions for the various environments exhibited a range of about 130 to 170 W/m^2 between the composites, differences between THL measurements made on the sweating manikin were only around 25 to 35 W/m^2. The reduction in heat loss in manikin tests can be mostly attributed to the thermal insulation of the additional gear worn (station uniform, underwear, socks, shoes, SCBA, respirator, thermal hood, helmet, and gloves) and to air layers that develop when the garment is dressed on a human form. Although the hot plate is a valuable tool for detecting material differences (because they are exaggerated by the elimination of naturally developed air layers), the manikin provides a better assessment of heat transfer in realistic wearing conditions.

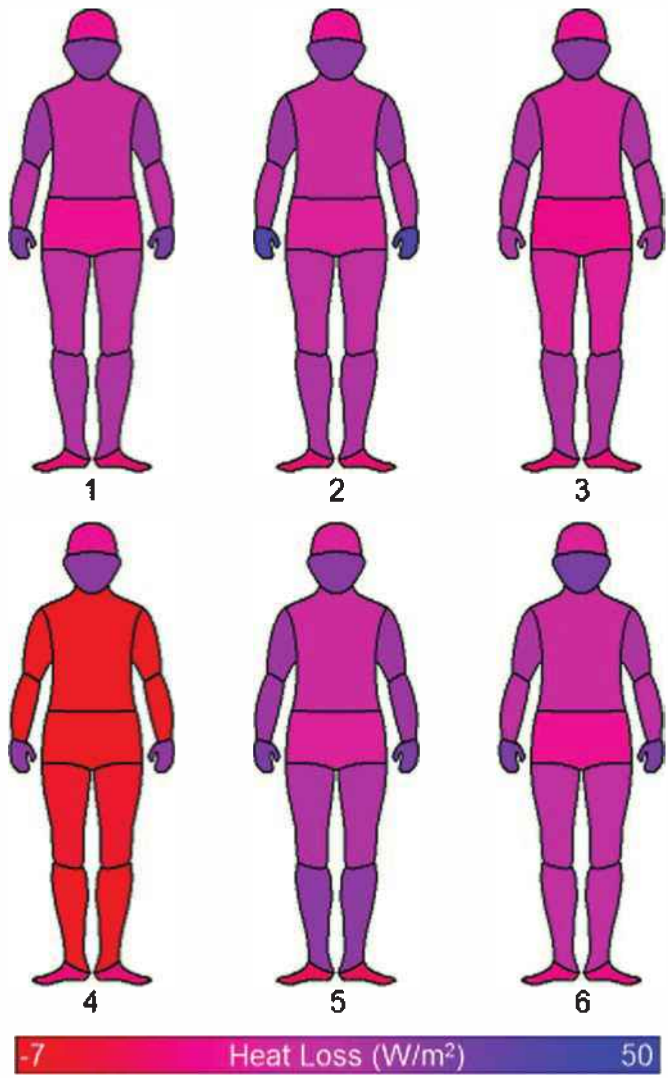

FIG. 7—*Heat loss predictions by section for test garments in 39°C and 35 % RH.*

Figure 6 shows that the three distinct heat loss levels predicted by sweating hot plate measurements are not apparent in the sweating manikin measurements. In the manikin tests, the turnout system with moisture barrier C (system 4) is easily distinguishable from all other systems. In contrast, the systems with moisture barriers A and B are not readily distinguishable from one another. Once again, the hot plate THL measurements accentuate the role of material properties by reducing the total air volume. In this case, the moisture mass transfer is limited mainly by the rate at which water can diffuse through the moisture barrier component of the layered turnout composite. At the garment level, however, air layers play a significant role in heat and moisture transfer. Coupled with the additional material layers, the relative impact of the moisture barrier permeability is much less when measured on the sweating manikin. For the "breathable" systems, the rate at which moisture travels through the other fabric and air layers has an equalizing effect. However, for the "non-breathable" systems, the moisture barrier permeability continues to have the greatest impact. As a result, the only clear distinction is between the non-breathable turnout and all other turnouts. Figure 7 shows a graphic representation of the heat loss from each section of the body predicted for warm environment conditions (39°C, 35 % RH).

For each of the predicted conditions on the manikin, the only turnout garment that was distinctly different from the others was the non-breathable garment (system 4). These findings are consistent with the results of the human physiological wear trials.

Conclusions

This study confirms that sweating manikin tests are more accurate predictors of the human heat stress associated with structural firefighter suits than sweating hot plate measurements. Sweating hot plate tests cannot account for the effects of clothing air layers, overlaps, outer shell attachments, or differences in the design and fit of a turnout garment, factors that play substantial roles in the actual heat stress of the ensembles. As a consequence, the heat stress reduction benefits measured using sweating plates might not always translate to the garment level. Despite this finding, THLs measured on flat fabric samples are useful predictors of the effects of turnout composites on potential heat stress. THL requirements have been appropriately incorporated into NFPA protective clothing performance standards for many years for this purpose. Sweating manikin tests simply provide more realistic simulations of actual wear conditions. They offer an intermediate objective instrument assessment that bridges the gap between plate measurements on materials and more elaborate and costly human subject wear testing, which will always be essential to the ultimate calibration and validation of any instrument measure, flat plate or manikin.

References

[1] TriData Corporation, "Firefighter Fatality Retrospective Study," Final Report presented to Federal Emergency Management Agency, Washington, D.C., 2002.

[2] NFPA 1971, 2007, "Standard on Protective Ensembles for Structural Fire Fighting and Proximity Fire Fighting," National Fire Protection Agency, Quincy, MA.

[3] Barker, R., Myhre, L., Scruggs, B., Shalev, I., Prahsarn, C., and Miszko, T., "Effect of Measured Heat Loss through Turnout Materials on Firefighter Comfort and Heat Stress. Part 1: Performance in a Mild Environment," *Performance of Protective Clothing: Issues and Priorities for the 21st Century*, ASTM STP 1386, Vol. 7, C. Nelson and N. Henry, Eds., ASTM International, West Conshohocken, PA, 2000.

[4] Myhre, L., Barker, R., Scruggs, B., Shalev, I., Prahsarn, C., and Miszko, T., "Effect of Measured Heat Loss Through Turnout Material on Firefighter Comfort and Heat Stress. Part 2: Performance in a Warm Environment," *Performance of Protective Clothing: Issues and Priorities for the 21st Century*, ASTM STP 1386, Vol. 7, C. Nelson and N. Henry, Eds., ASTM International, West Conshohocken, PA, 2000.

[5] Jones, B. W., *The Role of Material Properties in Reducing Heat Stress Associated With Fire Fighter Uniforms*, Institute for Environmental Research, Kansas State University, Manhattan, KS, 1989.

[6] Ross, K. A., 2006, "Evaluation of an Instrumented Sweating Manikin for Predicting Heat Stress in Firefighters' Turnout Ensembles," M. S. thesis, North Carolina State University, Raleigh, NC.

[7] Stull, J. O. and Duffy, R. M., "Field Evaluation of Protective Clothing Effects on Fire Fighter Physiology: Predictive Capability of Total Heat Loss Test," *Performance of Protective Clothing: Issues and Priorities for the 21st Century*, ASTM STP 1386, Vol. 7, C. Nelson and N. Henry, Eds., ASTM International, West Conshohocken, PA, 2000.

[8] O'Brien, C., Blanchard, L. A., Cadarette, B. S., Endrusick, T. L., Xu, X., Berglund, L. G., Sawka, M. N., and Hoyt, R. W., "Methods of Evaluating Protective Clothing Relative to Heat and Cold Stress: Thermal Manikin, Biomedical Modeling, and Human Testing," *J. Occup. Environ. Hyg.*, Vol. 8, No. 10, 2011, pp. 588–599.

[9] Gohlke, D. J., "History of the Development of the Total Heat Loss Test Method," *Performance of Protective Clothing: Issues and Priorities for the 21st Century*, ASTM STP 1273, Vol. 6, C. Nelson and N. Henry, Eds., ASTM International, West Conshohocken, PA, 1997.

[10] ASTM F1868-09, 2009, "Standard Test Method for Thermal and Evaporative Resistance of Clothing Materials Using a Sweating Hot Plate," *Annual Book of ASTM Standards*, Vol. 11.03, ASTM International, West Conshohocken, PA.

[11] NFPA 1971, 2000, "Standard on Protective Ensemble for Structural Fire Fighting," National Fire Protection Agency, Quincy, MA, 2000.

[12] NFPA, *NFPA 1971 Report on Proposals, 2005 Fall Revision Cycle*, National Fire Protection Agency, Quincy, MA, 2005.

[13] NFPA, *NFPA 1971 Report on Comments, 2011 Fall Revision Cycle*, National Fire Protection Agency, Quincy, MA, 2010.

[14] Meinander, H., "Experience with a Sweating Thermal Manikin—Ready for Standard Use?" *Proceedings of a European Seminar on Thermal Manikin Testing*, Stockholm, Sweden, Feb 12, 1997, National Institute for Working Life, Stockholm, Sweden.
[15] ASTM F1291-10, 2010, "Standard Test Method for Measuring the Thermal Insulation of Clothing Using a Heated Manikin," *Annual Book of ASTM Standards*, Vol. 11.03, ASTM International, West Conshohocken, PA.
[16] ASTM F2370-10, 2010, "Standard Test Method for Measuring the Evaporative Resistance of Clothing Using a Sweating Manikin," *Annual Book of ASTM Standards*, Vol. 11.03, ASTM International, West Conshohocken, PA.
[17] Flatau, P. J., Walko, R. L., and Cotton, W. R., "Polynomial Fits to Saturation Vapor Pressure," *J. Appl. Meteorol.*, Vol. 31, No. 12, 1992, pp. 1507–1513.

Performance of Protective Clothing and Equipment: Emerging Issues and Technologies
STP 1544, 2012
Available online at www.astm.org
DOI:10.1520/STP104118

ShuQin Wen,[1] *Guowen Song,*[1] *and Scott Duncan*[2]

Analysis of Physical and Thermal Comfort Properties of Chemical Protective Clothing

REFERENCE: Wen, ShuQin, Song, Guowen, and Duncan, Scott, "Analysis of Physical and Thermal Comfort Properties of Chemical Protective Clothing" *Performance of Protective Clothing and Equipment: Emerging Issues and Technologies* on April 16, 2011 in Anaheim, CA; STP 1544, Angie M. Shepherd, Editor, pp. 48–73, doi:10.1520/STP104118, ASTM International, West Conshohocken, PA 2012.

ABSTRACT: Research regarding chemical protective clothing (CPC) focuses on human comfort, clothing performance, and the heat strain associated with wearing protective materials. These studies are usually limited to one or two fabric/garment characteristics (e.g., garment weight, barrier permeability), and most of the research has been specific for certain tasks or garments. A systematic approach is needed in order to offer a comprehensive analysis on the performance of CPC and provide a technical basis for predicting comfort. This research measures the physical and thermal comfort related properties of CPC with available bench-scale methods and predicts the comfort level and heat strain based on the mechanical and physical properties of the material. Five articles of CPC and one fabric sample, with various chemical protective qualities, were evaluated with respect to mechanical and comfort related heat and moisture transfer properties. The results obtained were analyzed, and the physical burden and heat stress a human would experience when wearing these CPC fabrics were investigated. Comparisons and correlations between these properties and their contribution to clothing performance and human comfort are discussed. A full analysis of the physical and moisture related properties of the selected CPC fabrics is provided.

KEYWORDS: chemical protective clothing, comfort, physical burden, Kawabata, DMPC

Manuscript received June 10, 2011; accepted for publication February 27, 2012; published online September 2012.

[1]Dept. of Human Ecology, Univ. of Alberta, Edmonton, AB T6G 2N1, Canada.
[2]DRDC Suffield, Medicine Hat, AB T1A 8K6, Canada.

Introduction

Chemical protective clothing (CPC) is designed to prevent damage to the body and fatalities from the effects of chemical and biological substances. The provision of bulk and the use of enclosure are two common ways for protective garments to isolate humans from hazardous substances [1]. However, in both cases, comfort and work efficiency are compromised in achieving the desired protection. Work performance and mobility are impaired when bulky and thick fabrics are used to block or absorb chemicals and biological agents. When an impermeable clothing system is used, air and water vapor cannot circulate between the body and the environment, severely limiting the body's heat dissipating mechanisms [1,2].

Comfort is a complicated mix of subjective sensations. According to Slater [3,4], comfort involves physiological, psychological, and physical aspects. Psychological comfort is related to the subjective opinion of the clothing wearer and is therefore impossible to evaluate objectively. Physiological comfort (also referred to as thermo-physiological comfort or thermal comfort) relates to the way clothing buffers and dissipates moisture and heat [4]. When assessing thermal comfort, a variety of thermal and moisture management properties must be considered [5–7]; these include the fabric's thickness, weight, thermal insulation, resistance to evaporation, water repellence, air holding, and air permeability [5]. Physical comfort is correlated with the interaction of the clothing with the senses of the wearer [4,5]. Physical comfort can include not only the feel of the fabric against the skin but also the physical burden (weight, restriction of motion) of the whole garment. Tactile sensations such as prickliness, itchiness, stiffness, and smoothness are determined by the mechanical properties of the fabric or fiber and can be predicted by means of the mechanical simulation of skin–fabric interaction [8].

For a worker, thermal comfort relates directly to the heat stress experienced and the duration of a work shift; thus it is a critical attribute of the worker's clothing. A physical burden increases the work load and impairs work performance, resulting in a shortened work time and/or lower work efficiency. Tactile sensations, although they do not influence thermal or physical strain directly, contribute to the overall discomfort of the wearer and are therefore important factors in the endurance and work performance of CPC fabrics. The thermal and physical comfort of CPC can be measured directly through expensive, time-consuming, and poorly reproducible wear trials or predicted through correlated bench-scale laboratory tests [8–10].

In this study, several objective evaluation methods were chosen to characterize the physiological and physical comfort of CPC. The Kawabata Evaluation System (KES) was used to measure fabric's mechanical properties at low stress in order to evaluate the physical burden and tactile sensations a wearer would experience. A Measurement Technology Northwest sweating guarded hot plate and a dynamic moisture permeation cell (DMPC) were used to assess the transfer of heat and moisture through the test materials.

Materials and Methods

CPC Materials Tested

Six fabrics made from different materials and providing different levels of protection were investigated; three materials were double layered, and three were single layered. The material characteristics of the fabrics tested are outlined in Table 1. Fabrics S, V, M, C, and G are similar—hooded coveralls with a front zipper. Single layer fabrics S, V, and M have an identical design with elastic at the edges of the hood, wrists, and ankles. Fabrics C and G have more detailed designs including pockets on the chests, thighs, and upper arms and Velcro at the wrists and ankles; fabric G has a belt. The garment design of fabric P is still under development, and the tested material was received in swatches. Sketches of the garment designs are shown in Fig. 1.

These materials were selected not only for this study but also for a bigger project involving manikin tests, human trials, and comfort prediction. The variety of material types, protection levels, and different applications was taken into consideration, as were reasonable similarity and comparability.

Samples for tests (except P) were cut from the coveralls following the sampling rule that no two specimens for the same test could contain the same warp and weft yarns. The fabric samples were conditioned according to ASTM D1776 [11] at 20°C ± 1°C and 65 % ± 2 % relative humidity for at least 24 h prior to testing, unless otherwise specified.

TABLE 1—*Description of the fabrics used in this study.*

Fabric Type	Structure	Material Content	Thickness at 50 gf/cm^2(mm)	Mass (g/m^2)
S	Single layer	45 % polyethylene, 55 % polyester	0.26	55
V	Single layer	100 % high density polyethylene	0.18	45
M	Single layer	polyethylene-coated polythene	0.70	257
G	Double layer	Shell: 50/50 nylon cotton Adsorbent: activated carbon woven cloth (pyrolised polyacrylonitrile woven fabric)	1.21	478
P	Double layer	Shell: unknown Adsorbent: carbon coated unknown knit fabric	0.96	278
C	Double layer	Shell: 50/50 nylon/cotton Adsorbent: open cell carbon impregnated foam	2.83	533

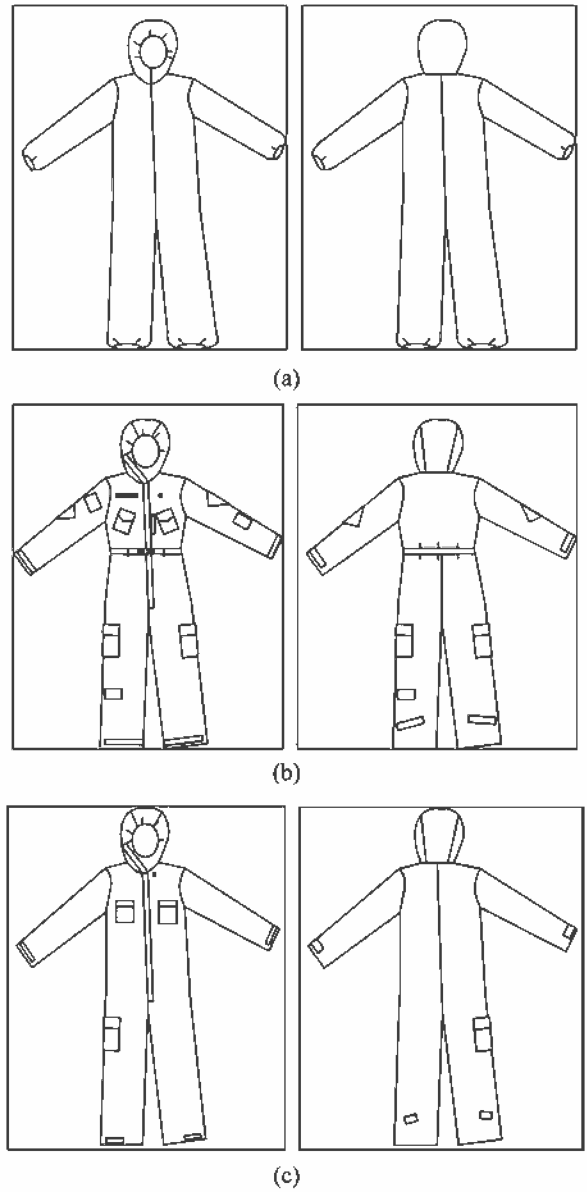

FIG. 1—*Sketches of garment designs: (a) front and back view of CPC S, V, and M; (b) front and back view of CPC G; and (c) front and back view of CPC C.*

Methods

Fabric Mechanical and Surface Properties—The KES was developed by the Japanese scientist Kawabata and his coworkers in 1970. This system measures the mechanical properties of fabric at low stress with high sensitivity, simulating the forces encountered when handling a fabric. Mechanical properties, including tensile, shearing, bending, compression, and surface properties, are tested in ways that imitate the effect of fingers and/or the entire hand while they touch and crumple the fabrics [12]. Table 2 shows the parameters that can be obtained from the KES.

The KES is used widely for testing fabric stiffness, thickness, extensibility, appearance retention, surface smoothness, and bulkiness [12–15]. It also provides "total hand" values and evaluates fabrics for specific end uses according to the recommended values [16]. In a few studies [17–19], fabric mechanical and surface property data from Kawabata tests were interpreted so as to predict the tactile comfort of the fabrics. Physical comfort is essentially a result of how much physical stress is generated in the fabric during wear and how stress is distributed over the skin and to the muscles. For example, when an individual is walking, the physical burden he or she encounters includes the weight of the fabric; friction between garment surfaces; and physical strains caused during stretching, bending, and shearing of the fabric. The heavier, rougher, and stiffer the fabric is, the greater the physical burden. Therefore, the physical comfort associated with wearing CPC has a strong relationship with the mechanical and surface properties of the fabric.

TABLE 2—*KES parameters and associated units of measure.*

Blocked Property	Abbreviation	Characteristic Value	Unit
Tensile	LT	Linearity	none
	WT	Tensile energy per unit area	N/m
	RT	Resilience	%
Bending	*B*	Bending rigidity per unit length	$\times 10^{-4}$ Nm/m
	2HB	Moment of hysteresis per unit length	$\times 10^{-2}$ N/m
Shearing	*G*	Shear stiffness	N/m/°
	2HG	Hysteresis at shear angle of 0.5°	N/m
	2HG5	Hysteresis at 5°	N/m
Compression	LC	Linearity	none
	WC	Energy required for compression	gf/cm^2
	RC	Resilience	%
Surface	MIU	Mean value of coefficient of friction	none
	MMD	Mean deviation of coefficient of friction	none
	SMD	Mean deviation of surface roughness	μm
Weight and thickness	*W*	Weight per unit area	g/cm^2
	TM	Thickness at 50 gf/cm^2	mm

In this study, the KES was used to determine the tensile, shearing, bending, compression, surface friction, and roughness properties of the CPC fabrics tested. The tactile sensation and physical burden of the fabrics were then predicted through the analysis of the individual attributes and comparisons of the fabric types tested.

Heat and Moisture Transfer Properties—Human body temperature is relatively constant at 37°C through continuous energy exchange with the environment. In order for a body to maintain thermal equilibrium, metabolic heat must be dissipated via moisture transfer (i.e., evaporation) and heat transfer (i.e., radiation, convection, and conduction). Conductive heat exchange is generally considered minimal and can be disregarded. Body heat loss at rest and in neutral environments is due to convection (10 % to 15 %), radiation (60 %), and evaporation (20 % to 30 %) [20]. In a warm environment or at high work intensity, evaporative heat loss plays a much more dominant role. Therefore, in evaluating the thermal comfort of CPC, the most important factors are the heat and moisture transfer properties.

Steady State Heat and Vapor Transmission—The sweating guarded hot plate, also called the "skin model," tests the thermal and evaporative heat transfer properties of a fabric system and the air layer above it. The resistance to dry heat transfer (R_{ct}) obtained from a dry test reflects the heat transfer properties of the whole fabric system—that is, the combined effects of conduction, convection, and radiation of heat from the hot plate surface through the material to the environment. The resistance to evaporative heat transfer (R_{et}) is related to the flow of moisture from the saturated hot plate surface through the material to the environment. This method has been widely used in comfort studies to simulate the heat and mass transfer conditions of a clothed body.

The dry and evaporative heat transfer properties of CPC materials were measured using a sweating guarded hot plate in an environment of 25°C and 65 % relative humidity, according to the test procedures described in Part C of ASTM F1868 [21].

Air Permeability—Air permeability is important for thermal comfort. High permeability allows air to access the skin surface, enhancing the evaporation of perspiration. The air permeability of the fabrics was measured according to ASTM D737 [22].

Diffusion/Convection Test Method—CPC materials can be partially or totally air impermeable [23]. In totally impermeable materials, air flow through clothing layers is not possible; thus moisture vapor can get out of the clothing system only through vapor diffusion. However, if the fabric is air-permeable and there is a pressure gradient across the fabric, air flow through the fabric (convection) will take place and will have an impact on vapor diffusion, as shown in Fig. 2. Air flow can be in a direction that is the same as or opposite to that of vapor diffusion; air flow is determined by the pressure gradient. Correspondingly, convection opposes or aids vapor diffusion flux.

The DMPC was developed by Gibson in 1997 [24]. This method measures water vapor diffusion resistance and air permeability (resistance to air flow) in the same test. In this test, the pressure drop across the sample is systematically changed in order to produce different air flows through the fabric [25]. Because there is a humidity difference across the sample, the water vapor diffusion property can also be determined from this test. At 0 pressure drop, the true water vapor diffusion resistance property and the true water vapor transmission rate are verified [24,26], as shown in Fig. 3. CPC materials are designed to offer different levels of protection and to serve in various environments. The DMPC can be used to simulate different environmental conditions such as hot or cold, dry or humid, windy or mild, or high or low humidity. The DMPC can also indicate the effect of air flow on water diffusion. Moreover, the DMPC test can be performed much faster and requires a much smaller specimen size than the sweating hot plate test. Therefore, the DMPC is a very useful and efficient test for evaluating the thermal comfort of CPC, especially in cases in which evaporative heat transfer is the main concern.

Air permeability, true water vapor diffusion, and true water vapor transmission rates were tested according to Part B of ASTM F2298 [26]. The test conditions were as follows:

Temperature = 30°C
Sample area = 10 cm^2
Flow rates on top and bottom = 2000 cm^3/min
Humidity on top = 0.95 (95 %); humidity on bottom = 0.05 (5 %)

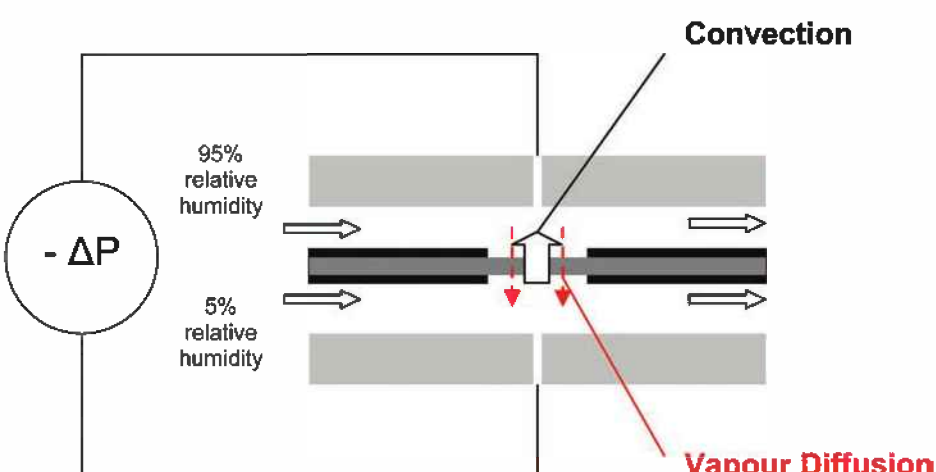

FIG. 2—*Schematic of vapor diffusion and convection through fabric.*

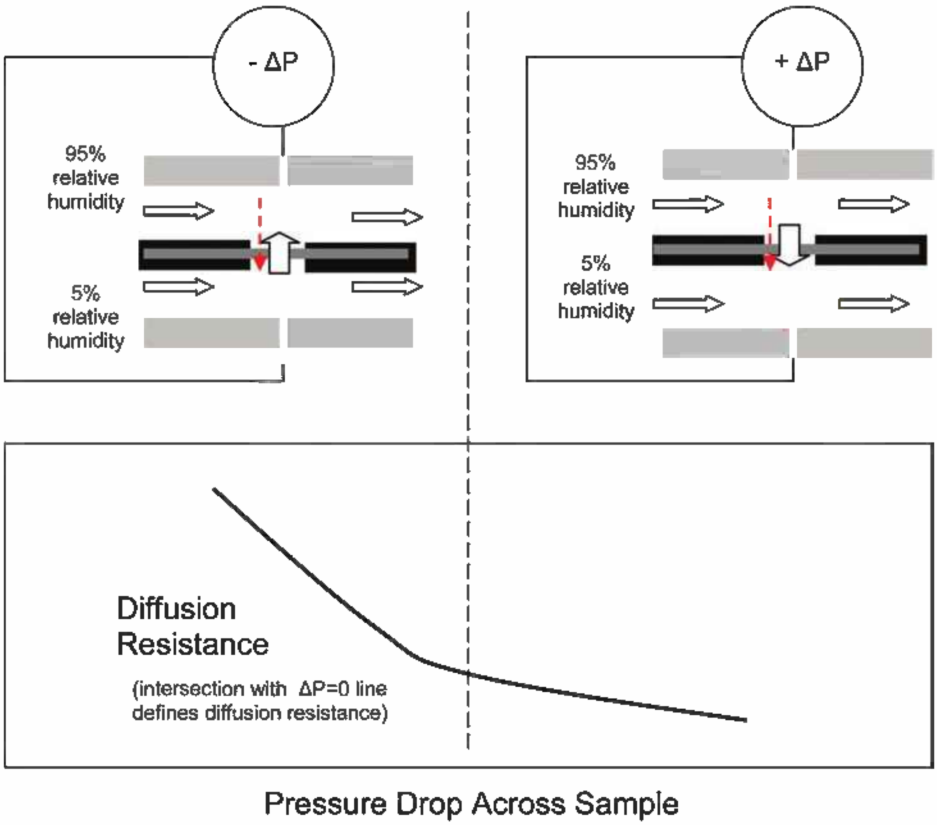

FIG. 3—*DMPC test, setup of Part B: convection/diffusion test.*

Pressure drop varied in increments between approximately − 150 and 150 Pa.

The liquid moisture management property is an important factor in thermal and sensorial comfort. As a textile material transports liquids away from the body, it reduces the sensation of wetness and creates more surface area for water to evaporate from. However, most CPC materials are not designed to be worn right next to the skin. Instead, undergarments with good liquid moisture transport properties are usually worn underneath CPC. Therefore, liquid moisture management associated with wearing CPC is not recognized as a main concern.

Results and Discussion

Fabric Mechanical and Surface Properties

Fifteen parameters describing the fabric mechanical and surface properties measured by the KES are shown in Table 3.

Tensile Properties—In the tensile test, tensile linearity (LT), tensile energy (WT), and tensile resilience (RT) were evaluated. LT is the linearity of the stress-strain curve, which reflects the elasticity of the fabric [27]. A higher value of LT represents a stiffer fabric. WT is defined as the energy required in order to extend a fabric, i.e., the ability of a fabric to withstand external stress during extension. The RT is defined as the ability of a fabric to recover after the application of tensile stress; it is a measure of the percentage of energy recovery from tensile deformation [27]. A reduced fabric RT value implies that it is difficult to restore the fabric to its original shape after releasing the applied tensile stress. With regard to CPC, fabrics with high WT and RT values, as well as with low LT values, possess excellent tensile strength and reasonable stretchiness to allow movement. As shown in Fig. 4, fabric G has the lowest LT and relatively high WT and RT values; thus the comfort-related tensile properties of fabric G are good. With the highest WT and a higher LT than the other fabrics tested, fabric P is stronger and stiffer than the other fabrics. Fabric V, with a low RT of 42.32 %, is the fabric mostly likely to become loose in

TABLE 3—*Mechanical properties measured using the Kawabata Evaluation System.*[a]

Fabric Type		S	V	M	G	P	C
Tensile[a]	LT	0.739	0.770	0.796	0.650	0.814	0.847
	WT, N/m	2.582	7.395	2.820	6.995	16.59	6.743
	RT, %	73.57	42.32	90.33	65.63	64.57	66.22
Bending[a]	B, $\times 10^{-4}$ Nm/m	0.085	0.099	4.260	0.315	0.364	0.474
	2HB, $\times 10^{-2}$ Nm/m	0.052	0.146	2.291	0.012	0.193	1.150
Shearing[a]	G, N/m/°	5.873	5.979	32.05	2.692	5.829	5.974
	2HG, N/m	3.927	6.805	31.32	4.099	6.130	15.73
	2HG5, N/m	22.57	23.59	91.86	8.819	12.41	39.48
Compression	LC	0.387	0.290	0.204	0.338	0.408	0.261
	WC, gf/cm^2	0.154	0.153	0.604	0.637	0.394	0.397
	RC, %	61.99	40.15	52.30	42.19	51.48	46.59
Surface[a]	MIU	0.161	0.201	0.192	0.174	0.152	0.195
	SMD, μm	2.871	2.598	1.229	4.325	7.777	5.607
Weight and Thickness	W, g/m^2	55.0	45.0	257	478	278	533
	TM, mm	0.26	0.18	0.70	1.21	0.96	2.83

[a]Tested in both warp and weft directions. Results are average values of warp and weft. For double-layered fabric systems, an average of shell fabric and adsorbent layer on tensile, bending, and shearing is taken to represent the whole system.

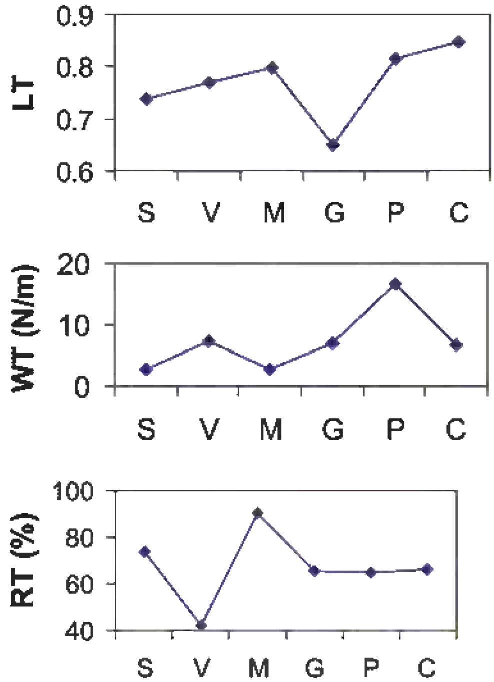

FIG. 4—*Tensile properties obtained via the KES test.*

shape due to tensile stress. The tensile and recovery behaviors of these fabric systems can also be compared with load-elongation curves, as demonstrated in Fig. 5. The curves of fabric V, lying to the right of the others, suggest its high extensibility, which is an advantage in terms of the freedom of motion of the person wearing the garment. The fabric M curves are on the very left of the chart, showing that it has the least extensibility of all the fabrics and might restrict the movement of the wearer. Compared with the other fabrics, fabric V has low tensile resilience and thus low appearance retention. This can affect both aesthetics and fit if the fabric is used to construct reusable CPC.

Bending—Bending rigidity (B) is defined as the ability of a fabric to resist the bending moment. Bending hysteresis (2HB) is defined as the ability of a fabric to recover after being bent. Bending properties affect both the handling and the flexibility of a fabric; B is related to the quality of stiffness when a fabric is handled. A higher B value indicates greater resistance to bending. Generally, a fabric with low B and low 2HB values has good bending properties [14].

As described in Fig. 6 and Fig. 7, fabric M has extremely high B and 2HB values compared to the other fabrics tested. This indicates that fabric M is hard to bend and, once bent, it is hard for fabric M to recover its original shape. Because walking, lifting, etc., require bending of the fabric, fabric M would be

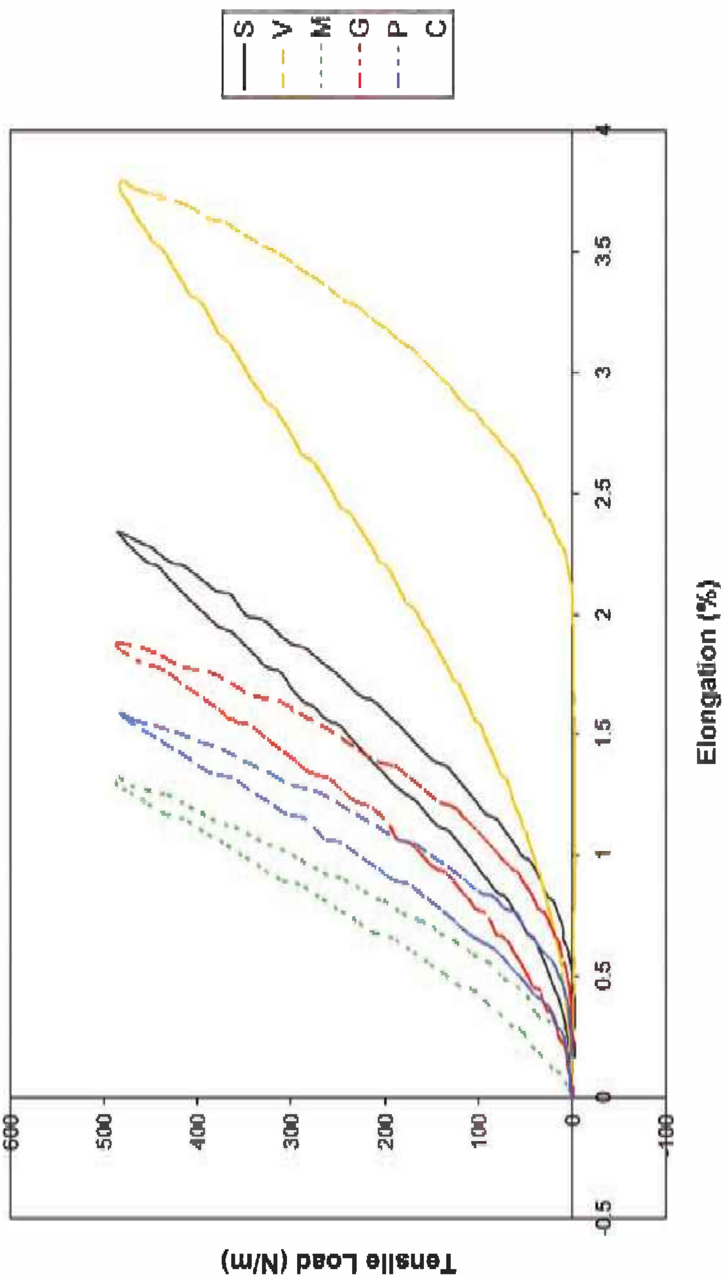

FIG. 5—*Warpwise tensile and recovery behavior. For double-layered fabrics G, P, and C, the behaviors of shell fabrics are shown.*

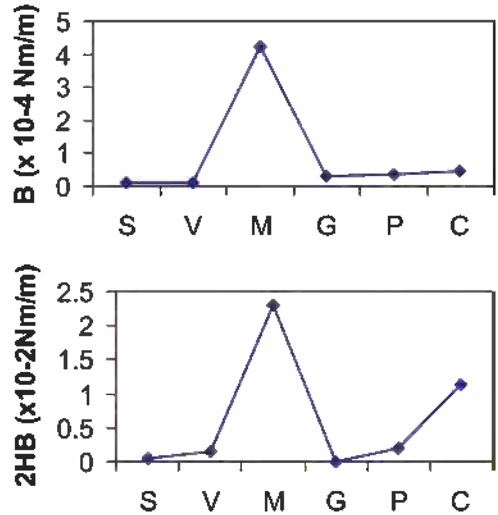

FIG. 6—*Bending properties obtained via the KES test.*

expected to resist these movements, placing a large mechanical burden on the wearer.

Shearing Properties—The shear rigidity G is defined as the ability of a fabric to resist shear stress. The shear rigidity of a fabric depends mainly on the mobility of the warp/weft threads within the fabric [27]. Lower values indicate less resistance to shearing, corresponding to a softer material having better drape [14,27]. In a KES standard measurement, 2HG and 2HG5 are the hysteresis of shear force at 0.5° and 5°, respectively. Shear hysteresis is the ability of a fabric to recover after receiving shearing stress. The smaller the shear hysteresis, the better the recovery. Therefore, fabric with low G and low shear hysteresis values has superior shearing properties, as it is easy for the fabric to shear and recover [27].

As presented in Figs. 8 and 9, the shearing behavior of fabric M is significantly different than that of the other fabrics tested. With high G, high 2HG, and high 2HG5, fabric M has the highest resistance to shearing of all the fabrics tested. That is, in order to perform movements that involve shearing of the fabric, the highest physical work will be needed when wearing CPC consisting of fabric M. Fabrics S, V, G, and P have good shearing properties. The higher 2HG and 2HG5 of fabric C compared to those of fabrics S, V, G, and P are mainly determined by the adsorbent layer of fabric C. The adsorbent layer is foam, which does not take much force to shear; however, the recovery of this foam from shearing is not as facile as the recovery of woven fabrics. Therefore, the overall shearing behavior of fabric C is relatively poor.

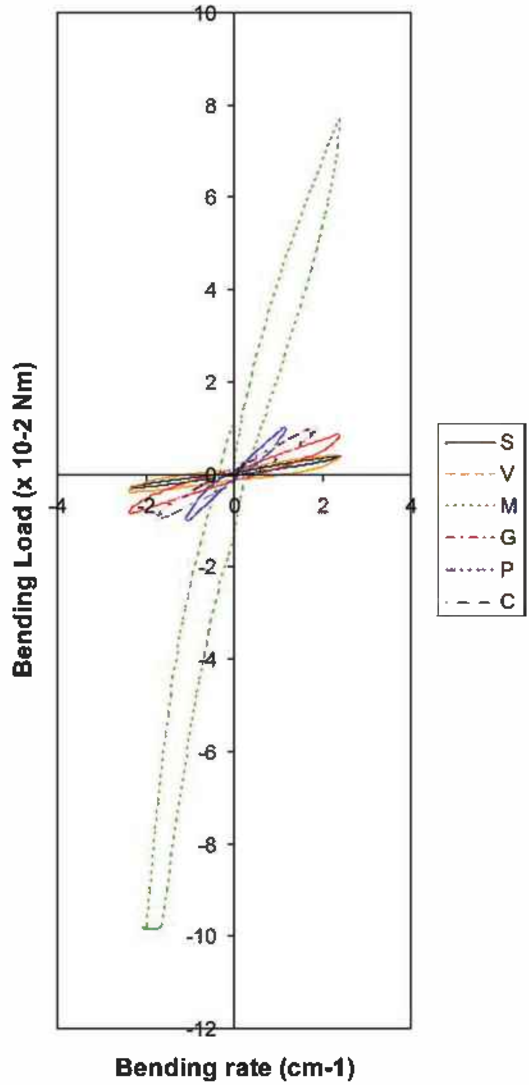

FIG. 7—*Warpwise bending and recovery behavior.*

Compression Properties—The compression properties of the tested fabric systems (double layers are measured as a whole)—compressional linearity (LC), compressional energy (WC), and compressional resilience (RC)—were measured at three distinct points on the specimens [27]. The results for LC, WC, and RC are shown in Fig. 10. LC shows the linearity of a compression-thickness curve. A high LC value indicates a fluffy fabric with high compressibility. WC is the work done in compressing a fabric. In the test, the highest compressing force is set up at 50 gf/cm^2 for all the fabrics. At the same force,

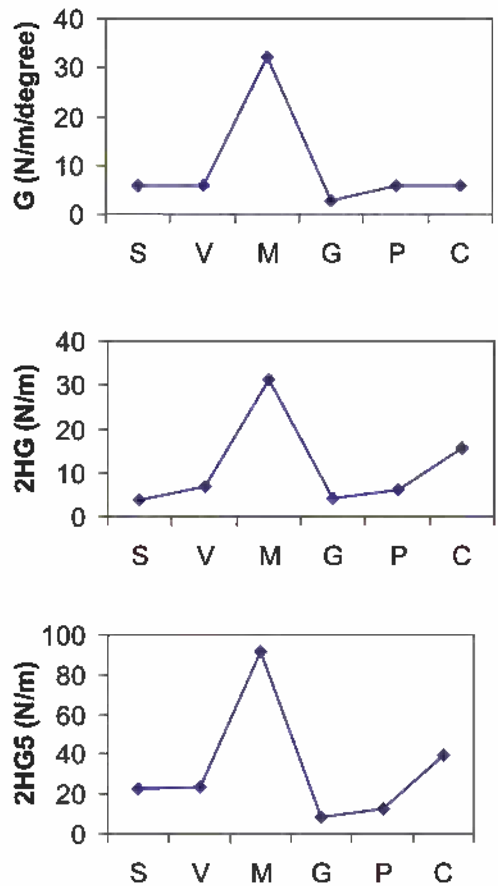

FIG. 8—*Shearing properties obtained via the KES test.*

when a fabric is easier to compress, the compressional sensor travels a longer distance across the thickness. Therefore, the higher the WC value, the higher the compressibility of the fabric. In addition, RC is defined as the ability of a fabric to retain its fullness after being compressed; i.e., RC indicates the recoverability of the fabric after the compression force is removed. A high RC value indicates good recovery from compression. Fabric with good compression properties usually possesses higher LC, WC, and RC values; the compressional properties are highly dependent on the thickness of the fabric. In Fig. 11, we see that at the same compressional load, fabrics M, C, and G are compressed more easily than fabrics P, V, and S. The reason that C and G can be compressed by about 1 mm is the adsorbent layer that increases their thickness. Fabric M is a single-layered laminated nonwoven sheet. The surface of M is smooth and flat; however, the back of M is fluffy like a thin layer of cotton batting. This structural feature is responsible for the compressional behavior of fabric M.

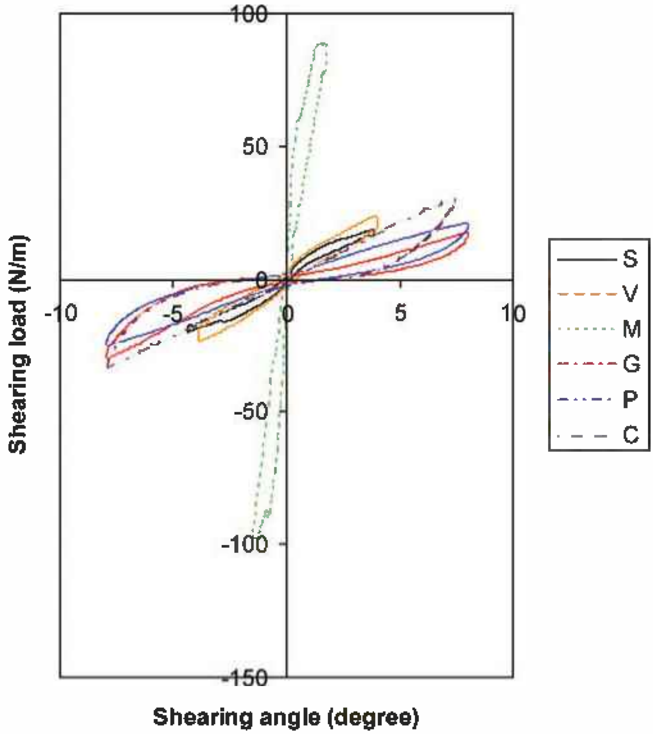

FIG. 9—*Warpwise shearing and recovery behavior.*

Surface Properties—Fabric surface properties, including the coefficient of friction (MIU) [27] and geometrical roughness (SMD), were measured. The MIU is the force required in order to move two surfaces over each other divided by the force holding them together; the former force is reduced once the motion has started. That is, the higher the value of MIU, the greater the friction force necessary to slide the fabric surface over an object. SMD measures the geometrical roughness of the fabric surface, or the fabric surface evenness characteristic [27]. The lower the SMD value, the more even the fabric surface will be. Generally, fabrics with low MIU and SMD values have surface properties that are more compatible with CPC. In this respect, fabrics S and G have better surface properties than the other fabrics tested, because they have lower MIU and SMD values, as demonstrated in Figs. 12 and 13. Fabrics V and M have relatively good surface roughness; however, the friction coefficients of these two fabrics are higher than those of S, G, and P. Friction between garment surfaces can be a physical burden when the wearer is involved in low intensity activities. Fabric C has a high MIU and a high SMD; therefore, the surface properties of C are poor with respect to CPC. Although fabric P has a low MIU, it has the highest surface roughness of the fabrics tested. This is probably because of the larger yarn diameter in fabric P,

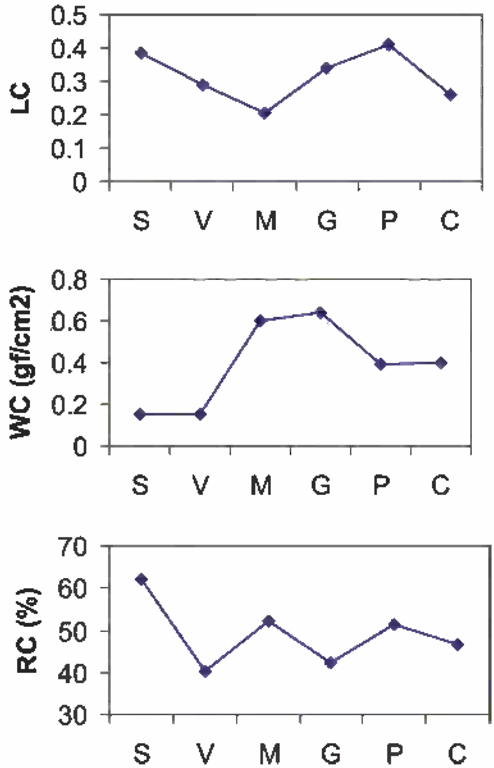

FIG. 10—*Compressional properties obtained via the KES test.*

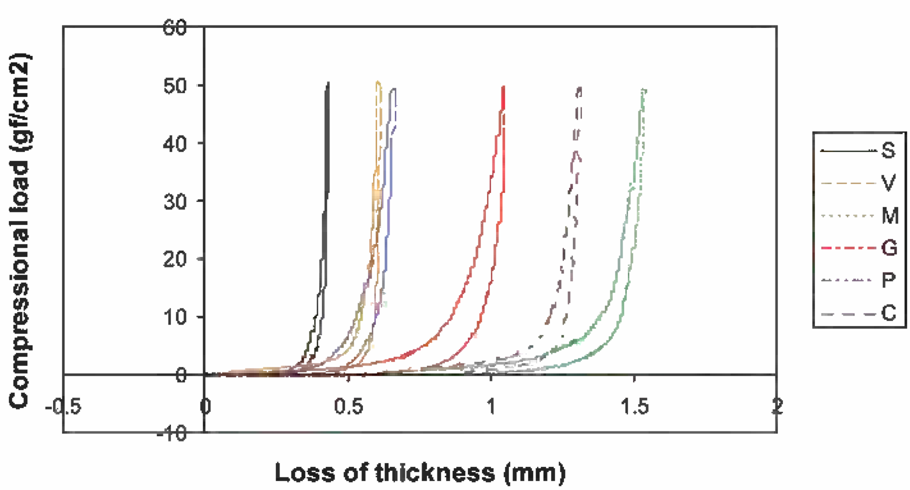

FIG. 11—*Compression and recovery behaviors.*

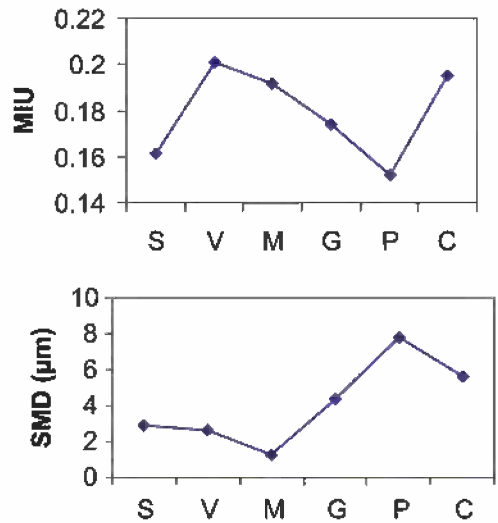

FIG. 12—*Surface properties obtained via the KES test.*

which makes its structure relatively loose and makes fabric P feel bumpier than the others.

Overall Physical Comfort

In the KES test, the total hand value was defined in order to give an overall assessment of the test fabric. The total hand value is a numerical scale from 0 (out of use) to 5 (excellent) that provides an evaluation of the primary quality of fabrics with regard to comfort and appearance [27]. The total hand value is correlated to and calculated based on the mechanical and surface properties of hundreds of sample fabrics [27]. It is a good indicator of the feel of a fabric for some conventional end uses—for example, men's winter suits and women's summer dresses [16,28]. However, desirable material properties for CPC deviate greatly from those of conventional fabrics; the total hand value defined by Kawabata does not represent the overall physical comfort quality of CPC materials.

A multiaxis radar graph (Fig. 14) was plotted based on LT, *B*, *G*, SMD, and weight (*W*). As discussed above, CPC materials with high LT, *B*, *G*, SMD, and *W* values will be stiff, rigid, rough, and heavy and will contribute negatively to the physical comfort of the CPC wearer. In Fig. 14, five properties of the six different fabrics tested are marked along the corresponding axes; the five marked dots of each fabric form a pentagon. By comparing pentagon areas, we can obtain the relative overall physical comfort ranking of these fabrics. Fabric M has the largest pentagon in the chart; therefore, it is predicted to perform the worst in terms of physical comfort. The double-layered fabrics C, P, and G have lower overall performance because of poor

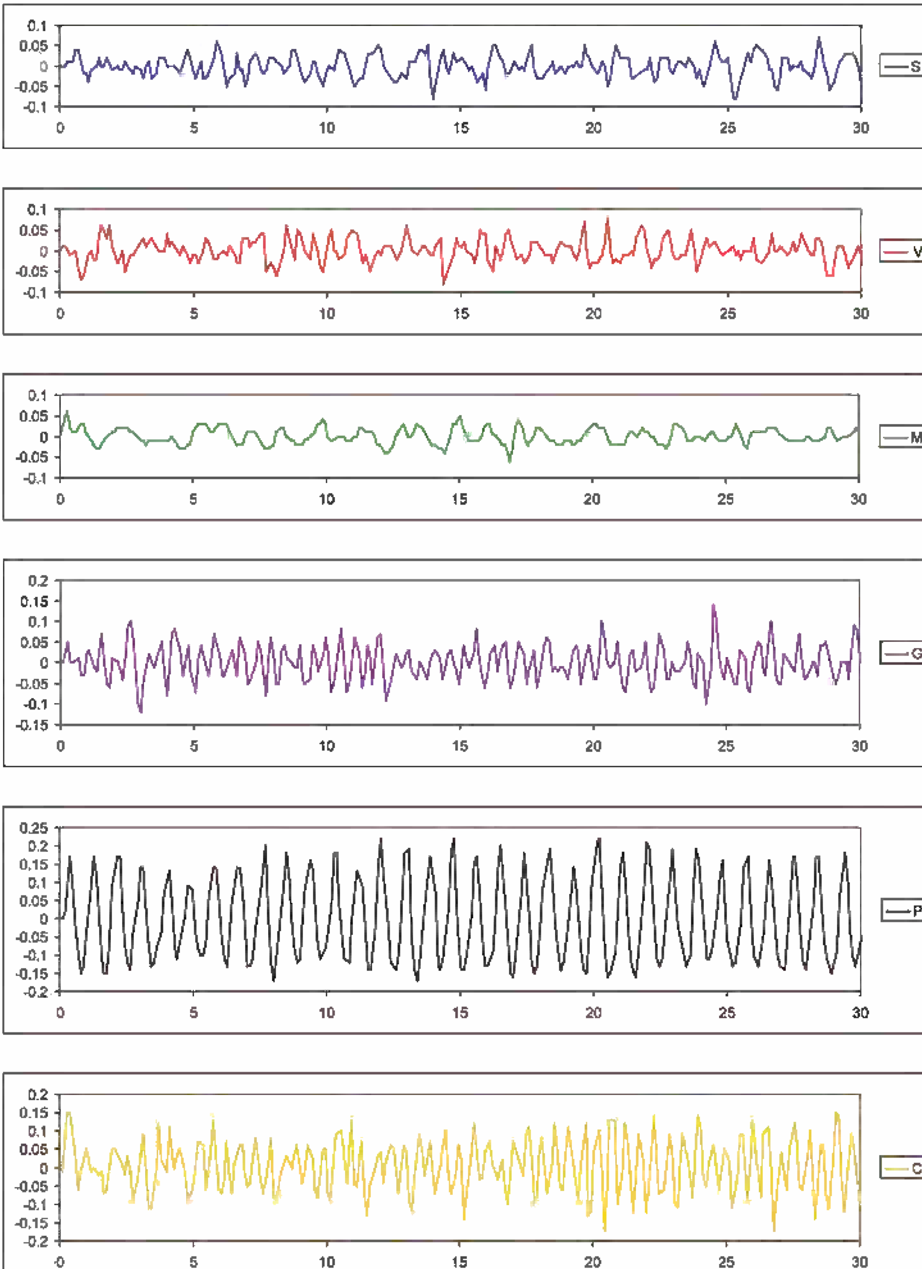

FIG. 13—*Surface roughness along the warp direction.*

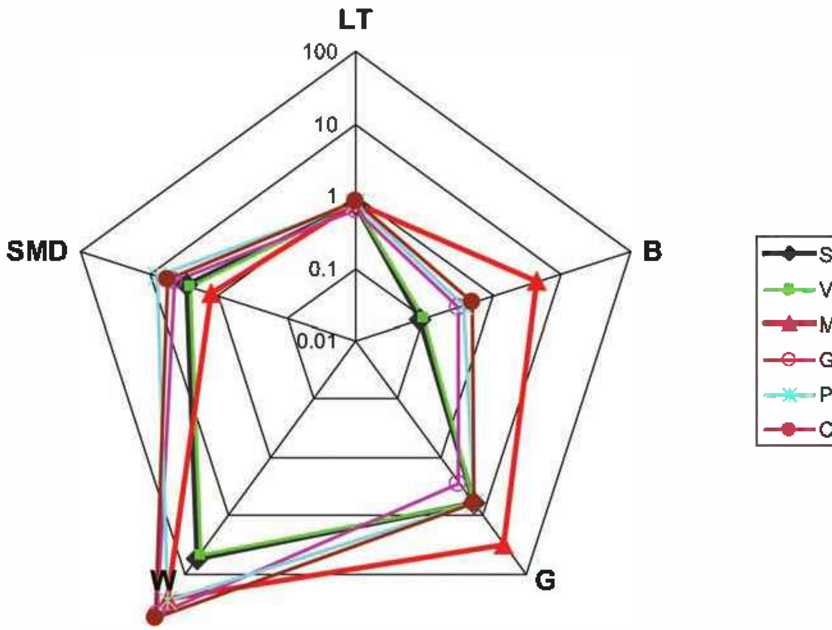

FIG. 14—*Overall physical comfort properties of CPC materials.*

weight and bending properties. The lightweight single-layered fabrics S and V are expected to present less physical burden to the wearer than the other fabrics tested.

Heat and Moisture Transfer Properties

Thermal and Evaporative Resistance—Dry and evaporative heat resistance results for fabrics S, V, M, G, and C are listed in Table 4. A still air layer, in which air movement does not take place, provides significant thermal

TABLE 4—*Thermal and evaporative heat transfer properties.*[a]

Fabric	Thermal Resistance of Fabric and Air Layer R_{ct}, m^2 K/W	Thermal Resistance of Fabric Only R_{cf}, m^2 K/W	Apparent Total Evaporative Resistance of Fabric and Air Layer R_{et}A, m^2 kPa/W	Apparent Intrinsic Evaporative Resistance of Fabric Only R_{ef}A, m^2 kPa/W
S	0.0823	0.0266	8.30	3.58
V	0.104	0.0483	14.0	9.33
M	0.108	0.0525	46.9	42.2
G	0.108	0.0523	10.8	6.10
C	0.151	0.0949	16.7	12.0

[a]Because the amount and size of received double-layered fabric P was limited, sweating hot plate tests were not performed on that fabric.

insulation [7]. The thickness of the still air layer on the surface of a fabric depends on the wind speed, temperature, and material surface properties. The layer of still air contributes to the total thermal resistance of the clothing. In Table 4, R_{ct} is the total thermal resistance of the fabric and air layer, and R_{cf} is the thermal resistance of the fabric only. R_{cf} was found to be correlated to the fabric thickness, $r = 0.93$, indicating that a thicker fabric normally provides higher thermal insulation. This is because for most clothing materials, the volume of air enclosed is far greater than the volume of the fibers [29]. Therefore, thermal insulation is highly dependent on the thickness of the material and less dependent on the fiber type. Among the CPC materials investigated, the thickest double-layered material (G) was found to have the highest thermal resistance. For thin fabrics S and V, the thermal resistances of the fabrics were even lower than the influence of the air layer. The influence on thermal resistance of materials S and V is minimal. During the design and engineering of CPC, control of the thickness is very important in the consideration of thermal comfort.

In order for a human being to be thermally comfortable, both heat balance and moisture balance have to be achieved. Similar to thermal resistance, evaporative resistance was also reported for the fabric only (R_{ef}A) and for the fabric and air layer (R_{et}A). With permeable materials, the thickness determines the major part of the evaporative resistance. Again, as the volume of fibers is usually low compared to the enclosed air volume, resistance to the transport of water vapor through the garment is mainly determined by the thickness of the enclosed air. Coatings, membranes, or other treatments added to the fabrics have a major effect on vapor resistance, as vapor molecules must diffuse through the treated material [29]. The results for R_{et}A and R_{ef}A were consistent with the theories described above. Fiber S, thin and permeable, had smaller values, whereas double-layered fabrics G and C and impermeable fabrics V and M—affected by thickness and/or membrane/coating—were observed to have greater evaporative resistances.

From an overall thermal comfort point of view, fabrics S and G, with smaller R_{ct} and R_{et} values, are predicted to perform better than the other fabrics tested. Fabric C, with a high R_{ct} value, prevents heat transfer to the environment; thus, more heat is captured in the fabric system, and perspiration could be accelerated. Heat stress will be aggravated in fabric M, which has the highest R_{et}, when it is worn in a hot environment in which heat transfer is limited or when the wearer is sweating heavily.

Air Permeability—Air permeability results from ASTM D737 [22] are given in Fig. 15. When comparing these data with the evaporative resistance data, it was found that, in general, the higher the air permeability, the lower the evaporative resistance. This is because air flow through the fabric system aids the removal of moisture. However, fabric V had very low air permeability, yet its evaporative resistance was relatively low. This fact indicates that a moisture diffusion mechanism was engineered

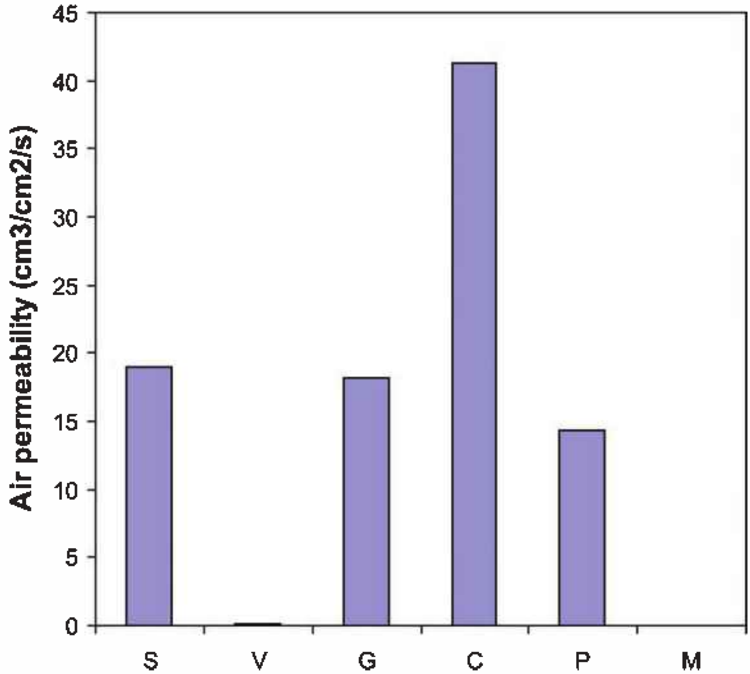

FIG. 15—*Air permeability obtained from ASTM D737.*

into fabric V to allow it to be impermeable to air but permeable to water vapor. This also implies that air permeability cannot be used alone to predict thermal comfort.

DMPC Diffusion/Convection Properties—A good correlation ($r = 0.99$) was found between the test results on water vapor diffusion resistance from the DMPC (Table 5) and R_{et}A values obtained in sweating hot plate tests. The air permeability calculated using the DMPC is also highly consistent with the results from ASTM D737. The DMPC is a much quicker test than the sweating hot plate (R_{et}) test. The other advantage is that the DMPC test specimen is

TABLE 5—*Water vapor transmission properties measured with a DMPC.*

Fabric	Water Vapor Diffusion Resistance, s/m	Water Vapor Flux, g/m^2-day	Air Flow Resistance, 1/m	Air Permeability, ft^3/min/ft^2
S	220	6712	4.12×10^7	33.5
V	394	5636	2.83×10^9	0.5
M	5023	469	1.00×10^{12}	0.0
G	448	2518	3.76×10^7	36.7
P	374	5711	4.60×10^7	30.0
C	878	887	1.25×10^7	110.3

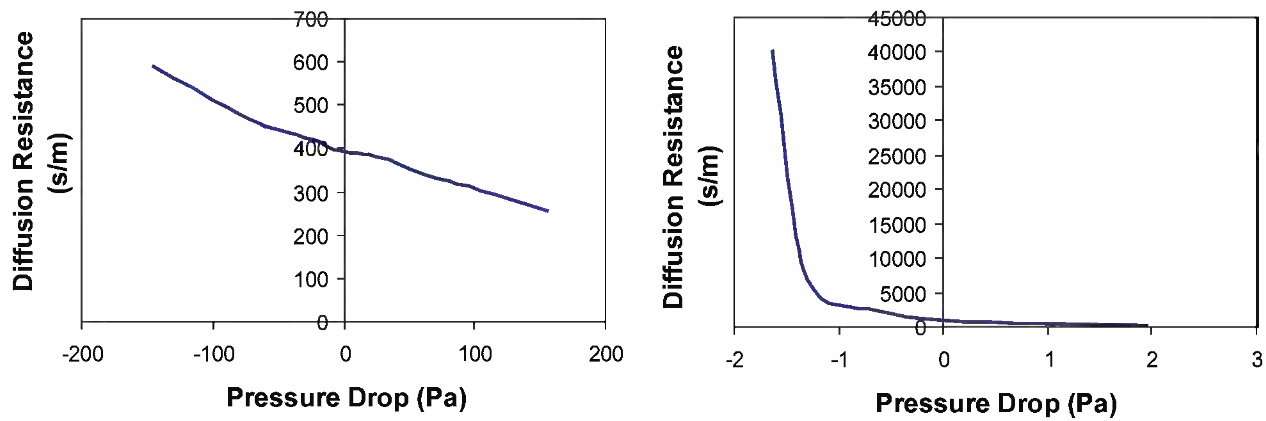

a) Fabric V b) Fabric C

FIG. 16—*Water vapor diffusion resistance across different pressure drops.*

much smaller. Fabric P was found to have a smaller water vapor diffusion resistance than the other two double-layered fabrics and is therefore predicted to offer better thermal comfort than fabrics G and C, especially when worn in hot environments or for high-intensity work.

The diffusion/convection test comprises a series of measurements at different pressure gradients that are used to determine the relationship between the water vapor diffusion resistance and a pressure drop. For fabric V, the relationship between vapor diffusion resistance and pressure drop was almost linear (Fig. 16). For fabric C, in contrast, the diffusion resistance dropped dramatically within the pressure drop range of -2 to -1 Pa. The change in the vapor diffusion resistance became much gentler when the pressure dropped to less than -1 Pa. This information has implications for the evaluation of CPC comfort in specific environments.

Conclusions and Future Work

Physical and thermal comfort properties were assessed for six CPC materials using bench-scale test methods. The six fabrics showed significant differences in low-stress mechanical and surface properties obtained from KES tests. The differences in the physical properties reflect differences in the level of physical burden on the CPC wearer during movement. The physical burden/discomfort was further summarized through the analysis of five physical properties in one radar graph. The properties of thermal and evaporative resistance, air permeability, and DMPC diffusion/convection were tested in order to characterize heat and water vapor transfer properties. Correlation was found between results from the resistance to evaporative heat transfer (R_{et}) test and the DMPC test. The thermal comfort performance of the six CPC fabrics was analyzed based on the results in these tests. Our continuing work on this project involves the investigation of the effects of garment size, fit, and design on the comfort of CPC. Thermal manikin tests and human trials will be conducted.

Acknowledgments

The writers express their gratitude to DRDC Suffield Canada for providing the materials used in this study. The writers also thank Dr. Phil Gibson for his assistance with this research.

References

[1] Slater, K, "Comfort or Protection: The Clothing Dilemma," *Performance of Protective Clothing*, ASTM STP 1237, J. S. Johnson and S. Z. Mansdorf, Eds., ASTM International, West Conshohocken, PA, 1996, pp. 486–497.

[2] Rossi, R., "Interactions between Protection and Thermal Comfort," *Textiles for Protection*, R. A. Scott, Ed., Woodhead, Cambridge, England, 2005, pp. 233–260.
[3] Slater, K., "The Assessment of Comfort," *J. Text. Inst.*, Vol. 77(3), 1986, pp. 157–171.
[4] Slater, K., "The Meaning of Comfort," *Human Comfort*, C.C. Thomas, Springfield, IL, 1985, pp. 3–11.
[5] Fourt, L. E. and Hollies, N. R. S., *Clothing: Comfort and Function*, Marcel Dekker, New York, 1970, Chaps. 4 and 6.
[6] Branson, D. H. and Sweeney, M., "Conceptualization and Measurement of Clothing Comfort: Toward a Metatheory," *Critical Linkages in Textiles and Clothing Subject Matter: Theory, Method and Practice*, ITAA Special Publication 4, S. B. Kaiser and M. L. Damhorst, Eds., International Textile and Apparel Association, Monument, CO, 1991, pp. 94–105.
[7] Saville, B. P. and the Textile Institute, "Comfort," *Physical Testing of Textiles*, Woodhead/CRC Press, Cambridge, England/Boca Raton, FL, 1999, pp. 209–243.
[8] Kilinc-Balci, F. S., "Testing, Analysing and Predicting the Comfort Properties of Textiles," *Improving Comfort in Clothing*, G. Song, Ed., Woodhead, Cambridge, England, 2010, pp. 138–162.
[9] Li, Y., *The Science of Clothing Comfort*, Textile Progress Series Vol. 31, Textile Institute, Manchester, UK, 2001.
[10] Barker, R. L. and Scruggs, B. J., "Evaluating the Comfort Performance of Fabrics for Nuclear Protective Apparel," *Performance of Protective Clothing*, ASTM STP 1237, J. S. Johnson and S. Z. Mansdorf, Eds., ASTM International, West Conshohocken, PA, 1996, pp. 327–346.
[11] ASTM D1776, 2008, "Standard Practice for Conditioning and Testing Textiles,"*Annual Book of ASTM Standards,*Vol. 07.01, ASTM International, West Conshohocken, PA, 2008.
[12] Jeguirim, S. E., Dhouib, A. B., Sahnoun, M., Cheickrouhou, M., Schacher, L., and Adolphe, D., "Sensory and Instrumental Techniques Evaluating the Effect of Structure Parameters on the Tactile Properties of Knitted Fabrics," *J. Texture Stud.*, Vol. 41(5), 2010, pp. 714–735.
[13] Avinc, O., Wilding, M., Gong, H., and Farrington, D., "Effects of Softeners and Laundering on the Handle of Knitted PLA Filament Fabrics," *Fibers Polym.*, Vol. 11(6), 2010, pp. 924–931.
[14] Lam, Y. L., Kan, C. W., Yuen, C. W. M., and Au, C. H., "Objective Measurement of Fabric Properties of the Plasma-treated Cotton Fabrics Subjected to Cocatalyzed Wrinkle-resistant Finishing," *J. Appl. Polym. Sci.*, Vol. 119(5), 2011, pp. 2875–2884.
[15] Liu, R., Kwok, Y., Li, Y., and Lao, T., "Fabric Mechanical-surface Properties of Compression Hosiery and Their Effects on Skin Pressure

Magnitudes When Worn," *Fibres & Textiles in Eastern Europe*, Vol. 18(2), 2010, pp. 91–97.

[16] Radhakrishnaiah, P., Tejatanalert, S., and Sawhney, A. P. S., "Handle and Comfort Properties of Woven Fabrics Made from Random Blend and Cotton-covered Cotton Polyester Yarns," *Text. Res. J.*, Vol. 63(10), 1993, pp. 573–579.

[17] Behera, B. K., Ishtiaque, S. M., and Chand, S., "Comfort Properties of Fabrics Woven from Ring-, Rotor-, and Friction-spun Yarns," *J. Text. Inst.*, Vol. 88(3), 1997, pp. 255–264.

[18] Cardello, A. V., Winterhalter, C., and Schutz, H. G., "Predicting the Handle and Comfort of Military Clothing Fabrics from Sensory and Instrumental Data: Development and Application of New Psychophysical Methods," *Text. Res. J.*, Vol. 73(3), 2003, pp. 221–237.

[19] Sztandera, L. M., "Predicting Tactile Fabric Comfort from Mechanical and Handfeel Properties Using Regression Analysis," *Proceedings of the 8th WSEAS International Conference on Applied Computer Science (ACS '08)—Recent Advances on Applied Computer Science*, Venice, Italy, November 21–23, 2008, WSEAS, Athens, Greece, 2008, pp. 217–220.

[20] White, M. K. and Ronk, R., "Chemical Protective Clothing and Heat-stress," *Prof. Saf.*, Vol. 29(12), 1984, pp. 34–38.

[21] ASTM F1868, 2009, "Standard Test Method for Thermal and Evaporative Resistance of Clothing Materials Using a Sweating Hot Plate," *Annual Book of ASTM Standards,* Vol. 11.03, ASTM International, West Conshohocken, PA.

[22] ASTM D737, 2008, "Standard Test Method for Air Permeability of Textile Fabrics," *Annual Book of ASTM Standards*, Vol. 07.01, ASTM International, West Conshohocken, PA.

[23] Truong, Q. and Wilusz, E., "Chemical and Biological Protection," *Textiles for Protection*, R. A. Scott, Ed., Woodhead, Cambridge, England, 2005, pp. 557–594.

[24] Gibson, P. W., Kendrick, C. E., Rivin, D., and Charmchi, M., "An Automated Dynamic Water Vapor Permeation Test Method," *Performance of Protective Clothing*, ASTM STP 1273, J. O. Stull and A. D. Schwope, Eds., ASTM International, West Conshohocken, PA, 1997, pp. 93–107.

[25] McCullough, E. A., Kwon, M., and Shim, H., "A Comparison of Standard Methods for Measuring Water Vapour Permeability of Fabrics," *Meas. Sci. Technol.*, Vol. 14, 2003, pp. 1–7.

[26] ASTM F2298, 2009, "Standard Test Methods for Water Vapor Diffusion Resistance and Air Flow Resistance of Clothing Materials Using the Dynamic Moisture Permeation Cell," *Annual Book of ASTM Standards*, Vol. 11.03, ASTM International, West Conshohocken, PA.

[27] Kawabata, S., *The Standardization and Analysis of Hand Evaluation*, 2nd ed., Hand Evaluation and Standardization Committee, Textile Machinery Society of Japan, Osaka, Japan, 1980.

[28] Rego, J. M., Verdu, P., Nieto, J., and Blanes, M., "Comfort Analysis of Woven Cotton/Polyester Fabrics Modified with a New Elastic Fiber, Part 2: Detailed Study of Mechanical, Thermo-Physiological and Skin Sensorial Properties," *Text. Res. J.*, Vol. 80(3), 2010, pp. 206–215.

[29] Havenith, G., Holmer, I., Den Hartog, E. A., and Parsons, K. C., "Clothing Evaporative Heat Resistance—Proposal for Improved Representation in Standard and Models," *Ann. Occup. Hyg.*, Vol 43(5), 1999, pp. 339–346.

Performance of Protective Clothing and Equipment: Emerging Issues and Technologies
STP 1544, 2012
Available online at www.astm.org
DOI:10.1520/STP104089

Kristen L. Hultzapple,[1] *Stephen S. Hirsch,*[2]
John Venafro,[3] *Stephen Frumkin,*[4] *Janet Brady,*[5]
Carole Winterhalter,[6] *and Scena Proodian*[7]

Chemical Protection Garment Redesign for Military Use by the Laboratory for Engineered Human Protecton Years 2005–2011

REFERENCE: Hultzapple, Kristen L., Hirsch, Stephen S., Venafro, John, Frumkin, Stephen, Brady, Janet, Winterhalter, Carole, and Proodian, Scena, "Chemical Protection Garment Redesign for Military Use by the Laboratory for Engineered Human Protecton Years 2005–2011," *Performance of Protective Clothing and Equipment: Emerging Issues and Technologies* on April 16, 2011 in Anaheim, CA; STP 1544, Angie M. Shepherd, Editor, pp. 74–107, doi:10.1520/STP104089, ASTM International, West Conshohocken, PA 2012.

ABSTRACT: The Laboratory for Engineered Human Protection (LEHP) at Philadelphia University investigated materials and developed design concepts to optimize the comfort, sizing, and protection of chemical protective

Manuscript received June 8, 2011; accepted for publication February 27, 2012; published online September 2012.

[1]Philadelphia Univ., School House Ln. and Henry Ave, Philadelphia PA 19144, email: hultzapplek@philau.edu

[2]Philadelphia Univ., School House Ln. and Henry Ave, Philadelphia PA 19144, email: hirschs@philau.edu

[3]Philadelphia Univ., School House Ln. and Henry Ave, Philadelphia PA 19144, email: JV611@yahoo.com

[4]Professor, Philadelphia Univ., School House Ln. and Henry Ave, Philadelphia PA 19144, email: frumkins@philau.edu

[5]Professor, Philadelphia Univ., School House Ln. and Henry Ave, Philadelphia PA 19144, email: bradyj@philau.edu

[6]Natick Soldier Systems Center, Kansas St., ATTN: AMSRD-NSC-SS-MS, Natick, MA 01760–5020, email: carole.winterhalter@us.army.mil

[7]Natick Soldier Systems Center, NCTRF, Attn: Scena Proodian/ Bldg 86, Kansas St., Natick, MA 01760, email: sproodian@nctrf.natick.army.mil

garments. Comfort was defined as ergonomic, biophysical, and tactile. This paper describes the iterative design methods used by LEHP's Garment Team (GT) and the results of those methods. Protective clothing is generally bulky, hot, and uncomfortable, adding to the physical burden a soldier endures. LEHP's goal was to develop a more comfortable uniform for use in environments threatened with chemical warfare. The GT designed and produced six prototype iterations described as Generations 1–6. Each included novel design concepts such as built-in kneepad pockets, strategic body/joint articulation, and a shaped structured hood. A novel hood/mask interface was also developed and refined. Two garment styles were produced. Generations 1 through 4 were a coverall with a fixed hood, while Generations 5 and 6 explored a two-piece jacket/trouser ensemble with two different hood designs—fixed and detachable. The two-piece style featured a mid-torso closure that integrated the two pieces into a system that could be doffed as a one-piece garment. This allows for various size jacket and trouser combinations and provides size flexibility to accommodate the fit for a wide range of body types and sizes. In all prototypes, the carbon layer was a separate component. This may reduce waste by allowing the expired carbon items to be removed, disposed, and replaced independent of the non-contaminated shell garment. This may increase the shell's wear life, where it could continue to function as a duty uniform and be returned to service for chemical protection. LEHP used outside testing facilities for Fluorescent Aerosol Screening (FAST), Contaminated Doffing (CD), and Human Factors (HF) studies. In-house evaluations included Sweating Manikin and Human Factors studies.

Introduction

The Laboratory for Engineered Human Protection (LEHP) was created at Philadelphia University using funds from Department of Defense University Research Initiative grants that were administered by the Natick Soldier Research Development and Engineering Center (NSRDEC). This paper describes the process that LEHP's Garment Team (GT) used during the past six years. Working closely with NSRDEC and the Navy Clothing and Textile Research Facility (NCTRF), the GT created uniforms intended for chemical defense. The goal was to produce garments that facilitate user comfort, mobility, performance, and functionality, while providing protection. The GT researched currently available chemical protective garments such as the Joint Service Lightweight Integrated Suit Technology (JSLIST) and the Joint Protective Air Crew Ensemble as well as commercially available garments in the fire, emergency rescue, and outdoor extreme sporting goods industries. The GT also worked closely with other LEHP teams to design, produce, and test prototype chemical protective garments. Those LEHP teams include the Materials Evaluation Team (MET), the Biophysics Team, and the Artificial Intelligence Team (AI).

Testing

The following tests were performed:

- Fluorescent Aerosol Screening Test (FAST)—This test was performed at Research Triangle Institute (RTI) in Research Triangle Park, NC. The participant was dressed in the prototype garment with ancillary equipment in Mission Oriented Protective Posture 4 (MOPP 4). MOPP levels from 1–4 describe the amount of protection that a user has donned. He then entered a large chamber and performed a series of motions for approximately one-half hour. A large fan distributed fluorescent fingerprint powder into the chamber throughout the duration of the test. The garment was doffed and any interface or closure infiltration of the simulant was assessed using a black light. This test provided valuable data about where contaminant penetrated the garments and reached the body through breaches at the interfaces.

- Contaminated Doffing—This test took place at Hazmat Science Applications in Santa Fe, NM. The test assessed ability to doff the contaminated garment without transfer of simulant to the wearer or assistant. During this evaluation the test participant was dressed in the prototype garment in MOPP 4 and covered in a fluorescent fingerprint powder as specified in the protocol and then processed through a proposed doffing sequence. Once the garment had been completely doffed a black light was used to reveal any contaminant that had been transferred onto the body.
- Human Factors (external)—This test was conducted at the NSRDEC. It included donning the garment in various MOPP levels, and performing a preselected motion routine. Participants also donned various ancillary pieces of equipment such as: helmets, backpacks, body armor, or tactical vests. These motion exercises provided an independent evaluation of the garment using military personnel who had received previous chemical/biological training.
- Human Factors (internal)—This series of tests was conducted at Philadelphia University in conjunction with the Biophysics Team. The motion routine exercises were based on guidelines provided by and consistent with the NSRDEC. Once the selected number of trials had been completed, the Biophysics Team analyzed the data for statistical validity. Results from each Generation prototype could then be compared to another Generation prototype. This test also proved invaluable to the GT for quick design changes before sending the garments for more sophisticated testing.

Design Overview

LEHP was launched in 2004 with a charter to design and produce comfortable, protective prototype garments intended for chemical defense. One goal was to reduce the amount of carbon components by evaluating various carbon design applications with advanced shell fabrics. Emphasis was placed on designing a carbon component that was separate from the external shell fabric configuration. This concept allowed the wearer to remove and dispose of an expired carbon layer and replace it with a fresh set, potentially extending the life of the non-contaminated shell garment. The Generation 2 and 3 outer garment prototypes incorporated a selectively permeable membrane (SPM) material. Through the design and evaluation process, this goal was expanded and the GT began using a breathable shell system supported by carbon component design.

Another goal was to design a suit that could be worn by all services and would be one-size-fits-many. Various design ideas resulted from brainstorming sessions that contributed to the development of the Generation 1 prototype.

Generation 1 Methods

The Generation 1 prototype (see Fig. 1) included an attached hood configured to interface with the Joint Service General Purpose Mask (JSGPM). The hood featured a removable carbon cord to help fill in the gaps between the mask and the actual hood fabric. Other features of the garment included an asymmetrical

FIG. 1—*Generation 1 prototype sketch.*

front zipper and a left arm zipper to facilitate the doffing process. A zipper was also included at the lower front torso; it opened completely from the center front waist to the center back waist to facilitate field waste relief.

To address the need for a garment to be "one size fits many," zippered lower arm and leg cuffs were added to accommodate different user heights. Shorter wearers could simply zip on a shorter cuff, and taller wearers could zip on longer versions. This idea allowed the garment to accommodate a variety of body heights and may reduce the core body design to fewer inventory size requirements. A waist cinching mechanism and a center back shoulder cinch were also included inside the garment to draw the garment closer to the body.

Hook and loop tape was used to secure the interfaces at the wrist, ankle, and mask opening to help minimize agent penetration.

The Generation 1 prototype was produced as muslin until a suitable SPM fabric was identified.

Generation 2 Methods

The Generation 2 prototype (see Fig. 2) was constructed using ultrasonic seaming methods with an SPM fabric sourced from a leading fabric company.

FIG. 2—*Generation 2 prototype.*

Carbon backup panels were placed behind all zippered closures, carbon cuffs were added at the wrist and ankles, and a carbon bib was located at the face openings to reduce penetration caused by bellowing of the garment. These backups were secured by hook and loop tape for quick and easy replacement when the carbon's usable life was spent. This design reduced the carbon fabric requirement, potentially reducing costs and disposal of material waste. Water resistant zippers were chosen because they provided moisture barrier protection and were not as bulky, stiff, noisy, and difficult to unzip as available waterproof zippers.

A Jentschmann ultrasonic seaming machine was used to seal the two layers of fabrics and the adhesive tape.

Because of limiting characteristics of the ultrasonic seaming system compared with conventional sewing methods, considerations were taken when designing the garment. Tight curves had to be smoothed, reduced, and streamlined to facilitate seaming with the ultrasonic method. This led to a raglan style sleeve configuration. Almost the entire garment was constructed using ultrasonic fabrication and subsequently seam sealed. The only sewn parts of the Generation 2 garment were small reinforcement bar tacks placed strategically at high stress points on the garment. These sewn bar tacks were then covered with small round, nickel-sized patches of the adhesive-backed SPM fabric that was bonded to the garment. This generation design was similar to the Generation 1 prototype that preceded it, with a few upgrades and revisions. The interface with the mask now included a draw cord to cinch the hood tightly to the mask to avoid agent penetration. Carbon backups were deemed necessary at the interface points and interface closures. Special attention was focused on the most important areas surrounding the head, neck, mask, and hood opening. A carbon bib was designed (see Fig. 3) that attached into the SPM shell hood with hook and loop tape. This interface was then secured around the mask using elastic. The bib was added to the design as a secondary backup when it was discovered that the hood/mask interface proved the most challenging area to seal.

The center front zipper, side doffing zipper, and the waste relief zipper all remained unchanged in the Generation 2 prototype. Underarm zippers were added to help alleviate heat buildup in the suit while not in MOPP 4. All zippers in this garment were backed up with removable carbon flaps.

The removable wrist and leg cuffs were retained but a zipper was added to ease the doffing process, particularly on the leg cuffs (see Fig. 4). An inner removable carbon cuff was attached to the wrists and ankles to reduce the impact of the bellows effect. The bellows effect occurs in almost all clothing, but more specifically in low air permeable fabrics due to the movement of the body drawing in air through breaches at the interfaces. Unless a hermetic seal is obtained at the interfaces, it was determined that a carbon cuff was necessary to provide additional protection. The hook and loop flaps on the shell could then be tightly fastened around the wrist and ankle, respectively, to create a secure closure. To enable a large size range of soldiers to use one garment,

FIG. 3—*Generation 2 carbon bib.*

elastic cords set into a channel with cord lock closures were placed on the back at the waist and shoulder areas.

An articulated shaped kneepad pocket was designed and included on the garment. This pocket contained a removable soft kneepad that provided comfort to the soldier while kneeling or crawling (see Fig. 4). The kneepad pocket also provided an extra layer of reinforcement to a high abrasion area. A similar system was attached onto the elbow to shoulder area, although this reinforcement patch did not contain a pocket for removable padding.

Generation 2 Results

FAST Evaluation

At RTI, three tests were conducted with the Generation 2 prototype in order to assess the amount of protection the garment provided and to evaluate the very first design in chemical protective fabric. Approximately 15–20 mins into the first test there was a bonding failure between the zipper tape and the SPM fabric (see Fig. 5). It was decided that for the two remaining tests the waste relief zipper would be secured with duct tape.

Some miscommunication resulted in the wrong gas mask being used in Tests 1 and 3. The interface of the hood with the incorrect masks was not ideal, and simulant was clearly present on the face and neck areas on all three tests (see Figs. 7 through 9). Of particular note, simulant, usually not seen without

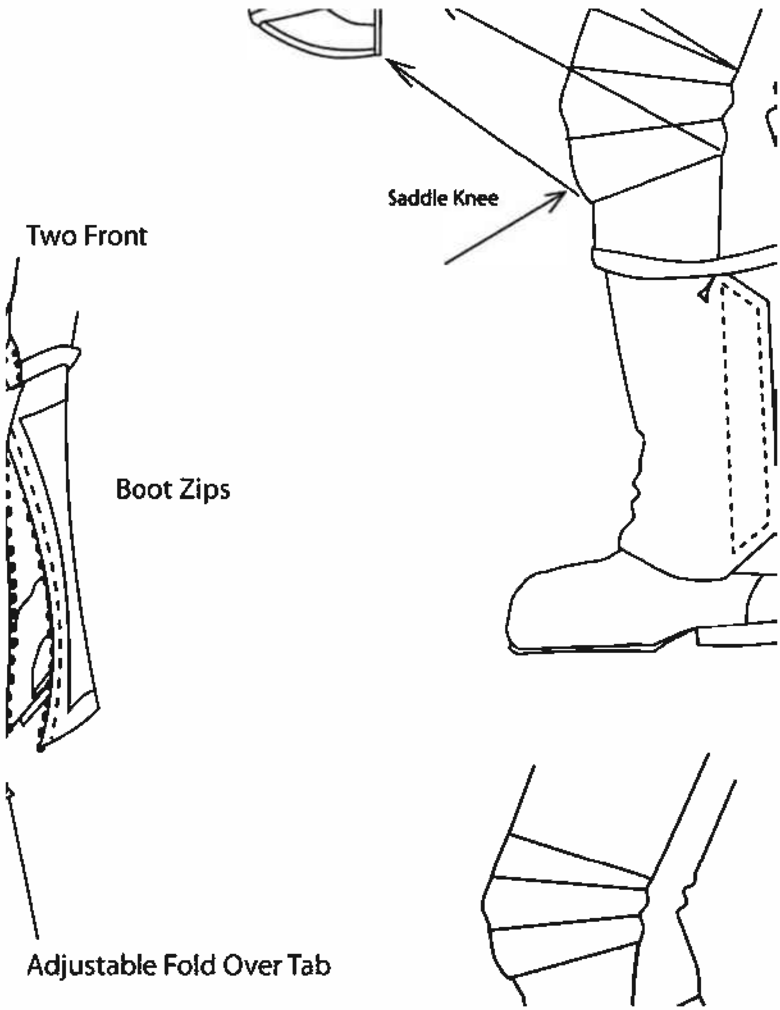

FIG. 4—*Generation 2 detailed sketch of zip off cuffs, carbon cuffs and kneepad pocket.*

the black light, was observed on Test 2 in the temple area. This is noteworthy because this particular test used the JSGPM, which appears to have a slight concavity at the temple area. This is a region to which LEHP continued to direct much focus for redesigning subsequent prototype hood openings to achieve a more satisfactory seal.

The first test saw high deposits of simulant on the body specifically around the crotch, lower torso, and upper leg areas; this was likely a result of the bonding failure at the relief zipper. The two subsequent tests saw significantly less simulant on the body. The outline of cleaner areas was clearly visible where

FIG. 5—*Generation 2 bonding failure.*

the bib ended and where the carbon flap backing up the center front zipper rested against the skin, as shown in Fig. 10. On this test there were also light hazes of simulant on the lower legs and arms.

In the second test, deposition of simulant on the torso was lighter than in the first, perhaps resulting from the fact that the correct mask was worn and thus a better seal was achieved at the hood/mask interface (see Fig. 11). The

FIG. 6—*Generation 2 relief zipper duct taped.*

FIG. 7—*Generation 2 Test 1 head.*

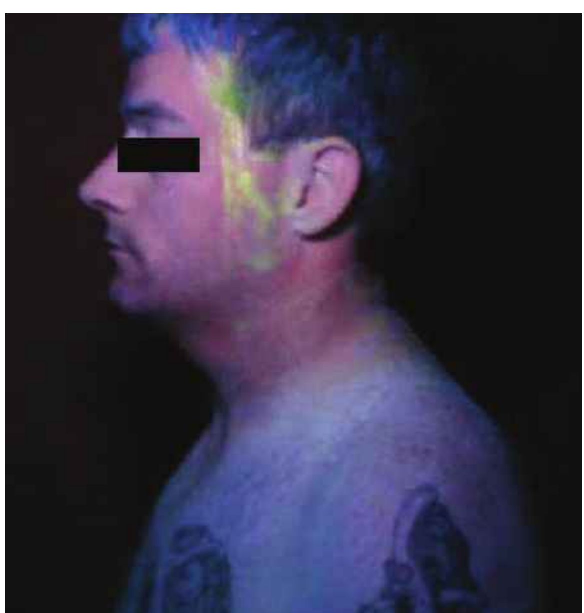

FIG. 8—*Generation 2 Test 2 head.*

FIG. 9—*Generation 2 Test 3 head.*

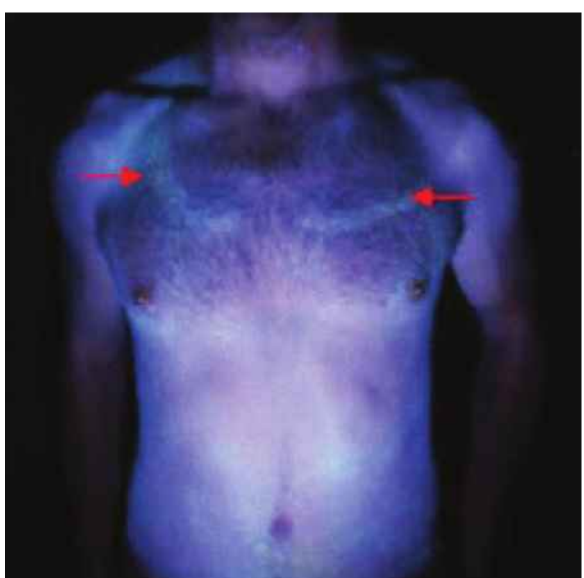

FIG. 10—*Generation 2 Test 1 torso.*

FIG. 11—*Generation 2 Test 2 torso.*

outlines of the bib and center front carbon flap are not visible, although heavier deposits were found on the forearms and lower legs.

The third test saw a light haze of simulant on much of the body. Again the outlines of the bib and center front carbon flap were visible, although fainter on this test (see Fig. 12).

Human Factors at NSRDEC

An evaluation was done of the Generation 2 prototype to assess fit, range of motion, and human comfort while wearing the ensemble. The results of this

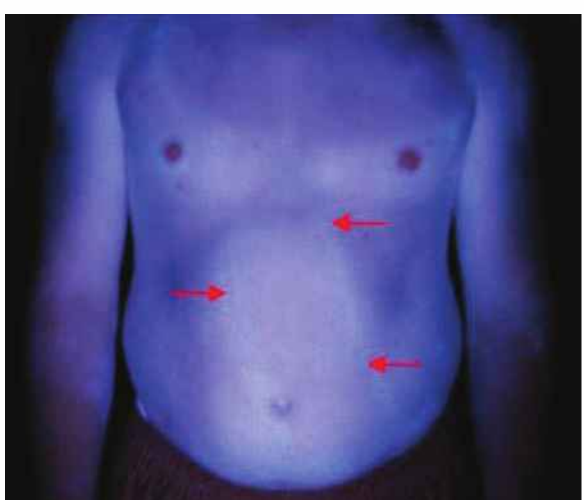

FIG. 12—*Generation 2 Test 3 torso.*

FIG. 13—*Generation 3 prototype.*

evaluation found that donning the Generation 2 garment was cumbersome and somewhat difficult; the sleeve/leg zippers were of concern, as soldiers had trouble closing them. After several trials they found that the garment was much easier to don when the left sleeve doffing zipper was closed. In

FIG. 14—*Generation 3 carbon balaclava.*

addition, the test subjects had difficulty securing the cinching mechanisms around the hood. Some reported discomfort with the cord locks because they created pressure points poking into their bodies. Overall, the garment was determined to be physically comfortable because it offered free range of motion without pinching or binding. The location of the left sleeve doffing zipper was well received by the soldiers; they felt it would substantially help to doff the garment when contaminated. Durability issues were evident in the form of hook/loop tape detachment and some seam or hem separation, prompting poor evaluation for this feature. Subsequent adhesive and machine bonding calibrations as well as hook/loop tape evaluations were performed in conjunction with the Jentschmann representative to eliminate these issues in future garments.

Generation 3 Methods

Continuing with the iterative development approach, the Generation 3 prototype built upon lessons learned from testing and feedback on the Generation 2 garment (see Fig. 13). Because of bonding issues during FAST evaluation and durability findings from Human Factors, much time was spent improving the ultrasonic seaming methods for the next prototype. In order to cut down on production time and increase flexibility, select portions of the ensemble were joined using conventional sewing techniques, such as overlapping outer edges that did not penetrate the body of the garment and hook and loop tape sewn onto wrist and ankle flaps. Improved machine settings were also found for affixing the hook and loop tape to the SPM fabric.

Design changes included a new hood configuration to improve the interface with the mask. Because soldiers found the carbon bib difficult to attach to the shell, a completely separate carbon balaclava was designed to replace it (see Fig. 14). The carbon balaclava differs from the carbon bib in that it completely covers the head, like a hood, with an opening for the mask, while the carbon bib only protected around the face and not the back of the head. Underarm zips were removed because of concern that soldiers might forget to close them when transitioning from a lower MOPP level to MOPP 4. The removable zip-off cuffs were also eliminated from the new design after being universally disliked during human factors testing; the cost benefit of eight fewer zippers was also a factor. The cinching mechanism at the shoulder was removed because of cord lock discomfort comments from human factors testing. The back waist cinch was changed to an internal elastic belt which improved the fit of the coverall waist. Kneepad pocket openings were reversed to open at the bottom instead of the top to reduce the risk of liquid agents pooling in the pocket. The most significant change was addition of an entire one-piece carbon body suit to be worn underneath the SPM shell.

Generation 3 Results

FAST Evaluation

Consistent with LEHP's original goal to reduce the amount of carbon components, during FAST one garment was tested using carbon cuffs as in Generation 2, and two garments were tested using the carbon undergarment to compare the difference in the systems' performance and protection. A significant reduction in the amount of simulant was found on the head demonstrating that the new hood configuration was effective. Only small bright spots were seen in the temple area, again possibly due to the concave nature of the JSGPM at this spot. In Test 1 bright spots were seen on both sides of the face, while in Tests 2 and 3 bright spots were only seen on one side of the face (see Figs. 15 through 17).

Aerosol simulant deposits were seen on the body and the faint line from the edge of the carbon balaclava could be seen on the torso in Test 1 (see Fig. 18). There was also a light haze of simulant on the forearms and lower legs. This configuration included the shell worn with carbon cuffs along with carbon backup flaps at each zipper, and the carbon balaclava. Tests 2 and 3 exhibited improved results with seemingly clean torsos, arms and legs (see Figs. 19 and 20). The shell garment in Tests 2 and 3 was worn with a one-piece stretch carbon body suit and the carbon balaclava. Carbon cuffs and carbon flaps were not necessary for these tests because the carbon body suit provided all over protection.

FIG. 15—*Generation 3 Test 1 head.*

FIG. 16—*Generation 3 Test 2 head.*

Contaminated Doffing

Generation 3 was the first LEHP prototype to be tested at Hazmat Science Applications to evaluate design of the garment and viability of removing the coverall without recontaminating the soldier. Because of the difference seen in FAST between the single garment that was worn with the carbon cuffs and

FIG. 17—*Gen 3eration Test 3 head*

FIG. 18—*Generation 3 Test 1 torso.*

closure flaps, and the outer garment worn with the full carbon undergarment, it was decided to conduct four tests of contaminated doffing. The first two tests would use the SPM shell with the carbon cuffs and closure flaps, and the last two would use the SPM shell with the carbon undergarment.

FIG. 19—*Generation 3 Test 2 torso.*

FIG. 20—*Generation 3 Test 3 torso.*

A significant difference was seen in performance of the two garment ensembles during the contaminated doffing evaluations. The two-garment configuration (SPM shell and carbon undergarment) was far superior to the single garment configuration with carbon cuffs and closure flaps. After doffing, simulant was seen at various points all over the body in both tests using the single garment system. In tests with the outer garment/carbon undergarment ensemble, one test had a spot of simulant on the temple and one speck on the chest, while the other test came out completely clean. These findings would impact future design changes.

Human Factors at NSRDEC

Results of human factors evaluations at NSRDEC showed that the carbon balaclava was an improvement over the bib style. The balaclava was more efficient to don than having to secure the bib into the hood. The hood was an improvement, but there was some difficulty in achieving a smooth attachment of the neck flaps under the chin. With removal of the zippers at the wrist and ankle areas, the hook and loop flaps were easier to secure and open. The wrist and ankle interfaces also did not move out of their original positions, indicating that they provided good coverage in those areas.

Generation 4 Methods

The Generation 4 garment saw many modifications based on the test results of the Generation 3 prototypes (see Fig. 21). The hood/mask interface design was streamlined to make it more comfortable and easier to use. The elastic belt that was introduced in Generation 3 was redesigned and an elastic shoulder strap

FIG. 21—*Generation 4 prototype.*

was added to the inside of the garment to stabilize shoulder fit, control equipment (i.e., backpack) positioning, and prevent neck pulling discomfort. Kneepad retention straps were also added to secure the kneepad into place while bending, running, or crawling, and to reduce noise.

Excellent results from the carbon body suit testing drove the design and fabric changes in this generation. The Garment Team continued to use separate carbon suits in all of the Generation 4 prototypes. In addition to the benefits of doffing separate garment layers, a discrete carbon layer has the potential to reduce costs and waste of chemical/biological ensembles. The current fielded JSLIST has a lifespan of 120 days once removed from the vacuum sealed pouch. The entire garment has to be disposed of upon expiration of 120 days whether it is contaminated or not. By separating the carbon and the outer shell layers, the user could retain the shell and replace only the carbon component in the Generation 4 design.

Two different carbon undergarment layers were designed; one a tight-fitting knit undergarment with stretch characteristics much like the one used in the Generation 3, and the other a loose-fitting woven non-stretch carbon layer that could be worn over a duty uniform. Either carbon layer could be used with the same shell or the shell alone could be worn as a duty uniform. All carbon layers were sewn.

On the basis of test participant comments and results, observations of participants wearing the garments, and high evaporative resistance properties measured using a Sweating Guarded Hot Plate (SGHP), the SPM fabric used in the Generation 2 and 3 prototypes was dropped from the evaluation.

LEHP collected a number of breathable fabric candidates for the Generation 4 prototype to be used in conjunction with the carbon-based one-piece undergarment. Generation 4 is a sewn garment without ultrasonic bonding and seam sealing. After an initial downselection by MET, four shell garments and four carbon undergarments were produced for human factors evaluation before being sent to FAST and contaminated doffing evaluations. Figure 22 is an overview of fabrics used in the Generation 4 prototypes. Two shell fabrics, 78C and 85M, were identical except for the addition of a tricot backer on 78C to protect the aerosol membrane. The GT wanted to experiment with this fabric to determine if the wearer could notice a difference in comfort between the two. None of the participants found any difference between the two materials.

Generation 4 Results

Human Factors at Philadelphia University

It was observed that the membrane of 85M began rubbing off during testing because it was not protected by the tricot; this led to removal of 85M from future garment evaluations.

Human Factors at NSRDEC

Overall, the improvements made to the design resulted in a more comfortable garment that was easier to don. The interface at the neck demonstrated continued improvement. This prompted a decision to move to a two-piece design version in Generation 5. Both test participants indicated they preferred the stretch undergarment to the non-stretch loose carbon undergarment.

Thermal Manikin

Thermal and evaporative resistance tests were performed in accordance with ASTM F1291 [1] and ASTM F2370 [2] on Generation 4 LEHP Garment ensembles. The results indicated that two of the ensembles, 63A liner/78C shell and 96X liner/31B shell exhibited improved cooling power compared to Generation 4 garments produced in current military fabrics.

MET also investigated thermal and evaporative resistance of two liner fabrics; each exhibited very different fabric mechanical properties. Specifically,

LEHP Code	LEHP Fabric Characteristics					
	Fabric Structure	Structure Type	Fiber Blend	Coloration Method	Functional Treatment	Weight (oz/sq. yard)
85M	laminate	330d Cordura shell with microporous ePTFE membrane	100% nylon 6,6 330 denier (Cordura)	jet dyed green	microporous ePTFE membrane, durable water repellent finish	5.00
78C	laminate	330d Cordura shell with microporous ePTFE membrane and tricot backing	100% nylon 6,6 330 denier (Cordura) polyester tricot knit backing	jet dyed green	microporous ePTFE membrane, durable water repellent finish	6.12
31B	woven	n/a	multiple fibers	universal camouflage print	durable water- and oil-repellent	5.20
61U	woven	n/a	flame-resistant	dyed green	durable water- and oil-repellent	5.30
63A	knit	active carbon filter material, polyester/ elastane 2-way stretch jersey knit material	polyester/ elastane carbon	dyed black knit	N/A	8.60
40C	laminate	spherical carbon with multiple fabrics	fiber combination with carbon	dyed green	N/A	5.84
54M	laminate	spherical carbon	multiple fibers with carbon	dyed black	N/A	6.74
96X	trilaminate	spherical carbon with multiple fabrics	fiber combination with carbon	dyed gray	N/A	11.42

FIG. 22—*Generation 4 fabric candidates.*

one was a stretch fabric (63A) and the second non-stretch (54M). Each fabric was produced in two garment designs, loose and tight fitting, with the goal of understanding the effect of garment design as well as fabric properties on thermal and evaporative resistance. The studies determined that the tight-fitting design, regardless of fabric properties, resulted in lower thermal and evaporative resistance [3,4]. Additionally, the stretch material exhibited greater tactile comfort through lower bending and shear rigidity properties, which lend themselves to a tight-fitting garment [4]. In summation, 63A liner fabric in the tight-fitting design was found to exhibit the lowest thermal and evaporative resistance [3,4]. Manikin tests described were all static.

Regression Analysis

Using fabric test data provided by MET the AI Team developed a regression analysis for tactile comfort [5]. This provided a tactile comfort ranking for the set of liner fabrics and the set of shell fabrics under investigation for garment development. On the basis of this analysis, the liner fabrics 63A and 96X, as well as shell fabrics 78C and 31B, were found to be the most comfortable. Garment evaluations and tests conducted later in the schedule and described in what follows supported these findings.

Fabric Downselection

After weighing the results from the previous four prototype evaluations, the team decided to use the 63A carbon fabric and 78C shell fabric for FAST and contaminated doffing evaluations for Generation 4. Carbon fabric 63A was ranked the most comfortable overall for an undergarment fabric and also received the highest tactile comfort score using AI regression analysis. The carbon liner was designed to be worn directly against the skin making 63A an appropriate fabric for further prototype development. In addition, shell fabric 78C was paired with 63A because of supplier requirements and guidelines.

FAST Evaluations

Overall results of FAST showed that the head and face were relatively clean (see Figures 23 through 25). Test 1 had a bright spot at the temple area on one

FIG. 23—*Generation 4 Test 1 head.*

FIG. 24—*Generation 4 Test 2 head.*

side along the mask. Test 2 showed a haze of simulant in the hair around the ears on both sides with clean lines where the mask straps sat. A slight modification was made to the carbon balaclava between Tests 2 and 3 by adding a knit semicircle insert into the temple area on each side. Results from Test 3 showed the best results in the head area with only a very slight haze around the ears.

FIG. 25—*Generation 4 Test 3 head.*

FIG. 26—*Generation 4 Test 1 torso.*

In all three FAST tests, the torso, arms, and legs were clean (see Figures 26 through 28). Only on the third test was a very slight haze of simulant observed on the upper back between the shoulder blades.

Contaminated Doffing

Overall, the test results from Contaminated Doffing were very positive. In two of the tests, the subjects were able to doff the garment without any contamination. In the remaining test, decontamination solution was observed on the right collar bone area and on the temple of the subject.

Generation 5 Methods

Production of Generation 5 garments proceeded using the same fabrics that were selected for Generation 4. This design retained many of the same features, but they were converted from a coverall to a jacket and trouser system (see Figure 29). This two-piece system allows for split sizing. For example, if a soldier wore a medium pant and a large jacket, the Generation 5 design would accommodate various size combinations. This flexibility in sizing lowers the logistical burden by reducing the need to produce custom-sized garments. Being a two-piece separate system, the jacket would be easier to remove than a coverall; therefore, the left sleeve doffing zipper was eliminated. Similarly, the relief

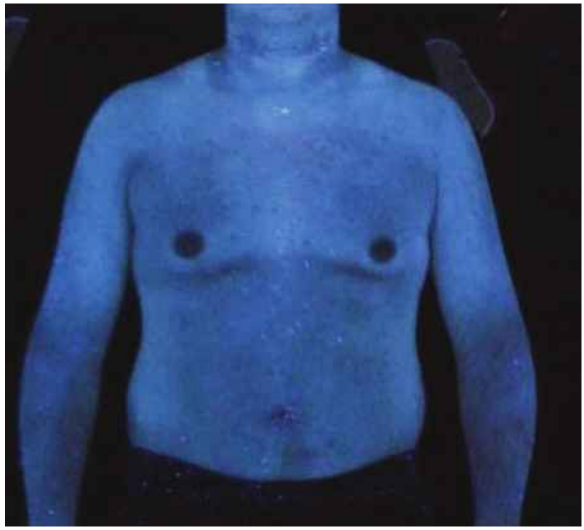

FIG. 27—*Generation 4 Test 2 torso.*

zipper was replaced by a fly zipper. Modifications were made to the hood design to again improve the interface with the mask. To facilitate range of motion in the arms a bi-swing back was integrated into the jacket design. Gripper fabric was added at the shoulders to prevent equipment slippage.

FIG. 28—*Generation 4 Test 3 torso.*

FIG. 29—*Generation 5 prototype.*

FIG. 30—*Generation 5 Test 1 head.*

FIG. 31—*Generation 5 Test 2 head.*

FIG. 32—*Generation 5 Test 3 head.*

Generation 5 Results

FAST Evaluations

In Test 1 there was a slight haze of simulant above the ear with clean areas where the mask straps sat on the right side of the face. In Test 2, blue haze was seen above the ears and the mask straps were again visible. There were also two bright spots of simulant on the upper jaw at the mask edge on both sides of the face. Slight haze was seen on both sides of the face in Test 3, and a brighter streak was present on the left cheek on the mask edge (see Figures 30 through 32).

A slight haze on the chest was seen in both Tests 1 and 2, so before Test 3 the possible breach points were duct taped to see the difference in performance. The duct tape sealed all the places where any simulant was penetrating the garment at the center front closure area, and no haze was seen on the body (see Figures 33 through 35).

Contaminated Doffing

A few drip marks of decontamination solution were viewed on the back left shoulder and the left shin in the first test of contaminated doffing. The second and third tests were clean except for a slight haze on the abdomen slightly above and to the left of the navel. These hazes were consistent with those seen at FAST, which led the GT to believe that there was a breach point at the center front closure where the jacket and pant overlap.

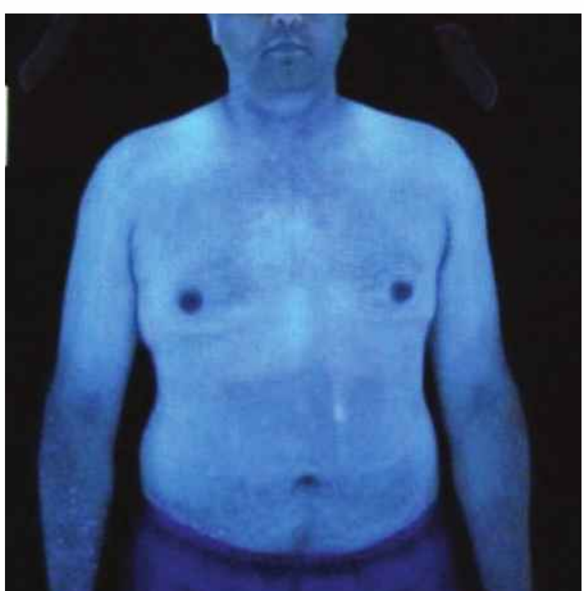

FIG. 33—*Generation 5 Test 1 torso.*

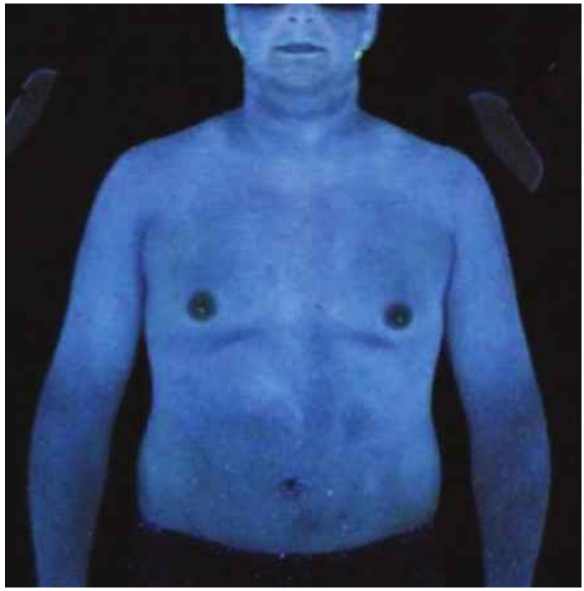

FIG. 34—*Generation 5 Test 2 torso.*

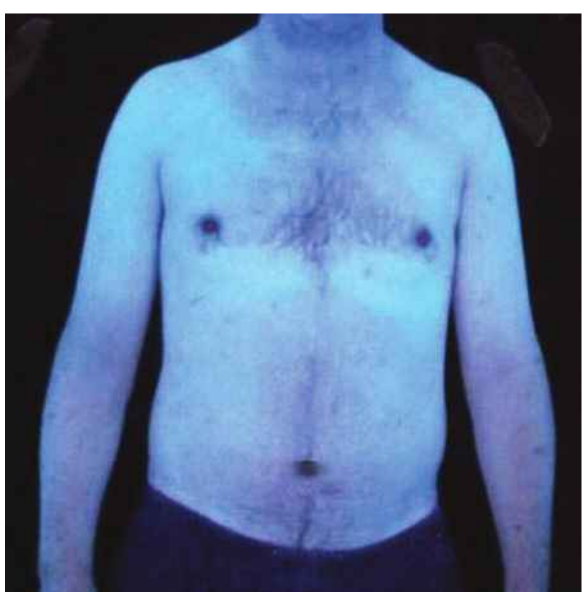

FIG. 35—*Generation 5 Test 3 torso.*

Human Factors at NSRDEC

The Generation 5 garment was viewed to be lightweight, easy to don, and comfortable. It also provided good range of motion. The main complaint was that the center front closure was somewhat confusing to attach and created uncomfortable bulk underneath the jacket during a stomach crawl. Overall the ensemble was favorably perceived.

Generation 6 Methods

Generation 6 was the evolution of the two-piece garment system introduced in Generation 5 (see Fig. 36). The new goal was to trim down the garment body to fit more closely to a duty uniform style ensemble. Two versions of the Generation 6 were developed. The Generation 6.1 jacket has a fixed (attached) hood. The Generation 6.2 jacket has a zip-off detachable hood with a fold-down collar neck that resembles a duty uniform when the hood is detached. Other modifications to both Generation 6 versions included the following: the amount of ease and fit over the body was slimmed down in the jacket and

FIG. 36—*Generation 6 prototype.*

trousers; both hoods were modified to reduce bulk to provide optimal fit when worn with a helmet; and stretch panels were inserted into a reshaped front neck shoulder area to increase neck range of motion and shoulder reach flexibility. These panels were backed up with shell fabric to prevent compromise of the protection capability of the garment. Further, the inside flap was redesigned as a dual layer overlapping the inner flap system that backs up the center front closure to create a deliberate path to channel any contaminant up and out of the system at the top neck area. This new configuration allows for improved interface with the jacket and trouser. This modification also resolved the breach point identified in Generation 5 FAST and contaminated doffing. The center front internal closure overlap was extended four inches to the right to shift the closure layers from center front and relieve the bulk discomfort noted in Generation 5 human factors testing. The pant received reshaped kneepad control tabs that contour to enhance fit and comfort. Pull strap elastic was revised for release ease into control channels.

Two versions of a two-piece knit carbon component were also designed. One adaptation is a carbon collared undershirt with an articulated shaped sleeve, an extended underarm gusset panel for increased reach and mobility, and a left side asymmetric shaped zipper to balance the distribution of the front closures and further eliminate layer bulk. A second undershirt has the same sleeve, gusset, and zipper components but also includes a funnel shaped neck shape design.

The Generation 6 jacket and trouser outer garment was produced in shell fabrics 78C and 31B. The two-piece carbon undergarments were produced in carbon fabrics 63A and 96X. All shell and carbon fabrics selected received high tactile comfort rankings as discussed previously.

Generation 6 Results

FAST Evaluations

The results showed that the torsos, arms, and legs for all tests appeared relatively clean (see Figures 37 through 39). Occasional areas of light deposition or haze were evident along the jawline and neck. They appeared to correspond to locations directly below and above the lower mask buckle. No simulant was evident above the ear or temple, which was an area of considerable focus from prior generation findings. Only two tests saw hazes of simulant near the sock line. One test also saw hazes of simulant on the side and back of the neck.

Contaminated Doffing

Overall, the doffing process proceeded very smoothly and the test participant in each test was able to remove the garment completely without contamination.

FIG. 37—*Test 5: 78C fixed hood.*

Only an occasional smudge of decon solution was evident. Head, face, and neck areas were clean. Run 1 exhibited very faint evidence of dotting on lower extremities. Runs 2, 5, and 6 were rated clean and free of any form of visible contamination. All other runs were virtually clean. In fact, the test proceeded

FIG. 38—*Test 4: 31B fixed hood.*

FIG. 39—*Test 10: 31B detached hood.*

so well that in Test 7, by our direction, the assistants eliminated the gross decontamination at the start of the process and only wiped down key interface areas of the ensemble, and the test participant was still able to doff cleanly. For Test 8, the GT instructed the test participant to self-decontaminate, which eliminated the gross decontamination and wipe-down by the assistants. Vital area wipe-down and doffing were performed solo by the test participant. Under black light evaluation, the subject emerged virtually clean.

Conclusions

- A separate carbon undergarment, when worn with an outer shell garment, provides better performance and also doffs more successfully than single garment systems. Even those systems with carbon cuffs and closure flaps were not as successful.
- Tighter carbon undergarments are cooler than looser versions, even when constructed of the same fabric.
- The hood/mask interface design allows less simulant penetration onto the body and face than LEHP garments used without this feature. This design also provides the wearer with unobstructed vertical and lateral vision during head movement.

- Generation 6 two-piece design accommodates multiple jacket/trouser sizing combinations that provide flexibility to address multiple body types and has the potential to reduce inventory stock requirements.

Acknowledgments

The writers thank Dr. David Brookstein, Dr. John Pierce, Dr. Les Sztandera, Dr. Niny Rao, Ms. Sara Beth Kane, Mr. Tim Rioux, Dr. Muthu Govindaraj, Dr. Brian George, Ms. Celia Frank, and Mr. Bill Hord for their significant contributions. The writers also thank Dr. Karla Allan for her expertise in Human Factors analysis at NSRDEC. Figs. 1 and 2, 4, 13, 21 and 22 by Philadelphia University. All others provided by Research Triangle Institute (RTI).

References

[1] ASTM F1291, 2010, "Standard Test Method for Measuring the Thermal Insulation of Clothing Using a Heated Manikin," *Annual Book of ASTM Standards*, Vol. 11.03, ASTM International, West Conshohocken, PA.

[2] ASTM F2370, 2010, "Standard Test Method for Measuring the Evaporative Resistance of Clothing Using a Sweating Manikin," *Annual Book of ASTM Standards*, Vol. 11.03, ASTM International, West Conshohocken, PA.

[3] Brady, J. L., Rioux, T., Rao, N., and Winterhalter, C., "Comparison of Evaporative Resistance Between Two Garment Designs Driven by Material Characteristics using a Sweating Thermal Manikin," *8th International Meeting for Manikins and Modeling*, Victoria, BC, Aug. 2010.

[4] Brady, J. L., Rioux, T., Rao, N., and Winterhalter, C., "Thermal Resistance Comparison Between Two Garment Designs Driven By Fabric Properties Using a Thermal Manikin," *AATCC International Conference and Exhibition*, Charleston, SC, March 2011.

[5] Sztandera, L. M., Cardello, A., and Winterhalter, C. (2011), "Identification of the Most Significant Comfort Factors for Textiles from Processing Mechanical, Handfeel, Fabric Construction, and Perceived Tactile Comfort Data," *Text. Res. J.* (accepted).

Performance of Protective Clothing and Equipment: Emerging Issues and Technologies
STP 1544, 2012
Available online at www.astm.org
DOI:10.1520/STP104100

John D. Pierce, Jr.,[1] *Stephen S. Hirsch,*[1] *Sara Beth Kane,*[1]
John A. Venafro,[1] *and Carole A. Winterhalter*[2]

Evaluation of Thermal Comfort of Fabrics Using a Controlled-Environment Chamber

REFERENCE: Pierce, John D., Jr., Hirsch, Stephen S., Kane, Sara Beth, Venafro, John A., and Winterhalter, Carole A., "Evaluation of Thermal Comfort of Fabrics Using a Controlled-Environment Chamber," *Performance of Protective Clothing and Equipment: Emerging Issues and Technologies* on April 16, 2011 in Anaheim, CA; STP 1544, Angie M. Shepherd, Editor, pp. 108–128, doi:10.1520/STP104100, ASTM International, West Conshohocken, PA 2012.

ABSTRACT: A critical characteristic of garments is thermal comfort, the ability to remain comfortable under conditions of elevated temperature and humidity. The traditional approach for assessing thermal comfort has required participants to exercise under conditions of elevated temperature and humidity while garbed in the candidate garments. The participants are subjected to stress, sophisticated equipment is required, and the measures, which have to be obtained in considerable numbers, require substantial time. In the present work, we report on the development of a potential alternate methodology to evaluate thermal comfort. Participants wore arm stockings of candidate fabrics and inserted their arms past the elbow in a controlled-environment chamber (CEC; Electro-tech Systems, Inc., Glenside, PA) under conditions of elevated temperature (40.5°C) and relative humidity (75 %). Participants assessed mittens made from eight different fabrics in 20-min testing sessions. Participants provided comfort ratings and judgments of specific perceptual experiences (such as warmth, sweatiness, stickiness, etc.) at separate specified times during the trial. Results revealed that fabric type was a significant predictor of thermal comfort ratings, with significant differences emerging after 10 min in the CEC. Further, thermal comfort was predicted by perceptual experiences of warmth, sweatiness, and stickiness. These results demonstrate the feasibility of the CEC approach in assessing

Manuscript received June 2, 2011; accepted for publication February 27, 2012; published online September 2012.

[1]Philadelphia University, 4201 Henry Ave., Philadelphia, PA, 19144.

[2]U.S. Army Natick Soldier Research, Development, and Engineering Center, Natick, MA, 01760.

relative fabric comfort as a viable alternative to whole-body testing under significant heat stress in an environmental chamber. This approach has further advantages of being more rapid, less stressful to participants, and not as complex as existing approaches.

KEYWORDS: thermal comfort, Psychophysics, clothing, labeled magnitude scale

Introduction

Successful design of garments for military and emergency first responders involves the optimal resolution of two opposing goals: protection and comfort. Whereas protection can be assessed effectively through laboratory-based and garment trial measures, assessing comfort is a more elusive goal because of both the multifaceted dimensions encompassing comfort and the perceptual nature of the experience. Considerable research efforts have been devoted to the study of apparel features that determine comfort and use of military garments through laboratory and perceptual measures, reflecting the considerable importance of comfort on performance in the military arena. In the present report, we detail efforts to develop a new methodology for the evaluation of thermal comfort in fabrics for potential use in military garments.

The scientific study of comfort in military and non-military fabrics extends over 80 years (reviewed Ref 1). Viewed broadly, comfort can be defined as a human emotional response that accompanies perception of the tactile and thermal environment. Important to this definition is recognition that the determinants of comfort are more than the fabric itself. Rather, the perception of comfort is a complex one [2], reflecting characteristics of three critical dimensions: the person, the garment, and the environment (e.g., see Refs 3–5). Further, the multidimensional nature of comfort is revealed when considering that overall garment comfort reflects the contributions of at least three major comfort factors: tactile, thermal, and psychological comfort [6,7].

Each of these three factors differs in its contribution to overall garment comfort and in the methodologies used for evaluation. Thermal comfort, for example, is satisfaction with the thermal environment, and the ability to remain comfortable under conditions of elevated temperature and humidity. Thermal discomfort, then, arises when individuals move out of range of normal "thermoneutrality" [8]. Thermal comfort involves interactions among clothing, climate, and physical activity [9]. Goldman [2] has identified six parameters affecting thermal comfort, including factors related to environment (air temperature, air movement, humidity, and mean radiant temperature), body-heat production, and clothing. Because thermal comfort involves interactions among these parameters of clothing and external environment, the traditional approach used to assess thermal discomfort has required human participants to exercise under conditions of elevated temperature and humidity while garbed in the candidate garments. Basic physiological measures are monitored during the exercise.

Typical of this approach to studying thermal comfort is the work by Santee et al. [10], evaluating thermal comfort of the standard battle-dress uniform (BDU) used by the U.S. military. Nine U.S. soldier participants wore BDUs made from four different military materials under two different testing conditions: a neutral condition of 20°C and 50 % relative humidity (RH) and a warm humid condition of at least 27°C and 75 % RH. In each condition, participants completed four 30-min periods of walking on a treadmill at 3 mph with a 10-min rest period between each period of walking. Heart rate, skin temperature, rectal temperature, and skin relative humidity were monitored throughout testing. Participants provided intensity ratings of overall thermal comfort and specific perceptual experiences of the garment (stickiness, clinginess, etc.) and their physiological state (sweatiness, skin wetness, etc.).

Although specific protocols differ in their methodological details, most approaches involve some form of physical activity under elevated environmental conditions in the garments to be evaluated. Wong et al. [11] had participants run on a treadmill for 20 min in a controlled-environment exercise chamber maintained at 29°C and 85 % RH. Sandsund et al. [12] exposed nine participants in full protective fire-fighting equipment with breathing apparatus to environments as hot as 130°C. Similar approaches have been used to evaluate thermal stress in saunas [13], heat stress in aircraft ground crews [14], cockpit thermal conditions [15], thermal conditions in German coal mines [16], and heat stress with different types of sportswear [17].

This traditional approach to evaluating thermal comfort presents several practical challenges and limitations. First, and most restrictive, is the need for specialized equipment: Typically, a full-scale environmental chamber and physiological monitoring capabilities are required. Second, because participants are usually subjected to some measure of heat stress, candidates must be carefully selected for participation and thoroughly monitored during the study (ideally by medical personnel). In many cases, approval by an institutional review board (IRB) may demand medical supervision of the experimental trials. Finally, the gathering of thermal comfort data is time and personnel intensive, with trials that can last several hours per assessed garment.

We sought to develop an alternative methodology that is briefer and less thermally stressful to participants. In the methodology that we assessed, participants wore long mittens of the fabrics to be evaluated and inserted their arms into a glove-box-like controlled-environment chamber. In this manner, evaluation of thermal comfort can be made among long mittens constructed from different materials under conditions of elevated temperature and RH in the chamber without placing participants in conditions of significant heat stress. In this report, we present the results of a full-scale experimental study to evaluate feasibility of this approach in assessing relative fabric thermal comfort as a viable alternative to whole-body testing under significant heat stress in a controlled-environment and instrumented exercise chamber.

Method

Participants—Testing involved 40 participants (mean age = 21.2) divided into two groups. Each group consisted of 15 median-size males and five median-size females recruited from students, faculty, and administrative personnel at Philadelphia University. All participants were treated in accordance with the American Psychological Association's Code of Ethics [18], and received compensation for their time. This study was approved by Philadelphia University's Institutional Review Board and by the U.S. Army Medical Research and Materiel Command (USAMRMC), Office of Research Protections (ORP), Human Research Protection Office (HRPO).

Equipment—The controlled-environment chamber (CEC) was purchased from Electro-tech Systems, Inc. (ETS), Glenside, PA, a leading manufacturer of environmental chambers (see Fig. 1). Working dimensions of the chamber are 39 in. wide × 20 in. deep × 21 in. high. The unit is equipped for adjusting the temperature and humidity from ambient to ca. 110°F and 90 % RH, and is designed to operate either isothermally at constant humidity or with both variables being ramped from ambient. The unit was installed by the manufacturer who provided training on its use to the testing proctor.

The chamber was placed on a hydraulic cart that enabled its height to be adjusted to each participant's preference and comfort while seated. A height-adjustable stool was also available to optimize each subject's position and comfort. Participants were seated so that they could insert their arms into the

FIG. 1—*The controlled-environment chamber (CEC) used to assess thermal comfort of the tested fabrics.*

chamber several inches beyond the antecubital (the interior of the elbow bend). A pair of lab jacks fitted with padded cloth covers was placed in the chamber to enable participants to rest the arms comfortably at a variety of heights and positions (for example, at the wrist, upper forearm, or elbow). The lab jacks served two functions. First, they helped participants avoid paresthesis (numbing, tingling, and "falling asleep" sensations). Second, they served to help position the upper arms to avoid contact with the porthole rims that could otherwise constrict blood flow and contribute to discomfort.

Scales—Participants were provided with two standardized labeled magnitude (LM) scales that have been extensively used in prior comfort assessment studies. LM scales, line-based scales with verbal labels to express the intensity of sensations, were originally developed by Borg [19–21] to measure perceived exertion. Subsequent applications have been made for diverse sensory experiences, including oral sensations from chemosensory irritants [22], gustatory and olfactory sensations [23,24], paradoxical heat sensations [25], and food preferences [26].

One scale, the Comfort Affective Labeled Magnitude scale, is a reliable and easy-to-use tool for quantifying the human experience of tactile comfort. The CALM scale is a standardized labeled magnitude scale, 200 mm in length and bounded by the labels "greatest imaginable discomfort" and "greatest imaginable comfort" (see Fig. 2). It was developed at the U.S. Army Natick

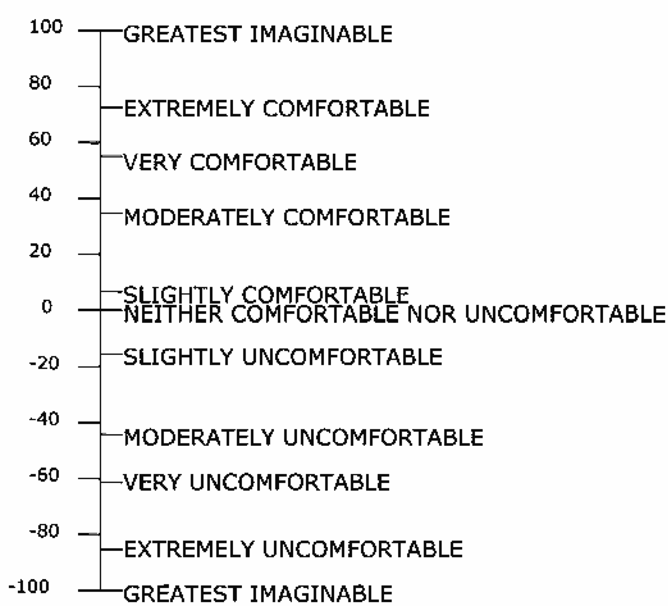

FIG. 2—*The comfort affective labeled magnitude scale used to provide psychophysical assessment of thermal comfort.*

Soldier RD&E Center (NSRDEC) to provide psychophysical assessments of comfort [1,27,28] and has been used extensively in fabric testing of tactile comfort [29–31]. Participants indicate their assessments of comfort by placing a mark across the vertical line scale at the point corresponding to the rating. The measurement from the bottom of the scale to the point marked by the participant provides the numeric estimate for comfort. This easy-to-use scale quantifies the human experience of thermal comfort and can readily be used to evaluate comfort perception and individual acceptance of fabrics.

The other scale used was the Labeled Magnitude Scale for Intensity (see Fig. 3) developed and used by the U.S. Army Research Institute of Environmental Medicine in conjunction with the NSRDEC [10]. This scale was used to express the intensity of specific perceptual experiences (such as warmth,

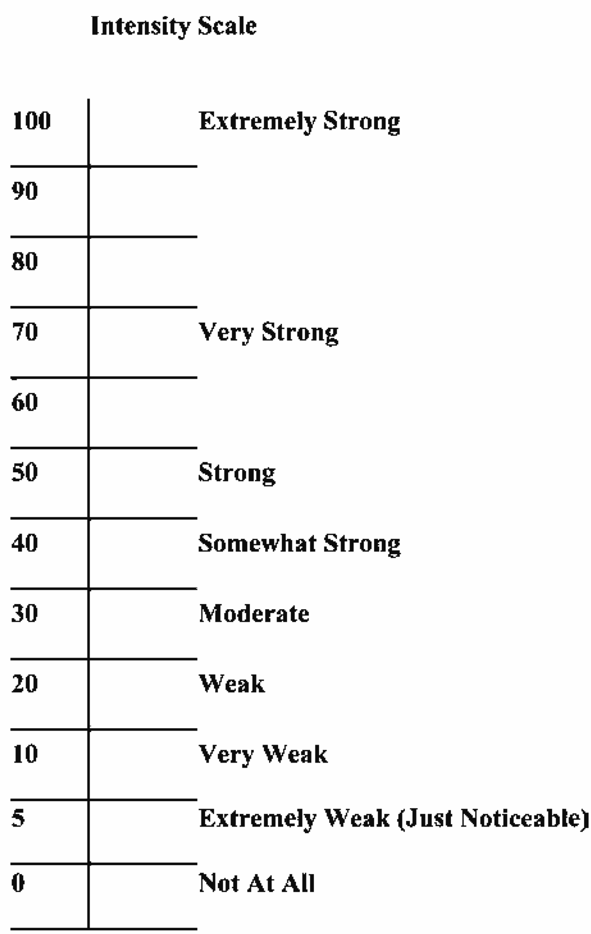

FIG. 3—*The labeled magnitude scale for intensity used to provide psychophysical assessment of selected perceptual characteristics.*

TABLE 1—*Dimensions for the eight fabrics evaluated for thermal comfort in the present study.*

Fabric Code	Fabric Structure	Fabric Content	Weight (oz/yard^2)	Moisture Vapor Transmission Rate (Grams per m^2 per day)
10R	Plain weave rip stop	50 % Combed cotton, 50 % nylon	6.90	762.11
11A	Oxford	50 % Cotton, 50 % polyester	5.60	771.55
17C	Plain weave	65 % Wool, 35 % polyester	6.40	761.78
19N	Oxford	92 % Nomex, 5 % kevlar, 3 % P140	7.50	752.76
11S	Plain weave	100 % Cotton	3.15	769.70
21K	Interlock knit	100 % Polyester	3.16	808.08
53H	Trilaminate	100 % Polyester woven shell 100 % ePTFE membrane tricot knit liner: polyester with some carbon yarns for dissipation	9.96	344.72
94K	Laminate	100 % FR polyester face, carbon beads, 100 % cotton back	13.92	702.45

sweatiness, stickiness, and clinginess; see below) at specified times during the protocol.

Fabrics—Eight fabrics were selected for testing (see Table 1). Each fabric was used to create long mittens with closure in two sizes. Larger mittens for male participants had a length from top to fingertips of 60 cm (23.5 in.), and a width at the widest point side to side when flat of 20 cm (7.9 in.). Mittens for female participants were slightly smaller, length from top to fingertips of 57 cm (22.5 in.), and widest point side to side when flat of 18 cm (7.1 in.). The mittens were manufactured in two sections. The first section was worn by the participant and reached to the top of the bicep area where it was closed with an elastic plus barrel lock device (enabling custom fitting to all participants). The second section, constructed from an impermeable fabric, was affixed directly to the chamber's ports, placed over the already donned mitten outside the chamber (see Fig. 1), and fastened so that a full seal was obtained. Seven pairs of mittens (five regular sized pairs and two smaller sized pairs) were constructed for each fabric; each pair was used a maximum of four times. Mittens were gently laundered and dried prior to first use and after each use in a testing session.

Procedure—All testing was done at CEC conditions of 40.5°C (105°F) and 75 % RH. These conditions were selected on the basis of extensive pilot testing with the CEC (Pierce, unpublished data).

The fabrics were divided into two sets. Set 1 consisted of fabrics 10R, 11A, 17C, and 19N, and were tested first by one group of 20 participants. Set 2 consisted of fabrics 11S, 21K, 53H, and 94K and were tested by the second group of 20 participants following the completion of Set 1 evaluation. Each participant within a group assessed each of the four test fabrics in individual experimental sessions, no more than one per day, in a repeated measures design. The order of presentation of each fabric was randomized for each participant.

The CEC was turned on 30 min before testing, so that the unit was at the proper temperature and humidity levels. Participants arrived at least 15 min prior to the session to acclimatize to the room conditions. They washed and thoroughly dried their hands in tepid (body-temperature) water with Ivory soap 5 to 10 min prior to the experiment. Upon arrival for their first session, participants received verbal instructions concerning the nature of the study and were asked to sign a written informed consent form.

Following informed consent, participants were read and shown a set of instructions that detailed proper seating and positioning for the CEC, the two scales used to provide perceptual evaluations, and the types of ratings to be provided. If there were no questions, the testing proctor recorded the temperature of the participant's forearm using a handheld surface thermometer. The proctor then helped the participant don the mittens. Participants inserted their arms into the CEC ports, while the proctor ensured the upper chamber sleeve covered each arm fully. Once the participant was seated properly, evaluations began according to the following schedule:

30-s Mark—CALM evaluation of overall thermal comfort. (Proctor question: *Please provide a rating of the level of thermal comfort and/or discomfort in the mittens that you are experiencing using the comfort scale on the left side of the chamber.*)

1-min Mark—Intensity rating of the warmth of the arms. (Proctor question: *Please provide a rating of the intensity of the warmth of your arms using the intensity scale on the right side of the chamber.*)

2-min Mark—Intensity rating of the level of sweatiness in the arms. (Proctor question: *Please provide a rating of the intensity of the degree of sweatiness in your arms using the intensity scale on the right side of the chamber.*)

3-min Mark—Intensity rating of the amount of stickiness in the palms and fingers. (Proctor question: *Please provide a rating of the intensity of the degree of dampness and stickiness in your palms and fingers using the movements we discussed from the intensity scale on the right side of the chamber.*)

4-min Mark—Intensity rating of the extent of fabric clinginess. (Proctor question: *Please provide a rating of the intensity of the extent to which the fabric is clinging to your skin—using arm lowering to the jacks and then raising as we discussed—from the intensity scale on the right side of the chamber.*)

For each rating, participants indicated their assessment by identifying the number corresponding to the appropriate point on the vertical line scale. The proctor, in turn, recorded the rating on the data sheet.

At 5, 10, and 15 min, the sequence was repeated, starting with the second CALM evaluation at 5 min. Participants were asked to perform simple hand exercises (such as clapping and waving their hands around the chamber) at selected intervals during testing to prevent paresthesis and help maintain experimental focus by the participant. The final evaluation, at the 20-min mark, was the last CALM evaluation of the study, followed by a rating of eagerness to exit the chamber: *Please rate how eager you are to remove your arms from the CEC*. The participant then removed each arm from the chamber, and the proctor immediately measured the temperature of the participant's forearm using the surface thermometer.

During each session, the proctor monitored the participant's performance and condition with the proviso that a testing session would be immediately discontinued if the participant showed undue effects from testing. None did, and no testing session was discontinued.

Results

Mean CALM ratings at the 20-min mark for each of the eight fabrics were calculated and are presented in Fig. 4. A multiple regression analysis was conducted to determine which factors significantly predicted thermal comfort ratings for the tested fabrics at the 20-min mark. In this analysis, the dependent variable was participants' CALM ratings of thermal comfort/discomfort at the 20-min mark. Fabric type, gender of the participant, and inter-participant differences were evaluated as potential predictors. The results, shown in Table 2, revealed that fabric type significantly predicted differences in CALM ratings. The analysis also revealed significant differences between participants in their ratings, although ratings by gender did not differ significantly.

Next, means were calculated for CALM ratings across all fabrics at each interval (beginning, 5-min, 10-min, 15-min, and 20-min marks) and are presented in Fig. 5. A time-series comparison using analysis of variance was used to assess changes in CALM ratings across the 20-min testing session. This analysis confirmed that CALM ratings significantly decreased during the 20-min testing session across all fabrics ($F\,[4{,}795] = 23.84$, $p < 0.001$). Post hoc Tukey HSD analysis revealed significant decreases across all time intervals compared to the initial CALM ratings (mean difference for initial

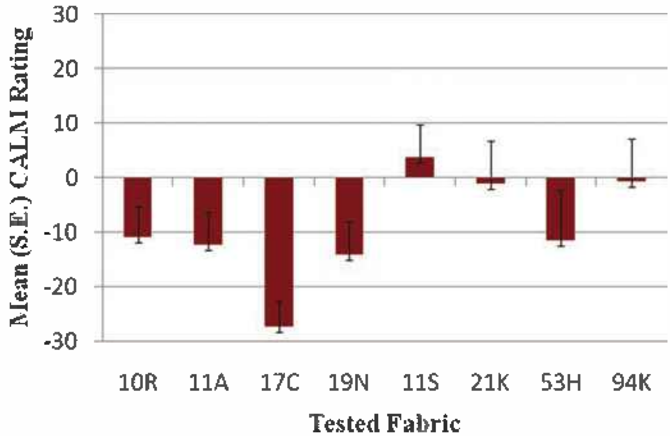

FIG. 4—*Mean CALM ratings with standard error bars for each of the eight fabrics at the 20-min mark.*

TABLE 2—*Regression analysis assessing predictors of thermal comfort CALM ratings at the 20-min mark for the eight tested fabrics in the controlled-environment chamber.*

Variable	Beta	*t* Value	Significance
Fabric	−0.390	−3.17	0.002
Gender of participant	0.005	0.06	0.950
Inter-participant differences	0.676	5.38	0.001

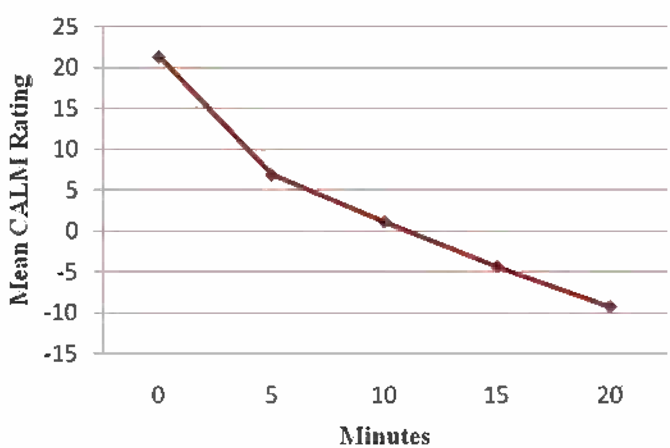

FIG. 5—*Mean CALM ratings for thermal comfort across all fabrics at each interval.*

TABLE 3—*Changes in CALM ratings across the 20-minute testing session for each individual fabric.*

Fabric Code	CALM Score at entry (Mean + SD)	CALM Score at 5 min (Mean + SD)	CALM Score at 10 min (Mean + SD)	CALM Score at 15 min (Mean + SD)	CALM Score at 20 min (Mean + SD)
10R	16.60 (25.6)	4.85 (25.4)	1.20 (26.2)	−4.35 (27.4)	−10.95 (25.1)
11A	13.95 (29.2)	−3.00 (27.5)	−5.80 (26.4)	−8.60 (25.8)	−12.30 (27.3)
17C	2.85 (37.5)	−8.40 (24.2)	−15.30 (26.3)	−18.80 (20.4)	−27.25 (20.7)
19N	18.60 (26.3)	4.40 (28.5)	−1.55 (31.0)	−10.40 (27.8)	−14.15 (27.3)
11S	29.15 (31.1)	16.30 (30.2)	9.60 (32.3)	7.45 (29.4)	3.85 (26.1)
21K	21.20 (31.6)	9.60 (33.0)	4.40 (32.4)	0.50 (34.0)	−1.10 (34.9)
53H	37.70 (29.9)	14.60 (32.7)	4.90 (32.2)	−5.15 (37.8)	−11.50 (41.1)
94K	30.75 (33.0)	16.95 (29.0)	11.70 (32.8)	4.30 (32.5)	−0.65 (35.2)

versus 10-min ratings = 20.21; initial versus 15-min ratings = 25.73; initial versus 20-min ratings = 30.61; all are significant at $p < 0.001$), except for ratings at the 5-min mark (initial CALM versus 5-min ratings = 14.44 mean difference, n.s.). Examination of CALM scores by fabric reveals consistent and uniform decreases during the 20-min session for each individual fabric (Table 3).

Multiple regression analysis was used to explore further the changes in CALM ratings across the 20-min session. Whereas the previous analysis analyzed CALM ratings collapsed across all fabrics, this analysis was based on mean CALM ratings for each fabric as the dependent variable, and fabric type, gender of the participant, and inter-participant differences as potential predictors. The results, presented in Table 4, reveal that significant differences in CALM ratings attributable to fabric type do not emerge until after 10 min of exposure in the CEC. These differences become more pronounced at the 15-min mark, and even more divergent at the 20-min mark. Inter-individual differences in CALM ratings were a significant predictor at each tested interval. However, gender of the participant was not a factor, as males and females did not significantly differ in CALM ratings at any assessed interval.

Means for the perceptual characteristics of warmth, sweatiness, stickiness, and clinginess of the fabric were calculated for each assessment interval and are presented in Fig. 6 across all fabrics and in Table 5 for each individual fabric. A time-series comparison using analysis of variance was used to assess changes in these perceptual characteristics across the 20-min testing session. This analysis confirmed that these perceptual ratings significantly increased during the 20-min testing session across all fabrics (warmth: $F\,[3,636] = 17.11, p < 0.001$; sweatiness: $F\,[3,636] = 20.51$, $p < 0.001$; stickiness: $F\,[4,795] = 18.77$, $p < 0.001$; and clinginess: $F\,[4,795] = 10.38, p < 0.001$).

TABLE 4—*Regression Analysis assessing predictors of Thermal Comfort CALM ratings at each assessment interval for the eight tested fabrics in the Controlled-Environment Chamber.*[a]

Time Point	t-Value Fabric	t-Value Gender	t-Value Inter-Participant Difference
Beginning	−0.32	1.68	2.78**
5-min Assessment	−1.58	1.05	4.11*****
10-min Assessment	−2.19*	0.77	4.42*****
15-min Assessment	−3.07***	0.14	5.13*****
20-min Assessment	−3.17****	0.06	5.38*****

[a]$*p < 0.03$, $**p < 0.006$, $***p < 0.003$, $****p < 0.002$, $*****p < 0.001$.

The relationship between CALM ratings and the other perceptual ratings was evaluated through multiple regression analysis with mean CALM ratings across all fabrics at the 20-min mark as the dependent variable, and the final ratings for warmth, sweatiness, stickiness, and clinginess as potential predictors. The results revealed that warmth ($t = -2.15$, $p < 0.033$), sweatiness ($t = -2.46$, $p < 0.015$), and stickiness ($t = 3.11$, $p < 0.002$) were significant predictors of CALM ratings, but clinginess ($t = -0.24$, n.s.) was not.

Finally, mean CALM ratings at the 20-min mark were evaluated against data derived from previous laboratory analysis and perceptual testing to determine if thermal comfort can be predicted by two physical characteristics of the fabric; fabric weight and moisture vapor transmission rate (MVTR; assessed using ASTM E-96 testing standards on a Gintronic GraviTest 6300). Neither physical characteristic was a significant predictor thermal comfort ratings (fabric weight: $t = -0.17$, n.s.; MVTR: $t = -1.26$, n.s.). However, CALM ratings of the tactile comfort previously gathered for these tested fabrics [29,30] did

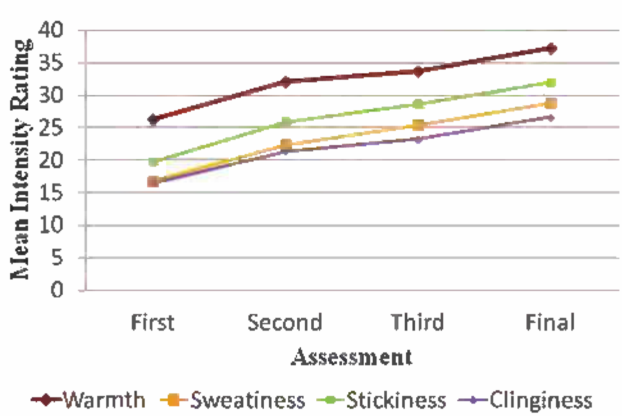

FIG. 6—*Mean intensity ratings for warmth, sweatiness, stickiness, and clinginess across all fabrics at each interval.*

TABLE 5—*Changes in ratings of sensory characteristics across the 20-minute testing session for each individual fabric.*

Warmth

Fabric Code	Warmth Rating at Entry (Mean + SD)	Warmth Rating at 5 min (Mean + SD)	Warmth Rating at 10 min (Mean + SD)	Warmth Rating at 15 min (Mean + SD)
10R	25.85 (9.2)	32.60 (8.78)	31.90 (9.9)	35.35 (12.2)
11A	28.80 (14.0)	34.65 (16.0)	32.15 (12.3)	35.50 (14.5)
17C	27.95 (12.2)	36.00 (17.8)	35.75 (14.9)	36.75 (14.4)
19N	24.10 (10.3)	27.70 (13.6)	31.25 (12.4)	37.10 (15.2)
11S	28.50 (15.1)	34.05 (13.3)	35.35 (15.3)	37.65 (14.3)
21K	27.95 (16.6)	32.60 (13.1)	36.00 (13.6)	38.35 (15.6)
53H	23.30 (14.7)	30.70 (14.5)	36.25 (16.1)	43.60 (17.1)
94K	23.90 (14.2)	28.35 (14.3)	30.95 (15.2)	33.65 (13.7)

Sweatiness

Fabric Code	Sweatiness Rating at Entry (Mean + SD)	Sweatiness Rating at 5 min (Mean + SD)	Sweatiness Rating at 10 min (Mean + SD)	Sweatiness Rating at 15 min (Mean + SD)
10R	16.25 (10.4)	22.85 (10.9)	25.05 (12.8)	27.86 (13.8)
11A	19.30 (14.1)	23.25 (12.4)	26.15 (13.5)	29.10 (13.7)
17C	16.85 (14.3)	25.95 (18.4)	26.30 (16.1)	28.80 (16.9)
19N	15.05 (8.5)	19.25 (12.5)	27.20 (15.1)	29.30 (15.4)
11S	17.35 (12.7)	23.35 (17.2)	24.40 (14.1)	26.90 (15.9)
21K	21.50 (13.7)	25.45 (14.4)	28.50 (13.7)	29.50 (14.9)
53H	16.00 (15.0)	22.50 (15.4)	27.10 (17.8)	35.00 (20.5)
94K	12.00 (11.7)	16.55 (12.1)	18.95 (12.0)	24.20 (12.3)

Stickiness

Fabric Code	Stickiness Rating at Entry (Mean + SD)	Stickiness Rating at 5 min (Mean + SD)	Stickiness Rating at 10 min (Mean + SD)	Stickiness Rating at 15 min (Mean + SD)
10R	19.25 (11.9)	24.20 (14.2)	27.75 (14.5)	30.63 (16.1)
11A	21.40 (17.9)	24.65 (17.6)	28.90 (17.1)	31.85 (17.8)
17C	21.55 (16.2)	26.80 (15.2)	29.75 (15.8)	33.30 (16.6)
19N	18.85 (10.6)	28.00 (13.6)	29.90 (13.4)	35.28 (16.9)
11S	22.15 (13.3)	28.45 (18.0)	28.95 (15.2)	31.20 (16.1)
21K	23.90 (16.5)	28.55 (16.5)	30.00 (15.8)	32.25 (16.3)
53H	15.95 (11.5)	25.45 (14.2)	29.90 (17.2)	36.20 (18.9)
94K	15.05 (10.3)	20.95 (11.9)	24.15 (13.1)	25.35 (12.7)

TABLE 5—*Continued*

Clingginess				
Fabric Code	Clinginess Rating at Entry (Mean + SD)	Clinginess Rating at 5 min (Mean + SD)	Clinginess Rating at 10 min (Mean + SD)	Clinginess Rating at 15 min (Mean + SD)
10R	19.95 (17.3)	25.55 (14.5)	25.30 (14.3)	28.85 (14.6)
11A	20.80 (17.3)	25.50 (16.2)	26.55 (17.1)	29.65 (15.2)
17C	19.40 (18.1)	20.05 (16.0)	21.75 (14.5)	28.40 (13.7)
19N	15.75 (11.7)	20.65 (12.1)	21.60 (11.0)	23.70 (12.7)
11S	11.65 (12.0)	20.85 (19.6)	21.80 (19.7)	24.50 (22.3)
21K	22.55 (15.8)	27.00 (17.9)	31.55 (18.7)	34.00 (19.6)
53H	12.70 (13.7)	20.80 (19.5)	26.40 (20.3)	31.65 (22.6)
94K	9.10 (11.0)	10.55 (11.1)	10.85 (10.5)	12.20 (11.4)

significantly predict mean CALM ratings of thermal comfort at the 20-min mark ($t = 2.80$, $p < 0.05$).

Discussion

These results provide an empirical demonstration of the feasibility of a proposed new methodology for the evaluation of thermal comfort in fabrics. Fabric type significantly predicted differences in CALM ratings of thermal comfort following fabric-covered arm exposure to elevated temperature and humidity conditions inside a controlled-environment chamber. Significant differences in thermal comfort ratings as a function of fabric type emerged after 10 min in the elevated environmental conditions, and continued for the duration of testing. Further, thermal comfort was predicted by perceptual experiences of warmth, sweatiness, and stickiness. Overall thermal comfort ratings significantly decreased, and the intensity of specific perceptual characteristics significantly increased, over the duration of the session. Ratings of thermal comfort were not predicted by laboratory measures of moisture vapor transmission rate or fabric weight, but were significantly associated with ratings of tactile comfort for the individual fabrics.

Although feasibility of the method was demonstrated in this initial study, much remains to be discovered concerning optimal testing conditions. Testing sessions were 20 min in length in the present work. However, significant differences in thermal comfort ratings as a function of fabric type were seen in as little as 10 min of testing. Whereas an argument can be made that a 10-min session is, therefore, sufficient, continued exposure led to thermal comfort differences that were even more pronounced. Further, intensity ratings for the other perceptual measures increased substantially with further exposure throughout the 20-min session. It may be that the general increase in discomfort seen may continue with testing beyond 20 min of exposure, and a nadir point, if any, remains to be identified.

Similarly, the effect of differing temperature and humidity levels in the CEC remain largely unexplored. In the current study, all testing was done at CEC settings of 40.5°C (105°F) and 75 % RH. These testing conditions were selected on the basis of extensive pilot evaluation of the CEC protocol (Pierce, unpublished data) in which participants evaluated four different fabrics in 20-min sessions at a constant temperature (105°F) under three different humidity conditions: 25, 50, and 75 % RH. As expected, a significant effect of humidity was observed, as CALM ratings of thermal comfort decreased significantly under moister conditions. Evaluations of the effects of differing temperature and humidity levels in the CEC await further study.

One area of concern is the marked and substantial inter-individual differences seen in CALM thermal comfort ratings (see Fig. 4 and Table 3). Inter-individual differences in CALM ratings of thermal comfort were a significant predictor at each tested interval. These differences are unlikely to be caused by gender differences in the participants in the present study, although the small number of females tested precludes a more definitive assessment. One possibility is that this pronounced inter-individual variation in ratings reflects the psychophysical nature of the evaluation technique. Previous psychophysical work has shown the potential for substantial inter-individual differences in ratings across various types of sensory scales, including category-rating and magnitude estimation scales [32]. This commonly seen inter-individual variation in scale use is perhaps attributable to differences across participants in perceptual contexts; that is, differences in the range of experiences of different participants [33]. Different experiences may provide a different frame of reference as to what represents; for example, "Moderately Comfortable," especially if, as in the present work, the scale is not anchored to a reference point. If so, providing a standard frame of reference (a reference anchor) may help minimize scale use differences across individuals. Another possibility related to scale use is that participants may interpret the verbal anchors of the scale differently (in this case, "greatest imaginable discomfort" and "greatest imaginable comfort"). Several studies have reported a shift in scale use with changes in the verbal labels used as end anchors. Cardello et al. [34], for example, noted compression in scale use with experimental changes in the verbal labels used as end anchors. In the present study, instructions provided to the participants regarding scale use did not include a definition of verbal labels to avoid biasing participant response. Thus, the substantial inter-individual variation seen in the present study may reflect differences in participant's prior perceptual experiences and their interpretation of the verbal labels used on the CALM scale.

Alternatively, inter-individual differences in thermal comfort ratings may, in fact, reflect actual inter-individual differences in perceived thermal comfort or thermoneutrality. It is a well-known phenomenon that individuals vary tremendously in their thermal sensitivity (hence, dual-control thermostat controls in cars, among other devices). Individual differences in thermal comfort may be, in part, attributable to demographic (age, gender, race, etc.) and cultural characteristics, as well as differences in physical fitness and metabolic rates [35]. If so, the significant inter-individual differences in thermal comfort observed in the present work may not be a consequence of the evaluation technique, but rather a meaningful finding worthy of further investigation.

That thermal comfort ratings were not predicted by either moisture vapor transmission rate (MVTR) or fabric weight illustrates the often frustrating difficulty of associating perceptual thermal comfort with laboratory-based measures. In general, previous work has found an inconsistent relationship between perceptual thermal comfort and numerous physical properties of the fabric. The most important physical properties for predicting thermal comfort appear to be fabric characteristics related to moisture transport [36]. Condensation, in particular, contributes greatly to thermal discomfort [37]. Santee et al. [10] related differences in evaporation (and, thus, potential for cooling) to fabric characteristics of moisture vapor permeability and insulation. These differences may underlie their observed fabric differences in thermal comfort. Similarly, Cardello et al. [38] reported that thermal properties were the most important predictor of overall comfort/discomfort of hot-weather BDUs. In that respect, failure to find the expected relationship between MVTR and thermal comfort in the present study is surprising. This lack of an observed relationship may be attributable to the relatively narrow range of MVTRs in the tested fabrics. Mean MVTRs ranged from 702.45 to 808.08 g/m^2 per day for seven of the eight tested fabrics on a scale that can vary from 0 (no moisture transfer) to approximately 1300 (no moisture barrier). Further testing with fabrics differing more substantially in their moisture vapor resistance would be needed to provide a clearer picture of the relationship of this laboratory measure to perceptual thermal comfort.

On the other hand, perceived thermal comfort was strongly related to previously obtained measures of tactile comfort. As noted earlier, perceptual comfort is a multidimensional comfort encompassing tactile, thermal, and psychological comfort [6]. Tactile comfort is typically conceived as a function of the feel of the fabric as it activates skin sensory receptors. Thermal comfort, the topic of the present paper, is satisfaction with the thermal environment. Psychological comfort encompasses a broad range of characteristics, including aesthetics, fit, and cognitive influences [39,40]. Whereas these components are viewed as separate parameters, this distinction may be artificial. There is potential for clear interactions among these comfort components. Tactile comfort of a particular garment; for example, may change dramatically with changes in the thermal environment. For example, a garment that feels comfortable under neutral thermal conditions may stimulate skin receptors differently and thus feel less comfortable tactilely when it absorbs sweat in a heated environment. Similarly, particular physical characteristics of a garment (such as scratchiness) may impact negatively across all three dimensions of comfort. An appreciation for the potential interactions among the three identified types of comfort (tactile, thermal, and psychological) may yield important benefits in understanding the complex relationships between fabric characteristics and their impact on fabric comfort.

The fabrics used in the current evaluation have been evaluated extensively in our materials evaluation laboratory. Their substantial differences across several critical fabric characteristics, such as MVTR, weight, and type (described in detail by Brady [41]) precludes a more systematic analysis of how these individual characteristics affect testing. A logical next stage of this research would be a more systematic evaluation of specific fabric characteristics as they affect performance in the current protocol. Such a systematic analysis would provide a rigorous assessment of the CEC protocol, as well as potentially helping to understand how fabric characteristics affect perceptual comfort.

One important limitation of the protocol described here is the lessened heat stress felt by participants. Two facets are critical here. One is the absence of an exercise component incorporated into the testing. Physical activity has been a central element of most previous research in thermal comfort evaluations, as activity impacts a host of physiological mechanisms in the body. Effects are evident most clearly in sweating and overall metabolic activity, but also seen with changes in heart rate, blood pressure, metabolic heat production by the muscles, and numerous other effects. Second, the heating only of the hands and lower arms allows for the dispersal of heat via the bloodstream throughout the body, potentially mitigating the effects of the elevated temperature and humidity conditions. Further, other body locations—or the body as a whole—may exhibit sensitivity to thermal/moisture challenge that is different from the hands/arms. Although the current approach is thus less robust than employing a whole-body exercise chamber, it remains to be seen whether the thermal conditions provided by the CEC environment provides an adequate substitute for the heat stress load incurred by vigorous exercise. It may be that the present methodology works best for a relatively rapid assessment of candidate fabrics, with final thermal testing to be done with the completed garment worn in a whole-body exercise chamber and complemented by laboratory analysis through use of a thermal manikin.

These results demonstrate feasibility of a controlled-environment chamber approach for assessing relative fabric comfort as a viable alternative to whole-body testing under significant heat stress in an environmental chamber. This approach has advantages of being more rapid, less stressful to participants, and not as complex as existing testing protocols. This modified CEC approach has potential applications in research and applied settings as a proxy for evaluating the thermal comfort of fabrics without methods that involve introducing the entire body into an environmental chamber.

References

[1] Cardello, A. V., Schutz, H. G., and Winterhalter, C., "Development and Application of New Psychophysical Methods for the Characterization of the Handfeel and Comfort Properties of Military Clothing Fabrics," *Technical Report No. NATICK/TR-02/022*, U.S. Army Solder and Biological Chemical Command Soldier Systems Center, Natick, MA, 2002.

[2] Goldman, R. F., "The Four 'Fs' of Clothing Comfort," *Environmental Ergonomics*, Y. Toschihara and T. Ohnaka, Eds., Elsevier, Amsterdam, 2005.

[3] LaMotte, R. H., "Psychophysical and Neurophysiological Studies of Tactile Sensitivity," *Clothing Comfort*, N. R. S. Hollies and R. F. Goldman, Eds., Ann Arbor Science, Ann Arbor, 1977.

[4] Li, Y., "Clothing, Comfort and Its Application," *Textile Asia*, Vol. 29, 1998, pp. 29–33.

[5] Slater, K., "The Assessment of Comfort," *J.Textile Inst.*, Vol. 77, 1986, pp. 157–171.

[6] Kilinc-Balci, F. S. and Elmogahzy, Y., "Testing and Analyzing Comfort Properties of Textile Materials for the Military," *Military Textiles*, E. Wilusz, Ed., CRC Press, Boca Raton, FL, 2008, pp. 107–136.

[7] Wong, A. S. W., Li, Y., and Yeung, P. K. W., "Statistical Simulation of Psychological Perception of Clothing Sensory Comfort," *J. Textile Inst.*, Vol. 93, 2002, pp. 108–109.

[8] Candas, V., "To Be or Not to Be Comfortable: Basis and Prediction," *Environmental Ergonomics*, Y. Toschihara and T. Ohnaka, Eds., Elsevier, Amsterdam, 2005.

[9] Li, Y. and Wong, A. S. W., "Psychology and Sensory Comfort," *Clothing Biosensory Engineering*, Y. Li and A. S. W. Wong, Eds., CRC Press, Boca Raton, FL, 2006, pp. 9–27.

[10] Santee, W. R., Berglund, L. G., Cardello, A., Winterhalter, C. A., and Endrusick, T. L., "Physiological and Comfort Assessment of Volunteers Wearing Battle-Dress (BDU) Uniforms of Different Fabrics during Intermittent Exercise," *Technical Report No. USARIEM/T06-06*, U.S. Army Research Institute of Environmental Medicine, Natick, MA, 2006.

[11] Wong, A. S. W., Li, Y., and Yeung, P. K. W., "The Influence of Thermal Comfort Perception on Consumer's Preferences to Sportswear," *Environmental Ergonomics*, Y. Toschihara and T. Ohnaka, Eds., Elsevier, Amsterdam, 2005.

[12] Sandsund, M., Winnberg, S., Finseth, H. W., Fossli, G. O., and Beinertsen, R. E., "Evaluation of Test Protocols for Smoke-Divers Working in the Heat," *Environmental Ergonomics*, Y. Toschihara and T. Ohnaka, Eds., Elsevier, Amsterdam, 2005.

[13] Szygula, Z., Pilch, W., Wnorowski, J., Sztwiertnia, J., and Torii, M., "The Influence of Various Methods of Fluid Ingestion on Changes in Selected Physiological Reactions during Thermal Stress in a Sauna," *Environmental Ergonomics*, Y. Toschihara and T. Ohnaka, Eds., Elsevier, Amsterdam, 2005.

[14] Tauri, H., Kanamaru, Y., Sakagami, J., and Ozaki, H., "Physiological Effects of Heat Stress on Ground Crew in the Japan Air Self-Defense Force," *Environmental Ergonomics*, Y. Toschihara and T. Ohnaka, Eds., Elsevier, Amsterdam, 2005.

[15] Ozaki, H., Ogawa, W., and Yokoyama, S., "Cockpit Thermal Conditions and Physiological Reactions in Flight: Effects of Mental Workload on Thermal Regulation of Aircrew While Flying Tasks," *Environmental Ergonomics*, Y. Toschihara and T. Ohnaka, Eds., Elsevier, Amsterdam, 2005.

[16] Kampmann, B. and Piekarski, C., "Assessment of the Risks of Heat Disorders Encountered during Work in Hot Conditions in German Hard Coal Mines," *Environmental Ergonomics*, Y. Toschihara and T. Ohnaka, Eds., Elsevier, Amsterdam, 2005.

[17] Shin-ya, H., Nakai, S., Yoshida, T., and Takahashi, E., "Effects of Sportswear on Thermoregulatory Responses during Exercise in a Hot Environment," *Environmental Ergonomics*, Y. Toschihara and T. Ohnaka, Eds., Elsevier, Amsterdam, 2005.

[18] American Psychological Association, "Ethical Principles of Psychologists and Code of Conduct," *Am. Psychol.*, Vol. 57, 2002, pp. 1060–1073.

[19] Borg, G. A., "Category Scale with Ratio Properties for Intermodal and Interindividual Comparisons," *Psychophysical Judgment and the Process of Perception*, H.-G. Geissler and P. Petxold, Eds., VEB Deutxcher Verlag der Wissenschaften, Berlin, 1982, pp. 25–34.

[20] Borg, G. A., "Psychophysical Scaling with Applications in Physical Work and the Perception of Exertion," *Scand. J. Work, Environ. Health*, Vol. 16, 1990, pp. 55–58.

[21] Borg, G. A., *Borg's Perceived Exertion and Pain Scales*, Human Kinetics, Champaign, IL, 1998.

[22] Green, B. G., Shaffer, G. S., and Gilmore, M. M., "Derivation and Evaluation of a Semantic Scale of Oral Sensation Magnitude with Apparent Ratio Properties," *Chem. Senses*, Vol. 18, 1993, pp. 683–702.

[23] Green, B. G., Dalton, P., Cowart, B., Shaffer, G., Rankin, K., and Higgins, J., "Evaluating the 'Labeled Magnitude Scale' for Measuring Sensations of Taste and Smell," *Chem. Senses*, Vol. 21, 1996, pp. 323–335.

[24] Mattes, R. D., "Effects of Linoleic Acid on Sweet, Sour, Salty, and Bitter Taste Thresholds and Intensity Ratings of Adults," *Am. J. Physiol.: Gastrointestinal Liver Physiol.*, Vol. 292, 2007, pp. G1243–G1248.

[25] Green, B. G., "Synthetic Heat at Mild Temperature," *Somatosensory Motor Res.*, Vol. 18, 2002, pp. 130–138.

[26] Schutz, H. G. and Cardello, A. V., "A Labeled Affective Magnitude (LAM) Scale for Assessing Food Liking/Disliking," *J. Sensory Stud.*, Vol. 16, 2001, pp. 117–159.

[27] Cardello, A. V., Winterhalter, C., and Schutz, H. G., "Predicting the Handle and Comfort of Military Clothing Fabrics from Sensory and Instrumental Data: Development and Application of New Psychophysical Methods," *Textile Res. J.*, Vol. 73, 2003, pp. 221–237.

[28] Schutz, H. G., Cardello, A. V., and Winterhalter, C., "Perceptions of Fiber and Fabric Uses and the Factors Contributing to Military Clothing Comfort and Satisfaction," *Textile Res. J.*, Vol. 75, 2005, pp. 223–232.

[29] Pierce, J. D., Jr., "Further Evaluation of the Reliability and Validity of the CALM Scale for Assessing the Tactile Comfort of Fabrics," *Technical Report No. PHILA-LEHP-ME-TR-08-01*, Philadelphia Univ. Laboratory for Engineered Human Protection, Philadelphia, PA, 2008.

[30] Pierce, J. D., Jr., Brady, J. L., and Hirsch, S. S., "Further Evaluation of the Comfort Affective Labeled Magnitude (CALM) Scale for Assessing Fabric Tactile Comfort," Poster, *Meeting of the Association for Psychological Science*, 2009, San Francisco, CA.

[31] Pierce, J. D., Jr., Hirsch, S. S., Kane, S. B., Brady, J. L., and Winterhalter, C.A., "Construct Validation of the CALM Scale for Assessing Fabric Tactile Comfort," Poster, *Meeting of the Association for Psychological Science*, 2010, Boston, MA.

[32] Wegener, B., "Category-Rating and Magnitude Estimation Scaling Techniques," *Sociolog. Methods Res.*, Vol. 12, 1983, pp. 31–75.

[33] Lawless, H. T., Horne, J., and Spiers, W., "Contrast and Range Effects for Category, Magnitude and Labeled Magnitude Scales in Judgements of Sweetness Intensity." *Chem. Senses*, Vol. 25, 2000, pp. 85–92.

[34] Cardello, A. V., Lawless, H. T., and Schutz, H. G., "Effects of Extreme Anchors and Interior Label Spacing on Labeled Affective Magnitude Scales," *Food Qual. Preference*, Vol. 19, 2008, pp. 473–480.

[35] Goto, T., Toftum, J., de Dear, R., and Fanger, P. O., "Thermal Sensation and Comfort with Transient Metabolic Rates," *Proceedings of Indoor Air, The 9th International Conference on Indoor Air Quality and Climate*, 2002, Monterey, CA, pp. 1038–1043.

[36] Endrusick, T. L., Julio A. G., and Gonzalez, R. R., "Improved Comfort of US Military Chemical and Biological Protective Clothing," *Environmental Ergonomics*, Y. Toschihara and T. Ohnaka, Eds., Elsevier, Amsterdam, 2005.

[37] Ghali, K., Ghaddar, N., and Jones, B., "Phase Changes in Fabrics," *Thermal and Moisture Transport in Fibrous Materials*, N. Pan and P. Gibson, Eds., Woodhead Publishing, Cambridge, U.K., 2006, pp. 402–423.
[38] Schutz, H. G., Cardello, A. V., and Winterhalter, C., "Perceptions of Fiber and Fabric Uses and the Factors Contributing to Military Clothing Comfort and Satisfaction," *Text. Res. J.*, Vol. 75, 2005, pp. 223–232.
[39] Cardello, A. V., "The Sensory Properties and Comfort of Military Fabrics and Clothing," *Military Textiles*, E. Wilusz, Ed., CRC Press, Boca Raton, FL, 2008, pp. 71–106.
[40] Das, A. and Ishtiaque, S. M., "Comfort Characteristics of Fabrics Containing Twist-Less and Hollow Fibrous Assemblies in Weft," *J. Text. Apparel Tech. Manage.*, Vol. 3, 2004, pp. 1–7.
[41] Brady, J. L., "Consolidated Data on Fabric Construction," *Technical Report PHILA-LEHP-ME-TR-08-0*, Philadelphia Univ. Laboratory for Engineered Human Protection, Philadelphia, PA, 2008.

Performance of Protective Clothing and Equipment: Emerging Issues and Technologies
STP 1544, 2012
Available online at www.astm.org
DOI:10.1520/STP104085

Carole Winterhalter,[1] Quoc Truong,[1] Thomas Endrusick,[2] Armand Cardello,[1] and Larry Lesher[1]

Effects of Overgarment Moisture Vapor Transmission Rate on Human Thermal Comfort

REFERENCE: Winterhalter, Carole, Truong, Quoc, Endrusick, Thomas, Cardello, Armand, and Lesher, Larry, "Effects of Overgarment Moisture Vapor Transmission Rate on Human Thermal Comfort," *Performance of Protective Clothing and Equipment: Emerging Issues and Technologies on* April 16, 2011 in Anaheim, CA; STP 1544, Angie M. Shepherd, Editor, pp. 129–157, doi:10.1520/STP104085, ASTM International, West Conshohocken, PA 2012.

ABSTRACT: The purpose of this study is to evaluate the effects of moisture vapor transport properties of four different groups of overgarments (OGs) on physiological, sensory, and comfort responses. These OGs were made from materials containing an impermeable film and three semi-permeable (or moisture vapor permeable) membranes with varying moisture vapor transmission rates (MVTR). The impermeable film had an MVTR of 5 $g/m^2/24$ h, and the three moisture vapor membranes had MVTRs of 360, 670, and 864. These four OGs were evaluated under two environmental and work/rest conditions. The environmental conditions consisted of a warm environment, $T_a = 29.2°C$, 51 % relative humidity, $V = 1.1$ m/s and a cool environment, $T_a = 18.4°C$, 50 % relative humidity, $V = 1.1$ m/s. Eight men wore the OGs while performing 4 h of intermittent exercise. Rectal temperature, an 8-point mean weighted skin temperature and heart rate were continuously recorded. Skin wettedness was calculated from dew point sensors under the OG. Mean body weight loss and moisture absorption by the OG, underwear, and footwear were measured from pre- and post-experiment weights. A sensory and comfort rating questionnaire was presented to the volunteers every 30 min. During prolonged intermittent exercise in moderate environmental conditions,

Manuscript received June 1, 2011; accepted for publication March 22, 2012; published online September 2012.

[1]U.S. Army Natick Soldier Research, Development and Engineering Center, Kansas St., Natick, MA 01760-5020.

[2]U.S. Army Research Institute of Environmental Medicine, Kansas St., Natick, MA 01760-5007.

volunteers wearing OGs with MVTR of 670 and greater produced less thermo-physiological stress, independent of changes in perceived comfort. Perceived comfort of the MVTR 5 OG was significantly lower than all other garments at 18.4°C. At 29.2°C, both the MVTR 5 and 360 OG produced lower comfort, but not significantly. At 29.2°C, volunteers were significantly warmer, sweatier, and experienced significantly greater moisture on their skin, undergarments, and inside their OGs than at 18.4°C, and these sensations increased over time. However, at 29.2°C, perceived comfort differences among MVTR levels were either not significant or not associated with MVTR level.

KEYWORDS: moisture vapor transmission rate, thermoregulatory responses, sensory comfort, semi-permeable membrane, protective clothing

Introduction

Military personnel perform in diverse missions and must be equipped with appropriate clothing to protect and empower them in complex and rapidly changing environments around the world. Military clothing systems are engineered from their basic materials to provide optimum user performance. Environmental protection against cold and wet climates is essential and the most commonly used materials are waterproof, moisture vapor permeable laminates composed of microporous membranes. In this study we investigated the effects of moisture vapor permeability on human thermoregulatory and sensory responses during prolonged intermittent exercise under warm and cool environmental conditions to determine which level of MVTR produced the least thermophysiological stress and highest perceived comfort.

Multi-layered protective clothing systems create resistance to both sensible and insensible heat transport. Resistance to dry heat transport is primarily determined by the amount of air trapped inside the layers and the velocity of the air measured at the outer surface of the ensemble [1]. The water vapor content of textiles is of minor importance in dry heat transport during steady-state conditions [2]. However, if air in the interstices between the fibers is replaced by molecular water, the thermal resistance of the clothing system is reduced because of the higher thermal conductivity of water. Excess water vapor can condense as liquid water, saturating inner layers of clothing and creating a water layer on the skin surface. Clothing systems with a high moisture vapor resistance can cause elevated skin and core temperatures as well as increased sweat rates, which can all contribute to general feelings of heat discomfort.

Military clothing developers have been utilizing a material that claims to provide superior water vapor transport along with the ability to completely protect the wearer from numerous environmental hazards. These waterproof/breathable membranes are rated according to the amount of moisture in the form of water vapor that can move through the membrane during a given time period. This value is referred to as the moisture vapor transmission rate (MVTR) and is measured in grams of water passing through a square meter of the membrane during a 24-h period ($g/m^2/24$ h). This standard procedure is described in ASTM Standard E96-80, Standard Test Methods for Water Vapor Transmission of Materials [3].

An earlier study [4] investigated the effect of moisture vapor permeability on the thermoregulatory responses of sedentary volunteers who wore permeable (MVTR 864) and impermeable (MVTR 5) overgarments in two environments: 18°C/50 % relative humidity; 29.7°C/52 % relative humidity. The results showed that a moisture vapor permeable overgarment reduced overall thermal strain, reduced underclothing absorption of sweat and increased evaporation of moisture vapor when compared with an impermeable overgarment.

This present study is a follow-on that investigates the effect of the level of MVTR (5, 360, 670, and 864) on volunteers wearing the same overgarments but under prolonged work/rest cycles, rather than sedentary conditions, and under the same environmental conditions to determine which provide the least thermophysiological strain and highest perceived comfort.

In addition to thermoregulation, a recent study [5] has shown that MVTR also affects cognitive and physical performance when using overgarments identical in design that differed only in MVTR (MVTR 5, 670, and 864) and the U.S. Army Advanced Combat Uniform (MVTR 915). Utilizing computerized cognitive tasks and a gross motor task (box lift and carry) MVTR was shown to affect human performance in terms of speed and accuracy even when core temperature did not vary significantly. After physical labor, lower MVTR levels were associated with increased perceptions of body warmth, sweat, discomfort, and exertion. During stationary activity, lower MVTR levels affected discomfort and perceived warmth.

Although physiological factors are important contributors to perceived comfort, the judgment of whether a garment or individual is comfortable is ultimately a subjective response based on environmental conditions, fabric properties, garment fit, physiological parameters, and psychological variables. Like other psychological constructs, the subjective nature of this judgment makes the measurement of perceived comfort more difficult than the assessment of objective, physiological responses.

Measures of thermal comfort involve individuals' assessment of environmental variables such as ambient air temperature and relative humidity. One of the most widely used measures, the McGinnis Thermal scale [6] asks subjects to rate their thermal sensations on a 13-point scale ranging from "I am so cold I am helpless" to "I am so hot I am sick and nauseated." Another scale is Gagge et al.'s Thermal Sensation scale [7]. Measures of tactile comfort involve individuals' perceptions of the feel of a garment against the skin and are usually measured through rating the intensity of a series of sensory attributes using a simple 5-, 7-, or 9-pt category scale, such as the Subjective Comfort Rating Chart [8], where subjects rate the intensity of each of 15 attributes describing various tactile sensations of garments, such as stiffness, smoothness, snugness, and clamminess. Measures of global comfort address the question of how comfortable (all things taken into account) an individual is at a given moment. In Gagge et al.'s scale [7] of comfort sensation, individuals evaluate their level of comfort on a 4-point scale ranging from comfortable to very uncomfortable.

All of the above approaches to measuring comfort rely on the use of category or partition scales, i.e., the comfort dimension is partitioned into a number of discrete categories. Such scales have long gone out of fashion in the field of psychophysics, primarily because newer methods have been developed that afford a better level of quantification of the data. For example, all of the above methods utilize verbal labels to define a set of intervals along the comfort dimension. However, there is no reason to assume that the semantic meaning of the verbal labels actually define an equal interval scale. As such, the data from such scales can only be considered ordered metric data and should be treated mathematically as non-parametric data. Even if considered equal interval scales, these scales suffer from other problems, including the fact that all category scales are compressed at the extremes of the scale, because once the highest or lowest category has been used, individuals know that they cannot accurately assess a subsequent sensation that is more intense, because they have no more extreme label to use. As a consequence there is an underuse of the end-categories with all category scales. Lastly, because category scales are, at best, interval scales, they do not allow ratio statements to be made about the data, i.e., a comfort level of 4 on a 7-point scale cannot be assumed to be twice as comfortable as a rating of 2 on the scale. It would be the same as trying to say that 40°F is twice as warm as 20°F. Ratio statements can only be made on a ratio scale, e.g., the Kelvin scale of temperature.

New psychophysical measures have been developed recently to evaluate perceived comfort variables using simple, ratio-level scales. Early work by Sweeney and Branson [9,10] utilized the method of magnitude estimation to measure comfort sensation. However, magnitude estimation can be difficult for untrained observers to use. Recently, simpler ratio methods have been developed that do not depend on the math skills of the observer. These methods are known as labeled magnitude scales and they are constructed by scaling the semantic meaning of word labels using magnitude estimation and then placing these labels at locations along a vertical line that represent the ratios in their semantic meaning. Once constructed, these scales can be used by observers who simply place a slash mark on the line to indicate the intensity of their sensation. Once collected, the obtained data constitute ratio level data, because the judgments were assigned using a ratio-level scale. In the present research, two such labeled magnitude scales were used. One scale was utilized to have individuals rate the intensity of a variety of thermal sensations using Borg's labeled magnitude scale of intensity [11–13]. The other scale was a labeled magnitude scale of comfort [14], and used to assess the global comfort of individuals.

Methods

Subjects

Eight healthy males volunteered for the intermittent exercise experiments. They had an average age of 22.3 years, weight of 74.3 kg, height of 171.5 cm, and DuBois surface area of 1.87 m^2. Before any testing, the volunteers were informed about the purpose of the study, any known risks, and their right to terminate participation without penalty. They expressed understanding by signing a statement of informed consent.

Test Clothing Description

All volunteers wore a clothing ensemble composed of the following components each test day: long underwear (separate top and bottom), socks and gloves composed of 100 % hydrophilic polyester fibers, which could theoretically transport liquid in the form of sweat away from the skin [15]; a one-piece protective overgarment with an integrated hood made from W. L. Gore & Associates, Inc., (Gore) Gore-Tex laminate material with a specific MVTR; and standard military combat boots. To eliminate air exchange between the overgarment and the environment, seams were sealed, and the hood, wrist, and ankle openings were elasticized for a close, snug fit. The center front zipper was covered with a flap. A large tariff of clothing component sizes was procured before testing began and volunteers were individually fitted after consenting to participate in the study.

Gore-Tex is a thin, microporous layer of polytetrafluoroethylene (PTFE). Specifically, the Gore-Tex membrane is a result of the rapid expansion of the TFE fluorocarbon and results in a standard material with 9×10^9 pores per square inch of area. Each pore is 20,000 times smaller than a water droplet, but 700 times larger than a molecule of water vapor. The first generation membrane (Gore-Tex I) is composed of pure PTFE. It is susceptible to contamination by sweat, oils, dirt, insect repellents, saltwater, etc. Second generation membrane (Gore-Tex II) is PTFE faced with a protective layer to prevent any of the above contamination.

To maintain both visual and textural similarity, Gore used the same inner and outer fabrics for each of the four test garment materials. The outer fabric was a 2.9-oz/yd^2 Taslite (a thin nylon fabric) in a woodland green camouflage pattern. The inner fabric was a 1.5-oz/yd^2 nylon tricot knit (a thin mesh-like synthetic material) in an olive green color. To control the MVTR in the three test materials with targeted MVTR values of approximately 0, 300, and 600 $g/m^2/24$ h, Gore modified the thickness and structural chemistry of the hydrophilic component in the bi-component Gore-Tex II membrane. To achieve a laminate MVTR value of 900 $g/m^2/24$ h, Gore used the hydrophobic Gore-Tex I membrane. The actual protective membrane was hidden by the above inner and outer fabrics. All overgarments looked the same to the volunteers prior to the start of each test day.

Gore verified the four levels of MVTR by conducting in-house testing of the materials prior to overgarment construction according to ASTM Standard E96-80 [3], Procedure B (upright cup method), $T = 23°C$, 50 % relative humidity. NSRDEC testing, using the same method, produced the following values (target and actual respectively): 0–5, 300–360, 600–670, and 900–864.

The cross-sectional thickness of the membrane portion of each three-layer laminate was measured using a scanning electron microscope (Model: Amray 1000A SEM). The MVTR 5 laminate was made with an impermeable membrane with a thickness of 64–79 μm and was the thickest membrane of all the laminates. The MVTR 360 membrane was hydrophobic and microporous, 16–24-μm thick, and was sandwiched between two hydrophilic urethane coating layers. The MVTR 670 was hydrophobic and microporous, 16-μm thick, and was urethane coated on one side. The MVTR 864 was 24–29 μm and not coated. Using the Handfeel Spectrum Descriptive Analysis [14], a tactile sensory handfeel method, panel ratings of the laminate handfeel attributes were tested and plotted in Fig. 1. The data show a highly significant difference in handfeel between the MVTR 5 and the other three fabrics. The MVTR 5 was perceived by the panel to be significantly thicker and stiffer than the other three fabrics, requiring greater force to gather and greater force to compress. This difference is sufficiently large that it may be perceived by a wearer who dons or doffs overgarments constructed from these materials. It also had greater compressional resilience (both intensity and rate) and greater fullness/volume than the other three fabrics.

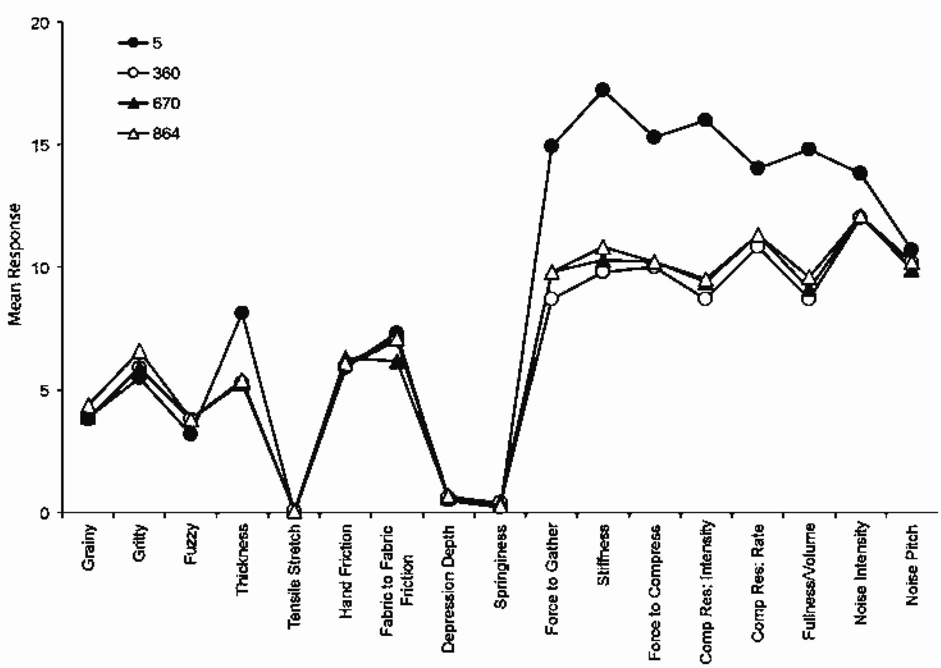

FIG. 1—*Results of laminated fabric handfeel analysis.*

Thermal Manikin Testing

The four clothing ensembles were previously evaluated for thermal resistance and evaporative heat transfer on a copper manikin as shown in Fig. 2. In the earlier study [16], the thermal resistances were decreased by the effects of increasing wind speed. Figure 3 shows that evaporative resistance (R_E) also declined as a function of wind speed, but the magnitude of the decrease depended on both category of MVTR and initial value assessed near still air conditions (0.4 m/s). The two ensembles with the least permeable MVTRs (5 and 360) displayed R_E values measured at 55.5 and 52 $m^2/Pa/W$, respectively. Each of these ensembles also declined precipitously by some 40 % with wind speeds elevated up to 2.4 m/s. The ensembles with MVTRs determined at 670 and 864 showed significantly lower initial R_E levels ($P < 0.0001$) and less steep declines from still wind speed to high wind speed (~34 %).

Experimental Protocol

The study was conducted in an environmental chamber. All volunteers wore a clothing ensemble (long underwear, socks, boots, gloves, and one-piece overgarment) that was visually identical in all respects. The overgarments, however, had four different levels of MVTR.

FIG. 2—*Thermal manikin: (a) dressed in long underwear, and (b) dressed in overgarment.*

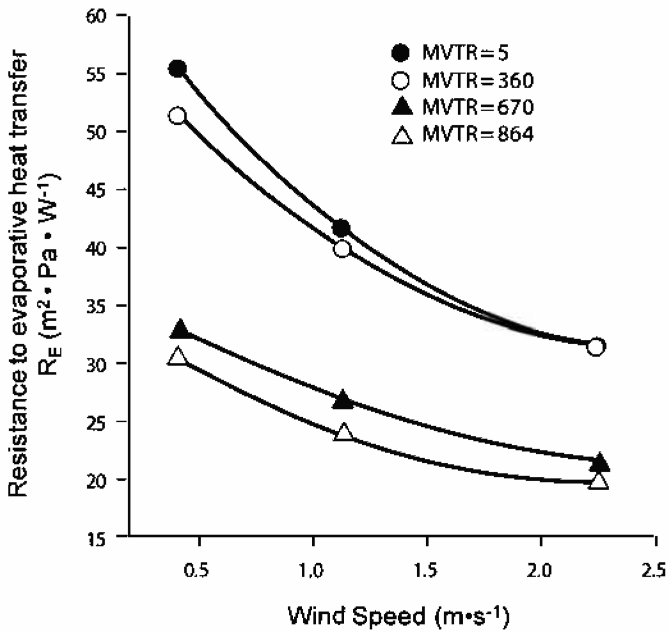

FIG. 3—*Thermal manikin assessment of MVTR overgarments.*

Volunteers were encouraged to eat their complete, normal breakfast in the morning before each test session. Volunteers were not allowed to eat any food in the test chamber. Volunteers were allowed to drink water ad libitum during the testing. All water consumed by volunteers was measured volumetrically. Upon arriving at the dressing room in the climatic chamber each morning at approximately 0700 h, the volunteers were weighed nude (without any clothing). Each volunteer then inserted his own rectal probe and then was assisted in the placement of three ECG electrodes and eight thermocouples on the skin surface. After the application of all instrumentation, each volunteer donned a complete test clothing ensemble. The four test uniforms with their different levels of MVTR were presented to the volunteers at random to avoid any ordering effect. The test overgarments were labeled for identification of MVTR level in a location and code known only by the Principal Investigator.

To control the heat and moisture content of all clothing ensemble components and eliminate this as a factor of variation for heat exchange in the body-clothing environment during the chamber tests, a rigid conditioning procedure was followed. Clothing ensemble components were stored in a conditioning room ($T_a = 29°C$ and 20 % relative humidity) for at least 15 h prior to use. Each clothing ensemble was weighed to the nearest 0.1 g before dressing and after removal by the volunteer each test day. This allowed for the calculation of the quantity of sweat accumulated within the clothing ensemble. Finally, after donning the clothing ensemble, but prior to beginning the test session, volunteers completed a questionnaire designed to measure their perceptions of the sensory characteristics of the test garment fabric, similarity of the test garment fabric to fabrics previously worn, garment fit, and overall acceptability of the test fabric and the test garment, as shown in Fig. 4. To assess the effect of garment wear on these subjective variables, volunteers also completed this questionnaire at the conclusion of each day's test.

After the 1-h instrumentation/dressing/questionnaire procedure, the volunteers were weighed again, entered the climatic chamber, and stood at designated positions on the treadmills in the chamber. While standing, a sensor was placed between the underwear layer and the overgarment layer to measure the relative humidity.

On test days 1–4, the chamber was maintained at 18.4°C, 50 % relative humidity and a wind speed of 1 m/s. On test days 5–8, the temperature was increased to 29.2°C, 51 % relative humidity and a wind speed of 1 m/s. When all volunteers were fully instrumented and all signals were being received by the data acquisition system (approximately 5 min standing baseline), the volunteers began walking on the treadmills (four per treadmill), which were controlled at 1.34 m/s as shown in Fig. 5. Volunteers attempted to walk for 40 min and then sat for 20 min on a wooden bench (four per bench) placed windward on the treadmill. This 1-h walk/rest cycle was attempted four times by each volunteer for a maximum total of 4 h in the climatic chamber.

Subjective measures of clothing sensations and comfort were taken every 30 min throughout the duration of the test. Immediately prior to the start of the test and at 30 min intervals throughout the test, labeled magnitude scales of

FIG. 4—*Test volunteers: (a) pre-test questionnaire, and (b) post-test questionnaire.*

FIG. 5—*Fully instrumented test volunteer on treadmill.*

clothing sensation and comfort were administered to all volunteers. Volunteers marked the clipboard-mounted questionnaires with pencils while walking on the treadmills and sitting on the benches. When a volunteer completed his daily chamber test, he exited the chamber, had his weight recorded, and then was assisted with the removal of the test clothing as well as all instrumentation. After the removal of the rectal probe, a nude weight (without any clothing) was recorded.

Physiological Variables

During all test sessions, rectal temperature was continually measured with the rectal probe, which was inserted 10 cm beyond the anal sphincter. This procedure ensured that no volunteer's core body temperature rose above the safety limit established for this study. Individual exposure would be terminated if the core temperature rose more than 0.6°C per 5 min of exposure or rose above 39.2°C when sitting or above 39.5°C when walking on the treadmill. Eight local skin temperatures obtained from standard, copper-constantan thermocouples were continually monitored to calculate a mean-weighted skin temperature (MWST) according to Gagge and Nishi [17]. The formula that was used to calculate MWST in this study is as follows: MWST = calf · 0.20 + thigh · 0.19 + forehead · 0.07 + abdomen · 0.175 + upper back · 0.175 + lower arm · 0.07 + upper arm ṡ 0.07 + hand · 0.05. All temperature measurements were recorded every 30 s using an automated data collection system.

The water vapor pressure and relative humidity were measured at the chest between the underwear layer and the overgarment as well as in the ambient air using small sensors. This allowed for the calculation of local skin wettedness (w) [18] using the following equation:

$$w = 100 \times \left(P_{sk,d} - P_a\right)/(P_{ssk} - P_a)(\%)$$

where $P_{sk,d}$ is the vapor pressure at the skin surface obtained from the sensor, P_{ssk} is the saturated vapor pressure at the local skin temperature, and P_a is the ambient water vapor pressure (Torr). Water vapor pressure readings were recorded every 10 min.

Heart rates were obtained from Polar brand radio transmitters that each volunteer wore around their chest. This procedure was necessary to ensure that no volunteer's heart rate exceeded the safety limit established for the study. Individual exposure would be terminated if a volunteer exceeded 80 % of his maximum predicted heart rate defined as 220 - age (in years) for a period of 5 min when sitting, or if a volunteer exceeded 90 % of his maximum predicted heart rate for a period of 5 min when walking on the treadmill. Individual heart rates were recorded every 5 min.

All volunteers were weighed in the nude and when fully-dressed pre- and post-test. The daily nude weights of the volunteers served as baseline measurements to detect possible day-to-day dehydration. Complete clothing ensemble weights pre- and post-test were also recorded. The weights were corrected for any volunteer water intake, urine production, and standard respiratory water and metabolic weight loss correction factors [19,20]. Because of the design of the clothing ensemble, any excessive sweating was probably absorbed within the clothing layers. Total non-evaporated sweat loss was measured as the difference between clothing ensemble weights pre- and post-test.

A volunteer's individual endurance time for each chamber exposure was measured to the nearest min. A master clock was started when all the volunteers entered the chamber. An initial period of 5 min was allowed for all volunteers to stand at their respective positions, to connect instrumentation, and to confirm that all instrumentation being used to monitor physiological responses (i.e., individual heart rate, rectal temperature, and skin temperatures) were transmitting properly. The end of this 5-min baseline period marked the beginning of the experimental exposure. The master clock was used to measure the total elapsed time of the exposure. A volunteer's endurance time was measured from the start of the master clock to the time he had his monitoring instrumentation disconnected to leave the chamber. Factors that could impact (i.e., shorten) individual volunteer endurance time included removal from the chamber because of rectal temperature or the heart rate reaching safety limits for the termination of an exposure established for this study. Endurance time could also be shortened as a result of volitional termination of an exposure by the volunteer because of discomfort, sickness, or for any other reason. Measuring individual endurance time was necessary to ascertain whether or not a volunteer could tolerate a 240-min exposure while wearing the various uniforms in the two environmental scenarios.

Sensory and Comfort Variables

Volunteers were asked to record their responses to a series of questions to ascertain their tactile sensations and thermal comfort. The questions included "how comfortable do you feel right now," "how hot or cold are you right now," "how sweaty are you right now," "how wet does your skin feel right now," "how wet does your undergarment feel right now," "how wet does your feet/socks feel right now." All ratings were made on labeled magnitude scales. The comfort/discomfort rating was made using the CALM (Comfort Affective Labeled Magnitude) scale [14]. All other ratings were made using a labeled magnitude scale adapted from the Borg Intensity scale. The rating questionnaires and the definitions of the various sensations were discussed in detail with each volunteer prior to the start of the study. Before and after each exposure, each volunteer was asked to give a detailed evaluation of the uniform worn that day.

Results and Discussion

Physiological

All volunteers completed the four 1-hr walk/rest cycles in the climatic chamber. The mean heart rates for volunteers under both cool and warm conditions are listed in Fig. 6. In the cool environment MVTR 864 showed slightly lower heart rates during exercise. In the warm environment, MVTR 5 produced higher heart rates during exercise.

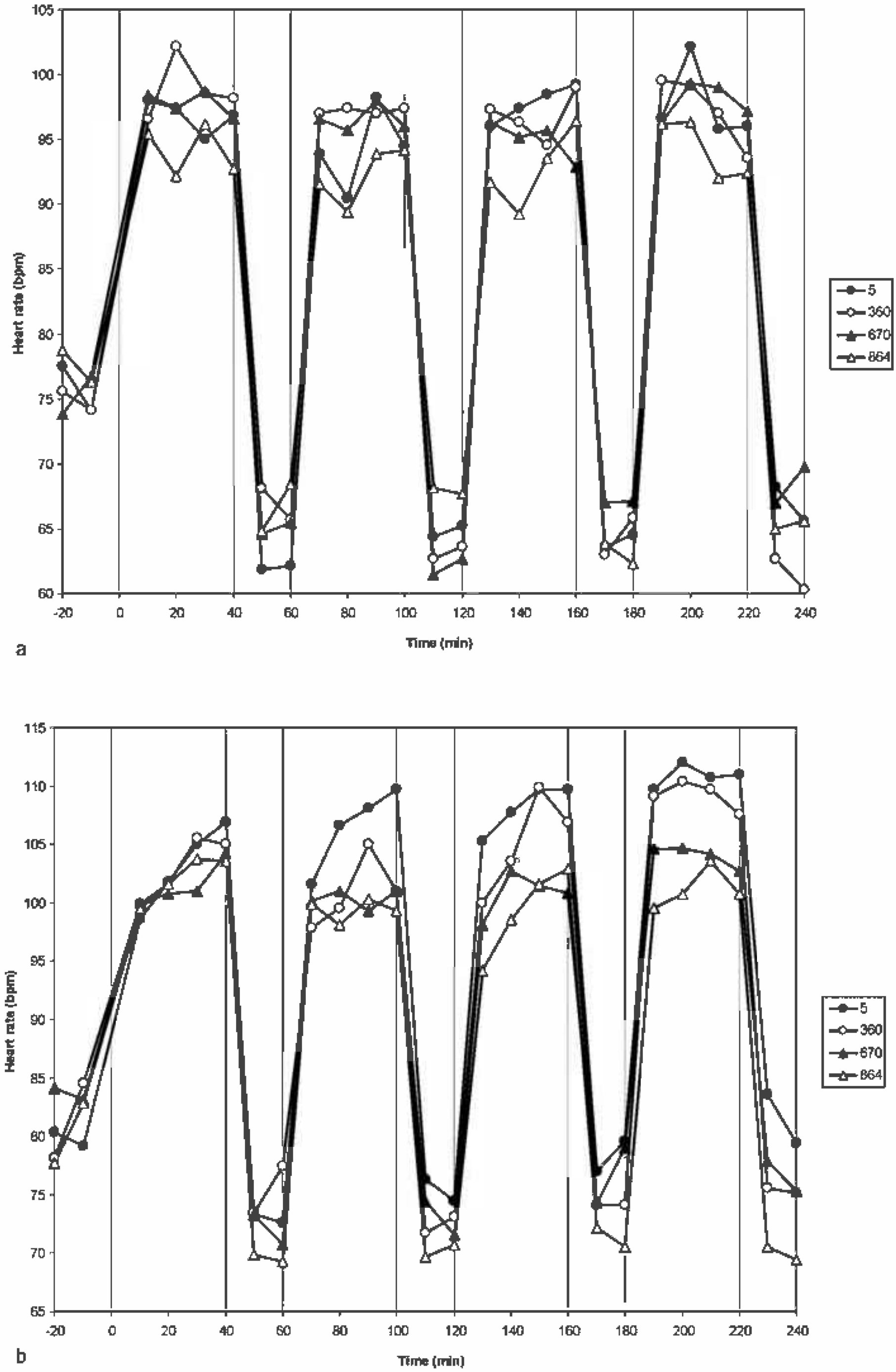

FIG. 6—*Mean heart rate of volunteers wearing overgarments: (a) at 18.4°C, and (b) at 29.2°C.*

Mean rectal temperatures of the volunteers were similar when tested under cool conditions but showed a clear divergence at 150 min under warm conditions as shown in Fig. 7. The rectal temperature when wearing the MVTR 5 overgarment eventually approached the termination temperature.

Most measures fell during the 20-min period of rest with the exception of skin temperature, which sometimes continued to rise even though the volunteers were sitting, as shown in Fig. 8. Under warm conditions MVTR 670 and 864 showed a lower mean weighted skin temperature than MVTR 5 and 360, and the MVTR 670 showed a relatively steady skin temperature throughout the work/rest cycles.

Mean weight gain of underwear, boots, and socks, which was caused by sweating, under both cool and warm conditions, is listed in Fig. 9. Under cool conditions the MVTR 5 ensemble showed higher mean weight gain, but under warm conditions both MVTR 5 and 360 gained much more weight than the higher MVTR overgarments. The higher weight gain of MVTR 5 and 360 and the steep drop in skin temperature indicated that when resting sweat cooled the body, lowered the skin temperature significantly, perhaps causing an after-exercise "chill." Whereas the MVTR 864, which had the lowest weight gain, demonstrated in Fig. 8 via a drop in skin temperature, that moisture in the suit dissipated when the volunteers began the exercise portion of the work rest cycle.

Under cool conditions volunteers wearing the MVTR 670 overgarment demonstrated the lowest body weight loss; however under the warm condition MVTR 360 showed the lowest body weight loss as shown in Fig. 10. Under both cool and warm conditions, the lower MVTR overgarments gained much more weight than the higher MVTR garments because they brought about a greater overall thermal strain, which required increased sweating to cool the body as shown in Fig. 11. The overgarments gained more weight under warm conditions than cool, as was expected.

With regard to mean sweat production, the lower MVTR overgarments demonstrated greater sweat production under both cool and warm conditions, and greater total sweat evaporation under cool conditions as demonstrated in Fig. 12. The total non-evaporated sweat, which is what was left in the overgarments, was significantly less in the higher MVTR overgarments. Because of the greater porosity of the higher MVTR overgarments, more sweat was evaporated under the warm condition.

When more than 50 %–65 % of the body surface is wet it is experienced as discomfort [21]. This level of wettedness was reached under the both warm and cool conditions for the MVTR 5 and 360 overgarments. Also, under the warm condition after 30 min, the lower MVTR overgarments behaved similarly and produced more wettedness than the higher MVTR overgarments, as shown in Fig. 13.

Sensory and Comfort Data

Figure 14 shows the data for how comfortable/uncomfortable the volunteers were as a function of time in both the cool and warm conditions. As can be

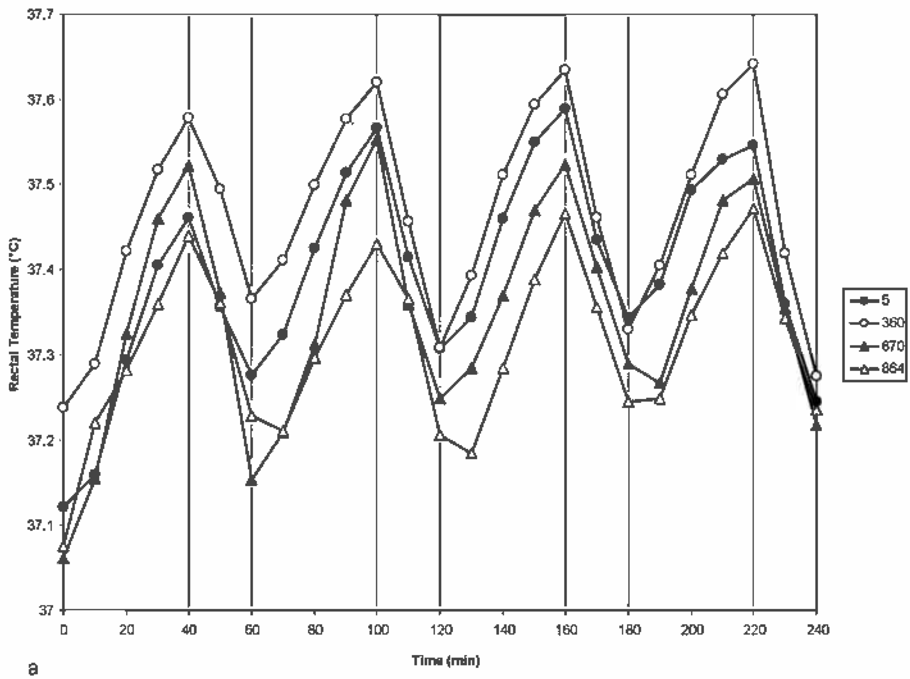

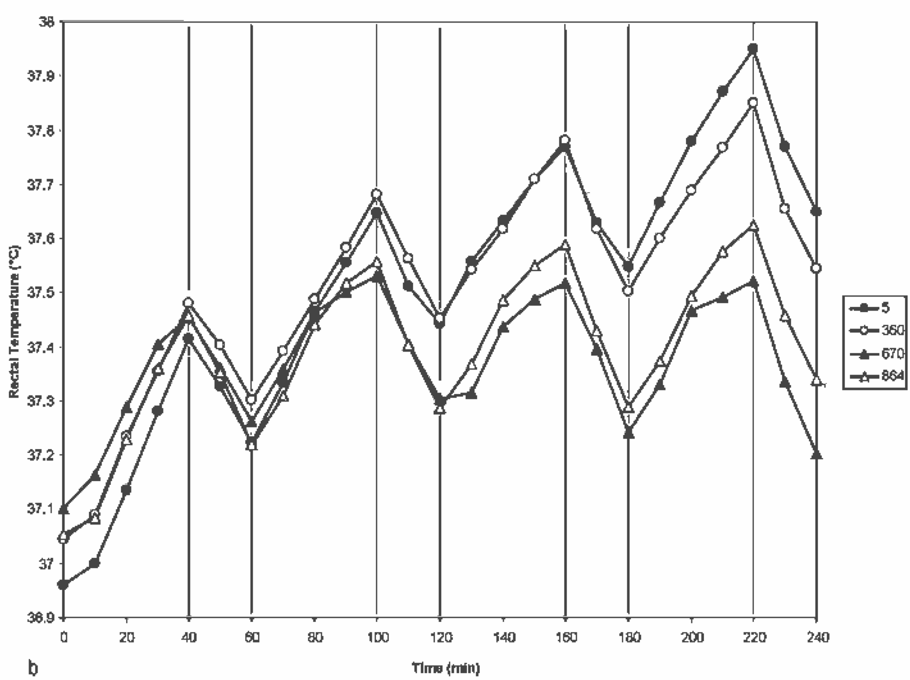

FIG. 7—*Mean rectal temperature of volunteers wearing overgarments: (a) at 18.4°C, and (b) at 29.2°C.*

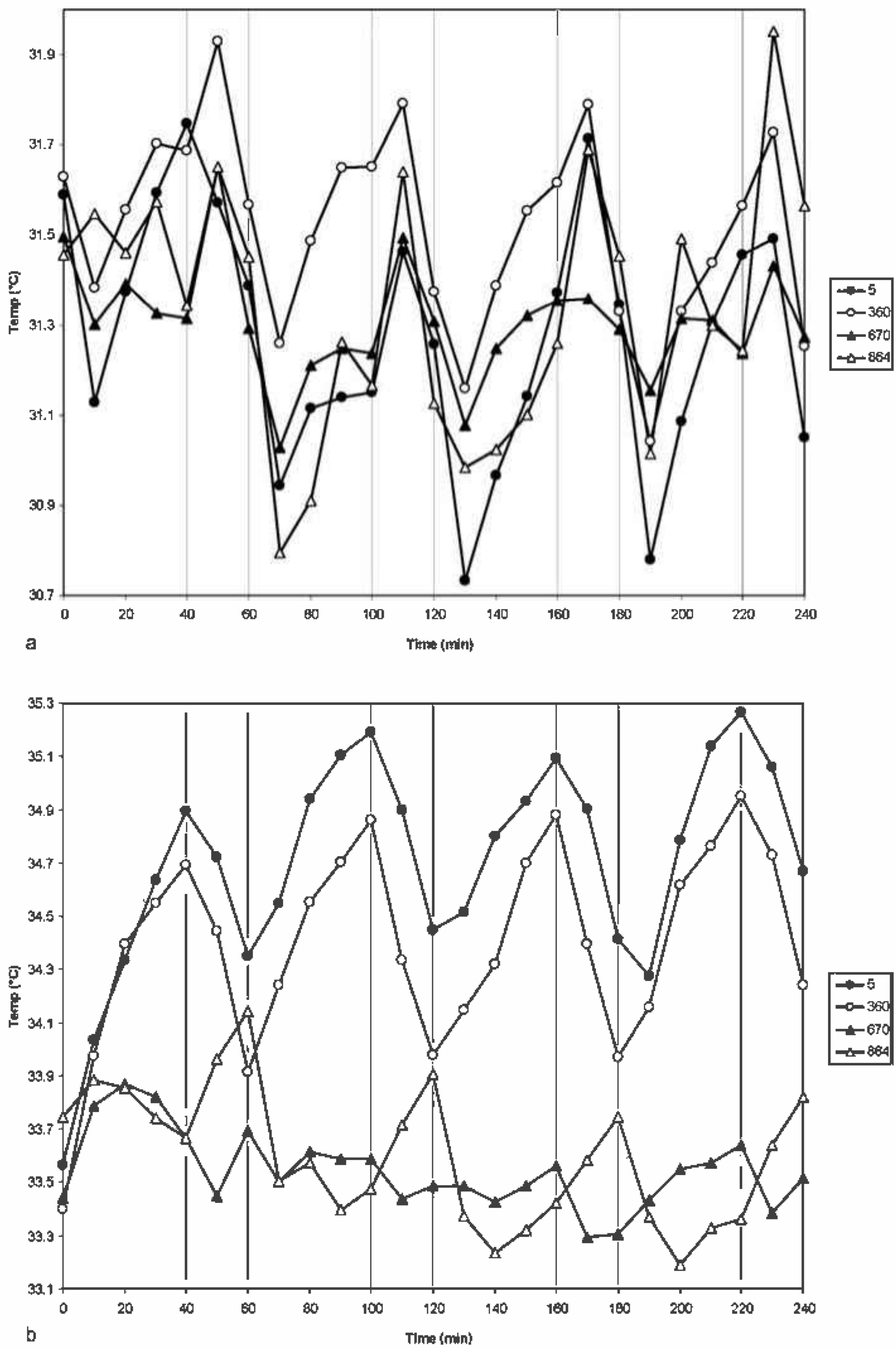

FIG. 8—*Mean weighted skin temperature of volunteers wearing overgarments: (a) at 18.4°C, and (b) at 29.2°C.*

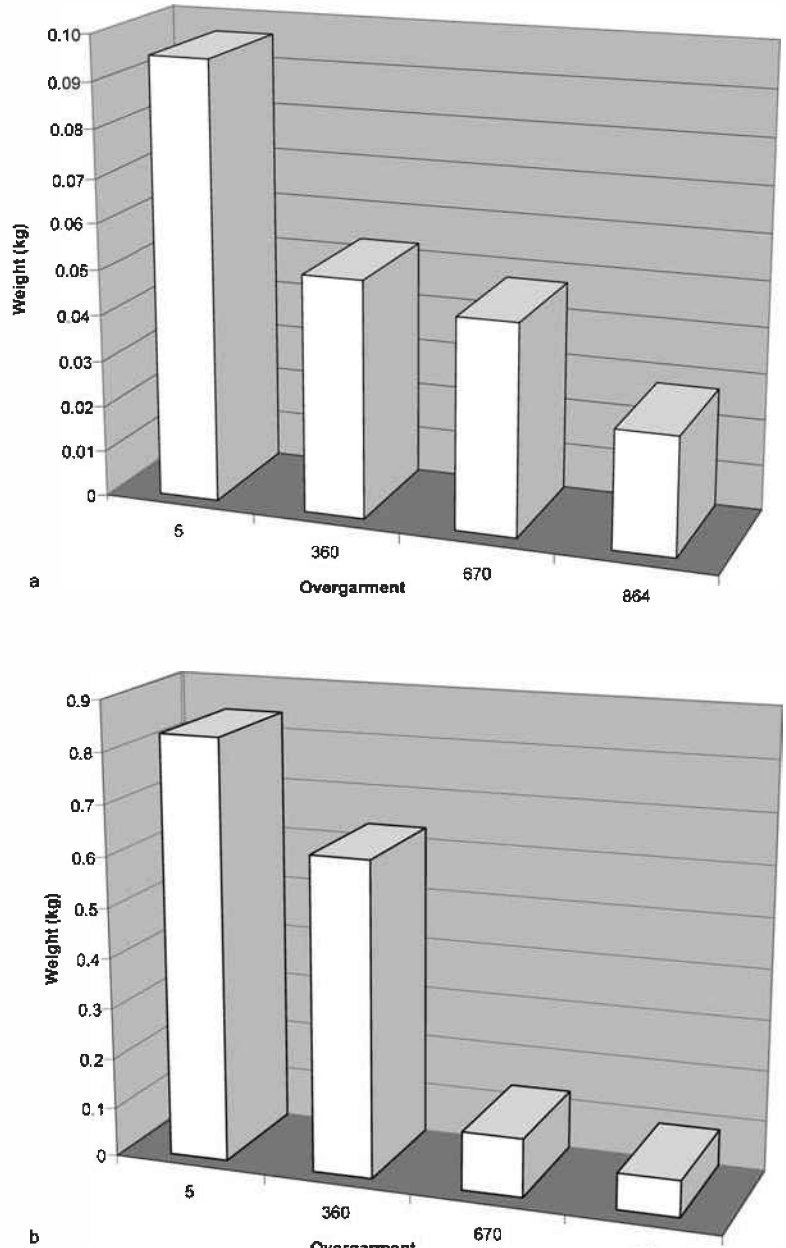

FIG. 9—*Mean weight gain of underwear, boots, and socks: (a) at 18.4°C, and (b) at 29.2°C.*

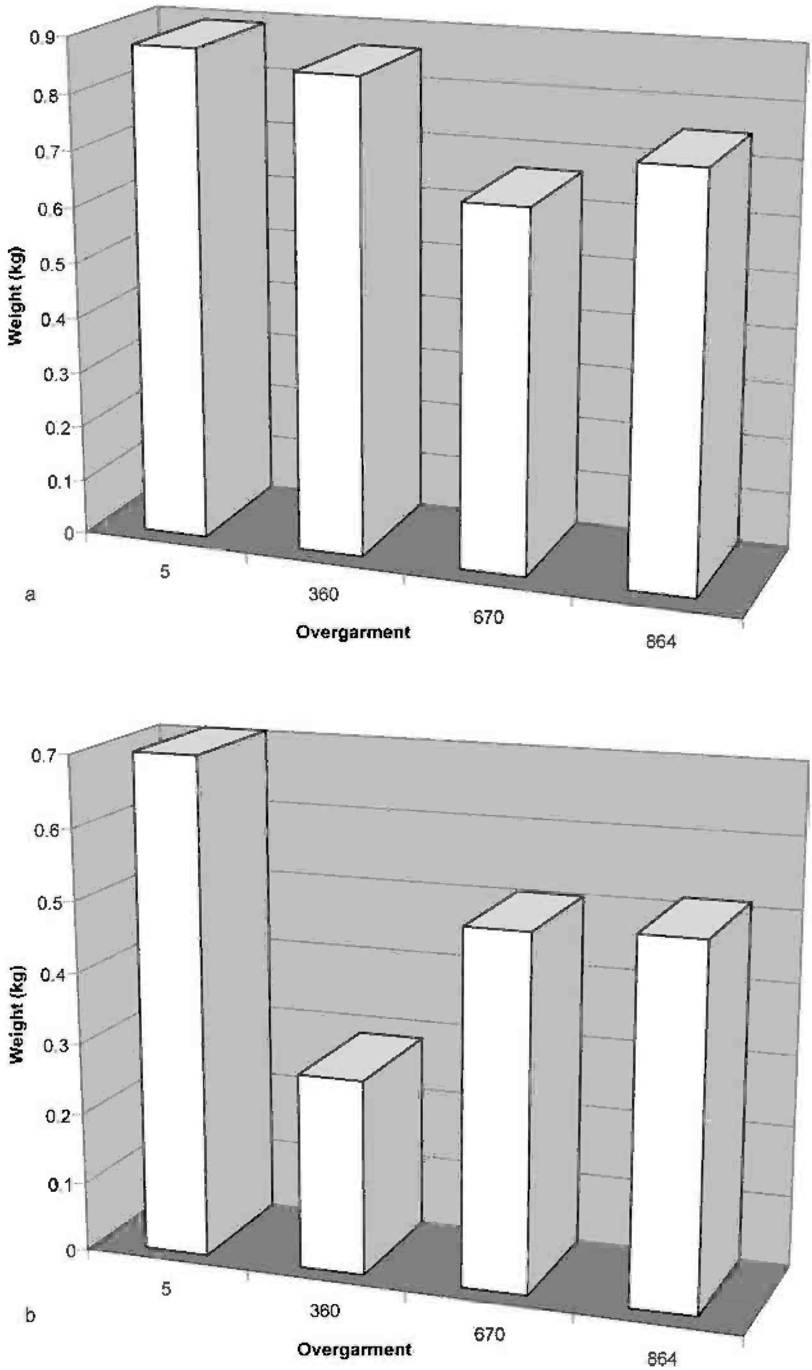

FIG. 10—*Mean body weight loss of test volunteers: (a) at 18.4°C, and (b) at 29.2°C.*

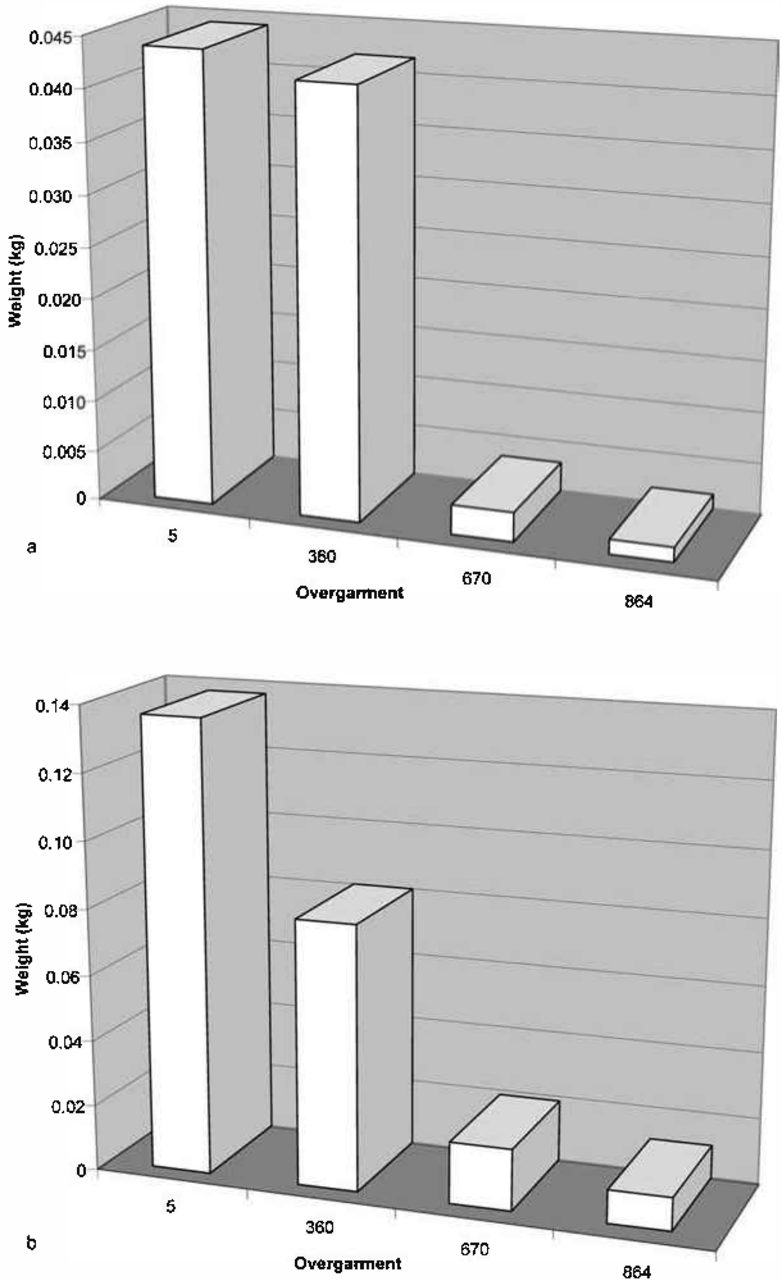

FIG. 11—*Mean weight increase of overgarments: (a) at 18.4°C, and (b) 29.2°C.*

seen, the MVTR 5 overgarment, which was objectively measured and subjectively perceived to be the thickest of all laminates, was significantly less comfortable (Tukey, HSD, $p < 0.05$) than any of the other overgarments at all time intervals in the cool condition. However, under the warm condition, comfort

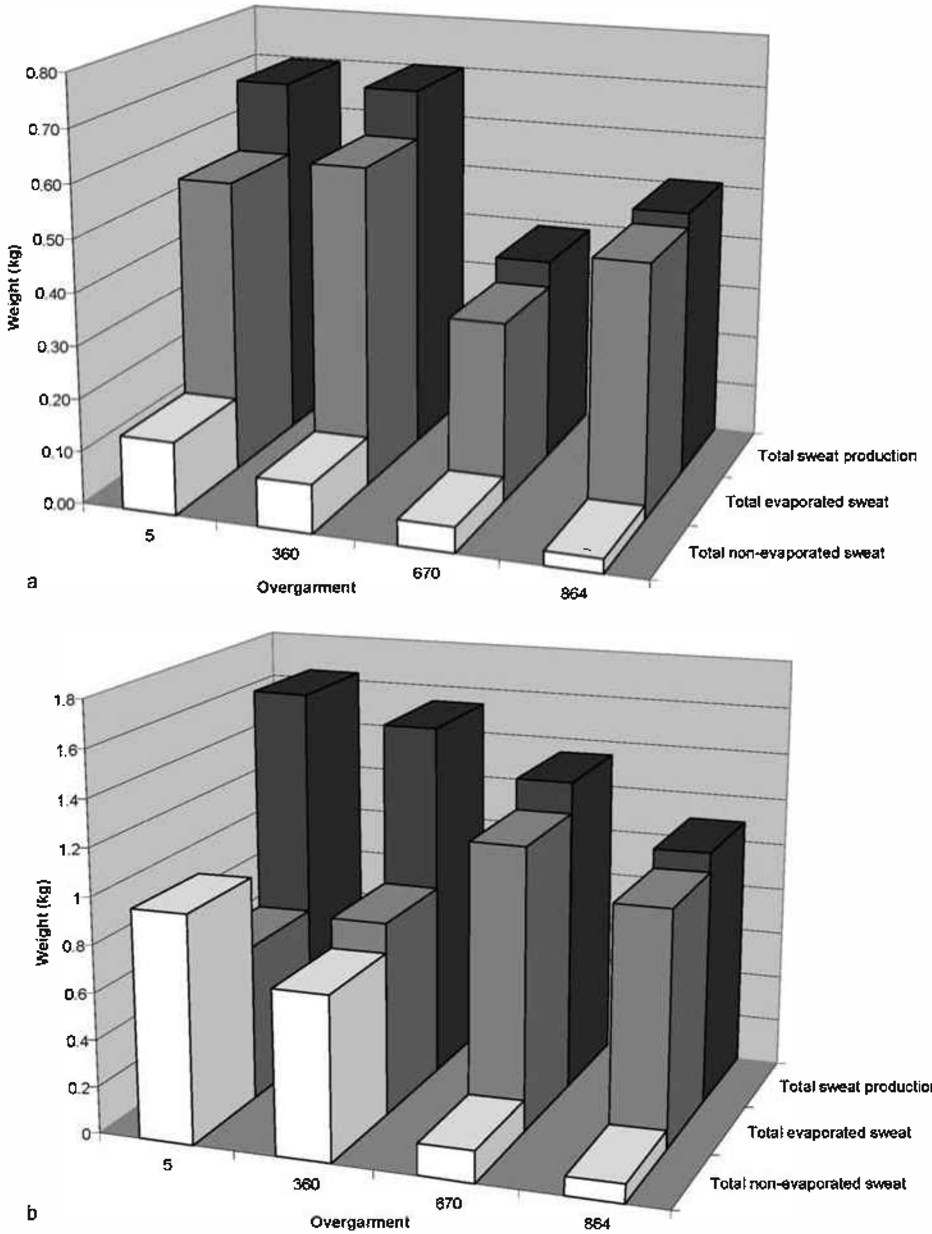

FIG. 12—*Mean sweat production: (a) at 18.4°C, and (b) at 29.2°C.*

levels were not significantly different among any of the MVTR levels. Whereas both the MVTR 5 and 360 overgarments reached the range of physiological wettedness associated with discomfort, the perceived discomfort was only statistically significant for the MVTR 5 overgarment under the cool condition.

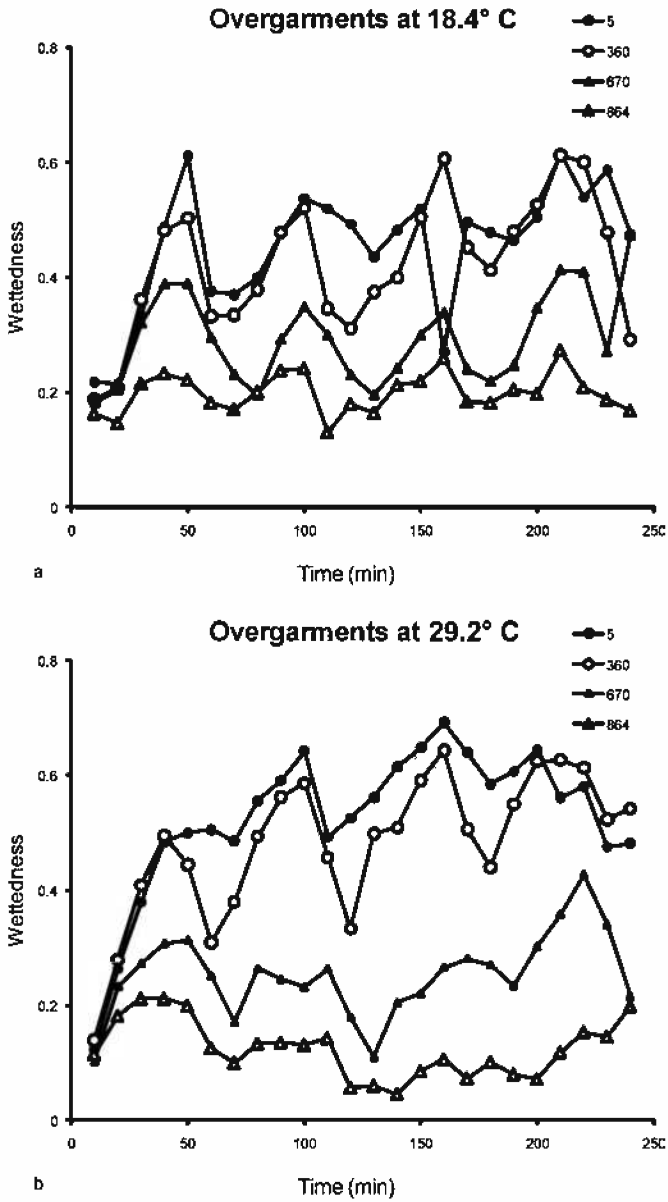

FIG. 13—*Skin wettedness of volunteers wearing overgarments: (a) at 18.4°C, and (b) at 29.2°C.*

Figures 15, 16, 17, and 18 show the data for perceived temperature (hot/cold), perceived sweatiness, perceived wetness of undergarment and perceived skin wettedness. Once again, whereas there was a significant difference in the thickness of the MVTR 5 laminate, which could impact thermal

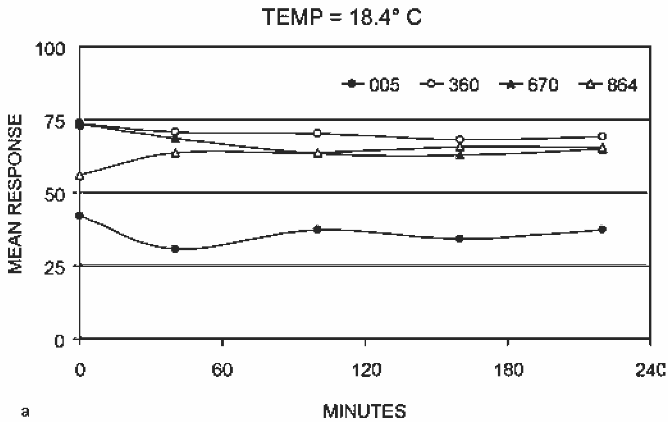

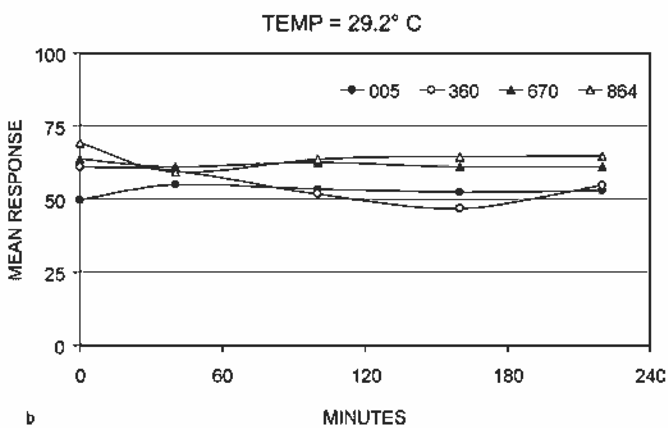

FIG. 14—*How comfortable/uncomfortable are you right now: (a) at 18.4°C, and (b) at 29.2°C.*

conductivity, there was no statistically significant difference in perceived thermal comfort between the overgarments. For all variables, there was a statistically significant difference between temperature conditions, with the warmer condition producing significantly ($p < 0.001$) greater perceived temperature, sweatiness, wetness of undergarments, and skin wettedness. These sensations increased over time in the chamber, especially in the warmer condition. However, there were no significant differences among garments of varying MVTR levels in either the cool or warm conditions.

Figure 19 shows the data for perceived perspiration collecting inside the overgarment. As can be seen, there was a clear and significant difference ($p < 0.001$) between temperature conditions, with greater perception of liquid perspiration in the warm condition. Whereas there was a significant effect of overgarment MVTR level in the warm condition, the data show the MVTR 360 overgarment to be significantly higher ($p < 0.001$) than the

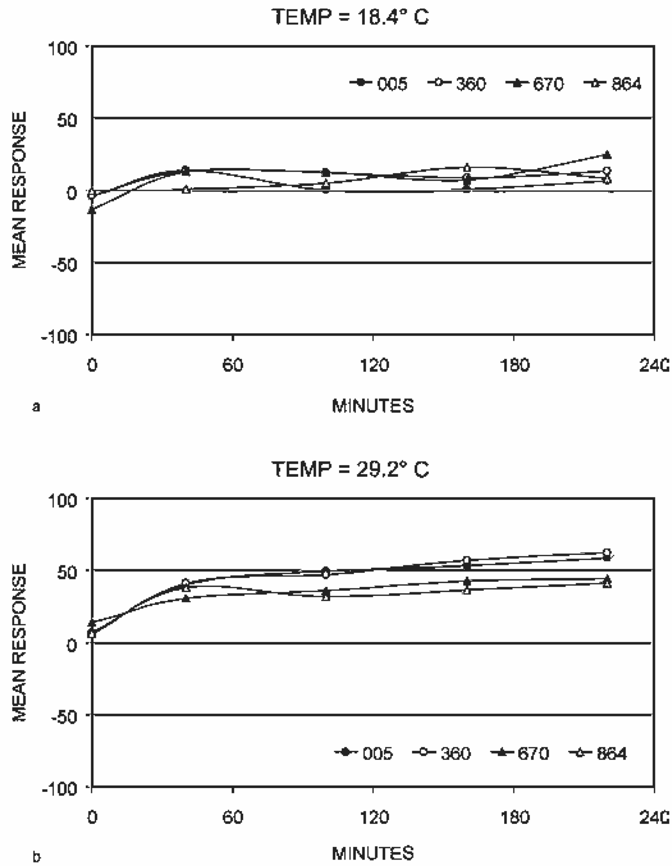

FIG. 15—*Are you hot, neutral, or cold right now: (a) at 18.4°C, and (b) at 29.2°C.*

MVTR 864 overgarment, especially after 2 h, but the MVTR 5 overgarment was intermediate between these two. There were no significant effects of either temperature condition or MVTR level for perceptions of wettedness of feet/socks.

Overall, the sensory data show significant effect of temperature on almost all measured variables, with greater perceptions of discomfort, temperature, and sweat-related variables at warmer temperatures. In addition, these variables show systematic increases as a function of time in the chamber, especially in the warm condition. Whereas the MVTR 5 overgarment produced significantly lower comfort than all other MVTR levels, this effect was only observed under the cool condition. This effect may be a result of the volunteers being somewhat cooler in this condition, which in a non-permeable garment would produce feelings of clamminess. The significantly greater perception of perspiration inside their garments for those wearing the MVTR

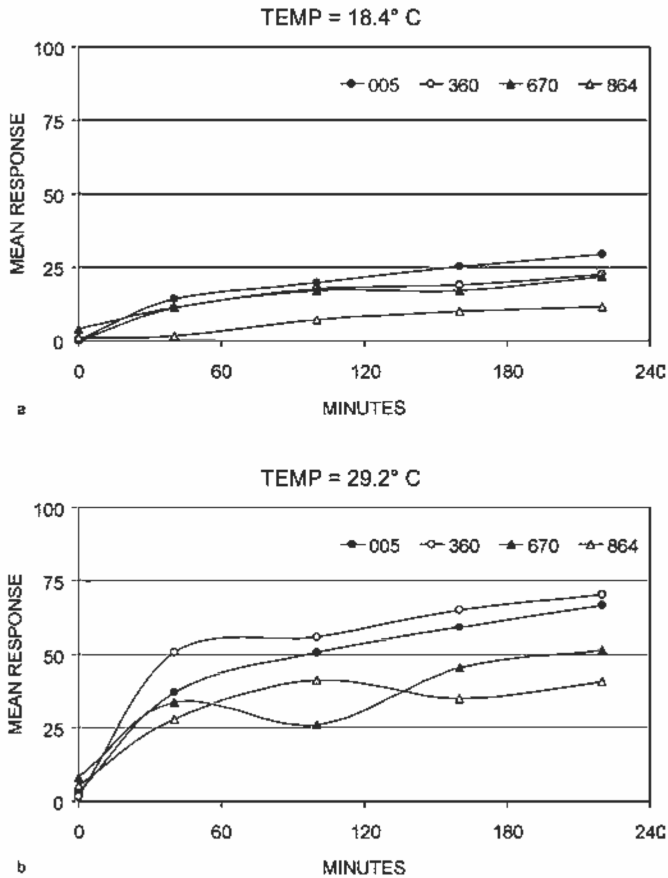

FIG. 16—*How sweaty are you right now: (a) at 18.4°C, and (b) at 29.2°C.*

360 overgarment versus those wearing the MVTR 864 overgarment appears to primarily be because of the precipitous drop in this sensation for the MVTR 864 overgarment after 2 h in the chamber. It is not clear why the MVTR 5 overgarment was intermediate to these two overgarments, but the data in Fig. 19(*b*) show a high degree of variability with time in the chamber.

Conclusions

Overall, volunteers wearing the MVTR 5 and 360 overgarments experienced greater thermal strain under warm conditions as indicated by elevated heart rate, rectal temperature, or skin temperature when compared to MVTRs of 670 and 864. As a result, volunteers produced more sweat to enhance evaporative cooling as measured by greater sweat production and skin wettedness. Because

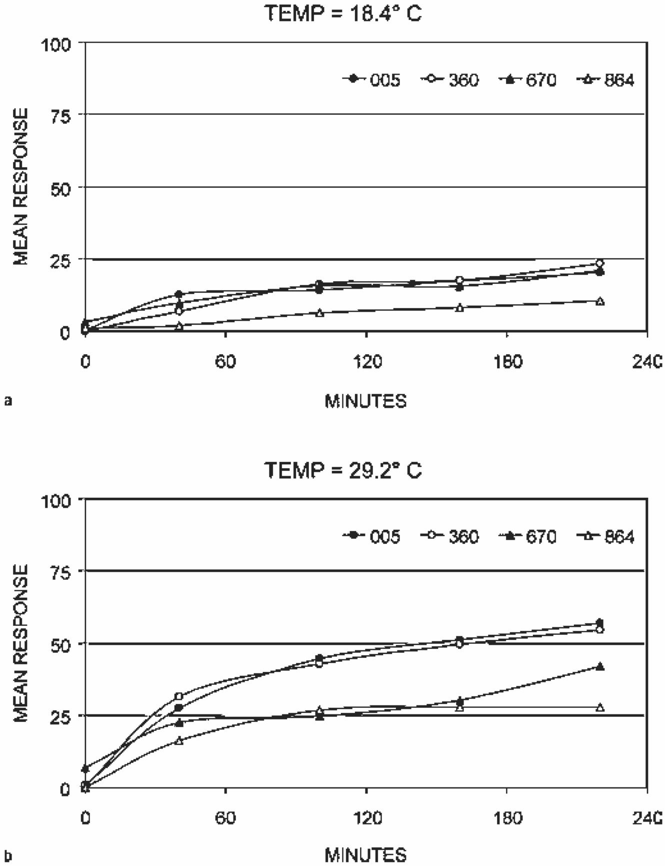

FIG. 17—*How wet does your undergarment feel right now: (a) at 18.4°C, and (b) at 29.2°C.*

of the very low microporosity of the MVTR 5 and 360 membranes, which prevented the moisture vapor from escaping, the weight of the overgarments, underwear, boots, and socks, was greater than those of higher MVTR. The MVTR 670 demonstrated the most steady skin temperature and lowest rectal temperature under the warm condition, and greatest sweat evaporation throughout the prolonged intermittent exercise. Although the sensory data generally support these findings, with the MVTR 5 producing greater mean discomfort levels than all other overgarments at both cool and warm conditions, the difference only reached significance in the cool condition. In addition, whereas sweat-related variables differed significantly between the cool and warm conditions and increased over time, there was only one significant difference among the overgarment MVTR levels. That effect showed that the MVTR 864 level produced less perspiration inside the overgarments than the MVTR 360 level overgarment, with no other differences being statistically significant.

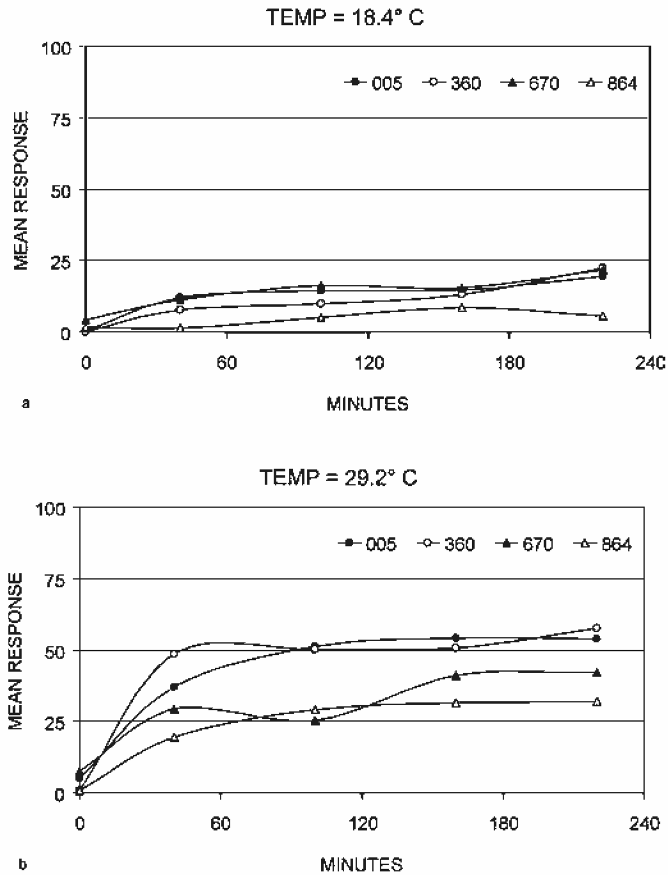

FIG. 18—*How wet does your skin feel right now: (a) at 18.4°C, and (b) at 29.2°C.*

Recommendations

The physiological findings clearly indicate that MVTR has an effect on the thermoregulatory responses of volunteers, and of the four evaluated, MVTR 670 was identified as the least stressful. Although the sensory data showed fewer differences, this may simply mean that the differences did not rise to conscious awareness. Now that an optimum MVTR material has been identified (from the group evaluated) it is recommended that follow-on studies focus on identifying the differences between physiological and sensory responses of overgarments made from semi-permeable (MVTR 670 or equivalent) and air permeable fabrics such as the U.S. Army Advanced Combat Uniform fabric (MIL-C-44436). These garments should be worn with a t-shirt and briefs rather than long underwear (as was used in this study) to measure and understand the effects of moisture vapor permeability and air permeability on tactile as well as thermal comfort.

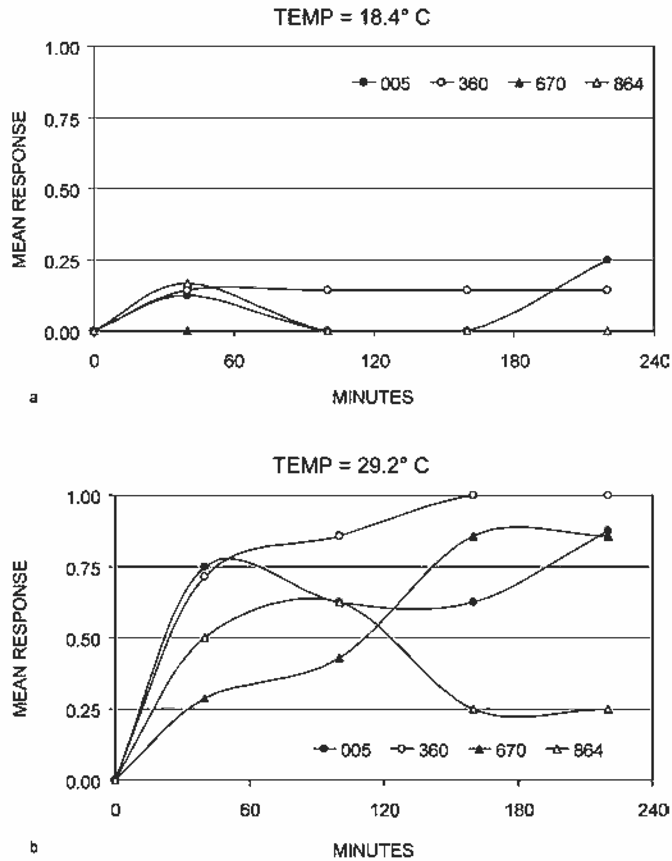

FIG. 19—*Liquid dripping inside your garment: (a) at 18.4°C, and (b) at 29.2°C.*

References

[1] Burton, A. C., and Edholm, O. G., *Man in a Cold Environment*, Edward Arnold, London, 1955.

[2] Rees, W. H., "The Transmission of Heat through Textile Fabrics," *J. Textile Inst.*, Vol. 32, 1941, pp. T149–T165.

[3] ASTM E96-80, 1984, "Standard Test Methods for Water Vapor Transmission of Materials," *Annual Book of ASTM Standards*, Vol. 04.04, ASTM International, West Conshohocken, PA pp. 368–375.

[4] Endrusick, T. L., and Gonzalez, R. R., "Effects of Wearing Impermeable and Permeable Protective Clothing on Thermoregulatory Responses While Sedentary," *Proceedings of the Eighth International Conference on*

Environmental Ergonomics, Orlando, FL, Defense Threat Reduction Agency, San Diego, CA, 1998, pp. 187–190.

[5] Allan, K., Brunye, T., and Kramer, F. M., "Influence of Moisture Vapor Transfer Rate on Cognitive and Physical Performance," *Chemical Biological Defense Science & Technology Conference*, 2010.

[6] Hollies, N. R. S., Custer, A. G., Morin, C. J., and Howard, M. E., "A Human Perception Analysis Approach to Clothing Comfort," *Textile Res. J.*, Vol. 49, 1979, pp. 557–564.

[7] Gagge, A. P., Stolwijk, J. A. J., and Hardy, J. D., "Comfort and Thermal Sensations and Associated Physiological Responses at Various Ambient Temperatures," *Environ. Res.*, Vol. 1, 1967, pp. 1–20.

[8] Hollies, N. R. S., "Investigation of the Factors Influencing Comfort in Cotton Apparel Fabrics," *Contract 12-14-100-7183(72)*, U.S. Dept. of Agriculture, New Orleans, 1965.

[9] Sweeney, M. M., and Branson, D. H., "Sensorial Comfort. Part I: A Psychophysical Method for Assessing Moisture Sensation in Clothing," *Textile Res. J.*, Vol. 60, 1990, pp. 371–377.

[10] Sweeney, M. M., and Branson, D. H., "Sensorial Comfort. Part II: A Magnitude Estimation Approach for Assessing Moisture Sensation," *Textile Res. J.*, Vol. 60, 1990, pp. 447–452.

[11] Borg, G., "A Category Scale with Ratio Properties for Intermodal and Interindividual Comparisons, *Psychophysical Judgment and the Process of Perception*, H.-G. Geissler and P. Petxoid, Eds., VEB Dentxcher Veriag der Wissencschaften, Berlin, 1982, pp. 25–34.

[12] Marks, L. E., Borg, G., and Ljunggren, G., "Individual Differences in Perceived Exertion Assessed by New Methods," *Percept. Psychophys.*, Vol. 34, 1983, pp. 280–288.

[13] Borg, G., and Ljunggren, G., "General and Differential Aspects of Perceived Exertion and Loudness Assessed by Two Methods," *Report No. 636*, Department of Psychology, Stockholm University, 1985.

[14] Cardello, V. A., Winterhalter, C. A., and Schutz, G. H., "Predicting the Handle and Comfort of Military Clothing Fabrics from Sensory and Instrumental Data: Development and Application of New Psychophysical Methods," *Textile Res. J.*, Vol. 73, No. 3, 2003, pp. 221–237.

[15] Gonzalez, R. R., "Biophysical and Physiological Integration of Proper Clothing for Exercise," *Exercise and Sport Sciences Reviews*, Vol. 15, K. B. Pandolf, Ed., Macmillan, New York, 1987, Chap. 9, pp. 261–295.

[16] Gonzalez, R. R., Endrusick, T. L., and Levell, C. A., "Biophysical Properties and Skin Wettedness of Garments with Variable Moisture Vapor Transmission Rates (MVTR)," *J. Thermal Biol.*, Vol. 23, No. 1, 1998, pp. 41–48.

[17] Gagge, A. P., and Nishi, Y., "Heat Exchange between Human Skin Surface and Thermal Environment," *Handbook of Physiology (Bethesda)*, Waverly, Baltimore, 1977, Chap. 9, pp. 69–92.
[18] Berglund, L. G., Cunningham, D. J., and Stolwijk, J. A. J., "The Resistance Type Dew Point Sensor for Moisture Measurements on Sweating Humans," *Proceedings of the Sixth Conference on Biometeorology and Aerobiology*, American Meteorological Society, Boston, 1983, pp. 6–9,
[19] Fanger, P. O., *Thermal Comfort*, McGraw-Hill, New York, 1970.
[20] Kerslake, D., McK., *The Stress of Hot Environments*, Cambridge University Press, Cambridge, 1972.
[21] Gagge, A. P., Stolwijk, J. A. J., and Hardy, J. D., "Comfort and Thermal Sensations and Associated Physiological Responses at Various Ambient Temperatures," *Environ. Res.*, Vol. 2, 1969, pp. 209–229.

Performance of Protective Clothing and Equipment: Emerging Issues and Technologies
STP 1544, 2012
Available online at www.astm.org
DOI:10.1520/STP104099

Jessica Barker,[1] *Lynn M. Boorady,*[2] *Shu-Hwa Lin,*[3]
Young-A Lee,[1] *Beth Esponnette,*[4] *and Susan P. Ashdown*[4]

Assessing User Needs and Perceptions of Firefighter PPE

REFERENCE: Barker, Jessica, Boorady, Lynn M., Lin, Shu-Hwa, Lee, Young-A, Esponnette, Beth, and Ashdown, Susan P., "Assessing User Needs and Perceptions of Firefighter PPE," *Performance of Protective Clothing and Equipment: Emerging Issues and Technologies* on 16 April 2011 in Anaheim, CA; STP 1544, Angie M. Shepherd, Editor, pp. 158–175, doi:10.1520/STP104099, ASTM International, West Conshohocken, PA 2012.

ABSTRACT: The purpose of this study was to evaluate user perceptions of firefighter personal protective equipment (PPE) to determine ways to improve PPE design and function for both male and female firefighters. No previous studies have included both male and female firefighters in identifying user needs. It is critical to consider the entire PPE that a firefighter wears in his or her work environments, due to the various items worn simultaneously, to ensure a system that is fully functional and minimizes impact on wearer work performance and comfort. A total of 12 focus group interviews were conducted of career and volunteer firefighters, utilizing 67 males and 22 females. Urban and rural companies were represented from five different states. To obtain more in-depth data than the focus group interviews allowed, three firefighters participated in individual follow-up interviews. All interviews were recorded, transcribed, and analyzed using thematic analysis methods to draw comparisons of perceptions and user needs shared by both male and female firefighters. Both male and female firefighters identified a number of similar concerns such as excessive weight of the PPE, heat stress, overprotection for non-fire calls, garment fit and restricted mobility, compression burns, and problems donning the PPE quickly. They also indicated concern about specific firefighter clothing features that did not function well for them,

---

Manuscript received June 2, 2011; accepted for publication May 16, 2012; published online September 2012.

[1]Dept. of Apparel, Educational Studies, and Hospitality Management, Iowa State Univ., Ames, IA 50011.
[2]Technology Dept., Buffalo State College, Buffalo, NY 14222.
[3]Dept. of Family and Consumer Sciences, Univ. of Hawaii at Manoa, Honolulu, HI 96822.
[4]Dept. of Fiber Science and Apparel Design, Cornell Univ., Ithaca, NY 14850.

including pockets, fasteners, knee and suspender padding, as well as the durability of the materials used in the PPE. Further study is needed to determine optimum design changes that can improve firefighter PPE to maximize wearer protection, performance, and comfort.

KEYWORDS: firefighter, turnout gear, personal protective equipment

Introduction

In 2010, there were more than 1.1×10^6 firefighters in the United States, approximately 800 000 volunteer firefighters and 350 000 career firefighters [1]. Firefighters respond daily to a diversity of emergency calls, including medical aid, fire, hazardous materials incidents, and vehicle incidents. Firefighters also encounter a variety of conditions, from freezing weather to blazing fire. Creating successful firefighter personal protective equipment (PPE) requires incorporating protection from multiple hazards while addressing users' physiological and task-related performance needs for varying environments [2]. The entire PPE system must be considered due to the different material properties of each component and how components interact on the body. Current PPE consists of thermally protective coat, pants, gloves, and boots. Some firefighters choose to wear suspenders. Firefighters also wear protective helmets with a protective hood under the helmet. A self-contained breathing apparatus (SCBA) is worn over the coat and attaches to a face-mask. Depending on department protocol and time of day, either station uniforms or casual clothing are worn under the PPE.

The National Fire Protection Association (NFPA) has established standards for structural firefighting [3], including the thermal protection provided by the materials, visibility (e.g., location and amount of reflective tape), and protective properties of the helmet, gloves [4], and boots. PPE components are regularly tested to ensure design and materials provide compliance to protective standards set by the NFPA.

A vast amount of research has been done related to firefighter PPE, including comparing protective properties of materials [5], optimal layers of fabric [6] and visibility provided by reflective components [7]. In order to determine the effectiveness of thermal protection provided by firefighter PPE, burn test manikins have been utilized to illustrate where protection may be inadequate [8]. These studies provide valuable information, but the data is limited by testing PPE on a static, inanimate figure. Movement and working positions, which greatly affect the level of heat protection, were not explored during these studies.

Testing has been done to determine differences in the physiological effects of PPE on firefighters. Research has evaluated the effect of specific types of PPE designs on firefighters [9], such as one-piece coveralls or two piece coat and pant designs. In addition, other research has tried to develop simulation methods to evaluate the effects of wearing PPE while firefighters complete simulated work tasks [10]. While such studies furthered understanding of the complex requirements of firefighter PPE, they cannot provide a comprehensive picture of the job-related experiences of firefighters.

A high percentage of firefighter deaths occur on the job due to overexertion and subsequent heart attacks, which are often attributed to trapped heat and the weight of the firefighting ensemble. In 2010, 61 % of firefighter fatalities were caused by stress and overexertion; 56 % of all fatalities were directly linked to heart attacks [1]. Only 2 % of all deaths were caused by burns or heat exhaustion [1]. The insulative properties of firefighter PPE cause it to be bulky, stiff, and heavy; thus the wearer experiences decreased mobility and comfort and increased physical stress [9,11,12]. The level of protection provided to keep firefighters safe in a fire can also increase the risk for responding to other types of emergency situations (e.g. medical calls), by increasing physical stress firefighters endure even in non-fire environments [13]. Wearing the PPE requires additional effort to complete even simple tasks such as walking and bending, creating additional physical stress for the user anytime the PPE is worn [9,13]. Understanding how firefighters perceive this stress and the impact of wearing their PPE could lead to improvements in firefighter PPE.

Rosenblad-Wallin [14] advocated a user-oriented product development approach for PPE because the user interacted as part of the PPE system. By including the end user in the development process through methods such as focus groups and interviews, problems could be identified and ranked by priority [15]. Research has indicated that PPE comfort and fit could be improved when employees actively participated in selection and testing [16]. Involving wearers in the design, selection, and testing process allowed their knowledge of PPE to increase; they became more accepting of the PPE and more likely to wear it [16]. The user-oriented design approach has been found to create garments that are desired by and acceptable to the end user [17].

No recent studies were found that explored firefighter needs and perceptions related to their PPE. Firefighter PPE should allow the necessary protection while minimizing impact on worker performance and comfort. This study was designed to identify firefighter perceptions related to their current PPE to serve as a guide for future PPE design and research efforts. This research also explored firefighter knowledge levels and behaviors regarding their PPE that could impact equipment performance and function, a critical piece of information for creating successful future designs.

Methods

This study was designed as an exploratory study of firefighters' needs and perceptions related to their PPE. To gain a broad representation of firefighters while still obtaining in-depth information, a two-part study was designed. In Phase I, focus groups were carried out with a wide variety of firefighter participants. A total of twelve focus group interviews were conducted utilizing 67 male and 22 female career and volunteer firefighters (Table 1). This follows the guidelines and recommendations set forth by Sandelowski [18] and Marshall [19] regarding sampling techniques and sample size for qualitative studies. Urban and rural companies were represented from five different states. An initial interview script was followed for each focus group interview to reduce interviewer bias. Follow-up questions were asked as needed for clarification of issues. The focus groups lasted from 60 to 90 min.

To obtain more in-depth data than the focus group interviews allowed, three firefighters were interviewed individually in Phase II. Each firefighter was interviewed using an extensive interview script that covered the topics of comfort, protection, mobility, function, donning, PPE design, and education over the course of about 80 questions. Although some questions required specific yes/no answers or responses to Likert-type scales, the majority of the questions were open-ended. Through the use of combined targeted questions

TABLE 1—*Focus group information.*

Site Number	Site	Date	Population Served	Type of Department	Total Number of Firefighters	Number of Male Participants	Number of Female Participants
1	Ames, IA	July 2008	Urban 58 000	Career	39	9	0
2	Ithaca, NY	June 2008	Rural 30 000	Career	65	7	0
3	Jefferson City, MO	August 2008	Urban 40 000	Career	75	6	1
4	Apache Flats, MO	August 2008	Rural 9500	Volunteer	40	10	0
5	Kawui, HI	July 2008	Urban 64 000	Career	100	8	0
6	Honolulu, HI	October 2009	Urban 902 168	Career	1200	21	0
7	St. Louis, MO	June 2009	Urban 350 000	Career	850	6	2
8	Gladstone, MO	August 2009	Urban 27 500	Career	82	6	5
9	Ames, IA	January 2009	Rural 17 333	Volunteer	73	0	3
10	Des Moines, IA	June 2009	Urban 450 000	Career	250	0	3
11	Honolulu, HI	October 2009	Urban 902 168	Career	1200	0	12
12	Ft. Worth, TX	August 2009	Urban 650 000	Career	900	0	2

and open-ended questions, data was obtained that provided further clarification than the focus group interviews allowed.

All interviews were recorded, transcribed, and analyzed using thematic analysis methods to draw comparisons of issues shared by both male and female firefighters from varying regions. The exploratory nature of the study allowed researchers to capture information about how current PPE is meeting firefighters' needs, as well as firefighters' perceptions and experiences while wearing their PPE.

Results

Due to the number and open-ended nature of the questions asked, both the focus group interviews and the three individual interviews produced a great deal of valuable data. Firefighters were encouraged to relate their experiences and issues with their PPE. Participants answered questions based on their individual PPE. Brands and styles of PPE worn by participants varied due to departmental and individual purchasing decisions. Despite variations in PPE brands and styles, regions of the country, or personal firefighter characteristics (e.g., male or female, body size), many of the areas of concern expressed were consistent among the firefighters. In addition, the issues identified through the in-depth interviews mirrored those related by participants of the focus group interviews, and provided additional clarification for better understanding of the firefighters' concerns.

This study was designed to capture issues common to all firefighters; thus only issues identified by both male and female, career and volunteer firefighters are reported. Issues identified specific to subgroups of firefighters are not identified within the constraints of this study. Through the use of thematic qualitative analysis methods, we identified three overarching concerns of firefighters: (1) the effect of the PPE on the wearer, (2) PPE features and function, and (3) the protective properties of PPE. For the purposes of this study, PPE was used to describe the whole system of protective clothing and gear firefighters wear, and firefighter clothing was used to describe the combination of protective coat and pants/bibs firefighters wear. Individual PPE components are referred to by their respective names (e.g., helmet, boots).

Effects on the Wearer

Firefighter PPE is designed with enough protection to allow an escape from otherwise unsurvivable conditions. While this function of the PPE is paramount to firefighter safety, the PPE is worn at all times firefighters are responding to calls, both fire and non-fire. Participants in our study therefore reported on how their PPE affects them throughout the range of activities they perform when wearing the PPE. Participants in the focus groups expressed unease about how their PPE affects them physically and physiologically. They were aware that the majority of firefighter fatalities are caused by cardiac arrest rather than more direct injuries from fighting fires (e.g., burns). In the focus groups, they indicated their concern that their PPE creates additional heat stress, muscle fatigue, and reduced mobility. These same issues were discussed in-depth by firefighters in the individual interviews.

Firefighters reported experiencing heat stress and discomfort from the firefighter clothing thermal barrier, which has very limited means of releasing the buildup of body heat. Physical exertion combined with the temperatures from a structural fire can bring the body temperature up to dangerously high levels, causing extreme thermal discomfort and eventually leading to heat stress. A participant from an urban Midwestern fire department wondered:

> "I do not see why we cannot incorporate some of that cool technology. We can manage in the winter time with the cold, but in the summer, 30 min into a working fire and you are overheating and there is nothing you can do about it. I mean, you could come out and drink all the water you want until you are ill, and you are still not going to recover, you know in 10 min. So it, definitely we're going to have to have something that gets the heat and the moisture away from you (Table 1, Site number 7)."

The firefighter clothing's thermal barrier can trap heat and absorb moisture. This causes additional issues for firefighters beyond heat stress when they sweat in their firefighter clothing or the outer shell of the clothing gets wet enough to soak through to the inner thermal barrier. One female firefighter described the effect of this in the winter:

> "If your shell is wet, the inner shell does not get dry. So, it is horrible putting on wet gear…, you know, a lot of people…, they will go into the house fire, wherever that fire was at, even though it may be out, to warm up because the house is still warm. But as soon as you come back outside, if you have been sweating, the inside of your gear will freeze and the outside of your gear will freeze and then you are colder and then you cannot get warmed up. So you will see a lot of people just stay outside and, you know, take the cold versus refreezing. … Because when you are in house fire and you are working and it is hot, you get to sweating. So your whole inner liner gets soaked. And then when you go outside and it is frigid cold outside, then the outer shell freezes and the inner shell freezes. … And then you are sweating so your inside clothes are wet. So you do not really have that layer of protection (Table 1, Site number 10)."

In the follow-up interviews, the firefighters all agreed that their PPE over-prepares them for nearly all of their non-fire calls (e.g., medical response calls). Each noted that temperature, perspiration rate, and heart rate all increased noticeably when they were in their PPE. The weight of the PPE makes it difficult to carry and the thermal protective qualities of the firefighter clothing traps large amounts of body heat, both of which contribute to elevated perspiration and heart rates. One of the firefighters expressed the over-preparedness succinctly: "street clothing is often more suitable" (Table 1, Site number 2). However, they think the benefits of suiting up for every call are worth the drawbacks, including the "false sense of security" (Site number 2) some firefighters develop when wearing their PPE. When asked, "Are you satisfied with suiting up for every call just in case it is worse than anticipated?" two answered that "usually [they] would prefer to wear the safety gear," and one responded that "it depends" (Site number 2).

Participants from seven different focus groups reported experiencing extreme muscle fatigue from the weight of their PPE, specifically in their neck muscles from wearing the helmets. One urban firefighter said,

> "It would be nice if our helmets were a little lighter…they are heavy. I mean, initially it does not feel that heavy, but then when you have to wear it for a while. I mean, that's one of the first things I want to take off is the helmet because your neck gets tired. It would be nice if they could be durable and a little lighter (Table 1, Site number 5)."

Despite the prevalence of this concern among focus group participants, it was not discussed in the follow-up interviews. Still, helmet weight warrants further investigation since it was identified as an issue in the majority of the focus groups.

The participants in both focus groups and individual interviews noted that they were often affected by reduced mobility when wearing their PPE. In general, firefighters believed this was caused by the bulkiness of the firefighter clothing. One male firefighter said, "I think it is too bulky. You know, you walk around, you cannot, you can barely move. They need to kind of make it a little bit better" (Table 1, Site number 9). Another echoed his sentiment, providing a more detailed description:

> "You have to bend your leg up over a sill if the garage does not open up enough, it is really hard to get your leg in the window. The joints, being able to move because it seems like just walking down the hall of a building takes a lot more work in turnout gear, because the legs are rubbing together as you are walking, joints are sometimes stiff (Table 1, Site number 2)."

The individually interviewed firefighters also commented that the knees of their firefighter clothing are typically hard to bend with all of the protective material, forcing the firefighters to expend more energy in movement.

Similarly, participants in both the focus groups and the follow-up interviews described frustration with the dexterity in their gloves. In order to protect against heat, there must be a certain amount of protective material, but in order to be flexible and dexterous, material at the joints needs to be minimized. Thinner gloves have been made available recently, but none of the participants in this study had been given the opportunity to adopt the improved gloves.

Features and Function

The second area of concern for firefighters in our study related to the features of the firefighter clothing and how the clothing functioned for firefighters performing their job-related tasks. The comments centered around two features of the clothing: closures and pockets. The function of closures affected the firefighters' ability to don the clothing quickly, a requirement of their job necessary for quick response times. The pocket design and function allowed firefighters to carry and access their tools more readily when responding to a call.

Participants from six focus groups (Table 1, Sites number 1, number 2, number 7, number 8, number 9, and number 12) related frustration with the design of the closures on their firefighter clothing. They felt the zippers were problematic for donning their clothing, while hook and loop tape was not durable enough. When asked what she would change about her firefighter clothing, a volunteer firefighter responded, "Sometimes the zipper. You know, getting it started is a little difficult. But part of that is the haste thing. But they are sometimes difficult to get started" (Site number 9). A career firefighter from another focus group responded similarly, "I would get rid of the zipper. I wish it was just like a snap, latch and Velcro [5] maybe, but not like the zipper" (Site number 12). Another stated, "Zippers and Velcro on everything are horrible and are the worst. The zippers all snag and unzip. The Velcro is off within four years." (Site number 8)

The durability of the hook and loop closures was mentioned by firefighters in both the focus groups and the follow-up interviews. In the focus groups, participants discussed that the stitching attaching the hook and loop tape does not hold up well, and the tape often becomes detached in places long before the firefighter clothing is ready to be replaced. In the follow-up interviews, firefighters talked about another area of concern related to hook and loop tape: when the firefighter clothing is washed, the hooks collect fibers, which is difficult to clean and is detrimental to the function of the tape. In general, the hook and loop closures were not viewed favorably by firefighters in our study.

Participants held strong opinions about the function of their pockets. They stated that radio pockets were too deep to easily remove the radio from, coat pockets were too small to accommodate gloved hands, and pockets with divided compartments were too small to store necessary equipment. One firefighter said of her pockets, "I hate them because they are divided. They are a big pocket, but then there's a divider so you cannot put your gloves in it. You cannot get your, you know, and so they are absolutely useless. And I do not use my coat pockets at all; just my inner one" (Table 1, Site number 12). Another firefighter said, "The pocket for the radio needs to be the proper size for the radio and the wire to get down in there and for you to have your mic[rophone] where you are not going to get hung up if you go in it" (Site number 7).

Protective Properties

The third area of concern for firefighters related to the protection provided by the PPE. Participants expressed unease about protection from burns, specifically from compression or direct exposure to heat, and the visibility their gear provided, a critical element when responding to calls in dark environments or vehicle incidents.

Compression burns, which are conduction burns that are intensified with a lot of pressure, are prevalent in fighting fires, as firefighters cannot avoid heat and pressure. These burns are common on the upper back and shoulder area in line with the SCBA straps, which weigh down on the back. Knees and elbows are also very prone to compression burns because of the pressure that is put on them during movement and crawling. The immediate contact between the skin, firefighter clothing fabric and external heat allows rapid conduction of the heat to the body. Each of the firefighters interviewed individually experienced this phenomenon. One firefighter interviewed received burns on the knees, elbows, shoulders, and upper back, while the others reported feeling intense amounts of heat in these areas.

Participants in the focus groups were also concerned about compression burns, and shared their desire for their PPE to have more padding in specific locations. Firefighters from eight focus groups (Table 1, Sites number 1, number 2, number 3, number 5, number 6, number 8, number 9, and number 10) indicated the padding on their knee pads was not adequate for comfort or protection from burns. These knee pads are most commonly rectangles of padded leather or cloth that snap or use hook and loop tape to attach onto the knees of the fighter clothing. Several firefighters indicated their desire for more protective padding on the knees and elbows, stating "It could have more padding because sometimes you have to crawl or get on your hands and knees" (Site number 6) and "Knee and elbow padding should be required" (Site number 8). Another firefighter remarked:

> "If you had knee pads built into the knees of the pants themselves, that would be wonderful, cause me, anymore less I have to crawl I do not. One, it is too slow, and two, I do not like to crawl. So unless I have to crawl because of visibility or heat, I will walk. But if I had knee pads built into it that would help out a lot. And then if you had knee pads maybe that would help give you more layers of protection for your knees to the floor and stuff (Table 1, Site number 3)."

There were also complaints of burns near the ears and face from exposure to high temperature. The protective hood is designed to protect these areas, but firefighters reported that their hoods often move out of place easily. The fabric is very light and has a stretch property to keep the hood in place around the face. This stretch property can lose the ability to recover over the life of the garment, causing the hood to stand away from the face when worn.

Participants in one focus group (Table 1, Site number 10) discussed this problem at length, noting that when their protective hood elasticity stretched out, it no longer created a proper seal around their face. They worried their faces would burn if they got into a fire situation where too much heat was coming through their protective hood edges. These same firefighters indicated that their protective hoods did not fit well from the start, which may cause undue strain on the elastic of their hoods.

The protective nature of the PPE can make it difficult for firefighters to sense when they have traveled too far into a hot situation. This creates a dangerous condition where the firefighter is deeper into the fire than the suit can protect. In the individual interviews, when asked: "I have heard that it is easy to be too protected and not realize when you are too far into the fire before it is too late. Have you experienced this?" all said "Yes." The most common location for firefighters to get burned in these situations is their ears, due to the protective hood losing its elasticity.

Firefighters in four focus groups (Table 1, Sites number 1, number 9, number 10, and number 11) also discussed the reflective tape used on their firefighter clothing. They indicated that the reflective tape soiled easily and was difficult to clean, diminishing their visibility when wearing the clothing at night. They also felt the reflective tape lost some reflective properties with multiple washings and expressed concern about whether civilians could see them in the dark. They suggested that more reflective tape could be incorporated in the clothing in different locations to enhance their visibility when working at night. They also indicated a desire for replaceable reflective tape, since the reflective properties of the tape do not last for the normal expected life of the clothing.

Discussion and Recommendations

The firefighters answered interview questions based on their own PPE, but the preferences of firefighters were still apparent despite inconsistencies in style and brand of PPE worn. Though all concerns that firefighters express deserve attention, the three concerns that came up most frequently during the focus groups and interviews were (1) the effect of the PPE on the wearer, (2) PPE features and function, and (3) the protective properties of the PPE.

Participants discussed ways in which the firefighter clothing creates additional heat stress, muscle fatigue, and reduced mobility while they were responding to calls. Firefighters were deeply concerned about the additional physiological stress they experienced when wearing their PPE. Although conscious of this stress and aware that their work does not always require the full protection of their PPE, they welcomed the protection and safety it provided. Yet the statistics of firefighter fatalities related to heat stress should not be ignored. Further work is needed to determine ways in which the breathability of the firefighter clothing can be improved. By doing so, firefighters will be able release heat more effectively and prevent the body from retaining heat.

Helmets deserve more research attention. Firefighters noted experiencing neck muscle fatigue after wearing their helmets for longer periods. Development of lighter weight materials for impact protection, as well as determining the best shape for protection with minimal weight is recommended to reduce the muscle fatigue firefighters currently experience. There are different helmet designs being worn by European firefighters that are closer fitting to the head and neck. This design may reduce neck muscle fatigue, and comparison testing is recommended between the two styles of helmets. Participants in our study expressed an unwillingness to consider the European helmet design, however, stating that it looked too "futuristic" (Table 1, Site number 2) and "did not look like a firefighter should look" (Site number 2). With this in mind, any changes to the traditional American firefighter look should be made gradually, with a great deal of education for firefighters to overcome misconceptions of new designs.

In addition, it is recommended that joint articulation be incorporated into all firefighter clothing design to enhance mobility. Firefighters in our study noted that they exerted more effort to move in their clothing, especially when trying to bend their knees, elbows, or fingers. Additional research needs to be conducted to reduce fabric bulk while still maintaining existing thermal protection.

Participants related a need for modifications to the closure systems on their firefighter clothing. The zipper laps, although crucial to fire protection, proved to be burdensome for the firefighters when donning their firefighter clothing. Participants in our study expressed a preference for clasp hook and latch closures for coats and pants, followed by hook and loop closures. While the hook and loop tape (e.g., Velcro) is harder to maintain, they reported that it was easier to fasten their coats and pants quickly with this tape than when trying to line up a zipper. Some participants owned firefighter clothing that had both a zipper closure with a flap that fastened down with hook and loop tape. This was the least preferred closure type. Based on our findings, it is recommended that further research be conducted to develop closure systems that are more durable and allow for faster donning of the PPE. The zippers are too arduous to fasten quickly, and the hook and loop tape is not durable enough. However, hook and loop tape is a sensible option to use for short closures (estimated at ten or fewer inches) with opposing pieces starting in a common seam to make alignment easier.

Pockets were also problematic for firefighters, and prove to be a more difficult problem to solve as preferences for pocket placement and design varied more between the firefighters. All manufacturers allow for customization of pocket placement on firefighter clothing, although many participants in our study were unaware of this option. Participants reported they utilized pants pockets more frequently than coat pockets because they were more accessible;

coat pocket access is often hindered by the SCBA straps. The majority of firefighters owned firefighter clothing with radio pockets that were designed to accommodate older styles of radios that were much longer than current radio designs; thus they struggled to remove their newer, smaller radios from the narrow, deep radio pockets on their coats. This design is simple to change; however, for many firefighters, they will have to wait several years before having the opportunity to replace their firefighter clothing. Furthermore, firefighters in our study expressed a desire to have divided pockets to stow items individually, but also recognized that the divided pockets were more challenging to recover items from when wearing their gloves. Some slight variations in the design of divided pockets could improve the function considerably for firefighters. In addition, firefighters need more education and information about the varying styles of gear and customizable features, such as pockets, that are available.

Participants in our study received compression burns and burns around their face and ears. With the prevalence of compression burns in firefighters, further investigation of how to protect firefighters' would be beneficial: how much space between the firefighter's skin and inner coat lining is optimal for the lowest amount of heat transfer and how to best keep the lining off of the firefighter's skin even with the pull of gravity are critical problems to solve. A recent study was done to determine the ideal air gap amount for a single layer garment, using the Thermal Protective Clothing Analysis System [20]. Similar research needs to be conducted regarding optimal gap values in the firefighter clothing's three layer system (outer shell, thermal layer, moisture barrier) to reduce compression burns. It is also recommended that padding at the knees and elbows be further evaluated to determine if enhancing the protective barrier would provide increased comfort and function for firefighters. Regarding face burns caused by stretched out hoods, it is recommended that further testing be done to determine ways to maintain the elasticity and wear life of the hood. In addition, firefighters need increased education regarding the shorter life span of protective hoods and the need to replace hoods more frequently.

Participants reported that the reflective tape on their firefighter clothing was easily soiled and difficult to clean, reducing their visibility when responding to calls in dark environments. Some participants in our study expressed a desire to have more reflective tape to increase their visibility. Without determining a way to keep the reflective tape clean from dirt and soot, however, this would only provide a temporary increase in visibility while the PPE was new. Material testing and development is recommended to develop reflective tape that can be easily cleaned.

Individual fit issues were identified in focus groups, but since fit is greatly determined by the individual's body shape and size of clothing worn, there were not common overarching problems to report. Some examples of ill-fitting firefighter clothing were documented for further examination (examples shown in

FIG. 1—*PPE on male firefighters of varying body proportions.*

Figs. 1–4). The NFPA has measurement standards for firefighter clothing sizes, but this does not ensure that firefighters select and wear the appropriately sized clothing for their body. Previous research has found that approximately 80 % of females and 20 % of male firefighters report fit issues with their PPE [21].

Participants in our study were selected from a variety of firefighting departments that represented the subgroups of firefighters in the United States (e.g., male and female, urban and rural, career and volunteer) to ensure that perceptions and user needs of each subgroup were captured through the focus groups. Due to the limitations of smaller sample sizes found in qualitative studies such as this one, the results of this research should not be generalized to the entire population of firefighters, but can be used to guide future research and firefighter PPE development. Further research will be needed to evaluate if the issues reported in this study are experienced by the larger population of firefighters.

FIG. 2—*Turnout gear pant length differences.*

FIG. 3—*Female firefighter illustrating large turnout gear pant waist.*

FIG. 4—*Female firefighter in oversized turnout gear pants.*

Firefighters in our study wore a variety of PPE styles and brand, and thus were able to provide feedback on a broad cross-section of the marketed PPE. For the purposes of this research, only issues common to multiple PPE styles and brands were reported. Follow-up studies will be needed to evaluate specific styles and brands of PPE in relation to the issues reported in this study.

Conclusion

This study evaluated firefighter PPE to identify ways to improve garment and equipment design and wearer comfort. User needs and perceptions of both male and female firefighters were collected through a two part study, utilizing both focus group interviews and individual interviews, to obtain a broad representation of firefighters and in-depth data. Participants represented volunteer and career firefighters from both rural and urban areas.

Firefighters identified a number of similar issues, including excessive weight of the PPE, heat stress, overprotection for most calls, garment fit and restricted mobility, compression burns, and problems donning the firefighter clothing quickly. They also indicated concern about specific garment features that did not function well for them, including pockets, fasteners, knee padding, and the durability of the materials used in the clothing. Although some of the problems noted by the firefighters, such as hoods stretching out and pocket placement issues, would seem to have solutions (i.e., replace hoods more frequently, order uniforms with custom pocket placement) it must be noted that many of these firefighters, particularly those in volunteer departments, do not have control over the uniform they are issued. Budget considerations affect the reality of firefighter equipment. Therefore consideration of design solutions to these problems, where possible, is reasonable.

These common issues of PPE affect firefighters, male and female, and warrant further investigation. This study is an excellent starting point for further, more specific research. There are also a number of functional and fit issues that should be examined more closely, in order to maximize wearer protection and performance. Further testing and analysis is needed to determine optimum design changes that will improve firefighters' PPE comfort and experiences.

References

[1] United States Fire Administration, 2010, In "Fire Statistics: Firefighters," http://www.usfa.dhs.gov/downloads/pdf/10_fatality_summary.pdf (Last accessed May 14, 2011).

[2] Forgue, J. M. "Respiratory Protection for Fire Fighters," *Prof. Saf.*, Vol. 37, No. 11, 1992, pp. 37–40.

[3] National Fire Protection Association, *NFPA 1971 Standard on Protective Ensembles for Structural Fire Fighting and Proximity Fire Fighting*, National Fire Protection Association, Quincy, 2007 Edition.

[4] Elliott, F. "Personal Protective Equipment, Safety Standards, Eye Protection, Headgear, Risk Assessment," *Occup. Health Saf.*, Vol. 72, No. 11, 2003, pp. 76–78.

[5] Bellingar, T., Shanley, L. A., Slaten, B., and Brady, P., "Use of Carbonaceous Fiber in Wildland Firefighter Protective Clothing," *Safety Protective Fabrics*, Vol. 4, 1995, pp. 20–24.

[6] House, J., Squire, J., and Staples, R., "Optimising the Number of Layers in Firefighters' Hoods," *Int. J. Clothing Sci. Technol.*, Vol. 14, 2002, pp. 111–118.

[7] Tuttle, S., Sayer, J., and Buonarosa, M., "The Conspicuity of First-responder Safety Garments," *J. Safety Res.*, Vol. 40, 2009, pp. 191–196.

[8] Kerber, S. and Madrzykowski, D., "Firefighting Technology Research at NIST: Technology Roundup," *Fire Eng.*, Vol. 161, No. 5, 2008, p. 68.

[9] Huck, J. and McCullough, E. A., "Fire Fighter Turnout Clothing: Physiological and Subjective Evaluation," *Performance of Protective Clothing: Second Symposium*, ASTM STP 989, C. Z. Mansdorf, R. Sager, A. P. Nielson, eds., ASTM International, West Conshohocken, PA, 1988, pp. 439–451.

[10] Webb, H., McMinn, D., Garten, R., Beckman, J., Kamimori, G., and Acevedo, E., "Cardiorespiratory Responses of Firefighters to a Computerized Fire Strategies and Tactics Drill During Physical Activity," *Appl. Ergon.*, Vol. 41, 2010, pp. 376–381.

[11] Stull, J. O., Connor, M. B., and McCarthy, R. T., "Protective Clothing and Equipment Performance Requirements for Fire Service Urban Search and Rescue Teams," *Performance of Protective Clothing: Fifth Volume*, ASTM STP 1237, J. S. Johnson and S. Z. Mansdorf, eds., ASTM International, West Conshohocken, PA, 1996, pp. 558 – 571.

[12] Coca, A., Roberge, R., Shepard, A., Powell, J. B., Stull, J. O., and Williams, W. J., "Ergonomic Comparison of a Chem./Bio. Prototype Firefighter Ensemble and a Standard Ensemble," *Eur. J. Appl. Physiol.*, Vol. **104**, 2008, pp. 351–359.

[13] Lawson, J. R., "Thermal Performance and Limitations of Bunker Gear," *Fire Eng.*, Vol, 151, No. 8, 1998, pp. 37–56.

[14] Rosenblad-Wallin, E, "Development of Protective Clothing Based on Demands of the User and His Environment," *Proceedings of the International Conference on Protective Clothing Systems*, Stockholm, Sweden, 1983, pp. 327–333.

[15] Rosenblad-Wallin, E., "User-oriented Product Development Applied to Functional Clothing Design," *Appl. Ergon.*, Vol. 16, 1985, pp. 279–287.

[16] Akbar-Khanzadeh, F. and Besesi, M. S., "Comfort of Personal Protective Equipment," *Appl. Ergon.*, Vol. 26, 1995, pp. 195–198.

[17] Ariyatum, B., Molland, R., Harrison, D., and Kazi, T., "The Future Design Direction of Smart Clothing Development," *J. Text. Inst.*, Vol. 96, 2005, pp. 199–212.

[18] Marshall, M. N., "Sampling for Qualitative Research," *Fam. Pract.*, 1996, pp. 522–525.

[19] Sandelowski, M., "Sample Size in Qualitative Research,", *Nurs. Health*, 1995, Vol. 18, pp. 179–183.

[20] Song, G., "Clothing Air Gaps Layers and Thermal Protective Performance in Single Layer Garment," *J. Indust. Text.*, Vol. 36, 2007, pp. 193–205.

[21] Hulett, D., Bendick, Jr., M., Thomas, S., and Moccio, F., 2008, "A National Report Card of Women in Firefighting," www.i-women.org (Last accessed on May 14, 2011).

Performance of Protective Clothing and Equipment: Emerging Issues and Technologies
STP 1544, 2012
Available online at www.astm.org
DOI:10.1520/STP104207

Alexander Hummel,[1] *Roger Barker,*[2] *Kevin Lyons,*[3]
A. Shawn Deaton,[4] *and John Morton-Aslanis*[5]

Developing a Thermal Sensor for Use in the Fingers of the PyroHands Fire Test System

REFERENCE: Hummel, Alexander, Barker, Roger, Lyons, Kevin, Shawn Deaton, A., and Morton-Aslanis, John, "Developing a Thermal Sensor for Use in the Fingers of the PyroHands Fire Test System," *Performance of Protective Clothing and Equipment: Emerging Issues and Technologies* on April 16, 2011 in Anaheim, CA; STP 1544, Angie M. Shepherd, Editor, pp. 176–187, doi:10.1520/STP104207, ASTM International, West Conshohocken, PA 2012.

ABSTRACT: This paper describes a thermal sensor developed for use in the fingers of the PyroHands Fire Test System. The PyroHands Fire Test System measures the thermal protective performance of gloves in laboratory controlled flash fire exposures. The development of the finger sensor presented several challenges; the first was that it required that a small thermal sensor fit into the finger of an anthropometrically designed hand. It was also important to ensure that the thermal sensor accurately measured heat flux incident on the finger. This required showing that the unidirectional heat flux measured by the sensor was unaffected by heat impinging on the sides and back of the finger. An experimental study was conducted in order to investigate the effects of lateral heating on sensor operation. Additional verification of the thermal sensor was provided

Manuscript received July 14, 2011; accepted for publication February 27, 2012; published online September 2012.

[1]Postdoctoral Research Scholar, Center for Research on Textile Protection and Comfort, North Carolina State Univ., Raleigh, NC 27695–7910.

[2]Professor, Dept. of Textiles Engineering, Chemistry and Science, North Carolina State Univ., Raleigh, NC 27695–8301.

[3]Professor, Dept. of Mechanical and Aerospace Engineering, North Carolina State Univ., Raleigh, NC 27695–7910.

[4]Special Projects Director, Center for Research on Textile Protection and Comfort, College of Textiles, North Carolina State Univ., Raleigh, NC 27695–8301.

[5]Research Assistant, Textile Protection and Comfort Center, College of Textiles, North Carolina State Univ., Raleigh, NC 27695–8301.

via the use of computer-aided design models to predict the temperature rise beneath gloves during PyroHands tests.

KEYWORDS: fire test manikins, thermal sensors, flash fires, heat transfer, fire resistant gloves, thermal protective performance

Introduction

The PyroMan full scale fire testing manikin at North Carolina State University (NCSU) has long been used to evaluate the thermal protective performance of clothing in laboratory controlled flash fire exposures. PyroMan, like other fire testing manikins, was not instrumented to measure or predict burn injury to the hands. Testing methods have not been available for measuring the thermal protective performance of whole gloves or hand protection systems. Thermal protection characterizations have relied on tests conducted on materials used in glove construction. This material testing cannot provide information on glove fit, construction, or gauntlet length, which are all factors that play a significant role in the thermal protection provided by gloves. Therefore, NCSU developed the PyroHands system to address the need for a whole glove fire testing method [1].

The PyroHands system (Fig. 1) incorporates 20 thermal sensors, 10 sensors in each hand, to measure the heat flux incident on the set of manikin hand forms. The thermal sensors are distributed in the palms, dorsum (back of the hand), and wrist area of the hand forms. However, these sensors are too large

FIG. 1—*Photograph of the PyroHands Fire Test System [1].*

to be fitted into the smaller space available in the fingers of the PyroHands system. A new smaller thermal sensor was needed for the slender, cylindrical fingers of the instrumented hand forms. This paper describes the design, heat transfer modeling, and experimentation conducted to develop a finger sensor for the PyroHands Fire Test System.

Finger Sensor Development

The cross sectional area of a human finger is smaller than that of any other part of the body. The small size and cylindrical geometry of a finger create two immediate challenges to the development of a finger sensor for the PyroHands system. The first challenge involves designing a thermal sensor using the demonstrated, robust technology of the sensors for PyroMan and PyroHands that is small enough to fit into the finger. The second challenge is to demonstrate that the sensor measures heat flux without excessive lateral heating from flames that impinge on the fingers from every direction. Heat flux analysis using computer-aided design (CAD) model techniques proved useful in the design phase.

Sensor Design

The thermal sensors used in the PyroMan and PyroHands systems are copper slug calorimeters, called PyroCal sensors, and were specially designed at NCSU for fire test manikins [2]. The PyroCal sensors used in PyroHands were previously modified so as to provide a smaller profile to fit into the breadth of the hands [1]. These PyroHands sensors were still far too large to fit into the finger. Therefore, a new sensor was designed and constructed to fit into the smaller, cylindrical fingers of the PyroHands hand forms. This sensor was designed to be located in line with the finger, essentially replacing the middle segment as seen in Fig. 2. This sensor placement would represent skin burns associated with the back (dorsal) side of the proximal interphalangeal joint, also known as the middle knuckle. The small size of the finger sensor required a smaller copper slug than previously used in PyroMan and PyroHands. Therefore, it was necessary to understand heat transfer in the sensor and determine the effects of reducing the diameter and surface area of the slug calorimeter on the estimated heat flux.

The PyroCal sensor, developed for PyroMan, measures the heat flux incident on the surface of the skin. The measurements are converted using a skin burn algorithm to predict burn injury [2]. The equation used to translate the temperature data to heat flux is

$$q = pc_pC_LL\frac{dT(t)}{dt} + K_L[T(t) - T_i], \quad (1)$$

FIG. 2—*Finger sensor showing its position in the finger of PyroHands.*

where:

q = heat flux, W/m^2,
ρ = density of copper slug, kg/m^3,
c_p = specific heat of copper slug, J/kg/K,
L = thickness of copper slug, m,
$T(t)$ = temperature of slug, K,
t = time, s,
C_L = dimensionless correction factor calibrated for sensor,
K_L = heat loss correction factor, W/m^2/K, and
T_i = initial temperature, K.

It can be seen from Eq 1 that the only size dimension of the copper slug used for calculating the incident heat flux is the thickness. Therefore, a reduction of the diameter of the copper slug does not change the estimated heat flux when the thickness of the slug is kept the same. This means that the diameter of the copper slug could be reduced from 0.44 in. (1.118 cm) to 0.30 in. (0.762 cm) for the finger sensor without affecting the heat flux measurement.

For the PyroCal sensors, the copper slug is embedded in a heat resistant ceramic housing, and the ceramic is held by a stainless steel shell [2]. For the finger sensor, the ceramic shell was modified to match the size and profile of the fingers of PyroHands, and the stainless steel outer shell was not used in order to reduce heat transfer to the sides and back of the sensor. The copper slug is held in place by two ceramic pins inserted into the top and bottom surfaces of the cylinder. A thermocouple wire is embedded into the copper slug, which then passes through the bottom of the sensor and into the hollow center of PyroHands. These features of the finger sensor can be seen in Fig. 3.

Heat Transfer Modeling

The heat flux sensors used in PyroMan and PyroHands are embedded into the manikin surface and are fully surrounded by heat resistant ceramic and other insulating materials. This insulation effectively acts to limit lateral and back-side heating, and it also restricts flame exposure to the surface of the thermal sensors. The fingers do not provide this insulation, and the flames can envelop the finger, resulting in heat flux to all exterior surfaces of the thermal sensor, and not just to the face of the sensor (copper slug side). This additional heat exposure is further compounded by the fact that the size of the finger is small compared to that of the hands and body, so there is less material insulating heat flow to the copper slug portion of the sensor. A main focus of this research was to model and coordinate tests to characterize the effects of lateral heating on the accuracy of the heat flux measurement of the finger sensor.

The *SolidWorks* [3] heat analysis package was used to simulate the heating effects to the finger sensor in the flash fire environment of the chamber. The model helped us visualize the temperature rise of the ceramic portion of the finger sensor and was also used to estimate the temperature increase in the copper slug for different heat flux exposure intensities. In order to simulate actual fire chamber conditions, three heat flux profiles were chosen from PyroMan sensor data. These PyroMan profiles represented heat flux

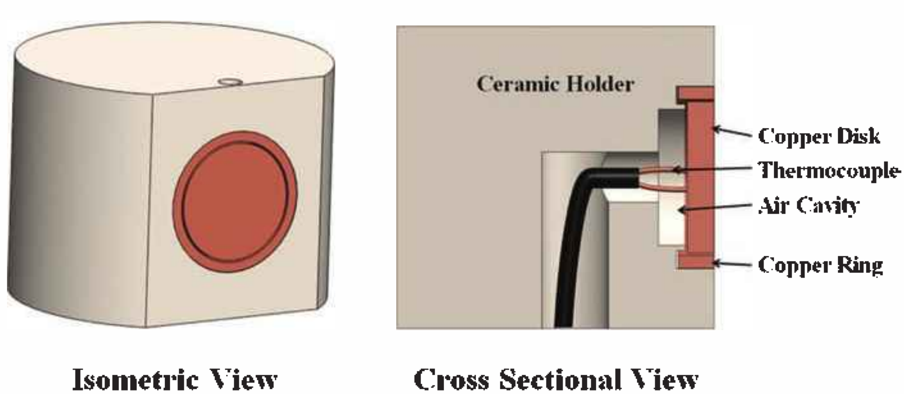

FIG. 3—*Isometric view (left) shows the cylindrical shape of the finger sensor, whereas the cross sectional view (right) shows the embedded thermocouple wire passing down through the bottom of the sensor.*

measurements that resulted in three different burn predictions: no predicted burn, second degree burn, and third degree burn. Temporal heat flux data from these three profiles were applied to the exposed surfaces. The top and bottom surfaces of the finger sensor model were not exposed to heat flux, so as to simulate the finger sensor as "in line" with the rest of the finger. The initial temperature of the entire finger sensor was set at 28°C (82.4°F) before heat flux was applied. Images of the heat flux modeling for the finger sensor can be seen in Fig. 4.

Figure 4 shows that for the lower two heat flux profiles, the inner parts of the sensor do not appear to experience significant heating. However, for the highest heat flux profile, the core of the sensor has a slightly higher temperature. The temperature of the copper slug was determined and Eq 1 was used to calculate the heat flux measurements for each of the three profiles. The same three heat flux exposures applied to the finger sensor model were applied to a model of the PyroCal sensor for comparison. For the PyroCal sensor, the heat flux was applied only to the face of the sensor (with the copper slug), in order to simulate the sensor's being embedded into the manikin. The heat flux calculations from the finger sensor model were compared to the PyroCal model for each of the three heat flux profiles, as well as to the input heat flux profiles taken from PyroMan test data (Figs. 5–7).

Figures 5–7 show that the heat flux values estimated by the finger sensor are nearly identical to the values measured by the PyroCal sensor. This is a good outcome because it indicates that the lateral heating experienced by the finger sensor when it is fully surrounded by flames will be equivalent to the heat measured by a front-facing sensor. Figures 5–7 also show that the heat fluxes calculated from both the PyroCal and finger sensor models are very similar to the input heat flux data. Therefore, the model forecasts that the finger sensor will provide an accurate measurement of the heat flux. Although the *SolidWorks* modeling data were promising, experimental verification is required in order to validate the model and to provide a full understanding of any effects due to lateral heating.

Experimental Verification

In order to experimentally characterize the lateral heating effects, it was important to heat the front and sides of the finger sensor. The fire test chamber environment is a combination of radiant and convective heat originating from high intensity flames produced by industrial propane torches. However, the main mode of heat transfer to a body within a simulated "fireball" condition is radiant heat [4]. Even when the hands are gloved, radiant heat transfer will dominate, so it was important to use radiant heaters for the experimental testing on the finger sensor. For these same reasons, radiant heat sources have been used to calibrate fire test manikin sensors as described in ASTM F1930 [5].

Three blackbody radiant heaters were used to heat the front and sides of the finger sensor. These heaters were positioned 90° apart and were all set at

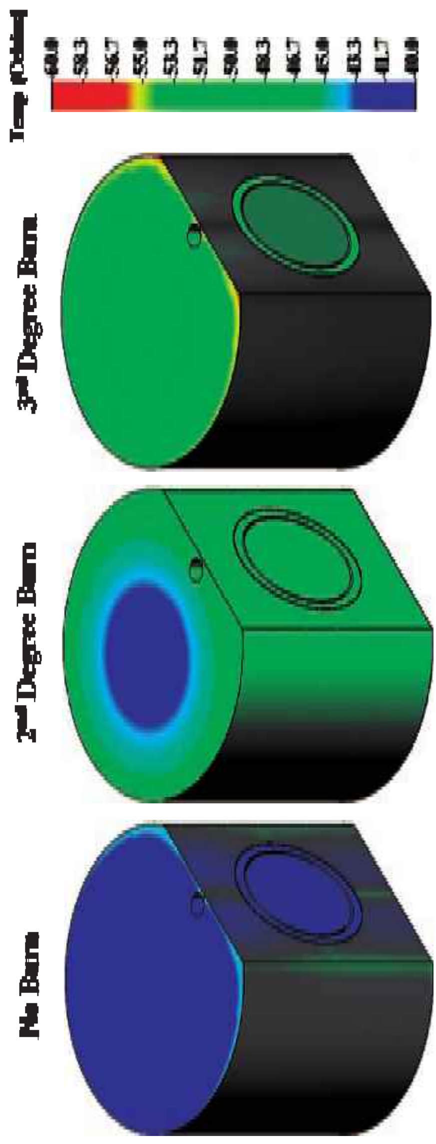

FIG. 4—*Computer model showing the temperature distribution of the finger sensor for three PyroMan profiles: no burn profile (left), second degree burn profile (middle), and third degree burn profile (right).*

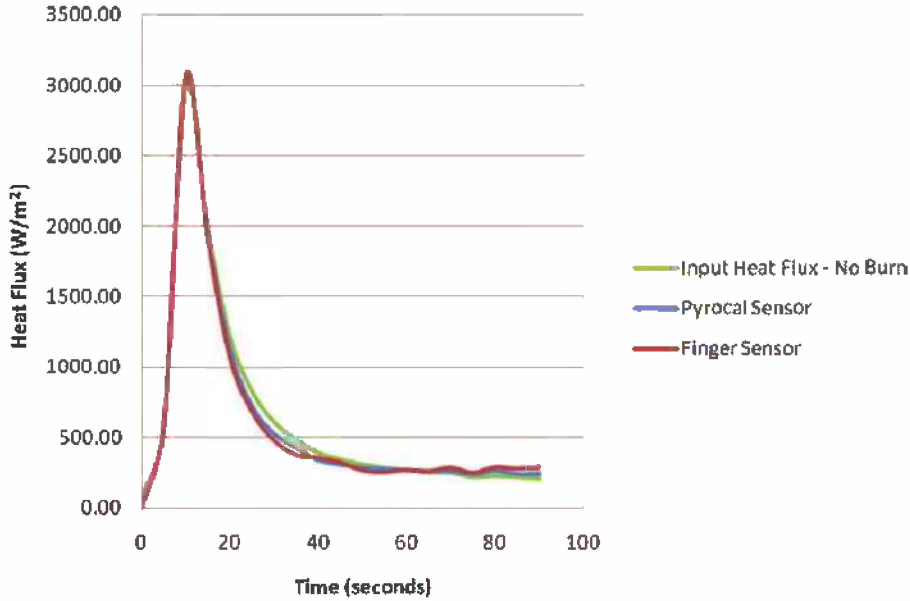

FIG. 5—*Model comparison of PyroCal and finger sensor response to heat flux (no predicted burn case).*

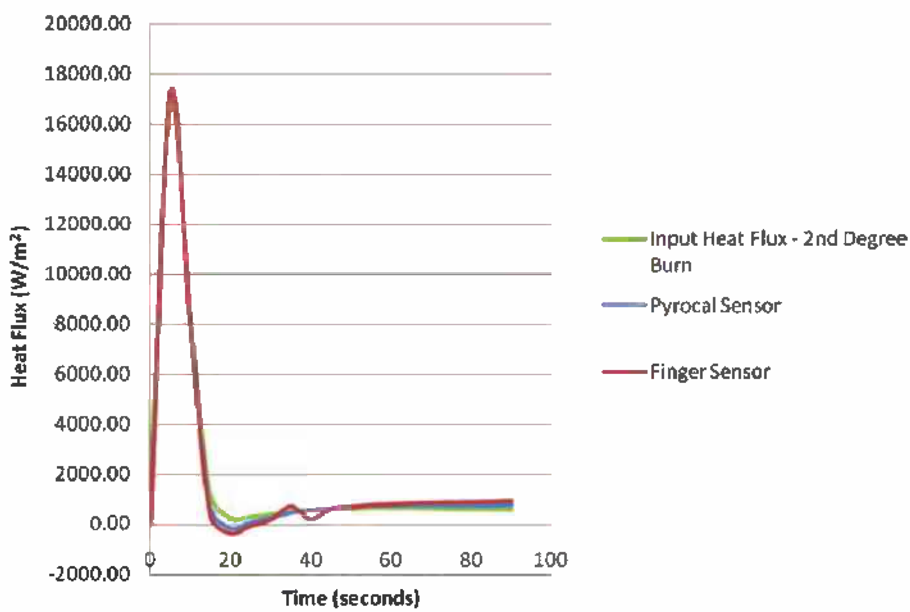

FIG. 6—*Model comparison of PyroCal and finger sensor response to heat flux (second degree burn case).*

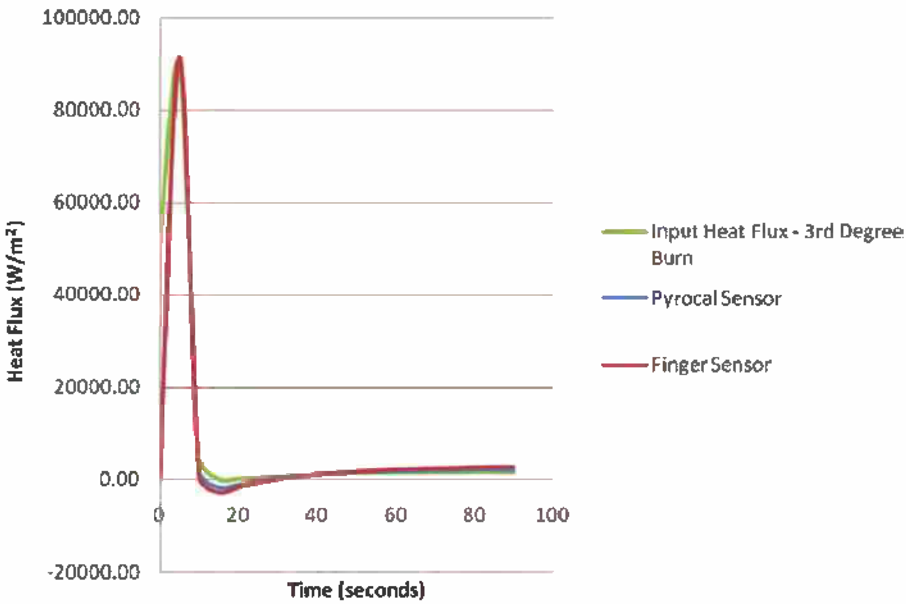

FIG. 7—*Model comparison of PyroCal and finger sensor response to heat flux (third degree burn case).*

the same temperature. This setup was adjusted to produce a combined incident heat flux of 14 kW/m^2 (0.34 cal/cm^2 s). A motorized actuator was used to move the sensor toward and then away from the heat source to simulate the dynamic heat flux profile that would occur underneath a test glove during a PyroHands test. The blackbody heater experimental setup is shown in Fig. 8.

Although the *SolidWorks* model demonstrated the equivalence of the heat flux measurements by the finger sensor and the PyroCal sensor, it was not possible to experimentally compare these two sensors. This is because a PyroCal sensor embedded into the ceramic block used with this test setup would have drastically altered the heat profile. This would mean that the two sensors would not be experiencing the same surface heating. Therefore, in order to ensure similar heating while evaluating lateral heating effects, a method of shielding was devised to insulate the sides of the finger sensor from additional heat. This built-in heat shield for the finger sensor consisted of 0.25 in. of additional ceramic material added to each side of the sensor. This shielded sensor had a square appearance, in contrast to the round shape of the functional finger sensor. Given that ceramic material is a very good insulator, the additional material on each side of the sensor should effectively reduce the lateral heating to the copper slug portion of the sensor. Figure 9 illustrates the "round" finger sensor and the "square," or shielded, finger sensor.

Three round finger sensors and three square finger sensors were built and used in the blackbody heater experiment. Each sensor was tested using the

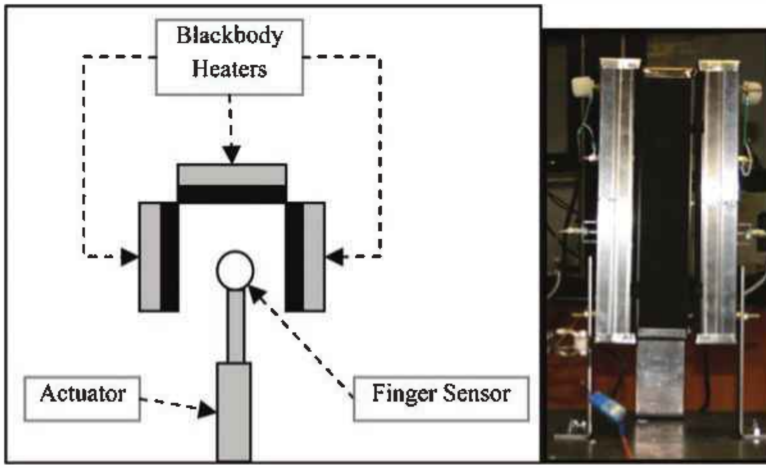

FIG. 8—*Dynamic blackbody heating setup used to assess finger sensor response to lateral radiant heating.*

setup seen in Fig. 8 for three repetitions at the same actuator speed and position. Data from the blackbody heater experiment, shown in Fig. 10, demonstrate that the heat fluxes measured by the round thermal sensor and the square (shielded) thermal sensor are nearly identical. This result shows that lateral heating from the sides of the sensors does not significantly affect the finger sensor's measurement of heat flux. This is in agreement with the *SolidWorks* modeling results (Figs. 5–7), which also showed that lateral heating does not affect the response of the finger sensor.

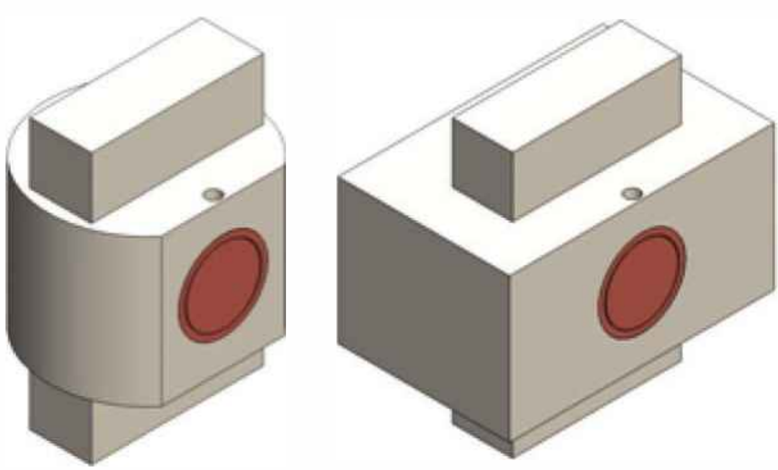

FIG. 9—*CAD images of the round finger sensor and the more insulated square sensor used for the blackbody heating experiments.*

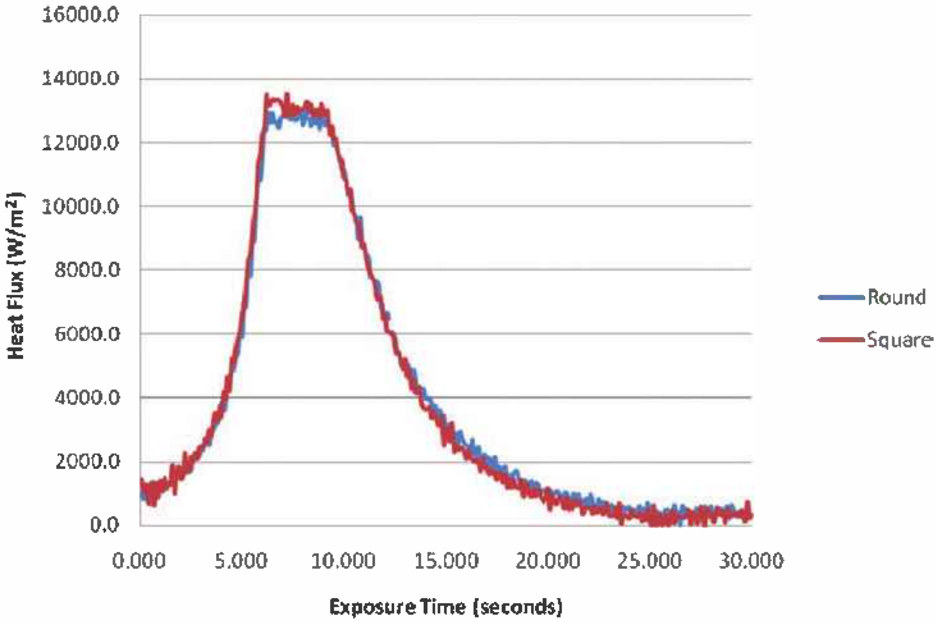

FIG. 10—*Average heat flux measured for the blackbody heater testing using the motorized actuator.*

Conclusions

This research has produced a new thermal sensor optimized for characterizing the heat flux incident on the fingers of the PyroHands instrumented hand forms. A model for translating the heat flux measured by the finger sensor in order to predict finger burn injuries has been developed and integrated into the data acquisition system. The PyroHands Fire Test System, upgraded with the addition of the newly developed finger sensors and burn model, is being used in ongoing studies of the thermal protective performance of gloves in flame exposures.

Acknowledgments

This research was funded by U.S. Army PM-SPIE, Contract No. W911QY-10-C-0106. The writers are grateful for their support and for the many contributions made by Celia Powell to this project. The writers would also like to recognize all of the contributions made by the staff of the Center for Research on Textile Protection and Comfort.

References

[1] Hummel, A., Barker, R., Lyons, K., Deaton, A. S., and Morton-Aslanis, J., "Development of Instrumented Manikin Hands for Characterizing the

Thermal Protective Performance of Gloves in Flash Fire Exposures," *Fire Technol.*, Vol. 47(3), 2011, pp. 615–629.

[2] Grimes, R. V., 1993, "The Design and Calibration of a Surface Heat Flux Transducer for Use in Fabric Thermal Protection Testing," M.S. thesis, North Carolina State University, Raleigh, NC.

[3] Hirschtick, J., *SolidWorks*. (2010). Dassault Systems S.A., Concord, MA.

[4] Prugh, R. W., "Quantitative Evaluation of Fireball Hazards," *Process Saf. Prog.*, Vol. 13(2), 1994, pp. 83–91.

[5] ASTM F1930, 2010, "Standard Test Method for Evaluation of Flame Resistant Clothing for Protection against Flash Fire Simulations Using an Instrumented Manikin," *Annual Book of ASTM Standards*, Vol. 11.03, ASTM International, West Conshohocken, PA.

Performance of Protective Clothing and Equipment: Emerging Issues and Technologies
STP 1544, 2012
Available online at www.astm.org
DOI:10.1520/STP104211

L. Deuser,[1] *R. Barker,*[2] *A. S. Deaton,*[3] *and A. Shepherd*[4]

Interlaboratory Study of ASTM F2731, Standard Test Method for Measuring the Transmitted and Stored Energy of Firefighter Protective Clothing Systems

---

REFERENCE: Deuser, L., Barker, R., Deaton, A. S., and Shepherd, A., "Interlaboratory Study of ASTM F2731, Standard Test Method for Measuring the Transmitted and Stored Energy of Firefighter Protective Clothing Systems," *Performance of Protective Clothing and Equipment: Emerging Issues and Technologies* on April 16, 2011 in Anaheim, CA; STP 1544, Angie M. Shepherd, Editor, pp. 188–201, doi:10.1520/STP104211, ASTM International, West Conshohocken, PA 2012.

ABSTRACT: This paper describes an interlaboratory study conducted using ASTM F2731, Standard Test Method for Measuring the Transmitted and Stored Energy of Firefighter Protective Clothing Systems. Five replications of six different composites representative of firefighting turnout gear materials were tested at six different laboratories equipped to conduct the test. Data collected were used to predict the time to second degree burn for each of the turnout composite test specimens. Statistical analysis showed good agreement between test sites. This interlaboratory study confirmed the repeatability and reliability of ASTM F2731, a test method used to measure an important property associated with the thermal protective performance of firefighter turnout materials.

KEYWORDS: firefighting, interlaboratory study, protective clothing, textiles, turnout gear, stored energy

---

Manuscript received July 15, 2011; accepted for publication November 18, 2011; published online February, 2012.

[1]Graduate Research Assistant, Center for Research on Textile Protection and Comfort, North Carolina State Univ., Raleigh, NC 27695.

[2]Professor, Dept. of Textile Engineering, Chemistry and Science, North Carolina State Univ., Raleigh, NC 27695.

[3]Special Projects Director, Center for Research on Textile Protection and Comfort, North Carolina State Univ., Raleigh, NC 27695.

[4]Protective Clothing and Ensembles Team Leader, NIOSH National Personal Protective Technology Laboratory, Pittsburgh, PA 15236.

Introduction

Skin burn injuries incurred during exposures to radiant heat at levels below flashover conditions are a cause for concern to firefighters. These burn injuries, often referred to as "stored energy burns," can involve several minutes of exposure to thermal energy levels not sufficient to degrade the outer shell of the turnout gear. They occur as a result of radiant heat transmitted from the firefighting environment and stored within the layers of the turnout suit composite. Subsequent compression of the layers exacerbates burns through rapid discharge of stored thermal energy within the layers of the garment. Studies have shown that these burns often occur in areas where moisture vapor impermeable layers, such as reflective trim, are attached to the outer shell of the turnout. The presence of moisture within the layers of the turnout suit has been shown to contribute to skin burn injuries [1,2].

An apparatus and test method for measuring the heat transmitted and stored in firefighting materials has been developed by NC State Univ. [2]. These test procedures are the basis for ASTM F2731, Standard Test Method for Measuring the Transmitted and Stored Energy of Firefighter Protective Clothing Systems [3]. As part of the development process, a limited interlaboratory study was conducted that involved two different test sites. The study showed the ability to reproduce test results generated at different test sites using a range of turnout composites [4]. The purpose of this paper is to describe the results of a more extensive interlaboratory study utilizing six different test sites.

Stored Energy Testing Apparatus

Figure 1 shows the stored energy testing (SET) apparatus used for this research. The testing apparatus consists of a specimen holder, a sensor assembly, data collection sensor, heat source, compressor assembly, and a data acquisition system/burn analysis program. The turnout composite specimen is loaded into the transfer tray and exposed to radiant heat supplied by a ceramic heating element for 120 s. The temperature of the heating element can be adjusted in one degree Celsius increments using a digital controller. The heat source is positioned 108 ± 5 mm away from the specimen holder. A water-cooled Schmidt-Boelter thermopile type sensor with a diameter of 25.4 mm measures the transmitted heat through the specimen. Water at 32.5 ± 1 °C is pumped through the data collection sensor to cool it at a constant rate [3]. Five seconds after the exposure phase, the specimen is compressed by a compressor assembly for a period of 60 s. Throughout the process, the data collection thermal sensor records the heat transmitted through the layers of the test specimen. This information is analyzed using Henrique's burn model to predict the time to second degree burn for the specimen [2]. Additional information about individual components of the apparatus can be found in Refs [2] and [5].

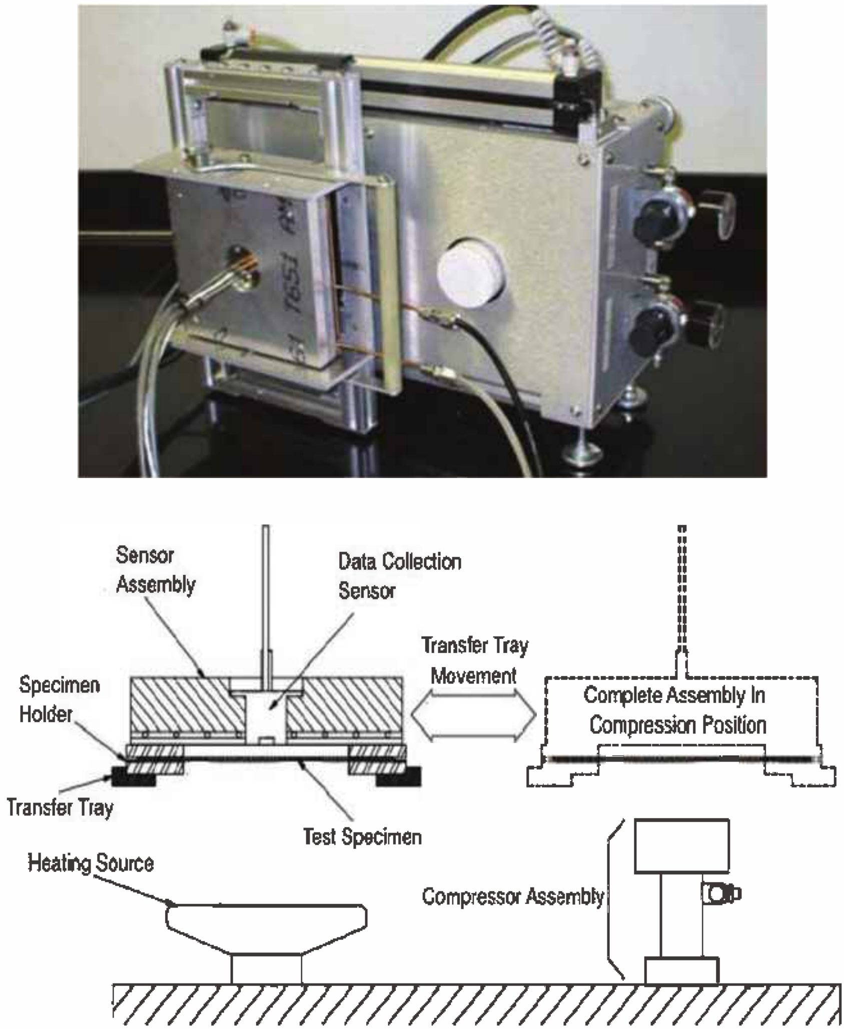

FIG. 1—*Photograph (top) and schematic (bottom) of stored energy testing apparatus [1,2].*

Stored Energy Test Procedure

6 in. × 6 in. test specimens are cut from the layers that make up a turnout suit. These layers are then assembled into a composite that is used for the testing procedure.

The turnout composite is moisture preconditioned as follows: two pieces of 152 × 152 mm (6 in. × 6 in.) AATCC blotter paper are submerged in distilled water for 10 s. Both sheets of blotter paper are then run through a wringer with 30 lb on the rolls. One piece of blotter paper is placed on one side of the innermost separable layer of the composite (closest to the user) and the other piece is placed on the other side of this layer. The entire test composite is then placed into a sealed plastic bag. The air is removed from the bag and the specimen is placed in an environmentally controlled room (21 ± 3 °C, 65 ± 10 % relative humidity) and allowed to equilibrate for 12–24 h [3].

The composite specimen is then removed from the bag and tested within 5 min. Specimens are exposed to 8.4 kW/m^2 (0.2 cal/cm^2–s) radiant heat for a period 120 s to simulate a firefighting environment with subflashover conditions. The data collection sensor measures the heat transmitted through the composite throughout the duration of the test. A 6.4 mm air gap (to emulate the spacer used in the thermal protective performance test [6]) is incorporated between the sensor assembly and the specimen. Two minutes after the start of the radiant heat exposure period, the turnout composite is compressed against the sensor assembly at a pressure of 13.79 kPa (2.0 psi) for a period of 60 s. The data collection sensor records the thermal energy discharged from the specimen during this time. A sample heat flux graph created by the stored energy program is shown in Fig. 2. Upon compression (≈120 s in Fig. 2), a distinct peak in the thermal flux indicates stored thermal energy discharged from the heated specimen.

Henriques burn model is used to translate the heat flux data to predict the time to second degree burn [1]. Additional description of the stored energy testing procedure can be found in Ref [3].

Interlaboratory Study

The objective of the interlaboratory study was to determine within and between laboratory variations, and assess the reproducibility of the stored energy test

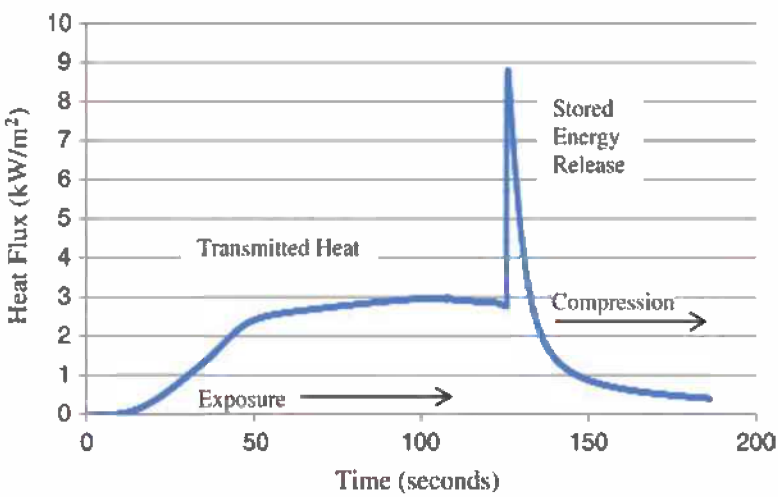

FIG. 2—*Typical measured heat flux during a stored energy test [2].*

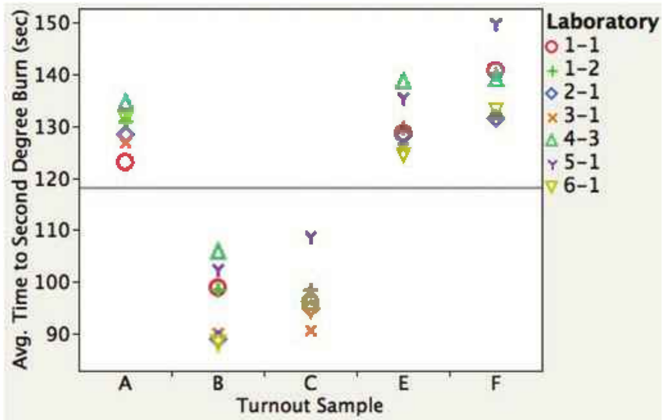

FIG. 3—*Predicted time to second degree burn (by turnout specimen).*

method. An additional objective was to identify sources contributing to variability in the test, or to the differences in results obtained at test sites.

Testing was conducted at NC State Univ. (NCSU) and at five other laboratories. Five of the six laboratories used the same testing apparatus used at NCSU. Test operators at each site were trained by NCSU on the setup of the stored energy apparatus, and on the standard testing procedures. Each laboratory site performed the testing in accordance with ASTM F2731. Testing conditions used at the test sites are summarized in Table 1.

Laboratory 4 was the only participating laboratory testing site that did not use the NCSU testing apparatus. However, they used an apparatus that also conforms to the requirements specified in ASTM F2731 [3].

NCSU (laboratory site 1) conducted two separate tests. The same operator on two different apparatuses conducted these tests over a 2-day period. The first set of data was collected using the instrument provided to the other participating laboratories (except site 4). The second data set was collected using a second apparatus that also complies with the specifications of ASTM F2731 [3].

Each laboratory calibrated the heat exposure as called for by ASTM F2731. The incident heat exposure is established by exposing the thermal sensor directly to the radiant heat source for a period of at least 70 s. The flux data recorded by the sensor was averaged over a 60 s period to determine the

TABLE 1—*Test conditions for interlaboratory study.*

Preconditioning	ASTM F2731 wet preconditioning procedure [3]
Radiant heat exposure	$8.5 \pm 0.5\,kW/m^2$
Exposure period length (before compression)	120 s
Compression period length	60 s
Total data collection time	190 s

average exposure. The temperature of the heat source was adjusted until an average thermal flux of $8.5 \pm .5\,kW/m^2$ ($0.2 \pm .012\,cal/cm^2-s$) was achieved [3].

Test Materials

Each laboratory tested six different firefighter turnout composite specimens. The turnout composites were selected to represent materials used in NFPA 1971 compliant firefighting turnout gear [7]. All consisted of a thermal liner, moisture barrier, and outer shell layer lay-up. Some of the composites incorporated an additional outer layer, including reflective trim or fabric reinforcement attached to the outer shell. The composites used are described in Table 2.

Two different weight outer shells were utilized in the sample set. All of the turnout composites used the same breathable, vapor permeable moisture barrier. Two different thermal liners, a two layer and one layer batting design, were represented in the sample set. Three of the turnout systems were base composites, or lay-ups without an additional layer added to the outer shell

TABLE 2—*Turnout materials tested.*

Specimen	Thermal liner	Moisture barrier	Outer shell	Additional layers
A (base composite)	two-layer spunlaced para- and meta-aramid/spun yarn meta-aramid	enhanced bi-component ePTFE/meta-aramid	$7.5\,oz/yd^2$ meta-aramid/ para-aramid	none
B (base + trim)	two-layer spunlaced para- and meta-aramid/ spun yarn meta-aramid	enhanced bi-component ePTFE/meta-aramid	$7.5\,oz/yd^2$ meta-aramid/ para-aramid	nonporous reflective trim
C (base + reinforcing layer)	two-layer spunlaced para- and meta-aramid/ spun yarn meta-aramid	enhanced bi-component ePTFE/meta-aramid	$7.5\,oz/yd^2$ meta-aramid/ para-aramid	$16\,oz/yd^2$ 100% para-aramid
D (base + additional outer shell)	two-layer spunlaced para- and meta-aramid/ spun yarn meta-aramid	enhanced bi-component ePTFE/meta-aramid	$7.5\,oz/yd^2$ meta-aramid/ para-aramid	$7.5\,oz/yd^2$ meta-aramid/ para-aramid
E	two-layer spunlaced para- and meta-aramid/ spun yarn meta-aramid	enhanced bi-component ePTFE/meta-aramid	$6.0\,oz/yd^2$ meta-aramid/ para-aramid	none
F	needle punched para- and meta-aramid/spun yarn meta-aramid	enhanced bi-component ePTFE/meta-aramid	$7.5\,oz/yd^2$ meta-aramid/ para-aramid	none

material. Each base composite represented different combinations of thermal liners and outer shells. Composite B consisted of a base composite with a 6 in. × 3 in. strip of nonporous reflective trim attached across the center of the outer shell. Composite C consisted of the same base composite with a layer of nonporous fabric, used to reinforce the knee and elbow areas of turnout suits, attached to the outer shell. Composite D incorporated the same base composite with an additional layer of outer shell fabric attached to represent reinforced shoulder areas.

Each laboratory tested five replicates of each turnout composite in a random order. Predicted time to second degree burn was recorded, as was average total energy, thickness, dry weight, and wet weight of each test composite.

Results and Discussion

Table 3 compares the average predicted second degree burn time for tests conducted at the participating laboratories. In the laboratory column, the first number denotes the participating laboratory while the number after the dash denotes the testing apparatus used. Figure 3 is a graphical representation of these data. Composite specimen D (base + additional outer shell layer) is not included because no second degree burn was recorded in the allotted exposure and compression period in over 70 % of the tests performed. A detailed table of results obtained by the interlaboratory study can be found in the Appendix.

Table 4 provides a summary of statistics calculated in accordance with ASTM E691, Standard Practice for Conducting an Interlaboratory Study to Determine the Precision of a Test Method [8].

The repeatability standard deviation (s_r), an index of within–laboratory variation, was calculated using

$$s_r = \sqrt{\sum_{1}^{p} s^2/p} \tag{1}$$

TABLE 3—*Average time to second degree burn at different laboratory sites for test turnout composites.*

	Predicted time to second degree burn, s				
Laboratory	A	B	C	E	F
1-1	123.0	98.9	95.9	128.2	140.7
1-2	130.8	98.3	98.2	129.5	140.0
2-1	128.3	88.8	94.6	128.1	131.4
3-1	126.8	89.9	90.3	125.7	131.6
4-3	134.4	105.8	96.9	138.5	138.9
5-1	132.5	102.3	108.4	135.2	149.7
6-1	131.4	88.3	94.2	124.4	133.0

TABLE 4—*Precision statistics (for predicted second degree burn time).*

Specimen	$\bar{x}$ Mean, s	$S_{\bar{x}}$ Standard deviation, s	s_r Repeatability std. dev., s	s_R Reproducibility std. dev., s	r Repeatability limit, s	R Reproducibility limit, s
A	129.6	3.9	8.5	8.5	23.7	23.8
B	96.1	7.0	9.4	10.9	26.2	30.6
C	96.9	5.7	4.7	7.0	13.1	19.7
E	129.9	5.1	3.7	6.1	10.3	17.1
F	137.9	6.6	7.9	9.6	22.1	27.0
Average	118.1	5.7	6.8	8.4	19.1	23.6

where:

p = number of labs and

s = standard deviations for each lab.

The repeatability limit (r) was estimated from the repeatability standard deviation by

$$r = 2.8 s_r \tag{2}$$

The repeatability limit defines the maximum expected difference (with 95% confidence) between two measurements taken by the same operator within one laboratory [8].

The reproducibility standard deviation (s_R) indicates the between-laboratory variation. It was calculated using

$$s_R = \sqrt{(s_{\bar{x}})^2 + (s_r)^2(n-1)/n} \tag{3}$$

where:

$s_{\bar{x}}$ = standard deviations of lab average,

s_r = repeatability standard deviations, and

n = number of replications.

The reproducibility limit, calculated using Eq 4 defines the maximum expected difference (with 95% confidence) between two measurements taken by different operators between two laboratories [8]:

$$R = 2.8 s_R \tag{4}$$

Table 4 shows that the standard deviation of the laboratory averages, a measure of overall data variation, ranged from 3.9 to 7.0 s. The largest amount of variation observed within the laboratory averages occurred in testing specimen B, the base composite turnout specimen with a layer of reflective trim added to the outer shell. Specimens that incorporate trim or reinforcement layers show a significant decrease in the predicted time to second degree burn. The composite specimen F (base composite with 1-layer needle punched thermal liner) showed the longest predicted time to second degree burn.

Test Repeatability and Reproducibility

Repeatability statistics quantify the within-laboratory variation while reproducibility statistics quantify the between-laboratory variation.

The repeatability standard deviations range from 3.7 to 9.4 s. These standard deviations range from 2.8 to 9.8% when compared to the overall means of each test specimen. Therefore these statistics demonstrate that the test is repeatable within a single laboratory.

The reproducibility standard deviations range from 6.1 to 10.9 s. These standard deviations range from 4.7 to 11.3% when compared to the overall means for each test specimen. These data show that there is higher variability from laboratory-to-laboratory than within a single laboratory.

Figure 4 provides a comparison of within-laboratory repeatability and between-laboratory reproducibility. The repeatability standard deviation for each composite is always slightly higher than then reproducibility standard deviation. This is an expected result because reproducibility measurements include within- and between-laboratory variation. The differences between the repeatability and reproducibility standard deviations indicate the variability added when measurements are made from laboratory to laboratory. The observation that the repeatability and reproducibility standard deviations vary from specimen to specimen indicates that the type of material tested affects the overall test variability.

The repeatability and reproducibility limits (r and R) shown in Table 4 quantify the expected maximum difference between two measurements (with

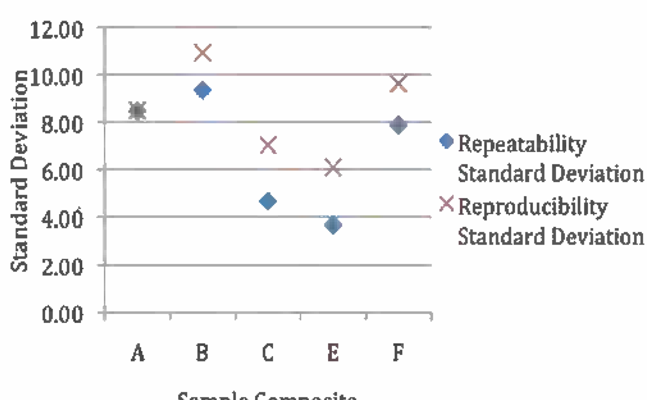

FIG. 4—*Repeatability and reproducibility standard deviations.*

95% certainty) taken within one laboratory and between laboratories [8]. These differences range from 10.3 to 26.2 s for repeatability, and 17.1 to 30.6 s for reproducibility. These values are a useful way to determine whether the amount of variation seen while performing a test in accordance with ASTM F2731 is within the range that has been established by this interlaboratory study.

To provide a mean normalized estimate of variability, the coefficient of variation of the test results obtained at each site (shown in Eq 5) was also computed. The standard deviation and means of all results across all laboratories were used to compute an overall %CV for each material:

$$C_v = \frac{\sigma}{|\mu|} \tag{5}$$

where:

σ = standard deviation and

μ = mean.

Figure 5 compares the % coefficient of variation (%CV) for each specimen. The %CV ranges from 3.0 to 7.3% over all of the turnout composites. These statistics show that variation within the test does depend on the type of composite tested. They also indicate a significant increase in the variation of specimens when additional impermeable layers attached to the outer shell (specimens B and C). However, the %CV are all under 10%, indicating a good overall agreement between laboratories.

Sources of Test Variability

This research investigated two possible sources of between-laboratory test variation: the variation in thermal exposure intensity and the moisture preconditioning procedure.

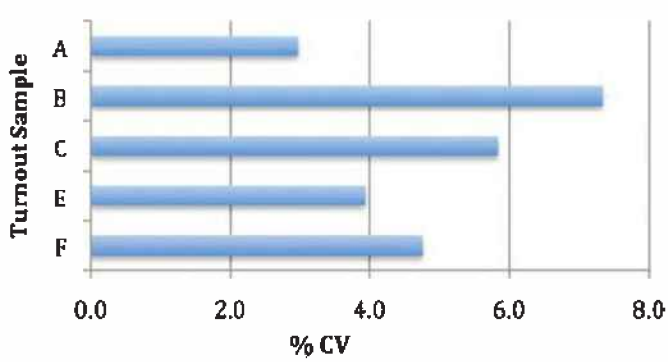

FIG. 5—*Coefficient of variation for turnout specimens.*

Because the stored energy test involves low-level radiant heat exposure for a long period of time, the total energy transmitted though the sample recorded throughout the test can vary over the test duration. Figure 6 compares the average total energy through each specimen composite recorded by each laboratory. Lower total energy values are reflected in the test results by a longer predicted time to second degree burn. Higher total energy values have the opposite effect on predicted time to second degree burn (see Table 3). It can therefore be concluded that the variation in total energy contributes to differences between laboratory estimates of time to second degree burn.

Previous studies have shown that moisture present within firefighter clothing materials has a complex and pronounced effect on its the thermal protective performance [6]. The moisture preconditioning procedure therefore may be a source of laboratory-to-laboratory variation. To study this effect, the dry and wet weights (moisture preconditioned) of each turnout composite tested were recorded. To quantify sources of variability, the average % moisture add-on after conditioning was calculated for each test material at each laboratory. Figure 7 shows the variability of the % moisture add-on between laboratories.

These data indicate good agreement between labs on the amount of moisture add-on for each composite. Although slight variation are observed from specimen to specimen as well as laboratory to laboratory, this study did not show a direct correlation between moisture add-on and the time to second degree burn. However, varying amounts of moisture within the test composite undoubtedly contributes to the variation in burn times within as well as between laboratories.

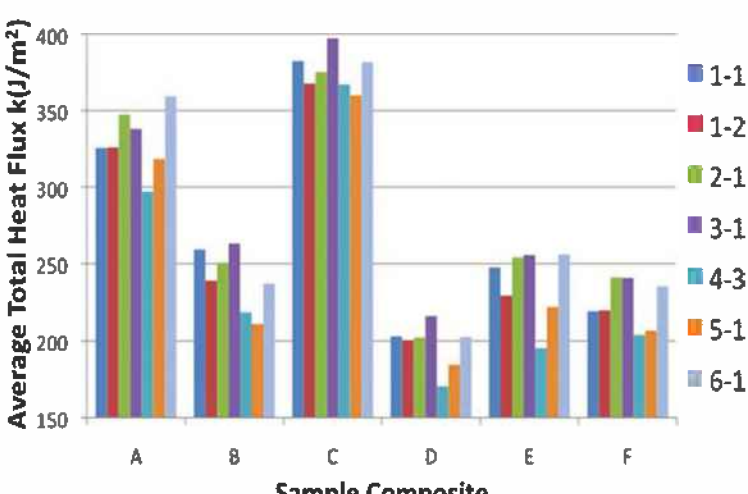

FIG. 6—*Average total energy transmitted per composite (by lab).*

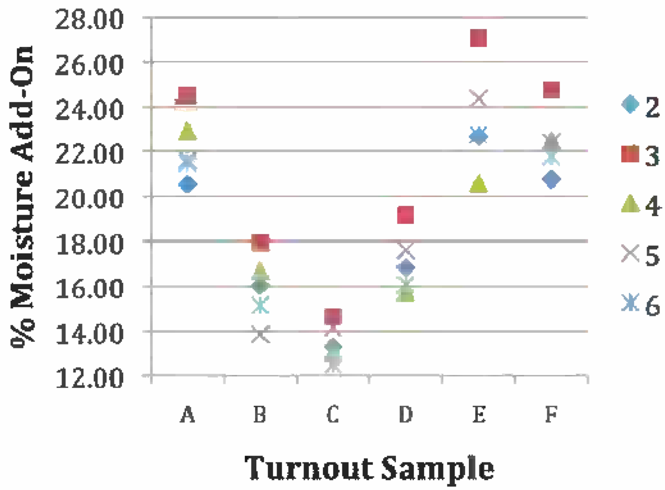

FIG. 7—*Moisture add-on versus material (per lab).*

Conclusions

Statistical analysis of the data obtained from this interlaboratory study showed good inter-laboratory agreement of the stored energy test method. Repeatability and reproducibility limits provide the basis on which to assess the variability of future tests run in accordance with ASTM F2731.

The study confirmed that some test variability can be attributed to differences in the turnout composite test specimens. Test specimens incorporating impermeable trim attached to the outer shell show an increase in within- and between-laboratory variability. Other sources of variability investigated were variations in thermal exposure intensity and moisture add-on after preconditioning, and heat source variations. However, these sources of variation did not directly correlate with test values obtained, nor did they cause any outlying observations in this study.

Acknowledgments

The writers wish to acknowledge the contributions of laboratories participating in this study including: Underwriters Laboratories, W.L. Gore & Associates, PBI Performance Products Inc., Globe Manufacturing Company, LLC, Lion Apparel Inc., and 3 M. The writers are grateful to the National Institute for Occupational Safety and Health (NIOSH) and the National Personal Protective Technology Laboratory (NPPTL) for their support of this research.

APPENDIX: COMPLETE RESULTS OBTAINED FROM THE INTERLABORATORY STUDY OF THE STORED ENERGY TEST METHOD ARE SHOWN IN TABLE 5 BELOW.

TABLE 5—*SET interlaboratory study data.*

	Time to second degree burn, s					
Laboratory	A	B	C	D	E	F
1-1	88.36	97.62	95.3	no burn	123.61	137.8
	128.16	95.96	100.71	no burn	128.72	132.9
	131.29	107.37	87.05	no burn	126.43	no burn
	137.95	105.02	101.13	no burn	130.47	134.53
	129.21	88.36	95.23	no burn	131.57	157.74
1-2	127.58	98.79	94.94	no burn	133.55	154.38
	127.64	88.85	96.8	143.2	128.6	132.65
	132.15	114.44	100.02	no burn	no burn	137.93
	134.92	88.11	100.62	no burn	130.92	134.95
	131.67	101.54	98.61	143.05	124.87	no burn
2-1	132.76	90.66	91.39	no burn	126.33	130.32
	122.53	90.46	93.44	no burn	129.85	131.46
	130.36	87.3	96.36	150.57	127.76	131.47
	125.15	89.18	95.45	no burn	126.19	130.35
	130.67	86.54	96.25	no burn	130.5	133.3
3-1	116.6	92.7	92.2	143.2	128.4	127.3
	130.5	88.1	89.7	138.9	128.3	133.1
	130.4	89.1	91.2	137.4	117.4	132.2
	127.6	92.3	90.8	151.9	126.8	130.9
	128.7	87.1	87.4	142.2	127.5	134.5
4-3	132.81	130.44	96.69	no burn	no burn	138.78
	135.9	123.24	92.57	no burn	137.02	138.21
	131.62	91.15	100.52	no burn	145.7	139.59
	133.13	100.78	103.35	no burn	134.84	no burn
	138.51	83.46	91.38	no burn	136.57	139.05
5-1	135.74	100.27	100.65	no burn	134.5	no burn
	no burn	104.22	112.16	no burn	136.24	no burn
	129.19	103.65	100.6	no burn	136.21	165.49
	no burn	102.61	108.41	no burn	138.59	139.88
	no burn	100.86	120.28	no burn	130.64	143.67
6-1	132.25	87.71	98.38	no burn	128.39	134.42
	130.31	89.57	90.19	no burn	119.5	131.57
	136.52	94.14	90.98	147.95	126.9	135.81
	123.91	85.06	96.35	140.31	122.1	130.26
	133.85	85.23	94.98	no burn	124.98	132.92

References

[1] Barker, R. L., Deaton, A. S., and Ross, K., "Heat Transmission and Thermal Energy Storage in Firefighter Turnout Suit Materials," *Fire Technol.*, Vol. 47, No. 3, 2010, pp. 549–563.

[2] Center for Research on Textile Protection and Comfort, NC State Univ., "Development of a Test Method for Measuring Transmitted Heat and Stored Thermal Energy in Firefighter Turnouts," final report presented to National Institute for Occupational Safety and Health (NIOSH) National Personal Protective Technology Laboratory (NPPTL) under Contract No. 200-2005-12411, April 29, 2008.

[3] ASTM F2731, 2011, "Standard Test Method for Measuring the Transmitted and Stored Energy of Firefighting Protective Clothing Systems," *Annual Book of ASTM Standards*, ASTM International, West Conshohocken, PA, 2011.

[4] Center for Research on Textile Protection and Comfort, NC State Univ., "Thermal Capacity of Firefighter Protective Clothing," presented to the Fire Protection Research Foundation, 2008.

[5] "Stored Energy Tester Operator's Manual," Measurement Technology Northwest, Seattle, WA.

[6] ASTM F2700, 2008, "Standard Test Method for Unsteady-State Heat Transfer Evaluation of Flame Resistant Materials for Clothing with Continuous Heating," ASTM International, West Conshohocken, PA, 2008.

[7] NFPA (1971), *Standard on Protective Ensembles for Structural Fire Fighting and Proximity Fire Fighting*, 2006 ed., National Fighting Protection Association, Quincy, MA, 2006.

[8] ASTM E691-09, 2009, "Standard Practice for Conducting an Interlaboratory Study to Determine the Precision of a Test Method," ASTM International, West Conshohocken, PA, 2009.

Performance of Protective Clothing and Equipment: Emerging Issues and Technologies
STP 1544, 2012
Available online at www.astm.org
DOI:10.1520/STP104097

Moein Rezazadeh[1] *and David A. Torvi*[2]

Non-destructive Test Methods to Assess the Level of Damage to Firefighters' Protective Clothing

REFERENCE: Rezazadeh, Moein and Torvi, David A., "Non-destructive Test Methods to Assess the Level of Damage to Firefighters' Protective Clothing," *Performance of Protective Clothing and Equipment: Emerging Issues and Technologies* on June 16–17, 2011 in Anaheim, CA; STP 1544, Angie M. Shepherd, Editor, pp. 202–226, doi:10.1520/STP104097, ASTM International, West Conshohocken, PA 2012.

ABSTRACT: During the service life of firefighters' protective clothing, individual aspects of its performance change due to factors such as thermal exposure. Although there are some standards for the inspection of firefighters' protective clothing, test methods that could be used to completely determine the level of damage and the remaining service life of such clothing have not yet been developed. In order to develop these test methods, it is necessary to understand how individual aspects of the performance of protective clothing deteriorate after exposure to fireground conditions. In this project, specimens consisting of an outer shell, a moisture barrier, and a thermal liner were thermally aged and tested using 20 kW/m^2 exposures in a cone calorimeter. Two different outer shell fabrics, one undyed (light brown in color) and one dyed (black), were tested. Changes in the tensile strength of the outer shell resulting from single and multiple exposures were measured. Changes in the color of the outer shell were also measured using digital image analysis. The study demonstrates that multiple exposures to this heat flux level were less destructive than a single exposure of the same total duration. Color measurements showed good potential as a possible non-destructive means of evaluating the condition of the outer shell fabric, as these color measurements could be correlated to the loss in tensile strength

Manuscript received June 3, 2011; accepted for publication May 7, 2012; published online July 2012.

[1]Ph.D. Candidate, Dept. of Mechanical Engineering, Univ. of Saskatchewan, Saskatoon, SK, Canada S7N 5A9.

[2]Professor, Dept. of Mechanical Engineering, Univ. of Saskatchewan, Saskatoon, SK, Canada S7N 5A9. (Corresponding author), e-mail: david.torvi@usask.ca

of the outer shell. Possible future work to evaluate other aspects of the performance of these materials is discussed.

KEYWORDS: firefighters' protective clothing, durability, non-destructive tests, color measurement, outer shell, service life, thermal aging, multiple exposures

Introduction

The characterization of the performance of firefighters' protective clothing over its entire lifetime is very important to firefighters. "Firefighters' protective clothing" is a general term that encompasses coats, pants, coveralls, helmets, gloves, footwear, and interface components. In this paper, the term "firefighters' protective clothing" is used to refer to coats and pants. Both coats and pants are made of similar fabrics and often include three layers: an outer shell, a moisture barrier, and a thermal liner (Fig. 1). The performance of each layer of firefighters' protective clothing has a significant influence on the level of protection provided by the entire ensemble. In general, the protection offered by firefighters' protective clothing is expected to deteriorate over time, but there is still uncertainty about how destructive different exposures are and how long a piece of firefighters' protective clothing can continue to protect a firefighter to an acceptable level.

FIG. 1—*Three layers of firefighters' protective clothing (from right: outer shell, moisture barrier, and thermal liner).*

"Useful life" (service life) can be defined as the period of time during which the firefighters' protective clothing provides acceptable protection. The useful life of firefighters' protective clothing depends on a number of factors, including the type of material from which it is constructed; the number, duration, and intensity of destructive exposures the clothing has faced; the amount of abrasion and wear; and the maintenance and storage procedures used [1]. A number of associations and manufacturers have developed standards or guidelines for determining the end of the useful life of protective clothing.

NFPA 1851 [2], one existing standard for the selection, care, and maintenance of structural firefighters' protective clothing, states that clothing shall be retired not later than ten years after its date of manufacture. In addition, NFPA 1851 mandates that fire departments discard a piece of protective clothing if it is so damaged or contaminated that its repair or decontamination is not cost effective. In the case of contamination by terrorism agents involving chemicals, biological agents, and/or radiological particulates, firefighters' protective clothing must be retired immediately, regardless of its physical appearance or repair cost. The standard suggests a typical guideline for retirement age based on a matrix that defines the reasonable repair cost of firefighters' protective clothing as a percentage of the replacement cost for each year of service life up to ten years. If the repair cost of firefighters' protective clothing is estimated to be higher than the specified cost in this matrix, it should be replaced with a new piece of firefighters' protective clothing.

Some manufacturers suggest a normal useful life of three to five years for firefighters' protective clothing, which might decrease to two to three years in an active fire department. Manufacturers suggest that the useful life is seldom more than seven years [3]. However, providing a definitive number of years of useful life for firefighters' protective clothing is problematic. Different firefighters, even in the same department, have different roles in firefighting, and their protective clothing is exposed to different conditions over the same period. In addition, fire departments in different areas might encounter different types and sizes of fires. For example, a fire department in a large metropolitan area might not be comparable with a fire department in a rural area in terms of the number and size of fires and the type of firefighting operations. In a study of the City of Montreal Fire Department in 1993–1994 [4], it was found that only 66 % of the personnel acted as first-line combat firefighters, and 10 % of personnel who were officially considered firefighters were not exposed to fire at all.

The standards for protective ensembles for structural firefighting, such as NFPA 1971 [5], describe the minimum requirements for new protective clothing and the test methods for evaluating clothing. Practically all of the test methods in these standards are destructive. As a result, measuring the performance of in-use firefighters' protective clothing without destroying that clothing is almost impossible. Performing the destructive tests listed in this or other standards on a limited number of pieces of protective clothing will not be representative of all clothing in a fire department and cannot completely assess the level of damage to individual pieces of clothing. Firefighters in the same department have different roles in firefighting, and their protective clothing is exposed to different conditions, so the use and maintenance histories of individual pieces of clothing might be different over the same period. This sampling procedure also might be too expensive for some departments. Therefore, there is a need to develop and improve non-destructive methods for evaluating the condition of in-use turnout gear.

Non-destructive techniques are being used extensively in many areas of engineering to evaluate in-use condition and as a predictive tool to estimate the remaining service life. In these techniques, some properties of the material serve as indicators of performance deterioration. If these properties can be measured, the level of material deterioration can be determined and used to help to estimate the remaining lifetime of the material. Two major issues should be addressed before a non-destructive method is chosen. The first issue is to identify the physical properties of the specimen that deteriorate with use, or the nature of the flaws that will appear in the specimen gradually during its service time. The second issue is to identify the physical process that the non-destructive method will be based on. These two issues will determine whether the non-destructive method is applicable to a particular test specimen [6].

Several non-destructive test methods have been proposed for the evaluation and inspection of fibers and protective clothing. For example, Raman spectroscopy was employed by Galiotis [7] to evaluate fibers, by Washer et al. [8] to evaluate strands of para-aramid (Kevlar), and by Thorpe and Torvi [9] to evaluate firefighters' protective clothing. A feasibility study on employing liquid penetrants to evaluate chemical protective clothing was conducted by Bray and Stull [10]. Active thermography was implemented by Gralewicz and Wiecek [11] for fire protective fabrics. In terms of qualitative evaluation, inspection by a light source or the penetration of a water–alcohol mixture is suggested in NFPA 1851 [2]. A more detailed review of previous work in this field can be found in a recent literature review [1].

Many standards and guidelines, including NFPA 1851 [2], suggest that regular visual inspections of protective clothing should be conducted. One particularly important step is to determine whether there are any areas with discoloration. One difficulty with evaluating discoloration is that color determination by individuals is subjective. Methods do exist to measure color. Thorpe and Torvi [9] measured changes in the color of specimens after exposure to radiant heat fluxes of between 5 and 30 kW/m^2. They found that color measurement using digital image analysis of images of fabrics obtained using a commercial scanner showed good potential as a non-destructive test method. In this paper, this method is also employed to evaluate specimens after different thermal exposures in the cone calorimeter.

Colorfastness is defined as the resistance of textile color to fading or removal during manufacturing, textile processes, service, storage, or aging by destructive agents [12]. For the protective fabrics considered in this study, changes in color during thermal exposure can be due to a loss of dye or to thermal decomposition of the fabrics. The depth of the dye in the fiber, binding forces between the dye and the fiber, and the nature of the thermal exposure are key factors in the analysis of colorfastness for these protective fabrics.

A new piece of thermal protective clothing must provide a certain level of thermal protection and meet specifications for mechanical properties, both of which are set by different standards such as NFPA 1971 [5]. When thermal protective clothing is employed in fire departments, it will be frequently exposed to deleterious agents such as elevated temperature, ultraviolet radiation, and chemicals during its service life. In most research studies, the level of damage to thermal protective fabrics is estimated by using simulated long-term exposures to harmful conditions. These simulations might not completely determine the real level of damage to thermal protective fabrics, because some factors, such as fatigue, are not considered. As some levels of thermal exposure occur on a regular basis during firefighting operations, simulating thermal aging with multi-stage exposures might be important. For example, Iyer and Vijayan [13] showed that for a certain length of exposure, the destructive effect of multi-stage aging is less severe than that of a one-stage (single) exposure. This was determined through comparison of the x-ray diffraction profile of a fabric exposed to 400°C for a continuous 10 h period with that of a fabric exposed to the same temperature for a total exposure time of 10 h divided into four 2.5 h stages.

In the current work, the effect of multi-stage thermal aging on one aspect of performance of firefighters' protective clothing, the tensile strength of the outer shell fabric, is considered. Specimens include three layers of firefighters' protective clothing: an outer shell, a moisture barrier, and a thermal liner. Two different outer shell fabrics, one undyed (light brown in color) and one dyed (black), were examined. Specimens were aged using a single exposure to a heat flux of 20 kW/m^2 for 15 to 150 s in a cone calorimeter, as well as multiple 30 s exposures at 20 kW/m^2. The tensile strength of the outer shell was then measured using destructive tests specified in ASTM and other standards for new clothing. Changes in the color of the outer shell fabric were also measured using digital image analysis.

This paper discusses the results of the destructive tensile tests of these fabrics, as well as the correlation between these results and the non-destructive color measurements. Results are also explained using measurements of the temperatures of the fabric layers made during cone calorimeter tests and the decomposition temperatures obtained from differential thermal analysis of these materials. Future work to evaluate other aspects of the performance of these materials, including tear strength, water penetration resistance, water vapor permeability, and flame resistance, are also discussed, along with the development of probabilistic and other models to determine the retirement age of firefighters' protective clothing.

Materials and Experimental Methods

Four protective fabrics used in the construction of the three layers of firefighters' protective clothing are considered in this work: Guardian 750, Guardian 790, Stedair 3000, and XE-289.[3] Guardian 750 and Guardian 790 are a blend of 60 % Kevlar and 40 % PBI with a surface weight of approximately 270 g/m^2 and are used as outer shell fabrics for firefighters' protective clothing. The Guardian 750 outer shell was undyed and therefore was the natural light brown color of these fibers. The Guardian 790 was a piece-dyed fabric (i.e., the fabric was dyed after being woven) and was black in color. Stedair 3000 is an expanded polytetrafluoroethylene–based moisture barrier laminated to Nomex E89. XE-289 is a three-layer fabric with a surface weight of 245 g/m^2 that is used as a thermal liner in firefighters' protective clothing and is made of Nomex E89. This thermal liner consists of two nonwoven layers and a dyed aramid face cloth. The orientation of the three layers of the specimen is the same as in firefighters' protective clothing (Fig. 1). The outer shell fabric is exposed to the heat source. The moisture barrier is placed in such a way that its substrate is in contact with the outer shell and its membrane is in contact with the thermal liner. The thermal liner's face cloth is on the unexposed side of the specimen.

Thermogravimetric analysis (TGA) of the Guardian 750 outer shell fabric in nitrogen showed that thermal decomposition of this fabric begins to occur at a temperature of about 450°C [14]. TGA tests of Stedair 3000 and XE-289 demonstrated that thermal decomposition of these fabrics begins at temperatures of approximately 275°C and 425°C, respectively.

In order to simulate the thermal exposures that firefighters face on the fire ground, a heat source and a range of intensities, durations, and numbers of exposures for thermal aging are required. Two methods of thermal aging are considered in this work. A cone colorimeter can generate a uniform heat flux over the surface of specimens, especially during short-duration exposures. A furnace can be used to expose fabrics to a high-temperature environment. However, the recovery time required in order for a furnace to reach its pre-set temperature after its door has opened is an issue, especially when fabrics are being

[3] Certain commercial products are identified in this paper in order to adequately specify the results of research. In no case does such identification imply recommendation or endorsement by the authors, nor does it imply that the product or material identified is the best available for the research purpose.

subjected to multiple short-duration exposures. Therefore, the conical heater of the cone calorimeter, which produces a primarily radiant heat flux, was selected as the heat source in this study.

In terms of the intensity of thermal exposure, one method for categorizing firefighting environments is to use three regions based on temperature and/or heat flux (Fig. 2): routine, ordinary, and emergency [15]. After an exposure to high heat fluxes in the emergency category, firefighters' protective clothing will likely be seriously damaged to the point that it is obvious that it will need to be retired. Also, exposures to low heat fluxes in the routine category might take a very long time to cause noticeable deterioration and discoloration in the specimens. Therefore, heat fluxes of 10, 20, and 30 kW/m^2 were selected for this part of the study, to represent the upper end of the ordinary category.

In order to interpret the changes in the performance of the fabrics evaluated during this study, the temperatures of the three layers during exposures to this range of incident heat fluxes were measured. For this purpose, specimens were cut from the aforementioned fabrics to dimensions of 10 cm × 10 cm (4 in. × 4 in.). Only the undyed brown Guardian 750 outer shell was used, as the other outer shell fabric was made of the same fibers. Specimens were conditioned in a chamber at 22°C ± 2°C and 65 % ± 2 % relative humidity for 24 h. The specimens were mounted on a specimen holder and restrained by pins attached to the holder (Fig. 3). Restraining the specimens restricts thermal shrinkage. The specimen holder is the same as that referenced in ASTM F2700 [16].

Type K thermocouples were chosen for temperature measurements. Thermocouple wires were soldered to each other to form a bead. In total, seven type K thermocouples (Omega, Laval, QC) with a wire diameter of 0.25 mm (36 AWG-GG-K-36-SLE) were sewn to the specimen to measure the temperature. The thermocouples were then sewn to the center points of the front and

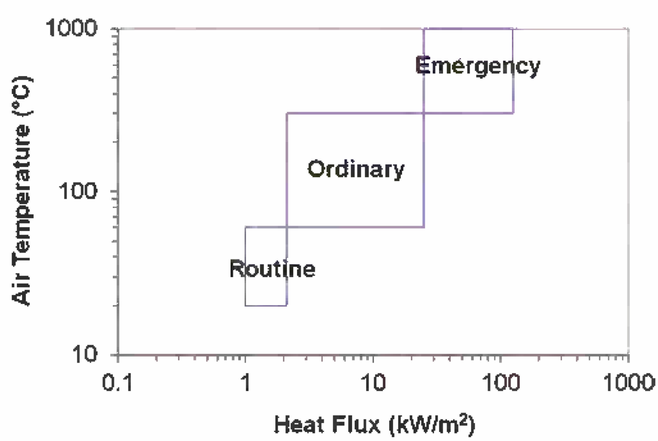

FIG. 2—*The range of thermal conditions faced by firefighters [15].*

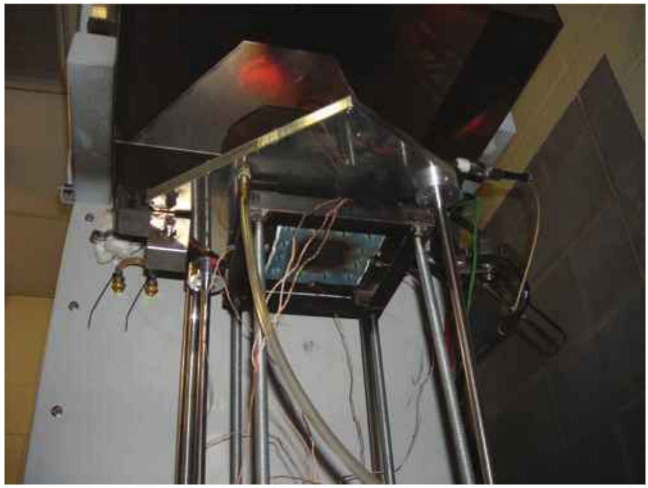

FIG. 3—*Test setup for measuring temperature of specimen layers.*

back sides of each layer of the specimen. One extra thermocouple was sewn to the middle layer of the thermal liner. The thermocouples were connected to a data acquisition system (HP Agilent 34970A, Santa Clara, CA) that recorded the temperature approximately every 0.3 s.

The specimen holder had a 5 cm × 5 cm (2 in. × 2 in.) cutout in the center, through which the specimen was exposed to a radiant heat flux. The specimen holder was placed on a stand, the height of which was adjustable. The height of the stand in this study was set such that the distance between the bottom of the conical heater and the surface of the specimen was 25 mm. Figure 3 shows the test setup.

The desired incident heat flux was produced by controlling the temperature of the conical heater of the cone calorimeter. The heat flux value was measured 25 mm below the center of the conical heater using a Schmidt-Boelter heat flux gauge (Medtherm, Huntsville, AL) cooled by a water flow. When the conical heater reached a steady-state condition and produced the desired heat flux, the heat flux sensor was removed from its place. Then, an air-cooled shutter was closed to protect the specimen from the conical heater. Although the shutter was closed, limited heat transfer occurred to the specimen through the shutter. This is why the specimen was not at room temperature at the beginning of the experiment or at the end of each stage of thermal exposure. The stand and the specimen holder were placed under the conical heater. After the shutter was opened, the specimen was exposed to the heat flux for the required duration. In the multi-stage exposure, the shutter was closed at the end of each stage. After the specimen cooled down, the shutter was reopened for the next stage of exposure.

The same procedure was used for the thermal aging of specimens prior to tensile testing. As noted earlier, a heat flux of 20 kW/m^2 was selected for this purpose, as it represents the ordinary range of conditions. It is also very similar to the 21 kW/m^2 heat flux that is used in several standards for flame resistant clothing [5,17]. Specimens for thermal aging were cut to 15 cm $\times$ 10 cm (6 in. $\times$ 4 in.) from the aforementioned fabrics. Each specimen consisted of all three layers of firefighters' protective clothing. Ensembles with both outer shell fabrics were tested. A peripheral margin of the specimen was covered with metal bars to constrain the exposed area to the central part of the specimen. The exposed area of the specimen, 8.5 cm $\times$ 5.8 cm, was used as the interrogation area later in color measurements.

Specimens were thermally aged using single and multiple exposures. In the single exposure, specimens were exposed to a heat flux of 20 kW/m^2 for a duration of between 15 and 150 s, whereas in multiple exposures the duration of each stage of exposure was 30 s. After each exposure, specimens were cooled to approximately the laboratory temperature for 5 min and then exposed to the heat source for the next 30 s exposure. Multiple exposures were done using two, three, four, and five stages. In order to provide an estimate of the consistency of the thermal aging of specimens, an infrared thermometer (Cyclops 300AF, Minolta/Land, Dronfield, UK) was employed to measure the temperature of the center point of the back side of the thermal liner. The infrared thermometer was connected to the same data acquisition system as in the previous temperature measurements, which recorded the temperature approximately every 0.2 s.

The tensile strength of the outer shells of the new and thermally aged specimens was measured using a procedure similar to those described in NFPA 1971 [5] and ASTM D5034-09 [18]. The employed tensile testing machine was of the constant-rate-of-extension type and operated at a speed of 200 mm/min. The jaw face was coated with an anti-slip coating. The jaw measured 25 mm (1 in.) perpendicular to the direction of the application of the force and 37.5 mm (1.5 in.) parallel to the direction of the application of the force.

Before the tensile tests were run, the outer shell surface color was evaluated using a commercial scanner (Epson Perfection V30, Markham, Canada) and a MATLAB code. The color was measured in the red-green-blue (RGB) system. In the RGB system, color is defined in three dimensions in terms of magnitudes of red, green, and blue components of the color. The [0,0,0] point describes black, and white is defined by [1,1,1].

The front side of the outer shell specimen, which was exposed to the cone calorimeter, was scanned with 24-bit color and 300 dpi resolution as a bitmap file. The code reads the image file and stores the color as an $m \times n \times 3$ matrix. The m and n values indicate the location within the interrogation area, and the third component of the matrix indicates which of the three colors in the RGB system is measured. The average value of each $m \times n$ submatrix represents the magnitude of each color component for the area of interest. Subsequently, the color of the thermally aged outer shell fabric is compared with that of the unexposed outer shell fabric. The color difference is calculated based on Eq 1 [19].

$$\Delta\text{Color} = \sqrt{(R_2 - R_1)^2 + (G_2 - G_1)^2 + (B_2 - B_1)^2} \quad (1)$$

R, G, and B denote the magnitudes of the red, green, and blue color components, respectively. The subscripts "2" and "1" signify exposed and unexposed conditions, respectively.

Results

The temperatures of different layers of ensembles with undyed brown outer shells were measured during exposure to incident heat fluxes of 10, 20, and 30 kW/m^2. Specimens were exposed to heat fluxes in three stages in each test. Individual tests were repeated three times. The averages of the values for the maximum temperature measured during each stage of exposure for each of the heat fluxes are presented in Table 1. The standard deviations for the recorded values shown in Table 1 for 10, 20, and 30 kW/m^2 heat fluxes are 4°C, 5°C, and 6°C, respectively. In addition to the uncertainty due to the measurement techniques used, the sizes of air gaps between the individual layers might vary between tests, affecting these maximum temperatures.

Figures 4–6 depict the temperature profiles of individual layers for the first two out of the three stages of exposure. As this part of the project is focused on the performance of the outer two layers, the temperature history of the thermal liner is not included in these figures. Stages of exposure to heat fluxes of 10, 20, and 30 kW/m^2 were 10, 6, and 1 min, respectively. After each stage of exposure, approximately 40 min were required in order for the specimen to cool down and reach the laboratory temperature.

TABLE 1—*Maximum temperatures (°C) achieved by different layers of the ensemble during exposure to various incident heat fluxes (undyed brown outer shell).*

Incident heat flux, kW/m^2		10			20			30		
Layer and orientation of the specimen \ Number of exposures		1	2	3	1	2	3	1	2	3
Outer shell	Front side	294	293	292	419	412	413	504	478	480
	Back side	288	289	288	411	402	402	506	470	472
Moisture barrier	Front side	258	257	257	384	370	372	497	434	434
	Back side	238	237	238	345	329	328	466	393	394
Thermal liner	Front side	195	194	196	282	274	274	392	337	338
	Second layer	175	175	175	258	250	250	342	295	296
	Back side	163	163	162	235	229	229	310	266	266

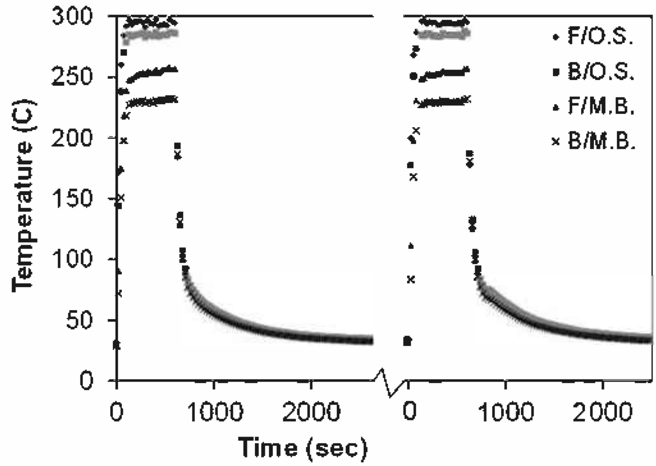

FIG. 4—*Specimen temperature profiles on the front (F) or back (B) side of the undyed (light brown in color) outer shell (O.S.) and moisture barrier (M.B.) (first two exposures to a heat flux of 10 kW/m*^{2}*).*

Specimens were then thermally aged using exposures to a heat flux level of 20 kW/m^2 in two ways. One group of specimens underwent a single exposure, and the second group was exposed multiple times. Specimens in the first group experienced single exposures for durations of 15, 30, 45, 60, 90, 120, and 150 s. Specimens in the second group were exposed to two, three, four, and five stages of 30 s thermal exposures; thus, these specimens underwent total thermal exposures of 60, 90, 120, and 150 s. This allowed the effects on the fabric performance of single and multiple thermal exposures of the same total

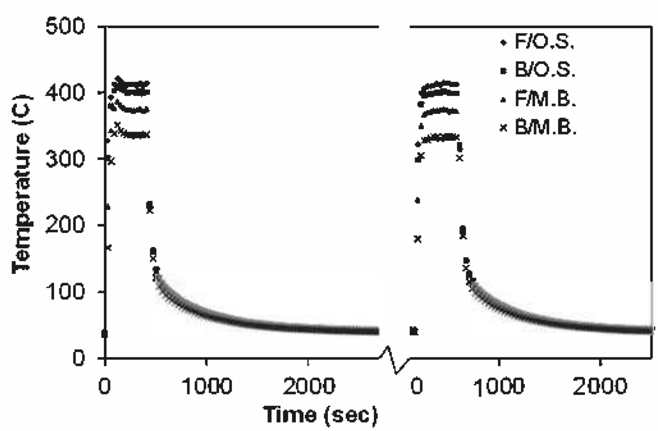

FIG. 5—*Specimen temperature profiles on the front (F) or back (B) side of the undyed (light brown in color) outer shell (O.S.) and moisture barrier (M.B.) (first two exposures to a heat flux of 20 kW/m*^{2}*).*

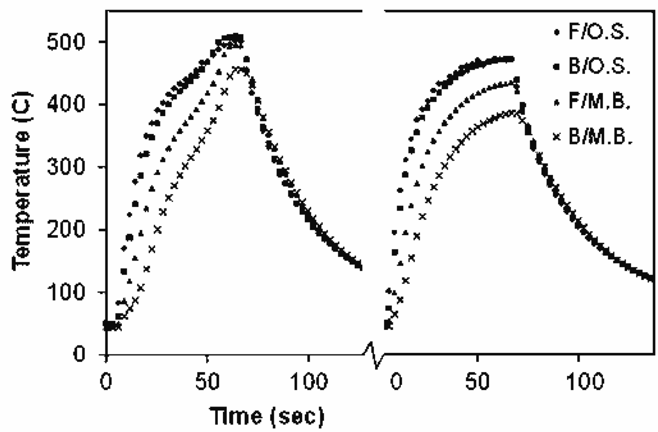

FIG. 6—*Specimen temperature profiles on the front (F) or back (B) side of the undyed (light brown in color) outer shell (O.S.) and moisture barrier (M.B.) (first two exposures to a heat flux of 30 kW/m*^{2}*).*

duration to be compared. Photographs of the specimens after single and multiple exposures are shown in the Appendix.

Because the mechanical strengths of fabrics differ in the warp and fill directions, specimen layers were cut from both directions. For each individual thermal exposure condition (the combination of the duration and number of exposures), four specimens were prepared: two specimens from the warp direction, and two specimens from the fill direction. Whereas NFPA 1971 [5] requires five specimens in each direction, average values based on measurements using two specimens in each direction were used in this study, as the emphasis of this work was on the change in tensile strength after exposure. After the thermal exposures, the tensile strength of the outer shell of the thermally aged specimens was measured. The average tensile strength of the outer shell fabric reported for each thermal exposure condition is the average tensile strength of the four outer shell specimens.

NFPA 1971 [5] mandates a minimum value of 623 N for the tensile strength of the outer shell layer of new firefighters' protective clothing. This requirement is shown in Figs. 7–12, which include the tensile testing results.

Figure 7 depicts the tensile strength of the outer shell fabrics after a single exposure for a certain duration (a duration of 0 indicates an unexposed outer shell fabric). Figure 8 shows the same results for multiple 30 s exposures. Figures 9 and 10 compare changes in the tensile strength of the undyed (light brown in color) fabric on an absolute and a percentage basis (compared with the initial tensile strength value), respectively, after single and multiple exposures for the same total duration. Figures 11 and 12 present the same information as Figs. 9 and 10 for the dyed (black) outer shell fabrics.

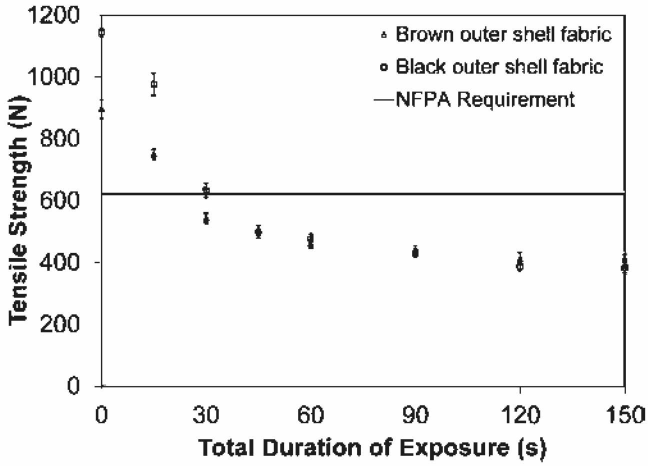

FIG. 7—*Tensile strength of the undyed (light brown in color) and dyed (black) outer shell fabrics after a single exposure to a 20 kW/m*^{2} *heat flux.*

Before destructive tensile testing, the discoloration of outer shell fabrics was quantified. In measurements of color, the whole exposed area was taken into account. After each thermal exposure, the outer shell color was compared with the color of unexposed fabric. This comparison led to the calculation of the color difference (Eq 1). Figures 13 and 14 illustrate the color differences of outer shell fabrics measured after single and multiple thermal exposures, respectively. Figures 15 and 16 compare the effects of single and multiple exposures on the discoloration of individual outer shell fabrics.

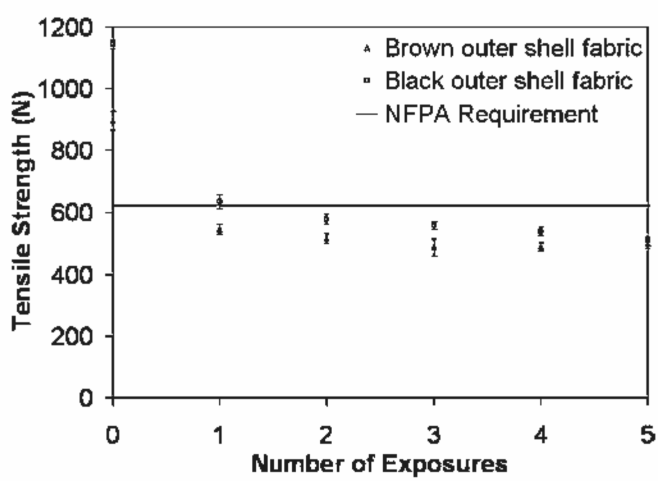

FIG. 8—*Tensile strength of the undyed (light brown in color) and dyed (black) outer shell fabrics after multiple 30 s exposures to a 20 kW/m*^{2} *heat flux.*

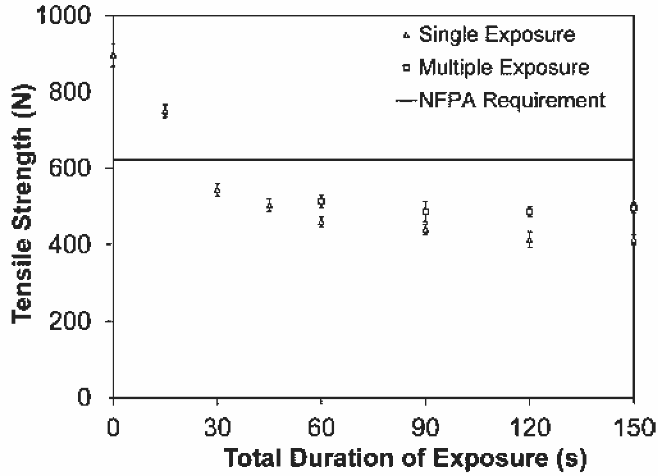

FIG. 9—*Tensile strength of the undyed (light brown in color) outer shell fabric after single and multiple exposures to a 20 kW/m^2 heat flux.*

Figures 17 and 18 show the correlation between the destructive tensile test results and the non-destructive color measurements. Test results for all replications, regardless of whether they were single or multiple exposures, are provided in Figs. 17 and 18. A curve fit was also plotted by eye for each of the individual outer shell fabrics.

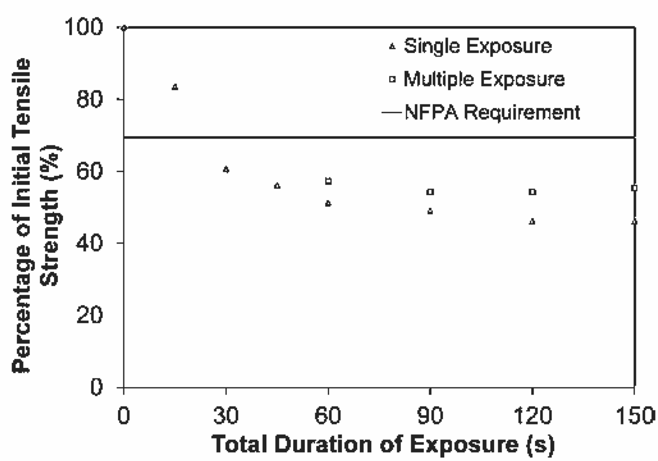

FIG. 10—*Percentage of initial tensile strength of the undyed (light brown in color) outer shell fabric after single and multiple exposures to a 20 kW/m^2 heat flux.*

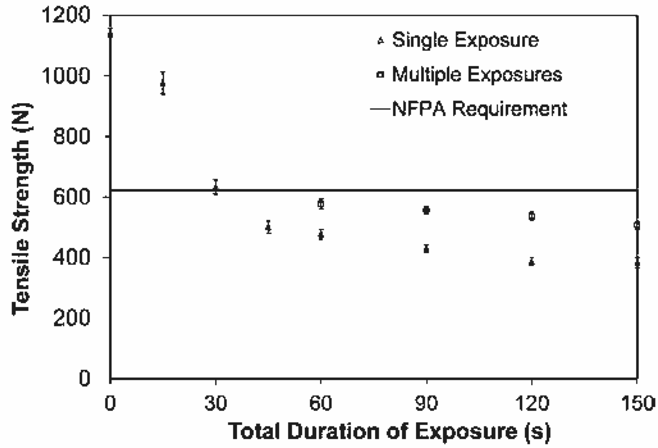

FIG. 11—*Tensile strength of the dyed (black) outer shell fabric after single and multiple exposures to a 20 kW/m^2 heat flux.*

Discussion of Results

As Fig. 4 illustrates, a heat flux of 10 kW/m^2 is of relatively low intensity, increasing the temperature of the outer shell of the specimen to around 300°C. The moisture barrier reaches a maximum temperature of 255°C. The only other difference between the responses of the two outer layers is that it takes longer for the moisture barrier to reach the steady-state condition than the outer shell because of the time required for conduction heat transfer from the outer shell to the moisture barrier.

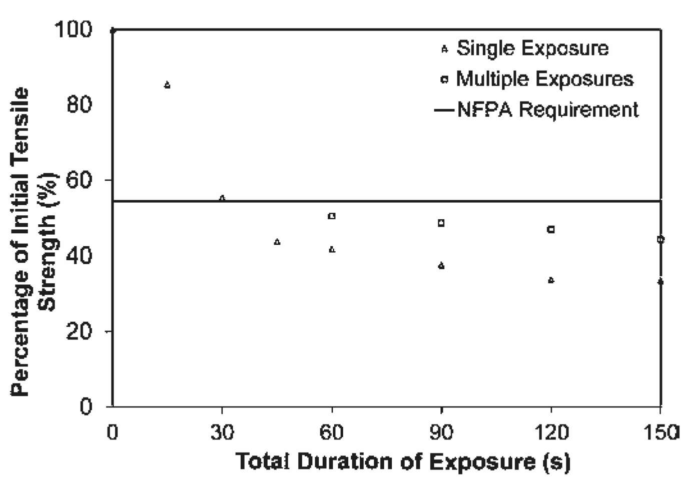

FIG. 12—*Percentage of initial tensile strength of the dyed (black) outer shell fabric after single and multiple exposures to a 20 kW/m^2 heat flux.*

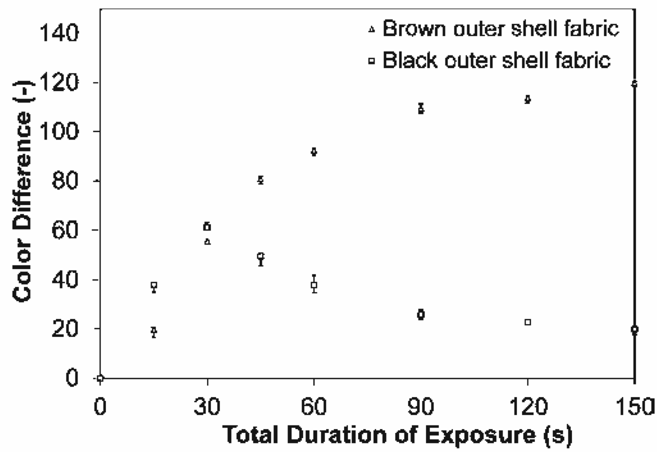

FIG. 13—*Discoloration of the undyed (light brown in color) and dyed (black) outer shell fabrics after a single exposure to a 20 kW/m² heat flux.*

Figure 4 indicates that there is a temperature gradient across each of the layers. The temperature difference is approximately 5°C and 20°C for the outer shell and the moisture barrier, respectively. The temperature difference across the interface between two layers of the specimen is appreciable. It is approximately 30°C across the interfaces between the outer shell and the moisture barrier. The layers were restrained by the peripheral pins on the specimen holder. They were also firmly pressed to each other before the tests were run to decrease any air gap between layers in contact. However, the significant temperature differences reveal that the thermal contact resistance between the

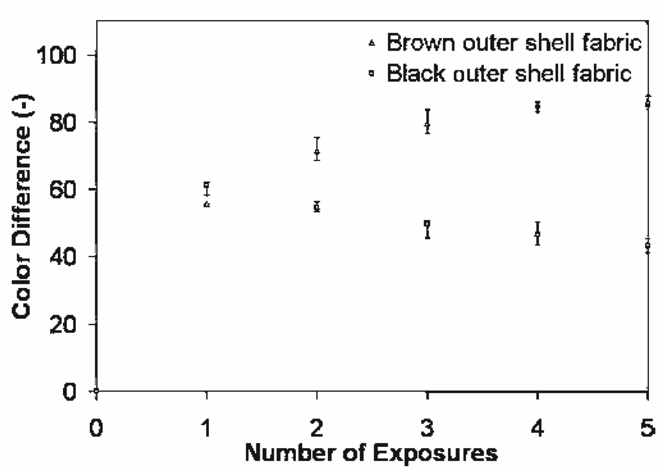

FIG. 14—*Discoloration of the undyed (light brown in color) and dyed (black) outer shell fabrics after multiple exposures to a 20 kW/m² heat flux.*

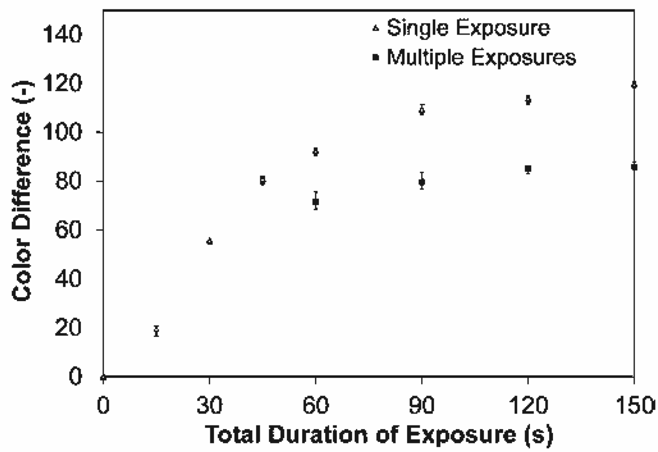

FIG. 15—*Discoloration of the undyed (light brown in color) outer shell fabric after single and multiple exposures to a 20 kW/m*^{2} *heat flux.*

layers cannot be neglected. Therefore, it is necessary to measure the temperature of both sides of the gap between layers in order to have a more accurate measurement of the temperature in each layer of the specimen. It is also unclear how much this thermal contact resistance is influenced by the presence of the thermocouples.

A comparison of the maximum temperature at each exposure to 10 kW/m^2 in Table 1 shows that there is no appreciable difference between the three exposures. This can be explained by the fact that the maximum temperatures of the individual layers in the specimen during the exposure to 10 kW/m^2 are

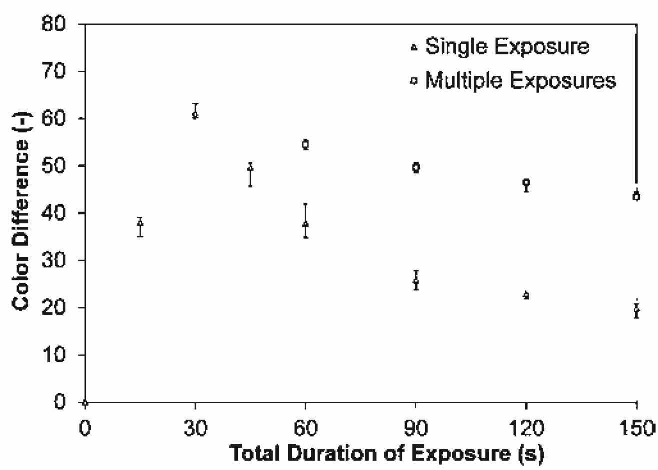

FIG. 16—*Discoloration of the dyed (black) outer shell fabric after single and multiple exposures to a 20 kW/m*^{2} *heat flux.*

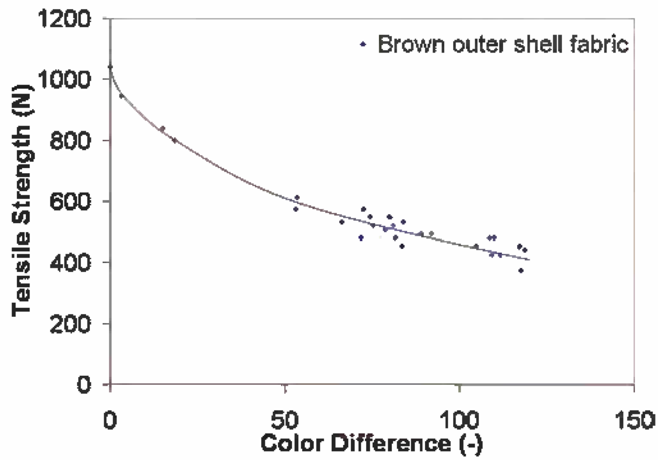

FIG. 17—*Comparison between tensile strength and discoloration for the undyed (light brown in color) outer shell fabric after exposure to a 20 kW/m^2 heat flux.*

lower than their decomposition temperatures. Therefore, such an exposure might not cause serious damage to the fabric in an exposure of relatively short duration. However, frequent exposure to a low heat flux might lead to thermal fatigue and gradual deterioration of performance properties of the fabrics.

Figure 5 represents the temperature profile of the specimen during an exposure to a heat flux of 20 kW/m^2. Such a heat flux increases the maximum temperature of all layers of the specimen by about 100°C as compared to the 10 kW/m^2 heat flux. The average maximum temperature of the outer shell is

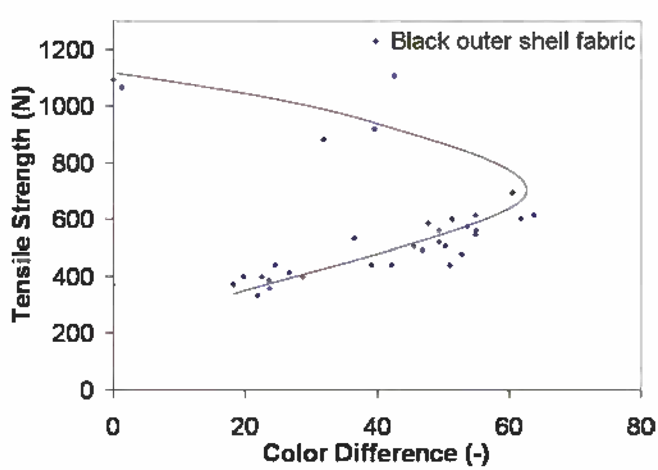

FIG. 18—*Comparison between tensile strength and discoloration for the dyed (black) outer shell fabric after exposure to a 20 kW/m^2 heat flux.*

approximately 415°C, which is closer to the temperature at which decomposition of the outer shell material is expected to begin based on TGA results [14].

The effect of the thermal exposure on the specimen in the first stage of exposure is different from that in the second and third exposures. First, a small temperature drop is observed in the first exposure before the steady-state condition is reached. This indicates that there is a possibility that the specimen has undergone some thermal degradation at this temperature. As a result of the drop, the temperature of the specimen decreases by about 10°C. Second, according to Table 1, the maximum temperature of the outer layer of the specimen in the second and third exposures decreases by approximately 7°C in comparison with that in the first exposure. Such a reduction in temperature is comparable with the measurement uncertainty; however, it might indicate the onset of decomposition of the outer shell in the first stage of exposure, because the maximum temperature of the first layer of the specimen is near its decomposition temperature. The maximum temperature of the underlying layers also decreases in subsequent exposures. This might indicate possible degradation of the inner layers of the clothing, especially as the maximum temperatures for these layers are greater than the temperatures at which decomposition began in TGA tests [14].

In Fig. 5, the temperature differences across the thickness of the outer shell and the moisture barrier are approximately 10°C and 40°C, respectively, which are larger than for the 10 kW/m^2 test. This is attributed to the higher incident heat flux. The same trend is observed for the temperature drop across the interface between two layers of the specimen—it is approximately 30°C for the interface between the outer shell and the moisture barrier.

Figure 6 depicts the first and second stages of exposure to a heat flux of 30 kW/m^2. Such a level of heat flux increases the temperature of the outer shell to 500°C, which is higher than the temperature at which decomposition begins in the TGA tests [14]. The temperature difference across the thickness of the moisture barrier at the end of the first exposure is approximately 30°C. The temperature drop across the interface between the outer shell and the moisture barrier at the same exposure is around 10°C and increases to 35°C in the following exposures, whereas that of the interface between the moisture barrier and the thermal liner is 75°C in the first exposure and decreases to 55°C in the subsequent exposures. The maximum temperature of the moisture barrier is well above the temperature at which decomposition begins in the TGA tests.

Figure 7 shows that the tensile strength of both outer shell fabrics decreases significantly from the value for new fabrics with exposures to 20 kW/m^2 for even 15 s. This implies that degradation in the tensile strength of the fabric starts at temperatures that are lower than the decomposition temperature of the fabric in TGA tests, given that the temperature of the undyed brown outer shell fabric reached 264°C after 15 s of thermal exposure to 20 kW/m^2. It should be noted that the environment during the cone calorimeter exposures was different from the environment in the TGA tests (100 % nitrogen), and heating rates in the cone calorimeter are much higher than the 20°C/min heating rate used in the TGA tests. In addition, the test results show that after approximately 30 s of exposure, the tensile strength of both outer shell fabrics did not meet the NFPA 1971 requirement for a new outer shell fabric.

Figure 8 indicates that, as noted above, the tensile strength of the outer shell fabrics decreased significantly after only one 30 s exposure. The tensile strength continued to decrease after each subsequent 30 s exposure. However, the incremental decrease after the subsequent exposures is much less than the initial decrease after the first exposure.

Figures 9–12 compare the decreases in tensile strength for single and multiple exposures of the same total duration for both outer shell fabrics on an absolute and a percentage basis. For both fabrics, a given total duration of thermal exposure produces a smaller reduction in tensile strength of the outer shell fabrics if the exposure is done in several stages rather than one stage. This result can be explained in terms of the higher maximum temperature that the outer shell fabrics reach in a single exposure of a given total duration relative to that reached in multiple 30 s exposures that produce the same total duration of exposure. For example, the temperature measurements shown in Fig. 5 and Table 1 indicate that the undyed brown outer shell fabric should reach a maximum temperature of approximately 410°C at the end of a 90 s exposure to 20 kW/m^2, whereas if the 90 s total duration exposure was carried out in three 30 s stages, the fabric should reach a temperature of approximately 350°C at the end of each 30 s stage. This difference in maximum temperature means that the fabric should undergo more thermal degradation in the single 90 s exposure than in three 30 s thermal exposures.

Figures 13 and 14 demonstrate the changes in color of the two outer shell fabrics during single and multiple exposures and can be compared with the photographs shown in the Appendix. As with changes in tensile strength, most of the changes in color occur during the shortest exposures, and there are only relatively small changes in color to the fabrics as the exposure time increases past 90 s. These figures also illustrate the differences in how the colors of the two fabrics change as a result of thermal exposure. The photographs in the Appendix indicate that there is a smaller change in color for a set of multiple exposures than for a single exposure of the same total duration. The color measurements shown in Figs. 15 and 16 also indicate this. This is not unexpected based on the temperature and tensile strength measurements discussed earlier.

The color changes for each individual fabric are dependent on the color of the undyed fabric, the initial dyed color of the fabric, and the color changes that occur when the fabric begins to undergo thermal degradation. The undyed brown outer shell fabric is the natural color of its fibers, and color changes are the result of thermal degradation of the fibers. During a thermal exposure, the color becomes darker and eventually would become black. The color of the black fabric first changes due to a loss of dye, tending toward the natural color of the fibers. After removal of the dye and the occurrence of thermal degradation, the color changes are similar to those of the undyed fabric. However, in the case of the black fabric, the color tends toward the original color of the fabric.

Figures 17 and 18 relate destructive and non-destructive test results for the brown undyed and the black dyed outer shell fabric, respectively. Both figures demonstrate how color difference can be correlated with changes in tensile strength due to thermal degradation. However, the two figures illustrate the importance of understanding the changes that occur during thermal exposures when developing a correlation for a particular fabric. As noted above, color continues to change during thermal exposure in the undyed fabric, and it would be relatively easy to develop a correlation for this particular fabric (Fig. 17). In the black dyed fabric, the color difference first increases and then decreases, and therefore more care would be needed in order to develop a correlation (Fig. 18). This difficulty was also noted by Thorpe and Torvi when they used the digital image analysis technique to evaluate differences in the tensile strength of fabrics that were dyed a dark brown color [9]. Preliminary results from a study of a larger range of colors of protective fabrics have also demonstrated the challenges in developing correlations between tensile strength and color difference [19].

Although the thermal aging of specimens was the focus of this study, the performance of protective fabrics is also influenced by other factors, such as exposure to ultraviolet radiation, dirt, soot, and chemicals. Laundering and abrasive and shear forces also affect fabric performance. Many of these factors can also contribute to the discoloration of textiles. This study examined the ability of color measurements to predict changes in tensile strength due to thermal exposure using a laboratory study in which the fabrics were exposed to only high heat fluxes. A challenge that would need to be overcome in order to use this, or any other, non-destructive technique in the field would be to determine the combined effects of different factors on the continuing performance of the fabric.

Conclusions and Future Work

The current work was done in three steps. In the first step, a series of tests were carried out in order to determine the effect of multi-stage aging on the temperatures of three layers of thermal protective clothing during and after exposure to heat fluxes of 10, 20, and 30 kW/m^2. In the second step, specimens including three layers of firefighters' protective clothing were exposed to a heat flux of 20 kW/m^2 using two types of exposures. Two fabrics, one undyed and one dyed, were chosen as outer shell fabrics. In the first set of exposures, specimens were exposed once for a duration of 15 to 150 s, and in the second set of exposures they were subjected to between two and five 30 s thermal exposures. In the third step, the discoloration of both outer shell fabrics was measured using a commercial scanner and a code for analyzing images. Color differences between thermally aged and unexposed outer shell fabrics were measured and compared.

It was shown that the tensile strength of the outer shell fabrics decreased more after a single exposure than with multiple exposures amounting to the same total duration of exposure as the single exposure. These changes in tensile strength can be correlated with changes in the color of the fabric. Such correlations could be of assistance in determining when to retire firefighters' protective clothing. Other heat flux levels and durations of exposure should be examined in future work to see whether more general trends can be determined.

A precise interpretation of the results also requires information about chemical reactions that thermal exposures might produce in the fibers and dyes, if applicable. As other factors contribute to the aging of protective fabrics, additional parameters, such as exposures to ultraviolet radiation and chemicals, laundering, and abrasive and shear forces, should be studied in order to determine whether color changes can be correlated with degradation in fabric performance. As only one fabric type was used here, this study should also be extended to other materials used for the construction of outer shell fabrics. Changes in other aspects of performance such as the tear strength of the outer shell and the moisture barrier, water penetration resistance, and water vapor permeability of the moisture barrier should also be examined. Statistical and probabilistic models, which could help to establish a relationship between the current condition of a piece of protective clothing and its condition after thermal exposure, should be investigated.

Acknowledgments

The writers would like to acknowledge the technical contributions of Mr. Hans-Jurgen Steinmetz, Mr. Rick Retzlaff, and Mr. Dave Deutscher of the Department of Mechanical Engineering at the University of Saskatchewan, as well as Difco Performance Fabrics Inc. and Stedfast Inc. for their donation of materials for this research. Financial support of this research from the Department of Mechanical Engineering, the College of Graduate Studies and Research, and the Natural Sciences and Engineering Research Council of Canada (NSERC) is also gratefully acknowledged.

Appendix

Photographs of undyed (light brown in color) outer shell fabric: single and multiple exposures.

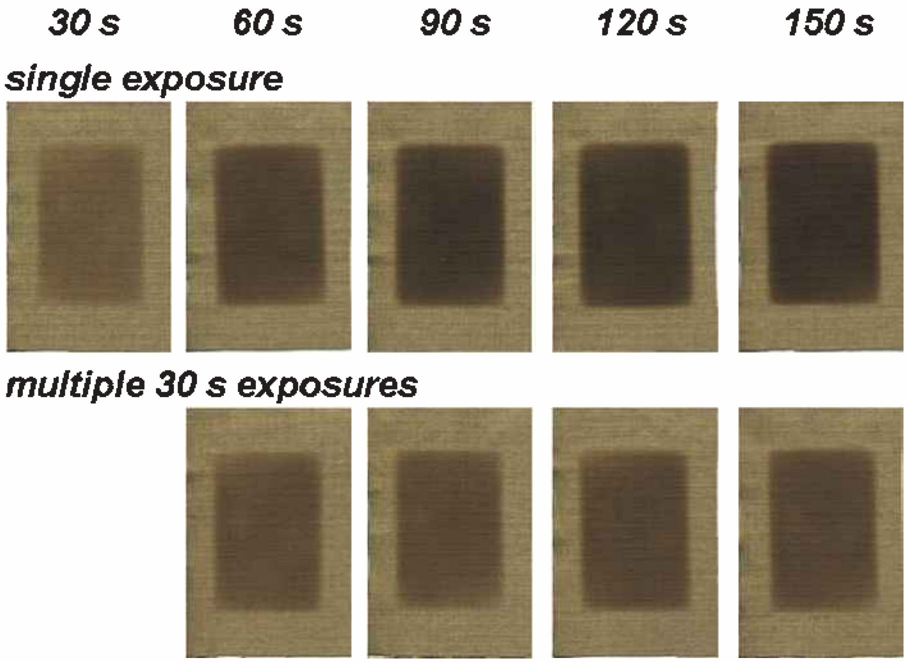

Photographs of dyed (black) outer shell fabric: single and multiple exposures.

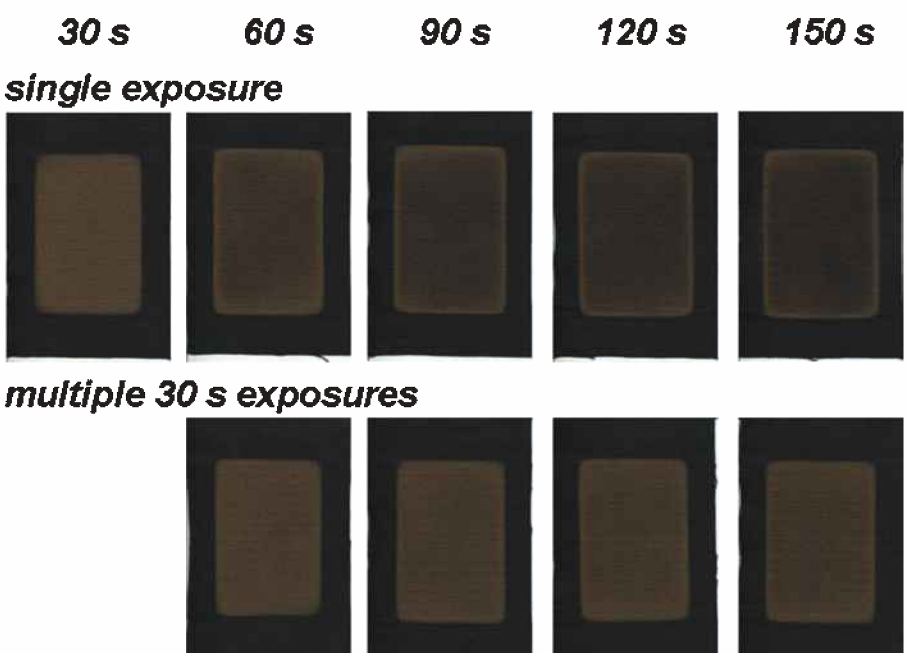

References

[1] Rezazadeh, M., and Torvi, D. A., "Assessment of Factors Affecting the Continuing Performance of Firefighters' Protective Clothing: A Literature Review," *Fire Technol.*, Vol. 47, 2011, pp. 565–599.

[2] NFPA 1851, 2008, "Standard on Selection, Care, and Maintenance of Structural Firefighting Protective Ensembles," National Fire Protection Association (NFPA), Quincy, MA.

[3] *User Instruction, Safety and Training Guide*, Lion Apparel, Dayton, OH, 2008.

[4] Austin, C. C., Dussault, G., and Ecobichon, D. J., "Municipal Firefighter Exposure Groups, Time Spent at Fires and Use of Self-contained-breathing-apparatus," *Am. J. Ind. Med.*, Vol. 40, 2001, pp. 683–692.

[5] NFPA 1971, 2007, "Standard on Protective Ensemble of Structural Firefighting," National Fire Protection Association (NFPA), Quincy, MA.

[6] Shull, P. J., "Introduction to NDE," *Nondestructive Evaluation: Theory, Techniques, and Applications*, Marcel Dekker, New York, 2002, pp. 1–15.

[7] Galiotis, C., "Raman Optomechanical Studies on Fibres, Composites and Fibre-matrix Interfaces," *Phase Interaction in Composite Materials*, Omega Scientific, Wallingford, UK, 1992, pp. 173–184.

[8] Washer, G., Brooks, T., and Saulsberry, R., "Characterization of Kevlar Using Raman Spectroscopy," *J. Mater. Civ. Eng.*, Vol. 21, 2009, pp. 226–234.

[9] Thorpe, P. A., and Torvi, D. A., "Development of Non-destructive Test Methods for Assessing Effects of Thermal Exposures on Fire Fighters' Turnout Gear," *J. ASTM Int.*, Vol. 1, 2004, JAI12119.

[10] Bray, A. V., and Stull, J. O., "A Non-destructive Inspection Method to Determine Fatigue in Chemical Protective Suit and Shelter Materials," *Performance of Protective Clothing*, ASTM STP 1237, Vol. 5, J. S. Johnson and S. Z. Mansdorf, Eds. ASTM International, West Conshohocken, PA, 1996, p. 281.

[11] Gralewicz, G., and Wiecek, B., "Active Thermography in Qualitative Evaluation of Protective Materials," *International Journal of Occupational Safety and Ergonomics*, Vol. 15, 2009, pp. 363–371.

[12] Klein, G. A., *Industrial Color Physics*, Springer, New York, 2010 , p. 192.

[13] Iyer, R. V., and Vijayan, K., "Identification of a New Parameter, Δt (T), Controlling the Thermally Induced Effects on Kevlar 49 Fibers," *Curr. Sci.*, Vol. 75, 1998, pp. 946–951.

[14] Rezazadeh, M. (unpublished), "Developing Non-destructive Techniques to Determine Retirement Age of Firefighters' Protective

Clothing," Ph.D. dissertation, University of Saskatchewan, Saskatoon, SK, Canada.

[15] Veghte, J. H., *Fire Fighter's Protective Clothing: Design Criteria*, 2nd ed., Lion Apparel, Dayton, OH, 1988.

[16] ASTM Standard F2700, 2008, "Standard Test Method for Unsteady-State Heat Transfer Evaluation of Flame Resistant Materials for Clothing with Continuous Heating," ASTM International, West Conshohocken, PA, DOI: 10.1520/F2700-08, www.astm.org.

[17] ASTM Standard F1939, 2008, "Standard Test Method for Radiant Heat Resistance of Flame Resistant Clothing Materials with Continuous Heating," ASTM International, West Conshohocken, PA, DOI: 10.1520/F1939-08, www.astm.org.

[18] ASTM Standard D5034, 2009, "Standard Test Method for Breaking Strength and Elongation of Textile Fabrics (Grab Test)," ASTM International, West Conshohocken, PA, DOI: 10.1520/D5034-09, www.astm.org.

[19] Fortner, B. and Meyer, T., *Number by Colors: A Guide to Using Color to Understand Technical Data*, Telos, New York, 1997, p. 266.

Performance of Protective Clothing and Equipment: Emerging Issues and Technologies
STP 1544, 2012
Available online at www.astm.org
DOI:10.1520/STP104062

Douglas L. MacTaggart,[1] *Sherry O. Farwell,*[1]
Zhongtao Cai,[1] *and Pauline Smith*[2]

Dual-mode Analytical Permeation System for Precise Evaluation of Porous and Nonporous Chemical Protective Materials

REFERENCE: MacTaggart, Douglas L., Farwell, Sherry O., Cai, Zhongtao, and Smith, Pauline, "Dual-mode Analytical Permeation System for Precise Evaluation of Porous and Nonporous Chemical Protective Materials," *Performance of Protective Clothing and Equipment: Emerging Issues and Technologies* on June 16–17, 2011 in Anaheim, CA; STP 1544, Angie M. Shepherd, Editor, pp. 227–246, doi:10.1520/STP104062, ASTM International, West Conshohocken, PA 2012.

ABSTRACT: The reliable determination of the permeation characteristics of chemical protective materials and material systems is vital for the development and assessment of effective personal protective clothing and equipment. ASTM F739 describes the necessary capabilities for rigorous testing of the permeation characteristics of protective materials. Currently available technologies are limited in their ability to test chemical protective materials for permeability to certain classes of hazardous substances such as toxic industrial chemicals, chemical warfare agents (CWAs), and CWA simulants. In an effort to overcome these limitations, a dual-mode Compact Integrated Analytical Swatch Testing System (C-IASTS) has been developed that combines an advanced test cell design with rigorous temperature, flow, and pressure control. The automated, dual-mode, five test cell instrument allows both convective (dynamic) and static tests of porous and nonporous chemical protective materials in a manner that is compliant with the requirements of ASTM F739. Performance characterization of the new dual-mode C-IASTS demonstrated sufficient detectability, measurement precision, and time resolution to allow the determination of breakthrough time, steady state and maximum permeation

Manuscript received May 28, 2011; accepted for publication March 29, 2012; published online August, 2012.
[1]EMCC Lab, LLC, 7103 Peaceful Pines Rd., Black Hawk, SD 57718.
[2]U.S. Army Research Laboratory, Materials Application Branch, Aberdeen Proving Ground, MD 21005.

rates, and cumulative permeation and an ability to produce a well-defined permeation curve. Current development and testing has been directed toward CWA simulants and military protective material systems, as well as commercial polymers, textiles, and other chemical selective barriers.

KEYWORDS: permeation testing, chemical protective clothing, personal protection, swatch test equipment, chemical warfare agent simulant

Introduction

The availability and use of testing methods with analytical features and performance specifications that either meet or exceed the requirements for a specific application are fundamental to the acquisition of reliable measurement-based information [1]. This analytical prerequisite is accentuated when considering a test methodology designed for the evaluation and selection of chemical protective materials (CPMs) [2,3]. Currently, the most commonly used standard methods for permeation and penetration testing of protective clothing materials are ASTM F739-07 [4], ASTM F1383-07 [5], BS EN 374-3 [6], ISO 6529 [7], and TOP 8-2-501 [8]. Data from these test methods for CPMs are often employed to link the measured barrier properties of tested material samples to a prediction of a material's protective effectiveness for toxic compounds, e.g., chemical warfare agents (CWAs), toxic industrial chemicals, and other hazardous materials.

Key analytical attributes for CPM test methods are limits of detection, precision (both reproducibility and repeatability), data acquisition frequency and time resolution, ruggedness, minimal analyte carryover effects between samples, operational safety, compatibility with both liquid and gas challenge chemicals, calibration efficiency and stability, and the capability for the evaluation of both porous (air-penetrable) and nonporous (air-impenetrable) materials. Central to the performance and functionality of analytical systems for CPMs is the design of the test cell. This mechanical cell assembly typically seals the test material securely between two chambers: one chamber functions to introduce the chemical challenge agent, and the other chamber is sampled and analyzed for challenge agent that permeates through the sample material as a function of testing time. Engineering, measurement and certification center (EMCC) Lab scientists have recently described the performance attributes and corresponding design criteria for permeation test cells and instrument control [9]. These combined analytical and test cell specifications have been incorporated in the development and characterization of a novel Integrated Analytical Swatch Testing System (IASTS) [10] and an advanced Compact IASTS (C-IASTS) [11]. The C-IASTS offers an improved test cell design, a smaller test-cell oven, an optimized flow path and flow control system, an internal permeation-based calibration cell, flexible event control and detection functions, and a significant reduction in system size, but it is designed primarily for static mode testing.

This paper summarizes the development and initial performance features of EMCC Lab's next generation instrument, a dual-mode C-IASTS with a demonstrated capability for the reliable evaluation of both nonporous and porous swatch materials in terms of their barrier properties when exposed to either liquid or vapor challenge agents. The experiments described here were conducted in order to determine the performance characteristics of the dual-mode C-IASTS for static mode permeation testing of nonporous materials and convective (also referred to as dynamic) mode testing of porous materials.

Experimental

Dual-mode C-IASTS Design and Construction

The dual-mode C-IASTS was based on research and development work using earlier permeation test instruments designed and constructed by EMCC Lab scientists. These earlier instruments were tested using a variety of materials, including nylon, different fluoropolymers, perfluorosulfonic acid fluoropolymers, sulfonated triblock copolymers, neoprene, butyl rubber, and various porous composite fabrics [9–11]. The earlier instruments were designed to meet the requirements of standard test methods [4–8] and to incorporate potential improvements. In particular, published research on standard test methods and equipment points out the importance of the permeation test cell design and of the associated flow geometry and temperature characteristics [12–19]. Also important is the analytical system connected to the output of the permeation test system. Several different analytical approaches have been used for permeation testing, including gas-phase infrared detection [20], liquid and ion chromatography [21], photoionization detection [14], and a variety of methods for combining gas chromatography with flame ionization (GC/FID) and flame photometric detectors [17,19,22].

The earlier IASTS and C-IASTS instruments incorporated a number of basic features that enabled the reliable testing of protective materials, including the following, all of which are included in the current dual-mode C-IASTS:

1. the optimization of multiple test cells for static mode operation;
2. test cell and internal instrument temperature control to 32.0°C ± 0.1°C;
3. precise instrument pressure control;
4. sweep gas air flow design and control (40 SCCM to each test cell [SCCM denotes cubic centimeters per minute at standard temperature and pressure]), including temperature (32.0°C ± 0.1°C) and humidity (0 % to 80 % relative humidity [RH]) of air flow;
5. a thermostated oven (105.0°C ± 0.1°C) housing the cell selection valve and gas sample valve;
6. programmed control of valve switching, collection loop heating, and detector start/stop events;
7. sensitive flame ionization detector (FID)-based detection, including a thermal preconcentration system that includes a heated capillary transfer

line to sweep helium at 40 SCCM through the preconcentration loop and directly into the FID (no chromatography is involved; the GC oven serves only to heat the transfer line before it reaches the FID);
8. quantitative analysis facilitated by a gravimetrically calibrated on-line standard permeation cell that allows system calibration including the flow paths from the cell selection valve and preconcentration loop to the FID; and
9. the ability to use new and existing challenge agent application methods.

Details of these instruments, including block and engineering diagrams, are available in earlier publications [9–11]. Also, this earlier work summarizes the results of experiments comparing C-IASTS [9–11] methodology with U.S. Army Aerosol, Vapor and Liquid Assessment Group and TOP 8-2-501 methodology [8].

The current dual-mode C-IASTS is depicted in Fig. 1. On the left side of the picture is the thermostated (32.0°C ± 0.1°C) flow and humidity control module. In the center is the thermostated permeation test cell module, with the Neslab CC-100 immersion cooler, which cools the preconcentration loop, visible underneath it. On the right is the Agilent 6890N GC/FID module. Figure 2 depicts the internal components of the permeation cell oven. The top of the thermostated copper block can be seen underlying the five aluminum test cells,

FIG. 1—*Picture of the dual-mode C-IASTS modules. From left to right are the thermostated flow and humidity control module, the thermostated permeation test cell module, and the GC/FID module, with the chiller unit for the preconcentrator visible underneath the central bench. As a scale reference, the length of the permeation test cell module is 66 cm.*

FIG. 2—*Internal picture of the dual-mode C-IASTS permeation test cell oven components, including the five aluminum test cells, aluminum blocks housing the vapor saturation vials, and standard permeation cell. As a scale reference, the length of the permeation test cell module is 66 cm.*

three aluminum blocks housing the vapor saturation vials, and standard permeation cell (aluminum circular device at the right-most edge). External controllers and gauges are mounted on the front panel below the oven lid to display system and vent pressures, cell selection and sample valve statuses, temperature of the copper block and attached test cells, temperature of the oven, valve oven temperature, and sample collection loop temperature. A close-up interior view of the dual-mode C-IASTS permeation oven compartment is depicted in Fig. 3, showing an opened test cell without a swatch sample. The open volume in the cell top allows incoming cell sweep airflow to spread out over the entire surface area of the test swatch when used in the convective mode. The small swept volume in the cell bottom (approximately 4 ml) underneath the ledge that holds the test swatch is also visible.

The dual-mode C-IASTS was designed and constructed to include the following enhancements:

1. Further optimization of the multiple test cell design for both convective and static mode operation. Both modes are varieties of the commonly used open collection flow path configuration. The difference between the two modes is illustrated in Fig. 4. The left-hand panel in Fig. 4 depicts the static mode, in which the cell sweep air enters the bottom of the cell, efficiently sweeps the area underneath the swatch (permeate side), and passes out of the cell. The convective mode is depicted in the right-hand panel, in which the cell sweep air enters the top of the cell,

FIG. 3—*Close-up view of the dual-mode C-IASTS permeation oven interior with an opened test cell. As a scale reference, the width of each test cell is 6.6 cm.*

passes through the porous or air-penetrable swatch, and exits through the bottom of the cell.

2. Improved flow path geometries as determined from detailed computational flow simulations [9].
3. Increased passivation of flow components.
4. Additional instrument pressure control via a digital pressure controller (Cole-Parmer Instrument Co. #68027-78) placed at the system vent.
5. Development of the saturated vapor challenge method.

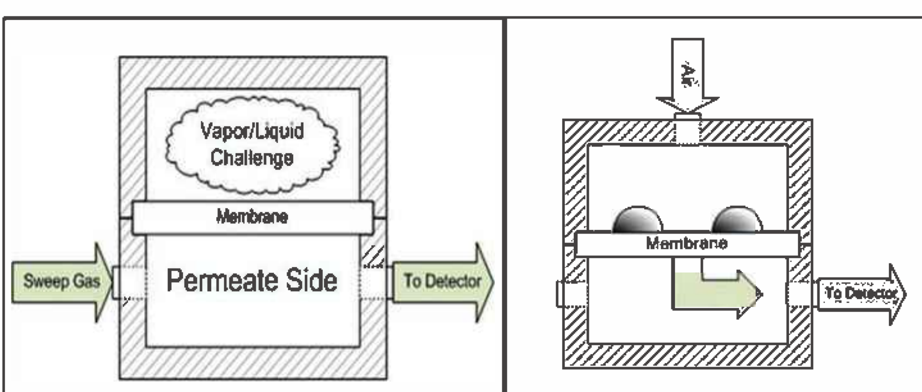

FIG. 4—*Block diagrams of static (left) and convective (right) test cell configurations.*

The dual-mode test cells are composed of the same bottom "permeate" part as the previous static mode test cells, with a newly designed top "challenge" part to accommodate convective mode testing. The height of the new tops is 0.9 in. (2.3 cm), as opposed to the previous 0.4 in. (1.0 cm) height, allowing for a homogeneous distribution of the sweep flow before it contacts the top side of the swatch material to be tested. Also, the height of the test cell oven was increased in order to allow connection of sweep gas flow (with or without the use of in-line vapor saturation vials) to the cell top. The design of these test cells was based on the optimization of flow dynamics from computational modeling performed at EMCC Lab (Fluent 6.3.2, Ansys, Inc.) [9].

The dual-mode C-IASTS is specifically designed and optimized for gas-phase testing, but it can also be used with bulk and droplet liquid challenge methods as detailed in earlier publications [9–11]. The current work focused on the use of methyl salicylate (MeS) as the challenge chemical because of the already developed and calibrated standard permeation cells charged with MeS and EMCC Lab's ongoing military material test contracts, which specify MeS as a simulant for certain CWAs. The current FID-based analytical system would work very well with a wide variety of organic challenge chemicals, and the system is also capable of being interfaced with other gas detection systems.

The C-IASTS accommodates 2 in. diameter swatch samples of various thicknesses. The multiple test cell design allows flexibility in carrying out permeation experiments. For maximum time resolution, a single test cell can be employed. The typical sample collection period is 0.5 min with the preconcentration loop held at ca. – 80°C, followed by rapid resistive heating of the loop to ca. 125°C. The preconcentration system serves to optimize peak size and shape, and thus analyte detectability. Accounting for the time required in order to cool the loop back down and for the desorbed sample to reach the FID, the typical total analytical cycle is 2 min. For concurrent replication in which the maximum time resolution is not needed, multiple test cells can be employed to increase the time efficiency of the experimental testing process.

Test Materials and Challenge Methods

One porous and two nonporous materials were tested in order to provide an initial assessment of the performance characteristics of the dual-mode C-IASTS. Static mode characterization was performed through permeation tests on nonporous neoprene and perfluoroalkoxy (PFA) fluoropolymer swatch materials. The neoprene material (Grainger Industrial Supply #2UPF3) used in these tests had a nominal thickness of 1/64 in. (0.397 mm), which is similar to the 0.44 mm average thickness neoprene used in the interlaboratory evaluation for ASTM F739-07 [4]. Several different neoprene formulations are available commercially. The choice of material for this study was based on the highest tensile strength neoprene product available from Grainger. The exact formulations of this and related materials were not available. The actual thicknesses of the swatches were measured with a Mitutoyo dial thickness gauge (#7326) that had a resolution of 0.0001 in. (0.00254 mm). The PFA material (DuPont PFA-200LP) had a measured mean thickness of 0.0022 in. (0.056 mm). Individual swatch thickness measurements were not obtained for the PFA experiments.

Convective mode characterization was performed through permeation tests on 2 in. swatch samples cut from semipermeable Lanx chemical protective undergarment (CPU) material (Lanx Type I activated carbon CPU drawer #CPU-D-48, Lanx Fabric Systems). The thickness of this breathable composite fabric exceeded the measurement range of the dial thickness gauge. Using a dial caliper with a 0.01 in. (0.254 mm) resolution (General #142), its thickness was measured as approximately 0.07 in. (1.8 mm). This measurement was an approximation due to the surface roughness and flexibility of the material. A microporous polytetrafluoroethylene (PTFE) membrane was placed on top of each of the nonporous and porous swatches in this study. The purpose of the PTFE membranes was to allow only vapor phase challenge to contact the top of the swatch samples. The PTFE membranes (Savillex #1150) had a pore size of 20 to 30 μm. A single o-ring for sealing the two halves of each test cell was placed on top of each microporous PTFE membrane.

MeS challenge for the static mode experiments was supplied by a porous polyethylene (PE) disk mounted in the top half of each test cell. The PE disks were cut from coarse grade porous fritware (Bel-Art Products, 1/16 in. thickness). For the static experiments, using a Microliter syringe (Hamilton Co. #710), 100 to 200 μl of MeS (Fisher Scientific #O3695-500, reagent grade, assay 99 % minimum MeS) was spread out across the exposed surface of the PE disk in droplets once the disk was mounted in the test cell top.

The convective mode challenge method utilized vapor saturation vials constructed from amber glass vials approximately 30 mm in diameter by 80 mm in height with a septum and screwcap seal. Approximately 10 mm of liquid MeS was placed in the bottom of each vial. The vials were subjected to the C-IASTS oven temperature of 32.0°C after being placed in aluminum blocks thermally connected to the thermostated copper block underlying the test cells. Inlet and outlet fittings for the vapor saturation vials consisted of 1/16 in. stainless steel Swagelok unions connected to short lengths of passivated stainless steel capillary tubing (Restek Corp.) that were plumbed through the vial septum. These vials placed within the aluminum blocks, with fittings on top of the vials, can be seen interspersed with the test cells in Figs. 2 and 3. The sweep air flow for each test cell was connected to the inlet fitting of the individual vapor saturation vial for each cell. This air flow of 40 SCCM picked up MeS vapor from the vial headspace and transported the MeS vapor through the vial outlet fitting to the top inlet fitting of the test cell. In theory, as long as there is excess MeS liquid in the vial, the constant vial temperature and sweep air flow rate will provide a constant mass transport rate of gaseous MeS to the test cells. The saturation vials were weighed before and after each experiment to enable the calculation of the vapor mass flow rate. In this study, the cell sweep air was dry (very near 0 % RH from the Aadco 737 Pure Air Generator) so as to not interfere with the gravimetric calibration of the vapor mass flow rates. However, controlled humidity levels could easily be achieved by decreasing the cell sweep flow before the vials and adding a known flow of humidified air between the vials and the test cells to make up the normal 40 SCCM. The current bank of ten mass flow controllers inside the flow/humidity control module of the C-IASTS provides the capability to do this for up to four test cells within an experiment.

Results and Discussion

Static Mode Neoprene Experiment

The neoprene experiment was designed so as to provide triplicate permeation data concurrently within a single test run. With the inclusion of a blank swatch (neoprene swatch and PTFE cover membrane with no challenge agent added), this design involved the use of four swatches mounted in individual C-IASTS test cells. For the neoprene experiment, 100 μl of MeS were charged on the PE disk in each of the first three cell tops as described above.

The triplicate neoprene experiment was conducted with 40 SCCM cell sweep air flows for the four active test cells, all humidified to approximately 80 % RH. The FID peak areas for each 0.5 min sample collection period in the experiment were converted to permeation rates using the calibrated standard permeation cell described above and the Cell 4 blank swatch data. To account for the remainder of the time in each 2 min analytical cycle, point-to-point interpolation was employed. This procedure enabled the calculation of cumulative permeation amounts in addition to breakthrough times and maximum permeation rates.

The resultant permeation rate profile for this experiment is shown in Fig. 5. Due to the very short time resolution, individual data points are not shown in this 20 h plot. The data are plotted with lines connecting point to point; i.e., no smoothing was employed. The excellent sensitivity and detectability of the system are illustrated in Fig. 6, in which the data from Fig. 5 are scaled to zoom in on the region around the standardized breakthrough time (SBT) defined by ASTM F739-07 [4]. From these data, MeS breakthrough can be detected well before the SBT permeation rate of 0.1 μg/cm^2/min is reached. Together, Figs. 5 and 6 demonstrate the capability of the dual-mode C-IASTS for determining permeation curves with a high degree of precision and time resolution.

The SBT, maximum permeation rate (Max PR), and 16 h cumulative permeation (CP) values for the neoprene experiment are presented in Table 1, along

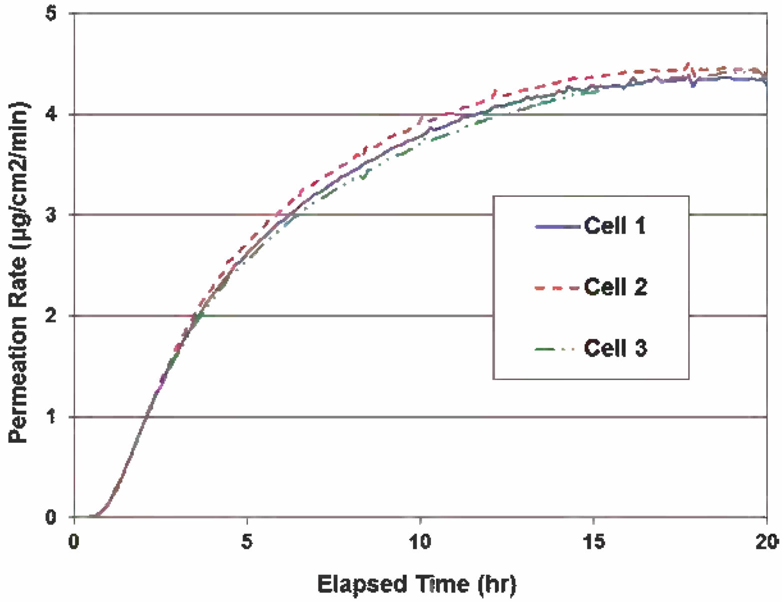

FIG. 5—*Static mode C-IASTS results for the concurrent triplicate test of nominal 1/64 in. neoprene swatches in a single experiment, demonstrating within day and between cell repeatability.*

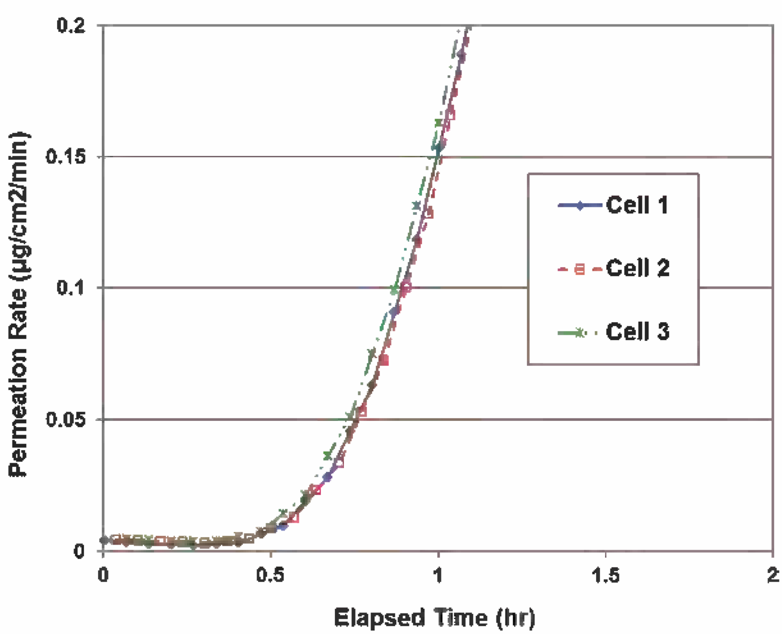

FIG. 6—*Figure 5 triplicate test results scaled to show the details of the time resolution, measurement precision, and sensitivity characteristics of the C-IASTS in the region of the standardized breakthrough time.*

TABLE 1—*Standardized breakthrough times (SBT), maximum permeation rates (Max PR), and cumulative permeation (CP) for the static mode triplicate neoprene experiment, along with summary statistics.*

C-IASTS Cell	Measured Neoprene Thickness, mm	SBT, min	Max PR, μg/cm^2/min	CP at 16 h, μg
Cell 1	0.368	53.59	4.352	28 202
Cell 2	0.354	54.23	4.443	29 129
Cell 3	0.362	52.33	4.431	27 799
Mean	0.361	53.38	4.409	28 377
Standard deviation	0.009	0.96	0.049	682
Relative standard deviation, %	2.35	1.81	1.12	2.40

with swatch thickness measurements and summary statistics in the form of means, standard deviations, and relative standard deviations (RSDs). The Max PR metric was used instead of the steady-state permeation rate (SSPR) because, as shown in Fig. 5, a true SSPR was not achieved in this experiment. The results summarized in Table 1 show that the precision as measured by the RSD for the three permeation curves within a single run was in the range of 1 % to 2 % for the SBT and Max PR. The RSD of CP values at 16 h was slightly over 2 %.

Static Mode Perfluoroalkoxy Experiments

In order to characterize the static mode behavior of the dual-mode C-IASTS over an extended time period, a set of experiments using PFA swatches was conducted. Four duplicate swatch experiments were interspersed with EMCC Lab's military contract testing over an 18 month timeframe. For each of these four experiments, either four or five of the C-IASTS test cells were employed. Two cells in each experiment were loaded with PFA swatches and microporous PTFE membranes in the bottom halves of the test cells as described above. The MeS challenge amount loaded onto the porous PE disks was 200 μl for the PFA experiments. In contrast to the neoprene experiment, the two or three blank test cells employed were not loaded with either PFA test swatches or PTFE membranes. For the blanks, the test cells were completely empty. The cell sweep air flow was humidified to approximately 80 % RH as for the neoprene experiments. Quantitation to obtain permeation rates was conducted as described above.

The resultant permeation rate profiles from the PFA experiments are plotted in Fig. 7. As in Fig. 5, individual data points are not shown. Also, in order to show profiles for all four experiments in one plot, data for the two replicates within each experiment were averaged. Figure 7 shows that for PFA, the Max PR values achieved are much less than the SBT permeation rate of 0.1 μg/cm^2/min.

Nevertheless, the sensitivity and time resolution characteristics of the dual-mode C-IASTS still allow one to obtain well-defined PFA permeation curves.

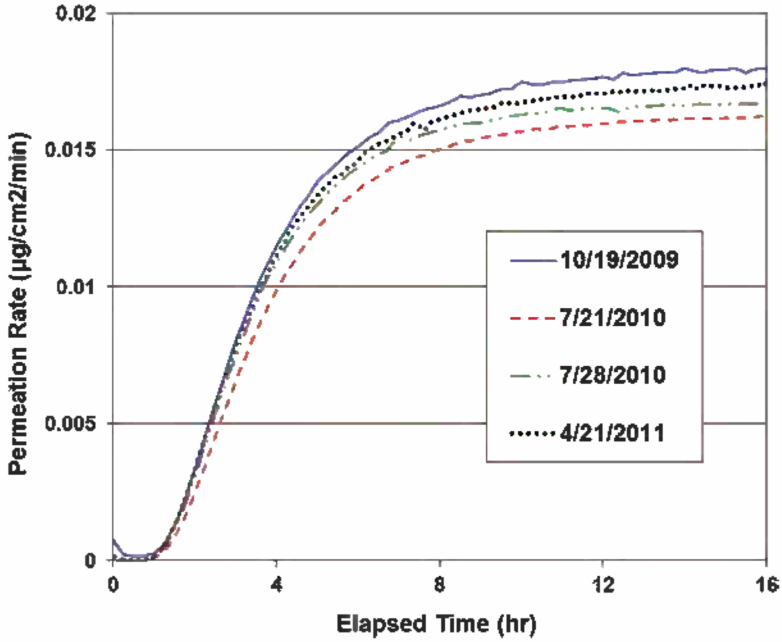

FIG. 7—*Static mode C-IASTS results showing average permeation curves for each of four duplicate tests of PFA-200LP swatches over an 18 month time period, demonstrating reproducibility over time.*

Nonstandardized breakthrough times (BTs) for this set of experiments were determined by means of a linear extrapolation method described by Rivin et al. [17,19]. In this method, the initial linear rise of a permeation curve is extrapolated back to the *x*-axis (time) intercept. This method is illustrated in Fig. 8, which shows the individual replicate data from the Apr. 21, 2011, experiment scaled to the region of the initial linear rise. Permeation rates from approximately 0.0015 to 0.007 μg/cm^2/min were regressed against time for each day/cell combination, and the regression lines were extrapolated back to the time axis.

BT results from this method, as well as Max PR and 16 h CP results, are presented in Table 2, along with summary statistics for each of the four experiments and for the set of experiments as a whole. The tabulated results exhibit within day precisions of typically 1 % to 3 % for BT, Max PR, and CP, with precisions over the 18 month time period of 3 % to 5 %. The permeation rates corresponding to the calculated BT values are in the range of 0.0005–0.001 μg/cm^2/min, which is between 0.5 % and 1 % of the ASTM F739-07 SBT permeation rate. These results demonstrate the short-term precision (repeatability), long-term precision (reproducibility), sensitivity, and detectability of the dual-mode C-IASTS when operated in the static mode.

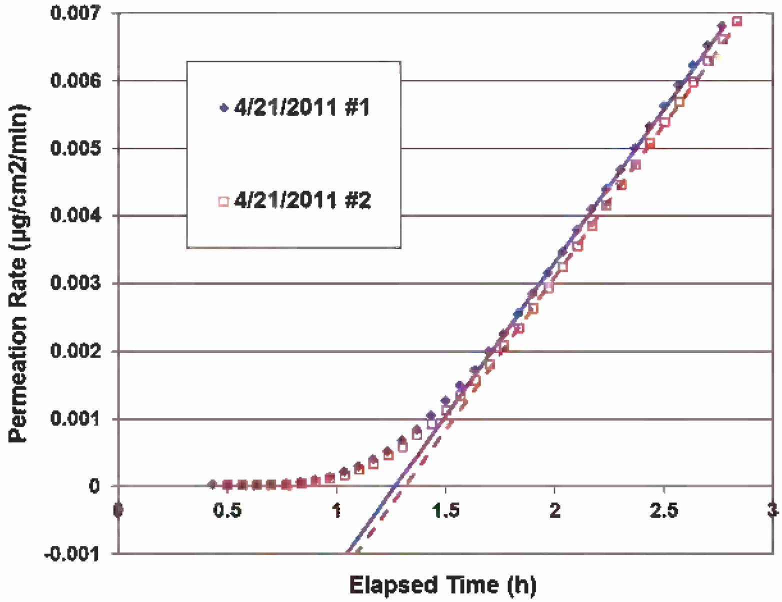

FIG. 8—*Detail showing extrapolation of the initial linear regions of the individual Apr. 21, 2011, permeation curves in order to calculate breakthrough times.*

A detection limit estimate in terms of the permeation rate of 0.00048 μg/cm^2/min for MeS was calculated from the variability of the combined baselines of the PFA experiments using the common three-sigma approach [23,24]. This permeation rate detection limit compares very well to the permeation rate range corresponding to the BT noted above, which employs a linear regression approach. This comparative result agrees with previous results for the calculation of detection limits when best practices are employed [25].

TABLE 2—*Breakthrough times (BT), maximum permeation rates (Max PR), and cumulative permeation (CP) for the set of static mode PFA experiments conducted over a timeframe of 18 months.*

	BT, min			Max PR, μg/cm^2/min			CP at 16 h, μg		
Date	Mean	SD	RSD, %	Mean	SD	RSD, %	Mean	SD	RSD, %
Oct. 19, 2009	78.15	0.69	0.89	0.0182	0.0005	2.82	129.3	2.7	2.09
July 21, 2010	83.84	1.55	1.84	0.0163	0.0003	2.00	116.3	1.8	1.57
July 28, 2010	80.05	2.02	2.53	0.0168	0.0008	4.55	121.3	7.3	6.02
Apr. 21, 2011	77.37	1.88	2.42	0.0175	0.0005	2.72	125.0	2.2	1.79
Mean	79.85			0.0172			123.0		
SD	2.89			0.0008			5.6		
RSD, %	3.61			4.78			4.52		

Notes: SD, standard deviation; RSD, relative standard deviation.

Convective Mode Experiments

Initial convective mode testing of the dual-mode C-IASTS was accomplished by means of a single cell experiment (110318) followed 1 week later by a multiple cell experiment (110325). The single cell experiment employed only one test cell. For the multiple cell experiment, composite fabric CPU swatches with microporous PTFE cover membranes were placed in each of the five test cells, including the blank. Cell 5 was used as a blank, i.e., its sweep air was directly connected to the top of the cell without connection to a saturation vial. As noted above, the cell sweep air flow was dry (very near 0 % RH) for the convective mode experiments. The individual sweep flow for each test cell was connected to a saturation vapor vial (except for the one blank cell in the multiple cell experiment) and then connected to each test cell's top fitting.

Permeation curves for the multiple cell experiment are shown in Fig. 9, and a comparison of the permeation curve for the single cell experiment with the mean permeation curve for the multiple cell experiment is shown in Fig. 10. As in Figs. 5 and 7, individual data points are not shown, and the permeation curves are not smoothed. These plots demonstrate that the permeation curves for these porous materials approach steady-state very gradually. After an elapsed time of 44 h, the permeation rates for these materials were on average 74 % of the vapor production rates (78 to 83 μg/min MeS), which were

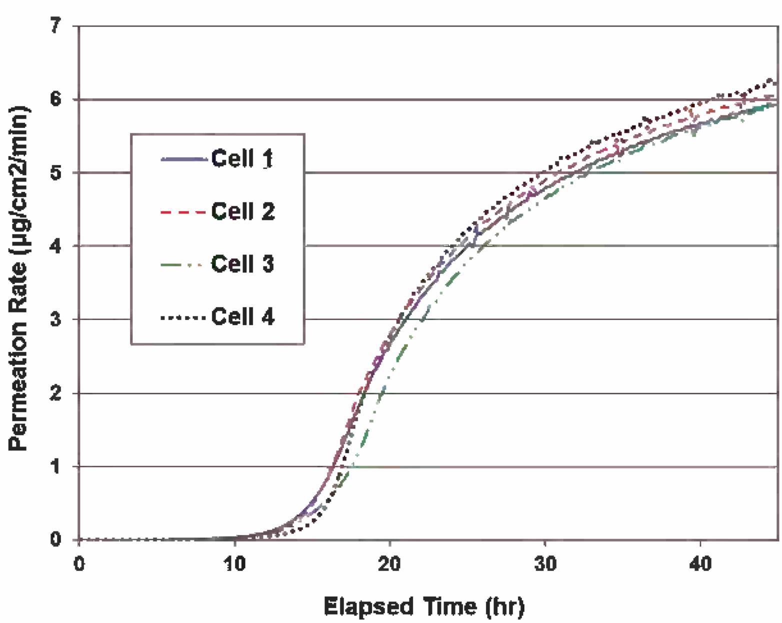

FIG. 9—*Convective mode C-IASTS results for the concurrent quadruplicate test of swatches from composite fabric CPU material in a single experiment, demonstrating within day and between cell repeatability.*

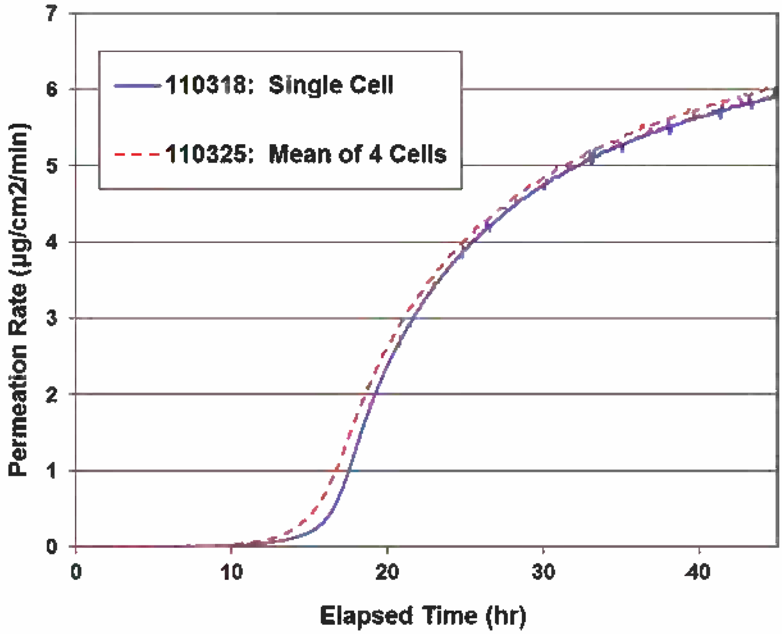

FIG. 10—*Comparison of convective mode C-IASTS results from single-cell and quadruplicate-cell tests of composite fabric CPU material, demonstrating reproducibility over a 1 week time period.*

calculated for the saturation vials based on the weights of the vials before and after the experiments. A mass balance can be calculated from the cumulative permeation amounts in conjunction with the vapor production rates. For the four replicates, the cumulative permeated amount over 44 h was on average 35 % of the total MeS vapor produced.

Table 3 presents the SBT, Max PR, and 44 h CP values for the two convective mode experiments, along with summary comparative statistics intended to provide a measure of the repeatability and reproducibility of the C-IASTS

TABLE 3—*Standardized breakthrough times (SBT), maximum permeation rates (Max PR), and cumulative permeation (CP) for convective mode CPU material experiments.*

	SBT, min			Max PR, μg/cm^2/min			CP at 44 h, μg		
Date	Mean	SD	RSD, %	Mean	SD	RSD, %	Mean	SD	RSD, %
Mar. 18, 2011	821.2	na	na	5.889	na	na	71 407	na	na
Mar. 25, 2011	749.4	41.3	2.42	6.021	0.146	2.43	74 278	2750	3.70
Mean	785.3			5.955			72 842		
SD	50.8			0.094			2030		
RSD, %	6.46			1.57			2.79		

Notes: SD, standard deviation; RSD, relative standard deviation; na, not applicable.

when used in this mode. The within day SBT, Max PR, and CP variabilities and the between-experiment Max PR and CP variabilities are well within the range of 1 % to 5 % observed for the static mode experiments, whereas the between day SBT variability of 6 % is slightly higher than for the static mode experiments. This small increase might be explained by the more heterogeneous nature of the CPU composite fabric material relative to the neoprene and PFA polymeric materials. Although neoprene products are known to be available in several different chemical formulations, material from a single lot or sheet should be relatively homogenous.

System Limitations and Potential Future Enhancements

Permeation Test System—Although the dual-mode C-IASTS is the fourth generation of this novel instrumentation developed by EMCC Lab, further design refinements might benefit specific applications. These possible enhancements include (a) additional electronics for the acquisition and storage of real-time data on all system temperatures, pressures, and RH values; (b) improved humidity generation techniques that allow a greater range, a more efficient transition, better integration, and automated feedback control of the RH setting; (c) dedicated software for more rapid and efficient transformation of the real-time detection data into selectable permeation formats; (d) test cells that are even easier to open and close yet which still completely seal after recurring use; (e) test cells optimized for use with swatch samples of several common sizes; and (f) the construction of different compact detection modules that can be integrated into the design of a future C-IASTS module and which can be selected by the user as a function of analyte detection characteristics and/or requirements. As an approach to determine accuracy, EMCC Lab is continuing to explore an independent method based on headspace analysis for comparison with the C-IASTS.

Detection Methodology—The dual-mode test cells were specifically designed and optimized for gas phase testing but are also capable of being used with bulk liquid and liquid droplet challenge methods. The tests in this study were conducted with MeS as the challenge agent. The current configuration with FID detection would also work well with a wide variety of volatile and nonvolatile organic chemical compounds. The current C-IASTS is also capable of interfacing with other commercially available gas chromatographic detectors to increase the range of applicable chemical agents or provide more specificity for certain compounds or compound classes. Many real-world protocols call for permeation testing under conditions of very high humidity (80 % RH and above), which can cause severe problems for many analyte-specific detector systems such as mass spectrometers. As one example, EMCC Lab is currently exploring proton transfer reaction mass spectrometry or the more recently available selected ion flow tube mass spectrometry as a potential continuous specific detection method for this application. These instruments are compatible with atmospheric pressure humid gas sample streams, as their inlet systems are at near-ambient pressures and their ionization schemes are based on H^+ transfer from water vapor continuously injected into their ionization sources [26,27]. The use of these instruments in an on-line configuration would potentially allow chemical speciation and the concomitant quantification of designated analytes in the output flow from the C-IASTS test cells.

Conclusions

The static and convective mode experimental results successfully demonstrate the performance characteristics of the dual-mode C-IASTS and its usefulness for the permeation testing of a variety of nonporous and porous materials under humid and dry conditions. Repeatability and reproducibility were measured based on the RSD within a day and over time periods of 1 week to 18 months and are typically in the range of 1 % to 5 %. A detection limit estimate in terms of a permeation rate of 0.00048 $\mu g/cm^2/min$ for MeS was calculated from the variability of the combined baselines of the PFA experiments in an 18 month timeframe. These performance characteristics were established with a time resolution of 2 min, demonstrating the capability of the dual-mode C-IASTS for measuring the permeation characteristics of materials with a high degree of precision, sensitivity, time resolution, and ease.

The instrumental details and experimental results demonstrate that the dual-mode C-IASTS is capable of performing permeation testing in conformance with ASTM F739-07 and other standard test methods. The instrument accommodates 2 in. diameter material swatches and controls the test cells and swatches at a defined temperature within $\pm 0.1°C$ throughout the duration of a test. The open-loop collection medium (test cell high purity sweep air) flow rate is precisely controlled at 40 SCCM, which is approximately ten swept collection area volumes per minute (ASTM F739-07 calls for at least five cell volumes per minute). The experimental results demonstrate that the system can easily produce reliable test metrics: SBT or BT based on the individual permeation characteristics of particular materials, SSPR (when achieved) or Max PR (when SSPR is not achieved), and CP. Also, the system produces well-resolved permeation curves for visual determination of the relative permeation characteristics of different materials. The gravimetrically calibrated on-line standard permeation test cell allows for convenient calibration of the entire system, and not just the detector.

In summary, the dual-mode C-IASTS has demonstrated substantial utility in the precise determination of the permeation characteristics of nonporous and porous materials using a variety of challenge introduction methods. The development and evaluation of this instrument and its predecessors have shown reliable application with CWA simulants and military protective material systems, as well as with commercial polymers and textiles. Thus, this novel technology has the performance characteristics and flexibility necessary for confident testing of a wide variety of CPMs and other chemical selective barriers. A U.S. patent application on this dual-mode C-IASTS technology has been filed [28].

Acknowledgments

This work was conducted in partnership with the South Dakota School of Mines & Technology with financial support from the U.S. Army Research Laboratory via Cooperative Agreement W911NF-08-2-0022. The writers appreciate the professional guidance of Dr. Gene A. Stark and the laboratory assistance of Mr. Gary O. Farwell.

References

[1] Ewing, G. W., *Analytical Instrumentation Handbook*, Marcel Dekker, New York, 1990, pp. 1–2.

[2] Forsberg, K. and Keith, L. H., *Chemical Protective Clothing Performance Index*, John Wiley & Sons, New York, 1999.

[3] Anna, D. H., *Chemical Protective Clothing*, American Industrial Hygiene Association Press, Fairfax, VA, 2003.

[4] ASTM F739-07, 2007, "Standard Test Method for Permeation of Liquids and Gases through Protective Clothing Materials Under Conditions of Continuous Contact," *Annual Book of ASTM Standards*, Vol. 11.03, ASTM International, West Conshohocken, PA.

[5] ASTM F1383-07, 2007, "Standard Test Method for Permeation of Liquids and Gases through Protective Clothing Materials Under Conditions of Intermittent Contact," *Annual Book of ASTM Standards*, Vol. 11.03, ASTM International, West Conshohocken, PA.

[6] BS EN 374-3:2003, 2003, "Protective Gloves against Chemicals and Micro-organisms. Determination of Resistance to Permeation by Chemicals," British Standards Institution, London.

[7] ISO 6529:2001, 2001, "Determination of Resistance of Protective Clothing Materials to Permeation by Liquids and Gases," International Organization for Standards, Geneva, Switzerland.

[8] Test Operations Procedure (TOP) 8-2-501, "Permeation and Penetration Testing of Air-permeable, Semipermeable, and Impermeable Materials With Chemical Agents or Simulants (Swatch Testing)," *AD-A322329*, U.S. Army Test and Evaluation Command, U.S. Army Dugway Proving Ground, UT, 2003.

[9] Verwolf, A., Farwell, S. O., Cai, Z., and Smith, P., "Performance-based Design of Permeation Test Cells for Reliable Evaluation of Chemical Protective Materials," *Polym. Test.*, Vol. 28, 2009, pp. 437–445.

[10] Farwell, S. O., Verwolf, A., Cai, Z., Smith, P., and Roy, W., "Design and Performance of an Integrated Analytical Swatch Testing System," *Instrum. Sci. Technol.*, Vol. 36, 2008, pp. 577–597.

[11] Verwolf, A., Farwell, S. O., Cai, Z., and Smith, P., "An Improved Compact Integrated Analytical Swatch Testing System," *Instrum. Sci. Technol.*, Vol. 38, 2010, pp. 220–233.

[12] Anna, D. H., Zellers, E. T., and Sulewski, R., "ASTM F739 Method for Testing the Permeation Resistance of Protective Clothing Materials: Critical Analysis With Proposed Changes in Procedure and Test-cell Design," *Am. Ind. Hyg. Assoc. J.*, Vol. 59, 1998, pp. 547–556.

[13] Schwope, A. D., Goydan, R., Reid, R. C., and Krishnamurthy, S., "State-of-the-art Review of Permeation Testing and the Interpretation of Its Results," *Am. Ind. Hyg. Assoc. J.*, Vol. 49, 1988, pp. 557–565.

[14] Bromwich, D., "The Validation of a Permeation Cell for Testing Chemical Protective Clothing," *Am. Ind. Hyg. Assoc. J.*, Vol. 59, 1998, pp. 842–851.

[15] Bromwich, D., 1999, "The Design of Permeation Cells for Testing Chemical Protective Clothing," Ph.D. dissertation, Griffith University, South Brisbane, Australia.

[16] Makela, E. A., Vainiotalo, S., and Peltonen, K., "Permeation of 70% Isopropyl Alcohol through Surgical Gloves: Comparison of the Standard Methods ASTM F739 and EN 374," *Ann. Occup. Hyg.*, Vol. 47, No. 4, 2003, pp. 305–312.

[17] Rivin, D., Lindsay, R. S., Shuely, W. J., and Rodriguez, A., "Liquid Permeation through Nonporous Barrier Materials," *J. Membr. Sci.*, Vol. 246, 2005, pp. 39–47.

[18] Chao, K., Lai, J., and Lin, H., "Comparison of Permeation Resistance of Protective Gloves to Organic Solvents With ISO, ASTM and EN Standard Methods," *Polym. Test.*, Vol. 26, No. 8, 2007, pp. 1090–1099.

[19] Rivin, D., Shuely, W. J., Palya, F., Lindsay, R. S., Rodriguez, A., and Bartram, P. W., 2008, "Estimating the Permeation Resistance of Nonporous Barrier Polymers to Sulfur Mustard (HD) and Sarin (GB) Chemical Warfare Agents Using Liquid Simulants," *DHHS (NIOSH) Publication No. 2008-141*, Atlanta, GA.

[20] Nelson, G. O., Lum, B. Y., Carlson, G. J., Wong, C. M., and Johnson, J. S., "Glove Permeation by Organic Solvents," *Am. Ind. Hyg. Assoc. J.*, Vol. 42, 1981, pp. 217–225.

[21] Makela, E. A., Vainiotalo, S., and Peltonen, K., "The Permeability of Surgical Gloves to Seven Chemicals Commonly Used in Hospitals," *Ann. Occup. Hyg.*, Vol. 47, No. 4, 2003, pp. 313–323.

[22] Boopathi, M., Singh, B., and Vijayaraghavan, R., "A Review on NBC Body Protective Clothing," *The Open Textile Journal*, Vol. 1, 2008, pp. 1–8.

[23] Long, G. L. and Winefordner, J. D., "Limit of Detection: A Closer Look at the IUPAC Definition," *Anal. Chem.*, Vol. 55, 1983, pp. 712A–724A.

[24] American Chemical Society Committee on Environmental Improvement, "Principles of Environmental Analysis," *Anal. Chem.*, Vol. 55, 1983, pp. 2210–2218.

[25] Burdge, J. R., MacTaggart, D. L., and Farwell, S. O., "Realistic Detection Limits from Confidence Bands," *J. Chem. Educ.*, Vol. 76, 1999, pp. 434–439.

[26] Lindinger, W., Hansel, A., and Jordan, A., "On-line Monitoring of Volatile Organic Compounds at pptv Levels by Means of Proton-transfer-reaction Mass Spectrometry (PTR-MS): Medical Applications, Food Control and Environmental Research," *Int. J. Mass Spectrom. Ion Process.*, Vol. 173, 1998, pp. 191–241.

[27] Freeman, C. G. and McEwan, M. J., "Rapid Analysis of Trace Gases in Complex Mixtures Using Selected Ion Flow Tube-mass Spectrometry," *Aust. J. Chem.*, Vol. 55, 2002, pp. 491–494.

[28] S. O. Farwell, "Chemical Permeation Testing Instrument," U.S. patent pending 10,326,248 (June 2011).

Performance of Protective Clothing and Equipment: Emerging Issues and Technologies
STP 1544, 2012
Available online at www.astm.org
DOI:10.1520/STP104205

R. Bryan Ormond,[1] *Roger Barker,*[2] *Keith Beck,*[3]
Donald Thompson,[4] *and Shawn Deaton*[5]

Factors Influencing the Uptake Rate of Passive Adsorbent Dosimeters Used in the Man-in-Simulant-Test

REFERENCE: Ormond, R. Bryan, Barker, Roger, Beck, Keith, Thompson, Donald, and Deaton, Shawn, "Factors Influencing the Uptake Rate of Passive Adsorbent Dosimeters Used in the Man-in-Simulant-Test," *Performance of Protective Clothing and Equipment: Emerging Issues and Technologies* on April 16, 2011 in Anaheim, CA; STP 1544, Angie M. Shepherd, Editor, pp. 247–265, doi:10.1520/STP104205, ASTM International, West Conshohocken, PA 2012.

ABSTRACT: The passive adsorbent dosimeter (PAD) is a critical component in the man-in-simulant-test (MIST). It is the only approved device for use in determining the localized and systemic protection factors for chemical protective ensembles. In MIST evaluation protocols, PADs are placed on test subjects underneath the protective suit, and then the test subject is exposed to a known concentration of methyl salicylate (MeS), a warfare agent

Manuscript received July 13, 2011; accepted for publication February 27, 2012; published online September 2012.

[1]Doctoral Candidate, Center for Research on Textile Protection and Comfort, College of Textiles, North Carolina State Univ., 2401 Research Dr., Campus Box 8301, Raleigh, NC 27695-8301, e-mail: rbormond@ncsu.edu

[2]Professor and Director, Center for Research on Textile Protection and Comfort, College of Textiles, North Carolina State Univ., 2401 Research Dr., Campus Box 8301, Raleigh, NC 27695-8301, e-mail: roger_barker@ncsu.edu

[3]Professor, College of Textiles, North Carolina State Univ., 2401 Research Dr., Campus Box 8301, Raleigh, NC 27695-8301, e-mail: keith_beck@ncsu.edu

[4]Associate Director, Center for Research on Textile Protection and Comfort, College of Textiles, North Carolina State Univ., 2401 Research Dr., Campus Box 8301, Raleigh, NC 27695-8301, e-mail: dthomps1@tx.ncsu.edu

[5]Special Projects Director, Center for Research on Textile Protection and Comfort, College of Textiles, North Carolina State Univ., 2401 Research Dr., Campus Box 8301, Raleigh, NC 27695-8301, e-mail: asdeaton@ncsu.edu

simulant. The purpose of the PADs is to collect the MeS vapors that enter the suit at seams, closures, or interfaces between the protective suit and gloves, boots, or the breathing apparatus. Given this key role, it is imperative that the diffusive uptake rates associated with the PADs are characterized. It is equally important to fully understand the factors influencing these rates. This research investigates two different categories of influential factors: the variation in adsorption rates associated with the simulant concentration and exposure time, and the relation to the effect of the time and temperature of the PAD's storage prior to extraction and analysis. For the first study, PADs were exposed, in the full scale MIST Facility at North Carolina State University, to concentrations ranging from 15 to 100 mg/m^3 for exposure times ranging from 1 min to 2 h in duration. In the second study, the effect of the storage time prior to analysis was determined by exposing PADs at a set condition and varying the amount of time before the PADs were extracted. In order to assess the effects of storage temperature on the uptake rate, PADs were exposed and stored at temperatures ranging from below −30°C to 4°C. The findings of this research help identify and explain a possible source of differences that have been observed in MIST results at different testing sites. This work also provides a deeper understanding of the characteristics of the PADs themselves.

KEYWORDS: passive adsorbent dosimeters, PADs, man-in-simulant-test, MIST, chem-/bio-ensemble, methyl salicylate, uptake rate, simulant concentration, adhesive, ASTM F2588

Introduction and Background

In the mid-1990s, a task group of the U.S. Army Chemical and Biological Defense Command developed the man-in-simulant-test (MIST) to aid in the assessment of chemical protective ensembles [1]. During the development of the test, multiple questions had to be answered, such as the following:

- What chemical could safely be used to simulate chemical warfare agents that are locally acting vesicants (e.g., sulfur mustard or lewisite) and also systemically acting nerve agents (e.g., Sarin or VX)?
- What is the most appropriate method for collecting any simulant vapors that might enter the garment while it is being tested?
- At what uptake rate does human skin absorb the warfare agents and the simulant?

A technical assessment of the MIST program was conducted and published in 1997 [1], and the answers to many of the task group's questions can be found in that evaluation. The most appropriate simulant for sulfur mustard (HD) was found to be methyl salicylate (MeS), commonly known as oil of wintergreen [1]. The work conducted in order to determine whether MeS could adequately serve as a simulant for HD mainly focused on the rates at which both chemicals permeate fabrics. According to the assessment [1], MeS was shown to permeate fabrics about 30 % slower than HD. However, due to the impermeable nature of the fabrics being tested, the amount of the vapor that enters the suit by permeating the material is much less than the amount that breaches the interfaces in the suit (e.g., zippers and seams). Riviere et al. have also investigated the use of MeS as a simulant for HD by analyzing its percutaneous absorption through the use of an isolated perfuse porcine skin flap, and they found that it was indeed an adequate simulant [2]. The technical assessment determined that although MeS was a good simulant for HD, its physical properties were too different from those of VX or Sarin for it to be said that it would simulate the nerve agents as well as the vesicants [1]. However, MeS was chosen to represent both classes of chemicals in order to simplify the test, rather than developing different tests for the two different simulants.

One of the biggest issues facing the development of the test was the method of vapor collection. Small packages of an adsorbent material that can be adhered to the test subject, referred to as passive adsorbent dosimeters (PADs), work through the process of passive diffusion. Therefore, no artificial airflows are generated inside the protective garment during testing, as would be the case with an active sampling system that pulled air into the sampler via the use of a pump or vacuum. The passive diffusion process allows for a sampling method that is more consistent with the process of percutaneous absorption. The main parameter that needs to be defined in order to ensure that the PAD is consistent with the percutaneous absorption of HD is the uptake rate or sampling velocity.

Two studies conducted in the early 1940s [3,4] looked at the absorption rates of HD into human skin. The first study exposed skin to liquid HD, and the second focused on vapor exposures. In a report for the Joint Service Lightweight Integrated Suit Technology (JSLIST) program in 1995, Fedele and Nelson [5] used both of these studies to develop a reasonable approximation for the uptake rate of HD into human skin. Their study makes it clear that because the thickness and sensitivity of human skin varies across the body, and because the uptake rate can increase with increasing skin temperatures, an ideal scenario would be to have multiple PADs with different uptake rates for each of these different body regions [5]. The technical assessment states that the observed variation in skin uptake rates can range between 1.0 and 4.0 cm/min [1]. However, due to the complexity of developing and dealing with multiple samplers, Fedele and Nelson recommended that a single passive sampler should be used with an uptake rate of 2.0 cm/min, which corresponds closely with the observed uptake rate for the forearm [5].

The PAD design that is currently used is referred to as the Natick Sampler and was developed by the U.S. Army Natick Soldier Research, Development, and Engineering Center. The PAD, seen in Fig. 1, is constructed of a permeable high density polyethylene (HDPE) film that is heat sealed against an aluminum foil backing and has an adhesive that allows the PAD to be attached to the test subject. The pocket inside the PAD contains approximately 40 mg of a polymer resin based on 2,6-diphenyl-p-phenylene oxide that adsorbs the simulant molecules as they diffuse through the HDPE membrane [6]. Detailed specifications for each component of the PAD are stated in ASTM F2588 [6].

In 2010, an ASTM subcommittee was tasked with responding to issues surrounding the calculated uptake rates of the PADs. The main issue was that

FIG. 1—*Passive adsorbent dosimeter used in MIST protocol. Dimensions of active sampling surface area are 2.5 cm × 1.8 cm according to ASTM F2588.*

different MIST facilities were reporting a wide range of calculated uptake rates of the PADs. As previously stated, the PADs were designed to have an uptake rate of 2.0 cm/min, but laboratories were reporting values as low as 1.0 cm/min and as high as 3.5 cm/min. Many manufactured products inherently have some degree of variability from lot to lot, and the PADs used for MIST testing are no different. In fact, the testing community had previously voiced concern with the manufacturing processes because the PADs varied significantly in the amount of adsorbent that they contained. In an attempt to resolve these inconsistencies, the supplier of the Natick Sampler transferred the manufacturing of the PADs from ITW Devcon[6] in Massachusetts to M&C Specialties Co.[7] in Pennsylvania in the latter part of 2010. The "new" PADs (used for this study) do appear to be more uniform and contain the appropriate amount of adsorbent, but the other physical properties have not been investigated. With knowledge of these previous issues, the quality control for PAD manufacturing was a logical starting point for determining the source of the observed inconsistencies in the uptake rates.

When discussing the uptake rate of the PADs, there are two different values that must be considered. For clarity, the first value can be referred to as the *film uptake rate* (cm/min). This parameter refers to the diffusion across the HDPE membrane and is dependent upon the thickness (standard value of 0.025 mm [6]) and other properties of the film. The film uptake rate most closely relates to the sampling velocity or flux referred to in the percutaneous

[6] ITW Devcon, 30 Endicott St., Danvers, MA 01923.
[7] M&C Specialties Co., 90 James Way, Southampton, PA 18966.

absorption process described by Fedele and Nelson [5]. Therefore, in order to achieve the suggested value of 2.0 cm/min, the thickness of the film and the diffusivity of MeS in the film are the main properties to consider. Whereas the film uptake rate is mainly dependent on these two properties, the second value, the *PAD uptake rate*, is dependent on both the film properties and the active sampling surface area of the PAD. The PAD uptake rate is expressed in units of cm^3/min and is a product of the active sampling surface area of the PAD and the film uptake rate. The PAD uptake rate is the value that the current version of ASTM F2588 refers to as simply the uptake rate. According to the standard, PADs with an active sampling surface area of 4.3 cm^2 should have a PAD uptake rate of (10 ± 2) cm^3/min [6]. Specifying the uptake rate in terms of cm/min describes the diffusion process in a one-dimensional direction and places tolerances on only the properties of the film. However, by incorporating the surface area of the PAD and setting criteria for the uptake rate in terms of cm^3/min, the three-dimensional diffusion process is better described. In other words, because the membrane thickness is held constant, diffusion occurs at the same rate (2.0 cm/min) over the whole surface of the PAD, but a larger surface area will allow more molecules to diffuse through the membrane and be collected by the adsorbent. The opposite would be true for a smaller active sampling surface area. If the surface areas of the PADs are not consistent and held to strict tolerances, the calculation of the film uptake rates can be incorrect.

The need for an understanding of the factors that affect the PAD uptake rate, manufacturing-related or otherwise, is best demonstrated by its importance to the MIST methodology. Testing according to the current ASTM F2588 standard requires that the uptake rate of each lot of PADs be measured prior to the conducting of MIST trials. The accepted practice is to expose at least four PADs in the MIST chamber for 30 ± 5 min to calibrate for the lot of PADs used in the specific trial [6]. The average uptake rate (cm/min) and average surface area (cm^2) for each lot of PADs being used in an individual MIST experiment are then applied to all of the PADs that are attached to the test subjects. The standard states that a set of PADs from the lot must be exposed, and the uptake rates are to be calculated using Eq 1 [6], in which u is the uptake rate in cm/min, m is the mass of the adsorbed MeS in ng, A is the active sampling surface area of the PAD in cm^2, and Ct is the chamber exposure dosage in mg·min/m^3. The Ct value is better defined as the exposure concentration multiplied by the time of exposure

$$u = \frac{m}{ACt} \tag{1}$$

$$PF = \frac{Ct_{\text{outside}}}{Ct_{\text{inside}}} \tag{2}$$

An average uptake rate is calculated for the lot of PADs, and then this average rate is used in Eq 1, along with the detected amount of MeS from each test PAD location, to calculate an exposure dosage or Ct_{inside} for each area under the garment. Then the Ct_{inside} for each PAD location is put into Eq 2, along with the exposure dosage for the chamber (Ct_{outside}), which for an ASTM protocol would be 100 mg/m^3 for 30 min, or a Ct_{outside} of 3000 mg·min/m^3. It is important to note that according to the ASTM standard, Ct_{outside} is not measured with PADs; instead, it is an average of the real-time chamber concentration measurements typically taken with Fourier transform infrared (FTIR) instrumentation [6]. The ratio in Eq 2 provides the raw protection factors for each PAD location. These protection factors are then converted to localized and systemic physiological protective dosage factors by multiplying them by body site specific weighting factors that reflect the varying susceptibilities of the different body regions to the chemical agents.

The purpose of this research is to answer questions that have been raised about the consistency of the PADs and to determine which factors affect the uptake rate that is observed. In this study, the physical dimensions of the PADs were measured and examined in order to determine the variation that exists in the surface areas. The variation in the film thickness was not measured due to a lack of instrumentation with the proper sensitivity. Also, the PADs were exposed to various concentrations for different lengths of time in order to determine the effect of the exposure dosage on the uptake rate. Other suspected sources of inconsistency that were investigated were the amount of time for which the PADs were allowed to sit after exposure and the temperature at which they were stored.

Experimental Methods

Measurement of the Passive Adsorbent Dosimeter Physical Dimensions

In order to determine the variability in the physical dimensions, 20 PADs from the same manufacturer-sealed package were measured with calipers along the PAD length and width (Mitutoyo Model No. CD-6" CS). The measurements were taken from the edge where the film was heat-sealed (shown in Fig. 1) and were not the same as the overall outer dimensions of the PAD.

Results from All Passive Adsorbent Dosimeter Exposures

In many of the experiments, a set of multiple PADs were exposed at each of the different conditions. In most cases, four PADs have been used to make a set of PADs, and any results mentioned in the discussion are the average of the values obtained for the four PADs in the set. Using multiple PADs at each condition provides replicate measurements for statistical importance.

Effect of Challenge Concentration and Exposure Time on Passive Adsorbent Dosimeter Uptake Rate

In order to determine how the calculated uptake rate of the PADs was affected by the challenge concentration and exposure time, a set of experiments was carried out in the full-scale MIST chamber at North Carolina State University. All of the PADs used in this study were the Natick Sampler type and came from the same manufacturing lot (P326). The MIST chamber was held at the conditions stated in ASTM F2588 (27°C, 60 % relative humidity, and a nominal wind speed of 1.65 m/s). The simulant concentration was set at five different levels for testing, and the average concentrations measured by a CIC Photonics Gas-Cell FTIR were 15.2, 24.5, 55.7, 71.2, and 97.5 mg/m^3. The PADs were exposed to each of the concentrations for 11 different exposure times: 1, 5, 10, 15, 30, 45, 60, 75, 90, 105, and 120 min. Each combination of concentration and time produced an exposure dosage (*Ct*) value, enabling the comparison of a short duration-high concentration exposure to long duration-low concentration exposure. In other words, a 30 min exposure at 100 mg/m^3 and a 100 min exposure at 30 mg/m^3 both produce a *Ct* value of 3000 mg·min/m^3. A set of four PADs were exposed for each of the 11 exposure times in order to ensure an accurate representation of the adsorption process. Each time the chamber was set to a new concentration, all 44 PADs for that experiment were placed in the chamber simultaneously. All four PADs in each set were adhered to individual aluminum plates for each exposure time. After being exposed for the desired amount of time, the plate was removed and the PADs were extracted immediately.

Due to concerns that the PADs might saturate under normal testing conditions (30 min at 100 mg/m^3), a set of four PADs was exposed overnight in the MIST chamber at 100 mg/m^3. This length of exposure was over 40 times the longest exposure required in the standard. After the PADs were exposed, they were extracted immediately and analyzed.

A second experiment was set up to expose the PADs to concentrations that were below the detection limit of the FTIR. The lowest range that was measurable via FTIR was approximately 10 to 15 mg/m^3. A VICI Metronics Dynacalibrator (Model 340) with a type D diffusion vial (National Institute of Standards and Technology traceable calibration and a diffusion path cut to 1 in.) was used to generate MeS vapor at concentrations in the range of 1–5 mg/m^3. The MeS flow out of the generator was directed to a glass chamber in which the PADs were placed. After the gas generator was allowed to stabilize, the PADs were placed in the glass chamber and exposed for 120 min. Four thermal desorption tubes packed with 200 mg of clean adsorbent (60/80 mesh) were placed at two tees in the flow path. A low vacuum drew 20 ml/min through each of the tubes during the 120 min exposure. Following the exposure, the PADs and tubes were extracted immediately and prepared for analysis.

Effect of Post-exposure Time on Passive Adsorbent Dosimeter Uptake Rate

A separate experiment was carried out in order to investigate the effect of the post-exposure storage time on the total adsorption of MeS. For this experiment, a set of PADs consisted of eight PADs, four with adhesive backing and four with the adhesive removed. The adhesive was removed manually from the back of the PAD by peeling it off, and isopropanol wipes were used to remove any residue that remained. Seven sets of PADs were placed in the MIST chamber simultaneously and exposed for 30 min at 100 mg/m^3. After exposure, one set of PADs was extracted immediately, and the other six sets were wrapped in aluminum foil, placed in individual sealed glass vials, and stored in a refrigerator at 4°C for six different time periods. The stored PADs were extracted after 30 min, 1 h, 2 h, 4 h, 1 day, and 3 days.

Effect of Storage Temperature on Passive Adsorbent Dosimeter Uptake Rate

The effect of the storage temperature on the total amount of adsorbed MeS was examined through two separate experiments. In the first experiment, three sets of four PADs were exposed for 30 min at approximately 94 mg/m^3. One set was extracted immediately, one set was stored under dry ice (below −30°C) for one day, and the final set was stored in the refrigerator (1°C to 4°C) for one day. Again, all PADs that were stored were wrapped in aluminum foil and placed in individual sealed glass vials. In the second experiment, three sets of six PADs were exposed for 120 min at an average concentration of 108 mg/m^3. One set was extracted immediately, one set was stored in the refrigerator (1°C to 4°C) for one day, and one set was stored in a freezer (−15°C to −20°C) for one day.

Passive Adsorbent Dosimeter Extraction Method

An extraction method developed at North Carolina State University was employed to recover the MeS from the PADs. After exposure, the adsorbent was removed from each PAD through the use of a vacuum and a modified empty 1 ml solid phase extraction (SPE) tube (Supelco) with a filter in the tip. The SPE tubes containing the adsorbent were then placed into a Supelco Visiprep DL Vacuum Manifold with autosampler vials to collect the extract. Each SPE tube had two 600 μL aliquots of acetonitrile (ACN) (Acros Organics HPLC Grade 99.9%) injected with a repeater pipet that had a 10 ml capacity pipet tip. The ACN was allowed to flow through the adsorbent to extract the MeS. A low vacuum (−5 in Hg) was turned on to drain the last drops out of the tubes, and the vials were capped and stored for later analysis. Internal method development with various solvents has shown a 99 % extraction of MeS with ACN.

Supplemental Extraction Methods for Desorption Tubes and Adhesive Film

The desorption tubes used to measure the MeS concentration for the 1 to 5 mg/m^3 PAD exposure had the adsorbent removed and placed in a glass vial with 2 ml of ACN. The specimens were allowed to sit for 30 min at room temperature. These extract specimens were then filtered into vials using 3 ml Luerlok syringes with 0.2 μm pore size Whatman filters attached. The adhesive film specimens from the overnight exposure were extracted in the same manner, but they were allowed to sit overnight before being filtered.

High Performance Liquid Chromatography Analysis Method

The PADs were analyzed on an Agilent 1200 Series high-performance liquid chromatograph (HPLC) containing a binary pump (model number G1312B), a standard autosampler (model number G1329B), and a diode-array detector (model number G1315C). The injector syringe was rinsed in ACN (HPLC grade 99.9%, Acros Organics) to prevent carryover, and the injection amount was 4 μL. For highly concentrated specimens, the injection amount was decreased to 0.5 μL in order to avoid overloading the detector. An Agilent Poroshell 120 EC-C18 column (3.0 mm $\times$ 100 mm, 2.7 μm particle size) heated to 45°C was used with a flow rate of 0.5 ml/min. A 40/60 H_2O/ACN isocratic method was used with a total analysis time of 4.0 min. The diode-array detector was set to monitor at 205 nm.

Results and Discussion

Variation in Physical Properties of the Passive Adsorbent Dosimeters

The first attempt to characterize some of the inter-laboratory variation involved investigating how well the active sampling surface areas of the PADs agreed with the tolerances stated in ASTM F2588. The ASTM standard specifies tolerance criteria only for the surface area, and not the individual length and width values. The active surface of a PAD is supposed to be 2.5 cm $\times$ 1.8 cm with a surface area of 4.3 $\pm$ 0.6 cm [6]. After measuring the dimensions of 20 PADs from one sealed pouch, it was observed that the average length was 2.38 cm, the average width was 1.78 cm, and the average surface area was 4.25 cm^2. The percent deviations from the standard length and width with their corresponding surface areas are shown in Figs. 2 and 3, respectively.

The dotted lines in Figs. 2 and 3 show the tolerance values for the surface area. For the most part, all but 3 or 4 PADs out of the 20 that were measured fall within the surface area tolerances. However, it is clear from the figures that the lengths of the PADs are much more variable than the widths. This might be an issue that the manufacturer could improve upon in order to produce a more consistent product. As it stands from this analysis, the average surface area for the lot of PADs that would be used in the uptake rate calculation is only 1.2 % smaller than the standard area that is specified. Even though the average of the

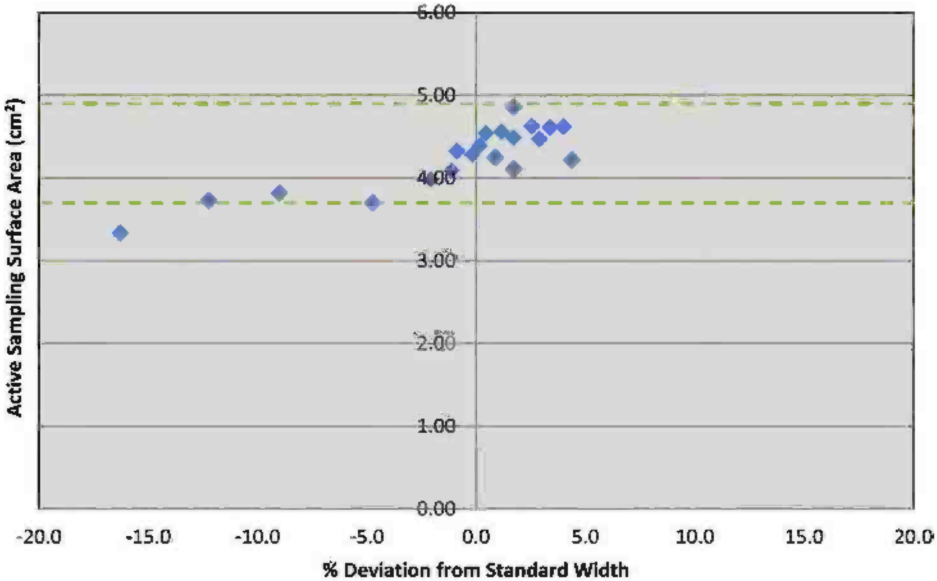

FIG. 2—*Calculated percent deviation from the standard length of 2.5 cm for 20 PADs.*

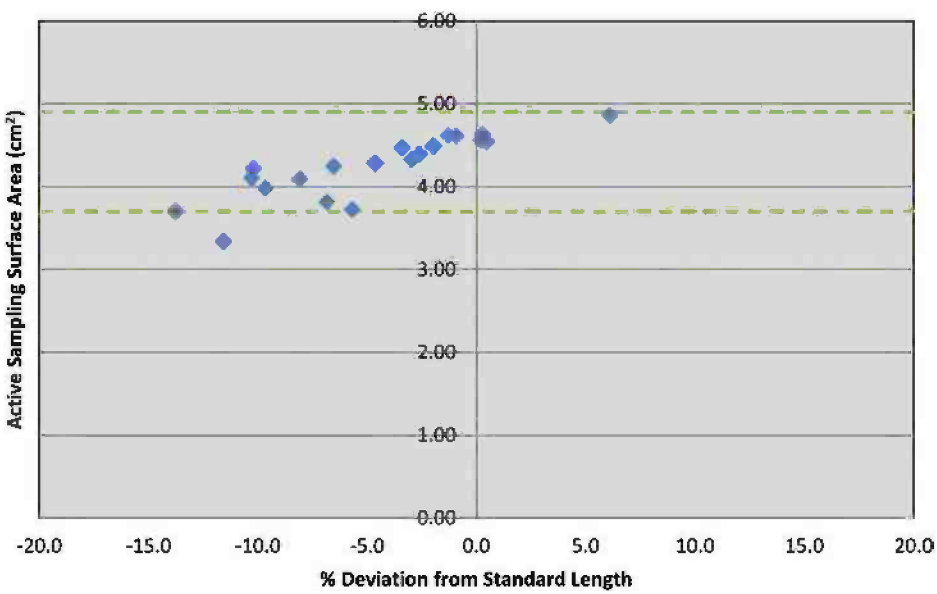

FIG. 3—*Calculated percent deviation from the standard width of 1.8 cm for 20 PADs.*

measured surface areas falls within the tolerance limits, there are a few data points that are as much as 20 % smaller or 13 % larger than the standard value.

The PAD with the smallest surface area (3.33 cm^2) should allow a lower total amount of MeS to diffuse across the membrane than a PAD with the standard surface area of 4.3 cm^2. If the standard surface area is used in the calculation, the lower diffused mass and the larger area could produce a slightly lower uptake rate than if the actual area of the PAD were used. For this reason, among others, not only should a PAD lot evaluation be conducted, but multiple PADs need to be used in an exposure to ensure a better representation of the actual exposure process. These results show that it is very important to use the average surface area for the specific lot of PADs that are being used in the test, as opposed to simply using the standard value.

Uptake Rate Variation with Challenge Concentration and Exposure Time

With over 200 PADs exposed and analyzed in the first set of experiments, a massive amount of data has been collected. There are numerous ways to organize the data in an attempt to pick out patterns and see which factors affect the PADs the most. It is possible to graph the total MeS adsorbed versus either the chamber concentration or the exposure time, but a significant amount of information is not gathered with regard to the uptake rate with that method. A graph of the total MeS adsorbed versus the exposure dosage is the best way to see whether the uptake rate stays constant over all of the conditions, because the *Ct* takes into account both the time of exposure and the challenge concentration.

In Eq 1, the PAD uptake rate (with the area included) is essentially the slope of the mass versus *Ct* linear relationship. The graph in Fig. 4 clearly shows that this rate is constant in the range of exposures used in this experiment. This relationship also confirms that a short duration–high concentration exposure is very similar to a long duration–low concentration exposure. Taking all points into consideration, the slope of the curve correlates to a PAD uptake rate of 14.3 cm^3/min and a film uptake rate of 3.4 cm/min if the previously measured average active sampling surface area of 4.25 cm^2 is used. Both of these rates are higher than the values required in the standard or suggested in the literature (10 cm^3/min and 2 cm/min). Because the measured surface areas for this particular lot of PADs are within the standard tolerances, it should be safe to conclude that the higher uptake rates are more likely due to a property of the film than to the surface area of the PAD. Therefore, for the remainder of the discussion, the uptake rates are expressed in terms of the film uptake rate (cm/min).

One important factor that affects the uptake rate can be noted if the rate is plotted against the time of exposure. Figure 5 shows that there is at least a 10 to 15 min equilibration time before the uptake rate reaches a steady state. This realization is very important because if one laboratory exposes PADs for 5 to

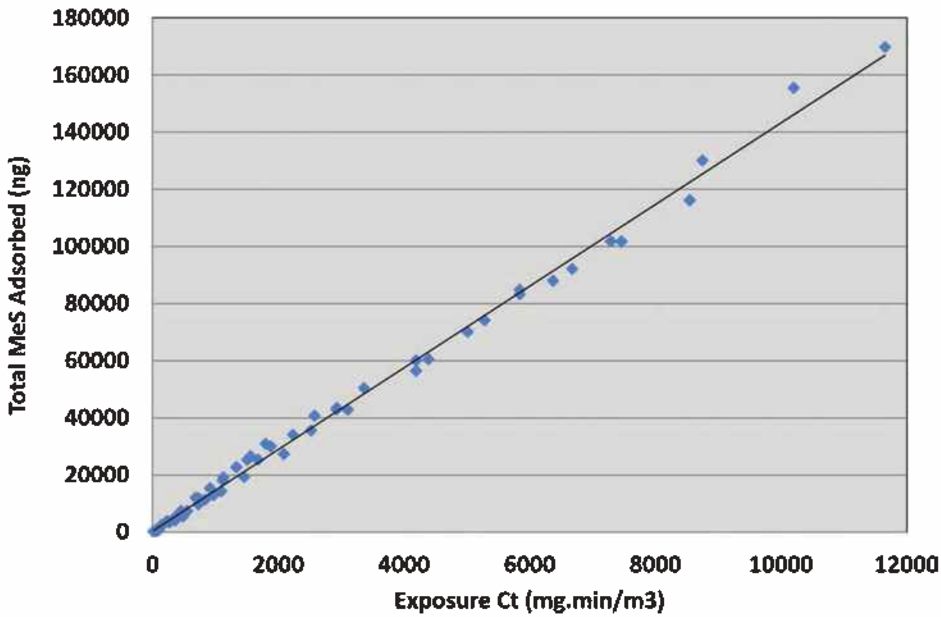

FIG. 4—*Total methyl salicylate uptake (ng) versus exposure Ct (mg · min/m^3). Each data point is the average of the values of four PADs exposed and extracted immediately. The slope corresponds to a PAD uptake rate of 14.3 cm^3/min and a film uptake rate of 3.4 cm/min.*

10 min to calculate the lot's average uptake rate and another laboratory exposes PADs for more than 30 min, the two calculated values might not agree. The first laboratory will generate uptake rates of around 1 to 2 cm/min, whereas the second laboratory will calculate the steady state uptake rates as around 3 to 4 cm/min. This relationship between the exposure time and the uptake rate could contribute significantly to inconsistencies between laboratories.

The values in Table 1 provide the averages, standard deviations, and coefficients of variation for all of the PADs that were exposed. The top portion of the table includes every data point, whereas the bottom portion includes the steady state data only for PADs exposed for more than 30 min. The total average uptake rate for all of the exposures was 3.3 cm/min with a standard deviation of 0.7 cm/min. The coefficient of variation around 20 % shows that many of the data points were not at an equilibrium steady state. When we consider only the PADs that were exposed for a longer period of time, the average uptake rate increases to 3.5 cm/min with a standard deviation of 0.4 cm/min, and the coefficient of variation is cut almost in half, from 20 % to 11 %. This coefficient of variation around 10 % is similar to what is normally seen with these PADs [7]. The best recommendation based on this relationship is that PADs should be exposed for at least 30 min in order to achieve a steady state.

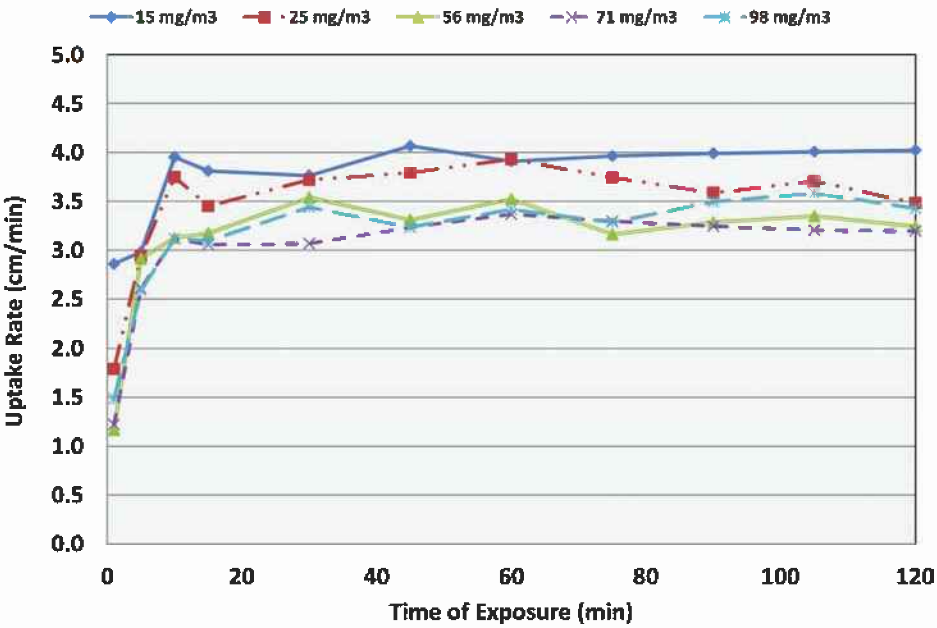

FIG. 5—*Average uptake rate (cm/min) versus the time of exposure (min). The average steady state uptake rate is approximately 3.5 cm/min.*

Therefore, the 1, 5, 10, and 15 min exposures are disregarded in most of the remaining discussion.

Another question that has been raised about the PADs that can be answered by Figs. 4 and 5 is whether unprotected/fully exposed PADs would saturate under normal test conditions. An ASTM standard test results in an exposure dosage of 3000 mg·min/m^3, and the military test operations procedure 10-2-022, which is a 120 min test at the same concentration, results in a 12 000 mg·min/m^3 exposure dosage. Neither of the figures shows any

TABLE 1—*Statistical values for the variation in the calculated uptake rates. Data for all exposed PADs are averaged from 44 total PADs at each concentration. Data for PADs exposed for 30+ min are averaged from 28 total PADs at each concentration.*

		Concentration, mg/m^3					
		15.2	24.5	55.7	71.2	97.5	Total
All exposed PADs	Average, cm/min	3.8	3.4	3.1	3.0	3.1	3.3
	Standard deviation	0.5	0.7	0.7	0.6	0.6	0.7
	% CV	14.6	20.2	21.8	21.7	20.7	21.6
PADs exposed for 30+ min	Average, cm/min	4.0	3.7	3.3	3.2	3.4	3.5
	Standard deviation	0.3	0.3	0.3	0.3	0.3	0.4
	% CV	6.5	8.7	7.6	8.1	8.9	11.0

indication of saturation during the test. The curve in Fig. 4 stays linear all the way to the 12 000 mg.min/m^3 mark, and a decrease in the uptake rate would be expected in Fig. 5 if saturation were present. The PADs that were exposed overnight adsorbed an average of 775 000 ng of MeS. Using the equation of the line in Fig. 4 to extrapolate the saturation point, the PADs most likely reached saturation after between 8 and 9 h of exposure, or at a *Ct* of approximately 54 000 mg·min/m^3. Without further investigation into the prolonged exposures, a more accurate exposure dosage for saturation cannot be stated.

A third observation that can be made from Fig. 5, as well as from the data in Table 1, is that the uptake rate slightly increases as the concentration decreases. The values go from approximately 3.4 cm/min at the highest concentration to around 4.0 cm/min at the lowest concentration. It is important to note that the standard deviation and coefficient of variation for each concentration level are very similar. This observed consistency shows that there is an increasing trend and that the difference is not simply part of the overall variability. This trend is a critical observation, because even though the MIST chamber is maintained at 100 mg/m^3 during testing, the microenvironment beneath the protective ensemble should be nowhere near as concentrated. The chamber concentrations used in this experiment spanned only 1 order of magnitude, and the uptake rate increased 0.6 cm/min. Simulant concentrations inside a protective ensemble might be closer to 2 or more orders of magnitude lower than the chamber concentration. If the uptake rate continues to increase at lower concentrations, then the protection factor calculations used in the MIST analysis might be incorrect, because those calculations assume that the uptake rate is constant at both the high chamber concentrations and the low concentrations underneath the protective ensemble.

To estimate the concentrations expected under a chemical protective garment, one can consider Eq 2. According to NFPA 1994 [8], a passing protection factor for a Class 2 ensemble should be 360. As Eq 2 is a ratio of Ct_{outside} to Ct_{inside} and the time of exposure is the same for both cases, the time cancels out, leaving only the concentrations outside and inside the protective suit as part of the equation. Using the 360 protection factor and the outside concentration of 100 mg/m^3, the potential internal concentration for a marginally protective garment is 0.28 mg/m^3, which is almost 2 orders of magnitude lower than the lowest concentration previously discussed. Although it would have been ideal to expose the PADs to concentrations on this level or lower, time and instrumentation constraints allowed for a lowest achievable concentration of only 4 to 5 mg/m^3 using the gas generator and small-scale chamber. For a 120 min exposure at 4.8 mg/m^3, the average calculated uptake rate was 4.1 cm/min with a standard deviation of 0.3 cm/min. Without further testing at even lower concentrations, it is impossible to determine how much more the uptake rate might increase.

Effect of Post-exposure Storage Time and Temperature on the Passive Adsorbent Dosimeter Uptake Rate

An easily overlooked factor that could be a major source of variation between laboratories is the handling of the PADs after exposure. The standard requires that the PADs be wrapped in aluminum foil, placed in sealed glass vials, and stored in the refrigerator at around 4°C [6]. Aluminum foil is used so that there is a solid surface attached to the adhesive during storage. The adhesive is most likely a polymeric substance that can allow the MeS to adsorb and then desorb while being stored. Placing the aluminum foil on the adhesive is an attempt by the standard committee to minimize mass transfer out of the adhesive and into the PAD. To slow this thermodynamic process even more, the PADs are stored at a cold temperature in the refrigerator.

In order to determine whether the storage time had any effect on the calculated PAD uptake rates, an experiment was carried out with the same conditions that a standard ASTM MIST would employ. A duplicate set of PADs had the adhesive removed in order to determine whether PADs with no adhesive would react similarly during storage. All of the PADs were handled in exactly the same way, except for the length of time that they were stored in the refrigerator. The results for this experiment are shown in Fig. 6. The normal PADs

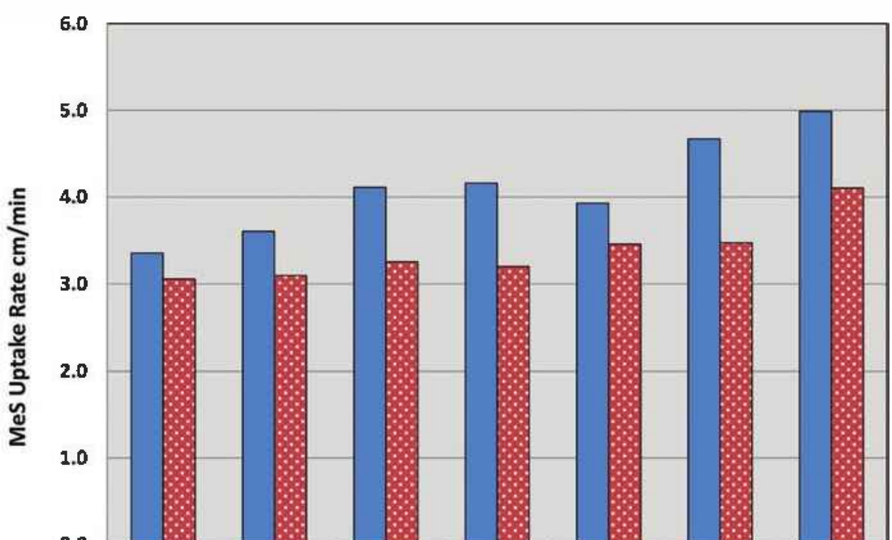

	Immediate	30 min	1 hr	2 hr	4 hr	1 day	3 day
Normal PADs	3.4	3.6	4.1	4.2	3.9	4.7	5.0
No Adhesive	3.1	3.1	3.3	3.2	3.5	3.5	4.1

FIG. 6—*Calculated uptake rate (cm/min) versus the post-exposure storage time for PADs with and without adhesive. All PADs were exposed for 30 min at 100 mg/m^3 and stored at 4°C.*

that were extracted immediately had the same uptake rate (3.4 cm/min) as the steady state rate mentioned previously.

In all cases, the PADs without adhesive adsorbed slightly less MeS and therefore had slightly lower uptake rates. From Fig. 6 it can be seen that the uptake rates for PADs with adhesive increased significantly during the storage time, from 3.6 cm/min immediately following exposure to 5.0 cm/min three days later. In contrast, the uptake rates for the PADs that had the adhesive removed stayed fairly constant over most of the storage time. The exception is the three day value, which increased to 4.1 cm/min but was still lower than the 5.0 cm/min observed for the normal PADs. This slight increase may be attributed to some residual adhesive left on the back of the PAD that was not completely removed with the isopropanol wipe. From these data, it can be assumed that MeS adsorbed into the adhesive can affect the calculated uptake rate of the PAD if stored at or above 4°C for more than an hour. It is important to note that the magnitude of the increase in the total amount of MeS adsorbed is probably a result of the PADs' being completely unprotected and exposed to the full challenge concentration during the test. Being exposed to such a high concentration allows the adhesive to adsorb more MeS during the test, so that during storage more MeS can transfer into the PAD. Preliminary data from some of the adhesive films that were exposed overnight at 100 mg/m^3 showed that the adhesive can adsorb over 190 000 ng of MeS.

Because wrapping the PADs in aluminum foil and storing them at 4°C in the refrigerator did not prohibit after-exposure MeS transfer from the adhesive to the PAD, a second experiment was conducted utilizing different storage temperatures. One easily accessible method for cooling the PADs to extremely cold temperatures is to pack them in dry ice. At atmospheric pressures, dry ice exists as a solid below −70°C, and it can be easily packed onto the PADs in the glass vials while they are being stored or transported. In order to test the efficacy of dry ice storage, it was compared to immediate extraction and refrigerator storage. The total amount of MeS adsorbed for each condition is shown in Fig. 7.

As previously determined in the concentration and time exposures, a 30 min exposure at 100 mg/m^3 should result in approximately 43 000 ng on the PAD (Fig. 4). This amount was consistent with the experiments, as seen for the immediately extracted PADs in Fig. 7. The cold temperature of the dry ice stops any mass transfer from occurring during the one-day storage. The total amount of MeS adsorbed (43 138 ng) from the PADs stored in dry ice was almost identical to the immediately extracted amount (43 057 ng). As expected, the values for the PADs that were stored in the refrigerator increased almost 42 %, with a total adsorption of 61 000 ng of MeS. These data prove that if the PADs cannot be extracted immediately, they should be stored under dry ice, or some other means should be used to reach extremely cold temperatures. The main theory behind the colder temperatures is that cooling the PADs below the

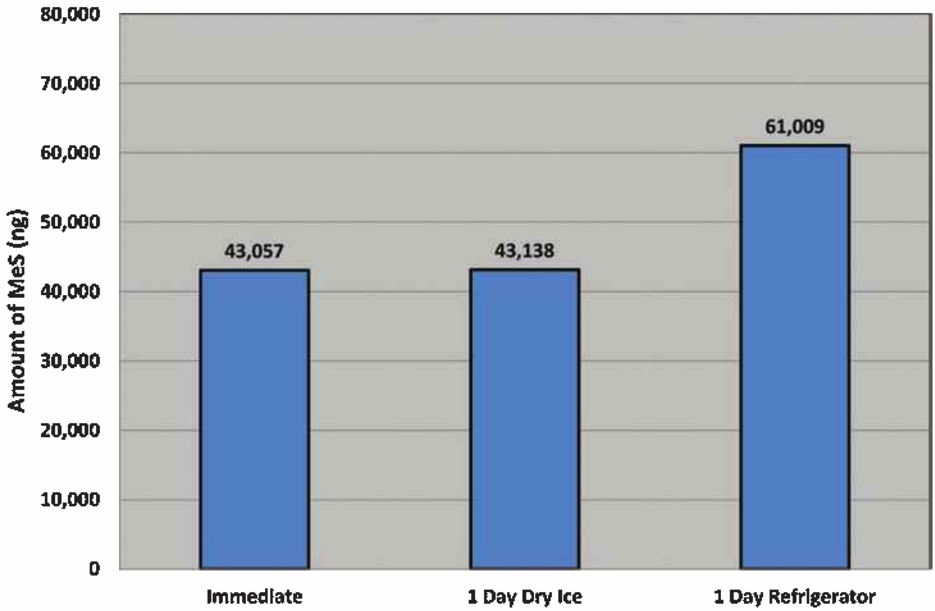

FIG. 7—*Total amount of MeS (ng) adsorbed for PADs exposed for 30 min at 100 mg/m*^{3}. *PADs were extracted immediately, stored below −70°C in dry ice for one day, and stored at 4°C in a refrigerator for one day.*

glass transition temperatures of the adhesive and the HDPE membrane greatly reduces the risk of any mass transfer. Further investigation into the most effective temperature needs to be conducted in order to confirm this theory.

Although the dry ice does an excellent job of preventing the desorption process from occurring, it is not the most convenient method for storing a large number of PADs, as would be required in an eight-subject MIST protocol. If a freezer could reach cold enough temperatures, it would be an ideal storage container for a large lot of PADs. In order to determine whether an ordinary commercial freezer would be sufficient, more PADs were exposed and stored under varying temperatures. After an exposure of 120 min at 108 mg/m^3, the PADs that were immediately extracted contained around 180 000 ng of MeS. The PADs that were stored in the freezer at an average temperature of −20°C for one day had an average of 190 000 ng, and the PADs stored in the refrigerator at 4°C for one day had an increased MeS amount of 208 000 ng. Therefore, the temperatures attainable in a normal commercial freezer are not sufficient to prevent the mass transfer from occurring. It is possible that special cryogenic freezers that can reach even colder temperatures could be used in the place of dry ice. Even though the temperatures in the freezer did not stop the process completely, it would still be beneficial to store the PADs in the freezer instead of in a refrigerator in the event that they could not be extracted immediately or packed with dry ice.

Conclusions

All the data that were gathered show that the best approximation for the steady state film uptake rate of this lot of Natick Sampler PADs is 3.5 ± 0.5 cm/min. Although this rate falls in the observed variability range of 1.0–4.0 cm/min reported for the different areas of the body [1], it is considerably higher than the 2.0 cm/min indicated by Fedele and Nelson [5]. Also, the corresponding average steady state PAD uptake rate is 15.0 ± 1.6 cm^3/min, which is considerably higher than the rate of 10 ± 2 cm^3/min specified in the standard. As all of the PADs in this study came from the same lot, it is also highly probable that there is significant variation among lots. Further analysis of the lot-to-lot variation in physical properties of the PADs such as film thickness and diffusivity or active sampling surface area might be able to identify any manufacturing problems that exist.

The most significant factors that affect the total amount of MeS adsorbed by the PADs are the challenge concentration and the time of exposure. This study shows that the total amount of MeS adsorbed follows a highly linear trend with the exposure dosage in the range of conditions that were tested. The slope of the linear relationship directly corresponds to the PAD uptake rate (cm^3/min), and dividing the slope by the surface area of the PAD yields the film uptake rate (cm/min). The film uptake rate was shown to increase slightly as the challenge concentration decreased. However, without further testing at much lower concentrations, no definitive conclusions can be made with regard to how high the uptake rate could increase.

Regarding the variability of the uptake rates, the data show that well-defined standard handling methods could eliminate many of the inter-laboratory inconsistencies. PADs used to calculate the lot uptake rate should be exposed for no fewer than 30 min, keeping in mind that even longer exposures ensure a steady state condition. In addition, there is no basis for the belief that the PADs saturate in testing conditions that fall below a *Ct* of approximately 54 000 mg·min/m^3. According to the results, if the PADs cannot be analyzed immediately following an exposure, they should be stored in dry ice or in a cryogenic freezer at extremely low temperatures (between $-30°$C and $-70°$C). This practice would help to minimize any transfer of MeS from the adhesive into the PAD.

With all things considered, the PADs used in the MIST standard methods from a single lot are very consistent, provided proper techniques are utilized to ensure that the actual amount of MeS that diffused through the membrane during the test duration is the amount actually being analyzed. Mass transfer during PAD storage can greatly affect the value that is calculated for the uptake rate. The insights gained from this research can help to improve the MIST standard methods and decrease the variability between laboratories.

Acknowledgments

The writers are grateful to U.S. Army RDECOM-STTC for providing support for this research.

References

[1] National Research Council Board on Army Science and Technology, *Technical Assessment of the Man-In-Simulant-Test (MIST) Program*, National Academies Press, Washington, D.C., 1997.

[2] Riviere, J. E., Smith, C. E., Budsaba, K., Brooks, J. D., Olajos, E. J., Salem, H., and Monteiro-Riviere, N. A., "Use of Methyl Salicylate as a Simulant to Predict the Percutaneous Absorption of Sulfur Mustard," *J. Appl. Toxicol.*, Vol. 21, 2001, pp. 91–99.

[3] Henriques, F. C., Moritz, A. R., Breyfogle, H. S., and Patterson, L. A., "The Mechanism of Cutaneous Injury by Mustard Gas: An Experimental Study Using Mustard Prepared with Radioactive Sulfur," National Defense Research Committee of the Office of Scientific Research and Development: Washington, DC, 1951.

[4] Bergmann, M., Fruton, J. S., Golumbic, C., Nagy, S. M., and Stein, W. H., "The Penetration of Vesicant Vapors into Human Skin," *J. Gen. Physiol.*, Vol. 29, 1946, pp. 441–469.

[5] Fedele, P. and Nelson, D. C., 1995, "A Method of Assessing Full Individual Protective System Performance against Cutaneous Effects of Aerosol and Vapour Exposures," U.S. Army Edgewood Research, Development and Engineering Center, Aberdeen Proving Ground, MD.

[6] ASTM F2588, 2007, "Standard Test Method for Man-In-Simulant-Test (MIST) for Protective Ensembles," *Annual Book of ASTM Standards*, Vol. 11.03, ASTM International, West Conshohocken, PA.

[7] Ormond, B., "Selection of a Manikin Skin Simulant for Use in the Man-In-Simulant-Test Phase 1: Development of a Lab-Scale Man-In-Simulant-Test Chamber," *AATCC International Conference*, Atlanta, GA, May 18–20, American Association of Textile Chemists and Colorists, Research Triangle Park, NC, 2010.

[8] NFPA 1994-07, 2007, "Standard on Protective Ensembles for First Responders to CBRN Terrorism Incidents," National Fire Protection Association, Quincy, MA.

Performance of Protective Clothing and Equipment: Emerging Issues and Technologies
STP 1544, 2012
Available online at www.astm.org
DOI:10.1520/STP103884

S. Kay Obendorf[1] *and Ellan F. Spero*[1]

Destructive Adsorption for Enhanced Chemical Protection

REFERENCE: Obendorf, S. Kay and Spero, Ellan F., "Destructive Adsorption for Enhanced Chemical Protection," *Performance of Protective Clothing and Equipment: Emerging Issues and Technologies* on April 16, 2011 in Anaheim, CA; STP 1544, Angie M. Shepherd, Editor, pp. 266–279, doi:10.1520/STP103884, ASTM International, West Conshohocken, PA 2012.

ABSTRACT: Destructive adsorption was studied as a mechanism to provide enhanced chemical protection for traditional textiles. A test procedure for chemical protective clothing fabrics using low volume contamination was used to focus on chemical protection by the mechanism of adsorption. Conventional woven fabrics were treated with two self-decontaminating textile treatments, N-halamine (chlorinated 1, 3-dimethylol-5, 5-dimethylhydantoin (DMDMH)) and MgO nanoparticles; a third treatment included starch in addition to MgO. Both N-halamine and MgO treatments demonstrated some degree of degradation of the toxin aldicarb. However, the MgO-treated specimens exhibited more degradative products and reduction of aldicarb than the N-halamine DMDMH. The fabric treatments containing the MgO nanoparticles resulted in destructive adsorption of aldicarb resulting in self-decontamination. Inclusion of starch with the MgO resulted in fabric that exhibited evidence of both physical adsorption and destructive adsorption of the toxin. The role of destructive adsorption to decontaminate traditional fabrics was clearly demonstrated. This self-decontamination enhances chemical protection at low volume contamination.

KEYWORDS: adsorption, MgO, N-halamine, self decontamination, protective clothing, aldicarb

Introduction

Textile surface interactions with a toxic liquid are determined by the chemical nature, surface configuration and fiber roughness, pore geometry of the textile,

Manuscript received March 27, 2011; accepted for publication February 27, 2012; published online September 2012.

[1]Fiber Science, Cornell Univ., Ithaca, NY 14853.

and liquid parameters such as surface tension and viscosity. Penetration of liquid toxins through non-barrier protective materials is governed by the basic mechanisms of repellency, sorption, and liquid flow through pores and capillaries. The process of surface wetting occurs upon exposure of a fibrous material to liquid leading to adsorbency and/or repellency. Penetration into or through the fabric can only occur if the material is "wettable," i.e., the fiber-air interface is displaced by a fiber-liquid interface. After wetting of fibers, capillary forces drive the spontaneous flow of the liquid through the porous substrate through a wicking process [1]. Liquid penetration is the flow of a chemical through pores, or other discontinuities in the material such as closures or other imperfections.

Textile structures have the ability to retain liquids and other chemicals via sorption. This property can provide protection by trapping a contaminant within a fibrous matrix limiting dermal contact. Adsorption is governed by inter- and intra-fiber spaces where liquids are retained through capillary forces. When fabrics have the same weave structure, yet different fiber contents, the adsorption capacity can be also quite different because of different fiber pore structures. Pore sizes for woven fabrics commonly have a bimodal distribution. Large sizes represent the inter-yarn spaces, whereas the inter-fiber spaces are reflected by smaller sizes [1,2]. Lee and Obendorf [3] observed pore sizes for a woven fabric of 6.5–114.4 μm, whereas the non-woven ranged from 0.3 to 6.2 μm.

Treatment of traditional non-barrier textiles with chemical finishes, such as starch, increase sorption properties, decreasing transfer by rubbing and enhancing removal of contaminants by laundering [4,5]. When thickness increases, there is a greater chance for liquids to be trapped within the fabric structure. Following this reasoning, layering of clothing materials has been shown to offer increased protection [6,7].

Textile treatments, such as renewable starch finish or durable carboxymethylation of cotton, increase the amount of toxins adsorbed by the fabrics [8]. Fabric weight also is a critical factor in adsorption of liquid toxins. Heavier materials such as denim retain more chemicals than lighter shirt-weight materials and may release contaminants over time. Cyclodextrins also have been used to enhance sorption of toxins on fibrous structures [9].

Toxins can be transferred from clothing with friction [10,11]. This is a critical factor when donning and doffing a contaminated garment because retained chemicals can be released to people and their immediate environment. Without successful decontamination, chemicals may accumulate over time and could be transferred to skin or other surfaces by friction [10,12]. In addition to protection from initial toxic exposure, limiting further contamination when doffing the garment or handling soiled garments is a critical factor for protective clothing. Self-decontaminating fabric treatments, which decompose toxins on contact, may provide enhanced dermal protection as well as limit garment-mediated contamination.

Materials with self-decontaminating treatments are a promising approach to attain comfortable yet protective clothing systems. This class of materials incorporates compounds capable of detoxifying reactions, such as oxidation and/or hydrolysis, onto protective textiles. By converting toxins to potentially less harmful forms on contact, the efficacy of porous materials for limiting dermal contamination may be enhanced. This project focuses on two such self-decontaminating treatments, N-halamine and metal oxide structures, used as finishes on shirt-weight plain woven cotton/polyester fabric.

N-Halamines

Oxidative properties of N-halamines are promising for development of self-detoxifying protective clothing. N-halamine compounds, which derive their efficacy from disassociation of chloramine bonds (N-Cl), have demonstrated the ability to oxidize commonly used carbamate pesticides that contain sulfur bonds such as aldicarb and methomyl [13]. Researchers have demonstrated their ability to convert alcohols to ketones, sulfides to sulfoxides and sulfones, and cyanides to carbon dioxide and water [14].

Three forms of chloramine bonds are imide, amide, and amine halamine. Bond stability is inversely related to reaction rate with aldicarb (imide halamine > amide halamine > amine halamine) [13,15]. The imide bond, which is present in 1, 3 dimethyol-5, 5-dimethylhydantoin (DMDMH), dissociates readily and reacts more rapidly with aldicarb than N-halamines containing amide and amine bond types. Researchers have shown the decrease in aldicarb concentration with exposure to N-halamines and the oxidation of the thio bond to sulfoxide (-SO-) and later sulfone (-SO_2-) [13]. The formation of these two oxidation products is illustrated in the overall scheme for degradation of aldicarb in Fig. 1.

N-halamine polymers have been grafted onto polyester/cotton and exhibit durable and rechargeable properties when reactivated with a chlorine treatment [15–17]. Higher temperatures contribute to a faster rate of oxidation [13].

Magnesium Oxide

Inorganic metal oxides, such as MgO are known for their high surface reactivity and adsorptive properties. In nanocrystalline form (particle size 8 nm, aggregate size 3.3 μm) with polyhedral shapes and high proportion of corner/edge sites, there is greater surface area available for reactions compared to typical polycrystalline material. This high surface area combined with high surface reactivity gives these materials great potential for use in decontamination of toxic substances by dissociative chemisorption or "destructive adsorption" [18]. Nano-MgO has been shown to destructively adsorb polar organics such as aldehydes, alcohols, ketones, and others in very high capacities [19].

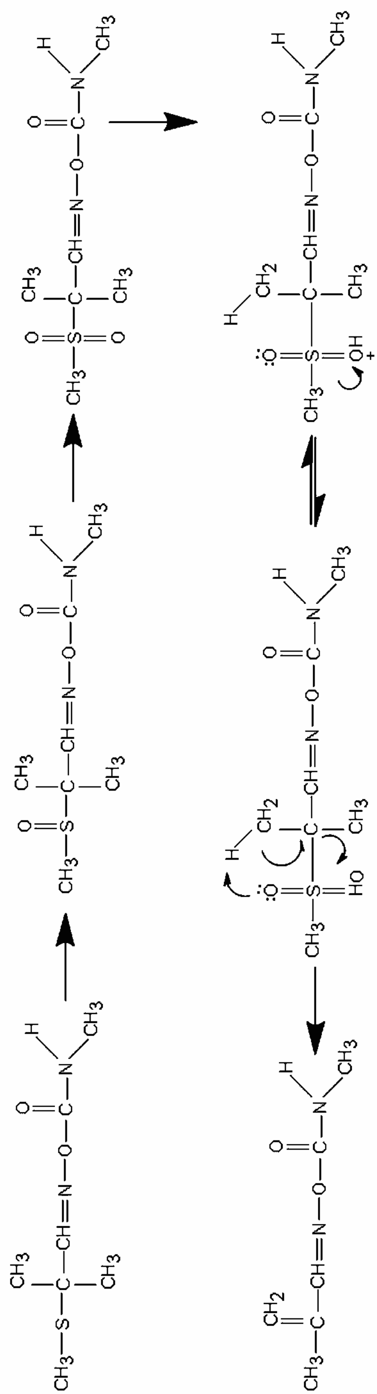

FIG. 1—*Degradation scheme for aldicarb [28].*

Whereas scientists have incorporated TiO_2 into non-woven polyester filtration fabrics and as a component in a silicone finish on cotton woven fabrics to aid in degradation of volatile organic compounds (VOC), this metal oxide acts as a photocatalyst requiring UV radiation [20,21]. Use of MgO nanoparticles is of interest because of its high adsorptive properties without the need for activation by UV radiation. Rajagopalan et al. [18] found that nanocrystalline MgO reacts faster and in higher capacity than activated carbon, a commonly used material for chemical and military protective clothing. Unlike activated carbon, which only physisorbs, MgO is able to immobilize organophosphate compounds by cleavage of P-O and P-F bonds. In the experiment that follows, MgO was tested both alone and with starch to combine properties of physical and destructive adsorption. Also, the self-decomposition functionality of MgO-treated fabric was compared to that of fabric treated with the N-halamine DMDMH.

Experimental Procedures

Experiments were designed to focus on the mechanism of destructive adsorption of the challenge toxin (aldicarb) by conventional woven fabrics treated with self-decontaminating and adsorbent finishes. N-halamine and MgO were chosen for their chemical reactivity and/or destructive adsorption [13,18,19], whereas starch was chosen for its physical adsorption [5,8]. A comparative study for untreated starch, chlorinated DMDMH (N-halamine), MgO/starch, and MgO was conducted at a low contamination load. Then, the effect of a higher contaminating load was studied for the MgO/starch-treated fabric.

N-Halamine

Because the imide structure is more effective in initially oxidizing aldicarb [13], DMDMH was chosen to represent the N-halamine class of compounds for comparison with the MgO-treated fabrics. 4 % DMDMH (1,3-dimethylol-5,5-dimethylhydantoin) treated 35 % cotton/65 % polyester plain weave textiles (#7409 Testfabrics, West Pittston, PA) were provided by Professor Gang Sun.

For grafting of DMDMH, a regular wet finishing process, pad-dry-cure, was employed [22]. Fabric specimens were immersed in a solution containing DMDMH, magnesium chloride, and anionic wetting agents. The *p*H value of the finishing solution was adjusted to 4.5–5.5 using citric acid. The fabric was padded (two dips and two nips) to the desired wet pickup rate (percentage weight increase on wet fabric). Then it was dried in an oven at 80°C for 5 min and cured at 160°C for 5 min. Finally, the fabrics were machine-washed and tumble dried to remove unreacted DMDMH. The weight of the grafted fabric was measured after the fabric was conditioned for over 24 h at 21°C and 65 % relative humidity. The add-on of the grafting was calculated to be 4 %.

The DMDMH-finished fabric was activated by immersing the specimens in a diluted chlorine solution containing 150 ppm of active chlorine for 30 min in a water/chlorine bleach ratio of 50:1 volume/volume [23]. The chlorinated fabric was then rinsed in de-ionized water and air dried in a drying cabinet. There was 863 ppm active chlorine on the fabric as reported by Qian and Sun [23].

Magnesium Oxide and Starch

MgO nanoparticles (crystallite size 8 nm, specific surface area 230 m^2/g from Nanoscale Materials, Inc., Manhattan, KS) and starch (Mallinckrodt acid-modified soluble) were applied to 35 % cotton/65 % polyester plain woven fabric (#7409 Testfabrics, West Pittston, PA) by saturating the fabrics via dipping into an aqueous slurry, then removing excess liquid using a wringer. There were three different slurries: 3 % MgO, 3 % starch, and a mixture of 3 % MgO/starch (1:1 weight/weight) in high performance liquid chromatography (HPLC) grade water. Fabrics were dried in a conditioned room at 21°C, relative humidity of 65 % for 24 h and weighed before and after application of nanoparticles and starch. Weight % finish contents were as follows: MgO 3.7 %, MgO/starch 3.6 %, starch 2.5 %. All fabrics, including the untreated 35 % cotton/65 % polyester plain weave, were placed in a conditioned room (21 ± 1°C, relative humidity of 65 ± 2 %) for 24 h prior to testing.

Aldicarb, [2-methyl-2-(methylthio) propionaldehyde O-(methylcarbamoyl) oxime], with a vapor pressure of 13 mPa at 20°C was used as the challenge toxin. Analytical reagent grade standard for aldicarb with 99 % purity was purchased from Chem Service (West Chester, PA). Aldicarb has a high potential for absorption through skin and gastrointestinal tract [24], and the Environmental Protection Agency has classified aldicarb in its highest toxicity category [25].

Aldicarb is susceptible to oxidation and hydrolysis. Its two primary oxidation products are aldicarb sulfoxide and aldicarb sulfone (aldoxycarb). Conversion to sulfoxide occurs relatively rapidly, 48 % of the parent compound is oxidized to the sulfoxide form within 7 days in soil, and oxidation can even be observed by simple exposure of a solution with air [26]. The second oxidized product, aldicarb sulfone, does not occur as quickly. Both of these metabolites are considered toxic [27]. They are further detoxified via hydrolysis to oximes and nitriles. Previous research with TiO_2 containing fibers showed that aldicarb was converted to aldicarb sulfoxide, aldicarb sulfone, and 2-propenal, 2-methyl-, O-[(methylamino)carbonyl]oxime (PMMCO) as illustrated in Fig. 1 [28].

Contamination Method

Because bulk liquid flow through porous media is a dominant mechanism for chemical penetration through a woven fabric, a low liquid challenge load was used to maximize adsorption without penetration through the fabrics. Five different textile finishing treatments were used: 4 % DMDMH, MgO, MgO/starch, starch, and untreated (control).

A modification of the ASTM F2130-09 [29] was used to contaminate and evaluate the treated fabrics. Specimens of chlorinated DMDMH, MgO, starch, and MgO/starch-treated fabrics as well as untreated control fabrics were cut into 3- × 3-cm squares. Each specimen was placed on a 3- × 3-cm collector layer of medical grade silicone elastomeric membrane (PharmElast, SF Medical, Trelleborg Sealing Solutions, Chase-Walton Elastomers, Inc., Hudson, MA) supported on a sheet of poly(methyl methacrylate) (PMMA). Fabrics were contaminated with 36 μL of 7.5×10^{-3} M aqueous aldicarb (0.27 μmol) delivered in a 3 × 3 (4 μL) drop formation delivered using a multiple-channel pipettor (Transferpette- S -8/-12, Brand GmbH and Co. KG imported by BrandTech Scientific, Inc., Essex, CT). Nine drops of aqueous aldicarb solution in a square pattern containing three rows of three drops each spaced 0.5 cm apart were delivered from a 1.0-cm height. After 10 min, a second silicone elastomer collector layer of equal size covered the test fabric/collector assembly for 2 min. The three layers were then placed separately into jars containing 10 mL of HPLC grade water. These jars were shaken at 200 rpm for 1 h using a wrist action shaker. Extracted liquids for specimens containing MgO were filtered with a nylon syringe filter (30 mm, 0.45 μm, Alltech Assoc., Inc., Deerfield, IL). Aliquots of 1 mL were removed from each jar and analyzed by HPLC (Agilent 1100, Santa Clara, CA). Specimens were tested in triplicate.

For the MgO/starch-treated fabrics, the effect of contamination load was studied using a higher challenge load of 180 μL (1.39 μmol). The challenge solution was 7.5×10^{-3} M aqueous aldicarb delivered in a 3 × 3 (20 μL) drop formation delivered by multiple-channel pipettor in three rows. The extraction and analyses were the same as for the study of fabric treatments with low contamination load (36 μL).

High Performance Liquid Chromatography (HPLC)

Because aldicarb degrades at temperatures above 40°C, analyses were performed using HPLC, which is effective at lower temperatures. An Agilent LC-MS system model LC1200 consisting of an autosampler, a binary gradient pump, diode array UV-vis detector (DAD), and mass spectra detector (MSD) consisting of a single quadrupole mass analyzer with multi-mode source atmospheric pressure chemical ionization (APCI) interface in positive ionization mode (PI) was used for detecting target compounds in the LC column effluent.

Specimens were placed into the autosampler and injected into the HPLC. The LC separation was effected on a 150 × 4.6 mm i.d. stainless steel C18 column (5-μm particle size) with flow rate 0.5 mL/min in isocratic mode (Restek Corporation, Bellefonte, PA). The column temperature was maintained at 15°C. The mobile phase was 40 % acetonitrile and 60 % water (pH 3 using H_3PO_4); 220/4 nm UV detector, flow rate 1 mL/min, with detection for 12 min was used for analyses. The equilibration time between injections was 6 min. The data acquisition was performed using Agilent Data Acquisition. Acetonitrile and water used were HPLC grade (Mallinckrodt Laboratory Chemicals, Phillipsburg, NJ).

Standard curves were created using known quantities of aldicarb, aldicarb sulfoxide, and aldicarb sulfone (purity 99 % from ChemService, West Chester, PA). An analytical standard was not available for 2-propenal, 2-methyl-, O-[(methylamino) carbonyl] oxime (PMMCO). Only peaks with heights greater than 1.0 mAu were included in analyses. Compounds analyzed are presented in Table 1.

TABLE 1—*Chemical structure and molecular weight of aldicab and the oxidized derivatives.*

Compound	Molecular weight	Chemical structure
Aldicarb	190	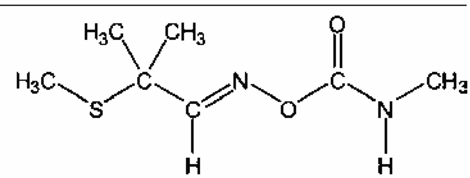
Aldicarb sulfoxide	206	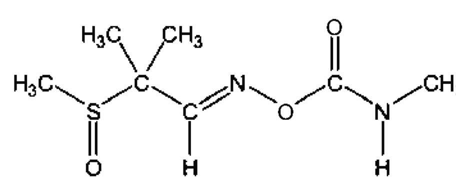
Aldicarb sulfone	222	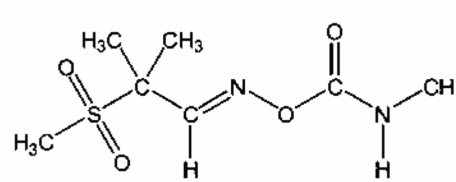
2-Propenal, 2-methyl-, O-((methylamino) carbonyl) oxime (PMMCO)	142	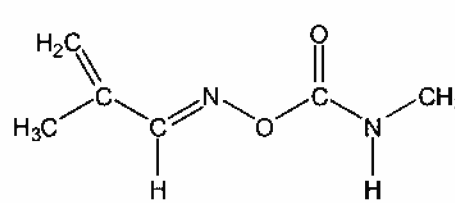

Results and Discussion

Aldicarb appeared at a retention time of 4.0 – 4.2 min. Aldicarb sulfoxide was located at 2.1 – 2.3 min, whereas aldicarb sulfone (aldoxycarb) produced a major peak at 2.5–2.8 min. Aldicarb, aldicarb sulfoxide, and aldicarb sulfone were identified by comparison to known analytical reagent grade standards. These HPLC peaks were consistent with those obtained with a mixture of known standard compounds of these three compounds. A third oxidized product appeared at retention time of 3.4–3.6 min. This retention time and the parent ion in the mass spectra of m/z 143 $(M+H)^+$ are consistent with that identified by Dixit et al. [28] as 2-propenal, 2-methyl-, O-[(methylamino)carbonyl]oxime (PMMCO) using LC/MS/MS.

No evidence of penetration or repellency was found for any of the fabrics at these contamination levels as indicated by an absence of peaks in the chromatographs from the extracted upper and lower membrane layers. Low contamination loads were chosen to focus on the mechanisms of physical and destructive adsorption of aldicarb in the fabric layer. Aldicarb was found in all fabric layers; the quantities of aldicarb (μmol) extracted from the fabric layers are summarized in Fig. 2. These values were determined by using the standard curve for aldicarb ($y = 45 \times 10^{-7} x - 1 \times 10^{-5}$, $R^2 = 0.99$). The extraction of aldicarb and any reaction product was conducted with a low volume of HPLC grade water (10 mL); this extraction method may contribute to the recovery of aldicarb observed in Fig. 2.

Aldicarb and its oxidized products were analyzed by HPLC; peak areas are presented in Table 2 because of the lack of a standard one of the reaction products (PMMC). The untreated control and starch treated fabrics showed similar

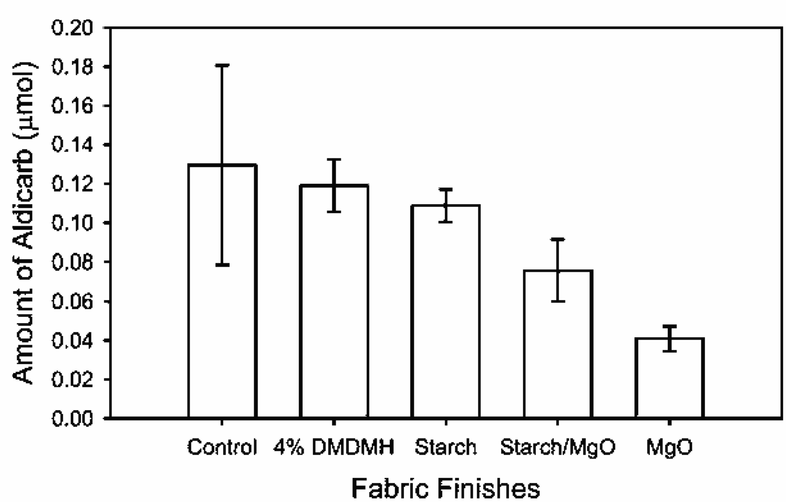

FIG. 2—*Aldicarb in treated fabric at low load (36 µL, 0.27 µmol).*

TABLE 2—*Presence of chemicals in the fabric layer contaminated with aldicarb (36 μL, 0.27 μmol; 180 μL, 1.39 μmol).*

Treatment	Contamination load, μL	Relative amount of compound peak area, mAu[a]			
		Aldicarb	Aldicarb sulfoxide	Aldicarb sulfone	PMMCO
Control	36	82 (12)	ND	ND	ND
4% DMDMH	36	80 (3)	32(1)	ND	ND
Starch	36	77 (2)	ND	ND	ND
MgO	36	60 (2)	ND	ND	12(2)
MgO/starch	36	69 (4)	ND	ND	23(3)
	180	245 (6)	ND	23(2)	396(82)

[a]Peak areas determined by HPLC (mAu), standard deviation in parentheses; ND, not detected.

results with aldicarb being the only chemical compound detected. Therefore, no degradation of aldicarb was observed for these two control fabrics.

The first oxidized product, aldicarb sulfoxide (degradation scheme shown in Fig. 1), indicated by a peak between 2.1–2.3 min retention time was found only in the extracted fabric layer treated with the N-halamine 4 % DMDMH. According to calculations using the standard curve ($y = 2 \times 10^{-7} x - 1 \times 10^{-6}$, $R^2 = 0.98$), there were 0.05 μmol (standard deviation 0.0016 μmol) of aldicarb sulfoxide present. There was no evidence of the second oxidized product, aldicarb sulfone, for any of the treatments with the 36-μL contamination load. However, the third oxidized product, PMMCO, was found in both the MgO and MgO/starch-treated fabric. This suggests destructive adsorption on fabrics treated with MgO and thus a self-decontamination process (oxidation/hydrolysis) resulting in more degradation products than observed for chlorinated fabric treated with 4 % DMDMH (N-halamine). Both chlorinated DMDMH and MgO treatments demonstrated an ability to convert aldicarb to one or more of its oxidized products.

When starch in addition to MgO nanoparticles was used to treat the fabric, at low contamination load (36 μL) similar degradation products were observed as for fabric treated with MgO nanoparticles (Table 2). However, more aldicarb was retained on the starch plus MgO-treated fabric than on the MgO-treated fabric.

At the contamination level of 180 μL, aldicarb, aldicarb sulfone, and PMMCO were found in the MgO/starch-treated fabric layer (Table 2). The first oxidized product, aldicarb sulfoxide, was not detected. Aldicarb sulfone was only observed for the MgO/starch-treated fabric at the higher contamination load (180 versus 36 μL). These observations are consistent with the degradation scheme (Fig. 1) and previous studies that show aldicarb sulfoxide to rapidly convert to the more stable aldicarb sulfone [30]. The amount of remaining aldicarb on the MgO/starch fabric was 65 % of that remaining on the untreated control fabric. These findings are consistent with destructive adsorption occurring in the treated fabric layer that could enhance chemical protection.

Conclusions

The objective of this study to examine adsorption with self-decontaminating surface treatments on traditional work clothing material was achieved by using a modification of the standard ASTM F2130-09 [29]. The relatively low contamination volumes produced neither penetration nor repellency, which made it possible to focus on the mechanism of adsorption. Results presented in this study were consistent with known schemes for the degradation of aldicarb (Fig. 1) [28].

Self decontamination was observed with fabric treated with both N-halamine (DMDMH) and MgO nanoparticles. Some degree of degradation was observed for textiles treated with N-halamine. Destructive adsorption was observed for textiles treated with MgO. Treatments including MgO nanoparticles resulted in more degradation products of aldicarb including the third oxidation product, PMMCO compared to fabric treated with chlorinated DMDMH. The degradation pathway is consistent with that previously observed with TiO_2 [28]. Reduction in the amount of aldicarb on the fabric was demonstrated with both N-halamine DMDMH and MgO nanoparticles, and incorporation of MgO nanoparticles resulted in a higher amount of the oxidation product PMMC. These functionalities may be useful to enhance chemical protection. Incorporation of MgO nanoparticles into a durable finish may be beneficial.

Acknowledgments

The writers thank the National Textile Center (C05-CR01); the Cornell Agricultural Experiment Station, North Central Regional Research Project NC 170 federal formula funds, Project NYC329407 received from Cooperative State Research, Education, and Extension Service, U.S. Department of Agriculture; and College of Human Ecology at Cornell University for the financial support. The writers would also like to thank Professor Gang Sun, University of California at Davis for providing the 4 % DMDMH (1,3-dimethylol-5,5-dimethylhydantoin) treated 35 % cotton/65 % polyester fabric and Tatyana Dokuchayeva and Vivechana Dixit from Cornell University for technical assistance.

References

[1] Lee, S. and Obendorf, S. K., "Statistical Model of Pesticide Penetration through Woven Work Clothing Fabrics," *Arch. Environ. Contam. Toxicol.*, Vol. 49, 2005, pp. 266–273.

[2] Miller, B. and Tyomkin, I., "Liquid Wetting, Transport, and Retention Properties of Fibrous Assemblies," *Text. Res. J.*, Vol. 64(1), 1994, pp. 55–57.

[3] Lee, S. and Obendorf, S. K., "Barrier Effectiveness and Thermal Comfort of Protective Clothing Materials," *J. Text. Inst.*, Vol. 98, 2007, pp. 87–97.

[4] Koh, Y.-K. C., Obendorf, S. K., and Derksen, R. C., "Pesticide Deposition Patterns on Protective Clothing during Vineyard Application Using Three Types of Sprayers," *Proceedings of the Second International Symposium on Consumer Issues: Safety, Health, Chemicals, and Textiles in the Near Environment*, St. Petersburg, FL, 1993, pp. 129–135.

[5] Obendorf, S. K. and Ko, L. L., "Effect of Starch on Reducing the Retention of Methyl Parathion by Cotton and Polyester Fabrics in Agricultural Protective Clothing," *J. Environ. Sci. Health, Part B*, Vol. 32(2), 1997, pp. 283–294.

[6] Laughlin, J. M., Easley, C. R., Gold, R. E., and Hill, R. M., "Fabric Parameters and Pesticide Characteristics that Impact on Dermal Exposure of Applicators," *Performance of Protective Clothing, ASTM STP* 900, R. L. Barker and G. C. Colletta, Eds., ASTM International, West Conshohocken, PA, 1986, pp. 136–150.

[7] Crossmore, D. G. and Obendorf, S. K., "Pesticide Protection through Layered Clothing Systems," *Performance of Protective Clothing: Fourth Volume, ASTM STP* 1133, J. P. McBriarty and N. W. Henry, Eds., ASTM International, West Conshohocken, PA, 1992, pp. 210–220.

[8] Csiszár, E., Borsa, J., Racz, I., and Obendorf, S. K., "Reduction in Human Exposure to Pesticide Using Traditional Work Clothing Fabrics with Chemical Finishing: Carboxymethylation and Starch," *Arch. Environ. Contam. Toxicol.*, Vol. 35(1), 1998, pp. 129–134.

[9] Martel, B., Thuaut, P. L., Bertini, S., Crini, G., Bacquet, M., Torri, G., and Morcellet, M., "Grafting of Cyclodextrins onto Polypropylene Nonwoven Fabrics for the Manufacture of Reactive Filters. III. Study of the Sorption Properties," *J. Appl. Polym. Sci.*, Vol. 85, 2002, pp. 1771–1778.

[10] Obendorf, S. K., Love, A. M., and Knox, T., "Use of a Crocking Test Method to Measure the Transfer of Pesticide from Contaminated Clothing," *Cloth. Text. Res. J.*, Vol. 12(2), 1994, pp. 1–5.

[11] Yang, Y. and Li, S., "Frictional Transition of Pesticides from Protective Clothing," *Arch. Environ. Contam. Toxicol.*, Vol. 25, 1993, pp. 279–284.

[12] Obendorf, S. K., Kasunick, R. S., Ravichandran, V., Borsa, J., and Coffman, C. W., "Starch as a Renewable Finish to Improve the Pesticide-Protective Properties of Conventional Workclothes," *Arch. Environ. Contam. Toxicol.*, Vol. 21(1), 1991, pp. 10–16.

[13] Fei, X., Gao, P., Shibamoto, T., and Sun, G., "Pesticide Detoxifying Functions of N-Halamine Fabrics," *Arch Environ Contam Toxicol.*, Vol. 51, 2006, pp. 509–514.

[14] Sun, G. and Worley, S. D., "Oxidation of Secondary Alcohols and Sulfides by Halamine Polymers," *Chem. Oxid.*, Vol. 6, 1997, pp. 134–144.
[15] Qian, L. and Sun, G., "Durable and Regenerable Antimicrobial Textiles: Chlorine Transfer among Halamine Structures." *Ind. Eng. Chem. Res.*, Vol. 44(4), 2005, pp. 852–856.
[16] Ko, L. L., Shibamoto, T., and Sun, G., "A Novel Detoxifying Pesticide Protective Clothing for Agricultural Workers," *Text. Chem. Color Am. D*, Vol. 32(2), 2002, pp. 34–38.
[17] Sun, Y. Y. and Sun, G., "Novel Regenerable N-Halamine Polymeric Biocides: I. Synthesis, Characterization, and Antibacterial Activity of Hydantoin-Containing Polymers," *J. Appl. Polym. Sci.*, Vol. 80(13), 2001, pp. 2460–2467.
[18] Rajagopalan, S., Koper, O., Decker, S., and Klabunde, K. J., "Nanocrystalline Metal Oxides as Destructive Adsorbents for Organophosphorus Compounds at Ambient Temperatures," *Chem.-Eur. J.*, Vol. 8(11), 2002, pp. 2602–2607.
[19] Khaleel, A., Kapoora, P. N., and Klabunde, K. J., "Nanocrystalline Metal Oxides as New Adsorbents for Air Purification," *Nanostruct. Mater.*, Vol. 11(4), 1999, pp. 459–468.
[20] Dong, Y., Bai, Z., Zhang, L., Liu, R., and Zhu, T., "Finishing of Cotton Fabrics with Aqueous Nano-Titanium Dioxide Dispersion and the Decomposition of Gaseous Ammonia by Ultraviolet Irradiation," *J. Appl. Polym. Sci.*, Vol. 99, 2005, pp. 286–291.
[21] Park, O. H., Kim, C. S., and Cho, H. H., "Development of a Photoreactive Fabric Filter for Simultaneous Removal of VOCs and Fine Particles," *Korean J. Chem. Eng.*, Vol. 23(2), 2006, pp. 194–198.
[22] Qian, L. and Sun, G., "Durable and Regenerable Antimicrobial Textiles: Synthesis and Applications of 3-methylol-2,2,5,5-tetramethylimidazolidin-4-one (MTMIO)," *J. Appl. Polym. Sci.*, Vol. 89, 2003, pp. 2418–2425.
[23] Qian, L. and Sun, G., "Durable and Regenerable Antimicrobial Textiles: Improving Efficacy and Durability of Biocidal Functions," *J. Appl. Polym. Sci.*, Vol. 91, 2004, pp. 2588–2593.
[24] Maibach, H. I., Feldman, R. J., Milby, T. H., and Serat, W. F., "Regional Variation in Percutaneous Penetration in Man," *Arch. Environ. Contam. Toxicol.*, Vol. 23(3), 1971, pp. 208–211.
[25] Ragoucy-Sengler, C., Tracqui, A., Chavonnet, A., Daijardin, J. B., Simonetti, M., Kintz, P., and Pileire, B., "Aldicarb Poisoning," *Hum. Exp. Toxicol.*, Vol. 19(12), 2000, pp. 657–662.
[26] Andrawes, N. R., Bagley, W. P., and Herrett, R. A., "Fate and Carryover Properties of Temik Aldicarb Pesticide [2-methyl-2- (methylthio) propionaldehyde O- (methylcarbamoyl) oxime] in Soil," *J. Agric. Food Chem.*, Vol. 19(4), 1971, pp. 727–730.

[27] "Environmental Health Criteria for Aldicarb," 1991, International Programme on Chemical Safety (IPCS) Report, http://inchem.org/documents/ehc/ehc/ehc121.htm (Last accessed 7 Oct 2008.
[28] Dixit, V., Tewari, J. C., and Obendorf, S. K., "Identification of Degraded Products of Aldicarb due to the Catalytic Behavior of Titanium Dioxide/Polyacrylnitrile Nanofiber," *J. Chromatogr. A*, Vol. 1216, 2009, pp. 6394–6399.
[29] ASTM F2130-09, 10, "Standard Test Method for Measurement for Measuring Repellency, Retention, and Penetration of Liquid Pesticide Formulation through Protective Clothing Materials," *Annual Book of ASTM Standards*, Volume 11.03, ASTM International, West Conshohocken, PA, pp. 449–454.
[30] Bartley, W. J., Andrawes, N. R., Chancey, E. L., Bagley, W. P., and Spurr, H. W., "Metabolism of Temik Aldicarb Pesticide [2-methyl-2(methylthio)propionaldehyde O-(methylcarbamoyl)oxime] in the Cotton Plant," *J. Agric. Food Chem.*, Vol. 18(3), 1970, pp. 446–453.

Performance of Protective Clothing and Equipment: Emerging Issues and Technologies
STP 1544, 2012
Available online at www.astm.org
DOI:10.1520/STP104483

Anugrah Shaw[1]

Protective Clothing for Pesticide Operators: The Past, Present, and Proposed Plans

REFERENCE: Shaw, Anugrah, "Protective Clothing for Pesticide Operators: The Past, Present, and Proposed Plans," *Performance of Protective Clothing and Equipment: Emerging Issues and Technologies* on 16 April 2011 in Anaheim, CA; STP 1544, Angie M. Shepherd, Editor, pp. 280–289, doi:10.1520/STP104483, ASTM International, West Conshohocken, PA 2012.

ABSTRACT: Pesticide operators have the risk of being exposed to chemicals while handling or spraying pesticides. Use of appropriate Personal Protective Equipment (PPE) is one of the methods for protecting the operators against harmful effects. This paper includes a historical perspective, current scenario, and proposed future plans. The historical perspective includes information on United States pesticide regulations; pesticide safety/stewardship programs; and protective clothing studies and standards. The current scenario provides information on PPE regulation and the challenges it poses in the selection of protective clothing. The section on proposed plans outlines the process for implementation of international performance standards as the basis for providing a risk-based approach to selection of protective clothing. The process could be used as a model to develop recommendations for other types of PPE.

KEYWORDS: Protective clothing, pesticide operators, PPE

Introduction

Promotion of safe and judicious use of pesticides is essential to safeguard the health and safety of individuals responsible for pesticide application. Use of engineering controls, appropriate clothing, and good occupational hygiene assists in reducing the hazards associated with pesticide application. The "ideal protective clothing" would provide adequate protection and comfort. In addition, it would be easily available, culturally acceptable, affordable, and easy to clean. In

Manuscript received October 28, 2011; accepted for publication March 20, 2012; published online September 2012.
[1]Univ. of Maryland Eastern Shore, Princess Anne, MD, 21853

reality, however, decisions have to be made that balance the need for protection with other factors such as comfort, availability, cost, safety awareness, and cultural acceptance. Thus, the concept of one-size-fits-all does not work well to meet the needs of operators (applicators, mixer/loaders, equipment maintenance personnel) throughout the world. In order to make sound decisions regarding protective clothing, a risk-based approach for the selection is recommended; higher protection is required when there is a greater potential risk.

This paper includes a historical perspective of protective clothing, describes some of the current challenges, and outlines a process for implementation of performance standards as the basis for providing a risk-based approach to selection of protective clothing. It also proposes a global approach to address some of the challenges addressing the health and safety of pesticide operators. The proposed process could also be used to develop recommendations for other types of Personal Protective Equipment (PPE). Ultimately, a global multidisciplinary approach with collaboration among stakeholders such as the crop protection industry, fabric and garment manufacturers, standard development organizations, regulatory agencies, researchers, educators, and international organizations is needed to address the unresolved issues related to PPE.

Historical Perspective

United States Pesticide Regulations

Federal mandates require the use of appropriate PPE while handling and spraying pesticides. In the United States the history of pesticide production spans more than 100 years. Given in what follows are the major milestones:

- In 1910 the Federal Insecticide Act was passed by the U.S. Congress to protect the buyer from fraudulent and substandard products [1].
- The law, administered by the U.S. Department of Agriculture (USDA), required that pesticide products conform to the statements printed on their labels.
- In 1947 the scope of the Insecticide Act was expanded and the name changed to Federal Insecticide, Fungicide, and Rodenticide Act (FIFRA). At that time the label did not require the use of PPE while mixing, loading, and spraying pesticides.
- By the mid 1960s, serious environmental and human health concerns led to a stricter control over pesticide use in the United States.
- In 1970 enforcement of FIFRA was transferred from USDA to the newly created Environmental Protection Agency (EPA).
- In 1972 significant changes were made to FIFRA that included the following: Major changes to the label, including a requirement for the labels to provide information on use of PPE during mixing and loading as well as application of pesticide. Requirement for pesticide

manufacturers to provide documentation including risk to humans and the environment as part of the registration process.

- In 1992, the federal Worker Protection Standards were enacted, which have requirements for training of pesticide handlers on PPE, such as providing, cleaning, and maintaining PPE. It also includes provisions for PPE for early entry workers.

Pesticide Safety/Stewardship Programs

Globally, crop protection companies/associations, academia, government, and non-government organizations are working to address the health and safety issues of pesticide workers. In the crop protection industry the health and safety issues are typically addressed by the groups responsible for product registration, risk assessments, and stewardship. Similarly, the regional and international crop protection associations are dealing with stewardship as part of sustainable use programs for pesticides. PPE is an important component in stewardship. The European Crop Protection Association (ECPA) has conducted studies as part of the Safe Use Initiative in Southern Europe in which cotton/polyester garments with repellent finishes were used.

In the United States, the topics of selection, use, care, and maintenance of PPE are included in the pesticide applicator training conducted as part of the Pesticide Safety Education Program (PSEP). PSEP trains applicators handling restricted use pesticides or those commercially applied. PSEPs are part of university Cooperative Extension Services located in each state. They are partially supported by state governments and the EPA; support funding has dramatically been reduced in the past 10 years [2]. In the 1980s and 1990s, the clothing and textile extension specialists developed the bulletins and brochures on PPE selection, use, and care. A majority of these individuals have since retired and in general, positions were eliminated as part of reorganization.

Protective Clothing Studies and Standards

In the late 1970s and early 1980s research projects were initiated in the United States and Canada that focused on protective clothing for pesticide applicators. Studies conducted ranged from survey studies to factorial, design-based laboratory studies to some field trials. In 1981 a southern regional research project entitled "Effects of Functional Textile Finishes on Comfort and Protection of Consumers" was approved [3]. Some of the studies conducted as part of the five-year project related to protection against pesticides. In 1982 a north central regional research project entitled "Limiting Pesticide Exposure through Textile Cleaning Procedures and Selection of Clothing" was initiated that focused on issues related to protective clothing [3]. A survey was conducted in several states to understand the practices and attitudes of farm workers towards selection, use, and care of clothing used for pesticide application, and the effectiveness of laundering in removing pesticides from garments was studied. The pipette method to contaminate fabrics to be laundered was developed as part of this project. In addition, field studies were conducted using different analytical techniques to measure pesticide penetration and distribution pattern. Funding for the majority of the projects, including regional research projects, was provided by the USDA, through the Agricultural Experiment Stations at various land-grant universities. Some projects were funded by the EPA. The studies conducted in the 1980s were presented at various conferences and published extensively. A majority of the laboratory studies were conducted on a limited number of fabrics using a variety of pesticides. The aforementioned clothing and textiles extension specialists used the findings of the research to develop informational brochures on selection, use, and care of protective clothing. In many instances the studies conducted in the 1980s and early 1990s are still being used today.

In 1993, the EPA published a comprehensive guidance document entitled "Guidance Manual for Selecting Protective Clothing for Agricultural Pesticides Operations." In Section 4.2, Measures of Chemical Resistance [4] of this manual, concerns were raised regarding research-based information available for whole-body garments. Inconsistent methodology, variability in the challenge liquid, and extrapolation of information from studies with limited data were issues identified in the report. Over the past two decades, these issues have been addressed as knowledge has evolved through scientifically and statistically-based inquiry. The resulting data have led to development of test standards, to development of an extensive database, and finally to development of performance specifications. Issues identified in the EPA guidance manual and actions taken to address them are discussed in what follows.

Issue I: "The penetration literature reviewed for and cited in this document was generated by less than a dozen research groups. Since there is no standard penetration test, each group has followed its own variation of the above generalized procedure" [4]. In the United States, university researchers involved in multi-state projects, funded by the USDA, developed pipette and spray methods to measure pesticide penetration through fabrics. In 1997, a project entitled "Occupational Safety and Health Through the Use of Protective Clothing" included as an objective "To propose standard methodology for industry-wide consensus standards for chemical protective clothing" [5]. The pipette method was refined through initial inter-laboratory tests conducted by members of this research project. A draft was submitted to ASTM for consideration as a standard. In 1999, a study was conducted to compare the percentage penetration of the pesticide through the materials, using three standards/proposed standards developed in the United States and Europe [6] with a follow-up study that compared the modified methods [7]. The modifications for the pipette method were incorporated in the proposed ASTM draft that resulted in the development of ASTM standard F2130 [8]. Subsequently, the pipette method was submitted to ISO for consideration. During the draft stage, a gravimetric method for analysis was added and another inter-laboratory study conducted to further refine the method. ISO 22608 was approved as a standard in 2004 [9].

Issue II: "Furthermore, the pesticide solutions used by different researchers are rarely the same and are, in most cases, not described in sufficient detail as to source and chemical composition. This situation makes comparison of published results very difficult" [4]. To address the issue regarding use of consistent challenge liquid, input from formulation chemists was sought and laboratory studies were conducted at the University of Maryland Eastern Shore to compare percentage penetration using a variety of pesticides with different physio-chemical properties and concentrations. On the basis of the data, a formulation was selected as the challenge liquid used to test all fabrics in the database as well as for inter-laboratory studies. The challenge liquid was also used for testing of materials and seams for the performance specifications. Information on studies conducted and data analyzed for selection of challenge liquid are included in this paper.

Issue III: "…definitive comparison of the fabrics is difficult because the agricultural clothing research community has no standard test for measuring barrier effectiveness. Furthermore, the difficulty of this situation is compounded by varied practices among the researchers for describing the fabrics that they tested. Examples include:

- Not reporting properties such as thickness, weight, and air permeability
- Not identifying trademarked fabrics……
- Not identifying trademarked treatments/finishes..." [4].

Properties of over 130 fabrics were measured using the standard test methods. This allows for the comparison of properties that affect the protection and comfort of various fabrics. Detailed information for source, trade names/trademarks, and the trademark of finishes/treatments was recorded. A database was developed to manage the extensive compilation of data. Data analysis of pesticide penetration was used to establish the minimum requirements for the pesticide penetration of the performance specification standards.

Current Scenario

PPE Regulations

The following process is currently used to determine PPE requirements on a pesticide label in the United States and Canada:

- Predictive models based on operator exposure studies data are used to determine potential exposure [10]. Exposure studies conducted by Agricultural Handlers Exposure Task Force (AHETF) and the Agricultural Reentry Task Force (ARTF) were used to develop the predictive models for agricultural workers exposed to pesticides during regular work activities. The exposure data comprises the amount of active ingredient measured in the whole body dosimeters worn under the garment (in earlier studies patches were used). For AHETF studies the long-sleeved shirt and long pants worn by the participants varied as they were asked to wear their own clothing.

- Predictive models as well as toxicity data are used to calculate potential risk.
- On the basis of the calculations, PPE required when applying the product is approved as part of the registration or re-registration process. The current requirements are based on the type of garment, as opposed to actual fabric performance. Typical garment requirements on pesticide labels on containers of EPA approved products sold in the United States are as follows:
  - Long-sleeved shirt and long pants
  - Coverall worn over short-sleeved shirt and shorts
  - Coverall worn over long-sleeved shirt and long pants
  - Chemical Resistant Coverall (no criteria to determine chemical resistance)

Garments in the above categories vary considerably in the protection provided due to the vast differences in material and garment performance.

PPE Challenges

A requirement based on garment type makes it difficult for the trainers and users to select the appropriate clothing. Information from the 1980s continues to be used for many training programs because the performance-based studies cannot be adopted unless the garment type based requirements are revised. Barriers identified to effective use of PPE include problems determining suitable PPE; problems in determining if a coverall is chemical-resistant; and problems in determining a suitable cleaning procedure.

Moreover, as PPE is a small component of the training program, the trainers often have limited knowledge of protective clothing materials. They require reliable information that can be incorporated into training material that focuses on selection, use, and care of protective clothing for pesticide applicators. The current information used for training and certification is varied and in some cases conflicting.

A third challenge is a frequent disconnect between the risk assessors and risk managers. According to a risk assessor colleague, there are "…two camps that seem to like to keep themselves separate from each other—the Risk Managers and the Risk Assessors." Risk and exposure assessors are responsible for risk and assessment, characterization of the assessment, and determining required mitigation factors. Risk managers are responsible for training/informing the users. The risk assessors use risk assessment as a basis for requiring PPE, whereas the risk managers often use exposure scenario, warning signs, and over protection as the basis for training. For example, chemical-resistant coveralls are recommended for orchard spraying even though the label may require just long sleeves and pants. Note: Chemical-resistant coveralls are very rarely required.

Proposed Future Plans

Performance Specification Standards

In the last two decades, a systematic approach to development of performance-based specifications has been undertaken that now provides the opportunity to implement performance-based protective clothing requirements. In 2009, an ASTM standard based on laboratory and field data was approved as a performance specification [11], and an equivalent ISO standard was approved in 2011 [12]. The Code of Federal Regulations (CFR) 170 and 171 are also undergoing revision. Therefore, an opportunity exists to use the recently approved ASTM standard as the basis for conformity in the assessment of garments for pesticide operators. With the proposed CFR revision, each pesticide label could clearly indicate the level of PPE required for safe use of the product (e.g., protection levels 1, 2, or 3). Performance specifications include minimum requirements for three levels of protection. Level 1 garments, with performance similar to those used for exposure studies, would be required for lower risk, and Levels 2 and/or 3 when higher levels of protection are necessary. The following are being proposed to address protective clothing issues in the United States:

- Development of a standard by ASTM International to certify protective garments as Level 1, 2, or 3
- Standard to be used to certify a garment. Standard would require information on use, care, and maintenance to be provided with the garment.
- Revision of the PPE requirements on pesticide labels. Risk assessors would specify garment level on the pesticide label to enable users to select appropriate PPE.
- Development of training materials based on revised standards to be used by risk managers for training.

The process, which includes development of a database, analysis of data, and development of minimal requirements based on laboratory and field data, can be used to develop simpler, research-based criteria for glove requirements.

Proposed Global Approach to Address PPE Challenges

While significant progress has been made in the area of protective clothing for pesticide operators over the past two decades, many unresolved challenges continue to compromise the health and safety of pesticide operators throughout the world. PPE for agricultural workers is often not high enough on the priority list for most organizations; resources allocated to address PPE are often limited. A global approach to address the health and safety issues of pesticide operators might provide the synergy required to pool several "limited resources" in terms of funds, expertise, and interest. Collaboration among government and non-government organizations, standards organizations, crop protection companies/associations, and academia to harmonize PPE regulations and standards may resolve many of the health and safety issues affecting pesticide operators. Recommendations based on laboratory and field data would facilitate the use of global information to create solutions acceptable at the local level (technical information based on global input, customized based on local needs). An interactive online system would serve as a vehicle to gather, analyze, and disseminate information, as well as highlight issues that need to be addressed.

The proposed consortium approach would do the following:

- Facilitate networking among groups that will assist in finding solutions for problems related to health and safety of pesticide operators;
- Improve communication between risk assessors and risk managers/trainers so that a risk-based approach can be used for selection of PPE;
- Establish a mechanism for decision-making at the local level based on accurate information available globally;
- Allow multinational organizations to identify solutions suitable for different regions/countries around the world;
- Establish a cost-effective system so that each group will not have the burden of gathering all the information; and
- Provide readily accessible garment details (including performance level, garment design, source, cost, country in which it is available) through an online data system.
- A universal communication system would provide accurate information on the use of performance-based specifications that take into consideration the protective properties of the fabrics. It would streamline the training materials, with the primary message being, "Select PPE based on requirements stated on pesticide label." Note: Use, care, and disposal of the PPE would be included as part of the user instructions provided with the PPE. Consistent and accurate information will assist the users and purchasers in making informed decisions. Development of standards would also establish compliance with the Food and Agriculture Oganization of the United Nations International Code of Conduct on the Distribution and Use of Pesticides, which states that "Government and industry should cooperate in further reducing risks by: promoting the use of proper and affordable personal protective equipment" [13]. Standards can also serve as a basis for PPE requirements for European and Global Good Agricultural Practices.

References

[1] U.S. Environmental Protection Agency, Sept 15, 2011, "FIFRA Statute, Regulations & Enforcement," http://www.epa.gov/compliance/civil/fifra/fifraenfstatreq.html (Last accessed May 15, 2012).

[2] "Scientists Point to Precarious State of U.S. Pesticide Safety Education Program," (2011), http://www.wssa.net/WSSA/PresRoom/WSSA-PSEP.htm (Last accessed May 15, 2012).

[3] Shaw, A., "CSRS-Funded Research on Pesticide Contaminated Textiles," *Book of Papers, International Conference, American Association of Textile Chemist and Colorist*, October 1–3, 1990, Research Triangle Park, NC, American Association of Textile Chemists and Colorists, Boston, MA, 1990, pp. 256–263.

[4] "Guidance Manual for Selecting Protective Clothing for Agricultural Pesticides Operations," U.S. Environmental Protection Agency, #EPA 736-B-94-001, Section 4.2.1, pp. 32–33, 1993.

[5] "Occupational Safety and Health through the Use of Protective Clothing," *NC170*, www.umes.edu/nc170 (Last accessed).

[6] Shaw, A., Cohen, E., Hinz, T., and Herzig, B., "Laboratory Test Methods to Measure Repellency, Retention and Penetration of Liquid Pesticides through Protective Clothing: Part I Comparison of Three Test Methods," *Text. Res. J.*, Vol. 71, No. 10, 2001, pp. 879–884.

[7] Shaw, A., Cohen, E., and Hinz, T., "Laboratory Test Methods to Measure Repellency, Retention and Penetration of Liquid Pesticides through Protective Clothing: Part II Comparison of Three Test Methods," *Text. Res. J.*, Vol. 74, No. 8, 2004, pp. 684–688.

[8] ASTM F2130-01, 2003, "Standard Test Method for Measuring Repellency, Retention, and Penetration of Liquid Pesticide Formulation Through Protective Clothing Materials," *Annual Book of ASTM Standards*, Vol. 11.03, ASTM International, West Conshohocken, PA, pp. 1558–1561.

[9] ISO 22608:2004, "Protective Clothing—Protection Against Liquid Chemicals—Measurement of Repellency, Retention, and Penetration of Liquid Pesticide Formulations Through Protective Clothing Materials," International Standards Organization, Geneva, Switzerland.

[10] "Pesticides: Regulating Pesticides," United States Environmental Protection Agency, Washington, DC, http://www.epa.gov/PR_Notices/pr2007-3.htm (Last accessed March 20, 2012).

[11] ASTM F2669-09, "Standard Performance Specification for Protective Clothing Worn by Operators Applying Pesticides," *Annual Book of ASTM Standards*, Vol. 11.03, ASTM International, West Conshohocken, PA, pp. 526–531.

[12] ISO 27065:2011, "Protective Clothing—Performance Requirements for Protective Clothing Worn by Operators Applying Liquid Pesticides," International Standards Organization, Geneva, Switzerland.

[13] Food and Agriculture Oganization of the United Nations, n.d., "Reducing Health and Environmental Risks," in *International Code of Conduct on the Distribution and Use of Pesticides* (Revised version), Publishing Management Service, Information Division, FAO, Rome, Italy, 2005, ftp://ftp.fao.org/docrep/fao/009/a0220e/a0220e00.pdf (Last accessed May 15, 2012).

Performance of Protective Clothing and Equipment: Emerging Issues and Technologies
STP 1544, 2012
Available online at www.astm.org
DOI:10.1520/STP104081

Sihong Yu,[1] *Megan Strickfaden,*[2] *Elizabeth Crown,*[2]
and Sara Olsen[2]

Garment Specifications and Mock-ups for Protection from Steam and Hot Water

REFERENCE: Yu, Sihong, Strickfaden, Megan, Crown, Elizabeth, and Olsen, Sara, "Garment Specifications and Mock-ups for Protection from Steam and Hot Water," *Performance of Protective Clothing and Equipment: Emerging Issues and Technologies* on June 16–17, 2011 in Anaheim, CA; STP 1544, Angie M. Shepherd, Editor, pp. 290–307, doi:10.1520/STP104081, ASTM International, West Conshohocken, PA 2012.

ABSTRACT: This work is part of a larger project to develop improved, innovative textiles and garments for workers in the oil industry. Use of steam and hot water in extracting bitumen from oil sands, in oilfields, and in plants has become extensive in recent years. Personal protective equipment (PPE) is currently well designed to protect against hazards such as flash fire and radiant thermal exposures; however, due to an increase in workplace injuries reported in the last five years, including incidents of steam and hot water burns, further protection for workers is considered a priority. Steam used at sites is up to 375°C and under extreme pressures of up to 13 500 kPa; hot water is under significantly less pressure but is 80°C–90°C, which is well above temperatures that result in partial thickness burns. This research presents several stages of the design process: (1) identifying specific tasks which expose workers to steam and hot water; (2) setting the criteria for determining the needs addressed in specific types of PPE; (3) developing specifications for PPE garment design; and (4) presenting a preliminary mock-up garment. A multi-method research approach was taken that included observing, photographing, interviewing, and analyzing the movements of workers in western Canada. Results indicate extreme workplace conditions both indoors (up to 40°C in summer) and outdoors (down to −30°C in winter). Hazardous activities include steam quality sampling, cleaning filters and sludge traps, loading and unloading hot water, opening traps

Manuscript received May 31, 2011; accepted for publication March 26, 2012; published online August, 2012.

[1]Dept. of Human Ecology, Univ. of Alberta, Edmonton, Alberta, Canada (Corresponding author), e-mail: sihong@ualberta.ca

[2]Dept. of Human Ecology, Univ. of Alberta, Edmonton, Alberta, Canada

and high pressure steam valves, working very close to hot valves and pipes, and spraying steam onto wellheads. Specifications for improved garment design and mock-up garments were developed based on analysis of interviews and observations. This work also contributes insights into the process for understanding the complexities of a workplace environment with specific hazards and worker needs.

KEYWORDS: multi-method, design process, hot water and steam hazards, oilfields, PPE

Introduction

The focus of this paper will consider a holistic approach to understanding worker protection from exposure to hot water and steam hazards within the context of task performance on the job site. This work is part of a larger project aimed at specifying and developing improved innovative protective materials, textiles, and garments for workers in the oil industry.

This research presents four parts of a process towards the design of personal protective equipment (PPE) to protect workers in the oilfields from steam and hot water exposure. These include: (1) identifying general environmental conditions and specific tasks exposing workers to environmental hazards; (2) understanding the needs of workers for specific types of PPE (e.g., physical, sociocultural); (3) developing specifications for PPE garment design; and (4) presenting preliminary mock-ups toward prototype development.

Recently the use of steam and hot water in extracting and producing oil has become extensive, especially in bitumen extraction from oil sands and in oilfields and plants producing heavy oil. PPE is currently well designed to protect against hazards such as flash fire and radiant thermal exposures; however, due to an increase in workplace injuries reported in the last five years, including incidents of steam and hot water burns, further protection for workers is considered a priority. Steam used at sites (Fig. 1) is up to 375°C and under extreme pressures of up to 13 500 kPa; hot water is under significantly less pressure but is 80°C–90°C, which is well above temperatures that result in partial thickness burns.

Research Problem

Workers engage in potentially hazardous tasks that require protection for safety, ease of mobility, and psychological comfort in the extreme environments encountered in the oil and gas sectors. Currently, workers are well protected from flash fire by PPE such as coveralls, gloves, and goggles; however, there is inadequate protection against steam and hot water, which puts them in danger of burn injuries when performing tasks such as manipulating high-pressure valves, checking steam quality, and spraying wellheads. Steam and

FIG. 1—*Oil plant is shown immersed in steam.*

hot water are commonly present in the ambient atmosphere around the pipes and valves in oil refining and extraction facilities as well as in the field. Although training practices and warnings to address these hazards are a regular part of administration, and workers are required to wear protective clothing as the last defense to ensure their safety, issues such as high cost, inadequate protection against steam and hot water, and lessened mobility with existent protective clothing all demonstrate a need for new protective clothing designs that complement current PPE.

Three key problems are identified in this user-centered research: the hazards in the working environment and conditions within; workers' needs and their attitudes towards protective garments; and design features and specifications for protective garments against steam and hot water.

Background

Clothing is the "portable" environment and is as intimate as the second skin to humankind [1]. A growing consciousness of function, protection, and comfort related to safety concerns contributes to an extensive body of research in functional and protective clothing. PPE covers a wide range of items: ensembles such as coveralls, coats, and pants; accessories such as hoods, boots, and gloves; equipment such as wireless radios; and special equipment such as gas masks [2]. Although there is little current research of the work environment and specific tasks particular to workers in the oil and gas sectors, there has been extensive research into protective clothing, including issues around mobility, functional fit, comfort, and some research into detail design. Understanding concerns around mobility, functional fit, comfort, and detail design relates directly to developing specifications for PPE and design outcomes.

Mobility

Mobility of the wearer is significant to the design of garments for protection. Prior research that uses wear trials and looks at real working environments showed that garments have the potential to impair the wearers' work productivity; layers of fabric add bulk and stiffness which leads to muscle stress when performing tasks [1–5]. Mobility impairment can be the result of fabric selection, garment ease, and garment construction. In garment design there are trade-offs between fabric stretch, stability, and durability. Fabrics used in protective clothing usually have low stretch ability, and this is often even lower when a protective coating is applied. In the case of designing for protection, according to Huck et al., garment construction for ease is *"the difference between the size of the garment and the size of the wearer"* [6]. Their research determined that placement of ease, in the form of extra fabric, can affect wear mobility and acceptance. Underarm ease is of vital importance for wearers who have to perform frequent arm and shoulder movements [1], which means both the width and length direction need to be taken into account. It is clear that the amount of ease and the allocation of ease in design can influence a person's level of mobility.

Functional Fit

Van Schoor [7] states that functional fit is relative to mobility and dependent on the purpose of the garment. For excessive range-of-motion, garments need to be loose fitting to accommodate a wider range of people; however, for protective wear there can be a dilemma between adding more ease and limiting fabric for safety concerns. Adams and Keyserling [8] note that undersized garments have significantly reduced hip flexion, while oversized garments (with too much fabric or ease) can create further safety issues.

To quantify wearers' mobility and functional fit, a method of measurement of range-of-motion (ROM) has been developed, which refers to the possible amount of movement at a joint [3,5]. ROM can vary from heredity, age, gender, physical and psychological factors, posture, and occupation [1]; besides a general ROM measurement, specific ROM data also need to be obtained when performing job-related movements. Research in ROM measured movement in reaching and squatting [9], shoulder flexion, and arm stretch [5] and identified that task-related movements were dynamic and could vary from static to general movement.

Comfort

Comfort is closely related with and affected by mobility and functional fit in the evaluation and design of protective clothing. Hollies and Goldman [10] define comfort as *"the sensation of contented well-being and the absence of* *unpleasant feelings*." While comfort is largely an individual, subjective measurement, several objective parameters can be referred to, such as thermal properties, moisture properties, fabric characteristics, and fiber characteristics. Some subjective parameters have also been defined relating to physical comfort (functional fit, mobility/restriction) by measuring ROM and physiological comfort (heat strain) and by measuring temperature, heart rate, and sweat loss.

Comfort factors may be evaluated subjectively by following ASTM practices for qualitatively evaluating the comfort of chemical-protective ensembles, where people are observed when performing routine work and asked to respond to evaluation questions [11]. Wear acceptance scales or evaluation protocols have been developed to include key factors such as flexibility, ease of donning and doffing, fit, likes/dislikes, etc.

Detail Design

The selection of specific features designed into a garment is significant to its success in a use environment. Along with a need for garments to support activities at work by not impeding mobility, people need garments to be comfortable and the garment needs to be functional. To better understand the effects of various detail designs, Tan et al. [6] and Huck and Kim [12] established interaction matrices for garment design for flight suits and grass fire fighting ensembles respectively, in which they demonstrate how detail design specifications may conflict with each other. Tan et al. showed an example of pockets on flight suits where pilots indicated that too many pockets affect the neat appearance, yet many pockets were preferred over neat appearance [6].

On the basis of the research reviewed above, it is evident that the design of protective clothing is an integral process that involves issues related to the use environment and to the interfaces between people and garments. Various techniques have been identified to better understand these issues, such as ROM measurement and interaction matrices. Even so, in order to develop garments or a garment system that fulfills the multiple layered issues, and design clothing that is innovative, an in-depth multiple method process is required to better understand workers' mobility and comfort needs.

Five-Fold Multiple Methods Approach

The research needs to take a holistic approach to clothing design in the development of special purpose apparel [8]. That is, developing a functional design must be user centered where, for example, specific measurements of mobility and understandings of use environment, including worker tasks, need to be explored [13]. Thus, a multiple method approach is taken; i.e., complex design problems and environments require various lenses toward understanding the depth and breadth of human interface that occurs within, in order to design a product that is suitable [14]. This approach involved five distinct techniques: focus group interviews (detail design), field observation with note taking and photography (use environment, task analysis), interviews (use environment, garment design), photography of mobility (garment-person interface), and precedent-based design research (existent designs).

Focus group interviews were completed at an early stage of the research process in order to identify key issues related to detail design (e.g., likes, dislikes) and to gain insights into workers' attitudes toward protective clothing. Male and female workers were recruited as participants and guiding questions aided discussions focused on personal experiences and opinions about PPE. Details on workers' perceptions around the work environment and their PPE is recorded on audiotape and transcribed verbatim.

Field observation was conducted at four worksites (two plants, two in the field) operated by two firms in two provinces in western Canada. During the field observation, notes were taken using observation sheets. Photographs were taken of routine tasks that involve steam or hot water exposure. Nearly 500 photographs were taken, which were analyzed in detail to understand sequences of working procedures, interfaces between different garments (e.g., gloves-sleeve, boot-pants), donning and doffing of garments, and more. Through extensive photo analysis, potential hazards such as sloppy use of current PPE and the challenges of using specialized garments for additional protection were revealed.

Interviews were completed with 13 participants at the four worksites following each field observation in order to gain a deeper understanding of the use environment and garment design. These interviews provide insights into the physical working environment and the cultural aspects of workers' perceptions of safety that play a role in designing protective clothing.

Precedent-based design research processes [15] were followed in order to better understand designs that are currently used and available on the market. Detailed documentation and analysis of industry workwear, firefighter garments, and outdoor wear were itemized in order to analyze similar garments and ones that incorporate innovative design solutions (Fig. 2).

Detail design, closure systems, and interfaces are the focus of this analysis. Precedent-based research includes looking at actual garments and photographing these being worn as well as the design details. Observation sheets are used to detail all aspects of the individual garment. The photographs and observation sheets are analyzed systematically.

Analysis of the data produced from this multiple method approach is data-driven where information is grouped, cross-referenced, and placed into themes (Fig. 3) to better understand worker needs.

This five-fold approach considers use environments, potential hazards, user activities, and user needs in a comprehensive and triangulated manner that reveals a great deal about current PPE, users, and the context of working within the oil and gas sectors.

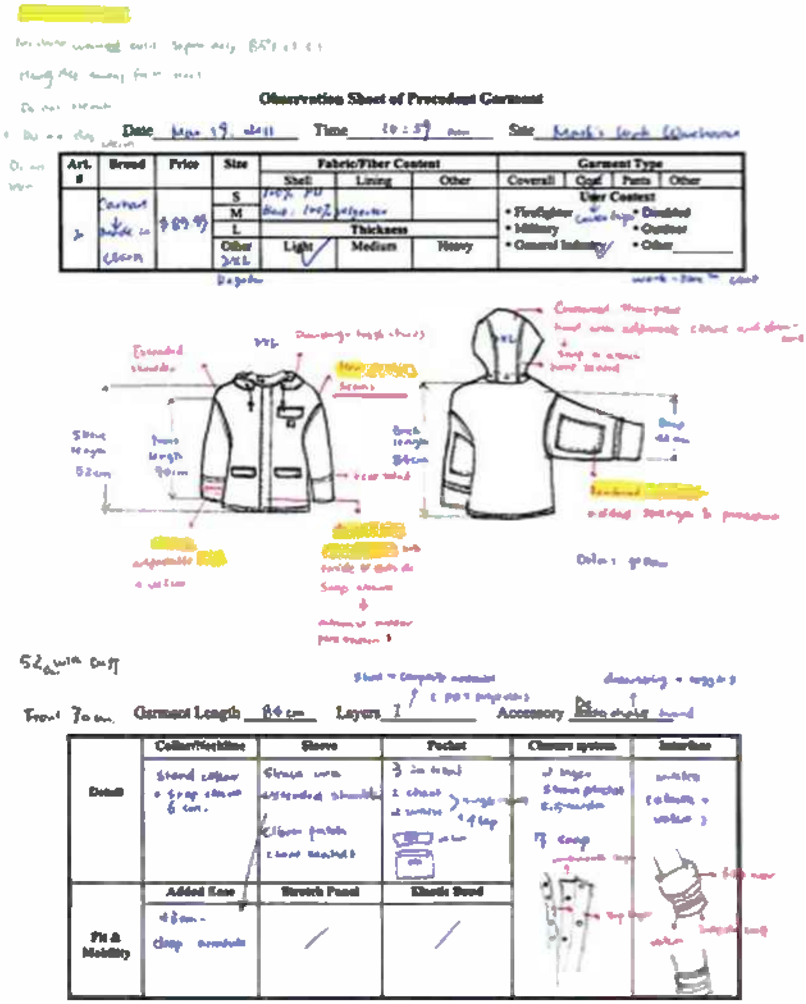

FIG. 2—*Observation sheets for precedent-based research.*

Results

On the basis of anecdotal information, industry reports, and this research, it is clear that it is highly probable that workers will encounter steam and/or hot water in the work setting sometime during their workday. There are routine activities that expose people to hazards, as well as tasks that are completed less often. Along with identifying the general work environment, our results identify specific work tasks, show how present PPE is used, recognize mobility requirements, and determine design details.

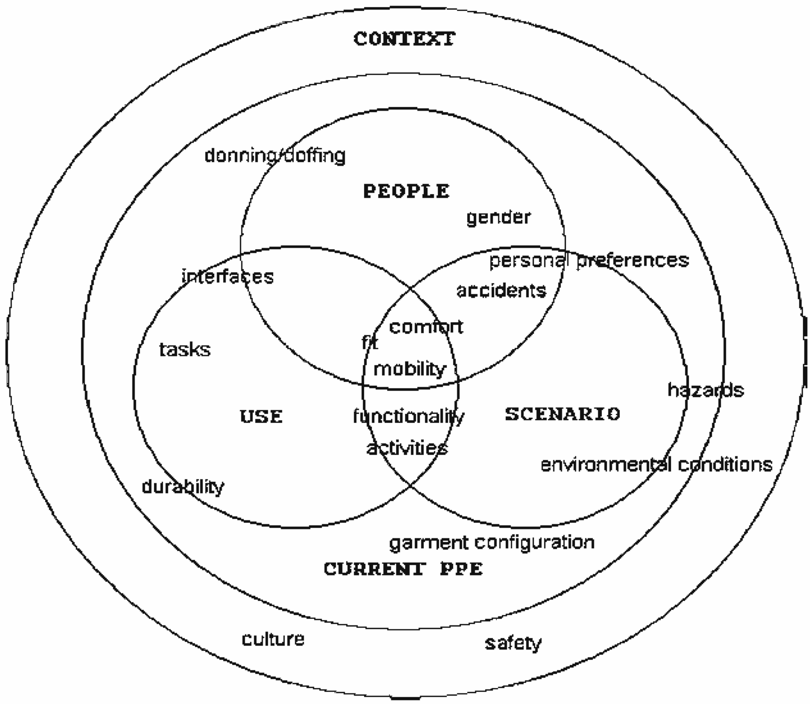

FIG. 3—*Data-driven themes derived from the five-fold research process.*

General Work Environment

Results indicate extreme workplace conditions both indoors (up to 40°C in summer) and outdoors (often down to −30°C and occasionally colder in winter). Workers frequently transition from inside to outside environments as well as getting in and out of equipment (e.g., trucks) to accomplish work duties. Participants wore regular aramid coveralls, or coveralls of aramid with PTFE membranes. Those wearing regular coveralls donned knee-length coats of aramid/PTFE for water handling and either coats or jacket and overalls of FR PVC/polyester for handling steam (Fig. 4). A variety of mostly cotton garments are worn under the PPE. Hardhats, protective leather or rubber boots, goggles, hearing protection, and insulated rubberized gloves are also worn, as are full-face shields for some tasks. The aramid/PTFE garments were generally considered comfortable in winter but too hot in summer if worn for more that 10–15 min. Participants indicated concerns about the effectiveness of aramid/PFTE after several cleanings. In general, the PVC garments are disliked for lack of comfort and stiffness in winter.

The overall work environment is complex because of the various workers, different tasks, and individual working styles. At the same time PPE is

(a)

(b)

FIG. 4—*Typical industry workwear and work environments.*

relatively standardized and involves extensive safety training. PPE is considered the last line of defense in protecting the worker from hazards, while being intrinsic to the use scenario (Fig. 5).

In work practice standard PPE are flame-resistant coveralls and steel-toed boots with additional protection being worn during certain tasks. For example, when loading water from a truck, workers are required to wear additional protection from hot water (e.g., long coat), eye protection (e.g., goggles), and gloves. Although protective equipment is a requirement on all worksites, not all employers provide it for free. Some employers provide financial support while most contract workers need to purchase their own PPE. For financial reasons, it is apparent that contract workers who have to buy protective clothing themselves may purchase the bare minimum. Workers who are on site within an intense safety culture are more likely to adhere to specific details on exactly how to use the PPE (e.g., putting cuff over or under gloves).

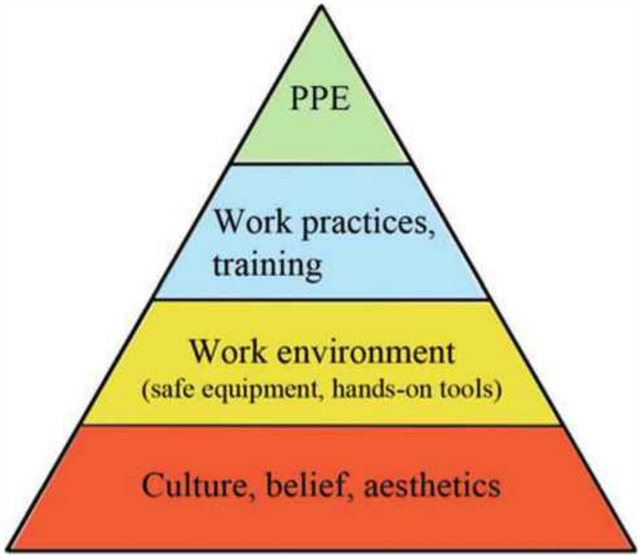

FIG. 5—*Different levels/defense lines of protection.*

Specific Work Tasks

Oilfields, refining, and extraction plants are places where steam and hot water injuries most likely occur in conjunction with specific work tasks. Six main work tasks are identified and described in Fig. 6.

These work tasks expose workers to a variety of different hazards for different lengths of time. Some tasks are high risk, such as spraying steam onto wellheads, which requires concentration and attention. In a recent industry report [16], a worker was severely burned during this activity. On the basis of analyzing the tasks and associated hazards, the most vulnerable parts of a worker's body while wearing current PPE are the wrists and hands, the feet and ankles, the neck and lower face, and most of the front of the torso.

Highlights of Observed Use

In observing how workers actually wore and used their PPE, some problematic areas were revealed. Workers who had to don and doff additional gear ran into challenges because of limitations of the garments, especially when footwear was involved. Figure 7 shows how the leg of a pair of overalls was torn when attempting to put them on and how the worker had to take his boots off to get into the gear.

It was also observed that workers frequently took off their gloves when performing certain tasks, such as connecting hoses. In several instances, workers were observed putting gloves on and off dozens of times during a single

#	Description of the task	Illustration
1	**Steam quality sampling** This requires the worker to perform with gloves on, and the sleeves and gloves should be adequately interfaced. The valves are required to be checked closed after sampling.	
2	**Cleaning filters and sludge traps** This work also requires worker to wear gloves, and in the illustration the worker is wearing a protective coverall over his working garments as a protection.	
3	**Loading and unloading hot water** This task is to load and unload hot water (connect and disconnect hoses) from boiler tank to truck and from truck to oil storage tanks. There's a danger if the hot water split out by pressure or by improperness to connect/disconnect the hoses.	
4	**Opening traps and high-pressure steam valves** As the positions of the valves are different it require different movement and position of the workers to manipulate on it. The danger comes from the high-pressure steam which has a tendency to blast and hurt directly onto workers.	
5	**Working close to hot valves and pipes** This task is hazardous for both conductive and radiant heat exposure near the hot valves and pipes. There is also the danger of steam blast during the task activity.	
6	**Spraying steam onto wellheads** This task is often performed in the field to defrost the wellheads in extreme cold weather, under which condition the protective clothing not only need to protect the worker from steam, but also to keep the wearer warm and comfort.	

FIG. 6—*Tasks exposing workers to steam and hot water.*

task because they apparently required additional dexterity for parts of the task. Along with being exposed during parts of the task, workers paid no attention to whether gloves were put over or under the cuffs of their coveralls or coat.

While performing certain kinds of tasks, workers carry, hold, or hang a significant amount of equipment. This equipment includes tool belts, safety harnesses, gas detectors, wireless radios, cell phones, pens, clipboards, and other miscellaneous equipment. Sometimes pockets are used for storage, while at other times additional PPE (gloves, ear and eye protection, etc.) is carried.

FIG. 7—*Worker having difficulty donning and doffing protective overalls.*

Finally, the overall aesthetic of people working in the oil and gas sector is of a strong and tough worker. That is, acceptable PPE has the aesthetic of being hardwearing, durable, and functional.

Mobility Requirements

Linked to the various tasks that are performed in the oil and gas sector is the need for a range of movement that poses a high demand of mobility on the protective clothing worn by workers. For instance, high-pressure swing/wheel valves are at different heights (e.g., at knee, at waist, above head), which means that working on valves involves climbing under, and even laying on backs to complete certain tasks. That is, workers need to climb, stretch, reach, and extend their bodies in a range of movement while wearing their protective garments. Figure 8 shows a sample of movement analysis of five different positions and the implications for garment design.

In general it was observed that workers had reasonable mobility while wearing their current PPE; however, for garments that are used by many workers (one size fits all) the fit causes mobility issues. On smaller workers the garment can be bulky and bunch up, which reduces movement and dexterity; and on larger workers the garment can tear, which causes a failure in protection. In addition, when workers bend down or squat when wearing an overcoat-styled garment, it opens at the front. This leaves a large gap that decreases the level of protection below the bottom closure (exposing the lower torso and upper legs) and above the upper closure (exposing the neck and a small portion of the upper torso).

Design Details

Design details were discussed by our participants and observed through use. For instance, interviews reveal that adjustable hook and loop to cinch or fasten sleeves is considered very functional and preferred over snaps or buttons. One of the main hazards we identified, while observing a worker spraying hot steam onto a wellhead, was an improper interface between coat sleeves and gloves.

#	Position & Design Implications	Movement
1	This position is to raise one arm to a 90-degree angle to the torso. The coverall will shift up, in which ease at the underarm is required. It is one of the most common movements when performing tasks like working on valves.	
2	This position is to extend arms to both sides. Ease at underarm is also necessary for wearer to extend their arms with least restriction. The chest width of the garment need to be adequate but not too much, which will leave bulky appearance at the front and lower the level of protection.	
3	This position is to fold two arms at the chest. Ease at the back and underarm is required for least restriction. This movement can cause a gap between garment front and the chest if there's no collar closure.	
4	This position is to turn to sideways with feet still on ground. Ease at the back is necessary for mobility. Also, this needs the adequate space for the armhole so that shoulder can move freely.	
5	This position is to stretch both arms to different angles. When performing tasks on overhead valves or pipes, the workers need to stretch their arms above head. This needs a large range of arm movement from down to up.	

FIG. 8—*Movement analysis and design implications.*

The resulting danger would be for steam or hot water to leak or flow into the sleeves. Other observed design details were improper closures at the neck and collar, workers not using hook and loop closures at wrists and ankles, and closures, in general, not being used. Finally, it was clear through observation that current PPE does not have adequate storage for equipment needed on the job.

Precedent-based design research revealed that there are many different details that are currently incorporated into overcoats and coveralls that protect various workers (e.g., firefighters, construction, oil). For example, various reinforced details assist in protecting workers, such as elbow and knee patches; functional fit is typically improved with elastic waistbands or tabs to cinch-in the garment and prevent bunching. Closure systems at the front of garments typically use double-front storm plackets and zipper/hook and loop combinations. More innovative solutions assisting in thermal comfort and regulation are underarm ventilation details and storm flaps on coat backs. Finally, solutions for protecting the wrists include cuffs that interface with gloves, including thumb-holds and multi-layered cuff details.

Specifications and Design Proposition

On the basis of our extensive user-centered research approach, design recommendations and specifications were developed. To begin, it is clear from our research that one garment will not fulfill the needs of all workers within this industry. As a result, specifications include a level 1 and level 2 garment or garment system. The level 1 system includes garment(s) that can be worn on site most of the workday, whereas the level 2 system is used for short-term situations (e.g., sampling) where workers only need to wear protection from steam or hot water for short periods of their workday. Current PPE uses a similar level 1 and level 2 system where workers wear standardized daily protection and put on overcoat-styled garments when they need additional protection.

Clothing Configuration

Design recommendations and specifications as a result of our study are as follows. The protective clothing shall provide the workers protection for upper and lower torso, neck, and extremities. Head, ears, hands, and feet shall be protected by other PPE, such as helmet, hood, face screen, protective glasses, protective gloves, boots, etc., but are excluded in the clothing requirement. The protective clothing shall comprise one of the following choices:

(a) one-piece coverall that covers upper and lower torso, neck, arms, and legs;
(b) two-piece suit provided with an interface area (i.e., short coat with bib pants); or
(c) a clothing assembly that has a series of outer and undergaments to be worn together.

Clothing Components

Collar—Coat collars shall remain vertical when rolled up and shall cover around the neck with a proper closure (e.g., snap, adjustable hook and loop, zipper). Any undergarment collar shall be either a stand collar or roll collar that can cover the neck when the garment is worn separately without the coat, and should also remain vertical when rolled up.

Front Placket—The front opening of the clothing shall have a form of closure with a hidden-button placket or an underneath extension to form an interface. Short/long coats shall be able to close at least from the neck to the waist when wearing overalls or coveralls underneath. Coveralls shall be able to close up to the collar.

Sleeves—Any sleeve hem shall have a proper form of closure (i.e., adjustable hook and loop, snap). Coat sleeves can have no cuff, but shall be able to go either over or inside the gloves. Coverall sleeves shall have a cuff and a closure or elastic tape that can be fit into gloves.

Pants—Any pants hem shall have a form of closure (usually adjustable hook and loop). The pants that are worn with coats shall have a bib (overall) that can provide adequate overlap with the coat.

Pockets—All external pockets shall have a means of fastening them in the closed position by (*i.e.*, flap, snap, hook and loop), to prevent entry of burning debris. They shall provide workers a convenient place for tools and other devises.

Adequate Interfaces

Upper Torso Interface—The upper torso shall be partly covered by a pant bib (overall) if wearing a coat. If wearing a coverall or coat over undergarments, they shall all close properly.

Lower Torso Interface—Our photo analysis revealed a high frequency of inadequate lower torso interface due to overcoat gaping open especially when walking, bending, or squatting down. In this case, the coat could provide more mobility than the one-piece coverall as it did not restrict the crotch area or the back; however, it shall be worn together with bib pants or coverall underneath it to form an adequate interface.

Glove and Sleeve Interface—The glove and sleeve interface may need to vary for different tasks that require different levels of protection. For general tasks, the glove tops or cuffs can go under the coat sleeve. For a more potentially hazardous task, the gloves shall be thicker and go outside the sleeve.

Pants Hem and Boots Interface—Currently the pants are worn over the boots, causing problems in donning and doffing. Design details such as an opening with snap or hook and loop, or godets with zipper shall be applied to improve the ease of donning and doffing.

Proper Closure System—The neck, front, sleeve, and hem shall have a proper form of closure system (i.e., adjustable hook and loop, snap, zipper) to ensure adequate protection for neck, chest, wrist, and foot.

Following the development of these specifications, they were itemized into a list of design criteria and a design brief was created in order to develop a mock-up. The design criteria are shown in an interaction matrix to better understand which items conflict with one another (Fig. 9).

As a result of these specifications and design criteria, a preliminary mock-up has been created for a level 2 overcoat as the first design proposition. The design features of this garment attempt to combine innovative solutions for the safety and practical needs of workers in this industry. Design details include the following:

- Standing collar with snap closure and chin guard
- Extended shoulders and deep armhole for extra room for layering
- Underarm stretch gusset for improved mobility and heat dissipation
- Interior cuff (neoprene or Kevlar) with adjustable hook and loop tab
- Larger or more storage pockets with cinch belt at waist
- Dropped hem to cover back waist
- Venting with storm flap at the upper back
- Wider pant leg with closure and/or flared insert with adjustable hook and loop tab

Figure 10 shows an illustration of the proposed design, which is to be used in combination with protective coveralls or overalls. This design incorporates many significant features including a unique cuff system that does not allow steam or hot water to flow inside the sleeve or glove, underarm and back venting to improve thermal comfort, a standing collar for improved protection, a

Design Criteria	1	2	3	4	5	6	7	8	9	10	
1. Protect from steam/hot water	0	0	0	0	0	0	0	1	0	0	
2. Cover torso and limbs	0	0	1	1	1	0	0	1	0	0	
3. Easy to don/doff	0	1	0	0	0	1	0	0	1	0	
4. Allow body movements	0	1	0	0	1	0	0	0	1	0	
5. Proper fit	0	1	0	1	0	0	0	0	0	0	
6. Provide neck protection	0	0	1	0	0	0	0	0	0	0	
7. Neat appearance	0	0	0	0	0	0	0	0	0	2	
8. Thermal comfortable	1	1	0	0	0	0	0	0	1	0	
9. Adequate interface at front, wrist and feet	0	0	1	1	0	0	0	1	0	0	
10. Many pockets and loops	0	0	0	0	0	0	2	0	0	0	

* *0 = no conflict 1= accommodation 2 = conflict*

FIG. 9—*Interaction matrix of design criteria.*

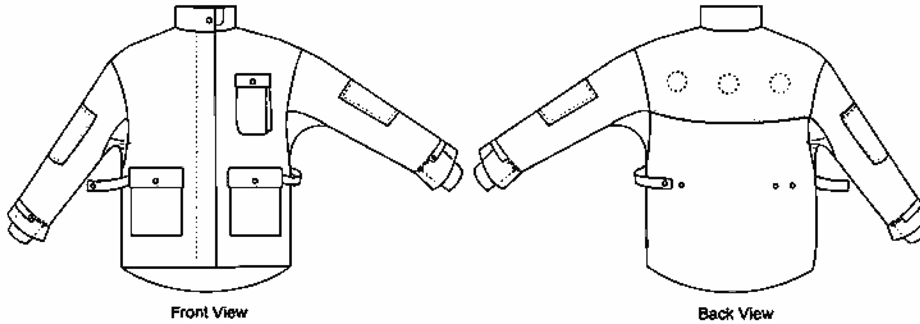

FIG. 10—*Sketch of preliminary overcoat design.*

dropped hem for comfort when sitting in vehicles or transitioning on work sites, and improved storage for personal and work equipment. The overall aesthetic of the overcoat maintains the hardwearing look of the workplace while adding sportswear-like features that provide additional functionality.

Conclusions and Future Research

Workers in the oil and gas sector are often exposed to hazardous materials and equipment, and as a result PPE is essential for protection. This paper represents ongoing research into the growing needs of oil industry workers and includes significant insights into the complexities of a workplace with specific tasks, hazards, and workers' needs. We have developed design recommendations and specifications to design better garments for higher levels of protection at the work place. Finally, we have presented an early design proposition that begins to address the various facets of oil industry workers' use environment, interfaces with current PPE, and addresses workers' needs, wants, and expectations. Future work on this project involves defining and developing the level 1 and level 2 garment systems. Work needs to include evaluating mock-ups through industry involvement, developing full-scale prototypes, and evaluating these prototypes in the lab and field.

Acknowledgments

The writers would like to thank the research participants and their safety supervisors. The writers would also like to thank Stephen Paskaluk who assisted in the field. This project is funded by Natural Sciences & Engineering Research Council of Canada (NSERC), Canadian Association of Petroleum Producers (CAPP), Imperial Oil Resources Ltd., Nexen Inc., Total E & P Canada Inc., and DuPont Canada Inc. The researchers would also like to thank the Protective Clothing & Equipment Research Facility (PCERF) and the Department of Human Ecology at the University of Alberta.

References

[1] Watkins, S. M., *Clothing: The Portable Environment*, 2nd ed., Iowa State University Press, Ames, IA, 1995.

[2] Coca, A., Roberge, R., Shepherd, A., Powell, J., Stull, J., and Williams, W. "Ergonomic Comparison of a Chem/Bio Prototype Firefighter Ensemble and a Standard Ensemble," *Eur. J. Appl. Phys.*, Vol. 104, No. 2, 2008 pp. 351–359.

[3] Huck, J., "Protective Clothing Systems: A Technique for Evaluating Restriction of Wearer Mobility," *Appl. Ergon.*, Vol. 19, No. 3, 1988 pp. 185–190.

[4] Huck, J., "Restriction to Movement in Fire-Fighter Protective Clothing: Evaluation of Alternative Sleeves and Liners," *Appl. Ergon.*, Vol. 22, No. 2, 1991 pp. 91–100.

[5] Coca, A., Williams, W. J., Roberge, R. J., and Powell, J. B., "Effects of Fire Fighter Protective Ensembles on Mobility and Performance," *Appl. Ergon.*, Vol. 41, No. 4, 2010 pp. 636–641.

[6] Huck, J., Maganga, O., and Kim, Y., "Protective Overalls: Evaluation of Garment Design and Fit," *Int. J. Clothing Sci. Technol.*, Vol. 9, No. 1, pp. 45.

[7] van Schoor, H. E., 1989, "Design and Evaluation of Protective Coveralls," Master's Thesis, University of Alberta, Edmonton, Alberta, Canada.

[8] Adams P. S. and Keyserling W. M., "The Effect of Size and Fabric Weight of Protective Coveralls on Range of Gross Body Motions," *Am. Ind. Hyg. Assoc.*, Vol. 56, No. 4, 1995 pp. 333–340.

[9] Tan, Y., Crown, E. M., and Capjack, L., "Design and Evaluation of Thermal Protective Flightsuits. I: The Design Process and Prototype Development," *Clothing Text. Res. J.*, Vol. 16, No. 1, 1998 pp. 47–55.

[10] Hollies, N.R.S. and Goldman, R. F. (Eds.), *Clothing Comfort*, Ann Arbor Science Publishers, Ann Arbor, MI, 1977.

[11] ASTM F1154-10, 2010, "Standard Practices for Qualitatively Evaluating the Comfort, Fit, Function, and Durability of Protective Ensembles and Ensemble Components," *Annual Book of ASTM Standards*, Vol. 11.03, ASTM International, West Conshohocken, PA.

[12] Huck, J. and Kim, Y., "Coveralls for Grass Fire Fighting," *Int. J. Clothing Sci. Technol.*, Vol. 9, No. 5, 1997, pp. 346–359.

[13] Jordan, P. W., *An Introduction to Usability*, Taylor and Francis, London, 1998.

[14] Callon, M. and Rabeharisoa, V. "Research 'in the Wild' and the Shaping of New Social Identities," *Technol. Soc.*, Vol. 25, 2003, pp. 193–204.

[15] Eilouti, B. H., "Design Knowledge Recycling Using Precedent-Based Analysis and Synthesis Models," *Des. Stud.*, Vol. 30, No. 4, 2009, pp. 340–368.

[16] Enform, "Worker Suffers Severe Burn to Foot, Safety Alert #27-2010 Oct 27," *Enform SafetyAlerts*, Calgary, Alberta, Canada, 2010. www.enform.ca/publications/SafetyAlerts (Last accessed November 16, 2011).

Performance of Protective Clothing and Equipment: Emerging Issues and Technologies
STP 1544, 2012
Available online at www.astm.org
DOI:10.1520/STP104104

M. Y. Ackerman,[1] *E. M. Crown,*[1] *J. D. Dale,*[1]
G. Murtaza,[1] *J. Batcheller,*[1] *and J. A. Gonzalez*[1]

Development of a Test Apparatus/Method and Material Specifications for Protection from Steam under Pressure

REFERENCE: Ackerman, M. Y., Crown, E. M., Dale, J. D., Murtaza, G., Batcheller, J., and Gonzalez, J. A., "Development of a Test Apparatus/Method and Material Specifications for Protection from Steam under Pressure," *Performance of Protective Clothing and Equipment: Emerging Issues and Technologies* on 16 April 2011 in Anaheim, CA; STP 1544, Angie M. Shepherd, Editor, pp. 308–328, doi:10.1520/STP104104, ASTM International, West Conshohocken, PA 2012.

ABSTRACT: Industrial steam presents a worker hazard that has not been addressed within the protective clothing industry to date, and traditional flame-resistant materials provide little protection against this hazard. A test method and associated equipment has been developed and evaluated against field measurements to ensure that the method is able to differentiate among materials and is representative of the actual hazard. A two-level system of ranking textiles has been suggested: Level 1—fabrics that would be used for everyday use, and Level 2—fabrics that could be used for higher risk operations. The two-level system proposed is based on energy transmitted through the material and time to the onset of a second-degree thermal injury

Introduction

Direct exposure to superheated water steam jets or to hot saturated environments is a potential hazard for workers in the oil sector and other heavy industries. Several incidents have been reported in which workers were seriously injured by steam and/or hot water condensate (Desruelle and Schmid [1], Fennel [2], and Kirsner [3]). These have brought into consideration questions

Manuscript received June 2, 2011; accepted for publication March 23, 2012; published online September 2012.
[1]Univ. of Alberta, Edmonton, Alberta, Canada

regarding the level of protection flame resistant (FR) work wear can provide against these two elements, the need for materials specifically designed to protect against them, and appropriate methods to evaluate materials intended for this application.

Textile materials used in manufacturing FR/steam protective clothing systems must be evaluated in terms of both steam/hot water permeation/penetration and energy transfer. Specifications for these clothing systems should be developed to prevent partial or full-thickness burns from energy transfer onto the skin during or after an exposure incident.

Limited reference was found in the literature to studies on the steam/hot water permeability of thermal protective clothing, its effects on FR properties of fabrics, or consequences for the wearer. Kirsner [3,4] reported several accidents involving hot steam at high pressure resulting in workers' death or seriously injured by full-thickness burns. A major reason why steam ruptures are very dangerous is because steam leaks may warm the surrounding ambient air rapidly in a confined space, and that steam can permeate such space very quickly. Condensing steam has a high heat transfer coefficient, making it a penetrating heat. Kirsner [5] reported that when the % steam (by volume) in the air surpasses 12 %, as it will quickly in a confined space, the condensing temperature rises above 45°C, and skin burns may result.

It is generally accepted that second degree burns may happen when the epidermis' temperature reaches 44°C (Stoll and Greene [6]). Moreover, the heat flux that skin can tolerate is an important factor to evaluate. Stoll and Chianta [7] established that the threshold of heat flux for skin burn is 2.51 kW/m^2 (0.06 $cal/cm^2/s$). Little fundamental investigation has been carried out since that time on the behaviour of human skin exposed to such hazards and as such the work of Stoll, Greene, and Chianta has largely been accepted as the basis for textile protection evaluation systems.

Watkins et al. [8] designed firefighting apparel that included an outermost layer that was FR and waterproof, and a liner comprising three fabric layers to protect the firefighter from heat transferred through the outer shell. These researchers hypothesized that, although steam would be able to penetrate the system, it would gradually move through the layers so that the skin would be acclimated rather than causing the pain threshold to be reached. Watkins et al. [8] stated that when condensation occurs, a clothing system for environments where high heat and moisture are present must insulate the wearer from the point at which condensation takes place. She also pointed out that to avoid injury, a clothing system that can control the heat flux or rate at which vapour reaches the body surface is required. Mell and Lawson [9] stated that wet garments may exhibit significantly higher heat-transfer rates than dry garments, that heating and evaporation of moisture trapped in protective clothing may result in scald or steam burns, and that moisture may help to store heat energy in protective clothing.

Lawson et al. [10] investigated the effects of moisture on heat transfer through materials comprising clothing systems worn by wildland firefighters, with particular attention given to source of moisture, location of moisture in the system, and timing of moisture application. They concluded that when moisture is a factor, heat transfer through thermal protective textiles differs among conditions of moisture application and among various layered fabric systems. They determined that for high heat flux exposures, external moisture generally decreased heat transfer through fabric systems, whereas internal moisture may increase it. At low heat fluxes, however, both internal and external moisture decrease heat transfer through the fabric systems, with internal moisture having the larger effect.

Rossi et al. [11] studied the transfer of steam through various layered textile systems. To simulate perspiration from the human body, a cylinder releasing defined amounts of moisture was used. The influence of different sweating rates on the heat and mass transfer during steam exposure was assessed. They determined that impermeable (waterproof) materials normally offer better protection to hot steam than semi-permeable ones. They also concluded that heat transfer during steam exposure depends on both the water vapour permeability of the material and its thermal insulation and thickness.

Desruelle and Schmid [1] at the Institut de Médecine Navale du Service de Santé des Armées (France) developed a set of tools to study the effects of exposure to hot water steam on human physiology and to evaluate the protective capacity of fabrics under steam stress. They also used a thermal mannequin to evaluate thermal protective capacity of garments. However, their work involved lengthy time scales (wherein the skin would likely be destroyed) and unrealistically held the skin surface at constant temperature, likely implying greater rates of heat transfer than would actually occur. They concluded that fabric thickness and water vapour diffusion have significant effects on protection against steam exposure.

Based on theoretical considerations including heat and mass transfer, and relationships to yarn and fabric structure/geometry, Sati et al. [12] developed a test protocol and a cylindrical (torso-like) test device with several skin-simulant sensors. They evaluated existing FR materials with different water vapour permeability properties, concluding that fabric structure, steam pressure and exposure distance significantly influence heat transfer during a steam exposure incident. Despite the differences in the two approaches, conclusions from this study supported and complemented those of Desruelle and Schmid [1] discussed above.

The need for more research is evident as several factors relevant to the steam/hot water permeability of FR protective clothing have not been thoroughly addressed. The study was intended to produce an apparatus and method to differentiate between materials and was limited to low pressure steam. Because studies completed to date have used relatively low-pressure steam exposures, up to 310 kPa (45 psi) compared to those found in industry. More work is needed to confirm the validity of tests using such pressures. As well, some new materials and applications currently on the market have not been evaluated.

The Protective Clothing Research Group at the University of Alberta recently concluded an initial investigation of steam/hot water permeability properties of FR protective clothing, in which we developed an evaluation device and procedures and evaluated some existing protective materials. This paper describes the test apparatus that was developed, its capabilities, and illustrates its utility through comparison of results among a representative set of materials as well as limited field data.

Fabric Selection

A series of permeable, semi-permeable, and impermeable fabrics (Table 1) were supplied by several manufacturers, based on our stated specifications. We attempted to find fabrics in each category that varied systematically on area mass, on thickness, and for thick fabrics, on compressibility. Initially, seven permeable (category A) fabrics, six semi-permeable (category B) fabrics, and two impermeable (category C) fabrics were selected for testing. Most were layered or multi-component fabrics. In preliminary testing, none of the permeable fabrics offered any significant thermal protection again steam under pressure; thus, most A fabrics were not used in final testing reported here. Fabric A2 was included because it is structurally identical to Fabric B9/10 except that it has no membrane. The structure of the semi-permeable fabrics includes either a PTFE or PU membrane.

Twenty meter rolls of each fabric were obtained. Each roll was cut into five large samples. Two replications of specimens for fabric characterization,

TABLE 1—*Fabric descriptions.*

Fabric	Description
A2	Quilted thermal liner: woven/non-woven/felt/non-woven (aramid face and non-woven; mainly aramid reprocessed felt)
B9	Aramid/carbon fleece/PU membrane/aramid/carbon fleece
B9/B10	Quilted thermal liner: woven/non-woven/felt/PU membrane (aramid face and non-woven; mainly aramid reprocessed felt)
B10	Tri-laminate: aramid/carbon woven/ptfe membrane/aramid fleece; WR finish on outer layer
B11	Tri-laminate: aramid/carbon woven/ptfe membrane/aramid jersey
B12	Woven aramid/PU membrane; fluorocarbon finish
B15/16	Tri-laminate: aramid jersey/FR PU membrane/aramid jersey
C18	Woven aramid treated with silicon
C20	Aramid/carbon non-woven with chemical barrier laminate

property testing, and small-scale steam testing were cut from two of the samples, while specimens for full-scale validity testing were cut from the remaining three samples.

The fabric samples were not laundered. All specimens for characterization and small-scale steam testing were conditioned for 24 h according to CAN/CGSB-4.2 No.2-M88 [13]. Specimens for full-scale testing were not conditioned. Fabric characteristics such as area mass and thickness, and performance properties such as air permeability, thermal resistance, evaporative resistance, and water-vapour permeability were determined following CGSB [14–16] and ISO [17] standard test methods as noted . These characteristics and properties are reported in Table 2, as means of ten specimens.

Test Apparatus—Protection against Steam Hazard

The development of a test apparatus was initiated with the development of a set of specifications, shown below:

- Provide a means of evaluating the protective performance of materials/composites against a low pressure steam hazard.
- Material sample—150 mm diameter, any number of layers.
- Sensor technology—measure energy transfer as a function of time, possibility of burn injury prediction.
- Steam conditions—saturated (10–90 psig, 69–620 kPa), superheated (10–90 psig, 69–620 kPa).
- Steam impingement—free jet with spacing between sample and jet of 50 mm to 150 mm.
- Steam impingement—enclosed jet (sample spacing fixed at 50 mm).
- Test duration—up to 10 s exposure time.
- Data acquisition—minimum five readings per second for duration of test, steam temperature, pressure, computer control of test.

The device developed to meet the specifications consists of a small 3 kW boiler with an added superheater, Fig. 1. The boiler produces saturated steam at a set pressure and the electrically heated super heater allows increasing the steam temperature above saturated conditions. The steam is routed to a 6.35 mm o.d. (4.6 mm inside diameter) nozzle that is positioned above the test specimen and the exposure time is controlled via a computer interface through a solenoid valve. The test platform, shown in Fig. 2 and in section view, Fig. 3, will contain pressure if the material has a liquid/vapor impermeable layer or alternatively will allow the condensate to flow through the specimen and out the bottom of the apparatus to a collection point. When the material composite contains an impermeable layer the pressure can rise above the specimen and will force the fabric against the teflon restraint and sensor. If this is not the desired condition (this will result in a buildup of pressure and condensate above the test specimen at a rate governed by the energy transfer from the steam to the

TABLE 2—*Fabric characteristics and properties.*

Fabric code	Mass[a] (g/m^2)	Initial thickness[b] (mm)	Thickness[b] —11.6 kPa (mm)	Density[c] (kg/m^3)	Density[c] —11.6 kPa (kg/m^3)	Air permeability[d] ($l/cm^2 \cdot s$)	Thermal resistance[e] ($m^2 \cdot C/W$)	Evaporative resistance[e] ($m^2 \cdot Pa/W$)	Water-vapour permeability[5] ($g/m^2 \cdot Pa \cdot h$)
A2	350	5.0	2.1	73.4	174	45	0.2	Not tested	not tested
B9	481	5.0	2.4	95.6	202	0.21	0.17	32	0.05
B9/B10	423	4.8	2.2	91.5	203	0.00	0.20	26	0.06
B10	507	2.5	1.7	202	309	0.13	0.12	32	0.05
B11	273	0.9	0.7	303	410	0.19	0.09	16	0.10
B12	261	0.7	0.5	389	541	0.00	0.17	22	0.07
B15/B16	203	0.9	0.6	224	320	0.20	0.10	36	0.05
C18	776	1.8	0.9	656	910	0.00	0.08	628	0.00
C20	273	1.7	0.8	166	334	0.00	0.10	591	0.00

[a]Measured following CAN/CGSB-4.2 No.5.1-M90 [14].
[b]Measured following CAN/CGSB-4.2 No.37-2002 [15].
[c]Calculated from mass and thickness measurements.
[d]Measured following CAN/CGSB-4.2 No.36-M89 [16].
[e]Measured following ISO 11092:1993 [17].

FIG. 1—*Apparatus for evaluation of material protection against steam hazard.*

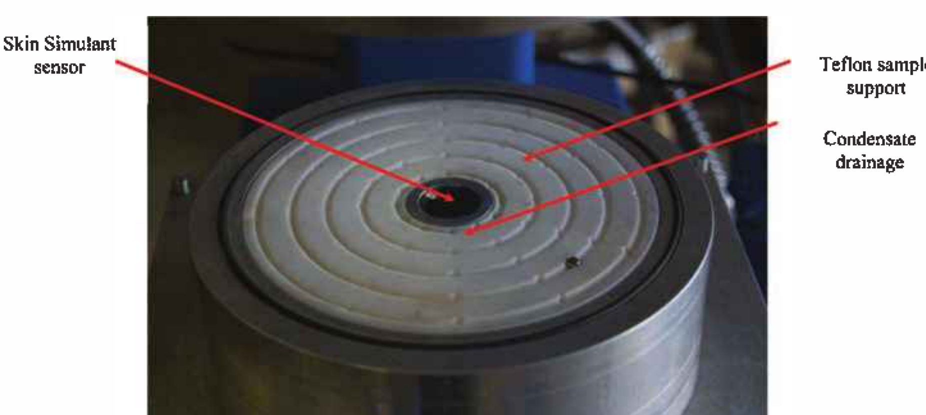

FIG. 2—*Sensor holder showing drainage channels and teflon sample support.*

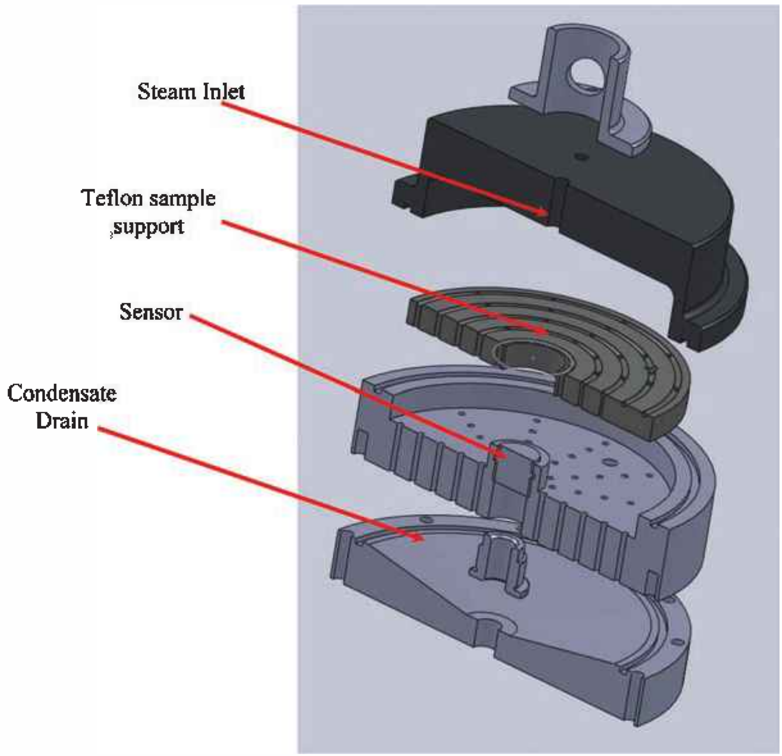

FIG. 3—*Section view of components.*

fabric and test chamber) the specimen restraint can be fitted with a series of holes around the perimeter that will allow the condensate to migrate to the outer rim of the test chamber and out of the apparatus. In this case, there will be little build up of pressure above the specimen. Preliminary tests have showed that under these conditions (with an impermeable fabric), there is no migration of condensate under the specimen to the sensor. If the fabric must be restrained a Teflon™ ring insert is used between the upper and lower platens to ensure no movement during the exposure. The Teflon™ ring had a series of holes around the perimeter (Fig. 4) that allows the steam to escape and at the same time restrains the fabric from moving during the exposure.

Operation of the apparatus is straight forward in that power is applied to the boiler and the unit requires perhaps 30 min to fully warm up and produce steam of the desired condition. A small amount of steam is allowed to continuously bleed though the system to ensure that all of the components are hot and the steam will not condense in the lines when the solenoid valve is first opened. The apparatus is kept open during this time to allow the sensor to cool and be dried if necessary (only necessary with permeable materials). After the desired steam conditions have been met, the sample is inserted, the unit is

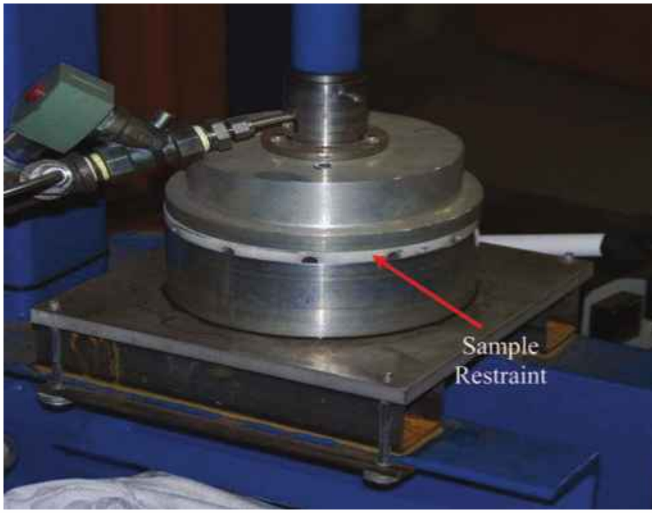

FIG. 4—*Platens closed with sample restraint in Pl.*

closed (Figs. 4 and 5) using the hydraulic pump (pressure set to maintain contact between the sample and apparatus), and the system is given over to computer control. The computer program controls the exposure time, monitors the sensor output and the steam conditions during the test (Fig. 6). If desired, the jet-sample spacing can be varied to approximately 150 mm by leaving the platens the desired distance apart, Fig. 7. In this case, it may be necessary to restrain the sample by other means or the steam jet can displace the material during the exposure, invalidating the test. Upon completion of the test period the computer will calculate the energy transfer as a function of time as well as the depth of damage in a predicted burn injury (if any).

The system is quite variable in the conditions that can be set for testing. The parameters that can be varied are:

- Steam pressure (69–620 kPa, 10–90 psig).
- Steam temperature (95–150°C).
- Open test jet spacing (50–150 mm).
- Closed test jet spacing fixed at 50 mm—with condensate flow or without—no sample restraint.
- Closed test jet spacing fixed at 62 mm with sample restraint.

Test results, small scale tests—selected fabrics.

The newly developed test device described above was used to test two replications of five specimens of each fabric. In addition, Fabric B9/10 was tested with either the face fabric or the membrane facing the steam. The apparatus was set to provide steam at 150°C and 200 kPa pressure.

FIG. 5—*Sample in place—no sample restraint.*

Heat flux sensor data were recorded at ten readings per second for both the 10-s exposure time and an additional 50 s after exposure to capture any effects of stored energy in the fabric. From the heat flux data total absorbed energy was determined. The heat flux history was used in a multi-layer skin model to estimate the time required to cause a second or third degree thermal injury. If there was no predicted thermal injury within the total 60-s data collection period, the result was indicated as >60 s. A summary of the test results is shown in Table 3. Note that, in some cases, the calculated burn injury exceeded 60 s in one or more of the five specimens tested in each group. In that case, the time to second or third degree thermal injury has been marked with an asterisk.

All tests were carried out with a sample restraint placed above the fabric to constrain the material during testing. Initial tests without the restraint allowed the fabrics to move and, in some cases, the steam jet was forceful enough to displace the fabric during the exposure. The use of the sample restraint means

FIG. 6—*Material under test, sample restraint in place.*

that the distance from the outlet of the steam jet and the sample is approximately 62 mm.

Comparison with Field Tests

Selection of test conditions for material or material composite evaluation can be done to provide maximum differentiation among materials or to be representative of a hazard that could be encountered under field conditions. Whatever the choice, one wishes to know that a protection rating or a performance ranking given to a material will in some way represent how the material(s) will perform under accident conditions. To compare field and test conditions, arrangements were made to visit a local refinery where process steam at a number of pressures was available. A test apparatus, Fig. 8, consisting of a nozzle, control valve, bleed valve, and a fiberglass cylinder containing five heat flux sensors was constructed and taken to the refinery. Steam at 650 kPa (125 psig) was piped to the apparatus and used to evaluate the same set of materials under 10-s exposure conditions. Spacing between the outlet of the steam jet and the sensors was set at either 150 mm or 250 mm. Steam flow was manually controlled and, as such, the exposure time varied somewhat from test to test. Figure 9 is a photograph of a typical exposure.

Steam jet—sample spacing was initially set at 100 mm, but it was found that this combination of distance and pressure was sufficient to damage some of the fabrics. Although this would be the case in reality, it would not have

FIG. 7—*Steam jet produced with apparatus open apparatus open.*

provided useful information for correlating small-scale and full-scale test results. Because the steam pressure was significantly higher at the refinery than the small scale, a large amount of fabric deformation caused by the stagnating jet was noted at the refinery. Figure 10 shows the deformation of a sample of material with a steam jet impinging on the surface. Both photographs are the same material but in one case the image has been converted to grey scale for clarity.

Data for the full-scale (refinery) tests are provided in Tables 4–6. It is notable that at the larger distance (250 mm) between jet and fabric, there are virtually no third degree burns; and except for fabrics A2, B9/10, and B12, the times to second degree burn are relatively long. On the other hand, at the more severe condition (150 mm), times to second degree burn are much shorter with only three fabrics having times of more than 6 s, while three fabrics have times to third degree burn under 20 s. Under both conditions, the two impermeable fabrics and fabric B10 appear to perform the best.

TABLE 3—*Steam apparatus test results with selected fabrics, 10-s exposure.*

Steam test apparatus, steam temperature 150°C, pressure 200 kPa				
Fabric	Rep	2nd Degree (s)	3rd Degree (s)	Absorbed energy (kJ/m^2)
A2	1	0.3	11.7	571
B9	1	25.9*	>60	173
B9	2	22.7*	>60	179
B9/10	1	1.0	14.9*	381
B9/10	2	1.0	14.4	430
B9/10R	1	8.3	>60	177
B10	1	>60	>60	137
B10	2	>60	>60	143
B11	1	5.0	46.7*	288
B11	2	5.1	46.2*	273
B12	1	1.3	15.3	404
B12	2	1.2	14.9	410
B15/16	1	6.5	>60	220
B15/16	2	5.9	>60	226
C18	1	>60	>60	161
C18	2	47.9*	>60	176
C20	1	>60	>60	80
C20	2	>60	>60	84

Note: An asterisk indicates that one or more of the five samples in the set did not show a thermal injury within the 60-s data collection period.

FIG. 8—*Experimental setup used to direct process steam at fiberglass form with heat flux sensors.*

FIG. 9—*Typical exposure using process steam at 650 kPa.*

The difference between Fabrics A2 and B9/10 are not great, largely because B9/10 was tested with the membrane against the sensor. When reversed and covered with a light-weight (262 g/m^2) aramid shell fabric (B9/10R) as it would be used in practice, this fabric performed quite well at 250 mm, but less well at the more severe 150 mm condition where its performance was similar to that of B9 and B12 and not as good as B15.

Statistical Analyses

Analyses were conducted using the statistical software package, SPSS Version 18 [18]. For both small-scale and large-scale testing, means and standard

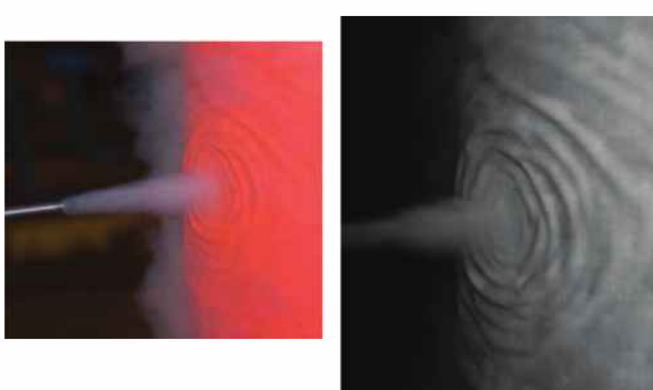

FIG. 10—*Fabric deformation under stagnation pressure developed when steam jet strikes surface*

TABLE 4—*Tests with process steam at 650 kPa, replication 1, 150-mm jet distance.*

10-s Exposure, ~650 kPa, 170°C, 150 mm from jet replicate 1					
Fabric code	Time to 2nd degree burn (s)	Time to 3rd degree burn (s)	Absorbed energy (kJ/m^2)	Peak temperature rise (°C)	Peak heat flux (kW/m^2)
A2-1	0.4	12.4	344	72.0	100.6
B9-1	2.2	25.4	265	55.0	33.7
B9/10-1	1.1	15.8	307	63.5	50.2
B10-1	6.3	>60	307	63.5	50.2
B11-1	3.4	47.6[a]	207	56.9	28.2
B12-1	1.0	16.5	253	62.7	49.3
B15/16-1	2.1	45.5[a]	191	58.6	40.6
C18-1	11.5	>60	108	21.9	10.9
C20-1	10.1	>60	99	23.0	12.0

[a]Indicates one or more of the three specimens in the set did not show a thermal injury within the 60-s data collection period.

deviations were calculated for time to second degree burn, time to third degree burn, and absorbed energy over 60 s. Two-way analyses of variance (fabric by replication) on the absorbed energy data demonstrated that there were no significant differences between replications, so pooled data were used in one-way ANOVAS, and Duncan's post-hoc tests were used to determine which fabrics differed significantly from one another. Correlations between absorbed energy and several fabric characteristics and properties were determined for both

TABLE 5—*Tests with process steam at 650 kPa, replication 2, 150 mm jet distance.*

10-s Exposure, ~650 kPa, 170°C, 150 mm from jet replicate 2					
Fabric code	Time to 2nd degree burn (s)	Time to 3rd degree burn (s)	Absorbed energy (kJ/m^2)	Peak temperature rise (°C)	Peak heat flux (kW/m^2)
A2-2	0.0	12.1	359	72.0	114.0
B9-2	2.9	47.5[a]	241	53.5	28.1
B9/10-2	1.0	15.4	308	63.7	59.5
B9/10R	3.2	38.6	251	52.8	30.2
B10-2	6.3	>60	136	33.4	17.0
B11-2	3.0	37.6[a]	208	59.5	29.2
B12-2	1.2	16.5	242	63.1	47.8
B15/16-2	3.3	>60	166	54.4	26.9
C18-2	27.4*	>60	103	21.3	10.9
C20-2	10.1	>60	96	22.8	11.9

[a]Indicates one or more of the three specimens in the set did not show a thermal injury within the 60-s data collection period.

TABLE 6—*Tests with process steam at 650 kPa, replication 1, 250 mm jet distance.*

10-s Exposure, ~650 kPa, 170°C, 250 mm from jet					
Fabric code	Time to 2nd degree burn (s)	Time to 3rd degree burn (s)	Absorbed energy (kJ/m^2)	Peak temperature rise (°C)	Peak heat flux (kW/m^2)
A2	1.0	37.4[a]	256	47.4	64.0
B9	>60	>60	90	14.2	6.8
B9/10	2.8	>60	200	37.5	31.6
B9/10R	>60	>60	64	10.6	5.0
B10	>60	>60	70	12.3	6.4
B11	9.7	>60	106	25.2	11.7
B12	3.6	>60	150	35.4	25.6
B15/16	6.4[a]	>60	85	21.2	11.8
C18	>60	>60	61	12.9	6.4
C20	>60	>60	29	7.8	4.0

[a]Indicates one or more of the three specimens in the set did not show a thermal injury within the 60-s data collection period.

small- and large-scale data. Correlations between small- and large-scale data were also determined.

Differentiation Among Fabrics

The differences discussed above are reflected in the results of one-way ANOVAs for the absorbed energy data (Table 7). Based on Duncan's post-hoc test, both the small-scale test and the large-scale test at 150 mm were able to

TABLE 7—*Analyses of variance (ANOVA): Fabric effect on absorbed energy for small-scale and large-scale tests.*

	Absorbed energy (kJ/m^2)		
Fabric code	Small-scale test	Large-scale test at 250 mm	Large-scale test at 150 mm
C20	81.9[a]	29.2[a]	97.4[a]
B10	140.0[b]	69.9[b,c]	138.3[b]
C18	168.6[c]	61.3[b]	105.9[a]
B9	175.9[c]	90.3[c,d]	253.0[e]
B9/10R	177.4[c]	64.1[b]	251.4[e]
B15	223.4[d]	84.8[b,c,d]	178.8[c]
B11	280.5[e]	106.0[d]	207.9[d]
B9/10	405.9[f]	199.5[f]	307.1[f]
B12	407.0[f]	149.9[e]	247.7[e]

Note: For each column, means with the same superscript do not differ significantly from each other when tested by Duncan's post-hoc test.

TABLE 8—*Rankings on 2nd and 3rd degree burn times (1 is best or highest; 10 is worst).*

	2nd Degree burn times			3rd Degree burn times		
Fabric	Small scale	150 mm	250 mm	Small scale	150 mm	250 mm
A2	10	10	10	10	10	10
B9	4	6–7	1–5	1–6	5–7	1–9
B9/10	9	8–9	9	8–9	9	1–9
B9/10R	5	4–5	1–5	1–6	5–7	1–9
B10	1–3	3	1–5	1–6	1–4	1–9
B11	7	4–5	7	7	5–7	1–9
B12	8	8–9	8	8–9	8	1–9
B15	6	6–7	6	1–6	1–4	1–9
C18	1–3	1	1–5	1–6	1–4	1–9
C20	1–3	2	1–5	1–6	1–4	1–9

differentiate the fabrics into six distinct groups. There is more overlap between groups for the large-scale tests at 250 mm; in other words, the differentiation is less clear. There are similar patterns among the three conditions; nevertheless, while it was noted above that C20, C18, and B10 appear to perform the best, B10 performs better than C18 in the small-scale test but not in the large-scale ones. Also, both B9 and B9/10R are grouped with C18 in the small-scale test, but do not perform as well in the more severe large-scale test at 150 mm. It should also be noted that only B10, C18, and C20 had times to second degree burn of over 60 s in the small-scale test, and also had the longest times to second degree burn in the more severe large-scale test (Table 8). These observations have implications for setting performance specifications based on the small-scale test data.

Time to both second and third degree thermal injury was examined for all fabrics in the three test conditions, bench scale, and full scale at two offset distances. In both bench scale tests and full-scale tests, a number of the fabric composites tested resulted in predicted burn times greater than 60 s. As a result, it was not possible to do analysis of variance and produce meaningful results. To get some idea of performance using burn injury as the metric, the fabrics were ranked in terms of time to produce second or third degree injury, Table 8.

As one would expect, the permeable fabric, A2, performed the worst in all cases with predicted time to second degree of 1 s or less in all cases. The semi-permeable (B-series) fabrics showed differing levels of protection (second degree injury) in both the small-scale and full-scale tests. While the ordering was different in the three tests, the ranking was generally the same with B10 performing the best and B9/10 (with membrane facing sensor) the worst. It was interesting to note that B9/10R provided better protection than B9/10 when the membrane was positioned to face the hazard (resulting in some thermal insulation between the hazard and the sensor). The impermeable (C-series) fabrics ranked the best (longest times to second degree thermal injury) in all test cases. Simply ranking the fabrics in terms of time to third degree injury did not provide as much differentiation in all cases—largely because the result was no third degree injury during the test period (10 s exposure, 60 s total data collection) in a number of cases. This was especially true in the full-scale refinery test at 250 mm jet spacing where a third degree predicted injury was only obtained with the permeable fabric, A2.

Proposed Specifications for Two Levels of Protection

Firms in the oil and gas industry have requested that specifications be set for two levels of protection from steam exposure: Level 1 garments that could be worn on site most of the workday, and Level 2 garment systems that could be worn for short-term but higher risk exposure situations. Based on the results of the large-scale field testing at 150 mm distance between the jet and fabric, we suggest tentatively that fabrics C18, C20, and B10 could be considered Level 2. Based on results of the large-scale field testing at 250 mm, Fabrics B9, B9/10R, B11, and B15 could be considered Level 1. To specify Levels 1 and 2 based on the small-scale test; therefore, the criteria for Level 2 could be a time to second degree burn of >60 s and absorbed energy of <200 kJ/m^2, while the criteria for Level 1 could be set at a time to second degree burn of >5 s and absorbed energy of <300 kJ/m^2.

Material Properties—Performance Correlations

Aside from the initial goal of establishing a test method that would provide differentiation in terms of protection, a secondary goal was to model the steam jet –fabric interaction to ultimately allow us to specify fabric characteristics to provide a set level of protection. While generally understood that the material must provide a barrier to the transmission of energy, the complex nature of the energy and mass transfer means that more than one material characteristic will affect the overall performance of a composite. The energy transfer through fabrics or fabric composites under an impacting jet of steam is a function of a number of variables such as mass, thickness, permeability, location of moisture barrier (if any), fabric construction, compressibility, and also the material characteristics such as thermal conductivity and density. To gain some understanding of which characteristics might be important, correlations were determined for each of the properties with absorbed energy as measured at the sensor. Table 9 shows the results of the analysis for both the full-scale refinery testing and small-scale testing. What is interesting about the results is that there appear to be significant differences in dependencies with each test condition. For example, the most severe test (refinery at 150 mm) show the strongest

TABLE 9—*SPSS correlations of material properties with absorbed energy.*

	Absorbed energy (kJ/m^2)		
	150 mm	250 mm	Small scale
Initial density (g/m^3)	−0.279	0.058	0.856
Density at 11.59 kPa	−0.184	0.046	0.887
Rct (m^2 C/W)	0.232	0.353	0.038
Ret (m^2 C/W)	−0.149	−0.207	−0.492
Water vapour permeability	0.005	0.539	0.438
Mass (g/m^2)	0.038	−0.067	−0.697
Initial thickness (mm)	0.489	0.212	−0.641
Thickness at 11.59 kPa	0.356	0.061	−0.730
Thickness change (%)	0.601	0.395	−0.440

correlation with thickness, compressed thickness, and thickness change—not surprising given the deformation of the fabric that was observed during testing. The full-scale refinery test at 250 mm showed the greatest correlation with water vapour permeability (not expected) and thickness change under pressure. The bench scale test results showed strong correlations with initial density, compressed density, and thickness under an applied pressure. The correlations from the full-scale tests unfortunately did not provide sufficient information to allow specification of fabric or fabric composites to provide a particular level of protection other than in the most general sense.

Summary and Conclusions

A test method for evaluating the performance of fabrics and composites has been developed and tested against a number of selected permeable, semi-permeable, and impermeable fabrics. The method allows for the evaluation of single-layer or multi-layer fabric systems and is able to differentiate among fabrics or systems. The equipment required to perform the method is relatively simple and laboratory based.

Fabrics were evaluated using the proposed bench scale test and in field trials using process steam. While the results were not identical because of differences in conditions between the process steam (temperature and pressure) and the bench scale conditions the ranking (protection in terms of energy transmitted or time to second degree thermal injury) determined with each method was very similar.

A two-level protection specification was developed from the test data. The two levels of protection were determined for (a) fabrics that would be used for everyday use, and (b) fabrics that could be used for higher risk operations. The two-level system proposed is based on energy transmitted through the material and time to the onset of a second degree thermal injury.

References

[1] Desruelle, A. V., and Schmid, B., "The Steam Laboratory of the Institut de Médecine Navale du Service de Santé des Armées: A Set of Tools in the Service of the French Navy," *Eur. J. Appl. Physiol.*, Vol. 92, 2004, pp. 630–635.

[2] Fennel, D. J., July 16, 2003 (unpublished).

[3] Kirsner, W., "What Caused the Steam System Accident that Killed Jack Smith?" *Heating, Piping Air Conditioning Eng.*, Vol. 67, No. 7, 1995, pp. 36–53.

[4] Kirsner, W., "Condensation-Induced Waterhammer," *Heating, Piping Air Conditioning Eng.*, Vol. 71, No. 1, 1999, pp. 112–122.

[5] Kirsner, W., "Surviving a Steam Rupture in an Enclosed Space," *Heating, Piping Air Conditioning Eng.*, Vol. 71, No. 7, 1999, pp. 39–41.

[6] Stoll, A. M., and Greene, L. C., "Relationship Between Pain and Tissue Damage Due to Thermal Radiation," *J. Appl. Physiol.*, Vol. 14, 1959, pp. 373–382.

[7] Stoll, A. M., and Chianta, M. A., "Method and Rating System for Evaluation of Thermal Production," *Aerospace Med.*, Vol. 40, 1969, pp. 1232–1238.

[8] Watkins, S. M., Valla, M. K., and Rosen, L. R., "The Development of Two Protective Apparel Systems for Firefighting," *Report No. 1978-03-01*, New York State College of Human Ecology, Ithaca, NY, 1978.

[9] Mell, W. E., and Lawson, J. R., "A Heat Transfer Model for Firefighters' Protective Clothing," *Fire Technol.*, Vol. 36, No. 1, 2000, pp. 39–68.

[10] Lawson, L. K., Crown, E. M., Ackerman, M. Y., and Dale, J. D., "Moisture Effects in Heat Transfer through Clothing Systems for Wildlands Firefighting," *Int. J. Occup. Safety Ergon.*, Vol. 10, No. 3, 2004, pp. 227–238.

[11] Rossi, R., Indelicato, E., and Bolli, W., "Hot Steam Transfer through Heat Protective Clothing Layers," *Int. J. Occup. Safety Ergon.*, Vol. 10, No. 3, 2004, pp. 239–245.

[12] Sati, R., Crown, E. M., Ackerman, M., Gonzalez, J. A., and Dale, J. D., "Protection from Steam at High Pressures: Development of a Test Device and Protocol," *Int. J. Occup. Safety Ergon.*, Vol. 14, No. 1, 2008, pp. 29–41.

[13] CAN/CGSB-4.2 No. 2, 1988, "Textile Test Methods—Conditioning Textile Materials for Testing," Canadian General Standards Board, Ottawa, Ontario, Canada.

[14] CAN/CGSB-4.2 No. 5.1-M90, 2004, "Textile Test Methods—Fabric Mass," Canadian General Standards Board, Ottawa, Ontario, Canada.
[15] CAN/CGSB-4.2 No. 37, 2002, "Textile Test Methods—Fabric Thickness," Canadian General Standards Board, Ottawa, Ontario, Canada.
[16] CAN/CGSB-4.2 No. 36-M89, 1997, "Textile Test Methods—Air Permeability," Canadian General Standards Board, Ottawa, Ontario, Canada.
[17] ISO11092, 1993, "Textiles—Physiological Effects—Measurement of Thermal and Water-Vapour Resistance under Steady-State Conditions (Sweating Guarded-Hotplate Test)," International Organization for Standardization, Geneva.
[18] *PASW Software; Version 18* (2009). SPSS Inc., Chicago, IL.

Performance of Protective Clothing and Equipment: Emerging Issues and Technologies
STP 1544, 2012
Available online at www.astm.org
DOI:10.1520/STP104098

S. H. Jalbani,[1] *M. Y. Ackerman,*[2] *E. M. Crown,*[1]
M. van Keulen,[1] *and G. Song*[1]

Apparatus for Use in Evaluating Protection from Low Pressure Hot Water Jets

---

REFERENCE: Jalbani, S. H., Ackerman, M. Y., Crown, E. M., van Keulen, M., and Song, G. , "Apparatus for Use in Evaluating Protection from Low Pressure Hot Water Jets," *Performance of Protective Clothing and Equipment: Emerging Issues and Technologies* on April 16, 2011 in Anaheim, CA; STP 1544, Angie M. Shepherd, Editor, pp. 329–339, doi:10.1520/STP104098, ASTM International, West Conshohocken, PA 2012.

ABSTRACT: Use of hot water has become extensive, especially in bitumen extraction from oil sands and in the production of heavy oil. The hot water is often under pressure and is 80–90°C, which is well above temperatures that result in immediate, potentially severe burn injuries. The ASTM F2701-08 apparatus consists of a funnel through which hot liquid is hand-poured to produce a 10 s exposure. Two 40 mm diameter copper calorimeters, mounted in an insulating sheet are positioned beneath the funnel outlet and are intended to measure the energy transfer through the fabric from the hot liquid. For this research, changes were made to the apparatus and procedures to more closely simulate low pressure hot water streams found in the oil industry and to improve reproducibility. The funnel producing the liquid splash was replaced with a small pipe directly fed by a circulating hot water bath via a small pump, through a hose and valve system, allowing for consistent application of a given quantity of water at a consistent temperature and flow rate. Water temperature, flow rate, and pressure can be altered as desired. A series of fabrics varying systematically on several parameters were tested with the modified equipment. Resulting heat transfer data suggest the system differentiates well among both semi-permeable and impermeable fabrics. Specifications for hot water protection are proposed.

KEYWORDS: hot water hazards, energy and mass transfer, test procedures, thermal protection

---

Manuscript received June 2, 2011; accepted for publication January 24, 2012; published online April 2012.

[1]Department of Human Ecology, Univ. of Alberta, Edmonton, AB T6G 2M7, Canada.
[2]Department of Mechanical Engineering, Univ. of Alberta, Edmonton, AB T6G 2M7, Canada.

Introduction

This research is part of a larger project aimed at specifying and developing improved, innovative protective materials and garments for workers in the oil industry. Use of both steam and hot water has become extensive in this industry, especially in bitumen extraction from oil sands and in the production of heavy oil. The hot water is often under pressure and is 80–90°C, which is well above temperatures that result in immediate, potentially severe burn injuries [1].

Over 5000 Workers' Compensation claims were made in Alberta for burns and scalds in 2008 and just under 4000 in 2009 [2]. These included all worksites; nevertheless, several injuries have occurred in oil production facilities in recent years. For example, one firm operating in the Province of Alberta and elsewhere in Canada [3] reported five serious accidents over a two-year period: a drilling rig-hand sprayed with steam and hot water when a hose failed, a swamper splashed with hot water while handling a hose, a tank truck driver sprayed with hot water when the wrong valve opened, a service rig-hand splashed with hot water that burped out of a well bore, and a plant operator checking the filter screen on the hot line softener during routine operation in the water reuse building. The latter was loosening bolts on a flange when a valve opened under pressure, spraying hot water at 99°C and sludge onto his face, chest, and arms. It took just under 1 min for this injured worker to get to the emergency shower and remove his saturated clothing. He received burns to 35 % of his body; burns were most severe (second and third degree) where his saturated flame resistant (FR) clothing remained against his skin. He was hospitalized for four months and spent five more months in physiotherapy.

While all workers in the oil industry in Alberta wear normal FR clothing, it does not protect from thermal injuries due to steam and hot water. While changes have been made to equipment and operating procedures following the accidents described above, a need remains to develop materials specifically designed to protect against the hazard of hot water, as well as appropriate methods to evaluate materials intended for this application. Huyer and Corkum [1] reported that water at 66°C will cause second degree burns within 3 s and third degree burns within 6 s, while water at 55°C will cause second degree burns within 30 s. Armstrong and Harris [4] compared the maximum temperature in a hot water jet to the maximum temperature in a steam jet as a function of distance from the nozzle. Steam under pressure cools considerably at a short distance from the nozzle compared to water under pressure; for example steam at 350 kPa and 140°C cools to 62°C at 14 cm and to 48°C at 25 cm while water at 910 kPa and 140°C cools to only 100°C at both 14 cm and 25 cm.

Purpose and Objectives

This research addressed the evaluation of hot water protection of textile materials. The objectives were as follows:

1. To develop appropriate test procedures, including parameters such as temperature and flow rate, for a modified ASTM F2701-08 [5] hot water protection apparatus;
2. To determine the ability of the new procedure to differentiate among fabrics;
3. To determine relationships between selected fabric characteristics and properties and measured heat transfer parameters; and
4. To make recommendations regarding material specifications for hot water protection and further alterations to the test apparatus and/or procedures.

Experimental Methods

Development of Test Device and Procedures

The current ASTM F2701-08 [5] apparatus comprises a funnel through which hot liquid is hand poured to produce a 10 s exposure (Fig. 1). Two 40 mm diameter copper calorimeters, mounted in an insulating sheet are positioned beneath the funnel outlet and are intended to measure the energy transfer through the fabric from the hot liquid. In preliminary experiments, a small number of permeable, semi-permeable and impermeable fabrics were tested following the procedures of ASTM F2701-08 with water at 75–80°C. The method was able to differentiate among fabric types in terms of peak temperature, time to peak temperature, and

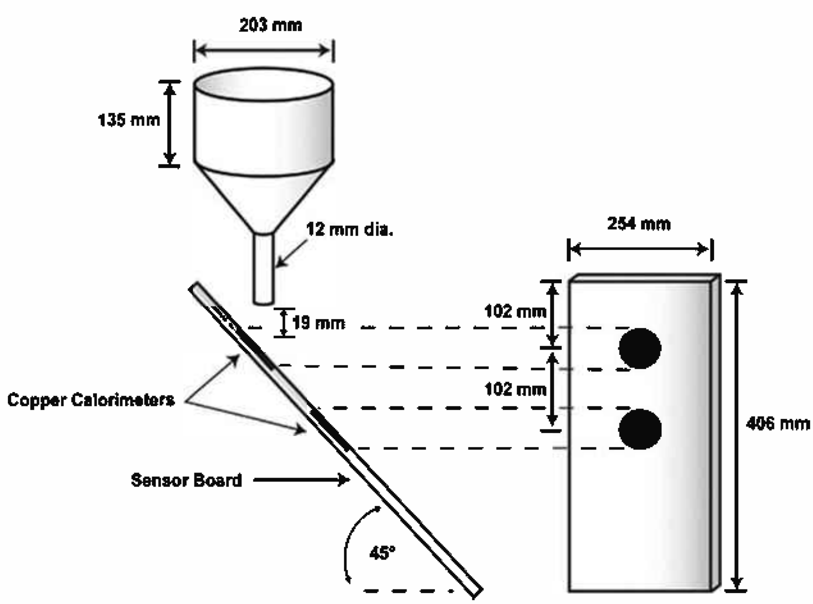

FIG. 1—*Apparatus for ASTM F2701-08.*

time to second degree burn. Not surprisingly, fabric permeability was a key factor in determining heat and mass transfer. Nevertheless, the pouring procedure is awkward, affecting flow rate and test repeatability, and risking burn injury to the operator. Data from the lower sensor were less consistent than data from the upper sensor located directly under the funnel outlet.

Changes to the method were made to more closely simulate low pressure hot water jets found in the oil industry and to improve reproducibility. The modified device is shown in Fig. 2. The funnel producing the liquid splash was replaced with a small pipe directly fed by a temperature-controlled circulating hot water bath via a small pump and through a hose and valve system, allowing for consistent application of a given quantity of water at a consistent temperature and flow rate. Water temperature, flow rate, and pressure can be altered as desired.

After a series of preliminary experiments with the modified test device varying flow rate and temperature, a flow of 1 l over 10 s (100 ml/s) and temperature of 85°C were selected for the main experiments. This temperature is similar to that of water commonly used in the oil and gas sectors.

Fabrics

A series of permeable, semi-permeable, and impermeable fabrics (Table 1) were supplied by several manufacturers, based on our stated specifications. We attempted to find fabrics in each category that varied systematically on area mass and thickness, and for thick fabrics, on compressibility. Initially, seven permeable (category A) fabrics, six semi-permeable (category B) fabrics, and two impermeable (category C) fabrics were selected for testing. Most were layered or multi-component fabrics. In preliminary testing, none of the permeable fabrics offered any significant thermal protection against the hot water stream; thus, most category A fabrics were not used in final testing reported here. Fabric A2 was included because it is structurally identical to Fabric B9/10 except

FIG. 2—*Modified test apparatus.*

TABLE 1—*Fabric descriptions.*

Fabric code	Description
Permeable	
A2	Quilted thermal liner: woven/non-woven/felt/non-woven (aramid face & non-woven; mainly aramid reprocessed felt)
Semi-Permeable	
B9	Aramid/carbon fleece/PU membrane/aramid/carbon fleece
B9/10	Quilted thermal liner: woven/non-woven/felt/PU membrane (aramid face & non-woven; mainly aramid reprocessed felt)
B10	Tri-laminate: aramid/carbon woven/PTFE membrane/aramid fleece; WR finish on outer layer
B11	Tri-laminate: aramid/carbon woven/PTFE membrane/aramid jersey
B12	Woven aramid/PU membrane; fluorocarbon finish
B15	Tri-laminate: aramid jersey/FR PU membrane/aramid jersey
Impermeable	
C18	Woven aramid treated with silicon
C20	Aramid/carbon non-woven with chemical barrier laminate

that it has no membrane. The structure of the semi-permeable fabrics includes either a polytetrafluoroethylene (PTFE) or a polyurethane (PU) membrane. Because Fabric B9/10 is intended to be used as a lining fabric, it was tested with both the lining and the membrane facing the hot water stream.

Twenty-meter rolls of each fabric were obtained. Each roll was cut into five large samples. Two replications of specimens for fabric characterization, property testing, and both steam and hot water testing were cut from two of the samples. (Specimens for full-scale steam testing were cut from the remaining three samples.) One replication of hot-water test specimens was used in preliminary testing. The second replication of five specimens was used in final testing reported here.

The fabric samples were not laundered. All specimens for characterization and hot water testing were conditioned for 24 h according to CAN/CGSB-4.2 No.2-M88 [6]. Fabric characteristics and performance properties, determined following CGSB and ISO standard test methods as noted, are reported in Table 2.

Test Procedures

Using the modified apparatus, the test specimens were clamped onto the test board within one minute of removal from the conditioning chamber, and were exposed to 1 l of hot water over 10 s. Note that the water stream was positioned to impact the fabric directly over the upper sensor. Temperature data were collected from the sensors for 60 s, including the exposure time. Only data from

TABLE 2—*Fabric characteristics and properties.*

Fabric code	Mass (g/m^2)[a]	Initial thickness (mm)[b]	Thickness @11 kPa (mm)[b]	Density (g/m^3)[c]	Density @11 kPa (g/m^3)[c]	Air permeability (l/cm^2 · sec)[d]	Thermal resistance (m^2 · C/W)[e]
A2	350	5. 0	2.1	73,377	173,550	44.81	0.20
B9	481	5.0	2.4	95,580	202,135	0.21	0.17
B9/B10	423	4.8	2.2	91,479	203,388	0.00	0.20
B10	507	2.5	1.7	201,517	307,837	0.13	0.12
B11	273	0.9	0.7	303,366	409,540	0.19	0.09
B12	261	0.7	0.5	389,177	540,572	0.0	0.17
B15	203	0.9	0.6	223545	320063	0.20	0.10
C18	776	1.1	0.9	656,124	909,516	0.00	0.08
C20	273	1.7	0.8	165,895	333,918	0.00	0.10

[a]measured following CAN/CGSB-4.2 No.5.1-M90 [7].
[b]measured following CAN/CGSB-4.2 No.37-2002 [8].
[c]calculated from mass and thickness measurements.
[d]measured following CAN/CGSB-4.2 No.36-M89 [9].
[e]measured following ISO 11092:1993 [10].

the upper sensor are reported here. The time to second-degree burn was calculated from the "Stoll Curve" as prescribed in ASTM F2701-08 [5]. If there was no predicted thermal injury within the total 60 s period, the result was reported as ">50 s." Other dependent heat transfer variables (peak temperature rise, peak heat flux, and net energy change) were calculated from the temperature/time curves. Typical curves are shown in Figs. 3 and 4.

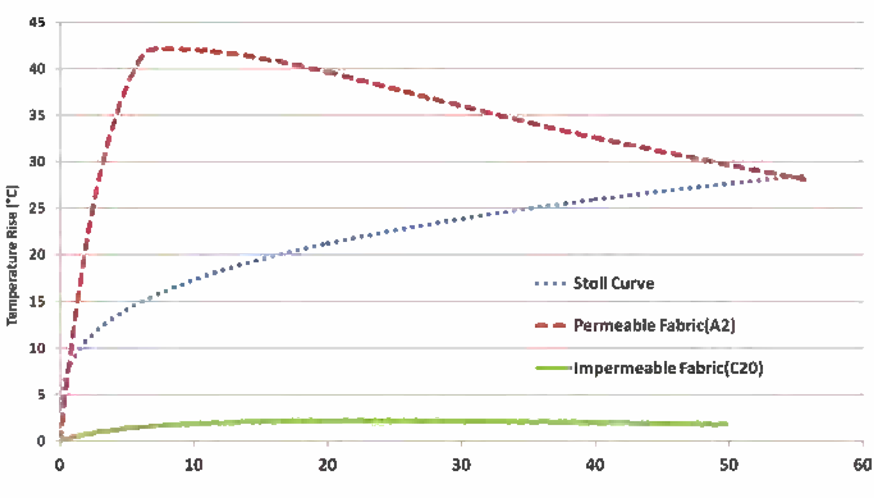

FIG. 3—*Temperature-time curve compared to Stoll curve for permeable (A2) and impermeable (C20) fabrics.*

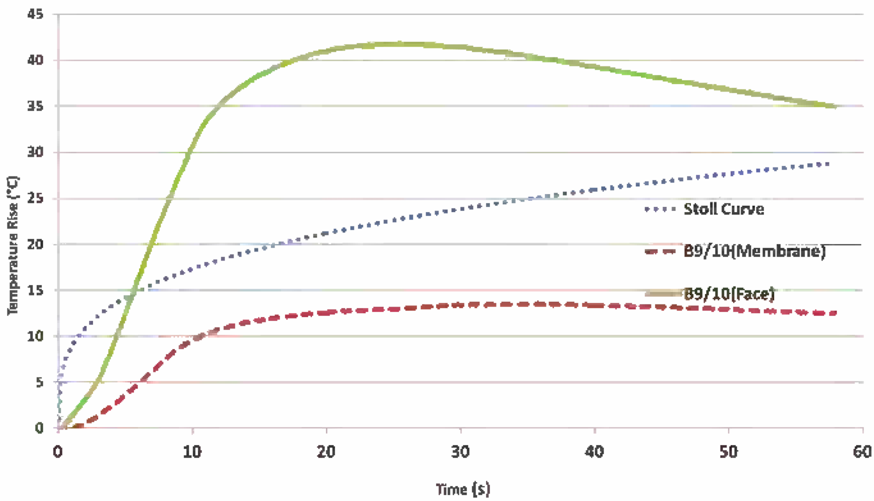

FIG. 4—*Temperature-time curve compared to Stoll curve for two orientations of Fabric B9/10.*

Statistical Analyses

Analyses were conducted using PASW (SPSS) Software, Version 18 [11]. Descriptive statistics were calculated for each dependent variable for each fabric. One way analyses of variance (ANOVAs) with Duncan's post hoc test were performed to determine differences among fabrics on peak temperature rise, net energy change, and peak heat flux.

Results and Discussion

Figures 3 and 4 demonstrate clear differences between the permeable Fabric A2 and the impermeable Fabric C20, and between the face and membrane orientations of Fabric B9/10. The calculated heat transfer variables are reported in Table 3, and ANOVA results on two of those dependent variables are reported in Table 4. It should be noted that only three of the fabrics, the permeable Fabric A2 and the semi-permeable Fabrics B12 and B9/10(F), allowed sufficient heat transfer to reach the second degree burn criterion. When tested with the membrane facing the water stream, and with insulating layers behind the membrane, Fabric B9/10(M) performed much better.

ANOVA results for peak temperature and net energy change (Table 4) demonstrate that the test is able to differentiate the most protective from the least protective fabrics quite well, but with considerable overlap among fabrics between the extremes. On all parameters, Fabrics A2 and B9/10(F) with the face oriented toward the water stream are clearly less protective than the other fabrics. The curves for both fabrics (Figs. 3 and 4) show a steep rise in

TABLE 3—*Heat transfer parameters.*

Fabric code	Time to second degree burn (s) mean (Standard deviation)	Peak temperature rise (°C) mean (Standard deviation)	Peak heat flux (kW/m^2) mean (Standard deviation)	Net energy Change @ 50 s (kJ/m^2) mean (Standard deviation)
A2	2.4 (0.7)	52.3 (2.0)	63.6 (8.7)	228.5 (14.4)
B9	>50	10.3 (2.2)	11.6 (1.7)	55.4 (11.7)
B9/10(F)[a]	6.4 (3.1)	39.0 (8.9)	25.4 (6.2)	192.5 (39.6)
B9/10(M)[b]	>50	4.7 (1.9)	13.4 (4.1)	12.9 (2.0)
B10	>50	6.4 (1.5)	12.2 (2.8)	33.8 (8.7)
B11	>50	15.0 (3.0)	17.4 (1.4)	70.9 (22.1)
B12	9.5 (1.0)	12.4 (3.9)	15.4 (4.7)	46.1 (13.1)
B15	>50	11.2 (0.7)	15.2 (3.1)	50.4 (2.2)
C18	>50	10.0 (0.6)	17.5 (3.2)	53.0 (3.2)
C20	>50	5.0 (0.8)	12.6 (3.5)	26.0 (4.3)

[a]Face (lining) side oriented toward hot water source.
[b]Membrane side oriented toward hot water source.

temperature, especially for Fabric A2. It was observed that B9/10(F) absorbed and held much water, likely contributing to stored energy that was later released; note that the temperature for this fabric does not drop much after it reaches its peak temperature rise. When the fabric is oriented as intended for use as in B9/10(M), with the membrane toward the water, the water does not penetrate the other layers and this fabric performs very well.

TABLE 4—*Analysis of variance: Differentiation among fabrics.*

Fabric	Peak temperature Rise (°C) (mean)	Net energy change @ 50 s (kJ/m^2) (mean)
B9/10(M)	4.74^{d}	12.84^{d}
C20	4.98^{d}	26.03^{d,e}
B10	6.40^{d,e}	33.82^{d,e}
C18	9.95^{e,f}	53.01^{f,g}
B9	10.32^{e,f}	55.40^{f,g}
B15	11.20^{f,g}	50.35^{f,g}
B12	12.38^{f,g}	46.09^{e,f}
B11	15.00^{g}	70.85^{g}
B9/10(F)	38.98^{h}	192.47^{h}
A2	52.26^{i}	228.47^{i}
	Corrected F Value = 107.25, ($p < 0.001$)	Corrected F Value = 95.64, ($p < 0.001$)

[a,b,c,d,e,f]Within each column, means with the same superscript do not differ significantly from each other according to the Duncan's test.

TABLE 5—*Correlations among selected dependent and independent variables (semi-permeable fabrics only).*

Fabric characteristics	Dependent Variables		
	Peak temperature rise	Net energy change @ 10 s	Net energy change @ 50 s
Mass	– 0.585[a]	– 0.863[a]	– 0.403[b]
Initial Thickness	– 0.558[a]	– 0.864[a]	– 0.393[b]
Thickness @ 11.6 kPa	– 0.583[a]	– 0.895[a]	– 0.404[b]
Thickness Change	– 0.324	– 0.777[a]	– 0.121
Initial Density	0.592[a]	0.820	0.437[b]
Density @ 11.6 kPa	0.548[a]	0.768	0.399[b]

[a]$P < 0.01$
[b]$P < 0.05$

On all parameters, Fabrics B9/10(M), C20, and B10 show the best protection, with C18, B9, B15, and B12 following for most parameters. B12 does reach the second degree burn criterion, but only after 9.5 s. While B11 does not reach the second degree burn criterion, its performance on other parameters may be of concern.

Correlations between selected fabric characteristics of the semi-permeable fabrics and two dependent variables (Table 5) show that, in general, while the heavier, thicker fabrics in this category are more protective than lighter, thinner ones, initial density has a major effect. Although significant, most of the correlations are far from perfect, due largely to the effect of other fabric structural characteristics.

Proposed Specifications for Two Levels of Protection

Firms in the oil and gas industry have requested that specifications be set for two levels of protection from hot water exposure: Level 1 garments that could be worn on site most of the workday, and Level 2 garment systems that could be worn for short-term but higher risk exposure situations. If for Level 2 the time to second degree burn criteria for this test were set at >50 s, and the net energy change criterion set at <35 kJ/m^2, fabrics B9/10(M), C20, and B10 could be recommended as Level 2 protection. If for Level 1 the time to second degree burn criteria for this test were set at >8 s and the net energy change criterion set at under 80 kJ/m^2, the remaining fabrics except A2 and B9/10(F) could be recommended as Level 1 protection.

Conclusions and Recommendations

A modified test apparatus and revised procedures have been developed that facilitate testing materials exposed to hot water under conditions that better simulate low pressure hot water streams found in industry. The apparatus is easy to operate safely. Testing materials using this device can provide data that will differentiate among them, screening unsuitable materials and allowing specification of requirements for two levels of protection against the hazard of hot water. Results suggest that water permeable fabrics cannot protect against hot water, and that the orientation of the membrane in semi-permeable fabrics is an important factor in determining the protection afforded.

Observations and correlations between test data and fabric characteristics and properties will inform the design and production of improved protective materials. For example, a layer of thermal insulation behind the membrane is important to avoid heat transfer even if the membrane protects from water penetration through the fabric.

Further modifications could be made to the test apparatus and procedures. Although preliminary testing included use of different flow rates before selecting one for this research, further testing with different flow rates and water pressures is recommended, as is evaluation of the reliability of the method. The original sensor board material absorbs water, which could interfere with the proper functioning of the sensor when testing permeable fabrics. Using a sensor board that will not absorb water would be an improvement. In addition, a modified system to hold fabric on the board would facilitate easier handling of specimens.

Acknowledgments

The writers wish to thank Dr. Jane Batcheller, Stephen Paskaluk, and Ghulam Murtaza for technical assistance; Dr. Tom Neal of Neal Associates for loan of the test apparatus; Davey Textiles for securing fabrics; and Dan King, Dr. J. Douglas Dale, and representatives of our funding partners for their valuable advice. Funding for this project is provided by Natural Sciences & Engineering Research Council of Canada (NSERC), Canadian Association of Petroleum Producers (CAPP), Imperial Oil Resources Ltd., Nexen Inc., Total E & P Canada Inc., and DuPont Canada Inc. The researchers would also like to thank the Protective Clothing & Equipment Research Facility (PCERF) and the Departments of Human Ecology and Mechanical Engineering at the University of Alberta for their support.

References

[1] Huyer, S. and Corkum, S., "Reducing the Incidence of Scalds: Strategies for Physicians," *Can. Med. J.*, Vol. 156, pp. 841–844, 1997.

[2] Workers' Compensation Board, "Workers' Compensation Board—Alberta 2009 Annual Report," Workers' Compensation Board, Alberta, Edmonton, AB, 2009, 87 pp.

[3] Fennell, D. J., "Flash and Splash—Protective Equipment for Our Workers,"Presentation to Petroleum Safety Conference, Banff, AB (sponsored by ENFORM), May 2009, available upon request from ENFORM at: safety@enform.ca or from the author at: dave.j.fennell@esso.ca.
[4] Armstrong, C. P. and Harris, W. S., "Temperature Distributions in Steam and Hot Water Jets Simulating Leaks," *ASHRAE Trans.*, Vol. 72, 1966, pp. 146–156.
[5] ASTM Standard F2701 – 2008, "Standard Test Method for Evaluating Heat Transfer through Materials for Protective Clothing upon Contact with a Hot Liquid Splash," ASTM International, West Conshohocken, PA, 2008. Available at: http://www.astm.org.
[6] CAN/CGSB – 4.2 No. 2, 1988, "Textile Test Methods—Conditioning Textile Materials for Testing," Canadian General Standards Board, Ottawa, ON.
[7] CAN/CGSB – 4.2 No. 5.1 – M90, 2004, "Textile Test Methods—Fabric Mass," Canadian General Standards Board, Ottawa, ON.
[8] CAN/CGSB – 4.2 No. 37, 2002, "Textile Test Methods—Fabric Thickness," Canadian General Standards Board, Ottawa, ON.
[9] CAN/CGSB – 4.2 No. 36 – M89, 1997, "Textile Test Methods—Air Permeability," Canadian General Standards Board, Ottawa, ON.
[10] ISO 11092, 1993, "Textiles—Physiological Effects—Measurement of Thermal and Water-Vapour Resistance Under Steady-State Conditions (Sweating Guarded-Hotplate Test)," International Organization for Standardization, Geneva.
[11] PASW Software, Version 18, SPSS Inc., Chicago, IL, 2009.

Performance of Protective Clothing and Equipment: Emerging Issues and Technologies
STP 1544, 2012
Available online at www.astm.org
DOI:10.1520/STP104096

Chantal Gauvin,[1] *Olivier Darveau,*[1] *Charlotte Robin,*[1] *and Jaime Lara*[2]

Analysis of Test Parameters and Criteria for Characterizing and Comparing Puncture Resistance of Protective Gloves to Needles

---

REFERENCE: Gauvin, Chantal, Darveau, Olivier, Robin, Charlotte, and Lara, Jaime, "Analysis of Test Parameters and Criteria for Characterizing and Comparing Puncture Resistance of Protective Gloves to Needles," *Performance of Protective Clothing and Equipment: Emerging Issues and Technologies* on April 16, 2011 in Anaheim, CA; STP 1544, Angie M. Shepherd, Editor, pp. 340–353, doi:10.1520/STP104096, ASTM International, West Conshohocken, PA 2012.

ABSTRACT: Needlestick injuries that expose workers to infection by blood-borne pathogens can be prevented by the use of appropriate protective gloves. Recently, an F23 ASTM task group developed the test method ASTM F2878-10, which defines needle puncture resistance as the maximum force recorded during tests using one of three hypodermic needle gauges. This study has two objectives: (1) to assess the effect of needle gauge on the ranking of glove puncture performance using the ASTM F2878-10 standard test method, and (2) to analyze the correspondence between maximum puncture force and puncture-through using an electrical detection device during needle penetration in protective gloves made of reinforced and multilayer composite materials. Two series of experiments were performed. In the first one, seven glove materials were characterized as described in the ASTM test method. The glove puncture resistance results were ranked after testing with the 21, 25, and 28 needle gauges. In the second experiment, a test device was used to electrically detect the force at which the needle tip punctures the material. Puncture tests were performed on seven glove materials following the ASTM F2878-10 test method and using this electrical device.

Manuscript received June 1, 2011; accepted for publication April 17, 2012; published online September, 2012.
[1]Institut de recherche Robert-Sauvé en santé et en sécurité du travail (IRSST), Montreal, Quebec, H3A 3C2, Canada.
[2]Institut de recherche Robert-Sauvé en santé et en sécurité du travail (IRSST), Montreal, Quebec, H3A 3C2, Canada (Currently at Univ. of Montreal, Quebec, H3C 3J7, Canada).

The maximum force and force at puncture-through criteria are discussed. In the first experiment, the needle puncture resistance ranking of the gloves was almost equivalent for all three needle gauges. For glove selection purposes, the use of a single needle gauge provides sufficient information on needle puncture resistance for a comparison of the performance of the protective glove materials. In the second experiment, for two of the seven glove models, needle puncture-through was detected before the maximum force was reached. For those cases, the force at puncture-through criterion provides additional information on the material resistance that is not fully captured by the maximum force criterion alone, but it requires a more complex experimental setup.

KEYWORDS: hypodermic needle, needle puncture resistance, protective gloves, standard test method

Introduction

Needlestick injuries from discarded syringes are associated with the risk of blood-transmissible infections such as human immunodeficiency virus and hepatitis B and C. This risk is widely recognized in the medical field [1–3]. The American Occupational Safety and Health Administration estimates that 5.6 million workers are at risk of occupational exposure to blood-transmitted disease in the healthcare field [4]. In addition, workers from other sectors such as law enforcement, corrections, maintenance, sanitation, and gardening services are also at risk for needlestick injuries from potentially contaminated needles or syringes [2,3,5,6]. For instance, 57 % of a sample of 803 law enforcement officers have reported having had needlestick injuries at least once during their work [7].

Standard testing methods for measuring the puncture resistance of protective material [8,9] use blunt probes to perforate samples. These methods are not appropriate for measuring the needle puncture resistance of a material [10] because the mechanism of hypodermic needle puncture differs completely from the mechanism of blunt probe puncture. Needle puncture is thought to involve gradual cutting by the sharp edge of the needle, whereas blunt probe puncture is a failure mechanism triggered by maximum deformation [11–14]. In order to fulfill the need for a test method to characterize the needle puncture resistance of protective gloves, studies have examined the effect of test parameters such as needle gauge, penetration angle, and puncture speed on puncture force with non-reinforced and fabric-reinforced elastomers [15–18]. These works have resulted in the proposal of a test method for measuring needle puncture resistance, which was used to characterize over 50 protective gloves [17,18].

The information obtained from these studies was used in the development of the new standard test method ASTM F2878-10 [19], intended to measure a protective material's puncture resistance to hypodermic needles, under the jurisdiction of the ASTM F23 committee. In this test method, a needle positioned perpendicular to the specimen is moved down at a constant speed of 500 mm/min until the tip of the needle perforates the backside of the material specimen. Hypodermic needles must be three-facet, regular bevel, regular wall, and one of the three following gauges: 21G, 25G, or 28G. A new needle is used for each test. The specimen is clamped between two flat support plates having one or more puncture guide holes measuring 10 to 25.4 mm in diameter, with no supporting structure behind the material specimen. The force required in order to puncture the specimen, measured with the compression load cell of the testing machine, is recorded against the needle displacement. The maximum force, averaged from 12 test replicates, is reported as the puncture resistance of the material.

Standard test methods are often used to obtain data for the purpose of comparing the properties of different materials, as is the case for cut resistance and puncture resistance (U.S. classification using ANSI/ISEA 105-2011 [20], European classification using EN 388 [9]). In the case of the needle puncture test method, needles of three different gauges are proposed as puncture probes, allowing one to perform the test in conditions close to those encountered in the workplace. However, it is unknown whether the choice of needle has an effect on the glove performance ranking, particularly when the gloves have very different material compositions or thicknesses.

Some studies have tried to simulate complex needle puncture situations. In one study, simulations were done at impact speed with conical needles on clamped fibrous structures [21]. In another study, experiments were performed with 12 to 22 gauge needles at very low speed on shear-thickening fluid-treated fabrics laid on foam backing material that simulated a hand [22]. These studies indicate that the perforation of a material sometimes occurs before the maximum puncture force is reached.

The objectives of this study are as follows:

(1) assess the effect of needle gauge on the ranking of glove puncture performance, and
(2) analyze the correspondence between maximum puncture force and puncture-through during needle penetration in protective gloves made of reinforced and multilayer composite materials.

Experimental

For each of the two objectives, a series of tests were performed on a selection of glove materials according to the ASTM F2878-10 test standard [19] using an MTS Systems testing machine equipped with a 25 N load cell (precision of $\pm$0.01 N) to record the puncture force. As suggested in the standard test method, 21G, 25G, and 28G needles were used (Table 1). For each glove material, 12 replicates were done on four samples, and these were used to calculate the average (Avg), standard deviation (SD), and coefficient of variation (CV).

Effect of Needle Gauge

In order to analyze the effect of the needle gauge on the puncture results, tests were performed on the seven glove models listed in Table 2. The diameter of the

TABLE 1—*Needles characteristics.*

Gauge	Outside Diameter, mm	Length, in.	Bevel	Manufacturer	Model Number
28	0.36	0.5	Three-facet, regular bevel	Becton Dickinson	329420
25	0.51	1.5	Three-facet, regular bevel	Becton Dickinson	305127
21	0.82	1.5	Three-facet, regular bevel	Becton Dickinson	305167

holes in the specimen support assembly was 10 mm. In accordance with ASTM F2878-10, the maximum force recorded during the test (F_{max}), averaged from 12 test replicates, was used as the puncture resistance of the material.

Force at Puncture-through

In this test method, the moment when the needle tip completely crossed the specimen was measured via the detection of an electrical contact between the needle and a 0.005 mm thick piece of aluminum glued under the specimen [Fig. 1(*b*)]. The piece of aluminum and the needle were both connected to an electronic box [Fig. 1(*a*)] that sent a signal to a computer when it detected the electrical contact between the needle and the piece of aluminum. This signal was also recorded against the needle displacement, allowing synchronizing force measurements and contact detection. The force recorded when the needle completely crosses the specimen is referred to below as the force at puncture-through (PT).

A series of puncture tests were done on seven protective glove models (Table 3) using the experimental device capable of detecting PT. We used 21G, 25G, and 28G needles for all models, except for models C1 and E1, for

TABLE 2—*Protective gloves used to analyze the effect of needle gauge.*

Manufacturer	Glove Model	Description	Thickness, mm
A	A1	Three layers of composite reinforced material (patented protective material) underneath one layer of cotton	2.5
	A2	Three layers of composite reinforced material (patented protective material) under nitrile dipped canvas shell	3.3
	A3	Two layers of composite reinforced material (patented protective material) and synthetic leather	1.8
B	B1	One layer of woven aramid fibers (patented technology of tight weave)	0.8
C	C1	Leather and 12 layers of woven nylon	2.8
D	D1	Coated nitrile-reinforced polyvinyl chloride on a cotton interlock liner	0.5
	D2	13-gauge cut-resistant high performance polyethylene engineered fiber with polyurethane coating	1.4

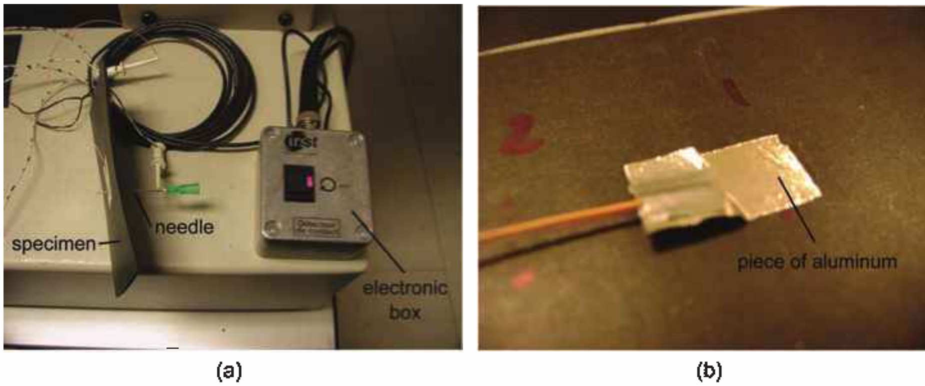

FIG. 1—*(a) Experimental device used to determine when the needle completely crosses through the specimen during a puncture test. (b) Attachment of a piece of aluminum to the specimen and wire.*

which only 25G and 28G needles were used for sample availability reasons. A specimen support assembly with holes 25.4 mm in diameter was used. This hole diameter value is the maximum allowed by the test standard, and it was chosen in order to facilitate the detection of the needle PT.

Results and Discussion

Effect of Needle Gauge

Figure 2 shows the ranking of the seven glove models according to the maximum force to puncture the material for each of the three needle gauges. For all

TABLE 3—*Gloves used to compare puncture resistance criteria.*

Manufacturer	Glove Model	Description	Thickness, mm
A	A1	Three layers of composite reinforced material (patented protective material) underneath one layer of cotton	2.5
	A2	Three layers of composite reinforced material (patented protective material) under nitrile dipped canvas shell	3.3
	A3	Two layers of composite reinforced material (patented protective material) and synthetic leather	1.8
B	B1	One layer of woven aramid fibers (patented technology of tight weave)	0.8
	B2	One layer of woven aramid fibers (patented technology of tight weave) under genuine leather	1.2
C	C1	Leather and 12 layers of woven nylon	2.8
E	E1	100 % Kevlar knit and leather palm	2.3

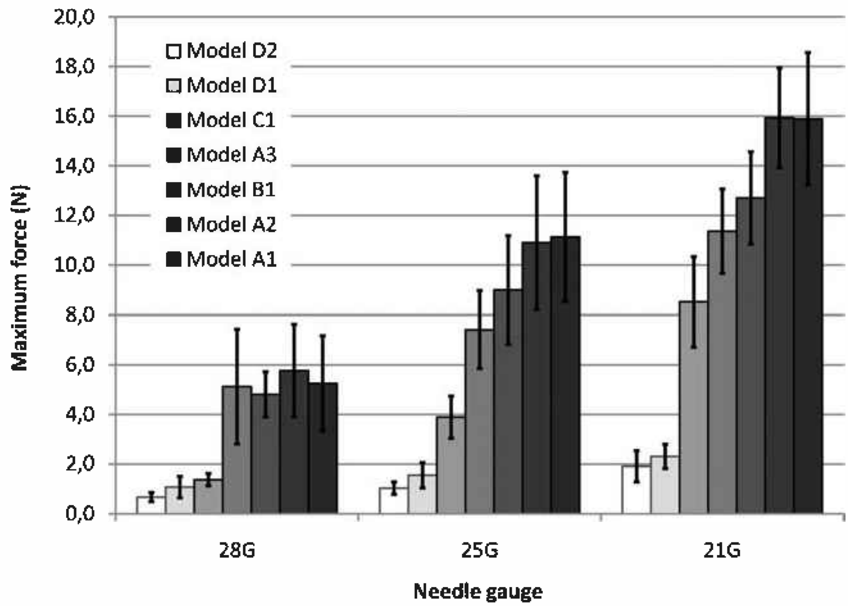

FIG. 2—*Maximum force for seven glove models using three needle gauges.*

glove materials, the maximum force increases with the needle diameter, as was observed for elastomers and fabric-reinforced materials tested in similar conditions [15]. For the tested glove models, the performance rankings are almost equivalent for the three needle gauges. Gloves A1 and A2 were more puncture resistant to any needle gauge than gloves D1 and D2. The differences between

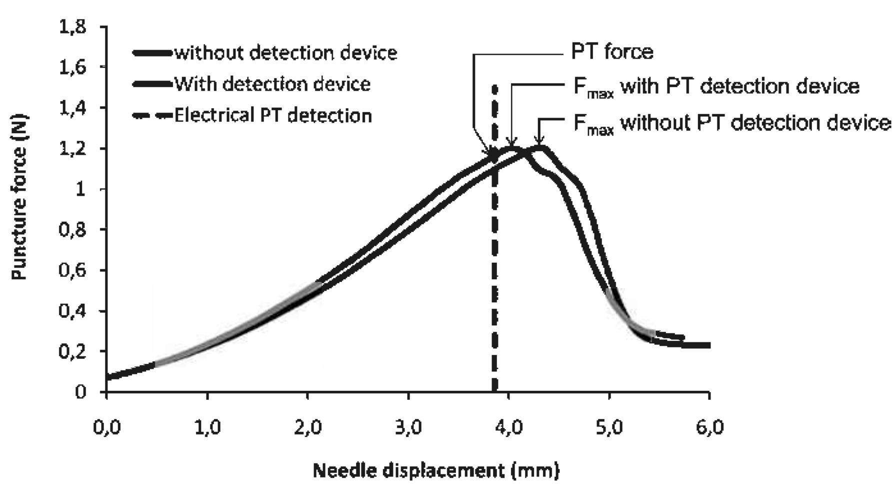

FIG. 3—*Examples of puncture force versus needle displacement curves obtained with and without the PT detection device (1.5 mm thick neoprene, 25G needle, 100 mm/min needle speed).*

TABLE 4—*Validation results for puncture-through detection device.*

			F_{max} without Detection Device, N		F_{max} with PT Detection Device, N		PT Force Detected with Electrical Device, N		Is Difference Significant between:	
Neoprene Thickness, mm	Needle	Speed, mm/min	Avg	CV, %	Avg	CV, %	Avg	CV, %	F_{max} without Detection Device and F_{max} with Detection Device	F_{max} with Detection Device and PT Force
1.5	21G	500	1.63	6.6	1.63	3.2	1.45	5.4	NS	S
	25G	100	1.12	6.3	1.12	4.7	1.09	4.8	NS	NS
	28G	5	0.71	3.5	0.72	4.7	0.71	4.4	NS	NS
	28G	500	0.98	7.7	1.03	4.3	0.99	4.5	NS	NS
0.4	25G	500	0.29	11.9	0.32	12.3	0.26	16.5	NS	S
	28G	500	0.27	7.8	0.28	4.4	0.22	13.6	S	S

Notes: NS, no significant difference between the two measures; S, significant difference between the two measures.

gloves are amplified and the CVs are smaller when using a needle with a larger diameter, such as the 21G. Glove models A1, A2, A3, and B1 had equivalent performance when tested with the smallest diameter needle (28G).

Based on these observations, one needle gauge seems sufficient for comparing or ranking glove resistance to needle puncture. It is important to point out that the needles most commonly encountered by non-healthcare workers are 28G, mainly used by drug users. However, a 25G needle is less difficult to manipulate than a 28G in the needle puncture test.

Force at Puncture-through

Validation of the Puncture-through Detection Device—Prior to the performance of tests on gloves, the PT detection device was validated using neoprene of 1.5 and 0.4 mm thickness, at speeds between 5 and 500 mm/min, with 21G, 25G, and 28G needles. *T*-test statistical analyses with a 95 % confidence interval were done in order to compare results with and without the PT detection device. The results showed that the piece of aluminum glued to the specimen did not significantly alter the needle force versus displacement curve

TABLE 5—*Maximum forces and PT forces for glove materials.*

		Maximum Force, N			PT Force, N			Maximum Force Prior to PT, N		
Glove Model	Needle	Avg	SD	CV, %	Avg	SD	CV, %	Avg	SD	CV, %
A1	21G	15.33	1.62	10.6	13.41	2.95	22.0	13.63	2.87	21.0
	25G	10.64	3.43	32.2	9.20	3.78	41.1	9.98	4.02	40.3
	28G	6.86	2.02	29.4	5.85	1.73	29.6	6.93	2.11	30.5
A2	21G	14.12	2.23	15.8	10.09	3.73	37.0	10.26	3.73	36.4
	25G	10.53	2.74	26.0	9.80	2.26	23.1	10.64	3.06	28.8
	28G	5.92	1.74	29.3	5.39	1.51	28.1	5.82	1.83	31.5
A3	21G	9.51	1.18	12.4	6.95	2.33	33.6	8.36	1.97	23.5
	25G	7.32	2.80	38.3	6.05	3.68	60.9	6.42	3.56	55.4
	28G	4.88	2.21	45.3	3.61	2.00	55.6	4.73	2.39	50.6
B1	21G	10.94	1.72	15.7	4.37	2.24	51.4	4.37	2.24	51.3
	25G	8.08	1.70	21.1	3.35	2.14	63.9	4.35	2.65	60.9
	28G	5.56	1.46	26.3	3.65	2.18	59.8	3.68	2.16	58.8
B2	21G	8.30	2.39	28.8	3.24	1.38	42.5	3.24	1.38	42.5
	25G	5.01	1.04	20.8	3.32	1.52	45.7	3.32	1.52	45.6
	28G	2.49	0.68	27.3	1.57	0.72	45.8	1.57	0.72	45.9
C1	25G	3.66	0.52	14.2	2.79	0.70	25.0	3.66	0.52	14.2
	28G	1.56	0.38	24.1	0.99	0.16	16.6	1.51	0.35	23.1
E1	25G	2.25	0.68	30.2	2.04	0.64	31.4	2.25	0.68	30.2
	28G	0.94	0.24	25.6	0.61	0.16	25.5	0.94	0.24	25.6

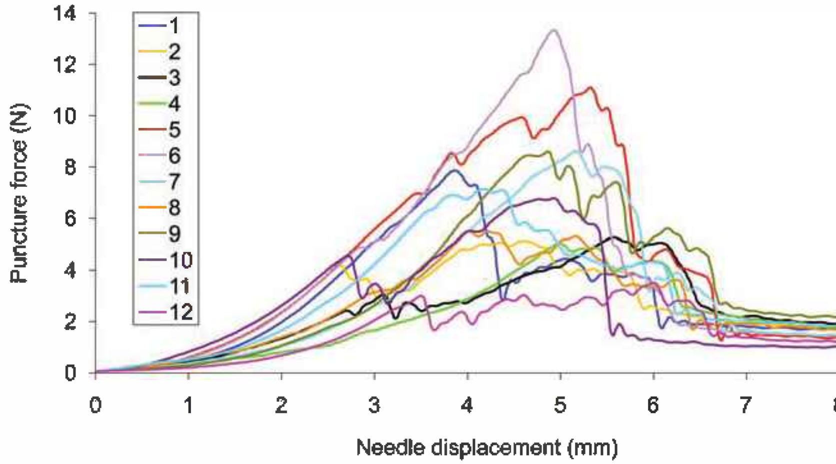

FIG. 4—*Sample results from 12 puncture test replicates for glove model A3 (25G needle, 500 mm/min speed).*

(Fig. 3), therefore leaving the maximum force value unchanged, as shown in Table 4. Moreover, this analysis has shown that the PT condition is detected at the same time as or slightly before the maximum force is attained. This means that there is no significant difference between the force at PT and the maximum force, as was shown for elastomers [15]. With the PT electrical detection device, the variability of the maximum force was less than 8 % for 1.5 mm thick neoprene, and less than 13 % for 0.4 mm thick neoprene.

Puncture Resistance Characterization Using Electrical Detection Device—The results of PT tests on gloves are presented in Table 5. The maximum force

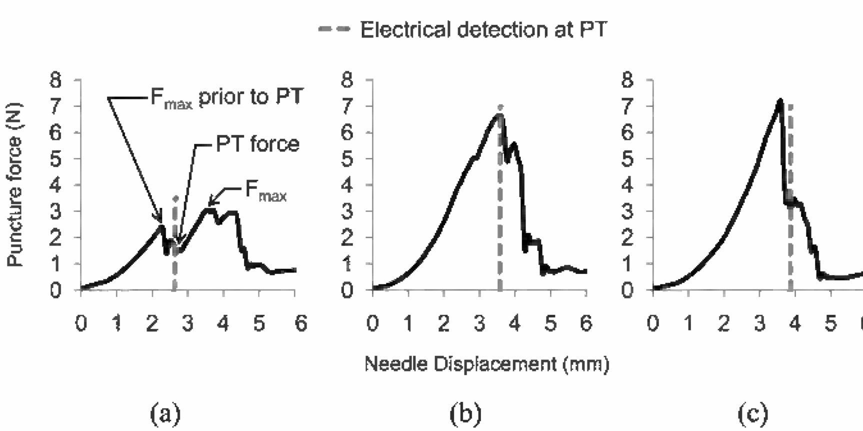

FIG. 5—*Specimen results from three puncture tests with glove model A1 and a 28G needle at 500 mm/min. PT occurs before (a), during (b), or after (c) the maximum force is reached.*

for gloves has a high variability (11 % to 45 %), probably because they are made of heterogeneous materials, as opposed to neoprene (CV between 3 % and 12 %; see Table 4), which is a homogeneous elastomer. The PT force has greater variability (17 % to 64 %) than the maximum force. Figure 4 shows examples of puncture force versus needle displacement curves for 12 replicates with glove model A3. These curves have multiple peaks, possibly because this glove model is made of two layers of heterogeneous materials.

Table 5 also shows that the maximum force does not always correspond to the PT force. In some cases, the PT force is clearly much lower than the maximum force, such as for glove models B1 and B2. It was also observed that the needle might puncture the specimen before, during, or after maximum force is reached. Figure 5 illustrates this behavior on three test replicates done on the same specimen (glove model A1).

PT timing, defined as the time at which PT is electrically detected with respect to maximum force, is presented in Table 6 for all glove models and all needle gauges. Whether PT occurs mostly before, during, or after maximum force seems to depend on the type of glove material rather than the needle gauge. For glove models A1, A2, and A3, each made of multi-layers of

TABLE 6—*Number of trials in which PT occurred during, before, and after maximum force.*

		Timing of PT Force/Number of Replicates			
Glove Model	Needle	During F_{max}	Before F_{max}	After F_{max}	Global Trend
A1	21G	8/12	4/12	0/12	During F_{max}
	25G	7/11	2/11	2/11	During F_{max}
	28G	7/10	0/10	3/10	During F_{max}
A2	21G	4/12	8/12	0/12	Before F_{max}
	25G	5/10	2/10	3/10	During F_{max}
	28G	8/12	1/12	3/12	During F_{max}
A3	21G	3/11	6/11	2/11	Before F_{max}
	25G	7/12	5/12	0/12	During F_{max}
	28G	7/12	1/12	4/12	During F_{max}
B1	21G	1/12	11/12	0/12	Before F_{max}
	25G	1/10	8/10	1/10	Before F_{max}
	28G	3/10	7/10	0/10	Before F_{max}
B2	21G	0/12	12/12	0/12	Before F_{max}
	25G	2/12	10/12	0/12	Before F_{max}
	28G	1/12	11/12	0/12	Before F_{max}
C1	25G	5/11	0/11	6/11	After F_{max}
	28G	2/11	0/11	9/11	After F_{max}
E1	25G	6/12	2/12	4/12	During F_{max}
	28G	0/11	0/11	11/11	After F_{max}

composite reinforced material, PT occurred mostly during maximum force. However, for glove models B1 and B2, made of one layer of woven aramid fibers, PT was almost always detected before maximum force. Such results have been reported in other studies [21,22].

For the purpose of characterizing and comparing glove performance, a greater needle puncture resistance of a glove means better protection against needles. The maximum force is shown to be an appropriate criterion of puncture resistance for glove models A1, A2, A3, C1, and E1. In other studies, maximum force also has been shown to be a sufficient criterion for characterizing the needle puncture resistance of elastomer materials, as PT was detected during maximum force [13–15]. However, for glove models B1 and B2 tested in this study, no correspondence was found between maximum force and PT. In fact, for those gloves, the needle PT is detected at a lower force than the maximum force recorded during the test. This could represent a risk of contact of the needle tip with the skin of the glove user. Consequently, maximum force recorded prior to PT could be another valid criterion of the puncture resistance of gloves.

The maximum force recorded prior to PT detection is reported in the last three columns of Table 5. The results show that the maximum force prior to PT and the PT force have similar CVs. Figure 6 shows the glove performance rankings obtained when the maximum force or the maximum force prior to PT criteria are used. The difference between these two performance criteria might be high enough to change the ranking of at least one of the seven glove models

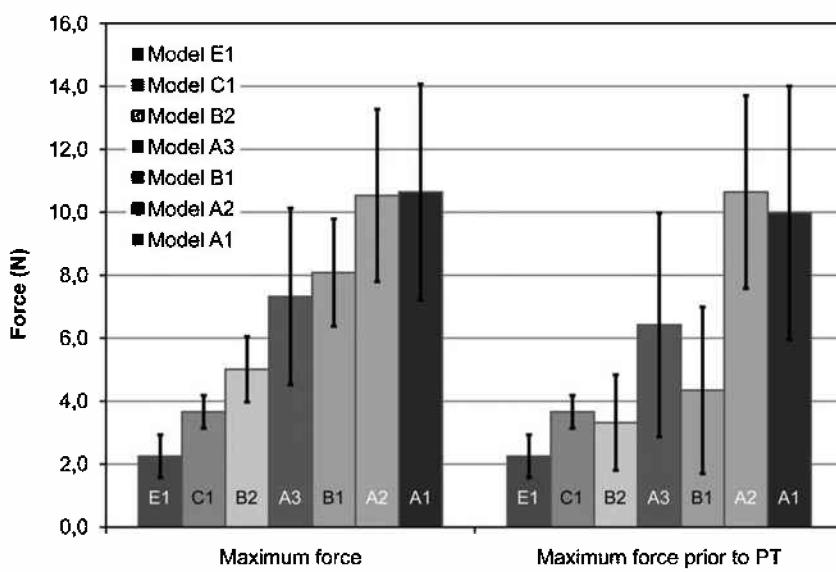

FIG. 6—*Glove models ranking according to the maximum force criterion and to the maximum force prior to PT criterion (25G needle).*

considered in this study. The maximum force prior to PT criteria deserves to be investigated further with other protective glove materials.

Conclusion

This study has shown that the ranking of gloves' performance according to the ASTM F2878-10 standard test method is similar for all needle gauges. Therefore, a single needle gauge seems sufficient to provide performance comparison data for glove models.

This study also has shown that for certain gloves, PT occurs before the maximum force is reached. Therefore, the use of maximum force prior to PT provides additional performance information that is not always fully captured by the maximum force criterion of ASTM F2878-10. However, the measurement of PT requires the use of a test device that can electrically detect PT.

Acknowledgments

The writers would like to thank Jérôme Boutin and Pierre Drouin for their help in the development of the electrical detection device and in the needle puncture testing, respectively.

References

[1] National Institute for Occupational Safety and Health (NIOSH), 1999, "Preventing Needlestick Injuries in Health Care Settings," *DHHS (NIOSH) Publication No. 2000-108*, NIOSH, Centers for Disease Control and Prevention, U.S. Department of Health and Human Services, Atlanta, GA.

[2] Chen, G. X. and Jenkins, E. L., "Potential Work-related Bloodborne Pathogen Exposures by Industry and Occupation in the United States Part I: An Emergency Department-based Surveillance Study," *Am. J. Ind. Med.*, Vol. 50, No. 3, 2007, pp. 183–190.

[3] Chen, G. X. and Jenkins, E. L., "Potential Work-related Exposures to Bloodborne Pathogens by Industry and Occupation in the United States Part II: A Telephone Interview Study," *Am. J. Ind. Med.*, Vol. 50, No. 4, 2007, pp. 285–292.

[4] Occupational Safety and Health Administration, 2009, "Bloodborne Pathogens and Needlestick Prevention—Hazard Recognition," www.osha.gov (Last accessed February 10, 2009).

[5] O'Leary, F. M. and Green, T. C., "Community Acquired Needlestick Injuries in Non-health Care Workers Presenting to an Urban Emergency Department," *Emergency Medicine*, Vol. 15, No. 5–6, 2003, pp. 434–440.

[6] Pagane, J., Chanmugam, A., Kirsch, T., and Kelen, G. D., "New York City Police Officers Incidence of Transcutaneous Exposures," *Occup. Med.*, Vol. 46, No. 4, 1996, pp. 285–288.

[7] Lorentz, J., Hill, L., and Samimi, B., "Occupational Needlestick Injuries in a Metropolitan Police Force," *Am. J. Prev. Med.*, Vol. 18, No. 2, 2000, pp. 146–150.

[8] ASTM F1342-05, 2005, "Standard Test Method for Protective Clothing Material Resistance to Puncture," *Annual Book of ASTM Standards*, Vol. 11.03, ASTM International, West Conshohocken, PA.

[9] EN 388, 2003, "Protective Gloves against Mechanical Risks," European Committee for Standardization, Brussels.

[10] Jackson, E. M., Wenger, M. D., Neal, J. G., Thacker, J. G., and Edlich, R. F., "Inadequate Standard for Glove Puncture Resistance: Allows Production of Gloves With Limited Puncture Resistance," *J. Emerg. Med.*, Vol. 16, No. 3, 1998, pp. 461–465.

[11] Nguyen, C. T., Vu-Khanh, T., and Lara, J., "A Study on the Puncture Resistance of Rubber Materials Used in Protective Clothing," *J. ASTM Int.*, Vol. 2, No. 4, 2005, pp. 245–258.

[12] Nguyen, C. T. and Vu-Khanh, T., "Mechanics and Mechanisms of Puncture by Medical Needles," *Procedia Engineering*, Vol. 1, No. 1, 2009, pp. 139–142.

[13] Nguyen, C. T., Vu-Khanh, T., Dolez, P., and Lara, J., "Puncture of Elastomers Membranes by Medical Needles. Part I: Mechanisms," *Int. J. Fract.*, Vol. 155, No. 1, 2009, pp. 75–81.

[14] Nguyen, C. T., Vu-Khanh, T., Dolez, P., and Lara, J., "Puncture of Elastomers Membranes by Medical Needles. Part II: Mechanics," *Int. J. Fract.*, Vol. 155, No. 1, 2009, pp. 83–91.

[15] Dolez, P., Vu-Khanh, T., Thang Nguyen, C., Guero, G., Gauvin, C., and Lara, J., "Influence of Medical Needle Characteristics on the Resistance to Puncture of Protective Glove Material," *J. ASTM Int.*, Vol. 5, No. 1, 2008.

[16] Nguyen, C. T., Dolez, P. I., Vu-Khanh, T., Gauvin, C., and Lara, J., "Resistance of Protective Gloves Materials to Puncture by Medical Needles," *J. ASTM Int.*, Vol. 7, No. 5, 2010.

[17] Gauvin, C., Dolez, P. I., Lara, J., Nguyen, C. T., Guero, G., and Vu-Khanh, T., "Glove Resistance to Hypodermic Needle Puncture—Method Development and Gloves Characterization," *1st International Conference on Personal Protective Equipment, CENTEXBEL, Brussels, Belgium, "For More (than) Safety*," Bruges, Belgium, May 21–23, 2008.

[18] Vu-Khanh, T., Dolez, P. I., Nguyen, C. T., Gauvin, C., and Lara, J., "Glove Resistance to Needle Puncture - Development of a Test Method," *Report R-711*, Institut Robert-Sauvé en santé et en sécurité du travail (IRSST), Montréal, PQ, Canada, 2011.

[19] ASTM F2878-10, 2010, "Standard Test Method for Protective Clothing Material Resistance to Hypodermic Needle Puncture," *Annual Book of*

ASTM Standards, Vol. 11.03, ASTM International, West Conshohocken, PA.

[20] ANSI/ISEA 105-2011, 2011, "American National Standard for Hand Protection Selection Criteria," International Safety Equipment Association, Arlington, VA.

[21] Termonia, Y., "Puncture Resistance of Fibrous Structures," *Int. J. Impact Eng.*, Vol. 32, 2006, pp. 1512–1520.

[22] Houghton, J. M., Schiffman, B. A., Kalman, D. P., Wetzel, E. D., and Wagner, N. J., "Hypodermic Needle Puncture of Shear Thickening Fluid (STF)-Treated Fabrics," *Proceedings of SAMPE*, 52nd International SAMPE Symposium and Exhibition (ISSE), June 3–7, 2007, Baltimore, MD, 2007.

Performance of Protective Clothing and Equipment: Emerging Issues and Technologies
STP 1544, 2012
Available online at www.astm.org
DOI:10.1520/STP104087

Patricia I. Dolez,[1] Mariem Azaiez,[2] and Toan Vu-Khanh[2]

Characterization of the Resistance of Protective Gloves to Pointed Blades

REFERENCE: Dolez, Patricia I., Azaiez, Mariem, and Vu-Khanh, Toan, "Characterization of the Resistance of Protective Gloves to Pointed Blades," *Performance of Protective Clothing and Equipment: Emerging Issues and Technologies* on 16 April 2011 in Anaheim, CA; STP 1544, Angie M. Shepherd, Editor, pp. 354–370, doi:10.1520/STP104087, ASTM International, West Conshohocken, PA 2012.

ABSTRACT: Hand lacerations account for a large percentage of occupational injuries. Wearing appropriate protective gloves has been shown to reduce these risks. However, the case of pointed blades, which include knife tips, metal sharps, and a large number of cutting tools, is still largely unexplored and calls for more research. This paper presents some initial results of tests performed with glove materials and several types of pointed blades used as a puncture probe. Tested glove materials include uncoated and polymer-coated Kevlar and Dyneema knits, leather as well as sheets of neoprene, nitrile rubber, and polyurethane. The effect of various parameters such as blade reuse, sample thickness, blade tip angle, probe displacement rate, blade lubrication, and sample support on the resistance of these materials to pointed blades was studied. The results show that the maximum force appears to increase in a non-linear way with the thickness of the membrane. A decrease in puncture force with decreasing tip angle was observed with all materials. In addition, measurements carried out at displacement rates between 1 and 500 mm/min eventually reveal in some instances the possible existence of two puncture regimes. Finally, the contribution of both friction and sample deformation on the pointed blade puncture process is evidenced by the large effect of lubrication and sample support on the maximum force. However, no correlation appears to exist between resistance to pointed blades and resistance to cutting or puncture measured with standard test methods. This

Manuscript received June 1, 2011; accepted for publication March 26, 2012; published online September 2012.
[1]École de Technologie Supérieure, Montréal, Québec H3C 1K3, Canada (Corresponding author), e-mail: patricia.dolez@etsmtl.ca
[2]École de Technologie Supérieure, Montréal, Québec H3C 1K3, Canada.

demonstrates the need for more research in that area and ultimately a dedicated standard test method.

KEYWORDS: protective gloves, puncture, pointed blades

Introduction

Hand lacerations account for 20 % of occupational injuries in Quebec [1]. More than half of them correspond to cutting/puncture-type lacerations. In some sectors like the meat processing industry, knife cuts even represent close to 30 % of all hand injuries [2]. Wearing appropriate protective gloves has been shown to reduce the risks of hand injuries. In the case of lacerations and punctures, it has been estimated that this reduction can reach 60 % to 70 % [3].

Among the mechanical hazards involved in hand injuries, some have already been the subject of large research efforts, which have led to the adoption of corresponding standard test methods: for example, ASTM F1790 and ISO 13997 for cutting [4,5], ASTM F1342 for puncture [6], and ASTM F2878 for needle puncture [7]. However, when several of these mechanical hazards are present simultaneously and because there is no correlation between the resistance of protective gloves to these different hazards [8], some have brought themselves to wearing two pairs of gloves over one another; for example, a cut-resistant and a puncture-resistant one [2]. This double-gloving practice is far from an ideal solution because of the reduction in comfort, dexterity, and manual performance and the increase in muscular fatigue associated with wearing protective gloves [9].

On the other hand, exposure to pointed blades like knife tips, metal sharps, glass splinters, and a large number of cutting tools, which occurs in a large number of occupational settings, for example in the food industry and in metal machining workshops, is currently not covered by glove selection criteria like those proposed by ANSI [10] or by ASTM test methods for protective gloves. It represents also a situation where combined resistance to cutting and puncture would be needed. However, it has been reported that cut-resistant gloves for example do not provide protection against stabbing [2]. In another survey performed in slaughterhouses and meat and poultry processing plants, 30 % of surveyed workers admitted not wearing metal mesh gloves in part because of their inefficiency against pointed blades [11].

Such lack of appropriate protection against pointed blades may be attributed in part to the absence of knowledge in that area. Indeed, very few papers in the literature deal with the fundamental aspects of the interaction between pointed blades and protective materials. One study looked at the resistance to stabbing of knitted structures based on poly (p-phenylenediamine terephthalamide) (Kevlar), high modulus polyethylene (Dyneema), polybenzazole (Zylon), and a blend of Kevlar and steel [12]. Blade displacement velocities ranged between 1.5 and 5.5 m/s. A reduction in blade penetration depth was recorded with the more flexible structures. This phenomenon was attributed by the author to the fact that flexible structures are able to follow the blade during its penetration in the plastiline used to simulate the response of the human body and thus absorb part of the impact energy. The best performances were observed with complex multilayer structures, especially with those displaying a low interlayer friction coefficient.

Another study reported the results of a finite element analysis of the penetration of knife through woven fabrics [13]. Based on energy and moment conservation, the proposed model leads to a complex mechanical behaviour of the textile structures during stabbing, with a non-linear response even in the elastic deformation zones. It was shown that the knife tip penetration mechanism involves fibre shear failure. Results obtained for a Kevlar plain weave fabric show that the knife penetration force is proportional to the yarn elastic modulus and increases with the yarn static friction coefficient and volume fraction.

Finally, no literature was found on the resistance to pointed blades of elastomers, which are often used as a coating for gloves against mechanical hazards. However, some research exists on cutting and puncture taken individually, which are thought to contribute to the pointed blade penetration mechanism. In the case of cutting, it has been shown that most of the energy is absorbed by the friction between the slicing blade and the material [14]. This friction can be divided into two parts: friction with the sides of the blade and friction at the cutting edge. These two contributions of friction have opposing effects on the cutting phenomenon. For its part, puncture resistance of elastomer membranes is controlled by the maximum local deformation [15]. That failure strain is an intrinsic property of the material.

This paper presents some initial results of tests performed with glove materials and several types of pointed blades used as puncture probe. In particular, it looks at the effect of blade reuse, sample thickness, blade tip angle, probe displacement rate, blade lubrication and sample support on the resistance of these materials to pointed blades.

Experimental

Method

The setup used for measuring the resistance of glove materials to pointed blades is similar to what is proposed in the ASTM F1342-05 puncture standard [6]. It includes two steel plates between which the sample is secured as illustrated in Fig. 1. Each plate contains a 38-mm diameter hole. The edge of the lower plate hole is rounded to avoid stress concentration. This setup was positioned in a mechanical test frame (Instron 1137) with a probe-holding pin chuck mounted on a 222N load cell calibrated with a 50 g weight.

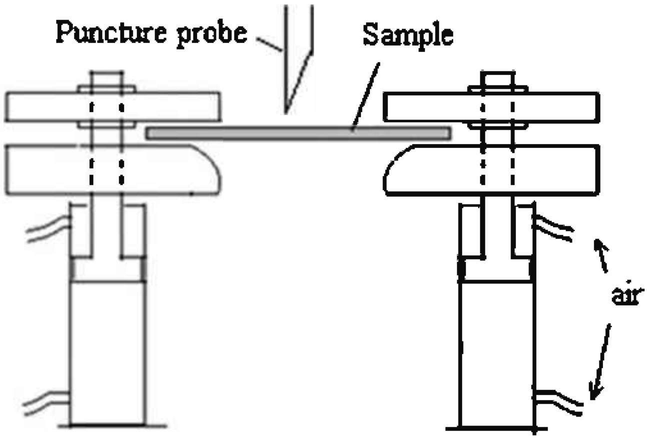

FIG. 1—*Schematic representation of the experimental measurement setup.*

Three models of pointed blades were used as puncture probes. Pictures are shown in Fig. 2. Blade #24 is a deburring blade with a 35° angle (Excel Hobby Blades Corp., NJ): Model 20024 (five-piece set) is lubricated and model 22624 (100-piece set) is non-lubricated. Blade #11 is a fine point blade with a 21° angle (Excel Hobby Blades Corp., NJ): Model 20011 (five-piece set) is lubricated and model 22611 (100-piece set) is non-lubricated. Finally, blade #10 is a lubricated curved edge blade (X-Acto, OH, Model X210).

During the tests, force-displacement data were recorded while the pointed blade was pushed through the sample at a constant rate. Values of probe displacement rate between 1 and 500 mm/min were used. An example of typical curve is illustrated in Fig. 3. A gradual increase in the force can be observed until brutal failure occurs. A small piece of thin aluminum foil glued under the sample was used to detect by electrical contact the point where the blade reaches the opposite side of the membrane. It can be seen in Fig. 3 that it corresponds to the location of the maximum force. Five replicates were measured for each condition. The reported puncture force corresponds to the average of the maximum value of the force-displacement curves obtained for these replicates.

For comparison purposes, measurements of materials resistance to puncture and cutting were also carried out. For puncture tests, probe B of the ASTM F1342-05 standard relative to puncture resistance of protective clothing

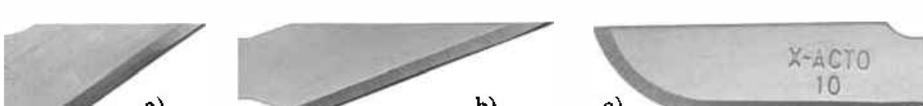

FIG. 2—*Picture of the pointed blades: (a) Blade #24, (b) Blade #11, and (c) Blade #10 (scale: blade width = 8.6 mm).*

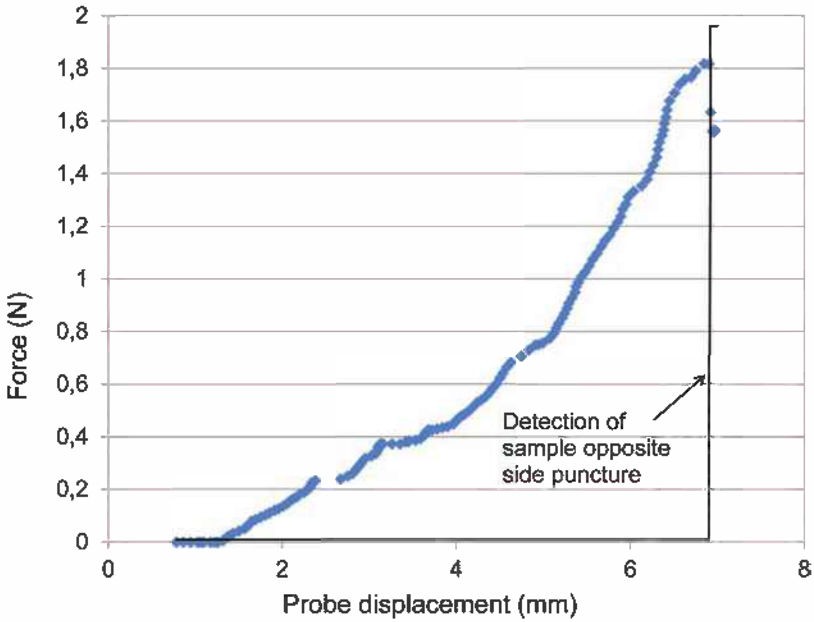

FIG. 3—*Typical force-displacement curve with detection of sample opposite face puncture (blade #11, nitrile rubber, probe displacement rate of 15 mm/min).*

was used [6]. It is a 1-mm-diameter stainless steel cylinder with a 0.5-radius-hemispherical head. Resistance to cutting was measured according to ASTM F1790 test method using a TDM-100 apparatus [4].

Materials

Tests were performed with two models of palm-coated protective gloves, a nitrile rubber/Kevlar knit one (Superior Touch S13KNT) and a polyurethane/Dyneema knit one (Superior Touch S13SXGPU). Samples were taken from the polymer-coated palm section as well as the uncoated back. Measurements were also carried out with sheets of the corresponding glove coating polymers, i.e., nitrile rubber (1.45, 1.6, 2.4, and 3.2 mm thick, McMaster Carr) and polyurethane (0.13-mm thick, McMaster Carr), as well as with sheets of neoprene (0.5-, 1.5-, 1.75-, and 3.2-mm thick, Fairprene Industrial Products). Finally, 1.5-mm-thick leather used for public works gloves was graciously provided by BCL Glove Ltd.

Results

Effect of Blade Reuse

Tests were performed to evaluate the possibility of blade reuse for multiple measurements. For that purpose, the effect of blade reuse on the puncture force

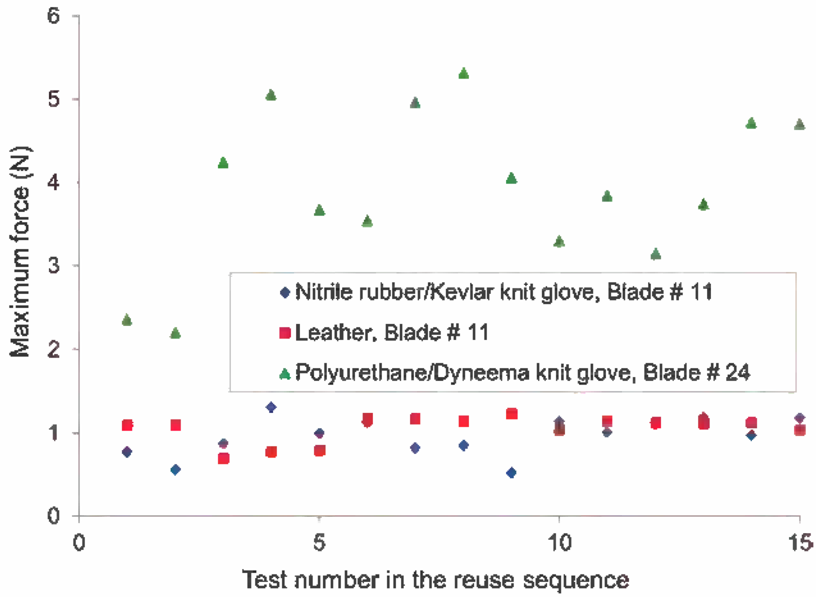

FIG. 4—*Effect of blade reuse on max force for nitrile rubber/Kevlar knit gloves and leather tested with blades #11 (lubricated) and polyurethane/ Dyneema knit gloves tested with blades #24 (lubricated) (probe displacement rate of 260 mm/min).*

was characterized. Figure 4 displays examples of results obtained for 15 successive reuses of blades #11 (lubricated) tested with nitrile rubber/Kevlar knit gloves and leather and of blades #24 (lubricated) tested with polyurethane/ Dyneema knit gloves. The rather large scattering in the maximum force data observed with polymer-coated gloves can be attributed to the inherently inhomogeneous nature of these materials.

No increase in maximum force indicative of a gradual wear of the pointed blade tip can be observed, contrary to what had been reported with hypodermic needles [16]. This indicates that for these types of materials, pointed blades may be reused a few times without affecting the quality of the results. Therefore, for the results presented in this paper, each blade was used for five successive measurements before being disposed of. It may be noted that in a few instances, some pointed blades broke during the tests. However, these cases were systematically related to a pre-existing defect in the blade tip (see Fig. 5), revealed by the much higher value of maximum force measured even during the first use.

Effect of Sample Thickness

The effect of sample thickness on the pointed blade puncture force was investigated with sheets of neoprene and nitrile rubber of different thickness values.

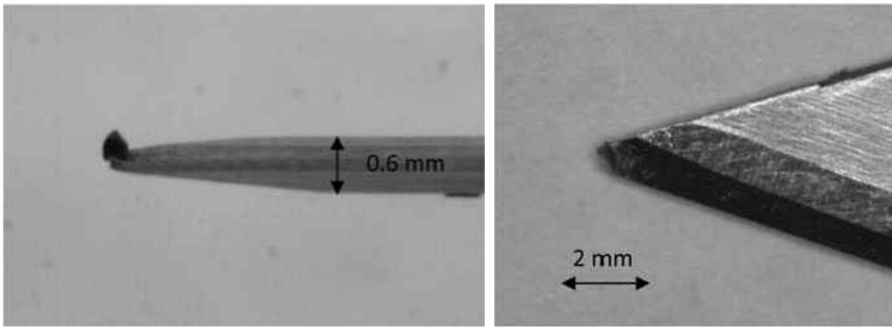

FIG. 5—*Pictures of a defective blade.*

The results for blades #24 (35° angle, non-lubricated) are displayed in Fig. 6. For both elastomers, the maximum force increases with the sample thickness. In addition, the relationship appears to be non-linear.

A non-linear behaviour has also been reported in the case of hypodermic needles [17]. It was associated with the non-linear nature of the elastomer needle puncture interaction, which involves a large contribution of cutting [18] and was satisfactorily described by a non-linear elastic fracture mechanics approach [19]. By comparison, in the case of hemispherical and flat tip probes, the puncture force was shown to be proportional to the material thickness [20]. In this case, more research is necessary to verify if the interaction between

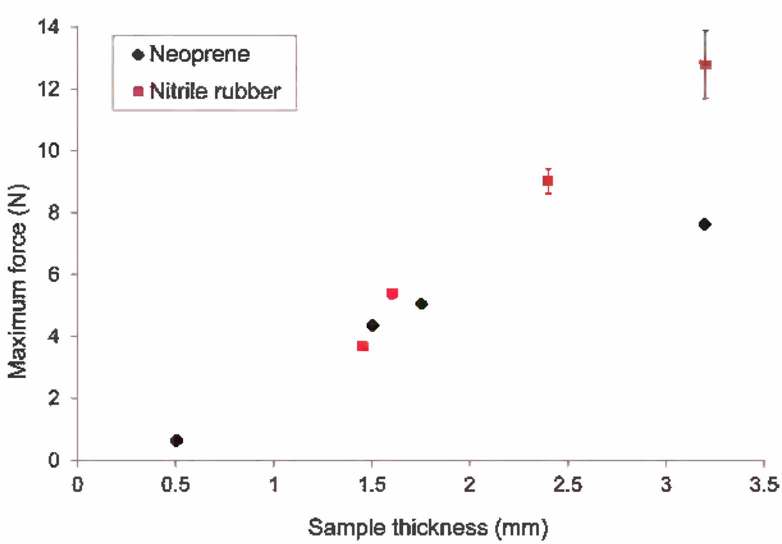

FIG. 6—*Variation of the pointed blade puncture force with the sample thickness for neoprene and nitrile rubber, blade #24 (35° angle, non-lubricated), and probe displacement rate of 150 mm/min.*

pointed blades and elastomers can be related to the shape of the crack generated by the pointed blade in the membrane and explained by the principles of fracture mechanics.

Effect of Blade Tip Angle

An analysis of the variation of the maximum force with the blade tip angle was carried out with the three types of pointed blades used in this study. In the case of blade #10, which is curved (see Fig. 2), an angle value of 60° was determined at the tip. Figure 7 displays the results obtained for leather, polyurethane, and nitrile rubber sheets. An increase in the maximum force as a function of the blade angle can be observed. This effect can be attributed to the decrease in blade acuteness as the angle increases, leading to a reduction in the cutting ability of the blade point. The same trend has been reported in the case of puncture by hypodermic needles [16].

The relationship between maximum force and blade tip angle appears rather linear with nitrile rubber. However, it is curved upwards for all other materials, including nitrile rubber coated Kevlar knit and Kevlar knit (see Fig. 8) and polyurethane coated Dyneema knit and Dyneema knit (see Fig. 9). This may indicate a difference in puncture mechanism for curved blades compared to triangular ones for these materials.

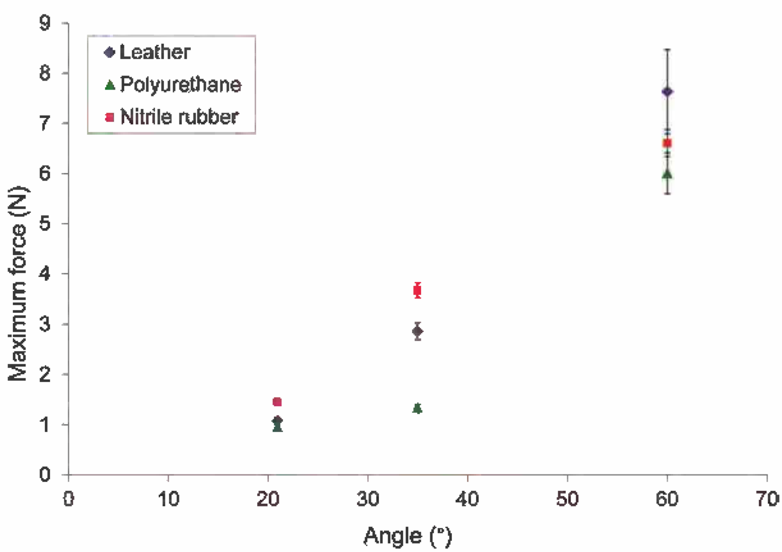

FIG. 7—*Variation of the max force with the blade tip angle for leather, polyurethane and nitrile rubber (1.45-mm-thick) sheets (lubricated blades, probe displacement rate of 150 mm/min).*

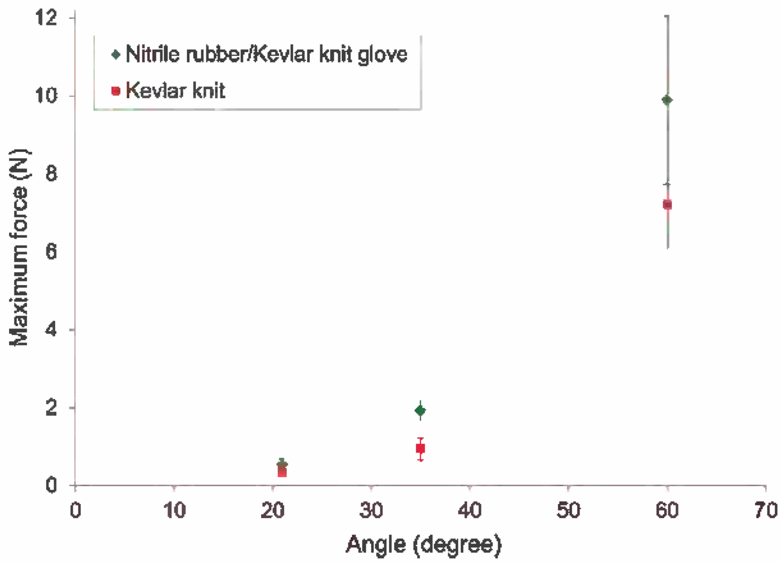

FIG. 8—*Variation of the max force with the blade tip angle for nitrile rubber/ Kevlar knit gloves and Kevlar knit (lubricated blades, probe displacement rate of 150 mm/min).*

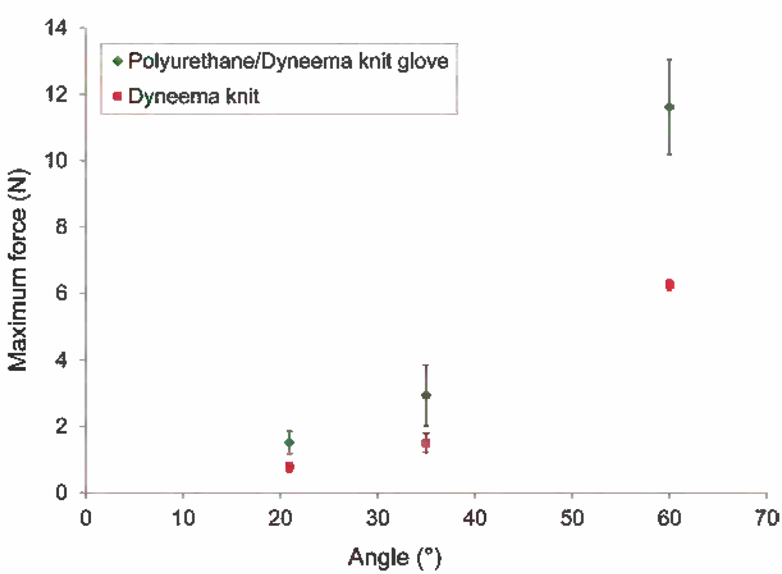

FIG. 9—*Variation of the max force with the blade tip angle for polyurethane/ Dyneema knit gloves and Dyneema knit (lubricated blades, probe displacement rate of 150 mm/min).*

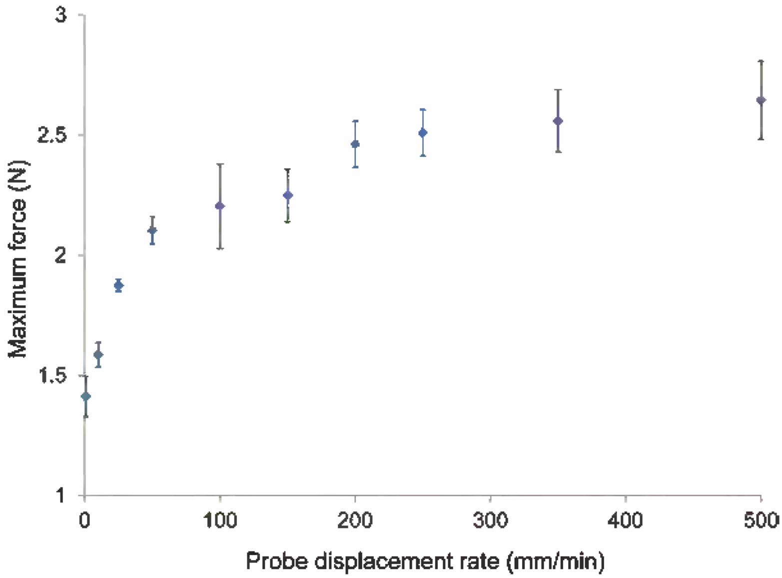

FIG. 10—*Variation of the max force with the probe displacement rate for 1.45-mm-thick nitrile rubber sheets (lubricated blades #24).*

Effect of Probe Displacement Rate

An investigation of the effect of the pointed blade displacement rate on the maximum force was carried out. The probe displacement rate was varied between 1 and 500 mm/min. Figure 10 displays the results obtained with 1.45-mm-thick nitrile rubber and pointed blades #24 (35° angle, lubricated). Below 100 mm/min, the puncture force increases rapidly with the probe displacement rate, then appears to reach a plateau. The shape of the curve is similar to what has been reported for the resistance of neoprene, fabric-reinforced nitrile rubber, and neoprene-coated cotton knit to puncture by hypodermic needles, which involves cutting and friction [17]. It agrees also with the behaviour observed for the cutting energy of elastomers in the absence of friction above the cutting threshold condition (crosshead displacement $>10^{-5}$ m/s) [21]. This may indicate that, as for cutting with or without friction, the resistance of elastomers to pointed blades includes a viscoelastic contribution.

When these data for nitrile rubber are expressed using a semi-logarithmic scale, a linear relationship is observed, except for the lowest value of blade displacement rate (see Fig. 11). This monotonous variation may indicate that the same mechanisms control the resistance of nitrile rubber to puncture by pointed blades between 10 and 500 mm/min. However, these values of probe displacement rate are much lower than adult hand quick grab velocity (250 m/min) [22] and stabbing velocities (up to 600 m/min) [23]. Therefore, it will be

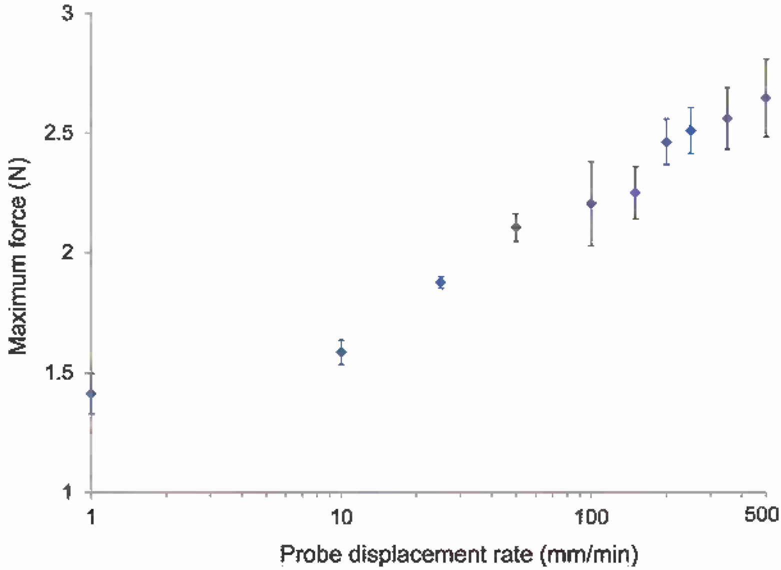

FIG. 11—*Variation of the max force with the probe displacement rate on a semi-logarithmic scale for 1.45-mm-thick nitrile rubber sheets (lubricated blades #24).*

necessary to verify if other mechanisms do not take place at more realistic impact-type blade displacement rates.

The same exercise was conducted with the other types of materials. A similar shape of the maximum force-displacement rate—sharp increase followed by a plateau—was observed, pointing toward the possible viscoelastic nature of the pointed blade interaction with these materials. On the other hand, in some instances, the semi-logarithmic representation of the force-displacement rate data appeared to display a succession of two straight lines. This is illustrated in Fig. 12 in the case of polyurethane coated Dyneema knit and Dyneema knit. This may indicate the existence of two different puncture regimes over that range of probe displacement rates. The value of displacement rate at which the shift of puncture regime occurs appears to depend on the material. It is located around 80 mm/min for the polyurethane coated Dyneema knit and around 130 mm/min for the Dyneema knit. A similar phenomenon of slope change might eventually have also happened with nitrile rubber just above the lowest value of blade displacement rate of 1 mm/min.

Effect of Lubrication

An investigation of the influence of lubrication on the interaction of pointed blades with polyurethane was conducted. Indeed, friction has been shown to play a major role in cutting [14]. As can be seen in Table 1, an increase in

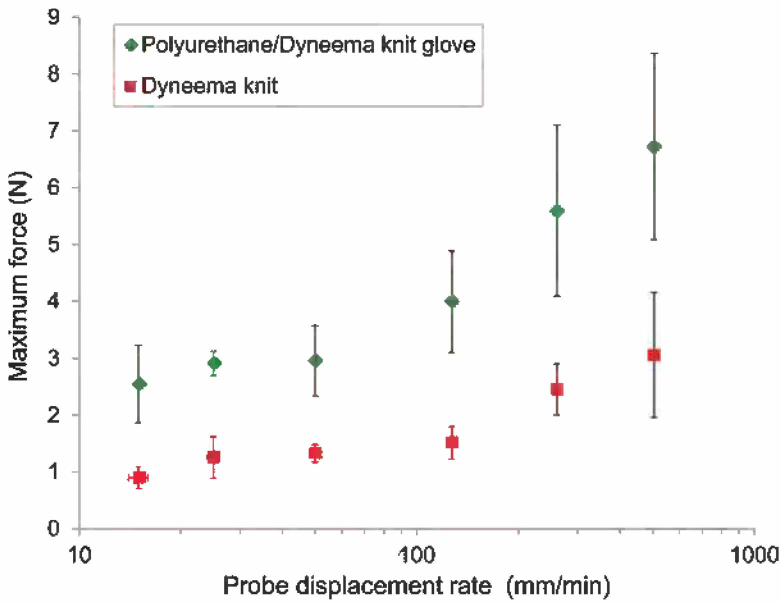

FIG. 12—*Variation of the max force with the probe displacement rate on a semi-logarithmic scale for polyurethane/Dyneema knit gloves and Dyneema knit (lubricated blades #24).*

maximum force was recorded with non-lubricated blades compared to lubricated ones of the same model and manufacturer. The same effect was produced by cleaning lubricated blades with methanol. This confirms that puncture by pointed blades involves a large contribution of friction.

Effect of Support

Since the presence of the hand inside the glove may restrict the deformation of the membrane during the puncture process and modify its resistance to puncture by pointed blades, a study was carried out to look at the influence of sample deformation on the pointed blade puncture process. For that purpose, a piece of aluminum foil positioned under the sample and firmly secured with it

TABLE 1—*Comparison between maximum force values measured with lubricated, non-lubricated and cleaned blades (polyurethane sheet, probe displacement rate of 250 mm/min).*

	Blade # 4		Blade #11	
	Lubricated	Non-lubricated	Lubricated	Cleaned
Maximum force (*N*)	1.38	1.97	1.02	1.35
Standard deviation (*N*)	0.06	0.19	0.05	0.12

TABLE 2—*Comparison between maximum force values measured with and without an aluminum foil support under the sample (2.4-mm-thick nitrile rubber, probe displacement rate of 15 mm/min).*

	No sample support	Aluminum foil as suppor
Maximum force (N)	1.80 ± 0.01	2.3 ± 0.071
Sample deformation at puncture (mm)	5.5 ± 0.2	2.9 ± 0.2

between the hole-bearing sample holder plates was used to restrict sample deformation during the puncture process. The moment when sample puncture occurred was detected by electrical contact between the aluminum foil and the blade. Table 2 presents the results obtained for nitrile rubber and blades #11 (21° angle, lubricated). An increase in maximum force and a large reduction in sample deformation at puncture were measured with the aluminum foil supporting the sample. By comparison, no effect of sample support on puncture force was obtained with hypodermic needles, while it strongly affected puncture by ASTM rounded probes [24]. These results show that puncture by pointed blades involves a much larger contribution of sample deformation than puncture by hypodermic needles.

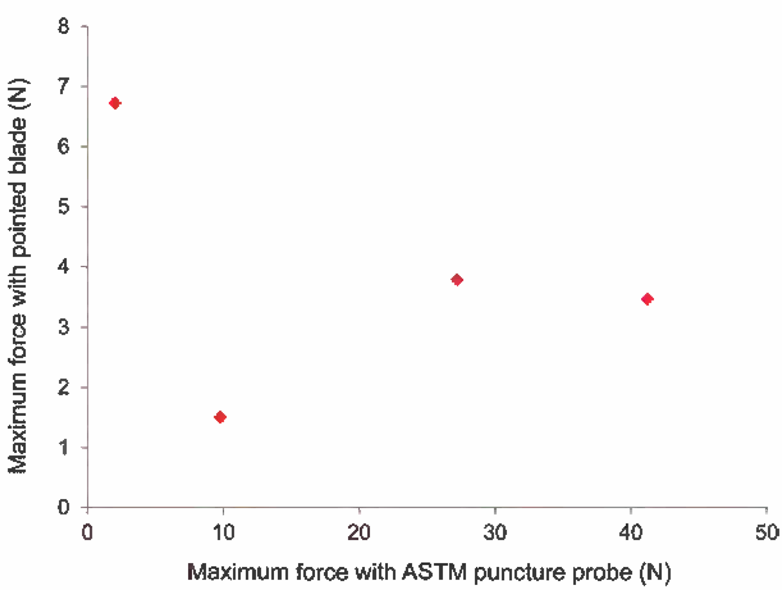

FIG. 13—*Variation of the max force measured with a pointed blade (lubricated blade #24) as a function of that obtained with the ASTM F1342-05 standard puncture test method probe B for polyurethane, polyurethane/Dyneema knit gloves, nitrile rubber/Kevlar knit gloves, and leather (probe displacement rate of 500 mm/min).*

Comparison with Puncture and Cutting Standard Test Results

These preliminary results with various types of protective materials have shown that both friction and sample deformation contribute to their resistance to pointed blades. Therefore, an analysis of the eventual correlations with the resistance to cutting and puncture measured using existing standard test methods appears relevant. The variation of the maximum force values measured with #24 pointed blades as a function of the corresponding maximum force values measured with the ASTM F1342-05 standard puncture test method probe B for polyurethane, polyurethane/Dyneema knit gloves, nitrile rubber/Kevlar knit gloves, and leather is displayed in Fig. 13. No correlation can be observed between the two sets of data. As it can be seen in Fig. 14, the same absence of correlation seems to prevail between the materials resistance to pointed blades (obtained with the setup described in Fig. 1) and the resistance to cutting measured according to the ASTM F1790-05 standard test method using a TDM-100 apparatus and a rectangular sliding blade. This indicates that none of these two existing standard test methods can be used to predict the performance of protective materials against pointed blades. As a result, a dedicated test method needs to be developed.

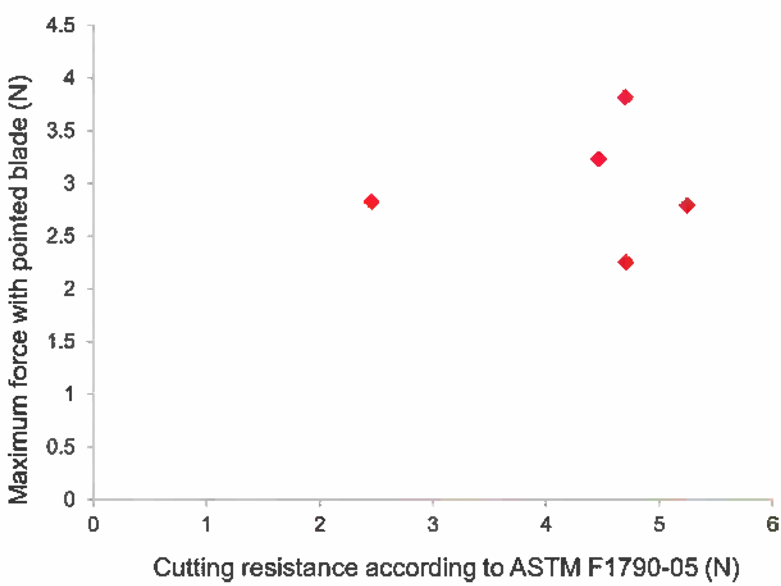

FIG. 14—*Variation of the max force obtained with a pointed blade (lubricated blade #24) as a function of the cutting resistance measured according to the ASTM F1790-05 standard cutting test method for polyurethane, polyurethane/Dyneema knit gloves, nitrile rubber/Kevlar knit gloves, 1.45-mm-thick nitrile rubber and 1.5-mm-thick neoprene (blade displacement rate of 150 mm/min).*

Conclusions

This paper presents some initial results of the measurements of protective glove materials resistance to several types of pointed blades. Tested materials include uncoated and polymer-coated Kevlar and Dyneema knits, leather as well as sheets of neoprene, nitrile rubber, and polyurethane. The effect of various parameters such as blade reuse, sample thickness, blade tip angle, probe displacement rate, blade lubrication, and sample support on the resistance of these materials to pointed blades was studied.

The results show that, in the case of elastomers, a non-linear increasing relationship seems to prevail between the maximum force, which corresponds to the point when the blade tip pierces the back side of the sample, and the thickness of the membrane. A decrease in puncture force for very pointed blades, i.e., with a small tip angle, was observed with all materials. In addition, measurements carried out at displacement rates between 1 and 500 mm/min point towards the existence of two puncture regimes for some materials, each one being characterized by a different value of the slope corresponding to the linear variation of the maximum force with the speed in a semi-log scale.

Finally, the contribution of both friction and sample deformation on the pointed blade puncture process was revealed by the large effect of lubrication and sample support on the maximum force. However, no correlation appears to exist between resistance to pointed blades and resistance to cutting or puncture measured with standard test methods. This demonstrates the need for more research in that area and ultimately a dedicated standard test method.

Acknowledgments

The writers would like to thank the companies Superior Glove Works Ltd. (Acton Ontario Canada) and BCL Glove Ltd (Saint-Pacôme Quebec Canada) for providing the gloves and the glove materials used in this study. They also want to acknowledge the help of Chantal Gauvin, Pierre Drouin, and the Institut de recherche Robert-Sauvé en santé et en sécurité du travail (Montréal Quebec Canada).

References

[1] Commission de la santé et de la sécurité du travail du Québec (Québec Occupational Health and Safety Commission), Occupational Lesion Database, Oct 2008.
[2] Caple, D., "Evaluation of Cut Resistance Gloves in the South Australian Meat Industry," South Australia WorkCover Corporation, Adelaide, Australia, 2000, 25 pp.
[3] Sorock, G. S., Lombardi, D. A., Peng, D. K., Hauser, R., Eisen, E. A., Herrick, R. F., and Mittleman, M. A., "Glove Use and the Relative Risk

of Acute Hand Injury: A Case-Crossover Study," *J. Occup. Environ. Hygiene*, Vol. 1, No. 3, 2004, pp. 182–190.
[4] ASTM F1790, 2005, "Standard Test Method for Measuring Cut Resistance of Materials Used in Protective Clothing," *Annual Book of ASTM Standards*, Vol. 11.03, ASTM International, West Conshohocken, PA, pp. 1602–1611.
[5] ISO13997, 1999, "Protective Clothing—Mechanical Properties—Determination of Resistance to Cutting by Sharp Objects," International Organization for Standardization, Geneva, 11 pp.
[6] ASTM F1342, 2005, "Standard Test Method for Protective Clothing Material Resistance to Puncture," *Annual Book of ASTM Standards*, Vol. 11.03, ASTM International, West Conshohocken, PA, pp. 1489–1493.
[7] ASTM F2878, 2010, "Standard Test Method for Protective Clothing Material Resistance to Hypodermic Needle Puncture," *Annual Book of ASTM Standards*, Vol. 11.03, ASTM International, West Conshohocken, PA, pp. 1–5.
[8] Harrabi, L., Dolez, P. I., Vu-Khanh, T., and Lara, J., "Optimization in the Selection of Protective Gloves for Resistance to Mechanical Risks," *Proceeding of the 2nd International Conference of Applied Research on Textile*, Monastir, Tunisia, Nov 30–Dec 2, 2006, 4 pp.
[9] Batra, S., Bronkema, L. A., and Wang, M. J., "Glove Attributes: Can They Predict Performance?" *Int. J. Indust. Ergon.*, Vol. 14, No. 3, 1994, pp. 201–209.
[10] ANSI/ISEA105, 2011, "American National Standard for Hand Protection Selection Criteria," American National Standards Institute—International Safety Equipment Association, Arlington, VA, 25 pp.
[11] Vézina, N., "Protection des mains dans l'industrie de la viande et de la volaille," *Profil-recherche 110*, Institut de recherche en santé et en sécurité du travail du Québec, Montréal, QC, Canada, 1990, 2 pp.
[12] Flambard, X., 2000, "Résistance à la coupure, à la perforation et au feu des structures textiles maillées," Ph.D. thesis, Université des Sciences et Technologies de Lille I, France.
[13] Wang, L., Zhang, S., Gao, W. M., and Wang, X., "FEM Analysis of Knife Penetration through Woven Fabrics," *Comput. Model. Eng. Sci.*, Vol. 20, 2007, pp. 11–20.
[14] Vu, T. B. N., Vu-Khanh, T., and Lara J., "Progress in the Characterization of the Cutting Resistance of Protective Materials," *J. ASTM Int.*, Vol. 2, No. 5, 2005, pp. 399–413.
[15] Nguyen, C. T., Vu-Khanh, T., and Lara, J., "Puncture Characterization of Rubber Membranes," *Theoret. Appl. Fract. Mech.*, Vol. 42, No. 1, 2004, pp. 25–33.
[16] Dolez, P. I., Vu-Khanh, T., Nguyen, C. T., Guero, G., Gauvin, C., and Lara, J., "Influence of Medical Needle Characteristics on the Resistance to Puncture of Protective Glove Materials," *J ASTM Int.*, Vol. 5, 2008, 12 pp.

[17] Nguyen, C. T., Dolez, P. I., Vu-Khanh, T., Gauvin, C., and Lara, J., "Resistance of Protective Gloves Materials to Puncture by Medical Needles," *J ASTM Int.*, Vol. 7, No. 5, 2010, 10 pp.

[18] Nguyen, C. T., Vu-Khanh, T., Dolez, P. I., and Lara J., "Puncture of Elastomer Membranes by Medical Needles. Part I: Mechanisms," *Int. J Fract.*, Vol. 155, No. 1, 2009, pp. 75–81.

[19] Nguyen, C. T., Vu-Khanh, T., Dolez, P. I., and Lara, J., "Puncture of Elastomer Membranes by Medical Needles. Part II: Mechanics," *Int. J Fract.*, Vol. 155, No. 1, 2009, pp. 83–91.

[20] Lara, J., Nelisse, N. F., Cote, S., and Nelisse, H. J., "Development of a Method to Evaluate the Puncture Resistance of Protective Clothing Materials," *Symposium on Performance of Protective Clothing: Fourth Volume, Montreal, QC, Canada, Jun 18–20, 1991*, ASTM International, West Conshohocken, PA, 1992, pp. 26–37.

[21] Cho, K. and Daeho, L., "Viscoelastic Effects in Cutting of Elastomers by a Sharp Object," *J. Polym. Sci., Part B (Polym. Phys.)*, Vol. 36, No. 8, 1998, pp. 1283–1291.

[22] McGuire, B. J., Sorrells, J. R., and Moore, J. D., "Resistance of Human Skin to Puncture and Laceration, *Report No. NBSIR 73-123*, U.S. Dept. of Commerce, NTIS Springfield, VA, 1973.

[23] Horsfall, I., Watson, C., Champion, S., Prosser, P., and Ringrose, T., "The Effect of Knife Handle Shape on Stabbing Performance," *Appl. Ergon.*, Vol. 36, No. 4 (Special issue), 2005, pp. 505–511.

[24] Nguyen, C. T., Dolez, P. I., Vu-Khanh, T., Gauvin, C., and Lara, J., "Effect of Protective Gloves' Use Conditions on Their Resistance to Needle Puncture," *Plastics, Rubber Composites: Macromolec. Eng.* (in press).

Performance of Protective Clothing and Equipment: Emerging Issues and Technologies
STP 1544, 2012
Available online at www.astm.org
DOI:10.1520/STP104482

Kevin Ross,[1] *Roger Barker,*[2] *Jessica Watkins,*[3]
and A. Shawn Deaton[4]

Methods for Measuring the Grip Performance of Structural Firefighting Gloves

REFERENCE: Ross, Kevin, Barker, Roger, Watkins, Jessica, and Deaton, A. Shawn, "Methods for Measuring the Grip Performance of Structural Firefighting Gloves," *Performance of Protective Clothing and Equipment: Emerging Issues and Technologies* on April 16, 2011 in Anaheim, CA; STP 1544, Angie M. Shepherd, Editor, pp. 371–391, doi:10.1520/STP104482, ASTM International, West Conshohocken, PA 2012.

ABSTRACT: Grip evaluation methods are compared in tests made on structural firefighter gloves selected to represent a range of materials and constructions. An investigation of the effects of pulling force orientation and wetting on grip performance in rope and rod-type grip tests is discussed. A new method developed to measure grip by measuring torque generated in twisting an acrylic glass rod with gloved hands is described. Comparative studies show that the newly developed torque test provides lower subject variability and enhanced resolution among different gloves based on measured grip performance. Factors of glove construction that influence performance in the torque grip test are discussed, including slip-stick phenomena observed in tests on some wet gloves.

KEYWORDS: grip, torque, gloves, slippage, structural firefighter gloves

Manuscript received October 28, 2011; accepted for publication February 27, 2012; published online September 2012.

[1]Research Associate, Textile Protection and Comfort Center, College of Textiles, NC State Univ., Raleigh, NC 27695–8301.

[2]Professor, Dept. of Textiles Engineering, Chemistry and Science, North Carolina State Univ., Raleigh, NC 27695–8301.

[3]Graduate Research Assistant, Dept. of Textile Engineering, NC State Univ., Raleigh, NC 27695–8301.

[4]Special Projects Director, Center for Research on Textile Protection and Comfort, College of Textiles, North Carolina State Univ., Raleigh, NC 27695–8301.

Introduction

There is a need for better laboratory test methods for measuring the grip performance of structural firefighter gloves. The 2007 NFPA 1971 Standard on Protective Ensembles for Structural Fire Fighting and Proximity Fire Fighting specifies that glove-grip performance be measured using a rope-pull method [1]. This method measures the force generated before slippage occurs when pulling on a horizontally oriented wet rope attached to a force gauge. Rope-pull methods can produce variable results, however, partly because glove-grip performance is affected by the stance and posture used by the test subject when pulling on the rope. Revisions in the method have included use of horizontal and vertical rope-pull configurations, and dry and wet test conditions. Despite the known influence of these testing factors, an analysis of the effects of methodology variations on the rope-pull test results has been lacking. Furthermore, there is ongoing need for grip test methods that provide less variable test results and more useful information about the performance of structural firefighter gloves.

This research was conducted, in part, to investigate the effects of modifications to rope-pull glove-grip testing protocols for testing firefighter gloves, including the use of a pole in place of a rope in the pull grip test. It also developed an entirely different testing approach for evaluating the grip performance. This method measures the torque that can be applied to a cylindrical rod by a gloved hand before slippage occurs. The torque grip test addresses the need for a measurement that better differentiates structural firefighter gloves based on their grip performance. The need for a test method that can measure differences in grip performance is of obvious importance to the development of performance standards for protective gloves. It is also crucial to understanding the effects of glove materials and designs on grip performance, and to the ultimate development of gloves with enhanced grip functionality.

Methods and Materials

Pull-Type Grip Test Methods

Rope- and rod-pull-type tests were used to assess glove-grip performance. Figure 1(*a*) shows the testing setup used in rope-pull tests. This rope-pull test apparatus consists of a three-strand, pre-stretched, 100 % polyester rope attached to a calibrated force-measuring device (Shimpo Model FGV-200HX digital force gauge). This test procedure is designed to measure the effects of gloves on the ability to grip a rope. It requires a person to pull a rope, one hand in front of the other with both feet planted firmly on the floor, exerting as much horizontal pulling force as possible. The pulling force is applied parallel to the rope while the gloved hands maintain control of the rope through a grasping

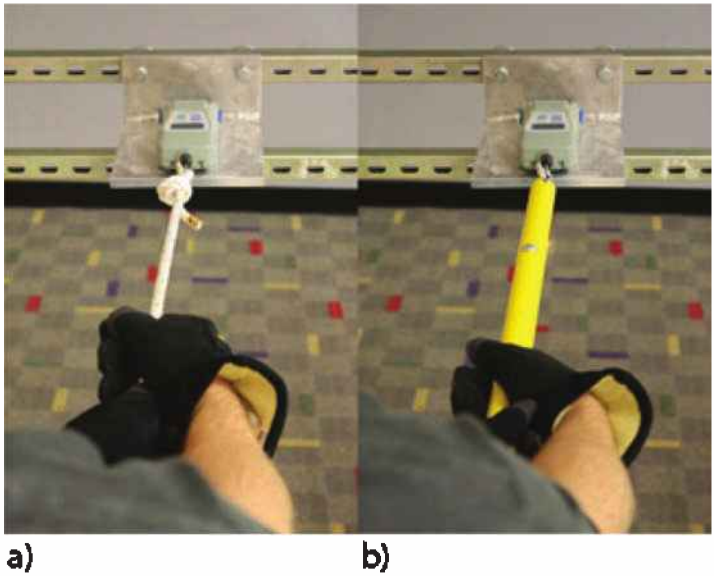

FIG. 1—*Pull test methods: (a) rope, and (b) pole.*

action. The maximum pull force is measured as the peak force before slippage, or when the pulling force exceeds the frictional force between the rope and gloves. The frictional force is a function of the normal grasping forces exerted on the rope, contact points, and frictional properties of the gloves and rope. An index of glove-grip performance is calculated as a ratio of gloved to bare-handed performance.

The pulling force was measured and a grip rating was determined for each set of gloves. Grip ratings were determined by comparing each subject's pulling force while wearing gloves to their bare-handed pulling force. The grip rating is defined as follows:

$$\text{grip rating} = \text{percentage of bare-handed control value} = \left(\mathrm{PF}_g / \mathrm{CV}_b\right) \times 100 \tag{1}$$

TABLE 1—*Pull test configurations.*

Test Protocol	Apparatus	Orientation	Condition	Stance
1	Rope	Horizontal	Wet	Restricted
2	Rope	Vertical	Wet	Restricted
3	Pole	Vertical	Wet	Restricted
4	Rope	Horizontal	Wet	Free
5	Pole	Vertical	Dry	Restricted

where:

PF_g = average pulling force with gloves, lbf, or N, and

CV_b = bare-handed control value, lbf, or N.

Higher grip ratings indicate better grip performance. A grip rating of 100 % signifies no difference between the gloved grip and the bare-handed grip. Table 1 shows the configurations and conditions that were used to study the effects of variations in pull grip-test protocols.

Protocol 1 is the horizontal-pull, wet-rope, grip-test method called for by the 2007 version of NFPA 1971 [1]. For wet-testing conditions, test gloves were wet conditioned by first being donned by the subject, then fully submerged into two containers of water at a temperature of 21°C, ± 3°C (70°F, ± 5°F) for 2 min + 12/−0 s. The gloves were then removed from the hand and hung vertically by digit 5 with the glove opening facing down for 2 min +/−12 s [2]. The test rope was wet conditioned by immersion in water at a temperature of 21°C, ± 3°C (70°F, ± 5°F) for 2 min and then drip-dried for 5 min. Multiple ropes were used to accommodate timing issues.

This research investigated an approach for reducing variability in the rope-pull grip test by introducing more control of the posture assumed by the human subject while executing the rope-pulling action. The NFPA 1971 standard requires that the test subject, with feet firmly planted, grasp the rope with both hands, one in front of the other without the thumbs overlapping the fingers. In an attempt to improve testing consistency, a test fixture was introduced to control the posture of the test subject by keeping their feet in a fixed place and shoulder width apart. The test fixture restricted the stance of the test subjects. It helped them maintain contact with the apparatus in the chest region, without falling forward during the pulling action. This restricted stance fixture was used in all cases except for Protocol 4. Protocol 4 used a free-stance pulling stance. In the free-stance pull, the subjects executed the pull while in a tug-of-war type stance without restriction on posture. As was the case with the fixture-restricted stance, the subject kept their feet shoulder width apart and firmly planted on the floor with hands placed one in front of the other while pulling in the free stance.

Protocols 2 through 5 are variants of the rope-pull method used to study the effects of wetting the apparatus and gloves, potential differences related to horizontal or vertical orientation of the pulling action, and differences related to the nature of the object being grasped.

A 1.25-in.-diameter fiberglass pole, similar to the pike poles used in firefighting, was used for Protocols 3 and 5 instead of a rope (Fig. 1(*b*)). The poles used in the test were wet conditioned by wiping them with a saturated wet cloth before each pull repetition. For testing in the vertical orientation, the rope or pole was securely attached to a steel structural beam in the ceiling, and the pull direction was downward. For all pull-type methods, the grip rating was determined for each test glove by comparing the gloved average peak force (three pulls) to the bare-handed baseline average peak force (three pulls) for each test subject (Eq 1). An average grip rating was calculated by averaging the ratings of five test subjects.

The Torque Grip Test

A new torque test method was developed to evaluate glove-grip performance based on the measured torque that can be applied to a cylindrical rod before slippage occurs between the gloved hand and the rod (Fig. 2). Similar to the pull methods, the grip rating is defined by comparing gloved to bare-handed performance as follows:

$$\text{grip rating} = \text{percentage of bare-handed control value} = \left(\mathrm{T_g}/\mathrm{CV}_b\right) \times 100 \tag{2}$$

where:

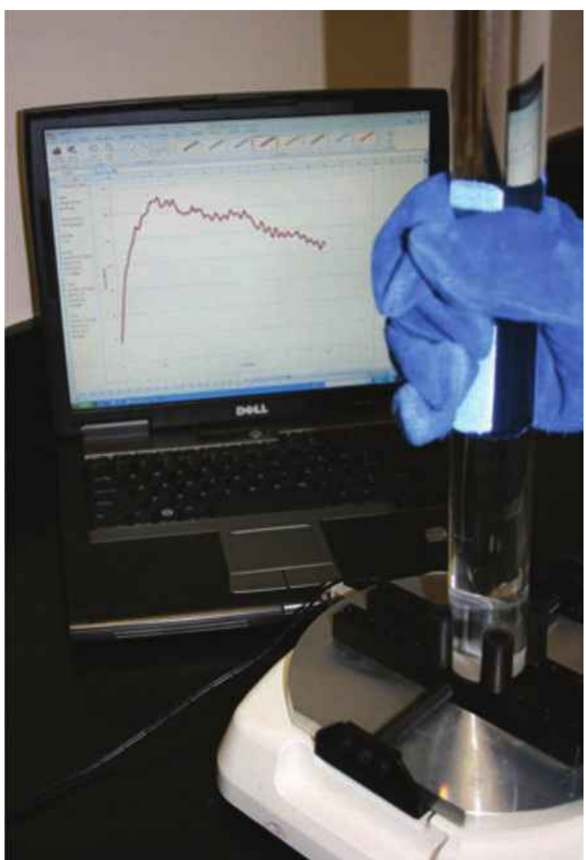

FIG. 2—*Torque tester and output.*

T_g = average torque with gloves, lbf·in., or N·m, and
CV_b = bare-handed control value, lbf·in., or N·m.

In this test, the subjects grasp an acrylic pole (1.625 in. diameter) with their dominant hand, so that the arm forms a 90° angle and the elbow is close to the hip. An inward grasping force maintains control of the test rod while torque is applied to exert a force tangential to the surface of the cylindrical rod. The subject turns the pole with maximum voluntary force in the "open" direction (counter-clockwise for right-handed subjects, clockwise for left-handed subjects) for 2.5 s. The acrylic rod is attached at its base to a Shimpo TNP-10 digital torque meter that measures the torque generated. Grip performance is measured by comparing the torque that can be maintained before slippage occurs, or when the force generated by twisting the rod overcomes the frictional force between the rod and gloves. The frictional force is a function of the normal grasping forces exerted on the rod, contact points, and frictional properties of the gloves and rod. Continuous torque measurements are recorded for the duration of the force application. The grip rating is determined by comparing the gloved average peak torque (three turns) to the bare-handed baseline average peak torque (three turns) for each test subject (Eq 2). An average grip rating was calculated by averaging the ratings of five test subjects. The test is carried out using both dry- and wet-conditioned glove samples (same wet-conditioning procedure as for pull-grip tests).

Test Subjects

Five test subjects performed the grip-test procedures, with the exception of the free-stance, rope-pull protocol, in which case three subjects were used for evaluation. Test subjects were right-hand dominant, 18- to 25-year-olds (four males and one female) selected to fit a size large glove. Because fit is an important factor affecting glove-grip performance, proper subject sizing was assured using the hand measurement procedures detailed in the NFPA 1971 standard [1].

Test Gloves

Test gloves consisted of 19 NFPA 1971-compliant firefighter gloves and five non-compliant gloves (Tables 2 and 3). The compliant glove samples were chosen to represent a range of state-of-the-art gloves used by structural firefighters. They incorporated different thermal liners, moisture barriers, and outer-shell components, and they used different composite layering and design concepts. Non-compliant gloves included an extrication glove (Sample V), a single-layer, leather work glove (Sample Q), an insulated hazmat glove (Sample R), a two-layer, leather, law-enforcement glove (Sample X), and a thin, knit glove with a rubber-coated palm designed for lab work (Sample W). Most of the non-compliant glove samples were chosen for the study, in part, because they were expected to have better functional performance than typically

TABLE 2—*Test glove materials.*

Glove	Shell[a] (Palm/Back if Different)	Moisture Barrier	Thermal Liner	Additional Materials
A	Cow	Intimate bicomponent ePTFE[g] and PU laminated to non-woven substrate[h]	Knitted, fleeced modacrylic liner	None
B	Same as glove A	Monolithic PU	Same as glove A	None
C	Same as glove A	Similar to glove A with substrate laminated directly to thermal liner	Thermal knit[h]	ePTFE-based film laminated to spunlace aramid substrate, between moisture barrier and back shell
D	Elk	Same as glove A	Same as glove A	None
E	Same as glove D	Same as glove B	Same as glove A	None
F	Same as glove D	Same as glove C	Same as glove C	Same as glove C
G	Cow	Same as glove A	Knitted, fleeced modacrylic and cotton liner	None
H	Cow	Same as glove A	Knitted, fleeced modacrylic liner	None
I	Cow	Monolithic PU[i]	Same as glove H	None
J	Pig/cow	ePTFE-based film laminated directly to thermal liner	Knitted, fleeced modacrylic liner	None
K	Cow/cow	Same as glove C	Same as glove C	Same as glove C
L	Elk	Same as glove A	Same as glove H	None
M	Same as glove M	Same as glove I	Same as glove H	Elk palm reinforcement band
N	Kangaroo[b]/kangaroo	Same as glove A	Knitted, fleeced para-aramid and meta-aramid	None
O	Cow/para-aramid[c]	Same as glove C	Same as glove C	ePTFE-based film laminated to non-woven substrate[h] and para-aramid/meta-aramid spacer fabric, between moisture barrier and back shell
P	Cow	Same as glove I	Same as glove H	None
Q	Pig	None	None	None

TABLE 2—*Continued*

Glove	Shell[a] (Palm/Back if Different)	Moisture Barrier	Thermal Liner	Additional Materials
R	Para-aramid[d]	PTFE-based film laminated directly to thermal liner	Knitted, fleeced aramid liner	None
S	Goat/goat and para-aramid /meta-aramid	Double layer PU	Knitted meta-aramid liner	1 – 2 layers knitted para-aramid, meta-aramid, or para-aramid/ meta-aramid blend throughout as well as a para-aramid, meta-aramid, and silicon carbide knuckle guard
T	Kangaroo/kangaroo and para-aramid/meta-aramid	Same as glove S	Same as glove S	Same as glove S
U	Cow	Same as glove A	Knitted para-aramid with silver fibers	para-aramid, silicone, and carbon knuckle, palm, and fingertip reinforcements
V	Synthetic leather/polyamide/spandex and synthetic leather and reflective[e]	None	Knitted terry[j] and nylon on back; knitted terry on finger side panels	Specialty para-aramid-based pads on palms, fingers, and PIP[k] joints as well as rubber back reinforcement
W	Rubber-coated nylon/nylon	None	None	None
X	Cow /cow and nylon and nylon/PU[f]	None	Knitted aramid liner	None

[a]All animals refer to leather type. All leathers have a napped texture (no top grain leathers). Leathers referenced as "Same as" have the same source and specification as indicated. Leathers that are the same animal type but not indicated "Same as" may or may not have similar properties.
[b]Digitally embossed.
[c]Simplex knit.
[d]Interlock knit, inner side fleeced.
[e]Specialty reflective fabric; unspecified fiber composition.
[f]Polyurethane.
[g]Expanded polytetrafluoroethylene.
[h]Flame resistant; fiber type unspecified.
[i]Similar but not the same as the PU barrier in glove B.

TABLE 3—*Test glove constructions and details.*

Glove	Pattern	Layers	Moisture Barrier to Thermal Liner Attachment	Moisture Barrier to Outer Shell Attachment	Thumb Style	Distinctive Features	Use (Intended)	Compliancy
A	2D	3	Glued along fingers	Liner sewn at fingertips	Modified straight		Structural firefighting	NFPA 1971
B	2D	3	Glued along fingers	Tabs glued to barrier and sewn to shell at fingertips	Modified straight		Structural firefighting	NFPA 1971
C	2D	2 – 3	Direct lamination	Tabs glued to barrier and sewn to shell at fingertips	Modified straight		Structural firefighting	NFPA 1971
D	2D	3	Glued along fingers	Liner sewn at fingertips	Modified straight		Structural firefighting	NFPA 1971
E	2D	3	Glued along fingers	Tabs glued to barrier and sewn to shell at fingertips	Modified straight		Structural firefighting	NFPA 1971
F	2D	2 – 3	Direct lamination	Tabs glued to barrier and sewn to shell at fingertips	Modified straight		Structural firefighting	NFPA 1971
G	2D	3	Tabs glued to barrier and sewn to thermal liner at side of fingertips	Liner sewn at fingertips	Wing		Structural firefighting	NFPA 1971
H	2D	3	Glued along fingers	Liner sewn at fingertips	Modified wing		Structural firefighting	NFPA 1971
I	2D	3	Glued along fingers	Liner sewn at fingertips	Modified wing		Structural firefighting	NFPA 1971
J	2D	2	Direct lamination	Tabs glued to barrier and sewn to shell at fingertips	Wing		Structural firefighting	NFPA 1971

TABLE 3—*Continued*

Glove	Pattern	Layers	Moisture Barrier to Thermal Liner Attachment	Moisture Barrier to Outer Shell Attachment	Thumb Style	Distinctive Features	Use (Intended)	Compliancy
K	2D	2 – 3	Direct lamination	Tabs glued to barrier and sewn to shell at fingertips and one on side of glove	Modified straight		Structural firefighting	NFPA 1971
L	2D	3	Glued along fingers	Liner sewn at fingertips	Modified wing		Structural firefighting	NFPA 1971
M	2D	3	Glued along fingers	Liner sewn at fingertips	Modified wing	Palm band	Structural firefighting	NFPA 1971
N	3D	3	Glued along fingers	Liner sewn at fingertips	Modified wing		Structural firefighting	NFPA 1971
O	2D	2 – 4	Direct lamination	Tabs glued to barrier and sewn to shell at fingertips	Wing	Fabric back; fingertip reinforcements	Structural firefighting	NFPA 1971
P	3D	3	Glued along fingers	Liner sewn at fingertips	Modified wing		Structural firefighting	NFPA 1971
Q	2D	1	N/A	N/A	Traditional keystone		Rescue/extrication	CE Rated
R	3D	2	Direct lamination	Tabs glued to barrier and sewn to shell at fingertips	3D keystone	All fabric construction	Hazmat	NFPA 1991/NFPA 1994
S	3D	5 – 6	Tabs glued to barrier and sewn to thermal liner at fingertips	Tabs glued to barrier and sewn to shell at fingertips	Winged keystone	Knuckle guard; partial fabric construction	Structural firefighting	NFPA 1971
T	3D	5 – 6	Tabs glued to barrier and sewn to thermal liner at fingertips	Tabs glued to barrier and sewn to shell at fingertips	Winged keystone	Knuckle guard; partial fabric construction	Structural firefighting	NFPA 1971
U	3D	3	Glued along fingers	Liner sewn at fingertips	Modified wing	Palm band, knuckle guard, and fingertip reinforcements	Structural firefighting	NFPA 1971

TABLE 3—*Continued*

Glove	Pattern	Layers	Moisture Barrier to Thermal Liner Attachment	Moisture Barrier to Outer Shell Attachment	Thumb Style	Distinctive Features	Use (Intended)	Compliancy
V	3D	1 – 3	N/A	N/A	Wing	Grip pads; knuckle guard; partial fabric construction	Extrication	None
W	Seamless 3D knit	1	N/A	N/A	Reversible	All fabric construction	General purpose work gloves	None
X	3D	2	N/A	N/A	Wing	Partial fabric back	Tactical law enforcement	None

associated with structural firefighter gloves (Samples V, Q, X, and W). These examples include a law-enforcement glove (Sample X), a single-layer, pigskin work glove (Sample Q), an extrication glove (Sample V), and a lightweight, knit glove with a rubber-coated palm (Sample W). Work gloves and extrication gloves are reportedly worn by structural firefighters for improved dexterity and grip performance. A hazmat glove (Sample R) was included, in part, because it is known for having poor grip performance.

Test gloves were selected with input from a technical panel consisting of firefighters and other knowledgeable individuals in the area of firefighter PPE technologies, testing methodologies, and NFPA 1971 requirements for structural firefighter gloves.

NFPA 1971-certified structural firefighter test gloves included examples of two-layer constructions, three-dimensional designs, and gloves that incorporate knit materials in the glove construction (Table 3). All the test gloves were commercially available gloves, purchased off the shelf.

Results and Discussion

Five variants of rope- or rod-pull grip tests (Table 1) and two variants of the torque test grip protocol (wet and dry test conditions) were used to evaluate the grip performance of the 24 sample glove study group. These data were statistically analyzed to compare the different grip-testing procedures based on the subject-to-subject testing variability of the test data produced, and on ability to differentiate among different NFPA 1971-compliant and non-compliant gloves.

Comparing Grip Test Procedures

A summary of the grip test ratings data produced by the procedures studied by this research is provided in the Appendix to this paper. Figures 3 and 4 show the grip ratings observed in the wet-conditioned, horizontal rope pull (Protocol 1) and wet-conditioned torque grip tests.

Table 4 provides a summary analysis of these data, showing the average, range, and % coefficient of variation for the grip ratings. It also shows the number of distinct levels of statistically significant differences observed among the glove test samples based on a series of Student *t* tests analyses performed at the 95 % confidence level.

These data show that a significant range of different grip ratings are obtained for the test gloves, depending on particular test method used for the evaluation. The most agreement among the different grip test protocols is observed for gloves having the highest (best) or lowest (worst) grip performance. For example, all the test procedures are able to identify the poor grip performance of the hazmat glove (Sample R). However, differences in grip ratings

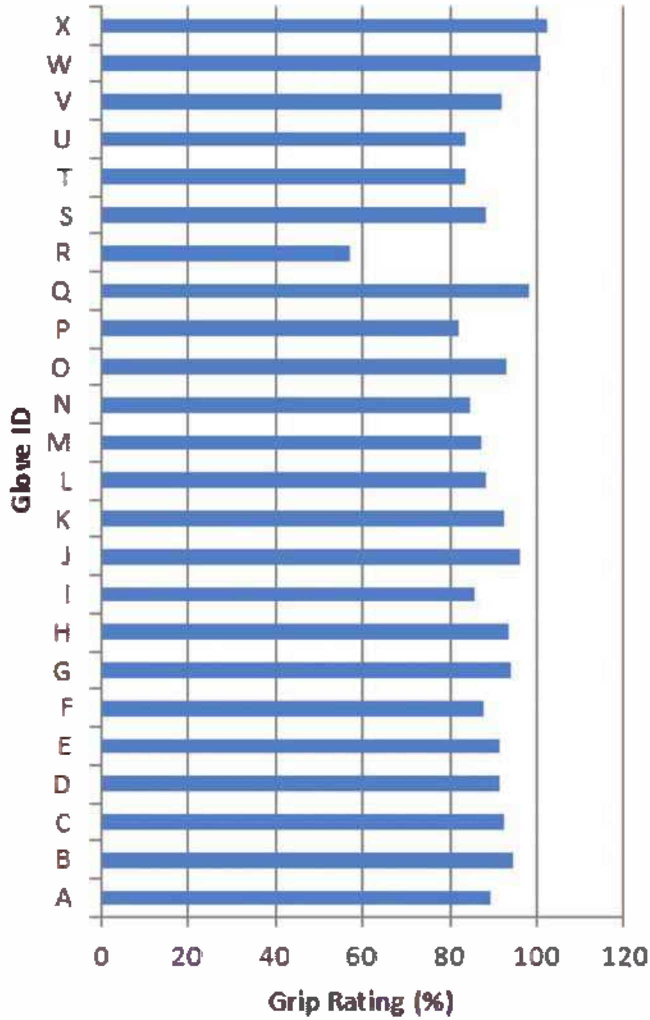

FIG. 3—*Grip ratings assessed via NFPA1971 horizontal wet rope-pull method (Protocol 1).*

can otherwise vary significantly by test method, especially for gloves whose grip performance is not at the either end of the performance spectrum. Some test-method-related differences can be attributed to the muscle mechanics involved in the gripping action, or to differences in the pulling or twisting forces applied in the tests. Other effects are undoubtedly because of differences in the orientation of applied forces, or to the physical interactions between a gloved hand and a rope, rod, or pole. Still others are because of the effects of wet test conditions. When considering the results of the rope- or pole-pull test variants over the 24-sample group, we observe that horizontally applied pulling forces and wet conditions tended to reduce glove-grip performance. There was

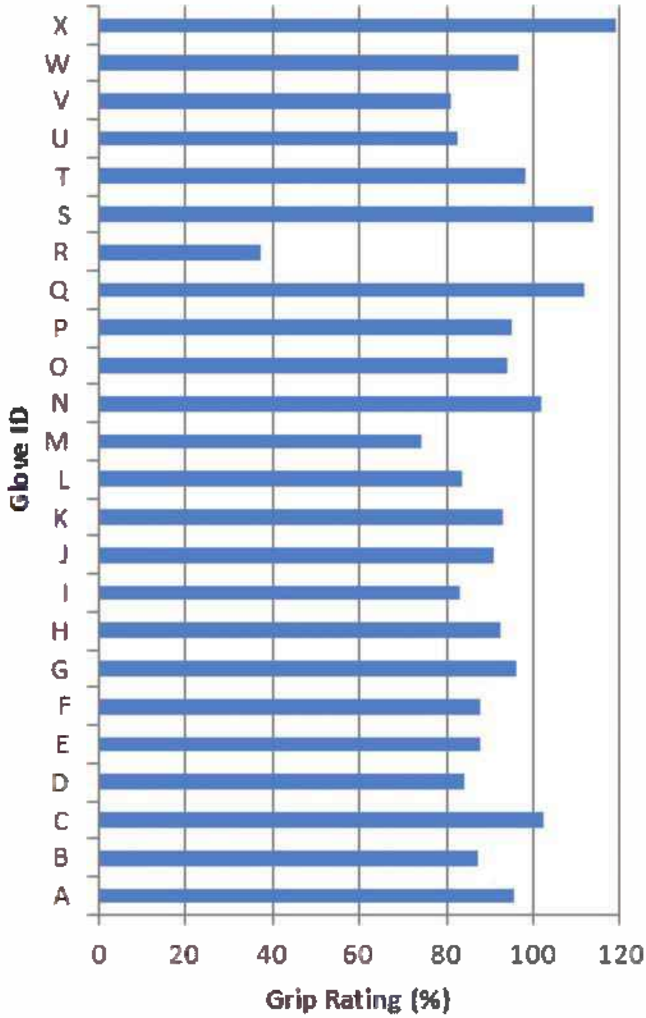

FIG. 4—*Grip ratings assessed via wet torque method.*

no general trend that could be observed regarding the effect of wet conditioning for the torque test; most gloves performed similarly whether tested in a wet or dry condition. A few gloves, however, performed significantly better or worse when wet, highlighting the potential for certain gloves to be more prone to the changes in the various surface interactions or glove properties when wet.

Difference observed in the grip ratings produced by different test methods must be weighed in light of the variability of the test data. In this regard, one of the most important finding of this study is related to the differences observed in the range and variability of grip ratings produced by the different test methods. Our research found a high level of testing variability in all the grip test methods studied, with the overall coefficients of variation ranging from 20 to 30 %

TABLE 4—*Summary results from different grip test methods.*

Test Protocol	Highest (Best) Grip Rating (%)	Lowest (Worst) Grip Rating (%)	Range (%)	CV[a] (%)	Levels of Discrimination
1	102.5	57.0	45.5	22.2	2
2	126.4	56.4	70.0	30.1	2
3	102.0	66.0	36.0	28.5	2
4	97.3	35.3	62.0	NC[b]	NC[b]
5	121.3	74.1	47.2	27.1	2
Wet torque	119.1	37.3	81.8	19.5	6
Dry torque	131.1	37.4	93.7	19.8	7

[a]Average coefficient of variation among subjects evaluating each glove.
[b]Values were not calculated because only three subjects evaluated gloves.

for all the gloves tested (Table 4). Figures 5 and 6 show that much of the source of test variability is caused by subject-to-subject variability in the grip rating data.

The data in Table 4 show that none of the protocol variants employed significantly reduced the variability provided by the rope- or pole-pull grip-testing methods. However, they also show that the newly developed toque test produced slightly lower subject-to-subject variability and the widest range

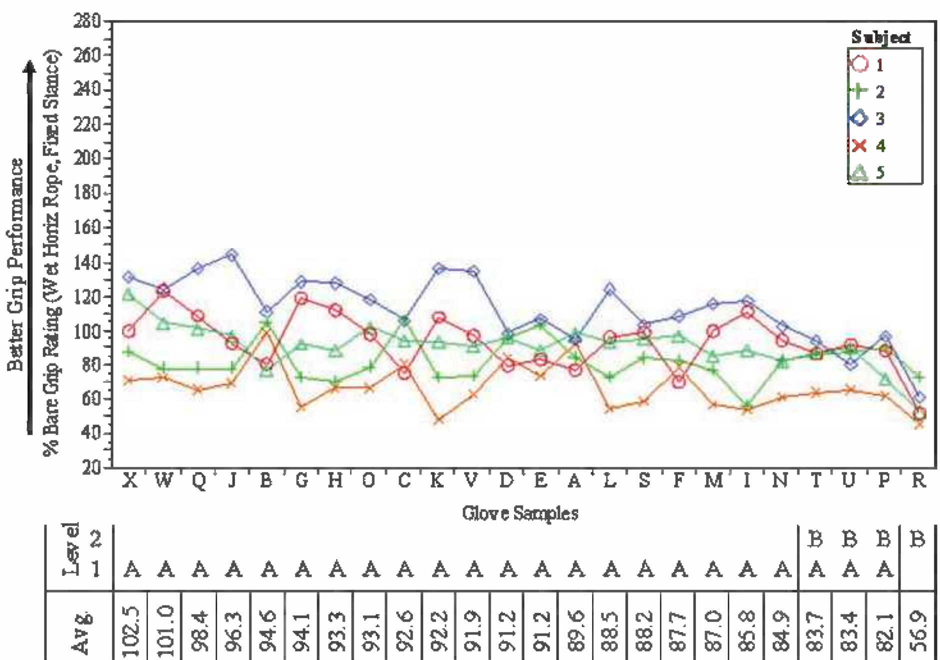

FIG. 5—*Subject-to-subject variability in NFPA1971 horizontal wet rope-pull method (Protocol 1).*

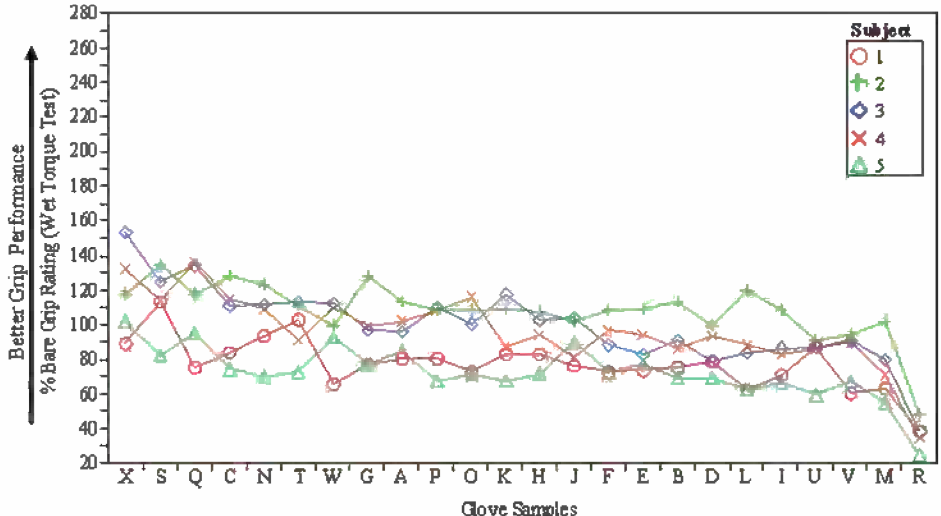

Level	X	S	Q	C	N	T	W	G	A	P	O	K	H	J	F	E	B	D	L	I	U	V	M	R
6																								F
5							E	E	E	E	E	E	E	E	E	E	E	E	E	E	E	E	E	
4				D	D	D	D	D	D	D	D	D	D	D	D	D	D	D	D	D	D	D		
3			C	C	C	C	C	C	C	C	C	C	C	C										
2		B	B	B	B	B	B	B	B	B	B	B	B											
1	A	A	A	A	A	A	A																	
Avg	119.1	113.8	111.7	102.5	101.6	98.3	96.4	95.9	95.7	95.2	94.2	93.1	92.3	90.9	88.0	87.5	87.4	84.2	83.5	83.2	82.5	80.8	74.5	37.3

FIG. 6—*Subject-to-subject variability in wet torque test.*

between the highest and lowest grip ratings. This small reduction in subject-to-subject test variability combined with the greater range in grip ratings to give the torque method significantly better ability to identify statistically significant differences in glove-grip performance, in comparison with any of the rope- or pole-pull procedures. The analysis summarized in Table 4 and Figs. 5 and 6 show that the rope- or pole-pull procedures are able to differentiate only two levels of glove-grip performance that are statistically significant at the 95 % confidence level. This is a remarkable finding that means that the grip performance of NFPA 1971 compliant gloves must be grouped with the non-compliant gloves by these pull-type test methods. In comparison, torque test procedures are able to distinguish six to seven statistically significant grip performance levels among the same group of test gloves.

The significance of the observed subject-to-subject variability in grip testing can be discussed in the context of the rope-pull method called by the 2007 version of the NFPA 1971 Standard. The NFPA 1971 rope grip-test method only requires two human evaluators, one selected to fit size-small and the other to fit size-large gloves [1]. Figure 5 shows the wide range of subject-to-subject ratings obtained when we used five human subjects in this method (Protocol 1). These data show that only about one-half of the certified NFPA 1971 gloves achieve the 90 % grip rating required to pass the current grip performance requirement when evaluated by our study. Many other NFPA 1971 certified gloves only marginally meet the current NFPA 1971 grip performance. Most significantly, our research demonstrates how different test subjects can give drastically different assessments while performing pull-type grip tests. The potential consequences of relying on two test subjects for glove-grip evaluations are apparent. In our study, Subject 3 would have passed 18 of the 19 NFPA 1971-compliant gloves in the test group (Fig. 5). In contrast, only two of the certified gloves would pass the grip requirement based on data from Subject 4's grip evaluation (Fig. 5).

Glove Performance in the Torque Grip Test

Additional validation for the torque grip test method was provided by observing how the method responds to expected difference in the grip performance of different gloves. We have established that, unlike pull-type grip tests, the torque test method is able to identify the best-performing glove samples. Several non-compliant gloves, including a two-layer leather work glove (Sample Q) and a law enforcement glove (Sample X) stand out for their good performance in the torque test (Fig. 5). NFPA 1971-compliant glove samples that used three-dimensional glove designs and thin kangaroo or goat leathers in the construction of the palm of the glove (Samples T, S, and N) also performed well in this test. The performance of the structural firefighter glove with the silicone-coated palm reinforcement (Sample U) indicates that the torque test is responsive to the detrimental effects of wetting on the grip performance of certain types of glove materials or treatments. This occurrence is even more drastic for the work glove that featured the rubberized palm and knit-fabric-back construction (Sample W), and shows how the torque method can be used to provide useful insights into the relationship between glove design and grip performance. As expected, the rubber-palmed glove provided superior grip when tested in the dry condition (Fig. 7). However, the performance rating of this glove is significantly lower when tested in the wet condition.

The dramatic difference between dry- and wet-state performance can be attributed to the effects of moisture on the interaction between the rubberized palm and the smooth, acrylic rod gripped in the torque test. The continuous-reading torque output provided by the torque test provides additional explanation. Figure 8 compares the torque recorded over the 2.5-s test interval for the rubber-palmed glove (Sample W) and a structural-firefighting glove made with a cow-leather palm (Sample I).

These data show that both gloves register near the same peak torque and, therefore, receive about the same grip rating in the wet-condition torque test.

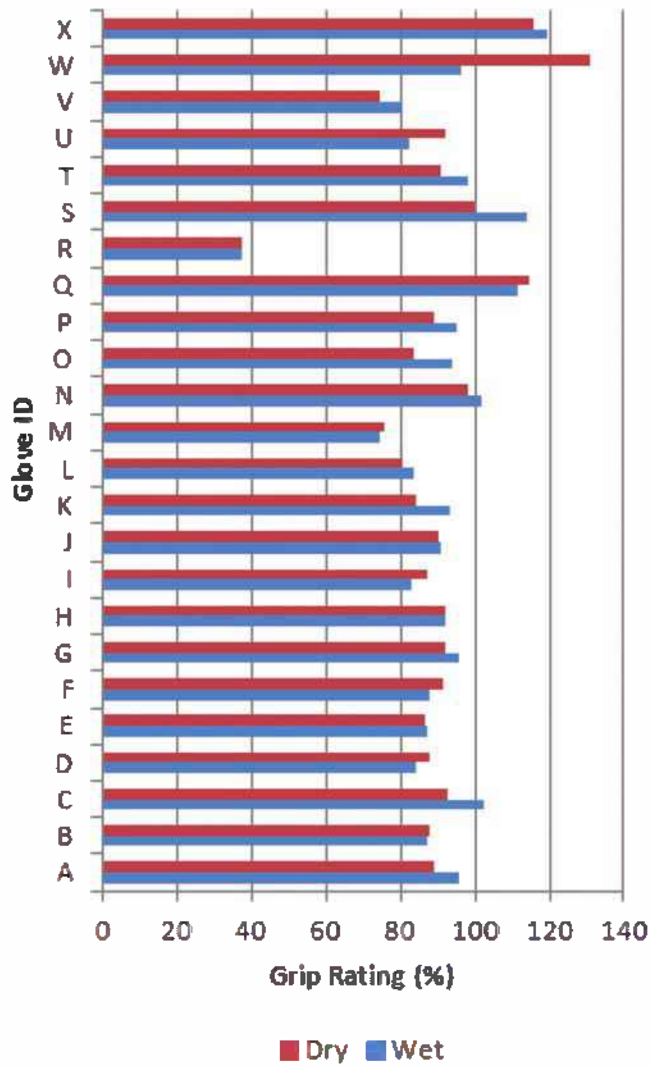

FIG. 7—*Grip ratings for torque method, dry and wet.*

However, these glove samples show a more complex behavior than is indicated by a simple comparison of peak gripping forces. The leather-palmed glove achieves a maximum gripping torque in about one second and maintains near-peak level throughout the remaining duration of the test. In contrast, the torque recorded by rubber-palmed glove exhibits a series of peaks and cascades from maximum torque levels throughout duration of the test.

The ability of the torque test to characterize "slip-stick" phenomenon may be of value in identifying gloves that have tendency for catastrophic grip failure when holding smooth surfaced implements such as an axe handle or pike

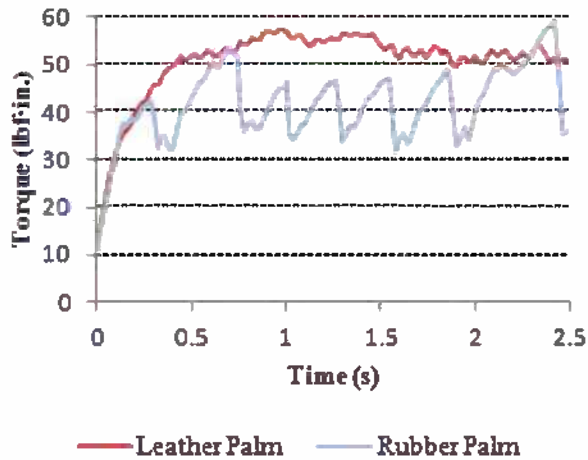

FIG. 8—*Stick-slip response observed in torque grip test (wet condition).*

pole. It should be pointed out that, aside from the rubber-palmed work glove, none of the other gloves in the selected test group exhibited slip-stick behavior in the torque test. Nor did any of the test gloves, including the rubber-palmed glove, show catastrophic grip failure in the vertical pull variant of the pole pull tests chosen for the baseline study. However, we were able to produce catastrophic failure in the rubber-palmed glove when using both metal and fiberglass poles in a variant of the wet-conditioned, pole-pull method that employed a horizontal "tug-of-war" stance to achieve a more aggressive pulling action. Further study of effects contributing to slip-stick, or to catastrophic grip failure, in structural firefighter gloves is clearly needed to better understand these phenomena and the relationship to hazardous grip failures that occur in firefighting.

Conclusions

This research has developed and demonstrated a torque-type test method for evaluating the grip performance of structural firefighter gloves. The new torque test is shown to provide less subject-to-subject variability and a greater range of measured grip ratings than any variant of rope- or pole-pull methods. Because the torque grip test is more simply performed, much of the observed improvements in testing variability can be attributed to reduction in subject-related differences typically associated with pull-type tests. These differences include subject variations in posture and pulling motions, and need for more detailed subject instruction and training in the technique for execution of pull-type methods.

This research shows that all grip-test methods are inherently variable because of the wide range of physiological response among subjects performing the tests. This study also shows how the use of only two evaluators in the 2007 NFPA 1971 rope-pull grip method can potentially result in entirely different conclusions about the compliance of structural firefighter gloves based on grip performance. Within practical limits, variability in human subject testing is typically counteracted by using more human test subjects for the evaluation.

This research shows the critical need for a better testing methodology for evaluating the grip of firefighter gloves. It has shown the inadequacy of the rope-pull method currently specified by the NFPA 1971 standard (2007 Edition). This method does not produce statistically significant differences in grip performance data in tests made on a wide range of NFPA 1971 certified gloves. Most significantly, the rope-pull grip test method does not identify differences in the grip performances, even in radically different gloves, including single-layer work gloves, extrication gloves, or gloves used for law-enforcement applications. This is a significant limitation because it means that pull-type

TABLE 5—*Average grip ratings and ranks.*

	Protocol 1		Protocol 2		Protocol 3		Protocol 4		Protocol 5		Dry Torque		Wet Torque	
	Mean	Rank	Mean	Rank	Mean	Rank	Mean	Rank	Mean	Rank	Mean	Rank	Mean	Rank
A	89.6	14	91.5	19	83.0	21	71.1	17	99.7	17	88.8	13	95.7	9
B	94.6	5	100.6	13	92.6	12	72.2	12	107.3	10	87.7	16	87.4	17
C	92.6	9	104.5	8	87.8	16	71.7	16	104.4	14	92.9	6	102.5	4
D	91.2	12	97.8	15	87.4	17	67.4	23	97.5	19	88.0	15	84.2	18
E	91.2	13	91.4	21	86.9	18	72.2	13	94.7	23	86.9	18	87.5	16
F	87.7	17	102.0	10	90.6	14	80.4	7	104.6	13	91.5	10	88.0	15
G	94.1	6	101.6	12	93.2	10	72.1	14	107.5	9	91.8	9	95.9	8
H	93.3	7	93.6	17	95.4	8	70.9	19	101.1	16	92.2	8	92.3	13
I	85.8	19	86.7	23	82.7	22	67.4	22	95.6	22	87.4	17	83.2	20
J	96.3	4	102.9	9	98.3	4	89.9	4	105.3	11	90.1	12	90.9	14
K	92.2	10	99.5	14	89.8	15	70.6	20	95.8	21	84.1	19	93.1	12
L	88.5	15	91.5	20	86.7	19	72.1	15	102.3	15	80.3	21	83.5	19
M	87.0	18	93.4	18	82.5	23	72.8	11	96.9	20	75.7	22	74.5	23
N	84.9	20	101.8	11	97.9	5	70.0	21	113.0	7	98.4	5	101.6	5
O	93.1	8	94.5	16	102.0	1	74.7	9	107.6	8	83.4	20	94.2	11
P	82.1	23	107.1	7	93.6	9	71.0	18	99.4	18	88.8	14	95.2	10
Q	98.4	3	115.1	4	95.5	7	97.3	1	113.6	6	114.4	3	111.7	3
R	57.0	24	56.4	24	66.0	24	35.3	24	74.1	24	37.4	24	37.3	24
S	88.2	16	122.0	2	98.6	3	87.7	5	118.7	3	100.1	4	113.8	2
T	83.7	21	107.6	6	101.6	2	78.5	8	121.3	1	90.7	11	98.3	6
U	83.4	22	90.9	22	91.1	13	74.5	10	117.2	4	92.4	7	82.5	21
V	92.0	11	110.1	5	83.7	20	81.0	6	105.2	12	74.4	23	80.8	22
W	101.0	2	116.6	3	93.2	11	92.0	2	120.7	2	131.1	1	96.4	7
X	102.5	1	126.4	1	95.8	6	90.1	3	114.3	5	115.7	2	119.1	1

grip test methods are blunt instruments that provide little guidance for future development of gloves with better grip performance.

Unlike rope- or pole-pull methods, the torque grip test method is capable of a measured response to different glove types and constructions. It also provides information on glove-grip performance associated with slip-stick grip behavior, a phenomenon possibly related to catastrophic grip failure. Because of its better test resolution, the torque grip test is being successfully used in our ongoing research to understand the role of material selection and glove design on the functional performance of structural firefighter gloves.

Work is being conducted to qualify the inter-laboratory reproducibility of the torque grip test method. However, its superior subject variability and resolution in comparison with rope- or pole-pull grip tests has been demonstrated, as has its value as a tool for guiding the development of more functional structural firefighter gloves.

Acknowledgments

The writers are grateful to the AFG Program of the Federal Emergency Management Agency (FEMA) at the Department of Homeland Security for providing funding for this research. They gratefully acknowledge the valuable input provided by the panel of firefighters and experts organized by Casey Grant of the National Fire Protection Research Foundation. They also wish to thank the NFPA 1971 Task Group on Gloves for their valuable correspondences as well.

APPENDIX

Seven grip test methods were evaluated (five pull methods plus dry- and wet-condition torque methods). Table 5 shows the mean grip ratings determined by each method for each glove and the relative rank of each glove within the test group (Best = 1).

References

[1] NFPA 1971, 2007, "Standard on Protective Ensembles for Structural Fire Fighting and Proximity Fire Fighting," NFPA, Quincy, MA.
[2] NFPA 1971, 2010, "Report on Proposals, 2011 Fall Revision Cycle," NFPA, Quincy, MA.

Performance of Protective Clothing and Equipment: Emerging Issues and Technologies
STP 1544, 2012
Available online at www.astm.org
DOI:10.1520/STP104094

Chantal Gauvin,[1] *Alexandre Airoldi,*[1]
Simon Proulx-Croteau,[1] *Patricia I. Dolez,*[2] *and Jaime Lara*[1,3]

A New Test Method to Characterize the Grip Adhesion of Protective Glove Materials

REFERENCE: Gauvin, Chantal, Airoldi, Alexandre, Proulx-Croteau, Simon, Dolez, Patricia I., and Lara, Jaime, "A New Test Method to Characterize the Grip Adhesion of Protective Glove Materials," *Performance of Protective Clothing and Equipment: Emerging Issues and Technologies* on April 16, 2011 in Anaheim, CA; STP 1544, Angie M. Shepherd, Editor, pp. 392–406, doi:10.1520/STP104094, ASTM International, West Conshohocken, PA 2012.

ABSTRACT: Protective gloves can reduce the number and severity of hand injuries but may also impair manual performance such as grip strength. A worker wearing poorly adherent gloves must apply additional muscular effort to retain the handled parts, leading to discomfort, pain, and possibly musculo-skeletal disorders. Glove grip depends on the coefficient of friction (COF) between the glove and handled object surfaces. Knowledge of COF values can be helpful to workers for selecting suitable gloves. However, existing standard test methods for measuring COF are not applicable to gloves. In a previous study, a test method was proposed to evaluate COF of glove materials, using a modified version of the TDM-100 test apparatus initially designed to characterize the cut resistance of protective materials. The test method consists in sliding a flat metal probe on a flat material specimen at a constant speed while applying a load perpendicular to the contact surface. The friction force is measured with a load cell attached to the probe. The friction force versus displacement curve typically presents an initial peak representing the static COF, followed by a plateau representing the dynamic COF. In this study, the effect of the applied load and probe roughness on the COF was characterized with neoprene and nitrile rubber as well as with six different thermoplastic

Manuscript received June 6, 2011; accepted for publication March 23, 2012; published online September 2012.

[1]Institut de Recherche Robert-Sauvé en Santé et en Sécurité du Travail (IRSST), Montreal, Quebec, Canada.

[2]École de Technologie Supérieure, Montreal, Quebec, Canada.

[3]Institut de Recherche Robert-Sauvé en Santé et en Sécurité du Travail (IRSST), Montreal, Quebec, Canada. (Presently at Univ. of Montreal, Quebec, Canada.)

materials. The study demonstrates that both of them affect the measured static and dynamic COFs. A normal load of 10 N, and a probe surface roughness of 1.0 or 2.0 μm gave the most reproducible results and seemed to be the more appropriate to perform testing with different polymer materials. The coefficient of variation of both static and dynamic COFs values obtained was generally lower than 15 %. This test protocol demonstrates to be well adapted to characterize the grip adhesion of glove materials.

KEYWORDS: grip, adhesion, coefficient of friction, glove materials

Introduction

Gloves designed to protect against a variety of occupational hazards can impair manual performance such as grip strength [1,2]. Studies have shown that a greater grip force is used to hold an object with gloves than bare handed [1,3]. This additional muscular effort can lead to fatigue, muscle pain, and eventually musculoskeletal disorders of the upper limbs. Gloves grip must be considered when selecting gloves best adapted to both the task and the hazard.

One way to evaluate glove grip is to measure the coefficient of friction (COF) between the glove material and the surface of the object. The COF is a dimensionless number representing the resistance to slip between two contacting surfaces, given by COF $= F_F/F_N$, where F_F is the friction force and F_N is the normal force. The static COF is measured when one surface starts to move relatively to the other, and the dynamic COF is measured during slipping.

Standard mechanical tests are defined to measure the COF of films and plastic sheets [4], of yarn to yarn in textiles [5], or yarn to solid materials [6], but none of these methods are applicable to protective gloves. Biomechanical methods involving functional gripping tasks with human subjects have been developed to study the effect of gloves on muscular gripping efforts [2,3,7–10]. In general, these methods only allow measuring the static COF.

In a previous study, a mechanical approach has been developed to characterize grip adhesion of protective gloves by measuring static and dynamic COFs [11]. It uses a modified version of the TDM-100 apparatus (RGI Industrial Products, St-Jean-sur-Richelieu, QC, Canada), originally designed to measure cut resistance of protective materials according to ISO 13997 [12] and ASTM F1790-05 [13]. It consists of sliding a flat probe at a constant speed on the glove material surface, while a so-called normal load is applied in the normal direction, i.e., perpendicular to the contact surfaces. Using this test method, the static and dynamic COFs of over 20 models of protective gloves have been measured using a flat stainless steel probe. The results have been shown to be in agreement with subject perceptions on the glove grip, and with COFs measured using a biomechanical approach [11]. The proposed mechanical method offers three advantages: (1) its variability is smaller than with a biomechanical method; (2) it is capable of measuring static and dynamic COFs for any material; and (3) it is simpler and less expensive to use.

Both static and dynamic COFs must be considered for task performance and safety when wearing protective gloves. An analogy can be made with the slip, trip, and fall research field. Although the static COF is measured at the beginning of a slip when walking on a surface, it is now recognized that the dynamic COF as well as the difference between the static and dynamic COFs are, by far, the parameters which reflect more accurately than the static COF the impression of safety felt by the subjects when they walk on slippery surfaces [14]. In the case of protective gloves, although an individual might need very adherent gloves to carry objects without dropping them, his tasks might also require complex manipulations of objects, involving controlled slip, which is highly related to dynamic COF.

Several phenomena involving slip friction in polymers have been studied, such as a tire on ground surface, a wiper on a glass surface, etc. The frictional behavior of a polymer is the combination of two physical phenomena: adhesion occurring at the contact zone, and deformation of the polymer surface asperities during friction [15,16]. The relative contribution of each of these two phenomena depends on many parameters, such as surface roughness and normal load applied.

The main goal of the current study is to investigate both the roughness of the stainless steel probe used in the mechanical test method [11] and the normal load applied to the probe-to-glove surfaces, to identify the best conditions for measuring COF of protecting gloves. Appropriate testing conditions would minimize COF sensitivity of the tested parameters, while ensuring good repeatability of the measurement.

Methods

As described in previous work [11], the TDM-100 apparatus was modified to allow measuring COF between polymer samples and steel. The blade was

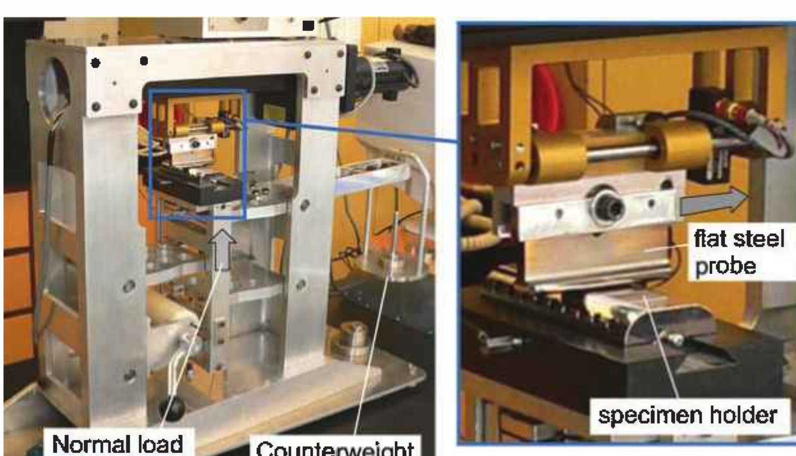

FIG. 1—*Experimental setup based on TDM-100 apparatus.*

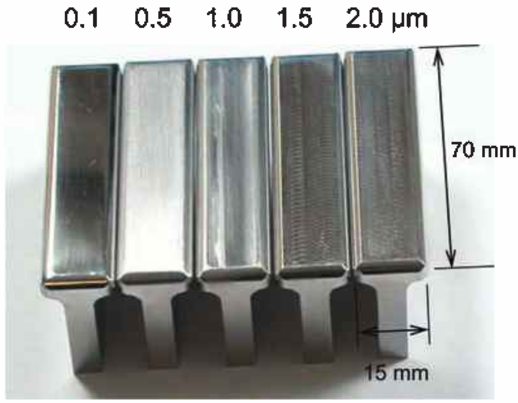

FIG. 2—*Probes of different roughness values.*

replaced by a flat probe, and the curved specimen holder was replaced by a flat specimen holder (Fig. 1). The probe and the specimen holder were secured so that their surfaces were perfectly parallel. The apparatus allows slipping the probe at constant speed of 150 mm/min over a specimen while a normal load (L), perpendicular to the contact surfaces, is applied on the specimen using a counterweight system. The friction force between the probe and the specimen is recorded using a 44-N load cell (MLP-10-C0, Transducer Techniques Inc., Temecula, CA) mounted on the probe holder.

This study was performed in two steps. In step 1, the best loads were identified by performing experiments with different loads (2.5, 5, 10, and 15 N) and different probe surface roughness values (0.1, 0.5, 1.0, 1.5, and 2.0 μm, see Fig. 2), using four polymer materials (neoprene, nitrile, HDPE, Delrin). In step 2, the best probe roughness values were identified by repeating the experiment with four additional polymer materials using the best load identified in step 1. The probes were all made out of grade 17-4 stainless steel (hardness Rockwell C: 30).

TABLE 1—*Polymer materials.*

Name	Full named	Model number	Hardness
Neoprene[a]	Neoprene rubber	N95550MVT062	Shore A: 50
Nitrile[b]	Oil-resistant Buna-N rubber	86795K31	Shore A: 60
HDPE[b]	High density polyethylene	8619K424	Shore D: 62–69
Delrin[b]	Polyoxymethylene	8575K411	Rockwell R: 120
PTFE[b]	Teflon PTFE	8545K42	Rockwell R: 58
PP[b]	Polypropylene	8742K431	Rockwell R: 79–115
Nylon[b]	Nylon 6/6	8539K91	Rockwell R: 108–121
ABS[b]	Acrylonitrile butadiene styrene	8586K452	Rockwell R: 100–109

[a]Obtained from Reeves Brothers Inc., Atlanta, GA.
[b]Obtained from McMaster-Carr, Cleveland, OH.

TABLE 2—*Test conditions used.*

Step objective	Probe roughness R, μm	Normal load L, N	Tested material
(1) Find best loads	0.1; 0.5; 1.0; 1.5; 2.0	2.5; 5.0; 10.0; 15.0	Neoprene; Nitrile; HDPE; Delrin
(2) Find best probe roughness values	0.1; 0.5; 1.0; 1.5; 2.0	Best found	Neoprene; Nitrile; HDPE; Delrin; PTFE; PP; Nylon; ABS

The eight polymer materials are listed in Table 1. They were in the form of 1.59 mm (1/16 in.) thick sheets. The testing protocol is summarized in Table 2.

For the tests, 5 by 10 cm specimens were cut into the material sheets. Because dirty surfaces may alter results, the specimens were washed with soft soap, wiped, dried with compressed air without oil, and stored away from dust and light under ambient conditions at least 24 h prior to the tests. The specimens were mounted on the specimen holder (Fig. 3) using double-sided adhesive tape. The contact surface for each test was approximately 2 by 1 cm. For rigid materials, the contact surface was larger because the specimen could not perfectly fit the shape of the specimen holder. For each testing condition, 18 tests were performed on locations evenly distributed on three specimens. It was ensured that the same surface section was never tested twice. Before each test, the probe was wiped with isopropanol and allowed to dry for 30 sec. Then, the probe was lowered onto the specimen and the normal load was applied. Twenty seconds later, the probe was moved parallel to the contact surface at constant speed over a distance of 20 mm.

For each test, the friction force was recorded as a function of the probe displacement. The static COF was defined as the peak COF value obtained at the beginning of the test, and the dynamic COF was obtained by averaging the COF values over 2 mm displacement after the peak. For each testing condition, averages and standard deviations for static and dynamic COFs were calculated over the 18 tests.

For studied parameters (normal load and probe roughness), ANOVA statistical analyses were performed with a significance level α of 0.05, followed by multiple comparisons Tukey-Kramer tests, to check for significant effects of the testing parameters. The repeatability of static and dynamic COFs measurements was evaluated using interquartile ranges IQR, which can be defined as IQR = Q3 - Q1, Q3 and Q1 being the third and first quartiles. The interquartile range spans 50 % of a data set and indicates the level of statistical dispersion of measurements.

Results and Discussion

Figure 4 shows typical friction force versus probe displacement curves for neoprene and nitrile elastomers, as well as for HDPE and Delrin thermoplastics.

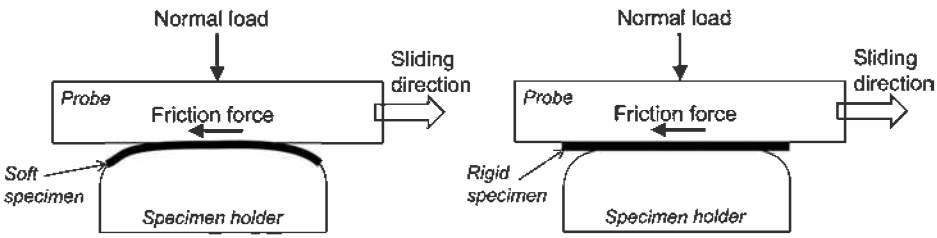

FIG. 3—*Use of modified TDM-100 apparatus for friction measurements, with soft and rigid specimens.*

The static COF was higher than the dynamic COF for all materials. The peaks for the static COF occurred at various probe displacements: around 0.2 mm for stiff thermoplastics, probably resulting from shearing of the double-sided adhesive tape, and around 1 mm for soft elastomers, mostly a result of shearing of the material itself and of the double-sided adhesive tape. The dynamic COF was obtained by averaging the COF values obtained from 3- to 5-mm probe displacement for elastomers, and from 1 to 3 mm for thermoplastics.

Friction of polymers is a complex phenomenon that is strongly affected by the material surface condition. For example, in some cases, the friction force

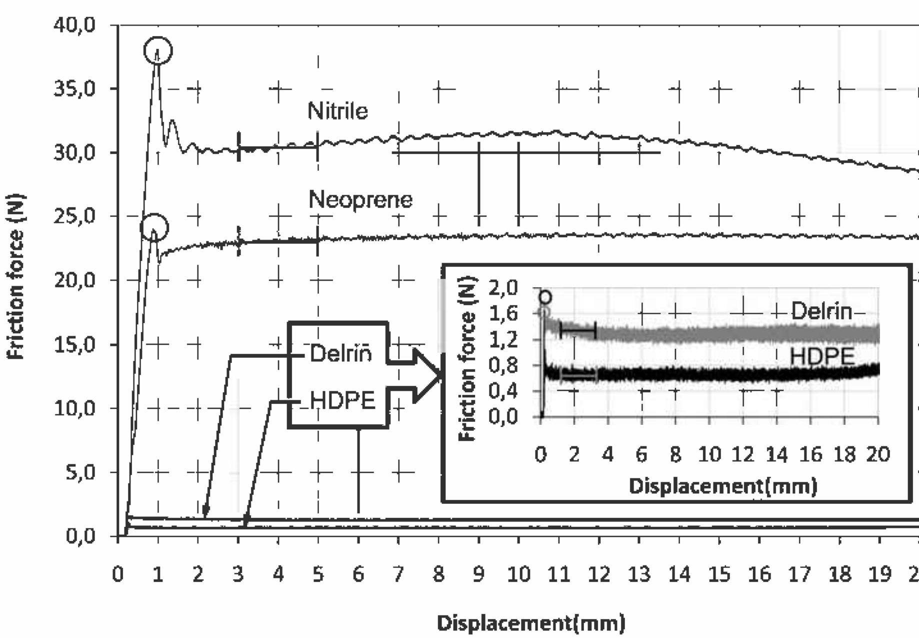

FIG. 4—*Typical friction force versus probe displacement curves, with a 10 N normal load and a 1.0 µm probe roughness, for neoprene, nitrile, HDPE and Delrin. The peaks and plateaus used to calculate the static and dynamic COFs are indicated by circles and by horizontal lines, respectively.*

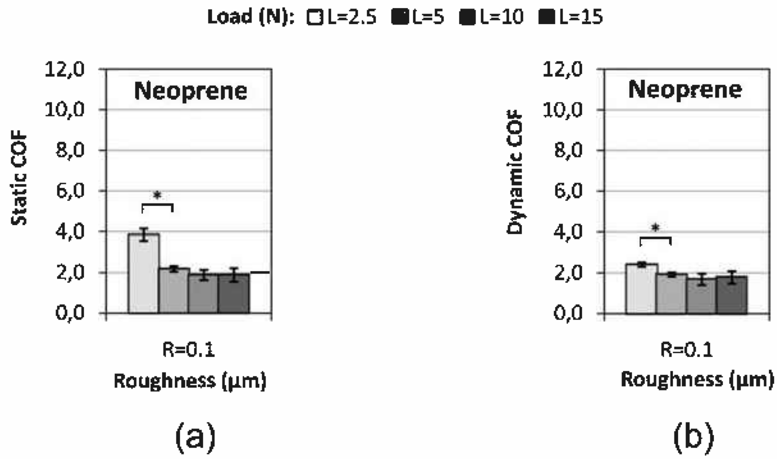

FIG. 5—(a) Static COF, and (b) dynamic COF for neoprene with different loads (L) and probe roughness of 0.1 µm.

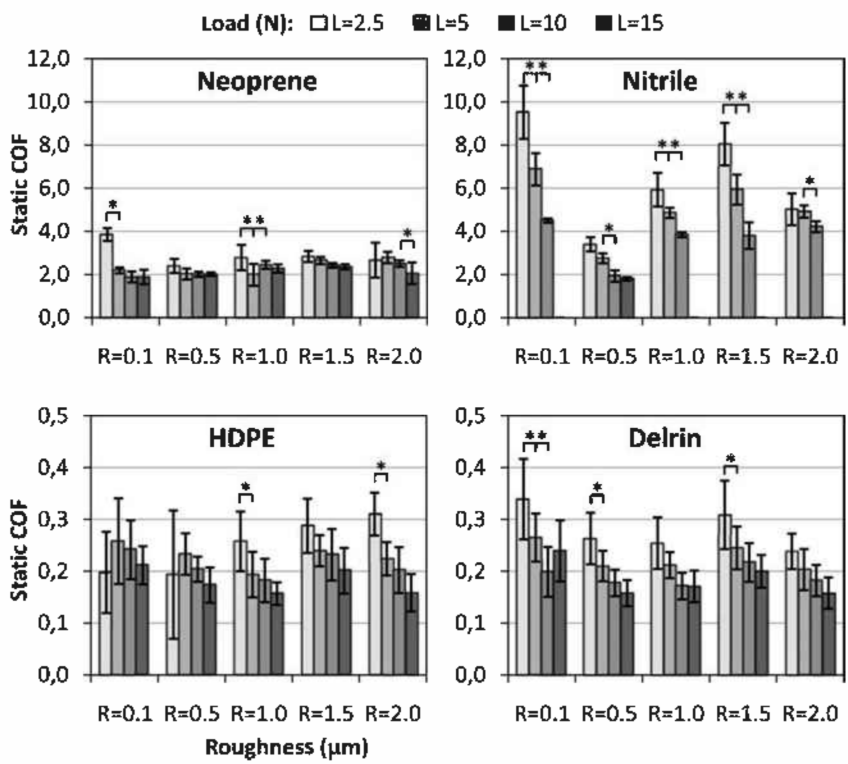

FIG. 6—*Static COF for neoprene, nitrile, HDPE, and Delrin with different loads (L) and probe roughness values (R). Notes: The vertical scale is different for elastomers and thermoplastics. Stars represent statistically significant differences between adjacent data bars only.*

continued to vary throughout the 20 mm displacement of the probe. This phenomenon could be caused by local temperature increases at the interface between the material and the probe, or to the material surface wearing, which would progressively alter the dynamic COF, as reported in other studies [16–19]. Also, the normal migration of low-weight molecules toward the polymer surface, could get torn during the friction test and be replaced by higher-weight molecules, therefore changing the nature of the material surface [20].

Effect of Load at Different Probe Roughness Values

Figure 5(*a*) presents an example of the static COF for neoprene obtained with loads from 2.5 N to 15 N using the probe roughness of 0.1 μm. The figure shows that the static COF decreases from 4 to 2 between 2.5 N and 5 N, and then remains unchanged up to 15 N. Figure 5(*b*) shows an example of dynamic COF for neoprene obtained with loads from 2.5 N to 15 N using the probe 0.1 μm. The dynamic COF is around 2 for all tested loads.

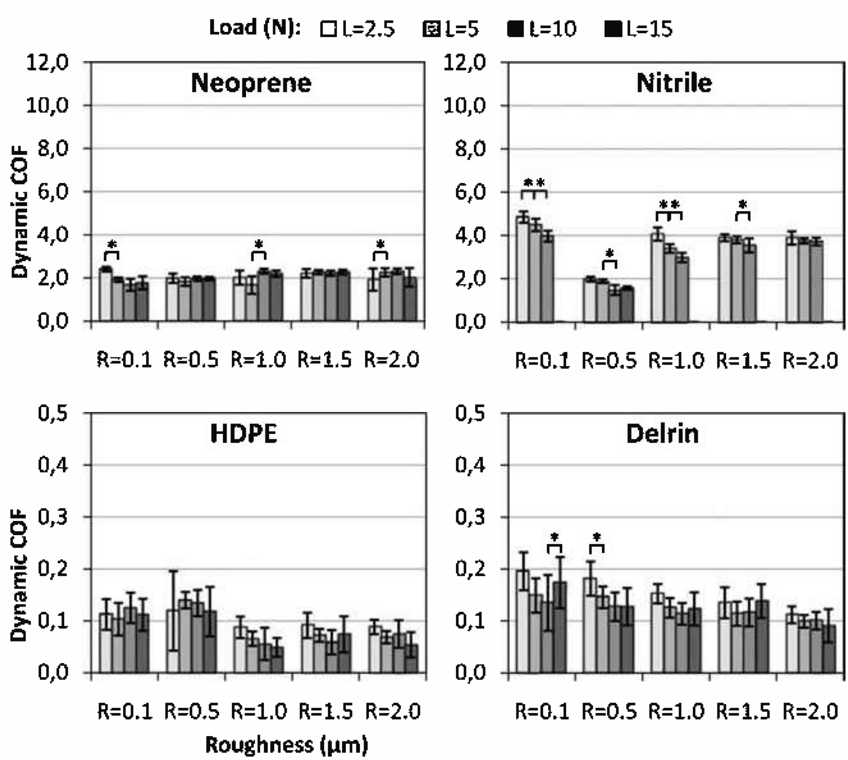

FIG. 7—*Dynamic COF for neoprene, nitrile, HDPE, and Delrin with different loads (L) and probe roughness values (R). The vertical scale is different for elastomers and thermoplastics. Note: Stars represent statistically significant differences between adjacent data bars only.*

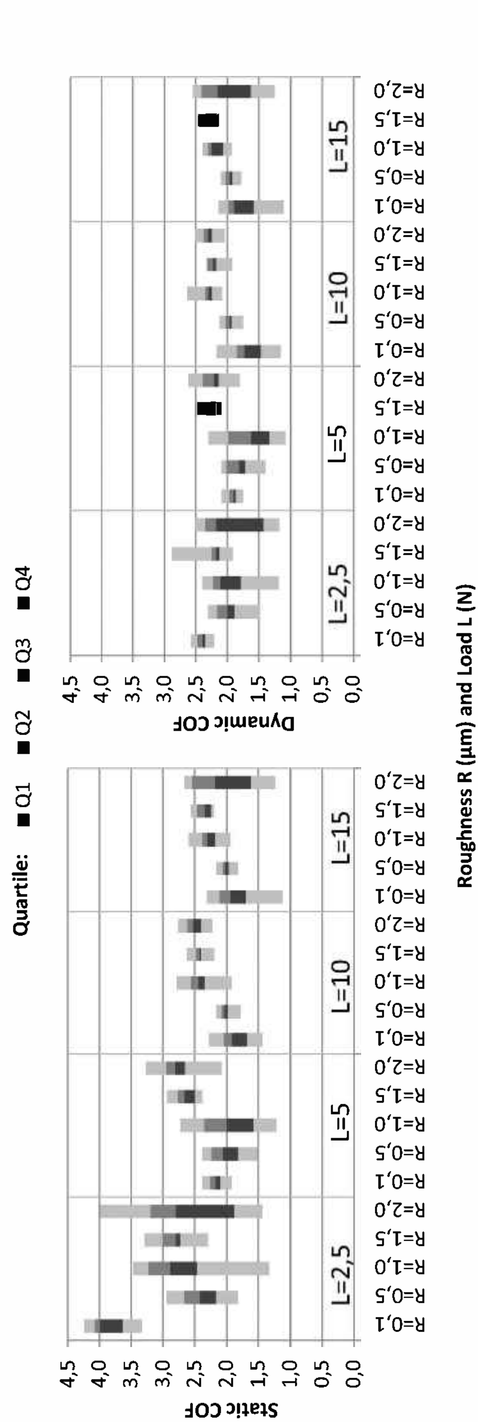

FIG. 8—*Quartile distribution of static and dynamic COFs for neoprene with different loads (L) and probe roughness values (R).*

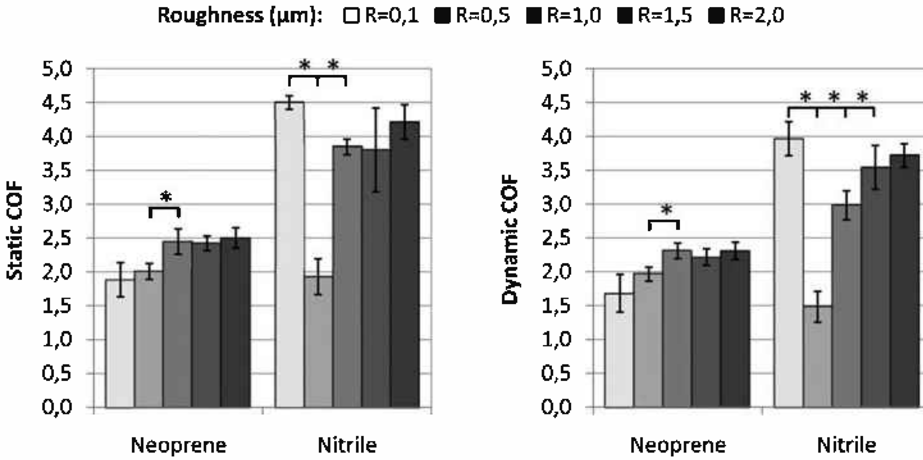

FIG. 9—*Static and dynamic COFs for elastomers with different probe roughness values (R) and a normal load of 10 N. Note: Stars represent statistically significant differences between adjacent data bars only.*

Figure 6 shows the static COF results for all the test conditions used in step 1 for neoprene, nitrile, HDPE, and Delrin materials. In the range of load tested (2.5 to 15 N), the static COF decreased when the load increased. However, these differences were not always significant, in particular between 5 and 15 N for neoprene, HDPE, and Delrin. This is in agreement with a literature review on friction of polymers, which reported that for several of those materials, the COF does not change with the load in the 10- to 100-N range [19].

Figure 7 shows the dynamic COF values obtained for the test conditions used in step 1 for the above-mentioned materials. The most significant changes

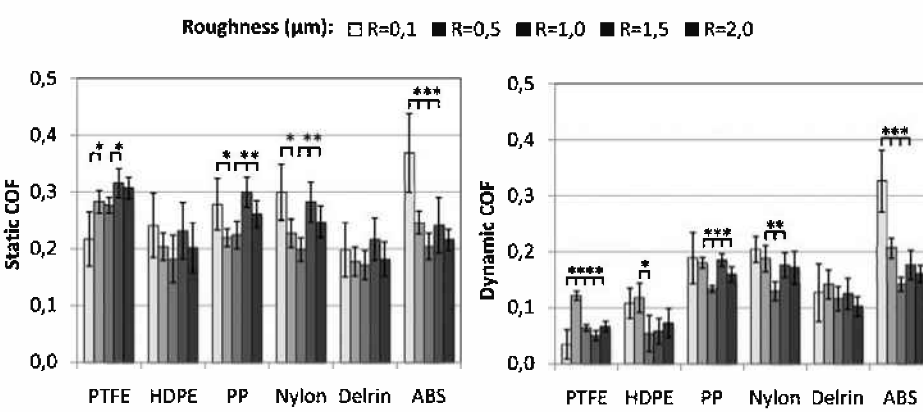

FIG. 10—*Static and dynamic COFs for thermoplastics with different probe roughness values (R) and a normal load of 10 N. Note: Stars represent statistically significant differences between adjacent data bars only.*

on dynamic COF are observed at low load (2.5 N) in particular for neoprene and nitrile elastomers. For the majority of the other conditions, the dynamic COF does not vary significantly with the load. Overall, COF is the least sensitive to load between 5 and 15 N.

Static and dynamic COFs had standard deviations between 0.08 and 1.20 for elastomers, and between 0.01 and 0.12 for thermoplastics. Most coefficients of variation were less than 15 % for elastomers and less than 25 % for thermoplastics. Preconditioning of the test specimens in a controlled temperature and humidity environment might have increased the measurement reproducibility. In most tested conditions, the statistical dispersion of static and dynamic COFs decreases with a load increase. The smallest interquartile ranges were mostly observed for the 10 N load, as can be seen for neoprene in Fig. 8. Overall, COF repeatability is best between 5 and 15 N.

For the purpose of characterizing the grip adhesion of protective gloves, 10 N appear to be a load value with a small sensitivity to load and a good repeatability for both static and dynamic COFs. This load was chosen for the step 2 of this study.

Effect of Probe Roughness

Figure 9 shows the results of static and dynamic COFs for elastomers under all the test conditions used for step 2, using a 10-N normal load. It was observed that both the static and dynamic COFs vary more with the probe surface roughness for nitrile than for neoprene. This is probably because of the characteristics

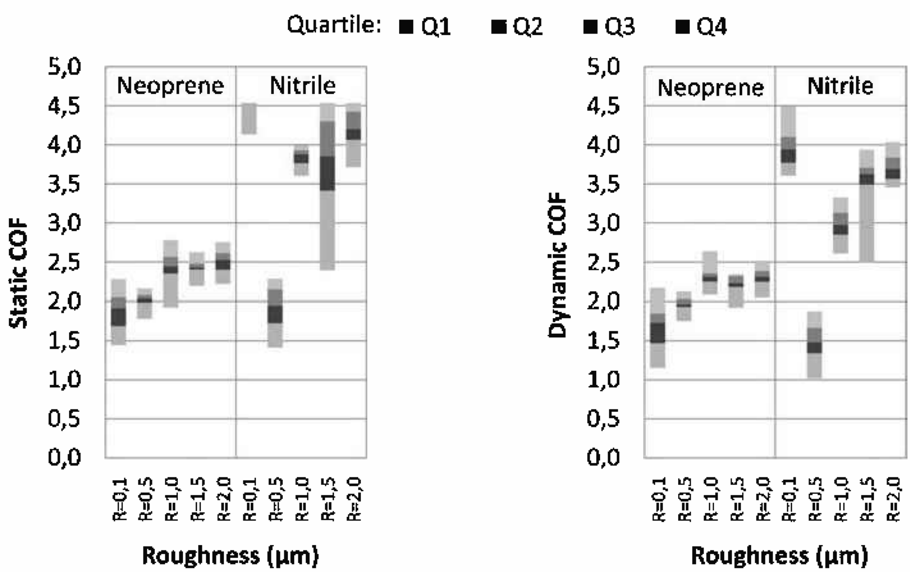

FIG. 11—*Quartile distribution of static and dynamic COFs for elastomers with different probe roughness values (R) and a normal load of 10 N.*

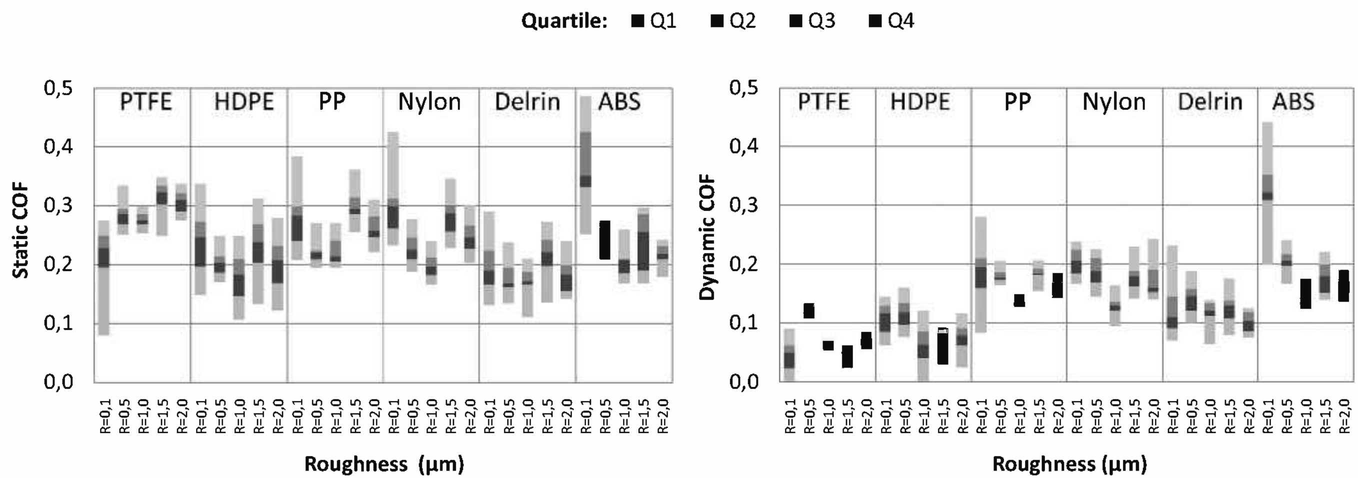

FIG. 12—*Quartile distribution of static and dynamic COFs for thermoplastics with different probe roughness values (R) and a normal load of 10 N.*

of the nitrile material used in this study, which presents a sticky surface. For static and dynamic COFs of neoprene, there were no significant differences between 0.1- and 0.5-μm probe roughness, as well as between 1.0-, 1.5-, and 2.0-μm roughness. For nitrile, there were no significant differences in static COF between 1.0-, 1.5-, and 2.0-μm roughness. The most important differences were observed on nitrile with probe roughness values of 0.1 and 0.5 μm.

Using the same experimental conditions, four other thermoplastics materials were characterized and the results of static and dynamic COFs are presented in Fig. 10. As shown in the figure, there appears to be no clear effect of the probe roughness on the static or dynamic COF for the tested thermoplastic materials.

For static and dynamic COFs of elastomers and thermoplastics, the largest interquartile ranges were obtained with 0.1- and 1.5-μm probe roughness, as shown in Fig. 11 and Fig. 12.

For the purpose of characterizing the grip adhesion of protective gloves, 1.0 and 2.0 μm are probe roughness values that seem to provide a good repeatability and a small sensitivity to roughness for both static and dynamic COFs. In those conditions, in which a 10-N normal load and a 1.0- or 2.0-μm probe roughness are used, the coefficients of variation of COF were less than 7.6 % for elastomers and less than 11.4 % for thermoplastics, except in the case of HDPE where it was equal to 23 %.

Conclusion

This study has confirmed that the static and dynamic COFs sensitivity and repeatability can vary with testing conditions. However, some conditions were identified as more suited for testing polymer materials. Out of all testing conditions used in this study, it was found that a normal load of 10 N and a surface roughness of 1.0 or 2.0 μm gave the best results for studied thermoplastics and elastomers. For these testing conditions, the coefficient of variation of the COF was smaller than 8 % for elastomers, which are often used in protective gloves. These parameters are suggested for testing protective gloves with this simple and affordable mechanical test method.

Other parameters could be examined to improve the repeatability of the measured COF, such as contact duration before starting the test, probe speed, temperature and humidity. In the next step of this research, the COF values for different available protective gloves will be characterized using the test method developed in this study.

Acknowledgments

The authors would like to thank Pierre Drouin and Christian Sirard for their help with the friction tests, and Dominique Desjardins for the pictures.

References

[1] Batra, S., Bronkema, L. A., and Wang, M. J., "Glove Attributes: Can They Predict Performance?" *Int. J. Indust. Ergon.*, Vol. 14, 1994, pp. 201–209.

[2] Buhman, D. C., Cherry, J. A., and Bronkema-Orr, L., "Effects of Glove, Orientation, Pressure, Load, and Handle on Submaximal Grasp Force," *Int. J. Indust. Ergon.*, Vol. 25, No. 3, 2000, pp. 247–256.

[3] Bronkema-Orr, L. and Bishu, R. R., "The Effects of Glove Frictional Characteristics and Load on Grasp Force and Grasp Control," *Human Centered Technology—Key to the Future. Proceedings of the Human Factors and Ergonomics Society 40th Annual Meeting*, Vol. 1, Philadelphia, PA, Sept 2–6, The Human Factors and Ergonomics Society, Santa Monica, CA, 1996, pp. 702–706.

[4] ASTM D1894-08, 2008, "Standard Test Method of Static and Kinetic Coefficients of Friction of Plastic Film and Sheeting," *Annual Book of ASTM Standards*, Vol. 08.01, ASTM International, West Conshohocken, PA.

[5] ASTM D3412-07, 2007, "Standard Test Method for Coefficient of Friction, Yarn to Yarn," *Annual Book of ASTM Standards*, Vol. 07.01, ASTM International, West Conshohocken, PA.

[6] ASTM D3108-07, 2007, "Standard Test Method for Coefficient of Friction Yarn to Solid Material," *Annual Book of ASTM Standards*, Vol. 07.01, ASTM International, West Conshohocken, PA.

[7] Kinoshita, H., "Effect of Gloves on Prehensile Forces during Lifting and Holding Tasks," *Ergonomics*, Vol. 42, No. 10, 1999, pp. 1372–1385.

[8] Mital, A., Kuo, T., and Faard, H. F., "A Quantitative Evaluation of Gloves Used with Non-Powered Hand Tools in Routine Maintenance Tasks," *Ergonomics*, Vol. 37, No. 2, 1994, pp. 333–343.

[9] Shih, R. H., Vasarhelyi, E. M., and Dubrowski, A., "The Effects of Latex Gloves on the Kinetics of Grasping," *Int. J. Indust. Ergon.*, Vol. 28, No. 5, 2001, pp. 265–273.

[10] Larivière, C., Plamondon, A., Lara, J., Tellier, C., and Boutin, J., "Biomechanical Assessment of Gloves. A Study of the Sensitivity and Reliability of Electromyographic Parameters Used to Measure the Activation and Fatigue of Different Forearm Muscles," *Int. J. Indust. Ergon.*, Vol. 34, No. 2, 2004, pp. 101–116.

[11] Gauvin, C., Dolez, P., Harrabi, L., Boutin, J., Petit, Y., Vu-Khanh, T., and Lara, J., "Mechanical and Biomechanical Approaches to Measure Protective Glove Adherence," *Proceedings of the Human Factors and Ergonomics Society 52nd Annual Meeting (HFES)*, Sept 22–26, New York, 2008, pp. 2018–2022.

[12] ISO 13997, 1999, Protective Clothing—Mechanical Properties—Determination of Resistance to Cutting by Sharp Objects," *International Organization for Standardization*, Geneva, Switzerland.

[13] ASTM F1790-05, 2005, "Standard Test Method for Measuring Cut Resistance of Materials Used in Protective Clothing," *Annual Book of ASTM Standards*, Vol. 11.03, ASTM International, West Conshohocken, PA, 2005.

[14] Tisserand, M., "Progress in the Prevention of Falls Caused by Slipping," *Ergonomics*, Vol. 28, No. 7, 1985, pp. 1027–1042.

[15] Rabinowicz, E., *Friction and Wear of Materials*, 2nd ed., Wiley, New York, 1995.

[16] Moore, D., *The Friction and Lubrication of Elastomers*, Pergamon, Oxford, 1972.

[17] Furuta, I., Kimura, S. I., and Iwama, M., "Physical Constants of Rubbery Polymers," *Polymer Handbook*, J. Brandrup et al., Eds., Wiley, New York, 2005.

[18] Schallamach, A., "Gummireibung (Friction of Rubber Vulcanizates)," *Gummi., Asbest., Kunststoffe.*, Vol. 28–3, 1975, p. 9.

[19] Myshkin, N. K., Petrokovets, M. I., and Kovalev, A. V., "Tribology of Polymers: Adhesion, Friction, Wear, and Mass-Transfer," *Tribol. Int.*, Vol. 38, 2005, pp. 910–921.

[20] Volynskii, A. L., et al., "Mechanism of the Migration of a Low Molecular Weight Component in the System Natural Rubber Vulcanizate—Low Molecular Weight Hydrocarbon," *Polym. Sci.*, Vol. 30–10, 1988, pp. 2220–2227.

Author Index

A

Ackerman, M. Y., 13-26, 308-328, 329-339
Airoldi, A., 392-406
Ashdown, S. P., 158-175
Azaiez, M., 354-370

B

Barker, J., 158-175
Barker, R., 27-47, 176-187, 188-201, 247-265, 371-391
Batcheller, J., 308-328
Beck, K., 247-265
Boorady, L. M., 158-175
Brady, J., 74-107

C

Cai, Z., 227-246
Cardello, A., 129-157
Crown, E., 290-307
Crown, E. M., 13-26, 308-328, 329-339

D

Dale, J. D., 13-26, 308-328
Darveau, O., 340-353
Deaton, A. S., 27-47, 176-187, 188-201, 371-391
Deaton, S., 247-265
Deuser, L., 188-201
Doan, D. R., 1-12
Dolez, P. I., 354-370, 392-406
Duncan, S., 48-73

E

Endrusick, T., 129-157
Esponnette, B., 158-175

F

Farwell, S. O., 227-246
Frumkin, S., 74-107

G

Gauvin, C., 340-353, 392-406
Gonzalez, J. A., 308-328

H

Hirsch, S. S., 74-107, 108-128
Hoagland, E. "Hugh" IV, 1-12
Hultzapple, K. L., 74-107
Hummel, A., 176-187

J

Jalbani, S. H., 329-339

K

Kane, S. B., 108-128

L

Lara, J., 340-353, 392-406
Lee, Y.-A., 158-175
Lesher, L., 129-157
Lin, S.-H., 158-175
Lyons, K., 176-187

M

MacTaggart, D. L., 227-246
Morton-Aslanis, J., 176-187
Murtaza, G., 308-328

N

Neal, T. E., 1-12

O

Obendorf, S. K., 266-279
Olsen, S., 290-307
Ormond, R. B., 247-265

P

Paskaluk, S., 13-26
Pierce, Jr., J. D., 108-128
Proodian, S., 74-107
Proulx-Croteau, S., 392-406

R

Rezazadeh, M., 202-226
Robin, C., 340-353
Ross, K., 27-47, 371-391

S

Shaw, A., 280-289
Shepherd, A., 188-201
Smith, P., 227-246
Song, G., 48-73, 329-339
Spero, E. F., 266-279
Strickfaden, M., 290-307

T

Thompson, D., 247-265
Torvi, D. A., 202-226
Truong, Q., 129-157

V

van Keulen, M., 329-339
Venafro, J., 74-107
Venafro, J. A., 108-128
Vu-Khanh, T., 354-370

W

Watkins, J., 371-391
Wen, S., 48-73
Winterhalter, C., 74-107, 129-157
Winterhalter, C. A., 108-128

Y

Yu, S., 290-307

Subject Index

A

adhesion, 392-406
adhesive, 247-265
adsorption, 266-279
aldicarb, 266-279
arc flash, 1-12
arc rated, 1-12
arc-flash hazard analysis, 1-12
ASTM F2588, 247-265

B

burn injury, 1-12

C

chem-/bio-ensemble, 247-265
chemical protective clothing, 48-73, 227-246
chemical warfare agent simulant, 227-246
clothing, 108-128
coefficient of friction, 392-406
color measurement, 202-226
comfort, 48-73

D

design process, 290-307
DMPC, 48-73
durability, 202-226

E

energy and mass transfer, 329-339
evaporative resistance, 27-47

F

fire resistant gloves, 176-187
fire test manikins, 176-187
firefighter, 158-175
firefighters' protective clothing, 202-226
firefighting, 188-201
flame resistant, 1-12
flash fire, 1-12, 176-187

G

glove materials, 392-406
gloves, 371-391
grip, 371-391, 392-406

H

heat stress, 27-47
heat transfer, 176-187
hot water and steam hazards, 290-307
hot water hazards, 329-339
hypodermic needle, 340-353

I

interlaboratory study, 188-201

K

Kawabata, 48-73

L

labeled magnitude scale, 108-128

M

man-in-simulant-test, 247-265
methyl salicylate, 247-265
MgO, 266-279
MIST, 247-265

moisture vapor transmission rate, 129-157
multi-method, 290-307
multiple exposures, 202-226

N

needle puncture resistance, 340-353
N-halamine, 266-279
non-destructive tests, 202-226

O

oilfields, 290-307
outer shell, 202-226

P

PADs, 247-265
passive adsorbent dosimeters, 247-265
permeation testing, 227-246
personal protection, 227-246
personal protective equipment, 1-12, 158-175
pesticide operators, 280-289
physical burden, 48-73
physiological response, 27-47
pointed blades, 354-370
PPE, 280-289, 290-307
protective clothing, 129-157, 188-201, 266-279, 280-289
protective gloves, 340-353, 354-370
Psychophysics, 108-128
puncture, 354-370

S

self decontamination, 266-279
semi-permeable membrane, 129-157
sensory comfort, 129-157
service life, 202-226
simulant concentration, 247-265
slippage, 371-391
standard test method, 340-353
stored energy, 188-201
structural firefighter gloves, 371-391
swatch test equipment, 227-246
sweating hot plate, 27-47
sweating manikin, 27-47

T

test procedures, 329-339
textiles, 188-201
thermal aging, 202-226
thermal comfort, 108-128
thermal manikin, 27-47
thermal protection, 329-339
thermal protective performance, 176-187
thermal resistance, 27-47
thermal sensors, 176-187
thermoregulatory responses, 129-157
THL, 27-47
torque, 371-391
total body surface area (TBSA), 1-12
total heat loss, 27-47
turnout gear, 158-175, 188-201

U

uptake rate, 247-265

www.astm.org

ISBN: 978-0-8031-7530-3
Stock #: STP1544